THE UNIVERSITY *of* EDINBURGH

Field-based evidence of sedimentary and tectonic processes related to continental collision: the Early Cenozoic basins of Central Eastern Turkey

Matthew Booth

Thesis submitted for the degree of Doctor of Philosophy

The University of Edinburgh

2012

I declare that the work presented in this thesis is entirely my own work, except where contributions have been cited or duly acknowledged.

Matthew Booth 2012

Abstract

Turkey is widely accepted to have formed from a collage of microcontinents that rifted from the northern margin of Gondwana and assembled from the Mesozoic to Mid Cenozoic in response to the closure, collision and suturing of numerous oceanic strands in the Eastern Mediterranean. Sedimentary-tectonic basins, which formed during ocean basin closure, can yield important information about the evolution, timing and processes related to the closure of these oceanic strands. The Darende Basin and the adjacent Hekimhan Basin are two sedimentary-tectonic basins which developed during the collision and suturing of the Neotethys Ocean in the Eastern Mediterranean.

The Darende and Hekimhan Basins developed as part of the northern margin of the Tauride microcontinent during the collision and suturing of Neotethys. Both basins exhibit a Jurassic to Cretaceous regional carbonate platform 'basement' overlain by a dismembered ophiolite, which was emplaced southwards during the Late Cretaceous. The basins then developed in two main phases: In the Darende Basin the first phase is characterised by non-marine clastic sediments, overlain by transgressive shallow-marine rocks. In the Hekimhan Basin, hemi-pelagic facies are deposited synchronously with the eruption of within plate-type alkaline basaltic-trachytic lavas and associated volcaniclastic sediments (later intruded by a syenitic pluton) under an extensional tectonic regime. A Paleocene-aged unconformity followed. A second phase of basin evolution during the Eocene is characterised in both basins by the deposition of variable sedimentary facies including conglomerate, sandstone, marl, shallow-marine nummulitic limestone and evaporites (and localised basaltic eruptions). These record successive deepening, shallowing and finally emergence of both basins during the Late Eocene. The Oligocene is represented by continental fluvial deposits that are only exposed in the Hekimhan Basin. The deposition of faunally diverse, shallow-marine, Miocene limestones, Pliocene subaerial basalts and Pliocene-Recent continental deposits in both basins completes the sequence.

The following tectonically and eustatically controlled stages of basin development are inferred: 1) Late Cretaceous extension initiated basin development (after ophiolite emplacement), possibly related to immediate isostatic compensation and on-going slab-pull during northward subduction of the remaining Neotethyan oceanic crust. The eruption of within-plate lavas and the intrusion of alkaline syenite bodies in the Hekimhan Basin reflect this extensional setting; 2) Emergence of the Darende and Hekimhan Basins in the latest Cretaceous was possibly controlled by regional flexural uplift as the down-going plate approached the subduction zone to the north (and was possibly also influenced by eustatic sea-level change); 3) Early Eocene flexural subsidence related to ‘soft collision’ of the Tauride microcontinent with Eurasia, coupled with a significant eustatic sea level rise, allowed sedimentation to resume; 4) Mid-Late Eocene ‘hard collision’ resulted in regional uplift, progressive isolation and subaerial exposure of the basins; 5) Suture tightening and compression, during the Late Eocene-Miocene, resulted in reactivation of pre-existing extensional faults and terminated marine sedimentation. Both basins were affected by predominantly sinistral strike-slip faulting during the Plio-Quaternary westward tectonic escape of Anatolia.

Acknowledgements

There are a number of people I would like to thank for their assistance and input into the project.

First and foremost thanks must go to my supervisor, Alastair Robertson. His enthusiasm for geology is unwavering (especially in the field) and he has been a true inspiration to me throughout my PhD. If ever I doubted the project or my role in it, a meeting with Alastair would fill me with optimism and enthusiasm which I hope has transferred across to the production of this thesis.

I would like to thank Stephen Vincent, my supervisor at CASP, for all his help in the field and with the write up and papers. I would like to thank Ulvi Can Ünlügenç of Çukorova University, Adana and his family for their hospitality. His help with logistics was crucial for all four field seasons in Turkey. Further to this, I would like to thank my field Assistants; Selim Solak, Gündüz Alp and special thanks to Süleyman Karahan and his family for looking after me during my final field season and who remains a valued friend.

Thanks go to Nurdan İnan and Kemal Taslı, of Mersin University, who provided crucial palaeontological analysis. Also, to Kemal Gürbüz and Osman Parlak, of Çukorova University, for their help and support.

Many thanks are extended to various members of the department of Geosciences at the University of Edinburgh; John Dixon, my second supervisor, for his useful input and dialogue regarding geochemical aspects; Hugh Sinclair, my advisor, for amazing field work opportunities and geological input; John Underhill for his support and financial assistance; Dick Kroon for 4 consecutively unique years on the Cyprus Fieldtrip; Nic Odling for patiently teaching me geochemical techniques and Mike Hall for preparing many, many thin sections. Thank you to Gillian McCay, Steve Nairn and Romesh Palamakumbura, my fellow Tethyan researchers.

Not so formal acknowledgements

"To those who helped me, thank you very much. To those who didn't, thank you very little." *–Kanye West, The College Dropout, 2004.*

Firstly, I would like to thank my Mum, who has supported me in everything I've done, and in every conceivable way, over the years. My step father who has been a rock at times of need. And, my recently reacquainted father and his wife Gale, you've made the past year much easier than it could have been.

I'd like to thank Pete Kokelaar and Richard Worden at Liverpool University for making me believe I could do this thing after completing my degree. Thanks again to Alastair who took me on for this PhD and is probably the best PhD supervisor you could ask for!

Special thanks go to those at Edinburgh who made this what it was. To Alex de Joux ne Kaye (and husband Andrew de Joux) from Liverpool to Edinburgh to Australia? May the good times continue! Niklas Heinemann for the one or two pints we had… and for so much more, Grant Nicoll for making me one of the Clan, Martin Hurst for the numerous rounds of golf and adventures in Cyprus, Laura Comeau for being a true star and for the love of goats cheese, Matthew Brolly for cinema trips, watching football and dub step (one day), Dave Lee for attempting golf (slappy slappy) and daily 11am KB coffee breaks, Jen Roberts for the unique individualism you will always bring to the table, Simon Haunch for always making things fun! Jamie Stewart (the Hoff) a thoroughly decent character, Andrew Miles for cycling and for giving me a home in the final months (and Matt Hiscock too), Mark Beaumont and Matt Clarkson for all the cycling chat, Geoff Bromiley for making Cyprus entertaining, and… memorable! Thanks to Polly Bulmer, for everything. And to everyone else who has made this an unforgettable experience; Rosie Jones, Simon King, Ian Bartholomew, Rudra Kapilla, Melanie Douarin, David Frankland, Nick Johnson, Rachel Kilgallon, Dan Hobley, Darren Wilkinson, Gillian McCay, Romesh Palamakumbura, Luke Ridley. Lastly, I'll be forever grateful to Lauren Clay.

Table of Contents

CHAPTER 1: INTRODUCTION 1

1.1 ORGANISATION OF THE THESIS 1
1.2 RATIONALE 2
1.3 AIMS 8
1.4 REGIONALLY IMPORTANT GEOLOGICAL UNITS AND PROCESSES 10
1.4.1 Niğde-Kırşehir Massif 10
1.4.2 The Tauride microcontinent 14
1.4.3 Ophiolite formation and emplacement 15
1.4.4 The Central Anatolian sedimentary basins 21
1.4.4.1 The Ulukışla Basin 23
1.4.4.2 The Sivas Basin 24
1.4.4.3 Kırıkkale Basin 25
1.4.4.4 Tuz Gölü Basin 26
1.4.5 The Pontide active margin 27
1.5 CONTRASTING TECTONIC MODELS OF BASIN DEVELOPMENT 30
1.6 METHODOLOGY 33
1.7 TURKISH PRONUNCIATION 35

CHAPTER 2. REVISED STRATIGRAPHY, LITHOLOGICAL DESCRIPTION AND INTERPRETATION OF THE DARENDE BASIN 37

2.1 INTRODUCTION 37
2.2 AIMS 44
2.3 PREVIOUS WORK 45
2.4 STRATIGRAPHY AND SEDIMENTOLOGY 47
2.4.1 Mesozoic 'Basement' 47
2.4.1.1 Mesozoic Platform Limestones (Geniz Formation) 47
2.4.1.2 Interpretation of the Mesozoic Platform Limestones (Geniz Formation) 51
2.4.1.3 Upper Cretaceous ophiolitic mélange (Hocalikova Formation) 52
2.4.1.4 Interpretation of the Upper Cretaceous ophiolitic mélange (Hocalikova Formation) 55
2.4.1.5 Ophiolite Geochemistry 55
2.4.2 Maastrichtian Sediments 58
2.4.2.1 Maastrichtian non-marine clastics (Ulupınar Formation) 58
2.4.2.2 Interpretation of the Maastrichtian non-marine clastics (Ulupınar Formation) 65
2.4.2.3 Rudist patch reefs (Tohma Member) 66
2.4.2.4 Interpretation of the rudist patch reefs (Tohma Member) 67
2.4.2.5 Maastrichtian transgressive shallow-marine carbonates (Kırankaya Formation) 68

2.4.2.6 Interpretation of the Maastrichtian transgressive shallow-marine carbonates (Kırankaya Formation). 73
2.4.3 Paleocene unconformity *75*
2.4.4 Interpretation of Paleocene unconformity *78*
2.4.5 Eocene sediments and volcanic rocks *79*
2.4.5.1 Early-Middle Eocene shallow-marine clastics (Korgantepe Formation) 79
2.4.5.2 Interpretation of the Early-Middle Eocene shallow-marine clastics (Korgantepe Formation) 89
2.4.5.3 Middle Eocene Volcanism (Karakayalar Member) 90
2.4.5.4 Geochemistry 93
2.4.5.5 Interpretation of the Middle Eocene Volcanism (Karakayalar Member) 98
2.4.5.6 Middle Eocene marine carbonates (Yenice Formation) 98
2.4.5.7 Interpretation of the Middle Eocene marine carbonates (Yenice Formation) 106
2.4.5.8 Middle Eocene shallow-marine carbonates (Asartepe Formation) 106
2.4.5.8 Interpretation of the Middle Eocene shallow-marine carbonates (Asartepe Formation) 115
2.4.5.9 Late-Eocene shallow-marine regressive facies (Darende Formation) 116
2.4.5.10 Interpretation of the Late Eocene shallow-marine regressive facies (Darende Formation) 123
2.4.6 Post Eocene *125*
2.4.6.1 Tahtalı Formation 125
2.4.6.2 Interpretation of the Miocene Tahtalı Formation 127
2.4.6.3 Kepez Formation 128
2.4.6.4 Interpretation of the Kepez Formation 129
2.4.6.5 Çaybaşı Formation 129
2.4.6.6 Interpretation of the Çaybaşı Formation 131
2.5 STRUCTURAL DEVELOPMENT OF THE DARENDE BASIN 132
2.5.1 Introduction *132*
2.5.2 Extensional features *133*
2.5.2.1 Extension within Mesozoic rocks 133
2.5.2.2 Extension within Eocene rocks 135
2.5.3 Compressional features *139*
2.5.3.1 Folding 139
2.5.3.2 Reverse faulting 145
2.5.4 Strike-slip faulting *151*
2.5.5 Interpretation of structural data 158
2.6 BASIN DEVELOPMENT 160
2.6.1 Latest Cretaceous *160*
2.6.2 Palaeocene-Early Eocene emergence *162*
2.6.3 Middle Eocene transgression *162*
2.6.4 Late Eocene shallow-marine carbonates *163*

CHAPTER 3. REVISED STRATIGRAPHY, LITHOLOGICAL DESCRIPTION AND INTERPRETATION OF THE HEKIMHAN BASIN 167

3.1 INTRODUCTION 167
3.2 AIMS 170

3.3 PREVIOUS WORK 173
3.4 STRATIGRAPHY 175
3.4.1 Mesozoic 'Basement' *175*
3.4.1.*1* Mesozoic Bolkar Carbonate Platform (Geniz Formation) 175
3.4.1.2 Interpretation of the Mesozoic Platform Limestones (Geniz Formation) 177
3.4.1.3 Upper Cretaceous ophiolitic mélange (Hocalikova Formation) 178
3.4.1.4 Interpretation of the Upper Cretaceous ophiolitic mélange (Hocalikova Formation) 182
3.4.1.5 Ophiolite Geochemistry 182
3.4.2 Maastrichtian sediments, volcanism and magmatism *185*
3.4.2.1 Maastrichtian non-marine clastics (Karadere Formation) 185
3.4.2.2 Interpretation of the Maastrichtian non-marine clastics (Karadere Formation) 192
3.4.2.3 Rudist bearing patch reefs (Tohma Member) 193
3.4.2.4 Interpretation of the rudist bearing patch reefs (Tohma Member) 195
3.4.2.5 Maastrichtian transgressive marine marls (Hekimhan Formation) 196
3.4.2.6 Interpretation of the Maastrichtian transgressive marine marls (Hekimhan Formation) 202
3.4.2.7 Maastrichtian volcanism (Hasançelebi Formation) 203
3.4.2.8 Geochemistry of the Maastrichtian volcanism (Hasançelebi Formation) 215
3.4.2.9 Geochemistry of the Maastrichtian inter-lava sediments (Hasançelebi Formation) 224
3.4.2.10 Interpretation of the Maastrichtian volcanism and inter-lava sediments (Hasançelebi Formation) 229
3.4.2.11 Maastrichtian Magmatism (Yüceşafak Member) 230
3.4.2.12 Geochemistry of the Maastrichtian Magmatism (Yüceşafak Member) 233
3.4.2.13 Interpretation of the Maastrichtian Magmatism (Yüceşafak Member) 234
3.4.2.14 Maastrichtian shallow-marine transgressive carbonates (Hüyük Formation) 235
3.4.2.15 Interpretation of the Maastrichtian shallow-marine transgressive carbonates (Hüyük Formation) 238
3.4.3 Paleocene–Eocene sediments and volcanic rocks *239*
3.4.3.1 Paleocene–Eocene evaporites (Ağharman Member) 239
3.4.3.2 Interpretation of the Paleocene–Eocene evaporites (Ağharman Member) 243
3.4.3.3 Eocene transgressive sediments (Akpınar Formation) 245
3.4.3.4 Interpretation of the Eocene transgressive sediments (Akpınar Formation) 250
3.4.3.5 Eocene basaltic volcanism (Kocaözü Member) 250
3.4.3.6 Geochemistry of the Eocene basaltic volcanism (Kocaözü Member) 251
3.4.3.7 Interpretation of the Eocene basaltic volcanism (Kocaözü Member) 254
3.4.3.8 Eocene andesitic volcanism (Leylek Member) 255
3.4.3.9 Geochemistry of the Eocene Andesitic volcanism (Leylek Member) 258
3.4.3.10 Interpretation of the Eocene Andesitic volcanism (Leylek Member) 258
3.4.4 Post Eocene *260*
3.4.4.1 Oligocene continental sediments (Kamatlar Formation) 260
3.4.4.2 Interpretation of the Oligocene continental sediments (Kamatlar Formation) 263
3.4.4.3 Miocene transgressive carbonates (Boyralı Formation) 263
3.4.4.4 Interpretation of the Miocene transgressive carbonates (Boyralı Formation) 265
3.4.4.5 Pliocene subaerial volcanism (Yamadağ Formation) 265
3.4.4.6 Interpretation of the Pliocene subaerial volcanism (Yamadağ Formation) 268
3.5 STRUCTURAL DEVELOPMENT OF THE HEKIMHAN BASIN 269
3.5.1 Introduction *269*

3.5.2 Extensional features *271*
3.5.3 Compressional features *277*
3.5.3.1 Folding 277
3.5.3.2 Reverse faulting 279
3.5.4 Strike-slip faulting *282*
3.5.5 Interpretation of structural data *287*
3.6 BASIN DEVELOPMENT 290
3.6.1 Latest Cretaceous *291*
3.6.2 Paleocene *293*
3.6.3 Eocene *294*
3.6.4 Post-Eocene *294*

CHAPTER 4. COMPARISON AND DISCUSSION 295

4.1 INTRODUCTION 295
4.2 COMPARISON OF THE DARENDE AND HEKIMHAN BASINS 298
4.2.1 Maastrichtian *300*
4.2.2 Paleocene *303*
4.2.3 Eocene *303*
4.2.4 Post Eocene *304*
4.3 EXISTING REGIONAL TECTONIC MODELS 306
4.4 DEVELOPMENT OF THE DARENDE AND HEKIMHAN BASINS 307
4.4.1. Regional context *307*
4.4.2 Evolution of the Darende and Hekimhan Basins *308*

CHAPTER 5. CONCLUSIONS 321

REFERENCES 323

APPENDIX 1: X-RAY FLUORESCENCE METHODOLOGY AND DATA I

APPENDIX 2: STRUCTURAL DATA X

Chapter 1: Introduction

Chapter 1: Introduction

1.1 ORGANISATION OF THE THESIS

This thesis is presented as a series of chapters representing individual papers currently accepted for publication, or intended to be submitted for publication. Chapter 2 concerns the description, analysis and interpretation of the Darende Basin and represents an extended version of a paper accepted for publication in the Geological Society of London, Special Publication Number 372 entitled 'The Geological Development of the Anatolian Continent and the Eastern Mediterranean Region'. The paper version is concise and many of the intricate details of the Darende Basin had to be omitted. However, the thesis version is comprehensive. Chapter 3 is a similar comprehensive description, analysis and interpretation of the Hekimhan Basin and is intended to be edited for journal publication in abbreviated form. To this end, Chapters 2 and 3 contain brief summaries of previous research contributions, and new descriptions of stratigraphic, sedimentary, geochemical and structural data for each formation. Short interpretations highlighting the main points of each formation build towards a complete interpretation of the basin evolution given at the end of each chapter. Chapter 4 compares and contrasts the Darende and Hekimhan Basins and explores their evolution in terms of the regional tectonic development of Anatolia and the Eastern Mediterranean as a whole. Summary conclusions are presented in Chapter 5. The remainder of this introductory chapter (Chapter 1) focuses on the project rationale and project aims, the regional geological context and the contrasting modes of basin formation as well as explaining the project methods.

Descriptions of the stratigraphy are defined by lithology, mineralogy, textures, structures, fossil content, boundaries, bed thickness and geographic extent. Interpretations are based on these observations, together with geochemical, palaeontological, structural and petrological analysis and inferred depositional processes and environments. Interpretations of advanced transport and depositional process are beyond the scope of this thesis. The timescale by Gradstein *et al.* (2004) is used throughout.

1.2 RATIONALE

Turkey forms part of the Alpine-Himalayan orogen, which extends ~7000 km from the Atlantic Ocean to the Himalayas and provides a remarkably well preserved and well exposed natural laboratory in which to research advanced tectonic concepts. Turkey and the adjacent countries benefit from substantial oil, gas and mineral reserves. Understanding the geology, and by inference the tectonic development, of the region will help to elucidate future exploration targets. Much research has been conducted on the subduction of a single oceanic basin, for example the Andes in South America (e.g. James 1971; Ramos & Kay 2006) and in orogenesis based on the closure of a single oceanic basin leading to continental collision (i.e. the Wilson cycle; Wilson 1966), for example, the Himalayas (e.g. Dewey *et al.* 1989; Yin 2006). However, some collisional environments are more complicated, for example, modern collisional zones, such as the Caribbean (e.g. Burke 1988; Meschede & Frisch 1998) and the Southwest Pacific (e.g. Charlton 2000; Milsom 2001; Hinschberger *et al.* 2005). There, tectonic evolution involves the interaction of several discrete microcontinental plates and associated small oceanic basins. Similar tectonic scenarios could apply to ancient oceans and collisional events. The Eastern Mediterranean region, and specifically Turkey, appears to have developed in this way. Turkey formed during the closure of the Palaeozoic-Mesozoic Tethys Ocean, located between Africa-Arabia (Gondwana) to the south and Eurasia to the north. The closure of this ocean led to the development of important suture zones (Fig 1.1). These suture zones mark the boundaries of oceanic basins, and previously separated lithospheric plates, which have proven crucial in the development of regional tectonic models (e.g. Şengör & Yılmaz 1981; Dercourt *et al.* 1986; Robertson & Dixon 1984; Okay & Tüysüz 1999; Robertson 2002; 2006; Robertson *et al.* 2009). The suture zones are associated with, and separated, by a variety of well-exposed tectonic units including continental fragments, ophiolites, metamorphic soles, magmatic arcs and sedimentary basins.

The evolution of the Tethys Ocean within the Tethyan realm can be divided into two overlapping phases: Palaeotethyan and Neotethyan (Old and New Tethys, respectively; Şengör & Yılmaz 1981). The Palaeotethys Ocean existed as a wedge-shaped oceanic basin, closing to the west and open to the east (Fig 1.2), which formed as a result of the break-up of Pangea during the Triassic and was a precursor to the development of

the Neotethys Ocean (Bullard *et al.* 1965; Kearey *et al.* 2009). Neotethyan oceanic lithosphere formed by rifting of the northern margin of Gondwana, to the south of the Palaeotethys Ocean (Fig. 1.2). The timing of this rifting, as well as the number of continental fragments, subduction zones and associated suture zones have been the subject of vigorous debate (Şengör & Yılmaz 1981; Robertson & Dixon 1984; Şengör *et al.* 1984; Görür *et al.* 1998; Stampfli 2000; Stampfli & Borel 2002; Gürer & Aldanmaz 2002; Okay *et al.* 2006; Mackintosh 2008; Mackintosh & Robertson 2009, in press). The Neotethys Ocean has been restored in different ways. The models can be summarised as: 1) a single oceanic basin, with ophiolites formed at one spreading centre (Fig. 1.3c; Ricou *et al.* 1984; Dercourt *et al.* 1986); 2) An oceanic basin split by a large continental fragment, the 'Cimmerian continent' (which includes the Tauride platform), which drifted northwards and opened the Neotethys Ocean during the Late Permian-Early Triassic. At the same time, an 'Anatolide block' rifted from Eurasia to collide with the Cimmerian continent. The Palaeotethys Ocean was simultaneously subducted northwards, beneath Eurasia (Stampfli 2000; Stampfli & Borel 2002; Moix *et al.* 2008). 3) Multiple oceanic sub-basins consisting of; 1) the Intra-Pontide Ocean, separating the Pontides from the Sakarya microcontinent; 2) the Northern Neotethys, separating the Pontides and Eurasia from the Tauride-Anatolide Block, and; 3) the Southern Neotethys, separating the Tauride-Anatolide Block from Africa-Arabia (northern Gondwana) (Fig. 1.3 a, b & d; Robertson & Dixon 1984; Şengör *et al.* 1984; Robertson *et al.* 2009). In the latter scenario, the Northern Neotethys can be subdivided into the İzmir-Ankara-Erzincan Ocean (IAEO), to the north, and the Inner-Tauride Ocean (ITO), to the south, separated by the Niğde-Kırşehir Massif (Fig. 1.3d; Dilek *et al.* 1999; Robertson 2007; Robertson *et al.* 2009). The origin and evolution of the Niğde-Kırşehir Massif is still debated and will be discussed later.

The Tauride Mountains in Central Eastern Turkey, specifically, are widely accepted to have formed by the amalgamation of several crustal fragments that rifted from the northern margin of Gondwana (modern-day North Africa) during Early Mesozoic time. (Şengör & Yılmaz 1981; Robertson & Dixon 1984; Robertson *et al.* 1991). During the Late Cretaceous, Tethyan oceanic lithosphere subducted northwards beneath Eurasia and also within Neotethys (Robertson & Dixon 1984; Görür *et al.* 1984; Dercourt *et al.* 1986; **2000**). Subduction instigated the collision and amalgamation of

microcontinents, leading to the formation of suture zones characterised by ophiolitic rocks and mélanges (Fig. 1.1). The suture zones are also associated with the development of distinctive sedimentary basins of latest Cretaceous–Eocene age. The 'syn-collisional' Darende and Hekimhan Basins in central eastern Anatolia, the subject of this thesis, are two such sedimentary basins. Some previous work on 'syn-collisional' sedimentary basins has tended to assume simple closure of an oceanic basin as a part of the classical plate tectonic Wilson Cycle (Dickinson & Seely 1979; Friedmann & Burbank l995). In this scenario, continental rifting was followed by spreading at a mid-ocean ridge to create oceanic crust that was later subducted, leading eventually to continental collision. However, it is now known that much of the preserved oceanic crust in orogenic belts, including the Tethyan orogen, formed by spreading above subduction zones rather than at mid-ocean ridges (Pearce *et al.* l984; Saunders & Tarney l984; Stern & Bloomer 1992; Robertson 2002; Takhanashi *et al.* 2007; Dilek & Furnes 2009; Stern 2010). In some cases, two subduction zones may be involved in ocean basin closure, one related to intra-oceanic supra-subduction zone spreading to form a supra-subduction zone-type ophiolite and another related to the closure and suturing of the oceanic basin (Shervais 2001; Robertson 2006). This type of tectonic setting has some important implications for related sedimentary basin development (Robertson 1994) of which the Arabian Gulf and specifically the Oman Makran region is the type example (e.g. Mann *et al.* 1990; Robertson *et al.* 1990; Warburton *et al.* 1990).

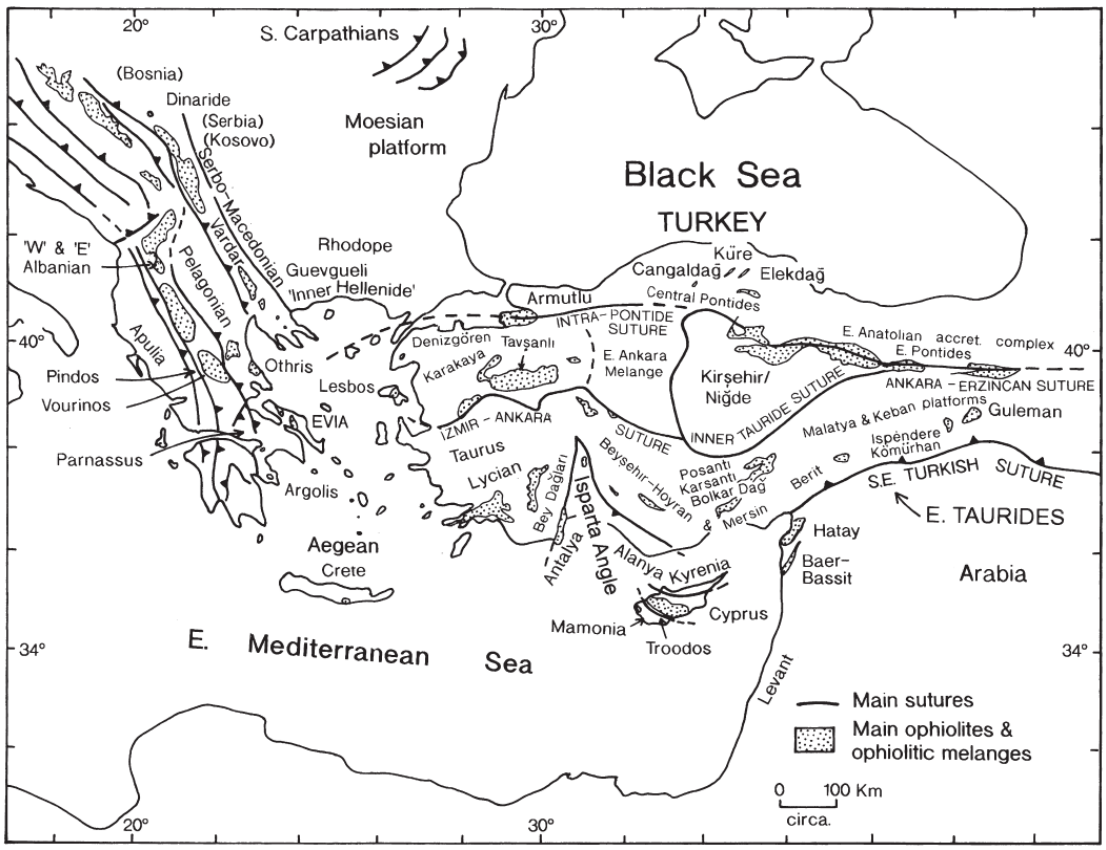

Figure 1.1. Outline tectonic map showing the main suture zones and associated ophiolite locations in the Eastern Mediterranean region (from Robertson 2007).

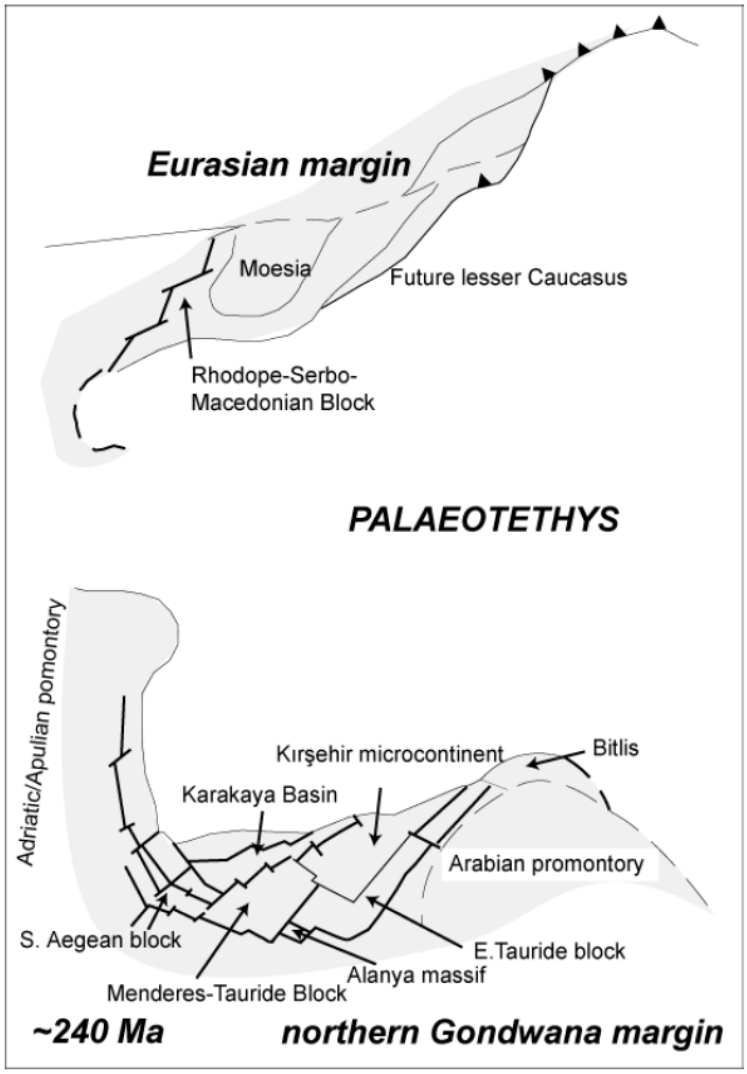

Figure 1.2. Schematic palaeotectonic map of the Eastern Mediterranean region at ~240 Ma (Triassic) showing rifting of the Gondwanan margin to the south of the Palaeotethys Ocean (after Robertson & Dixon 1984, redrawn by Nairn 2010).

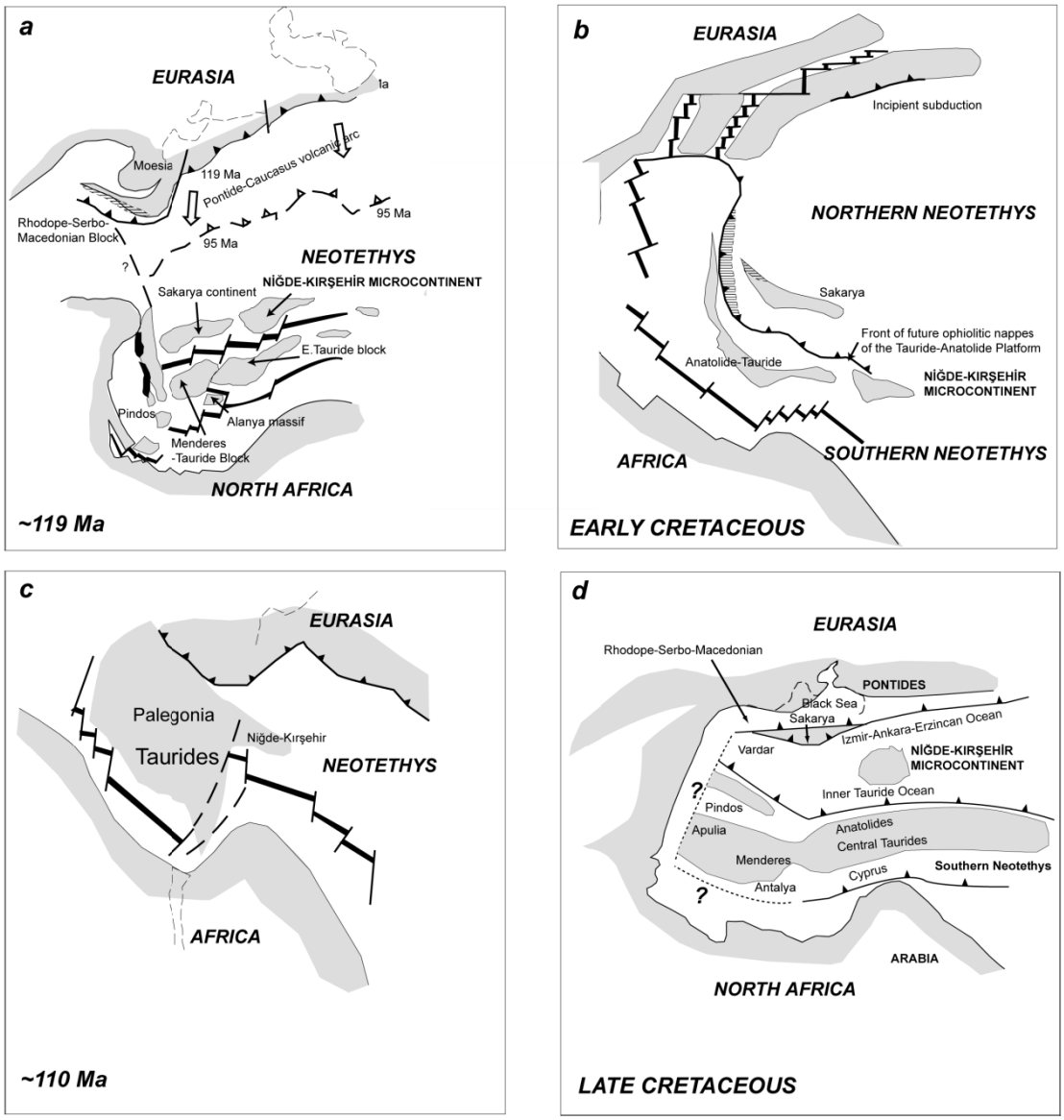

Figure 1.3. Schematic palaeotectonic reconstructions of the Eastern Mediterranean throughout the Cretaceous. a, Northward subduction of the northern Neotethys Ocean beneath the Eurasian margin and the northwards movement of continental fragments rifted from Gondwana. Ophiolites were formed above subduction zones (after Robertson & Dixon 1984); b, Northward drift of continental fragments (Cimmeria) towards a Eurasian passive margin (after Şengör *et al.* 1984b); c, One evolving Tethys Ocean in which Neotethyan ocean crust formed in a single ocean basin to the north of Gondwana where Cretaceous ophiolites were formed at spreading ridges (after Dercourt *et al.* 1986). See Robertson *et al.* (1996) for further discussion; d, Palaeotectonic reconstruction showing the positions of the Izmir-Ankara-Erzincan Ocean and the inferred Inner Tauride Ocean (after Robertson et al. 2009, figures redrawn by Nairn 2010)

1.3 AIMS

Sedimentary-tectonic basins to the north, south and west of the Niğde-Kırşehir Massif are well documented. However, comparatively little research has been conducted on sedimentary-tectonic basins to the east of the Niğde-Kırşehir Massif. The aim of this study is to examine the sedimentary-tectonic basins situated to the east of the Niğde-Kırşehir Massif in order to test whether the regional geodynamic evolution models of Central Turkey are applicable to Central Eastern Turkey. Specifically, the project aimed to seek evidence for the existence and evolution of the Inner Tauride Ocean during Maastrichtian-Eocene times. Two basins were chosen for this study, the Darende Basin and the Hekimhan Basin. The analysis of a single basin would not have provided enough information for the regional geological evolution. More than two basins would have been too much work. The two basins studied here provide the ability for direct comparison and comparison with other basins as well as the construction of a more thorough geological model.

This study builds on the work of previous authors. However, a complete, integrated geological analysis of either the Darende Basin or Hekimhan Basin, or a coherent tectonic evolution model have never been attempted. It is therefore crucial to asses and interpret the evolution of these basins, and then discuss their evolution in terms of a regional tectonic model.

This was achieved by a modern, multi-method geological approach involving: 1) four data collection field seasons; 2) detailed electronic remapping using a combination of software; 3) measurement of stratigraphic sections; 4) primary structural fault and fold data collection and analysis, and synthesis with kinematic indicators; 5) detailed micropalaeontological analysis in conjunction with specialists from Mersin University, Kemel Taslı and Nurden Inan; 6) geochemical analysis of igneous rocks and; 7) palaeocurrent analysis.

The findings of this work will help to illuminate the processes involved in continental collision and, more directly, the processes involved in incipient microcontinental collision and basin formation within this tectonic setting. The results are

relevant to other orogens (i.e. the Himalayas or the Iapetus orogens) and can also be used to elucidate less well known tectonic environments (e.g. parts of SE Asia).

1.4 REGIONALLY IMPORTANT GEOLOGICAL UNITS AND PROCESSES

In order to understand the potential importance of research into the syn-collisional sedimentary-tectonic basins in Turkey, it is necessary to fully appreciate the tectonic setting of the various crustal units in the region. Regionally important geological units are summarised below, including their evolution and the processes which lead to their formation.

1.4.1 Niğde-Kırşehir Massif

The Niğde-Kırşehir Massif (also termed the Central Anatolian Crystalline Complex (CACC); Göncüoğlu *et al.* 1991) is located in Central Turkey between the Pontide mountain range to the north and the Tauride mountain range to the south. It has a triangular-shaped geometry, covering ~250x250x250 km of modern Turkey. It is bounded to the west by the Tuz Gölü fault zone and in the east by the Ecemiş fault zone. The Niğde-Kırşehir Massif consists of a Palaeozoic-Mesozoic metamorphic basement composed of platform metasediments (marbles, calc-silicates and mica-schists), amphibolites and garnet gneisses (Seymen 1981), overlain by ophiolite-related rocks. This sequence was intruded by upper Cretaceous plutons of mainly granitic, granodioritic, monzonitic and syenitic composition. The intrusives have been dated as ~74-92 Ma by a range of methods including U/Pb SHRIMP giving ages of 85-92 Ma (Whitney *et al.* 2003), U/Pb titanite giving ages of 74.0±2.8 and 74.1±0.7 Ma (Köksal *et al.* 2004), K/Ar cooling ages of hornblende and biotite are 66.6±1.1 Ma to 79.5±1.7 Ma (Ilbeyli *et al.* 2004) and, $^{40}Ar/^{39}Ar$ biotite cooling ages are 77.6±0.3 Ma (Kadıoğlu *et al.* 2003). The Niğde-Kırşehir Massif is overlain by Cretaceous–Cenozoic basin deposits.

The tectonic setting of the Niğde-Kırşehir Massif has been the subject of some debate. It has been restored as: 1) a northern promontory of the Tauride-Anatolide continent (Fig. 1.4a; Yaliniz *et al.* 1996; Floyd *et al.* 2000; Göncüoğlu *et al.* 2006); 2) as part of the southern margin of Eurasia (Kazmin & Tikhonova 2006); 3) as an allochthonous block transferred laterally, via strike-slip faulting, during the Triassic (Stampfli *et al.* 2001), or; 4) as a microcontinent within the Northern Neotethys Ocean (Fig. 1.4b; Görür *et al.* 1984; Robertson & Dixon 1984; Whitney *et al.* 2001; Robertson *et al.* 2009; Lefebvre 2012). The latter interpretation is becoming widely accepted thanks to

a large amount of field, geochemical and palaeomagnetic research. One of the main points in favour of the Niğde-Kırşehir Massif representing a separate microcontinent (and, therefore, supports the existence of the Inner-Tauride-Ocean to the south) is that the northern margin of the Anatolide–Tauride continent experienced regional HP/LT metamorphism (Candan *et al.* 2005). This contrasts with the Niğde-Kırşehir Massif, that experienced Barrovian metamorphism (at up to 5–6 kbar, 700^{o}C) (Whitney & Dilek 1998; Fayon *et al.* 2001). The Niğde-Kırşehir Massif is, therefore, likely to have been located in an over-riding plate with the Tauride-Anatolide margin located on a subducting plate. Furthermore, if the Niğde-Kırşehir Massif were a promontory of the Tauride-Anatolide microcontinent, the ophiolitic rocks must, therefore, have been derived from a supra-subduction zone located in the İzmir-Ankara-Erzincan Ocean to the north. Thus, they would have been transported >500 km southwards, which seems excessive (Andrew & Robertson 2002).

The Niğde-Kırşehir Massif has recently been subdivided into three crustal units, which restore as a single elongate NE–SW trending microcontinent during the Cretaceous (Fig. 1.5; Lefebvre *et al.* 2012). Collision of this microcontinent with the Pontide margin to the north began in the Late Cretaceous and initiated the block rotations that culminated in the present triangular geometry of the Niğde-Kırşehir Massif. The collision of the Niğde-Kırşehir microcontinent with the Pontide margin caused the oroclinal bending of the Eurasian continental margin, as demonstrated by palaeomagnetic data (Meijers *et al.* 2010). Taken together, the collision-induced block rotations and oroclinal bending suggest that Late Cretaceous–Paleocene deformation was concentrated on the Niğde-Kırşehir microcontinent and surrounding areas. However, it is likely that the İzmir-Ankara-Erzincan Ocean was not completely closed, both to the west and to the east of the Niğde-Kırşehir microcontinent, until Late Paleocene–Early Eocene time. Collision was, therefore, progressive and diachronous.

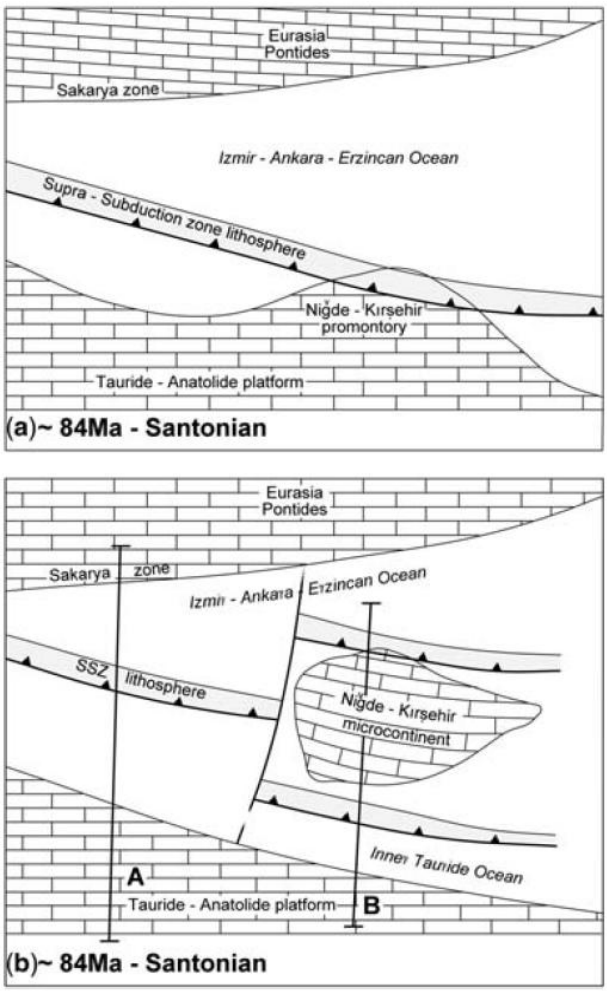

Figure 1.4. Alternative regional tectonic reconstructions of the Niğde-Kırşehir Massif. (a) The Niğde-Kırşehir Massif as a promontory of the northern margin of the Anatolide–Tauride continent; (b) The Niğde-Kırşehir Massif as a separate microcontinent (Robertson *et al.* 2009).

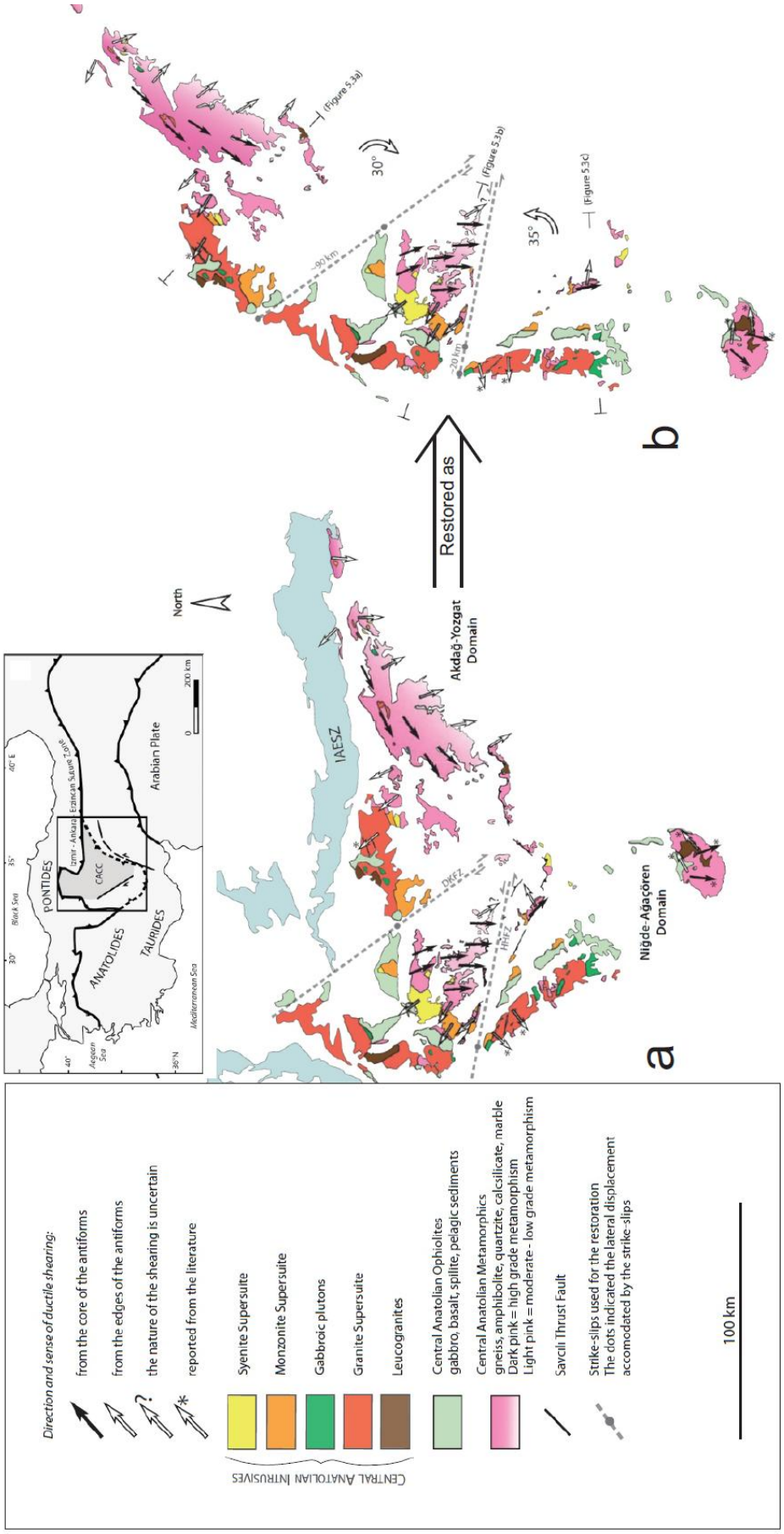

Figure 1.5. a, Simplified geological map of the Niğde-Kırşehir Massif; b, Late Cretaceous restoration of the Niğde-Kırşehir Massif using a combination of structural, metamorphic and palaeomagnetic data (after Lefebvre 2011).

1.4.2 The Tauride microcontinent

The Tauride microcontinent (also known as the Tauride-Anatolide microcontinent) consists of an unmetamorphosed *Tauride* part situated generally to the south and a metamorphosed *Anatolide* part generally situated to the north. It represents an E-W trending elongate terrane running the length of Turkey. The Tauride microcontinent is widely interpreted to represent a continental fragment that rifted from Gondwana (modern N Africa) during the Triassic, followed by re-amalgamation during Late Mesozoic-Early Cenozoic time (Şengör & Yılmaz 1981; Robertson & Dixon l984; Robertson *et al.* in press). It is generally split into three approximately autochthonous regions, the West, Central and Eastern Taurides. The Darende and Hekimhan Basins are developed within the Eastern Taurides. From south to north the Eastern Taurides represents a transition from a Tauride continental unit across a deep-water continental margin to an oceanic basin (Collins & Robertson 1998; Robertson *et al*. in press). The Western and Central Taurides share a similar structure and tectonic development to the Eastern Taurides. The Eastern Taurides experienced a common tectonic development during the Mesozoic-Early Cenozoic with the Central and Western Taurides (Robertson *et al.* in press). The main differences are: the Western Taurides experienced intense, southward directed re-thrusting during the Late Miocene (Collins & Robertson 1998; Okay *et al.* 2001) in contrast to the Central and Eastern Taurides where thrusting took place in the Late Cretaceous and again in the Mid-Late Eocene (Booth *et al.* in press; Robertson *et al.* in press), and; the northern margin of the Central Taurides (the *Anatolide* part) have undergone high pressure/low temperature (HP/LT) metamorphism due to subduction (and subsequent exhumation) beneath the Niğde-Kırşehir Massif (Dilek & Whitney 2000; Okay et al. 2001; Robertson *et al*. 2009; Oberhansli *et al.* 2010; Pourteau *et al.* 2010). The northern margin of the Tauride-Anatolide microcontinent is represented by neritic platform carbonates which were deposited during Mid-Late Triassic to Late Cretaceous time. The platform and its margins were probably initiated due to rifting to form the Inner Tauride Ocean (Robertson *et al.* in press). These platform carbonates form the ‘basement’ rocks of both the Darende Basin and the Hekimhan Basin (Geniz Formation).

1.4.3 Ophiolite formation and emplacement

Ophio is Greek for "snake", *lite* means "stone" from the Greek *lithos,* after the often green-coloured rocks (e.g. serpentinite) that make up many ophiolites.

An ophiolite may be described as "an oceanic magmatic complex comprising ultramafic rocks at the base, with variable amounts of harzburgite, lherzolite and dunite (commonly serpentinised), overlain by layered/non-layered gabbroic rocks, then by mainly basaltic extrusive rocks, with, or without, a sheeted dyke complex, and including a cover of pelagic deep-sea sediments" (Anonymous 1972; Robertson 2002). A classic, example is the Troodos ophiolite in Cyprus (see e.g. Robertson & Xenophontos 1993) although the emplacement/uplift mechanisms of the Troodos are uncharacteristic of most ophiolites.

Wakabayashi & Dilek (2003) usefully defined four sub-types of ophiolite relating to their emplacement mechanisms. Of these, Cordilleran and Tethyan ophiolites are the best known and best represented in the geological record. 'Cordilleran'-type ophiolites are associated with ocean-ocean subduction zones (Fig. 1.6a). Material is scraped off the down-going slab to form an accretionary wedge complex (Fig. 1.6b). Ophiolite emplacement is continuous as the accretionary complex grows (Fig. 1.6c). The Coast Range ophiolite in California and the Rocas Verdes ophiolite in the Pacific Northeast are two well known examples of Cordilleran-type ophiolites. The Coast Range ophiolite was emplaced in the upper plate of the east-dipping Franciscan subduction zone at 165-160 Ma (Robertson 1989; Wakabayashi & Dilek 2000). The subduction continued for over 140 Ma, resulting in progressive accretion of units scraped off the down-going plate (Wakabayashi 1992). It is estimated that at least 25% of the exposed Franciscan complex was metamorphosed under HP-LT, blueschist-facies conditions. Basin sediments were deposited in a forearc setting whilst the Franciscan subduction complex was forming structurally beneath the ophiolite (Wakabayashi & Dilek 2003). The Coast Range ophiolite began to be exhumed during the Eocene, while subduction was still active (Nilsen & McKee 1979; Robertson 1989), and was completely unroofed by the Miocene when the subduction zone ceased and converted into a transform plate boundary (Cole & Armentrout 1979).

'Tethyan' ophiolites are collisional in origin and are typically defined as "the thrusting of an ophiolite over a continental margin and/or a crystalline complex of a microcontinent" (Dewey & Bird 1970, 1971; Coleman 1971; Robertson 2002, 2006; Wakabayashi & Dilek 2003; Whattam & Stern 2011). Tethyan ophiolites form above a subduction zone (also termed supra-subduction zone ophiolites) with a high rollback vector creating a 'space' which is filled by mantle derived magma (Fig. 1.7a), with a geochemical signature significantly different to Mid Ocean Ridge Basalt (MORB). The ophiolitic material is initially emplaced onto a continental margin in response to the collision of a subduction trench with a passive continental margin (Fig. 1.7b). After ophiolite emplacement the ocean basin remains partially open and there is, therefore, an opportunity for a distinctive type of sedimentary basin to form on the emplaced continental margin, prior to suturing of the ocean basin (Fig. 1.7c). The majority of ophiolites in the Eastern Mediterranean, and specifically Turkey, are formed in this manor and are often exposed along elongate structural lineaments associated with the suture zones (Fig. 1.8). The latest Cretaceous-Eocene basins of central Anatolian record this type of supra-ophiolite tectonic setting (Görür *et al.* l984, l998; Clark & Robertson 2002; 2005; Booth *et al.* in press Nairn *et al.* in press).

A classic non-sutured counterpart of the central Anatolian basins is developed in northern Oman. Supra-subduction zone-type ophiolites in this region were emplaced onto the Arabian continental margin during latest Cretaceous time. This was followed by the development of tectonically and volcanically active extensional basins bordering the Gulf of Makran to the northeast (Lippard *et al.* 1986; Robertson & Searle l990; Glennie *et al.* 1990). A more modern example, with active sedimentary basins, is New Caledonia in the South Pacific. There, ophiolites were initially emplaced onto a down-going margin in a subduction zone via thrusting during the Late Cretaceous and then exhumed during extensional tectonism during the Mid-Late Eocene, associated with a second subduction zone initiating to the north. A period of compression followed, deforming the tectonostratigraphic terrane into megafolds. Basin and range style normal faulting unroofed the HP/LT metamorphosed ophiolite components to form the basement of the active sedimentary basins (Rawling & Lister 1999; Milsom *et al.* 2009).

Two further types of ophiolite can occur; where emplacement of ophiolite results from complex processes involving the interaction of a spreading ridge and a subduction zone (ridge-trench intersection), or; where oceanic crust is exposed as a result of shifts in plate boundary configurations, for example, where spreading ridge segments are converted to transform boundaries (Macquarie Island-type ophiolites) (Wakabayashi & Dilek 2003). However, ophiolite emplacement is not limited to destructive (or transform) plate settings (Dilek & Furnes 2011). For example, it has been shown that extension and thinning of the continental lithosphere can produce ophiolitic rocks at the surface. For example, slow extension rates within a continental margin can unroof ophiolites in a nonvolcanic setting, as in Newfoundland (Bédard 1999). Alternatively, high rates of extension and thinning can induce adiabatic upwelling and decompression melting of the asthenosphere to produce a MORB-type melt which is readily ponded and fractionated, as in the Alps (Rampone *et al.* 2005; Bernoulli & Jenkyns 2009; Piccardo *et al.* 2009).

The majority of ophiolite examples in the Eastern Mediterranean, and specifically Turkey, are preserved in a highly dismembered state due to tectonic and sedimentary emplacement processes. Where a dismembered ophiolite is observed in a highly mixed state, that is, components from all structural levels occurring together (e.g. ultramafic, basaltic and chert lithologies), it may be termed an ophiolitic mélange. The ophiolitic rocks beneath the Darende and Hekimhan Basins are defined as ophiolitic mélange.

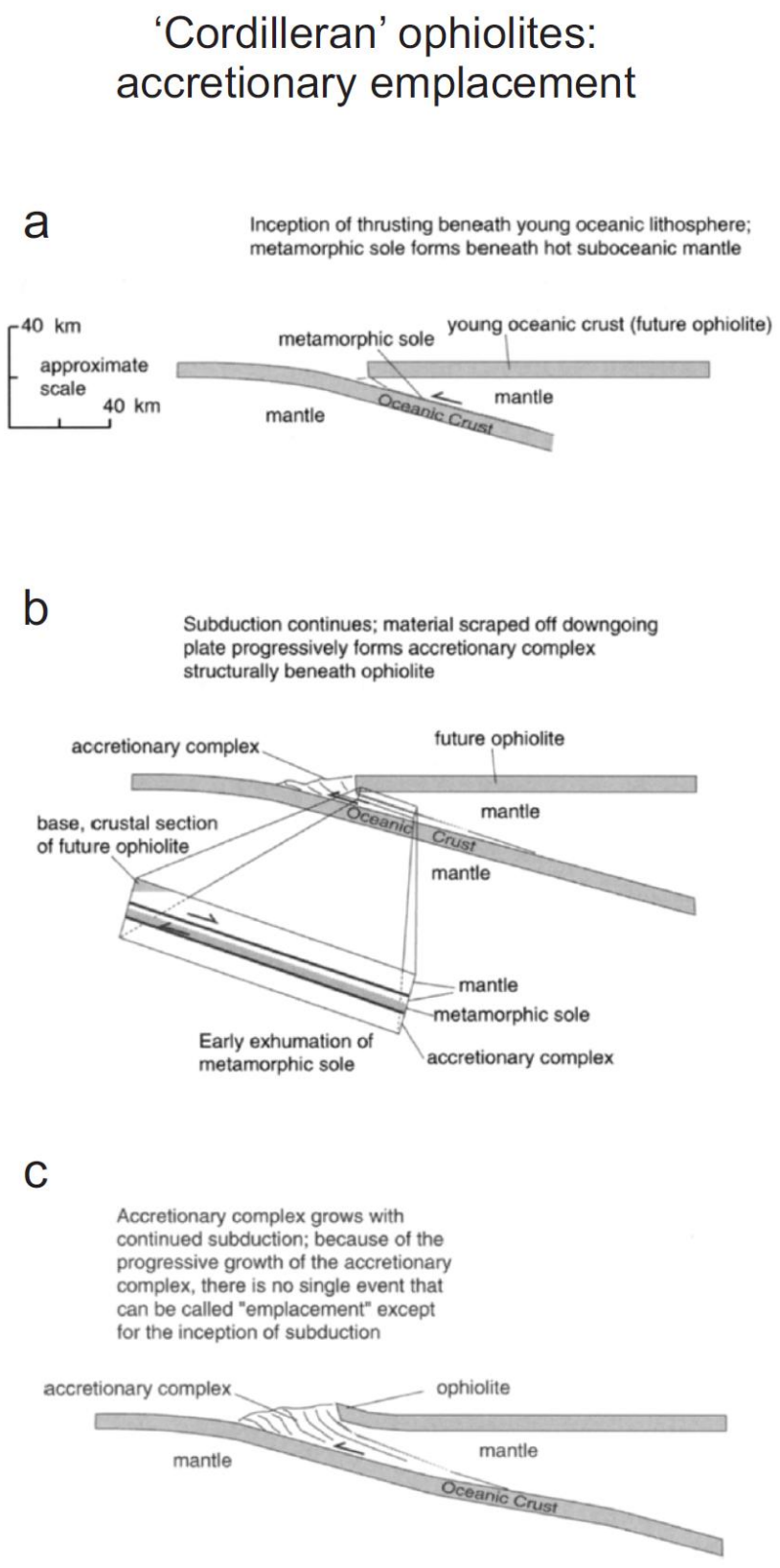

Figure 1.6. Emplacement of a typical Cordilleran-type ophiolite (adapted from Wakabayashi & Dilek 2003).

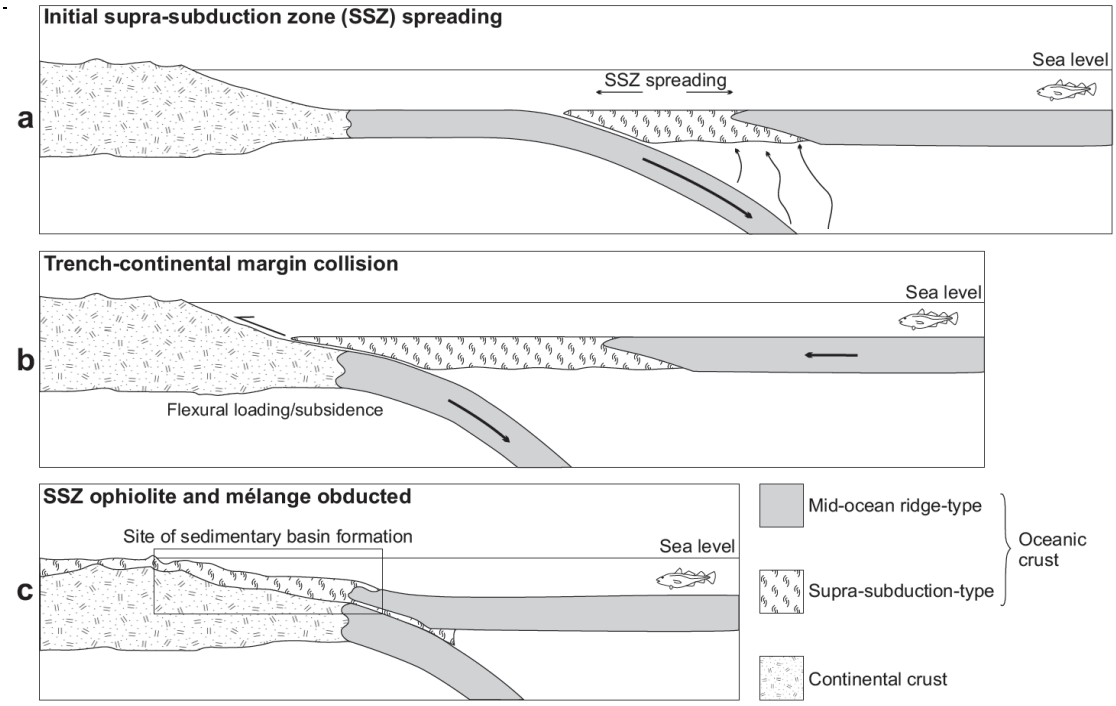

Figure 1.7. Cartoon showing the potential for formation of a distinctive type of sedimentary basin above ophiolite and related mélange after they were emplaced onto a continental margin (Booth *et al.* in press); a. the ophiolite formed by spreading above an intra-oceanic subduction zone; b. the ophiolite was emplaced when the subduction zone collided with the passive continental margin; c. the ocean remained partially open allowing the basin to evolve until final suturing. The evolution of the Darende and Hekimhan Basins generally conform to this model, as discussed in this thesis.

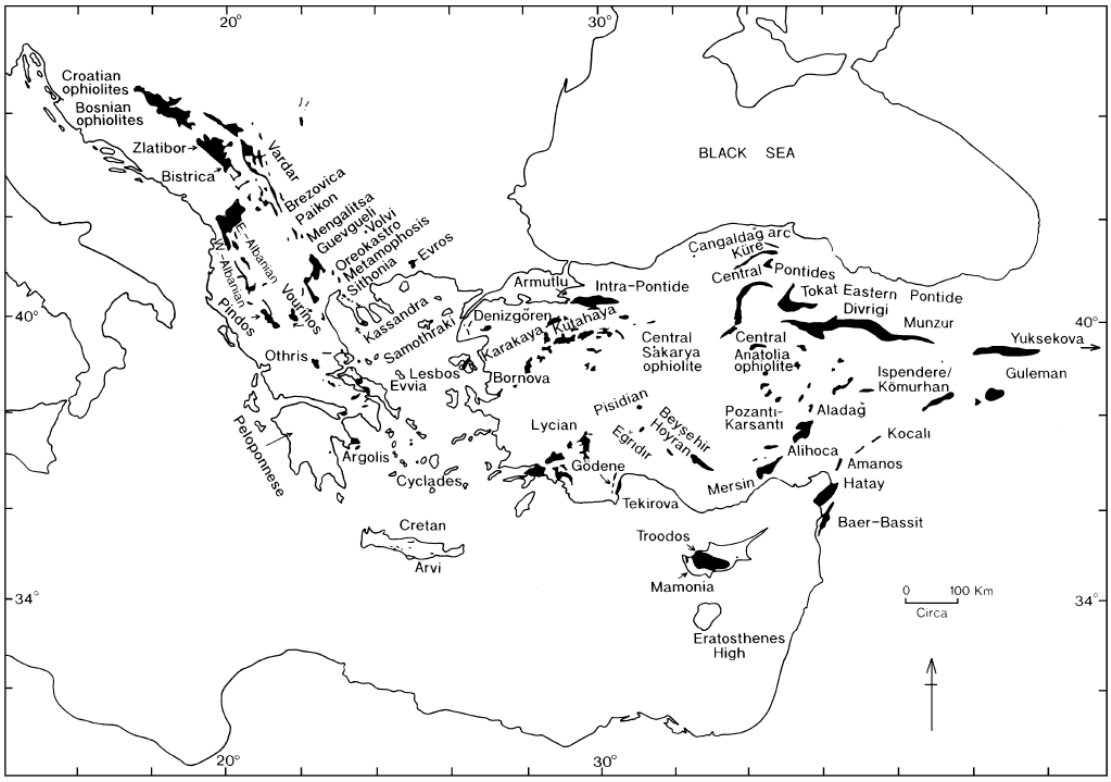

Figure 1.8. Outline map of the Eastern Mediterranean region showing the main occurrences of ophiolite (Robertson 2002).

1.4.4 The Central Anatolian sedimentary basins

Basins developed during the collision and suturing of oceans often preserve a critical record of the tectonic and sedimentary processes related to the collision. The Cretaceous-Cenozoic Darende and Hekimhan Basins which border the eastern margin of the Niğde-Kırşehir Massif can usefully be compared to other Cretaceous-Cenozoic tectono-sedimentary basins in Central Anatolia (Kelling *et al.* 2005). Some of the key basins developed during the suturing and collision of Turkey at this time are outlined below and are located in Figure 1.9. The basins can be subdivided into two main groups: One type of basin formed on the northern margin of the Tauride microcontinent (usually Tauride carbonate platform rocks) associated with the closure of the Inner Tauride Ocean. These basins are located to the south and east of the Niğde-Kırşehir Massif. Examples include the Ulukışla (Göncüoğlu 1986; Clark & Robertson 2002; Alpaslan *et al.* 2004; Clark & Robertson 2005; Alpaslan *et al.* 2006; Kurt *et al.* 2008; Zorlu *et al.* 2011) and Sivas Basins (Kavak *et al.* 1997; Cater *et al.* 1991; Gürsoy *et al.* 1997; Dirik *et al.* 1999; Yılmaz & Yılmaz 2006), as well as the Darende and Hekimhan Basins. The second type of basin formed on a variable mixture of metamorphic, magmatic or accretionary wedge complexes overlain by ophiolite-related lithologies. These basins are associated with the northern margin of the Niğde-Kırşehir Massif and evolved during the collision and suturing of the Northern Neotethys Ocean, situated between the Niğde-Kırşehir Massif to the south and the Pontides to the north (southern margin of Eurasia). Examples include the Kırıkkale (Norman 1972; Norman 1973a; Norman 1973b; Akyürek *et al.* 1984; Akyürek *et al.* 2001; Nairn 2010) and Tuz Gölü Basins (Rigo de Righi & Cortesini 1959; Arikan 1975; Uğurtaş 1975; Dellaloğlu & Aksu 1984; Görür *et al.* 1984; Çemen *et al.* 1999; Derman *et al.* 2000; Genç & Yürür 2010; Nairn 2010).

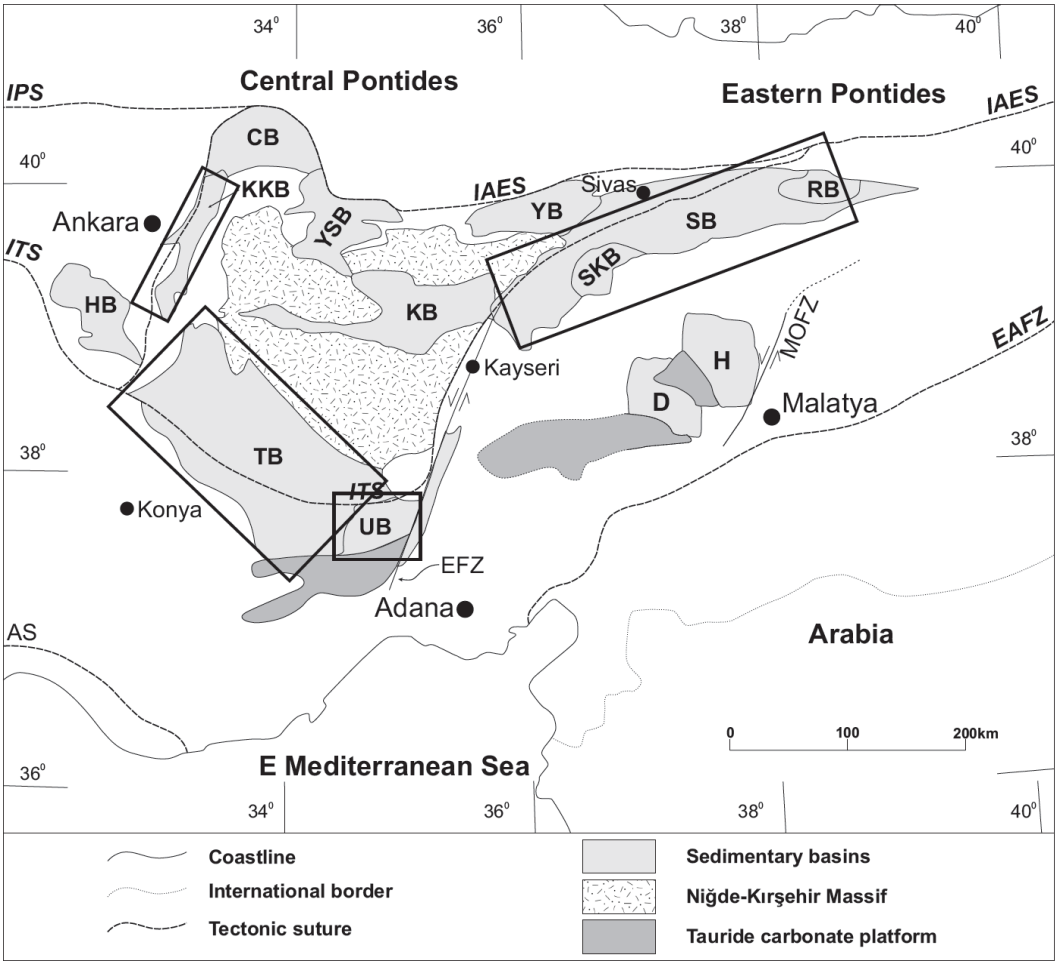

Figure 1.9. Regional outline map of Central Eastern Anatolia showing the extent of the Niğde-Kırşehir Massif and some key sedimentary-tectonic basins surrounding it denoted by the black rectangles (KKB, Kırıkkale Basin; TB, Tuzgölü Basin; UB, Ulukışla Basin; SB, Sivas Basin), as well as the major suture zones and fault zones (IPS, Intra Pontide Suture; ITS, Inner Tauride Suture; AS, Antalya Suture; IAES, İzmir-Ankara-Erzincan Suture; EAFZ, East Anatolian Fault Zone; MOFZ, Malatya-Ovacık Fault Zone; EFZ, Ecemiş Fault Zone). Other sedimentary basins are also highlighted (HB, Haymana Basin; CB, Çankırı Basin; YSB, Yozgat-Sorgun Basin; KB, Kızılırmak Basin; YB, Yıldızeli Basin; SKB, Şarkışla Basin; RB, Refahiye Basin; D, Darende Basin; H, Hekimhan Basin). Modified from Görür *et al.* (1998). See text for explanation.

1.4.4.1 The Ulukışla Basin

The Ulukışla Basin (Blumenthal 1956; Oktay 1973; 1982; Demirtaşlı *et al.* 1975; 1984; Atabey *et al.* 1990; Çevikbaş & Özuntali 1991; Görür *et al.* 1998; Clark 2002; Clark & Robertson 2002, 2005) is the most southerly of the Central Anatolian sedimentary basins, lying between the Bolkar carbonate platform (the northern margin of the Tauride microcontinent) to the south and the Niğde-Kırşehir Massif to the north. The Ulukışla Basin initiated during the Maastrichtian soon after ophiolites and ophiolite-related mélange was emplaced southwards on to the Tauride margin (Clark & Robertson 2002). Extensional (or transtensional) tectonics initiated basin development (Clark & Robertson 2005; Alpaslan *et al.* 2006; Zorlu *et al.* 2011) as recorded by transgressive sediments including the shallow-marine carbonates of Maastrichtian-Early Palaeocene age. These sediments pass upwards into slope-facies carbonates, with localised sedimentary breccias and channelised units. Subsidence during the Paleocene and Eocene resulted in a transition from neritic, mainly carbonate, deposition to relatively deep-water clastic turbidites of Middle Palaeocene–Early Eocene age (Clark 2002; Zorlu *et al.* 2011). This was synchronous with the eruption of up to 2000 m of alkaline, within-plate type basic volcanic rocks during the Late Cretaceous to Early–Mid Eocene time (Alpaslan *et al.* 2004; 2006; Kurt *et al.* 2008; Kalelioğlu *et al.* 2009). Coral-bearing neritic carbonates and Nummulites-rich shelf sediments accumulated along the northern and southern margins of the basin once volcanism had ceased. A basin-wide regression during the latest Eocene lead to the deposition of gypsum deposits, as well as turbidites, debris flows, and sabkhas, which effectively ended marine sedimentation in the basin (Altay *et al.* 2010). Regional folding and faulting affected the Ulukışla Basin during the Late Eocene and was followed by a regional Oligocene unconformity (Clark & Robertson 2005).

The Ulukışla Basin probably developed during an intermediate stage of continental collision, after the northwards subduction of remaining oceanic crust had ceased (termed ‘soft collision’), but before the opposing Tauride and Eurasian continental units forcefully collided (termed ‘hard collision’). This Late Eocene hard collision terminated sedimentation in the Ulukışla Basin and preceded the post Mid-Miocene uplift of the Tauride Mountains (Clark & Robertson 2002; 2005; Robertson *et al.* 2009; Nairn *et al.* in press).

1.4.4.2 The Sivas Basin

The Sivas Basin is an ENE-WSW trending sedimentary-tectonic basin located towards the eastern margin of the triangular shaped Niğde-Kırşehir Massif. However, it is also bounded to the north by elements of the Niğde-Kırşehir Massif and to the south by the Tauride microcontinent (Kavak *et al.* 1997; Yılmaz & Yılmaz 2006). The basin is floored by Jurassic-Lower Cretaceous platform carbonates of the Tauride margin and overthrust by Upper Cretaceous ophiolites and HP/LT metamorphic rocks presumably related to the Anatolide part of the Tauride microcontinent (Dirik *et al.* 1999). This sequence is intruded by felsic monzonitic/syenitic, mafic gabbroic/doleritic and monzogabbroic/monzodioritic rocks with K-Ar cooling ages ranging from 77–68 Ma (Yılmaz & Yılmaz 2004; Boztuğ *et al.* 2007; 2008a). These are variably overlain by Maastrichtian-Paleocene continental clastics and shallow-marine deposits and then fully marine siltstone, shale and pelagic limestone. Volcanic rocks and associated volcaniclastic material with a geochemical within-plate signature were also developed on the basement unit (Dirik *et al.* 1999). A mixture of Eocene-aged fossiliferous, reefal-limestones, marl, sandstone turbidites and massive debris flows record a basin-wide transgression related to a phase of extension (Cater *et al.* 1991; Dirik *et al.* 1999; Yılmaz & Yılmaz 2006). Variable evaporite sequences cap this sequence which are likely to have been deposited during the Late Eocene to Miocene (Ocakoğlu 2001; Gündogan *et al.* 2005; Kayseri & Akgün 2008). A phase of compression followed, which may have lasted until the Early Miocene, reactivating previously extensional lineaments (Dirik *et al.* 1999). The Sivas Basin has been shown to consist of a number of palaeotectonic sub-basins bounded by NE-SW orientated oblique-slip faults (probably reactivated) based on geophysical and palaeomagnetic analysis (Gürsöy *et al.* 1997; Temiz 2004; Onal *et al.* 2008) and basin-wide variations in the stratigraphy (Yılmaz & Yılmaz 2006).

The stratigraphic and structural evidence for the Sivas Basin indicates a syn-to post-collisional, intra-continental basin evolution (Dirik *et al.* 1999; Yılmaz & Yılmaz 2004; 2006; Boztuğ *et al.* 2007).

1.4.4.3 Kırıkkale Basin

The Kırıkkale Basin is a relatively small, NE-SW striking, elongate sedimentary basin located on the NW margin of the Niğde-Kırşehir Massif (Norman 1972; Norman 1973a, 1973b; Akyürek et al. 1984; Akyürek et al. 2001; Delibaş & Genç 2004; Dönmez et al. 2008). Unlike the Ulukışla and Sivas Basins, which are developed on carbonate platform rocks associated with the northern margin of the Tauride microcontinent (Clark & Robertson 2005; Yılmaz & Yılmaz 2006), the Kırıkkale Basin is developed on the İzmir-Ankara Accretionary Complex (also termed the Ankara Mélange). The İzmir-Ankara Accretionary Complex is an accretionary prism composed of deep-sea sediments, oceanic crustal fragments and also seamounts thought to have developed during the Early Cretaceous, and is associated with the northward subduction of oceanic crust (to the north of the Niğde-Kırşehir Massif) beneath the southern margin of Eurasia (Nairn 2010). Supra-subduction zone ophiolite-related lithologies were generated in an extensional setting above an intra-oceanic subduction zone. They were then obducted onto the northern margin of the Niğde-Kırşehir Massif during Turonian-Campanian time (Floyd *et al.* 2000; Yalınız *et al.* 2000; Göncüoğlu 2006). Similar to the Sivas Basin, granite and monzonite plutons were emplaced into the sequence prior to the onset of basin sedimentation (Kuşcu *et al.* 2002; Delibaş & Genç 2004; Nairn 2010). Sedimentation into a relatively stable (non-tectonic) basin began during the Maastrichtian and was variable across the basin, consisting of relatively deep-marine mudstone, sandstone, chert, pelagic silt, marl and limestone together with metalliferous sediments (Nairn 2010). Relatively deep-marine sedimentation persisted throughout the Paleocene. However, the Late Paleocene is characterised by compression relating to the collision of the Niğde-Kırşehir Massif with the Pontide (Eurasian) margin (Kaymakcı *et al.* 2003). The Eocene is represented by a shallowing up sequence of limestones and intercalated conglomeratic mass flows which culminate in evaporite deposition during the late Eocene (Nairn 2010).

The Kırıkkale Basin probably evolved initially in a forearc setting after ophiolite-related rocks were obducted onto an accretionary complex which formed as a result of the ‘soft collision’ of the Niğde-Kırşehir Massif with the southern margin of Eurasia (the Pontides) during the Cretaceous (Robinson *et al.* 1995; Boztuğ *et al.* 2008b). Sedimentation continued above this complex until ‘hard collision’ probably fully sutured

the basin in Late Eocene-Oligocene times (Rice *et al.* 2009). Unlike basins to the east of the Niğde-Kırşehir Massif (e.g. Darende and Hekimhan Basins), no shallow-marine Miocene transgressive sequence was observed in the Kırıkkale Basin indicating that regional uplift occurred post Eocene-Oligocene.

1.4.4.4 Tuz Gölü Basin

The Tuz Gölü Basin is relatively poorly exposed in central Turkey as the Maastrichtian-Eocene basin depocentre is covered by post-Middle Eocene to recent sediments that are composed of continental clastics, evaporites and lacustrine limestones (Görür et al. 1984; Tekin *et al.* 2007; Kutluay *et al.* 2010). The basin is also dissected by a major sinistral strike-slip fault zone (the Tuz Gölü Fault Zone; Aydemir & Ateş 2006; Genç & Yürür 2010). However, more information on the sub-surface (e.g. seismic sections) exists in unpublished hydocarbon company records. The basin initally developed under an E-W orientated extensional tectonic regime during the Late Cretaceous, as evidence by terrestrial conglomerates composed of the unroofed Niğde-Kırşehir Massif (Görür & Derman 1978; Nairn 2010). A Maastrichtian transgression instigated the deposition of marginal rudist-bearing patch reefs, with turbidite and marl alternations in deeper parts of the basin. Transgressive sedimentation continued into the Paleocene with variable coralgal and benthic foraminiferal-bearing limestones and marls with turbidites and debris flows in deeper parts of the basin. Eocene sediments record deep-water lithofacies. Nummulites-bearing shelf-type carbonates sequences are absent from the Tuz Gölü Basin unlike the majority of sedimentary basins in Turkey (Nairn 2010; in press). During the Mid-Late Eocene, E-W orientated extension shifted to E-W orientated compression, as indicated by thrust repetition (Çemen *et al.* 1999; Nairn 2010). Compression and eustatic sea level fall (Miller *et al.* 2005) effectively ended marine sedimentation in the basin. Evaporites cap the sequence. Basin margin folding occurred during the Late Eocene (Aydemir & Ateş 2005; Aydemir 2008; 2009; Nairn 2010).

Previously the Tuz Gölü and Ulukışla Basins were thought to be extensions of the same sedimentary basin (Görür *et al.* 1984; Çemen *et al.* 1999). However, there are sufficient differences in the stratigraphy and structure (e.g. up to 2000 m of volcanism in

the Ulukışla Basin, not known in the Tuz Gölü Basin) that they have since been interpreted as individual basins (Görür *et al.* 1998; Clark 2002).

The Tuz Gölü Basin probably evolved during the Late Cretaceous due to extension above emplaced ophiolite-related sequences and an accretionary complex developed on the NW margin of the Niğde-Kırşehir Massif. Extension occured synchronously with deep-marine sediments until the Mid-Late Eocene when the margin collided with the Pontides (southern margin of Eurasia) to the north shifting the basin to a compressional setting.

1.4.5 The Pontide active margin

The Pontides are an E-W trending mountain range located in northern Turkey. The range can be roughly split into the Western Pontides (represented by the amalgamated Sakarya microcontinent and the Istanbul-Zonguldak zone; Robertson & Ustaömer 2004), Central and Eastern Pontides (Fig. 1.10; Şengör & Yilmaz 1981; Okay & Şahintürk 1997; Topuz *et al.* 2004). The Western Taurides are considered to represent the closure and suturing of an Intra-Pontide Ocean leading to the accretion of two microcontinents to the north of a wider Northern Neotethys Ocean by Maastrichtian time. The western Taurides are mainly composed of high and low grade metamorphic facies, overlain by sediments and volcanogenic lithologies interpreted to have deposited in a flexural foredeep ahead of ophiolite emplacement, collision and suturing (Yilmaz *et al.* 1997; Robertson & Ustaömer 2004; Rice 2005). The timing and evolution of the Western Pontides is still debated (e.g. Robertson & Ustaömer 2004; Okay & Göncüoğlu 2004). However, the evolution of the Western Pontides is independent of the topic of this thesis and is thus not discussed further here.

The basement of the Central and Eastern Pontides is partly represented by the Pulur metamorphic complex, a mixture of schists and gneisses intruded by Early Carboniferous granites (Eyüboğlu *et al.* 2010). This sequence is over-thrust by a Palaeotethyan accretionary complex associated with the subduction of Palaeotethys from Permian to Late Triassic (Topuz *et al.* 2004; Ustaömer & Robertson 2010). This complex is overlain by Upper Jurassic continental, to shallow-marine sediments, together with

non-subduction-influenced basalts. This was followed by extension-related deposition of pelagic carbonates and mixed terrigenous, biogenic and volcaniclastic gravity flows (Rice *et al.* 2006; Ustaömer & Robertson 2010). During the Late Cretaceous, calc-alkaline magmatism (termed the Eastern Pontide magmatic arc) and associated volcaniclastic successions were emplaced in the Eastern Pontides (Şengör & Yilmaz 1981; Robinson *et al.* 1995; Yilmaz *et al.* 1997; Rice *et al.* 2006). The Eastern Pontide magmatic arc is generally interpreted as a continental margin volcanic arc formed above a northward subducting slab of Neotethyan lithosphere (Robertson 2004; Rice *et al.* 2009; Ustaömer & Robertson 2010). No evidence for this arc is observed on the Eurasian continental rocks of the Central Pontides leading some workers to postulate oblique subduction of the Neotethyan lithosphere beneath a geometrically irregular Eurasian margin (Ustaömer & Robertson 1997). In addition, a Late Cretaceous volcanic arc and associated accretionary complex overlying ophiolitic basement is observed to the south of the Central Pontides (Şengör & Yilmaz 1981; Tüysüz 1990; Keskin 2003). The sequence has been interpreted as an intra-oceanic volcanic arc and later accretionary complex developed in response to intra-oceanic, northward subduction of northern Neotethys (Tüysüz 1990; Ustaömer & Robertson 2010). This was later thrust northwards (during Late Cretaceous-Early Paleocene time) and imbricated with elements of the Pontide continental margin (Rice 2005).

Collision of the Niğde-Kırşehir Massif with the Pontides during the Late Cretaceous to Paleocene caused indentation tectonics and resulted in the oroclinal bending of the Central Pontide margin (Kaymakcı *et al.* 2000; 2003a; 2003b; Meijers *et al.* 2010; Çınku *et al.* 2011). Supra-subduction zone-type ophiolites were emplaced onto both margins at this time (Ustaömer & Robertson 2010), followed by northwards directed Eocene thrusting (Rice *et al.* 2009; Ustaömer & Robertson 2010) and post-collisional magmatism (Çamur et al. 1996; Arslan et al. 1997; Arslan & Aslan 2006; Eyüboğlu *et al.* 2011; Kaygusuz *et al.* 2011; Topuz *et al.* 2011; Temizel *et al.* 2012).

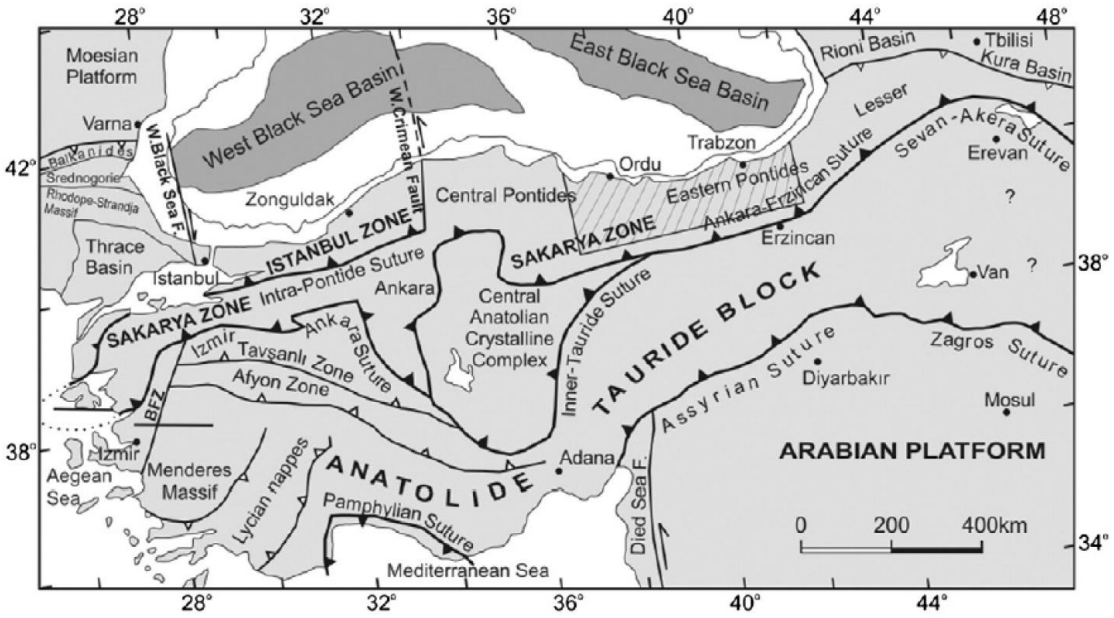

Figure 1.10. Tectonic map of the NE Mediterranean region showing the major continental blocks, including those constituting the Pontides. Sutures are shown by heavy lines with the polarity of former subduction zones indicated by filled triangles. Heavy lines with open triangles represent active subduction zones. Small open triangles indicate the vergence of the major fold and thrust belts. BFZ denotes the Bornova Flysch Zone (originally from Okay & Tüysüz 1999, adapted by Temizel *et al.* 2012).

1.5 CONTRASTING TECTONIC MODELS OF BASIN DEVELOPMENT

There are two main tectonic models which have been proposed for the Late Cretaceous-Cenozoic tectonic development of the Eastern Mediterranean. In one model, the Northern Neotethys was palaeogeographically uncomplicated, forming a single ocean whose lithosphere subducted northwards beneath the Eurasian margin (Şengör & Yılmaz 1981; Göncüoğlu 1986; Gürer & Aldanmaz 2002). In this model, the Niğde-Kırşehir Massif formed a promontory of the Tauride microcontinent and should, therefore, share similar lithological attributes. Ophiolites associated with a single subduction zone were emplaced southwards for several hundred kilometres across the northern margin of this singular terrane. Sedimentary basins developed initially as forearc basins along the northern margin and then as post-collisional basins once collision of the Tauride microcontinent and the Eurasian margin occurred. The evolution of a single oceanic basin indicates that there should be few differences in the characteristics of the Central Anatolian sedimentary basins, indeed, they should be genetically 'linked'. Volcanism in the basins could, therefore, relate to contemporaneous subduction. The Cenozoic was characterised by thrusting of ophiolite-related 'basement', platform rocks and sedimentary basin material followed by suture tightening.

In the second model, the Neotethys was palaeogeographically complex and included at least one microcontinent, the Niğde-Kırşehir Massif, which rifted from the Tauride continent to the south during the early Mesozoic and evolved independently from the Tauride microcontinent (Görür *et al.* 1984; Görür *et al.* 1998; Görür & Tüysüz 2001). In this model, Neotethyan oceanic lithosphere was subducted northwards via two subduction zones. One subduction zone was situated to the south of the Niğde-Kırşehir Massif, which emplaced ophiolites on to the northern margin of the Tauride continent (Robertson 2002; Robertson *et al.* 2009). Another, was situated to the north of the Niğde-Kırşehir Massif (with oceanic lithosphere subducting northwards beneath the Eurasian margin), which emplaced ophiolites onto the northern margin of the Niğde-Kırşehir Massif (Robertson 2004; Rice *et al.* 2009; Ustaömer & Robertson 2010). The ophiolites are of supra-subduction zone origin and were mainly emplaced as sedimentary and tectonic mélanges when subduction trenches collided with microcontinental margins (Robertson *et al.* 2009). The subduction zones were associated with the development of

an intra-oceanic magmatic arc situated to the north of the Niğde-Kırşehir Massif (Ustaömer & Robertson 1997), accretionary forearc-type basins to the west of the Niğde-Kırşehir Massif (Koçyiğit 1991; Nairn 2010), as well as an active continental volcanic and magmatic arc situated on the southern margin of Eurasia (the Pontide magmatic arc; Şengör & Yilmaz 1981; Robinson *et al.* 1995; Yilmaz *et al.* 1997; Rice *et al.* 2006). In this regard, the Neotethys Ocean is split in two, a northern İzmir-Ankara-Erzincan Ocean (developed between the Niğde-Kırşehir Massif and the Eurasian margin) and a southern Inner Tauride Ocean (developed between the Niğde-Kırşehir Massif and the Tauride microcontinent). Sedimentary basins developed on the northern margins of both the Niğde-Kırşehir Massif and the Tauride microcontinent and they show significantly different tectono-stratigraphic evolution. Sedimentary basins were developed as convergent, accretionary-type basins on the northern margins of the Niğde-Kırşehir Massif associated with closure of the İzmir-Ankara-Erzincan Ocean and the collision of the Pontide margin (Ustaömer & Robertson 2010; Nairn *et al.* in press). Sedimentary basins associated with the northern margin of the Tauride microcontinent developed as a result of closure of the Inner Tauride Ocean initially, followed by the convergence of the Niğde-Kırşehir Massif with the Eurasian margin (Clark & Robertson 2002). The İzmir-Ankara-Erzincan Ocean was partially closed by the latest Cretaceous. However, some parts remained open until the Early-Mid Eocene.

In the latter, favoured, scenario, the main questions to be resolved are:

1) How far east does the Niğde-Kırşehir Massif extend? If the Niğde-Kırşehir Massif terminates under the western part of the Sivas Basin (e.g. Fig. 1.9), the Darende and Hekimhan basins could solely reflect the evolution, closure and suturing of the İzmir-Ankara-Erzincan Ocean. However, if the Niğde-Kırşehir Massif extends further east (such that the eastern margins are situated roughly north of the Darende and Hekimhan Basins), as is likely, due to outcrop observations of Niğde-Kırşehir Massif rocks within the Sivas area to the north (MTA 2002). The Niğde-Kırşehir Massif could then extend further eastwards in the subsurface. In this scenario, the Darende and Hekimhan Basins could represent composite basins recording the evolution, closure and suturing of both the Inner-Tauride Ocean and the İzmir-Ankara-Erzincan Ocean.

2) An important question associated with the eastern extent of the Niğde-Kırşehir Massif is: What happens to the southerly subduction zone (associated with the closer of

the Inner-Tauride Ocean) to the east of the Niğde-Kırşehir Massif? The options are: 1) The subduction zone terminates at a transform boundary (potentially reactivated as the sinistral Ecemiş Fault Zone), transferring subduction over to the northern subduction zone (associated with the closure of the İzmir-Ankara-Erzincan Ocean), as has been proposed in one tectonic reconstruction to the west of the Niğde-Kırşehir Massif (Fig. 1.4b; Robertson *et al.* 2009). In this scenario, ophiolites in Central Eastern and Eastern Turkey must be derived from one source; 2) The subduction zone continues eastwards as an intra-oceanic subduction zone. In this scenario, evidence of an intra-oceanic arc and associated accretionary complex might be expected. Some evidence for ophiolite-related mélange and granite intrusions has been observed in the Divriği area (Parlak *et al.* ongoing work).

1.6 METHODOLOGY

This thesis revolves around the collection and interpretation of geological fieldwork. To that end, seventeen weeks spread over four separate field seasons (September/October 2008, April/May 2009, September 2009 and September/October 2010) were spent in the field areas in central Eastern Turkey, with the time split roughly equally between the Darende and Hekimhan Basins. Fieldwork included; detailed description and analysis of each formation encountered, detailed stratigraphic logging (at varying scales), photographing and sketching key localities, partial remapping of important areas as well as gathering large datasets of structural and palaeocurrent data. Additionally, over 300 sedimentary, igneous and palaeontological samples were collected.

As well as field work, a multi-method approach was utilised at the University of Edinburgh in order to fully analyse and interpret the sedimentary-tectonic basins. Methods included:

- Petrographic analysis of both sedimentary and igneous thin sections using a Nikon Eclipse e2000 petrological microscope with a Nikon Coolpix SLR camera.
- Whole rock analysis of igneous samples using X-Ray Fluorescence (XRF). See Appendix 1 for methodology and data
- Great effort was made to digitally remap the field areas, based on field observations, using a combination of: 1) military-grade, regional topographic maps, 2) Turkish General Directorate of Mineral Research and Exploration (MTA) geological maps, 3) ASTOR satellite data, and 4) Digital Elevation Models (DEM). This multi-method approach utilised ArcGIS software to ensure geological boundaries, fault zones, streams, towns, roads and GPS locations were located as accurately as possible. The maps were ultimately constructed in Corel Draw.
- Structural data (faults and folds and kinematic indicators) were analysed using a combination of TectonicsFP (Ortner *et al.* 2002), Steronet7 (Allmendinger 2011) and FaultKin5.2 (Allmendinger 1992; 1995). See Appendix 2 for methodology and data.

- Palaeocurrent indicators (groove casts, flute casts and imbricated clasts) were rotated to horizontal where they were located on bedding surfaces dipping greater than 10^{o} and plotted onto rose diagrams.
- A preliminary microfossil analysis was undertaken at the University of Edinburgh in order to identify the best thin sections. These were sent to Prof. Nurdan İnan and prof. Kemal Taslı of Mersin University, Turkey where a detailed analysis was conducted. The ages provided are presented in this thesis and integrated with other data in order to construct detailed basin chronostratigraphic evolution models. The timescale used is from Gradstein *et al.* (2004), as noted previously.

Frequently, specific formation names do not extend beyond individual basins in the Turkish geological literature, as they often do elsewhere. For example, The Grés d'Annot Formation in the French Alps is interpreted to extend for hundreds of kilometres across many sub-basins based on facies analysis and palaeogeographic determination (e.g. Apps *et al.* 2004). However, in Turkey, Maastrichtian-aged, non-marine, reddish sandstone and pebbly sandstone deposits are called the Ulupınar Formation (Akkuş 1971) and the Karadere Formation (Gürer 1994) in the Darende and Hekimhan Basins, respectively. Wherever possible, the original formation names have been preserved. However, some modifications to the stratigraphic nomenclature were necessary in order to preserve stratigraphic continuity between the two basins or where formal stratigraphic names were absent entirely.

1.7 TURKISH PRONUNCIATION

The Turkish alphabet is based on the Latin alphabet, although some letters are pronounced differently, and there are a number of additional letters. Those differences and additions are listed below together with their phonetic sounds.

Differences:

Aa: as in f**a**r
Cc: Pronounced ‘j’ as in **J**elly
Ee: as in b**e**t
Gg: as in **g**et
Hh: as in **h**en, never silent
Ii: pronounced ‘ee’ as in L**ee**
Jj: pronounced ‘zh’ as in plea**s**ure
Oo: as in n**o**te
Uu: as in bl**u**e

Additions:

Çç: pronounced ‘ch’ as in **ch**at
Ğğ: a silent ‘g’ and lengthens the sound of the preceding vowel
İı: unstressed vowel similar to the vestigial sound between the **b** and **l** of probable
Öö: pronounced ‘ur’ as in b**u**rn
Şş: pronounced ‘sh’ as in **sh**ape
Üü: pronounced ‘ew’ as in f**ew**

Towns:

Balaban: (Bala-ban)
Darende: (Dar-en-dey)
Hasançelebi: (Hassan-chel-ebee)
Hekimhan: (Heki-Man)

Key words:

Aşağı: down or under
Bahçe: garden
Cık: used after a noun to make it smaller, e.g. Hisarcık (Little Castle)
Çay: stream or small river
Dağ: mountain
Dere: river/stream
Gazı: warrior of the (Islamic) faith
Hacı: honourific of someone who has made the pilgrimage to Mecca
Hisar: castle or fort
Hoca: teacher in charge of religious instruction for children
Ilıca: spring
Irmak: river

Kale:	castle or fort
Kapı:	gate or door
Köy:	village
Pınar:	spring
Saray:	palace
Taş:	stone
Tepe:	hill
Yeni:	new, e.g. Yenipınar (New Spring)
Yeşıl:	green, e.g Yeşılkale (Green Castle)

Chapter 2: The Darende Basin

Chapter 2. Revised stratigraphy, lithological description and interpretation of the Darende Basin

2.1 INTRODUCTION

This chapter focuses on an extensive geological analysis and interpretation of the Darende Basin. This chapter is an extended version of a paper to be published in the Geological Society of London for the Special Publication 'The Geological Development of Anatolia in the Eastern Mediterranean Region'. The Darende Basin is a composite basin recording two separate stages of tectonic development during the latest Cretaceous (Maastrichtian) and then during the Eocene (Lutetian-Priabonian). Maastrichtian strata were deposited under an extensional tectonic regime, following ophiolitic mélange emplacement, whereas the Eocene strata reflect a syn-collisional tectonic setting. The Darende Basin was chosen for this study because comparatively little work has been carried out on sedimentary-tectonic basins of Central Eastern Anatolian. These basins highlight the later stages of continental collision in the Tethyan region. Much of the centre of the basin is occupied by latest Eocene sediments and Neogene cover. However, some complete successions are well exposed along the NE and SW basin margins.

Geographically, the Darende Basin is located in central eastern Turkey ~100 km NW of the city of Malatya (Fig. 2.1) The basin is located on the Tauride-Anatolide micro-continental unit, to the east of the Niğde-Kırşehir Massif and to the south of the Izmir-Ankara-Erzincan Suture Zone (Fig. 2.2), which marks the remnants of the Izmir-Ankara-Erzincan ocean which closed during Late Cretaceous-Late Eocene times (see chapter 1; Şengor & Yılmaz 1981; Robertson & Dixon 1984). The Darende Basin occupies an area of ~1000 km^2 making it comparitively small compared with some other Upper Mesozoic-Cenozoic basins in central Turkey (*e.g.* Çankırı Basin, see e.g. Nairn *et al.* in press).

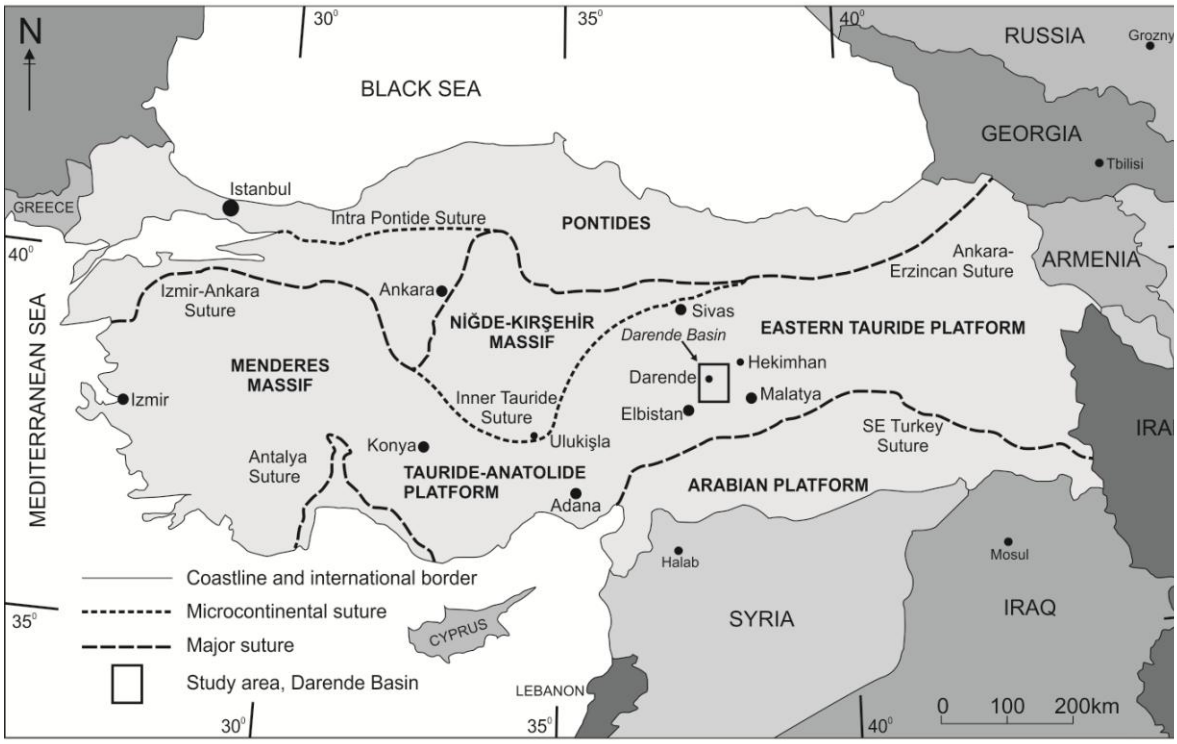

Figure 2.1. Location map and outline of the tectonic suture zones of mainland Turkey (modified from Clark & Robertson 2002). The Darende Basin in central eastern Anatolia is marked by the rectangle.

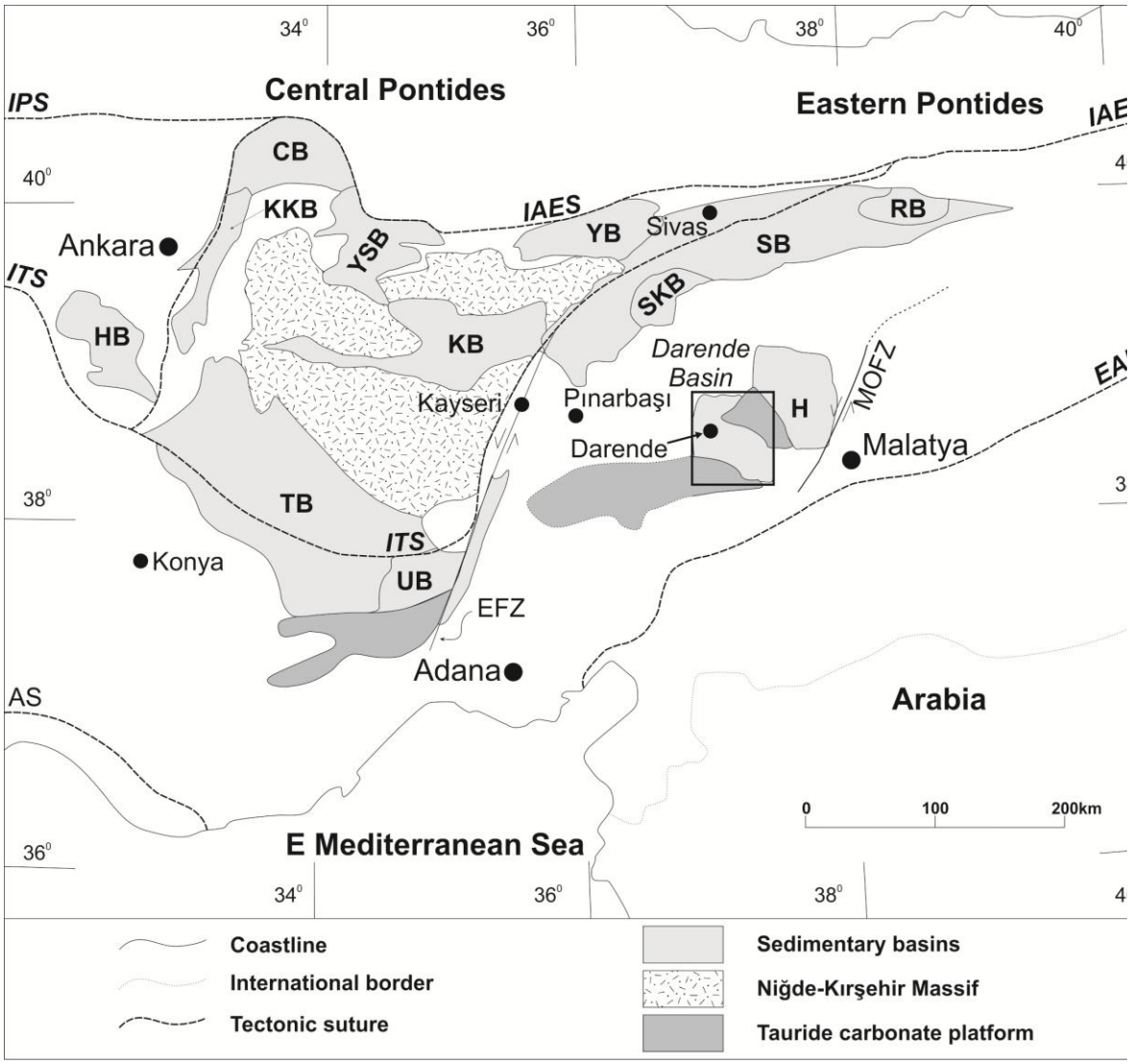

Figure 2.2. Regional outline map showing the major suture zones and fault zones (IPS, Intra Pontide Suture; ITS, Inner Tauride Suture; AS, Antalya Suture; IAES, İzmir-Ankara-Erzincan Suture; EAFZ, East Anatolian Fault Zone; MOFZ, Malatya-Ovacık Fault Zone; EFZ, Ecemiş Fault Zone) and the major sedimentary basins (HB, Haymana Basin; KKB, Kırıkkale Basin; CB, Çankırı Basin; YSB, Yozgat-Sorgun Basin; KB, Kızılırmak Basin; YB, Yıldızeli Basin; SKB, Şarkışla Basin; SB, Sivas Basin; RB, Refahiye Basin; TB, Tuzgölü Basin; UB, Ulukışla Basin; H, Hekimhan Basin) in Central Eastern Anatolia. Study area shown by black rectangle. Modified from Görür et al. (1998).

The Darende Basin (Fig. 2.3) comprises sedimentary and subordinate volcanic rocks up to ~1000 m thick, ranging from Late Cretaceous to Late Eocene in age (Akkuş 1970, 1971; Gürbüz & Gül 2005; this study). The basin is bowl shaped, bounded to the north, south and west by Jurassic and Cretaceous carbonate rocks of the Bolkar Carbonate Platform, part of the regional Eastern Tauride Block (Robertson *et al.* in press). The basin stratigraphy unconformably overlies parts of this Mesozoic carbonate platform together with regionally emplaced ophiolite mélange, particularly in the south of the basin. Parts of the basin margins are characterised by fault lineaments that played an important role in

the formation and later deformation of the Darende Basin. These features are expressed in three cross sections located near the basin margins. Fig. 2.4a (X^1-X^2) shows a NE-SW trending cross section through the Karakayalar region, near the NE basin margin. There, the sediments and the volcanic rocks dip to the south and are juxtaposed with Mesozoic carbonate platform rocks via a Neotectonic sinistral strike-slip fault. Fig. 2.4b (Y^1-Y^2) shows a cross section through the SW basin margin. There, the sediments dip towards the north and are folded, probably as a result of northward thrusting of the Mesozoic carbonate platform. Fig. 2.4c (Z^1-Z^2) shows a cross section through the south of the basin where basin sediments onlap the Mesozoic carbonate platform at the southernmost point but have been folded into an anticline and subsequently breached by northwards thrusting of Mesozoic carbonate platform rocks over ophiolite related units which probably acted as a décollement surface.

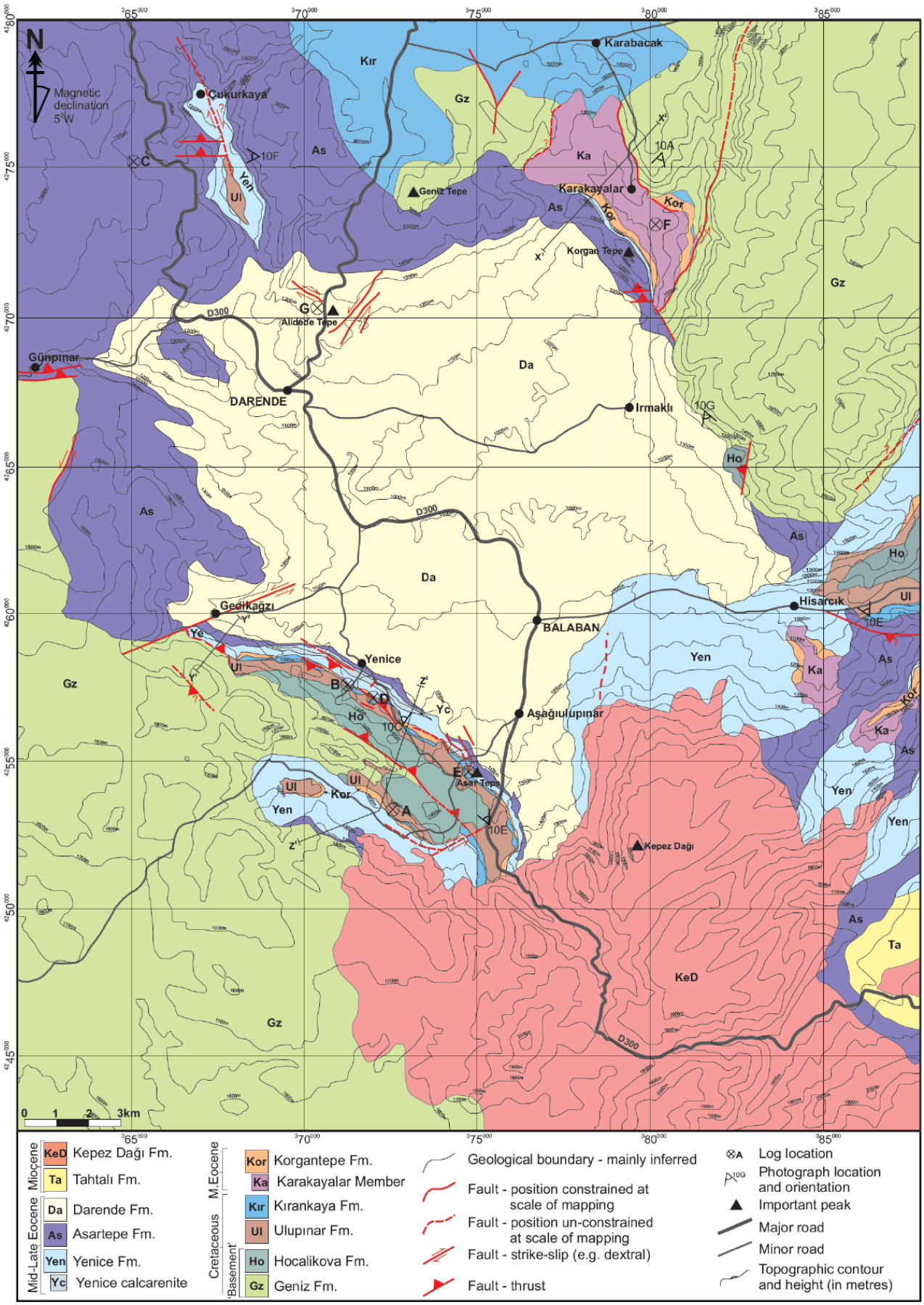
N
Magnetic declination 5°W
Çukurkaya
Karabacak
Kır
Gz
As
Ka
Yen
Ul
Kor
Ho
Da
Genç Tepe
Karakayalar
Korgan Tepe
Alidede Tepe
Günpınar
DARENDE
Irmaklı
Gedikağzı
BALABAN
Hisarcık
Yenice
Aşağıulupınar
Asar Tepe
Kepez Dağı
KeD
Ta
D300
10A
10C
10D
10E
10F
10G
0 1 2 3km
Mid-Late Eocene
Miocene
M.Eocene
Cretaceous
'Basement'
KeD Kepez Dağı Fm.
Ta Tahtalı Fm.
Da Darende Fm.
As Asartepe Fm.
Yen Yenice Fm.
Yc Yenice calcarenite
Kor Korgantepe Fm.
Ka Karakayalar Member
Kır Kırankaya Fm.
Ul Ulupınar Fm.
Ho Hocalikova Fm.
Gz Geniz Fm.
Geological boundary - mainly inferred
Fault - position constrained at scale of mapping
Fault - position un-constrained at scale of mapping
Fault - strike-slip (e.g. dextral)
Fault - thrust
Log location
Photograph location and orientation
Important peak
Major road
Minor road
Topographic contour and height (in metres)

Figure 2.3. Geological map of the Darende Basin (above). The map includes the main geological boundaries between the units, the lithostratigraphy and the main fault lineaments. The locations of the photographs, the type sections/areas and cross section orientations are also shown. Modified and partially re-mapped during this study after Akkuş (1971) and Gürbüz & Gül (2005).

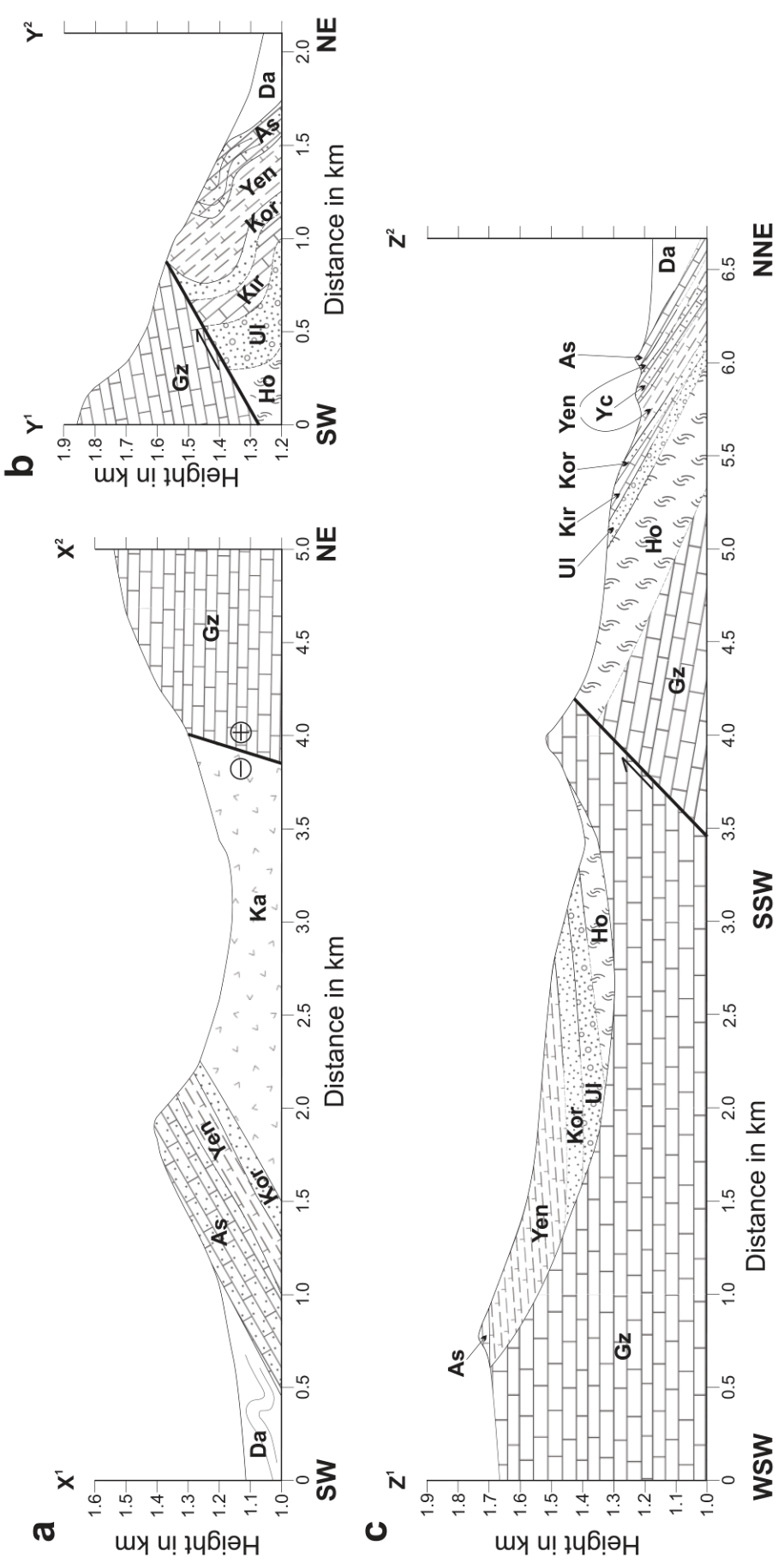

Figure 2.4. Cross sections. a, Cross section of the northeastern basin margin in the Karakayalar area (X^1-X^2 in Fig. 2.3) showing basin sediments and associated volcanics (Karakayalar Member) dipping ~southwestwards, together with a steeply dipping Neotectonic sinistral strike-slip fault bounding Mesozoic limestones. b, Cross section of part of the southwestern margin of the basin, near Gedikağzı (Y^1-Y^2 in Fig. 2.3) showing basin sediments dipping ~northeastwards. Mesozoic limestones are folded and thrust northeastwards over basin sediments. c, Cross section of part of the southern margin of the basin (Z^1-Z^2 on Fig. 2.3) showing Mesozoic limestones unconformably underlying the basin sediments. These sediments are folded into an anticline that was cut and breached by a thrust.

2.2 AIMS

The objective of this chapter is to discuss new sedimentary, stratigraphical, palaeontological, geochemical and structural data gathered during the course of this study. This detailed, multidisciplinary approach has hitherto not been undertaken for the Darende Basin. The geological map of the Darende Basin utilises a combination of regional 1:500,000-scale geological maps prepared by the General Directorate of Mineral Research and Exploration (MTA) (2002), together with detailed remapping of key field localities during this work. Previous contributions concerning some parts of the basin have been assimilated (*e.g.* Akkuş 1970; 1971; Gürbüz & Gül 2005). Mapping was enhanced and boundaries edited by utilisation of Digital Elevation Models (DEM) and projection software (ArcGIS and Google Earth) in a combined approach at remapping the Darende Basin in its entirety for the first time and as accurately as possible (Fig.2.3).

The basin includes Mid-Eocene (Lutetian) lavas that are apparently unique to the Central Anatolian basins which span the Izmir-Ankara-Erzincan suture zone. Eocene-aged lavas are not normally found as far south as the Darende Basin and are, therefore, poorly represented in the literature. Geochemistry of these lavas has been undertaken for the first time here. Palaeogeographic reconstructions, together with regional-scale tectonic evolution figures based on the geochemical results and basin-wide sedimentary and stratigraphic analysis are presented at the end of this chapter.

2.3 PREVIOUS WORK

The Darende Basin was initially investigated by the Turkish General Directorate of Mineral Research and Exploration (MTA) during the regional geological mapping of Turkey (~1936). Since then several MTA reports have referred to this area, including those by Stchepinsky (1944), Wirtz (1955), Gattinger (1958), Kurtman (1961) Baykal (1965) and Yazgan & Chessex (1991). Akkuş (1970, 1971) prepared the first detailed geological map and produced an initial lithostratigraphy and nomenclature supported by dating of microfossils (Fig. 2.5). More recently (Gürbüz & Gül 2005), based on a study of the central and southern part of the basin, produced a revised lithostratigraphy (Fig. 2.5). This was supported by additional microfossil dating, coupled with the first detailed sedimentological description and interpretation. Information on Eocene foraminifera and ostracods, in particular, was provided by Nazik (l993) and by Nazik *et al.* (2006). A revised lithostratigraphy is presented here (Fig. 2.5; this work) that incorporates new micropalaeontological dating and the analysis of the important unit of Eocene volcanic rocks in the northeastern part of the basin, together with the results of substantial re-mapping and integration on a regional scale. The Darende Basin has previously been known as the Darende-Balaban Basin (Akkuş 1970, 1971; Gürbüz & Gül 2005; Nazik *et al.* 2006) but for simplicity is here termed the Darende Basin.

Akkuş (1971) separated the Darende Formation (Fig 2.5) into two separate formations, the widespread Darende Formation composed of sandstone, siltstone and marl alternations with evaporitic horizons, and the Balaban Formation, located south of Balaban, and composed of similar mixed lithologies but dominated by conglomerates. Akkuş (1971) included the lower marls of the Darende Formation as the upper part of the Asartepe Formation (Fig 2.5). More recently, Gürbüz (2005) concluded from palaeontological evidence that the marls are of Upper Lutetian age and thus not part of the Asartepe Formation. Furthermore, it was seen as unnecessary for the Darende and Balaban Formations to exist as separate formations because conglomeratic lenses of the Balaban Formation are interleaved with other lithologies in the Darende Formation; thus, the Balaban Formation was included in the Darende Formation.

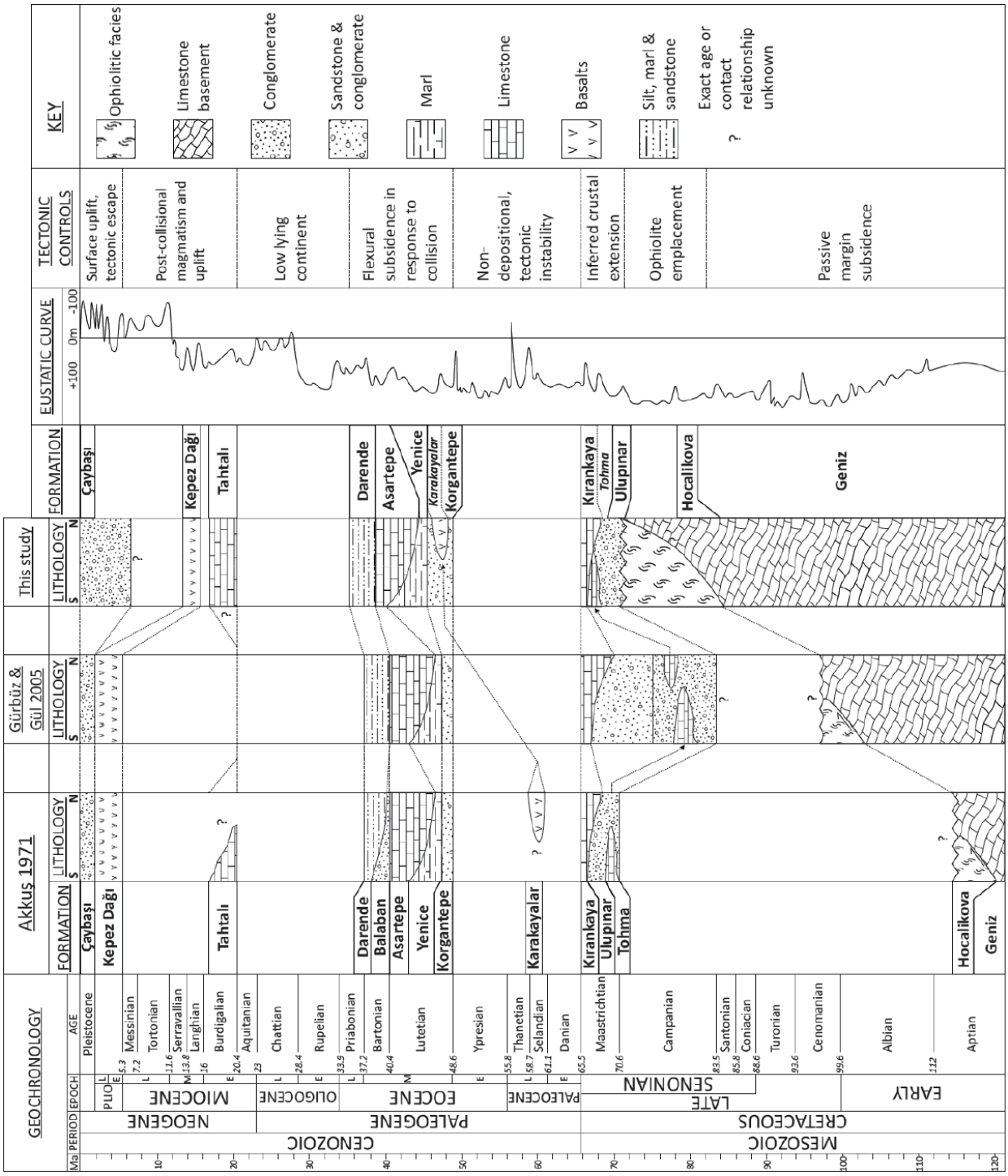

Figure 2.5. Previous and revised stratigraphic nomenclatures of the Darende Basin. An initial stratigraphy by Akkuş (1971) was revised by Gürbüz & Gül (2005) and is further revised here. The revision takes account of improved knowledge of the Mesozoic carbonate platform and emplaced ophiolite-related mélange (Robertson *et al.* in press), the dating of microfossils during this work and also of recent radiometric dating of Miocene volcanic rocks (Gürsoy *et al.* 2011). A global eustatic sea level curve (Miller *et al.* 2005) is included on the right to aid discussion of the controls of sediment deposition (i.e. tectonics versus sea level change). The main inferred controls of deposition are also summarised.

2.4 STRATIGRAPHY AND SEDIMENTOLOGY

In this section, new stratigraphic and sedimentary data are presented based on measured stratigraphic logs, new field-mapping and the geochemical, petrological and palaeontological study of rock samples collected in the field. New lithofacies analysis is presented here and defined in terms of grain size, bed thickness, sedimentary structures and lithology. The stratigraphic units are described here in geochronological order.

2.4.1 Mesozoic 'Basement'

2.4.1.1 Mesozoic Platform Limestones (Geniz Formation)

Name: Probably derived from Geniz Tepe which is located approximately 5 km west of Karakayalar in the northern part of the Darende basin (Fig. 2.6).

Type locality: High ridge to the south of Yenice (Fig. 2.6)

Lithology: The Geniz Formation is composed of light-grey, white to pink, recrystallised, microcrystalline limestone with a sugary texture. Some of these features can be seen in Figure 2.7a. These rocks are typically thickly bedded to massive, heavily fractured, faulted, folded and exhibit several generations of calcite veining (Fig. 2.7b). Indeterminate, fragmented bivalve, gastropod and large foraminifera are visible as etchings on weathered surfaces.

Boundaries: The basal contact is not observed in the field area. The formation is believed to overlie Triassic sediments to the south of Pınarbaşı (approximately 80 km SE of the Darende basin (Akkuş, 1971). The upper contact is not well exposed in the field area. On the SW margin of the basin, ophiolite mélange was emplaced above and, in turn, over thrust by the Geniz Formation. To the north, the upper contact is more difficult to define. In some areas to the northwest it appears that Upper Cretaceous limestone (Kırankaya Formation; See below) lies directly on top of the Geniz Formation. The two lithologies are difficult to distinguish and an accurate contact could not be established. In the northeast the present contact between the Geniz Formation and the Cretaceous-Eocene

basin fill sediments appears to have been partially controlled by Neotectonic sinistral strike-slip faulting. Crucially, the Asartepe and Darende Formations appear to onlap the Geniz Formation along this margin, as seen to the southeast of Irmaklı.

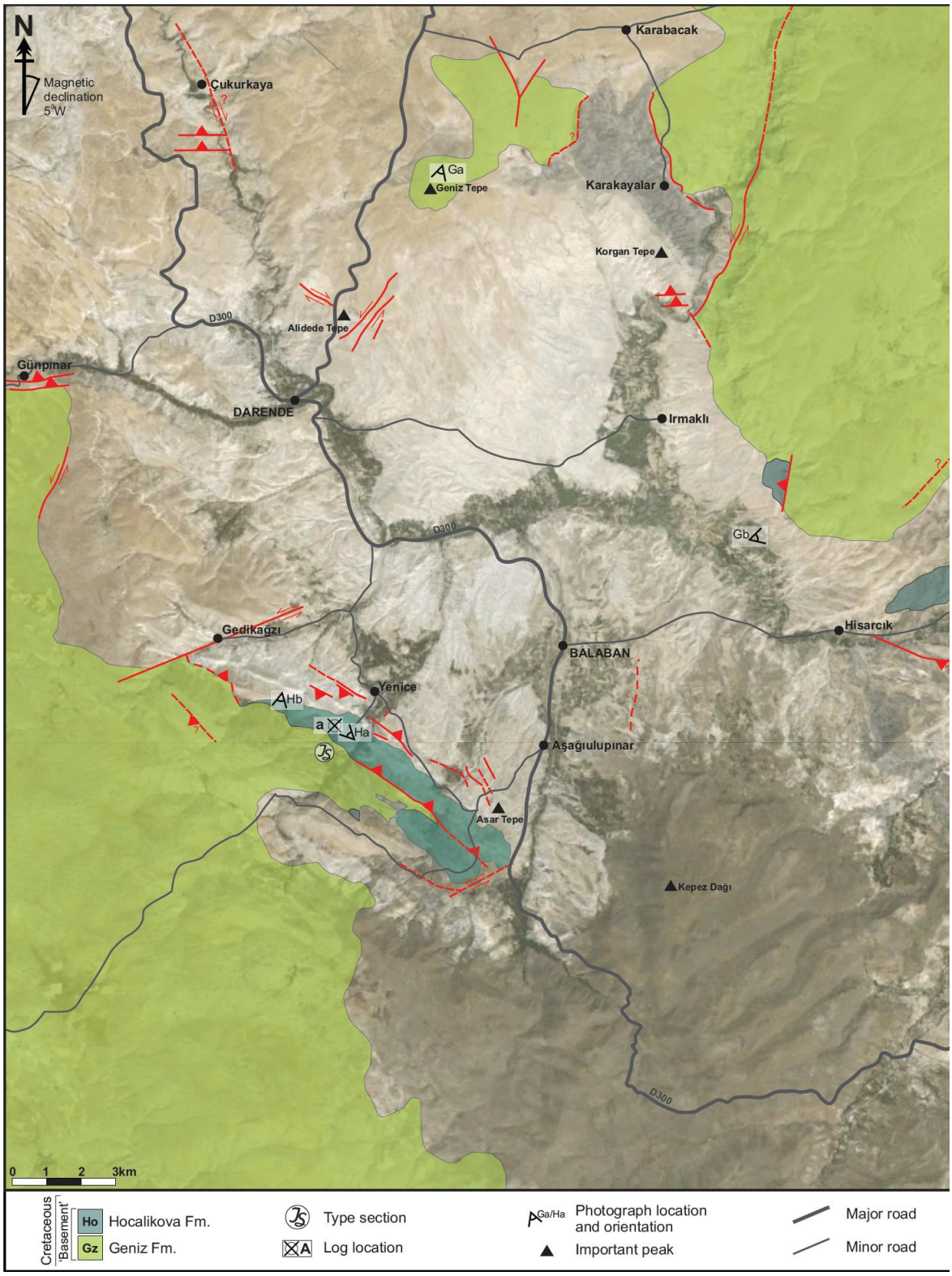

Figure 2.6. Simplified geological map showing the extent of the Geniz and Hocalikova Formations draped over a satellite image of the Darende Basin. Also shown are logged section locations together with the location and approximate bearings of landscape photographs.

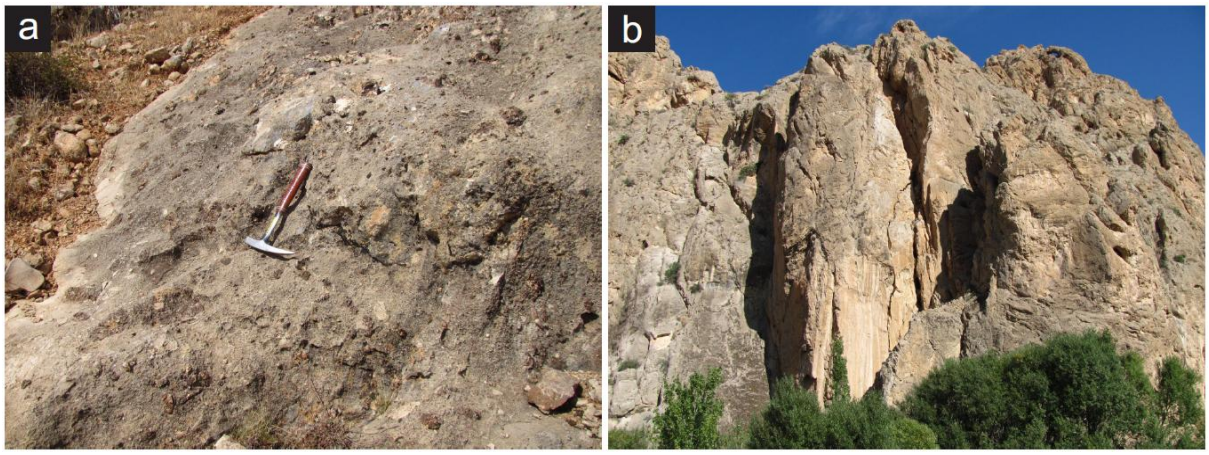

Figure 2.7. Field photographs of the Geniz Formation. a, showing grey-to-pink colour of crystalline limestone; b, showing scale of outcrop and degree of faulting, fracturing and weathering.

Thickness and extent: The maximum stratigraphic thickness of the outcrop is ~500 m, as seen along the southwest margin of the basin. However, the base of the platform carbonate succession is not exposed in the study area. Elsewhere, the equivalent of the Geniz Formation, known regionally as the Tauride Carbonate Platform, is typically up to several kilometres thick (e.g. Perınçek & Kozlu l984). For example, shallow-water carbonates overlie Triassic sediments to the south of Pınarbaşı (~100 km west of the Darende Basin), where they exceed 1000 m in thickness (Akkuş 1971). A borehole to the NW of the field area is recorded as reaching 2090 m within neritic carbonates before terminating (Akkuş 1971; Table 2.1, exact location unspecified). The Geniz Formation is well exposed and well represented in and around the field area. Similar limestone outcrops ~50 km north of Darende, near Gürün, are believed to be a structural extension of the regional Tauride carbonate platform 'basement' unit (Robertson *et al.* in press).

Geochronology	Thickness	Lithology	Fossils
Maastrichtian	89	Reef limestone	*Orbitoides media, O. apiculata, Siderolites calcitrapoides, Lepidorbitoides socialis.*
Cenomanian-Senonian	541	Brecciated limestone, marl-interbedded with sandstone, partly chalky and cherty and dolomitised limestone	*Globotruncana fornicata, Gl. Stephani, Gl. Lapparenti, Gl. Apenninica, Cuneolina pavonia, Dicyclina sp.*
Aptian-Albian	230	Partly chalky and fractured limestone	*n/a*
Neocomian-Barremian	250	Partly dolomitised limestone	*Hensonella cylindrica, Salpingoporella sp. Actinoporella podolica.*
Dogger-Malm	550	Partly chalky and dolomitic limestone in the upper levels	*Clypeina jurassica, Valvulinella jurassica, Bankia striata, Favreina salevensis.*
Lias	925	Partly chalky and fractured limestones, interbedded with marl in the upper and lower levels	*Macroporella pigmaea, Lituola sp., Cayeuxia sp., Solenopora spicules.*

Table 2.1. Summary of the borehole drilled through Mesozoic limestones to the west of the field area, from Akkuş (1971). Note that total thickness exceeds 2000m.

Age: The age of the Geniz Formation is Mesozoic and it is believed to have been deposited from the Late Jurassic to Mid-Late Cretaceous basin on foraminifera (Table 2.1) (Akkuş, 1971, Perincek & Kozlu l984, Robertson *et al.* in press).

2.4.1.2 Interpretation of the Mesozoic Platform Limestones (Geniz Formation)

The stratigraphically lowest unit, the Jurassic-Cretaceous carbonate platform (Geniz Formation), is interpreted as part of the regional Eastern Tauride carbonate platform. The Taurides are traditionally divided into three contiguous parts, the Western Taurides (Collins & Robertson 1998; Okay *et al.* 2001), the Central Taurides (Özgül l984, l997; Göncüoğlu *et al.* 2003; Mackintosh & Robertson 2009) and the Eastern Taurides (Perincek & Kozlu l984, Robertson *et al.* in press). The Eastern Taurides, east of the ~NE-SW striking Neotectonic Ecemiş fault zone (Fig. 2.2) developed after Triassic rifting during a phase of passive margin subsidence of the Tauride-Anatolide

microcontinent bordering Neotethys (Demirtaşlı *et al.* l984; Perincek & Kozlu l984; Özgül l996 Taslı *et al.* 2006; Robertson *et al.* in press).

2.4.1.3 Upper Cretaceous ophiolitic mélange (Hocalikova Formation)

Name: Possibly derived from a mountain in the Hekimhan Basin region (~70 km east of Darende; see Hekimhan Basin chapter).

Type locality: To the SE of Yenice.

Lithology: Typically, the Hocalikova ophiolitic mélange in the Darende Basin occurs as a sheared sedimentary mélange (see Raymond l984 for definition of mélange) with ophiolitic derived clasts ranging from granular, to pebbly, to very large blocks tens of metres in diameter termed olistoliths. The lower ~50 m of the mélange mainly consists of ophiolite-derived blocks, up to tens of metres in size. The blocks are dominated by highly altered gabbro, pillow basalt (Fig. 2.8a, 2.9), red radiolarian chert and neritic limestone, typically set in a dark grey, clay-rich, sheared sandy matrix. The upper ~100 m of the mélange comprises sheared, dark grey, matrix-supported conglomerates and sandstones. The conglomerates are composed of sub-rounded granule-to cobble-sized clasts of ophiolite-related lithologies, set in a clay-rich matrix (Fig. 2.8b).

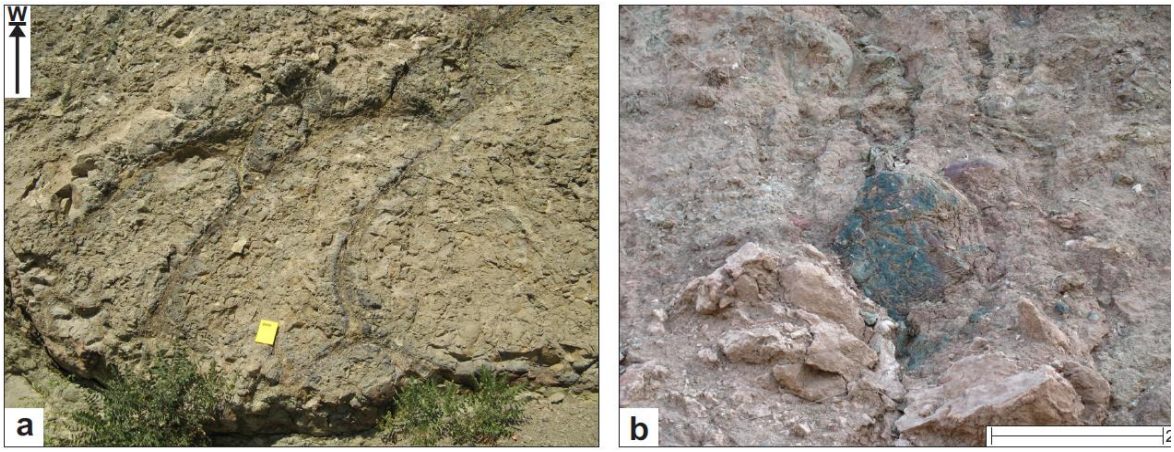

Figure 2.8. Field photographs of ophiolite in the Darende Basin. a, part of an olistolith composed of altered pillow basalt. Dark, devitrified hyaloclastite glass bands mark the boundaries of pillows, notebook for scale; b, clast of hydrothermally altered chloritised material set in a sheared, clay-rich matrix.

Boundaries: The lower boundary is an unconformable contact above the Geniz limestone Formation which is often affected by tectonics. The upper boundary forms an unconformity onto which Maastrichtian aged clastics and marine limestones were deposited (see below). However, the boundaries between the mélange and other formations are often seen as tectonic and as such, are discussed in the structure section of the Darende Basin (Chapter 2.5).

Thickness and extent: The mélange is extremely localised in the Darende Basin. It mainly crops out along the NW-SE striking southern basin margin, south of Yenice (Fig. 2.6), where it reaches a maximum thickness of ~150 m. The thickness is variable along strike reflecting the mode of emplacement and its susceptibility to erosion. The mélange is not exposed along the northern margin of the basin; however, localised outcrops were observed in the east of the basin, near Hisarcık, where the exposure is controlled by tectonic structures (see Chapter 2.5).

Age: The Hocalikova ophiolitic mélange forms part of a region-scale supra-subduction zone (SSZ) type ophiolite which is believed to have been obducted during the Late Cretaceous (Parlak et al. 2000; 2004; Robertson et al. 2009; in press).

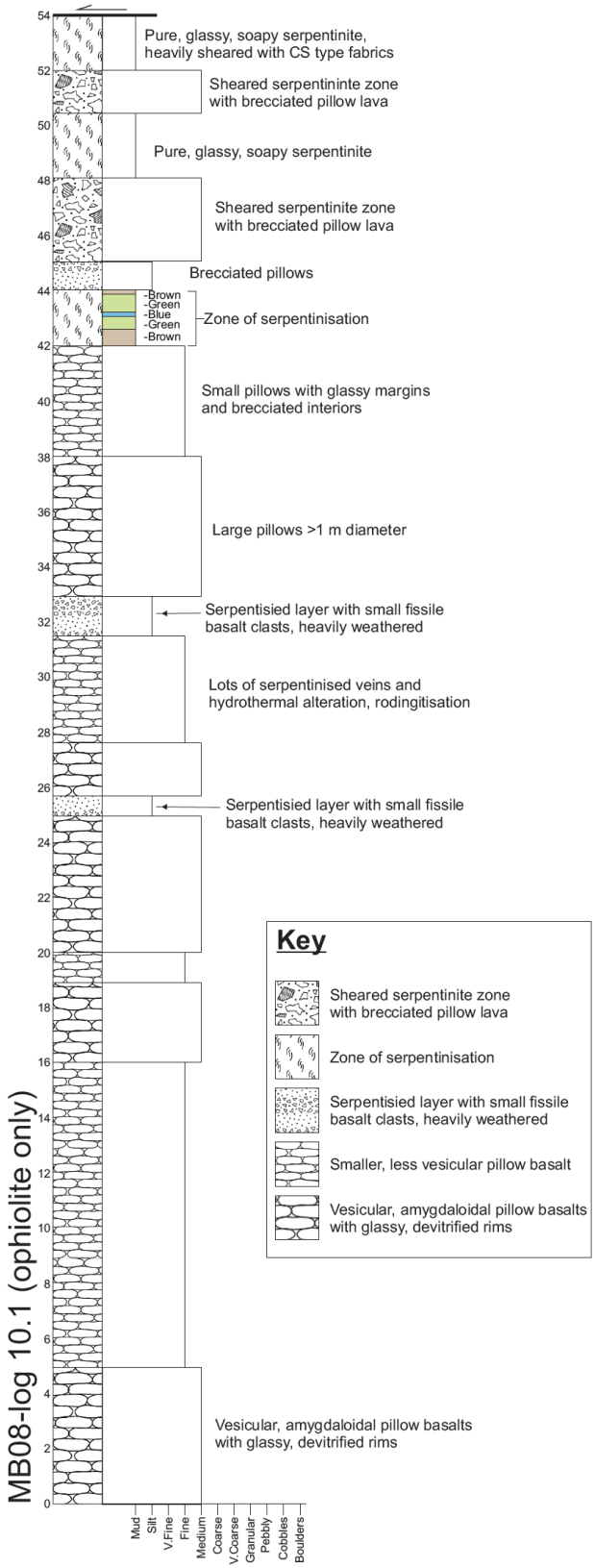

Figure 2.9. Logged succession of part of the ophiolitic mélange exposed to the west of Yenice. Most of the section is pillow lava. Lava breccia intervals are also present. Many horizons are heavily affected by hydrothermal alteration.

2.4.1.4 Interpretation of the Upper Cretaceous ophiolitic mélange (Hocalikova Formation)

The ophiolite-related mélange (Hocalikova Formation) was formed by a combination of tectonic and sedimentary processes, although the localised outcrops are too small to permit detailed interpretation. Elsewhere in the region (e.g. in the Gürün area, northwest of the Darende Basin) similar mélange was emplaced onto the northern margin of the Tauride platform during Campanian-Maastrichtian time (Perinçek & Kozlu, l984; Robertson *et al.* in press). The lithologies are interpreted to have accreted above a northward-dipping subduction zone within Neotethys and then emplaced southwards onto the Tauride carbonate platform during latest Cretaceous time (Robertson *et al.* in press). The ophiolitic rocks themselves are likely to have formed in a supra-subduction zone setting, probably the Inner Tauride ocean (Görür *et al.* 1984), as inferred for other ophiolites overlying the Tauride-Anatolide microcontinent (Robertson, 2002, 2006; Parlak *et al.* 2000, 2004, 2009).

2.4.1.5 Ophiolite Geochemistry

Three samples of basalt from the Hocalikova Formation were collected and analysed using X-Ray Fluorescence (XRF). Care was taken in the field to collect relatively unaltered hand specimens. However, the ophiolite has been subjected to alteration including sub-surface and surface chemical weathering. Only one ophiolitic sample was found to be suitable for geochemical analysis and is shown on the ‘spider plot’ (Fig. 2.10, Table 2.2) normalised to Mid Ocean Ridge Basalt (MORB). The result shows enrichment in the lighter more mobile elements. Thorium to Scandium plot close to MORB indicating a geochemical affinity with MORB. However, the relative depletion in Nickel and Chromium may indicate some degree of fractionation.

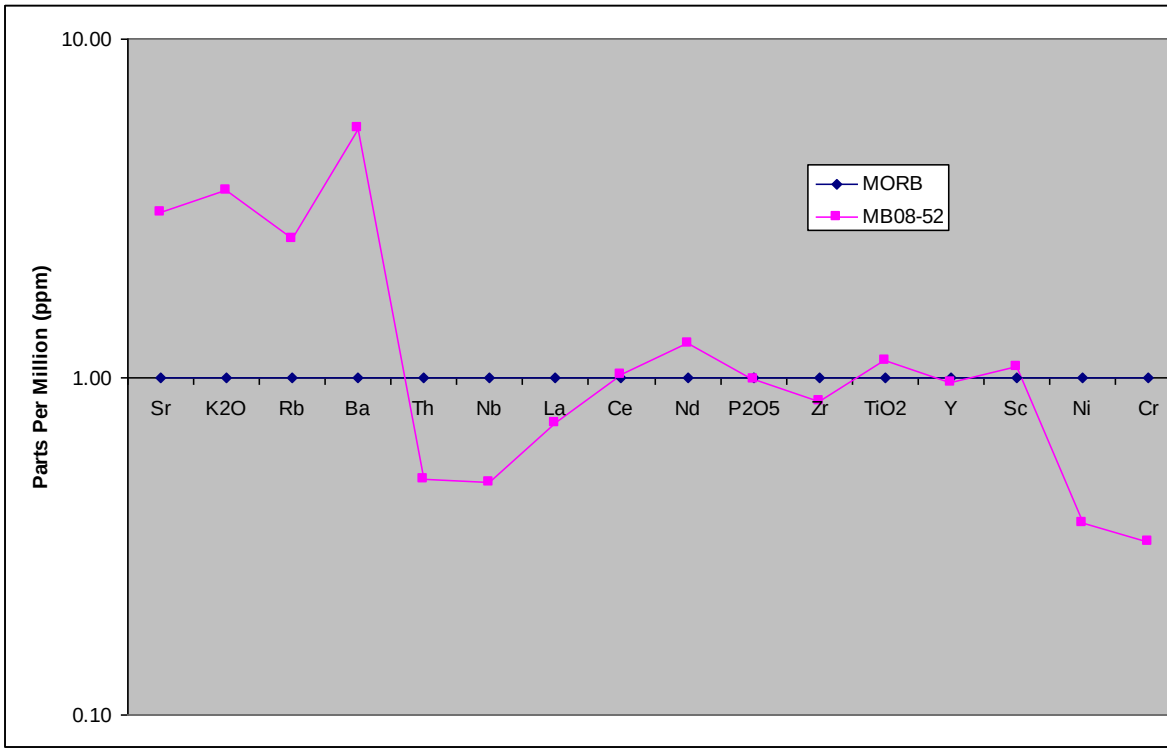

Figure 2.10. MORB normalised 'spider plot' of geochemical XRF data from ophiolitic basalt of the Hocalikova Formation.

Sample	MB08-52
Latitude	38.4456
Longitude	37.5183
Majors	
SiO2	49.67
Al2O3	16.04
Fe2O3	12.54
MgO	5.69
CaO	8.10
Na2O	2.67
K2O	0.518
TiO2	1.628
MnO	0.180
P2O5	0.115
LOI	2.38
Total	99.53
Total - LOI	97.15
Minors	
Zn	89.8
Cu	59.3
Ni	50.9
Cr	81
V	351.8
Ba	109.3
Sc	42.8
La	2.2
Ce	10.2
Nd	10.1
U2	n.d.
Th	0.1
Pb	0.7
Nb	1.7
Zr	76.4
Y	29
Sr	369.2
Rb	5.1

Table 2.2. Raw data (Majors recalculated for LOI) for ophiolite sample MB08-52.

2.4.2 Maastrichtian Sediments

Sedimentation in the Darende Basin, as defined here, began during the Maastrichtian with the deposition of red conglomerates, sandstones and mudstones, termed the Ulupınar Formation (Fig. 2.5). The formation is unfossiliferous but is inferred to be of Maastrichtian age owing to its position between the Campanian-Maastrichtian ophiolite-related mélange, below (Perinçek& Kozlu l984; Robertson *et al.* in press) and overlying shallow-water carbonates that are dated as Maastrichtian. These sediments are dominated by a succession of light grey marls and finely laminated limestones, termed the Kırankaya Formation (Fig. 2.5). These are dated as Late Maastrichtian, based mainly on benthic foraminifera (Akkuş 1970, 1971; Gürbüz & Gül 2005). The formation includes distinctive carbonate build-ups rich in rudist bivalves that are distinguished as the Tohma Member (Fig. 2.5). The Upper Cretaceous sediments unconformably overlie the ophiolite-related mélange or the Mesozoic platform carbonates in different areas (Fig. 2.3, 2.4). The Maastrichtian sedimentary rocks are commonly faulted and folded especially near some parts of the basin margin.

2.4.2.1 Maastrichtian non-marine clastics (Ulupınar Formation)

Name: Named after the village of (Aşağı) Ulupınar (Akkuş 1971) situated approximately 3.5 km south of Balaban along the D300 highway (Fig. 2.11).

Type locality: ~2.5 km SW of Asar Tepe (location b on Fig. 2.11).

Lithology: The Ulupınar Formation has a distinctive red colour and is generally composed of poorly sorted, texturally immature, fine-to-granular, erosive-based sandstones and conglomerates that exhibit an overall fining-upward trend. Fig. 2.12 is a sedimentary log of a small part of the Ulupinar Formation at Yenice (Log locality d on Fig. 2.11). This mainly consists of alternations of sandstone and pebbly, lenticular and erosive-based conglomerates. Imbricated clasts are common. Fig. 2.13 is a sedimentary log of part of the Ulupınar Formation measured near the southern margin of the basin (log locality a on Fig. 2.11). This shows the erosive nature of the conglomerates. Fig. 2.14 is a

sedimentary log of part of the Ulupinar Formation from the Çukurkaya valley area to the north of the Darende Basin (Log location c on Fig. 2.11). Although the section is shorter, the bedding and lithology are similar. Palaeocurrents were restored to horizontal by rotation about the bedding plane. Palaeocurrents from this section trend towards the NNW.

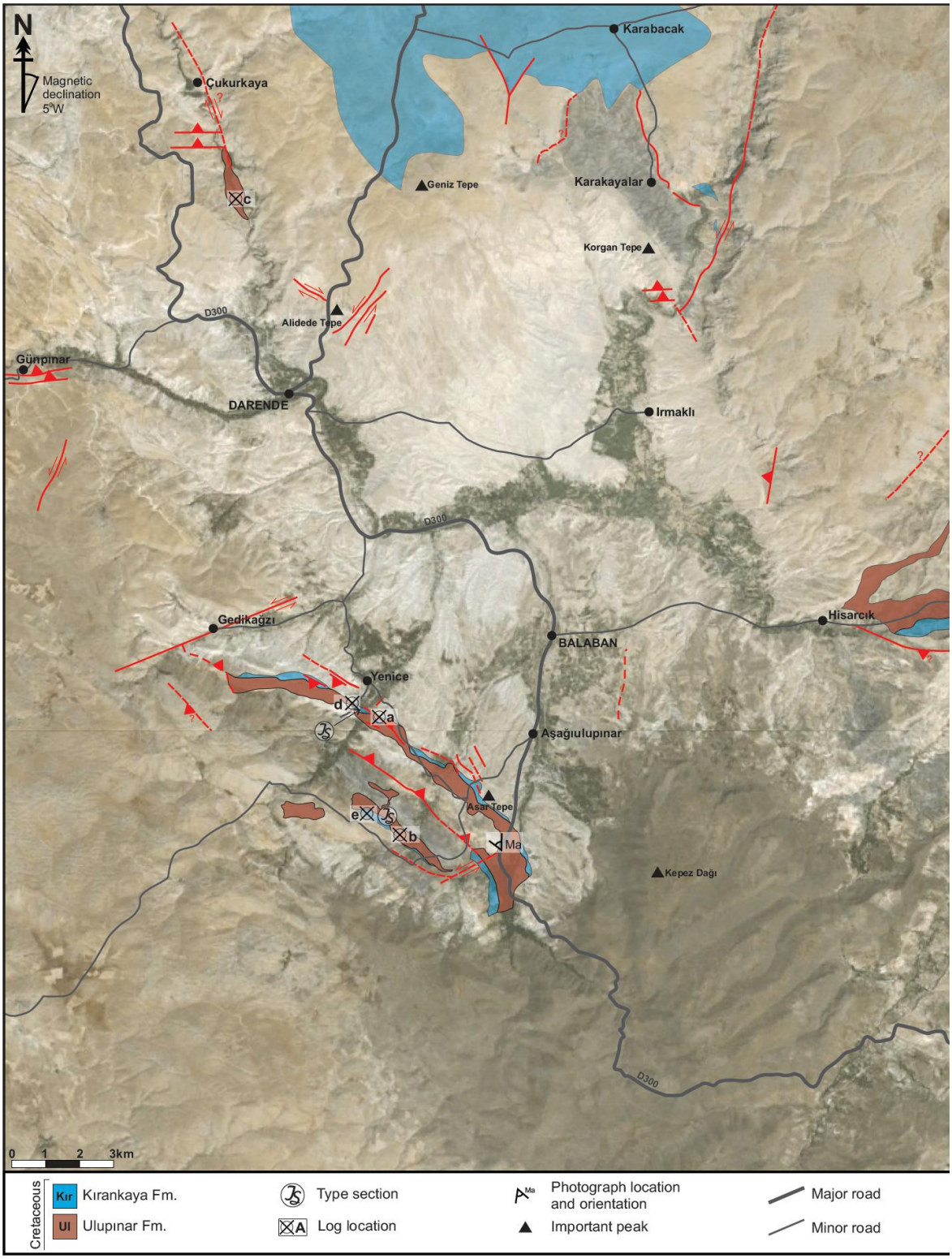

Figure 2.11. Simplified geological map showing the extent of the Ulupınar and Kırankaya Formations draped over a satellite image of the Darende Basin. Also shown are logged section locations together with the location and approximate bearings of landscape photographs.

Pebble-to cobble-grade, cross-bedded sandstones are frequent in the lower to mid parts of the succession. Red mudstone-shale interbeds and lenses commonly occur in the

upper part of the succession, particularly in the north of the basin (e.g. Çukurkaya area). Clasts are predominantly sub-rounded, to rounded, with the larger clasts being more rounded. The clasts encompass a wide range of lithologies, including Mesozoic neritic limestone and ophiolite-related clasts; e.g. radiolarite, chert, altered basalt, gabbro and serpentinised ultramafic rocks (Fig. 2.15). However, the ratio of Mesozoic limestone to ophiolite-derived clasts varies across the basin and up section. A relatively greater abundance of Mesozoic limestone clasts was observed at the base of the sequence and in all areas of the basin. In the south of the basin, the mid-to-upper levels of the formation have a greater ratio of ophiolite-derived lithologies, whereas similar stratigraphic levels in the northern parts of the basin retain a higher ratio of Mesozoic limestone clasts. The clasts are arranged into erosive-based, lenticular packages several tens of centimetres thick and on average ~20 m in width, which erode a few centimetres into the underlying layers.

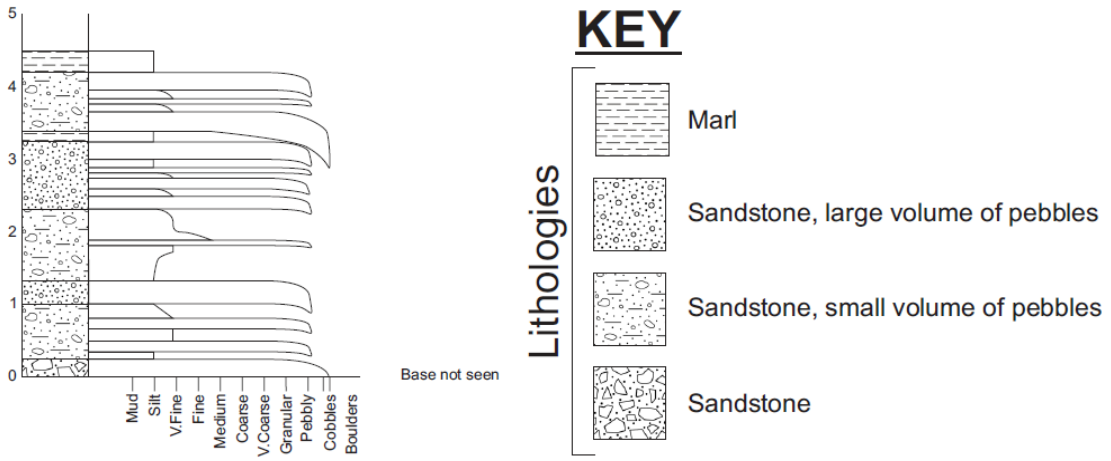

Figure 2.12. Sedimentary log of part of the Ulupinar Formation measured in the Yenice type area (Log locality d on Fig. 2.11).

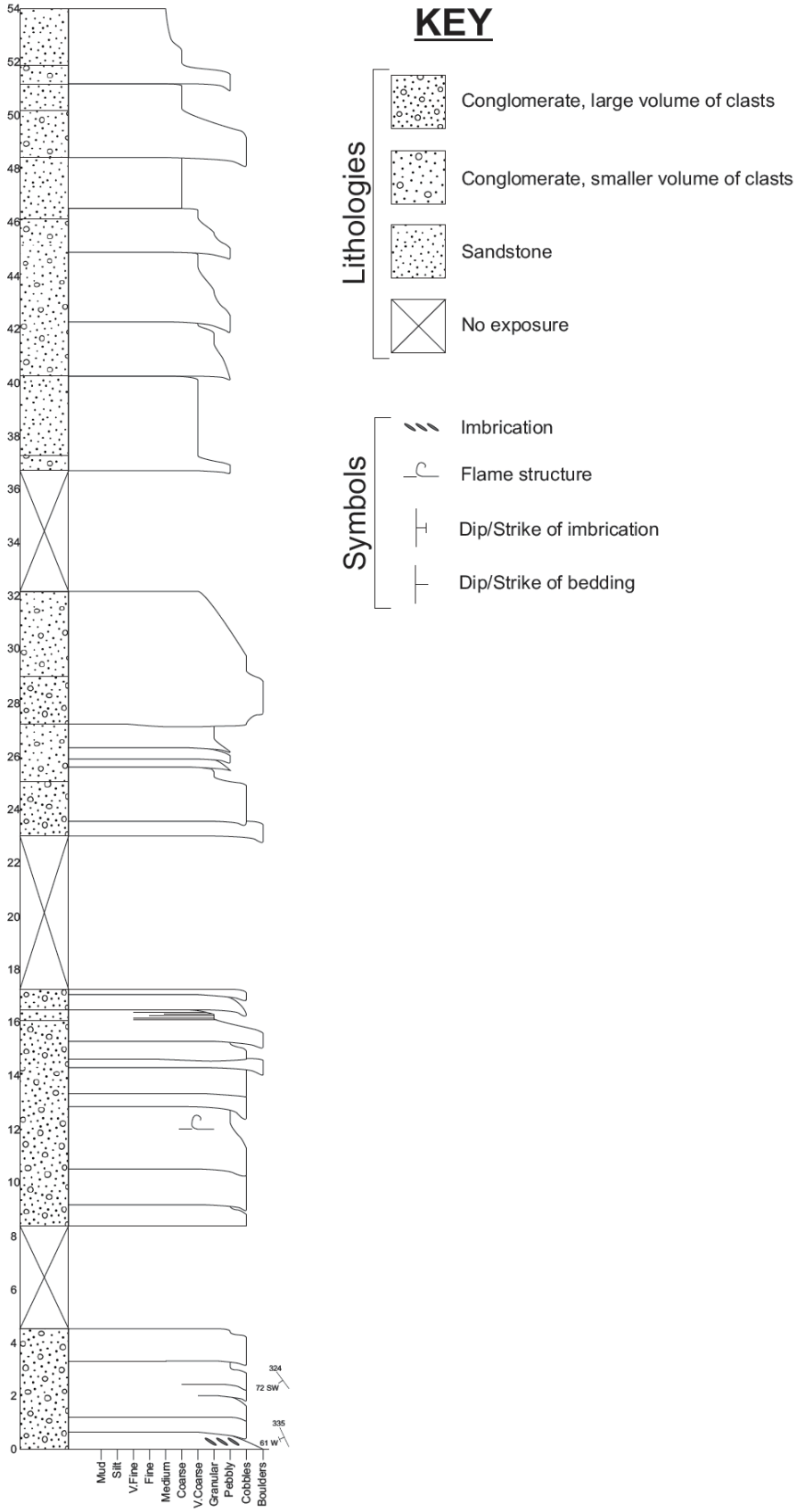

Figure 2.13. Measured sequence of part of the Ulupınar Formation, as logged at locality a on the geological map (Fig. 2.11).

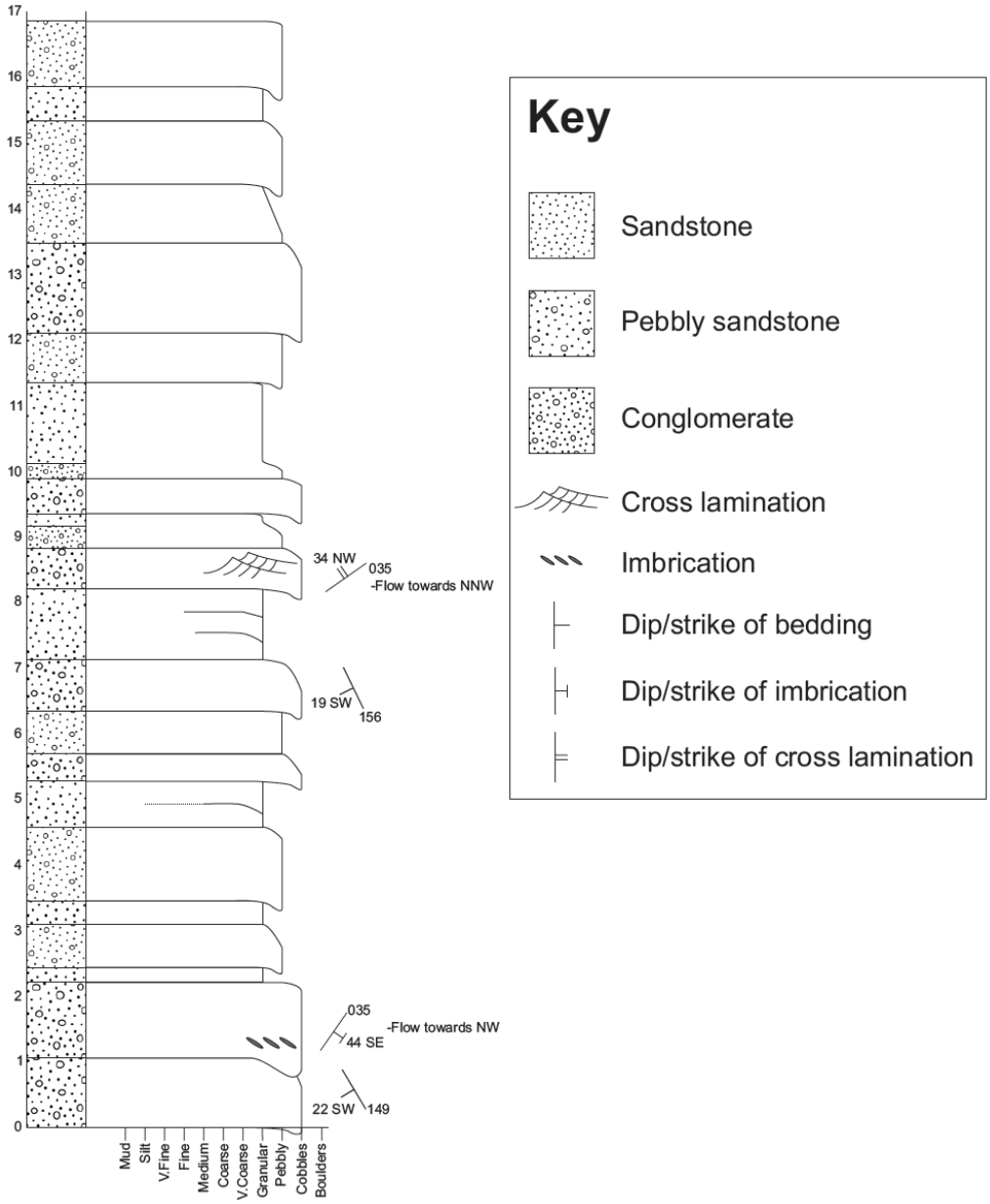

Figure 2.14. Measured section of part of the Ulupinar Formation taken from the southern part of the Çukurkaya valley area to the north of the Darende Basin (log location c on Fig. 2.11). Bedding geometries and lithology are similar to the Ulupinar Formation exposed around Yenice in the south of the Basin (see Fig. 2.13).

Figure 2.15. Field photograph showing tilted outcrop of the Ulupınar Formation at locality b on Fig. 2.2.11, showing well-rounded clasts of various lithologies.

Boundaries: The lower boundary is unconformable on the ophiolitic mélange and displays varying degrees of angular discordance along the contact. The upper boundary is represented by a marine transgression.

Thickness and extent: The occurrence and thickness of the formation varies considerably around the margins of the basin. It reaches a maximum thickness of ~150 m south of Asar Tepe and thins northwestwards to ~50 m (northwest of Yenice). To the north of Darende, the Formation is ~75 m thick and wedges out northwards along the Çukurkaya valley. It is absent from the northeasternmost part of the basin.

Age: The Ulupınar Formation is unfossiliferous but is dated based on its position between the ophiolite-related mélange below that was regionally emplaced during latest Cretaceous (Campanian-Maastrichtian) time (Perınçek& Kozlu l984; Robertson *et al.* in

press) and the overlying shallow-water carbonates of the Kırankaya Formation and the Tohma Member which are dated as Maastrichtian (Akkuş 1970; 1971).

2.4.2.2 Interpretation of the Maastrichtian non-marine clastics (Ulupınar Formation)

Erosion of the Mesozoic carbonate platform and the poorly consolidated ophiolite-related mélange was followed by deposition of the Maastrichtian reddish, non-marine sediments of the Ulupınar Formation. Fluvial deposition in a braided system is indicated by the erosive, channelised and cross-bedded nature of many of the beds, coupled with the ubiquitous clast rounding. Local changes in sediment thickness reflect deposition over a variable palaeotopography including 'highs' and 'lows' (Fig. 2.16). The lithology of the formation, particularly the ratio of ophiolite related grains to carbonate grains reflects the localised source areas. Deposition was initiated in the south of the basin within topographic depressions created by erosion or faulting indicated by the thickness variations within the formation. The relatively thin deposits found in the northwest of the basin together with northwestwards trending palaeocurrents indicate a braided fluvial system prograded generally northwestwards across the basin. Similar red continental clastic sediments of variable thickness accumulated in the east of the basin (Hisarcık area), where palaeocurrents trend westwards.

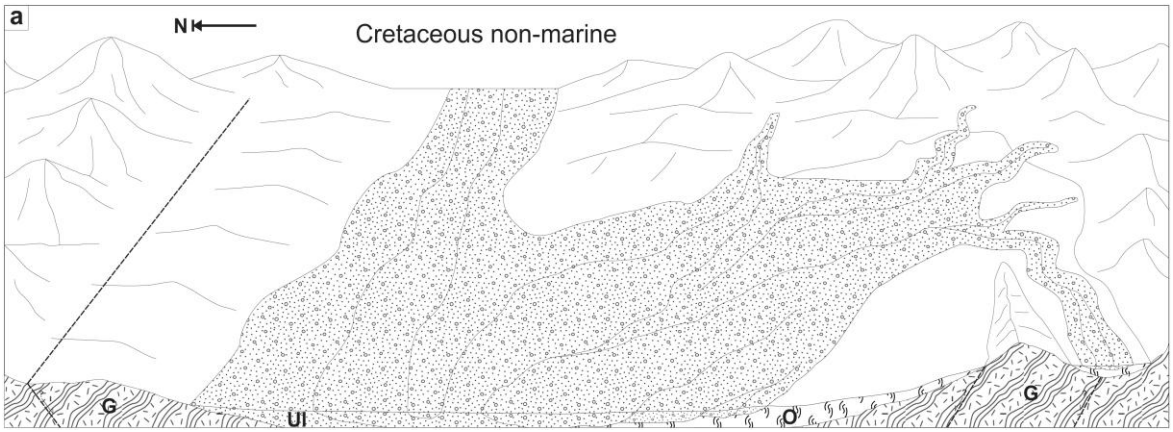

Figure 2.16. Palaeogeographic reconstruction of the latest Cretaceous (Maastrichtian) clastic deposition (Ulupınar Formation). G, Geniz Formation; O, Hocalikova ophiolite Formation; Ul, Ulupınar Formation.

2.4.2.3 Rudist patch reefs (Tohma Member)

Name: Named after the Tohma River which flows from the northwest of the field area towards the southeast and then due east across the centre of the field area.

Type locality: 1.5 km west of the village of Hisarcık on the eastern side of the Darende area.

Lithology: The Member is characterised by an abundance of rudist bivalves (Fig. 2.17) (e.g. Steuber & Löser 2000; Özer *et al.* 2009). Many of the hand specimens are of the species *Hippurites* sp. (Özer 1988; Steuber 2002). The rudists range in size from <5 cm to 30 cm and occur in great abundance within poorly lithified silty to micritic limestone. The associated macrofauna include gastropods and other bivalves. The shells of the rudist bivalves are made of calcite and consequently have a high preservation potential. However, portions of the inside of the test were made of aragonite and have subsequently been recrystalised to calcite spar (Falini *et al.* 1996; Steuber 1999).

Boundaries: The lower boundaries of the Tohma Member are unconformable. The unit is either found directly overlying ophiolitic lithologies or the Ulupinar Formation. The upper boundary is not well exposed within the basin but in most instances it appears to be transitional with micritic marls of the Kırankaya Formation within which occasional rudists are present, although usually as individual, small shells.

Thickness and extent: The rudist-rich units commonly form elongate, ridge-like outcrops, ranging from <10 m long x <2 m wide, to >150 m long x 20 m wide, and are up to 30 m high. The size and abundance of rudists decrease in outcrops containing relatively high proportions of terrigenous clastic material compared to carbonate material.

Age: Rudist bivalves existed throughout the Jurassic and Cretaceous and were particularly widespread during the Maastrichtian. Many of the rudists found in the Tohma Member are characteristic of the Maastrichtian (Steuber & Löser 2000).

Figure 2.17. Field photograph showing a large rudist bivalve within a patch reef; near Hisarcık to the east of the field area (Fig. 2.11); pencil for scale.

2.4.2.4 Interpretation of the rudist patch reefs (Tohma Member)

Rudist-bearing carbonate sequences are common in the Tethyan realm (and are an important hydrocarbon reservoir rock for the region) (Demirel & Kozlu 1997; Sarı & Özer 2009). Rudist bivalves as a whole flourished in shallow-marine, tropical waters with low siliciclastic input, in similar conditions to tropical corals, before becoming extinct at the Cretaceous-Tertiary boundary (Steuber & Löser 2000; Stössel & Bernoulli 2000). The marine transgression during the Maastrichtian in the Darende Basin was characterised by the development of rudist-rich patch reefs on elongate topographic highs. The rudist reefs nucleated on relatively immobile non-marine clastic sediments of the Ulupınar Formation or the ophiolitic mélange of the Hocalikova Formation. These sessile, epibenthic rudists grew on top of each other to form mounds and acted as reef bafflers, trapping sediment and other organisms between there shells as they grew.

2.4.2.5 Maastrichtian transgressive shallow-marine carbonates (Kırankaya Formation)

Name: *Unknown (not on available maps).*

Type locality: The type locality is along a northwest-southeast-striking ridge to the south of Yenice (locality d on Fig. 2.11).

Lithology: The Formation begins with thin micritic limestones, interbedded with silty, fissile, micritic marl. There is then a passage over ~20 m to well-bedded, finely, often wavy laminated micritic limestones. These sediments are ~30-50 m thick in the south but are up to ~100 m thick in the northern part of the basin. The fine-to-wavy lamination is attributed to microbial (algal) binding of fine-grained sediment (Fig. 2.18a). In the southern part of the basin, contemporaneous sedimentary breccias (autobreccias), gypsum pseudomorphs and bird's eye structure (Fig. 2.18b) are common in the upper part of the succession but these are absent in the northern part of the basin. Large bivalves (e.g. *Gryphea sp*.) are common in the eastern parts of the basin. Well-exposed limestones in the upper part of the Kırankaya Formation can be seen in the lower to middle part of Figure 2.19 in the south of the field area (*e.g.* ~59m on Fig 2.20). These are commonly wavy-to cross-laminated and become silty and flaser laminated upwards. The limestones pass into red, wavy-laminated, bioturbated, muddy, to-pebbly, sandstones. Occasional palaeosols in the highest parts of the sequence contain rootlets and caliche nodules. These are typically interbedded with white, wavy-laminated microbial limestones (*e.g.* ~72m on Fig 2.20). The logged section shown in Figure 2.21 also shows a marine sequence represented by shallow-marine limestones. There, the sequence begins with subaerially influenced facies (red mudstone interbedded with white limestone ~4-8 m) and progresses through marine deposits of limestone, sandy limestone and marl, of marine origin, as indicated by the presence of foraminifera and bivalves. The top of the sequence is not present due to an erosive unconformity. Above the unconformity comes thick (>1 m), lenticular conglomerates with well-rounded clasts which are sub-matrix supported.

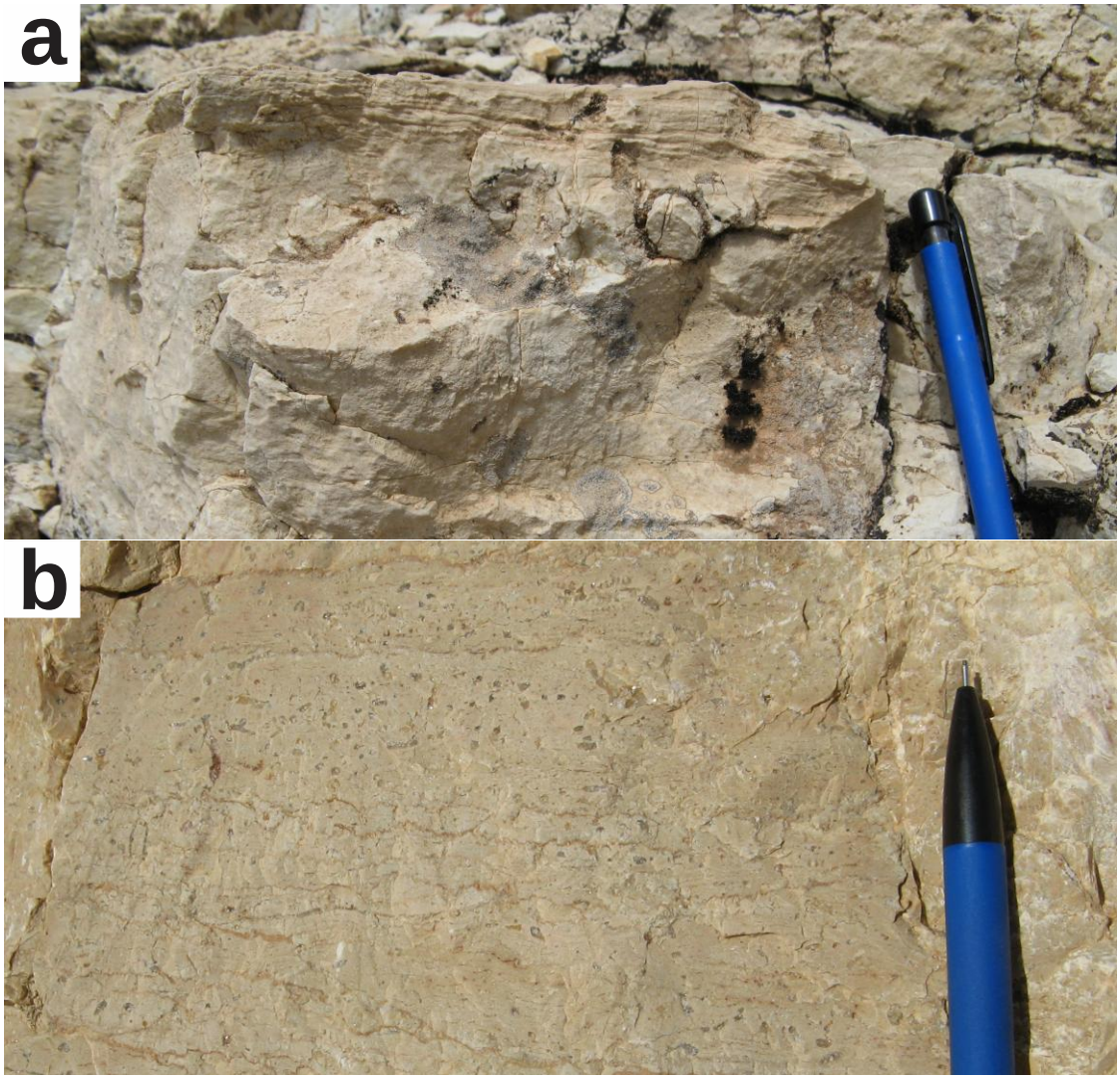

Figure 2.18. Field photograph. a, Microbial (algal)-laminated limestone of the Kırankaya Formation from location d in Fig. 2.11; b, Bird's-eye texture within limestone in the upper part of the Kirankaya Formation at location d on Fig. 2.11. Pencil for scale in both.

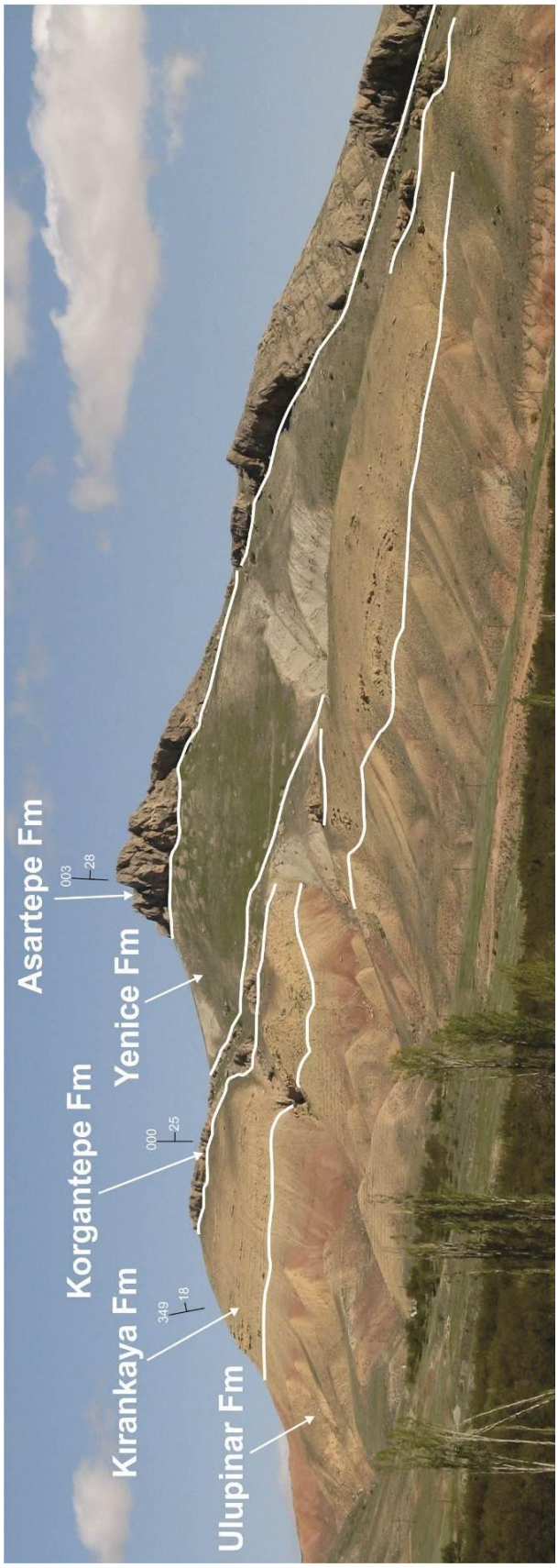

Figure 2.19. View northwestwards to Asar Tepe (location on Fig. 2.3 & 2.11) showing basin-filling sediments near the southwestern margin of the Darende Basin.

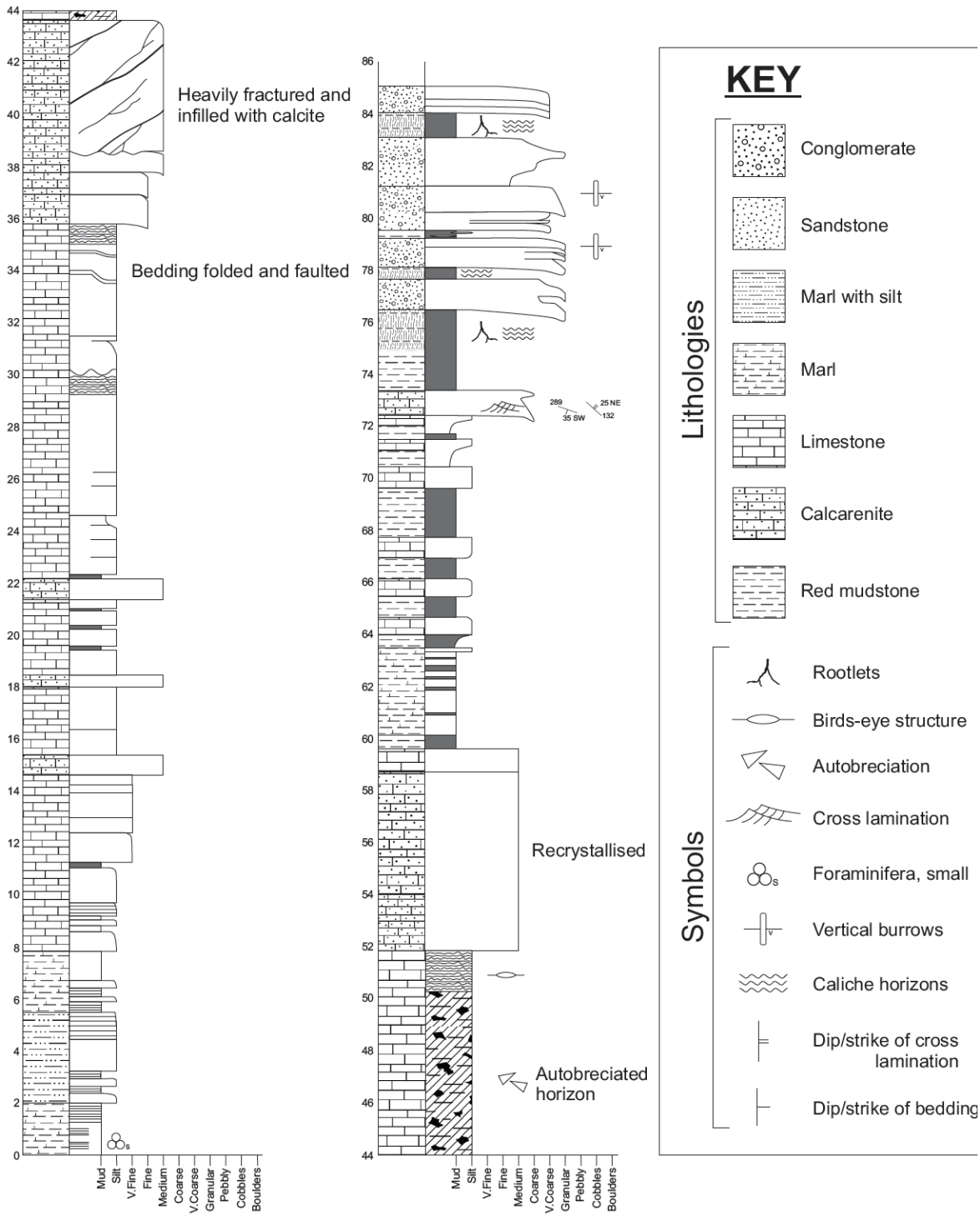

Figure 2.20. Sedimentary log of the Kırankaya Formation (location d on Fig. 2.11). Note the transition from shallow-marine limestones in the lower to middle part of the section, to marls and lacustrine limestones, followed by mudstone, palaeosols and conglomerates in the upper part. See text for explanation.

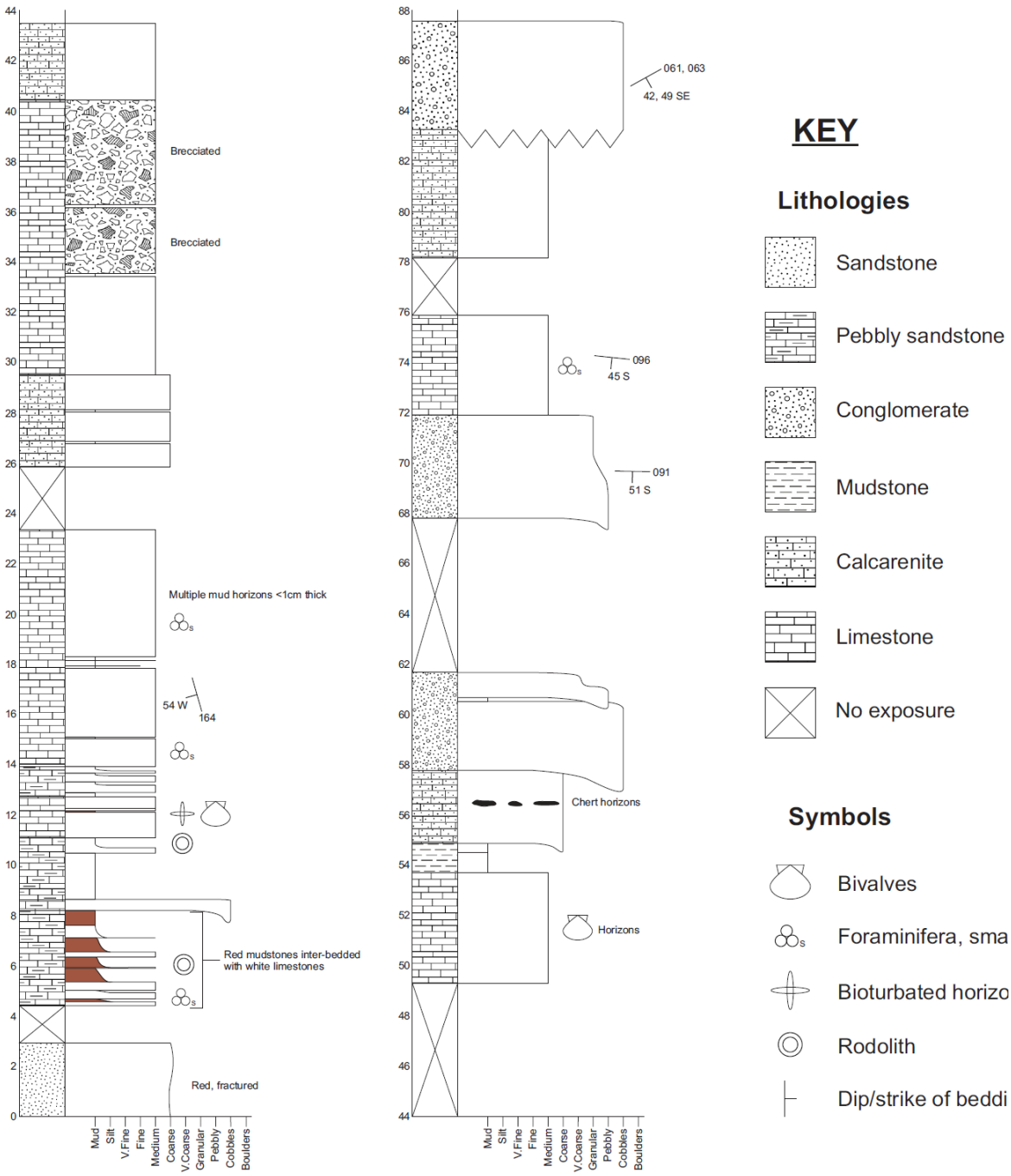

Figure 2.21. Sedimentary log of the Kırankaya Formation (location e on Fig. 2.11). Notice the transition from subaerially influenced red mudstones interbedded with limestones at the base of the sequence into a marine sequence before being unconformably overlain by fluvial conglomerates.

Boundaries: The lower boundary is transgressive on the Ulupınar Formation. This can be seen in many locations in the south of the basin (e.g. Asartepe, Yenice and Gedikağzı). However, in the north of the basin, the contact between the Ulupınar and the Kırankaya Formations is only evident at one locality, the Çukurkaya valley. There, the facies change from red, poorly sorted, immature, continental sandstones and pebbly conglomerates

(Ulupınar Formation) through sandy and silty dark grey marl, to pure light grey marl (Kırankaya Formation) and into white microbial micritic limestones over ~ 15 m. The upper boundary is represented by a basin-wide low-angle unconformity (~5^{o}). In the south, the unconformity is situated on continental and lacustrine facies whereas in the north the unconformity directly overlies white micritic limestone. In many cases the formation is transitional with rudist reefs of the Tohma formation.

Thickness and extent: The total thickness ranges from 30 to 100 m across the basin. The formation is at its thinnest and with greatest facies variations in the southern part of the basin around the villages of Asartepe, Yenice and Gedikağzı. In northern and eastern areas the formation is thicker (up to 100 m) with less facies variation and is predominantly composed of white microbial micritic limestone. The Kırankaya Formation is widespread in the northern and southern parts of the field area.

Age: The Kırankaya Formation is Maastrichtian-aged (Akkuş 1971) based on the identification of Foraminifera and the presence of isolated rudist bivalves.

2.4.2.6 Interpretation of the Maastrichtian transgressive shallow-marine carbonates (Kırankaya Formation)

The Kırankaya Formation varies in thickness and lithology considerably across the basin. In northern areas the formation is thickest (~100m) and least variable being mainly composed of micritic limestone. In the south the formation is less well developed with the greatest lithological variability. This is because the southern part, representing the marginal facies of the formation (Fig. 2.20) is made up of micritic limestones in the lower part, overlain by a variable shallow-marine to non-marine sequence. The sequence culminates in fluvially deposited conglomerates interbedded with caliche and rootlet bearing palaeosols. This succession was not observed in other areas of the basin which could be attributed to erosion associated with the Paleocene unconformity (see 2.4.3 below). This relatively thin marine succession is again observed in the logged section in Figure 2.21 and likely suggests a localised marine transgression. No evidence of syn-sedimentary deformation was observed in the Kırankaya Formation suggesting that deposition was controlled by eustatic sea level change rather than active tectonics. Figure

2.22 shows a palaeogeographic reconstruction of the Kırankaya Formation that highlights the relatively thin sequence at the margins of the basin, with a thicker sequence filling the basin depocentre.

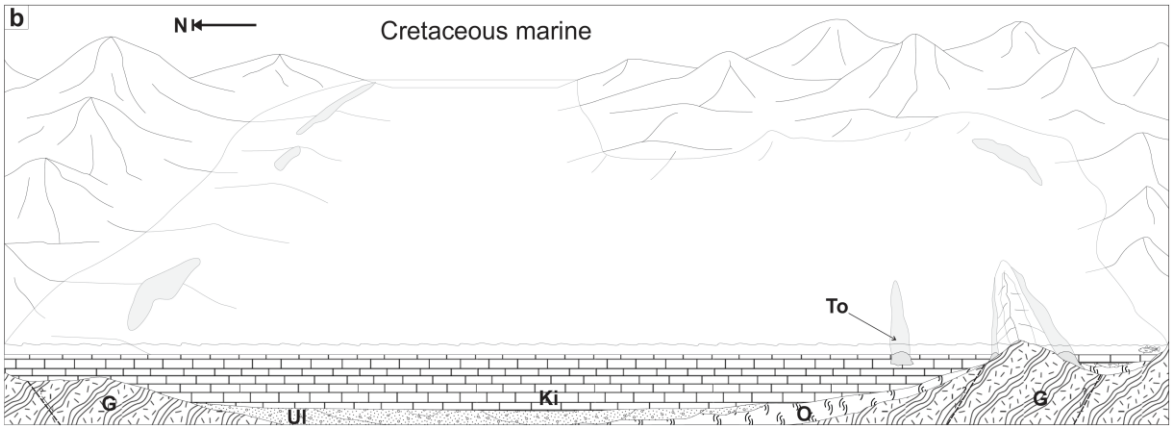

Figure 2.22. Palaeogeographic reconstruction of the latest Cretaceous (Maastrichtian) marine Kırankaya Formation and Tohma Member deposition. Kı, Kırankaya Formation; To, Tohma Member; G, Geniz Formation; O, Hocalikova ophiolite Formation; Ul, Ulupınar Formation.

2.4.3 Paleocene unconformity

No fossils of Paleocene age have been recognised in the Darende Basin based on palaeontological studies (Akkuş l9711; Gürbüz & Gül 2005; Booth *et al.* in press). By the time sedimentation resumed during the Early-Middle Eocene, the Darende Basin as a whole had been tilted by ~5-10^{o} on average. Figure 2.19 shows Asar Tepe where well exposed Cretaceous sediments are overlain by Eocene sediments above an angular unconformity, reaching ~10^{o}. Where Cretaceous sediments are exposed in the northerly parts of the basin the unconformity is typically a similar, shallow angle (~5-10^{o}). However, prominent angular discordances (up to ~ 45^{o}) are present in places along the southern margin of the basin (e.g. near Yenice). Figure 2.23 is a field photograph and line-pic showing prominent topography and important geological information taken ~1.5 km southeast of Yenice village (locality a on Fig. 2.11). This shows horizontally bedded Cretaceous conglomerates and limestones (Ulupınar and Kırankaya Formations) overlain by Eocene sandstones and marls (Korgantepe and Yenice Formations), dipping at ~40^{o}. Neptunian dykes approximately 3 cm wide and up to 25 cm depth were observed penetrating down from the Eocene sandstones into the Cretaceous conglomerates (Fig. 2.24).

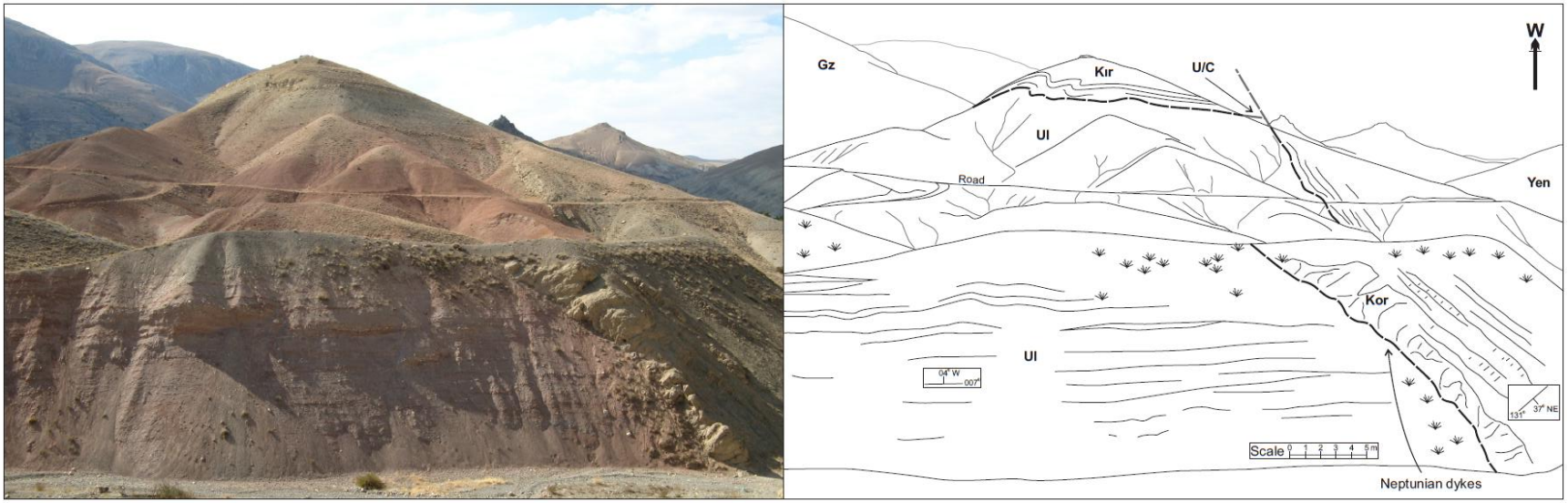

Figure 2.23. Field photograph (location a on Fig. 2.11) and line drawing showing sub-horizontally bedded Upper Cretaceous red sandstones and conglomerates (Ulupınar Formation) and overlying Upper Cretaceous limestones (Kırankaya Formation), both unconformably overlain by relatively steeply dipping Eocene sandstones (Korgantepe Formation). These unusual relations imply tilting by ~40^0 (related to extension (?), followed by transgression and then a reversal of the tilting by nearly the same amount (compression related).

Figure 2.24. Field photograph showing neptunian dykes composed of Ilerdian-Lutetian (Eocene)-aged brown sandstones of the Korgantepe Formation penetrating into Maastrichtian-aged red sandstones of the Ulupınar Formation. Hammer for scale. Picture taken from location of arrow in Fig 2.23.

2.4.4 Interpretation of Paleocene unconformity

No rocks of Paleocene age were observed within the Darende Basin. The basin appears to have remained emergent throughout Paleocene-Early Eocene time. A less likely alternative is that sediments of this age range were deposited but then completely eroded. The implied hiatus contrasts with some other basins in central Anatolia that include Paleocene sediments, namely the Ulukışla (where relatively deep-marine mudstone and turbidite associations have accumulated), Kırıkkale, Tuz Gölü, Çankırı and Sivas basins (e.g. Nairn *et al.* in press). The absence of Paleocene deposition in the Darende Basin could be explained by sedimentary infill of the shallow Late Maastrichtian basin (infill of accommodation space), coupled with eustatic regression (Miller *et al.* 2005). However, tectonics must also have played a role as evidenced by localised Maastrichtian sediments tilted by up to ~40^0 prior to the deposition of the overlying Early-Middle Eocene facies (Fig. 2.23).

Figure 2.21 is a sedimentary log of part of the Kırankaya Formation from location e on Figure 2.11. This shows an angular unconformity, ~83 m above this there are thick (>1 m), lenticular conglomerates with well-rounded clasts which are sub-matrix supported. These conglomerates could be the only known example of possible Paleocene-aged fluvial rocks identified in the Darende basin. The conglomerates are discordant with the underlying Maastrichtian-aged rocks by approximately 030^0 of strike and up to 09^0 of dip. It was not possible to establish the boundary between this conglomeratic unit and the overlying Korgantepe Formation. However, basal breccias of the Korgantepe Formation found in other areas contain angular clasts predominantly composed of Kırankaya Formation limestone which are clearly distinguished from this conglomerate. Therefore, the conglomerate unit may not be part of the Kırankaya Formation or the Korgantepe Formation and could thus be of Paleocene age. However, no fossils were found in the conglomerate so that dating them was not possible.

2.4.5 Eocene sediments and volcanic rocks

Sedimentation resumed with the accumulation of unconformably overlying, faunally diverse, brown to grey sandstones and siltstones of the Korgantepe Formation. The Korgantepe Formation is dated as Ilerdian-Lutetian (Early-Middle Eocene) based on numerous benthic foraminifera and a smaller number of planktic foraminifera. Subaerial, to submarine alkali basalt volcanism interrupts the Korgantepe Formation in the northeast of the basin (Karakayalar Member). The Korgantepe Formation is conformably overlain, and in places contemporaneous with, light grey hemipelagic, to pelagic marls, defined as the Yenice Formation (Fig. 2.5, this work). Distinctive yellow calcarenites interrupt the marls and characterise the southern part of the basin. The Yenice Formation is dated as Lutetian (Mid-Eocene), based on a combination of benthic foraminifera and planktic foraminifera. Above this, the conformably overlying, faunally diverse Asartepe Formation is dated as Early Lutetian (Mid-Eocene) to Late Bartonian-Early Priabonian (Late Eocene), mainly because of a rich assemblage of benthic foraminifera (including *Nummulites* sp.). This was finally succeeded by the Darende Formation, a mixture of carbonate, clastic and evaporitic facies (Fig. 2.5; this work) that is dated as Late Lutetian to Early Priabonian (Late Eocene) based on benthic foraminifera. Both of the Late Eocene formations (Asartepe and Darende Formations) transgressively onlap older lithologies around the basin margins, including Mesozoic limestones.

2.4.5.1 Early-Middle Eocene shallow-marine clastics (Korgantepe Formation)

Name: Possibly derived from the northwest-southeast trending ridge with a peak called Korgan Tepe, located to the south of Karakayalar (Fig. 2.25) in the northeast of the field area.

Type locality: The type section is around the village called Yenice, although this location is affected by faulting (location b on Fig. 2.25)

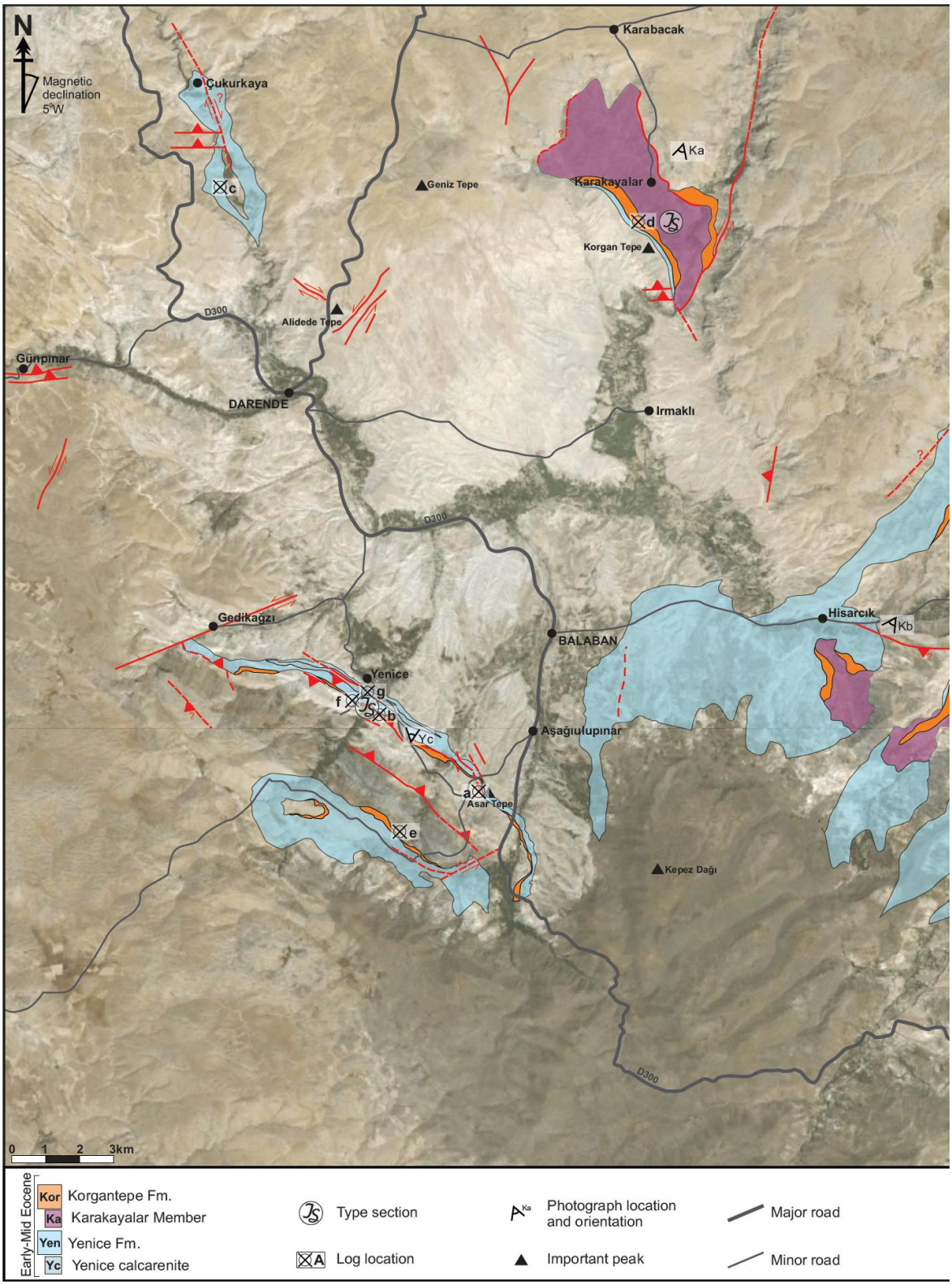

Figure 2.25. Simplified geological map showing the extent of the Korgantepe Formation, Karakayalar Member, Yenice Formation and Yenice Member draped over a satellite image of the Darende Basin. Also shown are logged section locations together with the location and approximate bearings of landscape photographs.

Lithology: The Korgantepe Formation is predominantly composed of poorly sorted, texturally immature, terrigenous sandstones and siltstones. The formation begins with a prominent basal breccia ~1 m thick (Fig 2.26a, base), only observed in the south of the basin, near Asartepe (locality a on Fig. 2.25) and in the north of the basin, east of Irmaklı (Fig. 2.25). This breccia is almost entirely composed of angular, pebble-to cobble-sized clasts of finely laminated (microbial?) limestone, set in a calcareous matrix of similar composition (Fig. 2.27a, base). Additionally, the northern outcrop contains ~10-20% ophiolite-derived lithologies such as basalt, gabbro and serpentinised ultramafics, together with red radiolarite and chert. Dark–brown to green, texturally immature, poorly sorted pebbly sandstones overlie the conglomerates (Fig 2.27b). The sandstones are medium grained to granular in the lower part of the succession but fine upwards, overall. These sediments are rich in ophiolite-related grains, including variable amounts of altered basalt, gabbro, chert, serpentinite and ultramafic rocks. The sandstones are interbedded with less well-cemented, commonly fissile, dark grey, sandy siltstones. Up-section, the sandstones thin, become finer grained and relatively less abundant. The sequence then becomes more silty and marl-rich, eventually passing into fissile hemipelagic marls of the Yenice Formation.

The Korgantepe Formation, particularly the sandstones, is faunally diverse, with bivalves (e.g. small pectins), echinoid debris (especially spines), gastropods and abundant foraminifera (Fig. 2.28) including *Nummulites* sp. (Fig. 2.27c & d). Trace fossils include *Thalassinoides* and *Skolithos*. Cross lamination and imbrication of large foraminifera were observed around Yenice in the southern part of the basin and indicate local palaeoflow towards the west (Fig. 2.26b). Erosive, scoured bases and rip-up clasts are also commonly developed. Neptunian fissures, up to 50 cm long and 3-4 cm wide, occur around Yenice, penetrating downwards from the base of the Korgantepe Formation into the underlying Maastrichtian Ulupınar Formation.

In the far south of the basin the Korgantepe Formation appears to be similar to the Yenice Formation type section. Coarse pebbly sands were deposited first and then fine upwards over ~50 m into medium sands (Fig. 2.29). An important north verging slump fold was observed in the upper part of the sequence (Fig. 2.29, ~51 m).

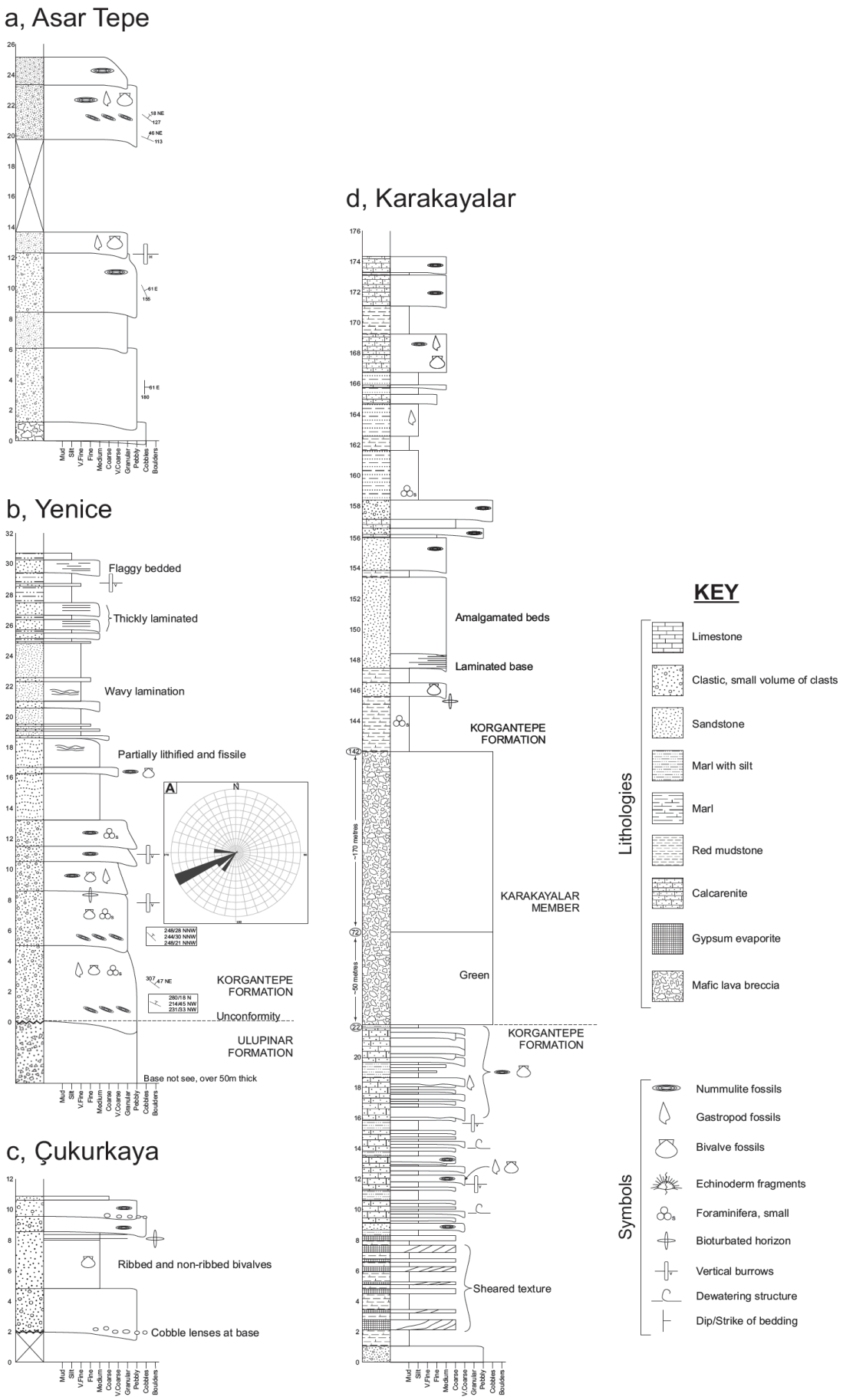
a, Asar Tepe
b, Yenice
Flaggy bedded
Thickly laminated
Wavy lamination
Partially lithified and fissile
KORGANTEPE FORMATION
Unconformity
ULUPINAR FORMATION
Base not see, over 50m thick
c, Çukurkaya
Ribbed and non-ribbed bivalves
Cobble lenses at base
d, Karakayalar
Amalgamated beds
Laminated base
KORGANTEPE FORMATION
~170 metres
KARAKAYALAR MEMBER
~50 metres
Green
KORGANTEPE FORMATION
Sheared texture
Mud
Silt
V.Fine
Fine
Medium
Coarse
V.Coarse
Granular
Pebbly
Cobbles
Boulders
KEY
Lithologies
Limestone
Clastic, small volume of clasts
Sandstone
Marl with silt
Marl
Red mudstone
Calcarenite
Gypsum evaporite
Mafic lava breccia
Symbols
Nummulite fossils
Gastropod fossils
Bivalve fossils
Echinoderm fragments
Foraminifera, small
Bioturbated horizon
Vertical burrows
Dewatering structure
Dip/Strike of bedding

Figure 2.26. Measured sequences of the Korgantepe Formation logged at: a, Asar Tepe, b, Yenice, c, Çukurkaya and d, Karakayalar (locations a, b, c & d respectively on Fig. 2.25). Note the relatively similar thicknesses of the Korgantepe Formation in the Yenice, Asar Tepe and Karakayalar locations compared to the much-reduced thickness (~10m) at Çukurkaya in the northeast of the basin. The rose diagram utilises palaeocurrent data from Yenice and indicates palaeoflow to the west-southwest. Also note the ~220 m-thick volcanic interval (Karakayalar Member).

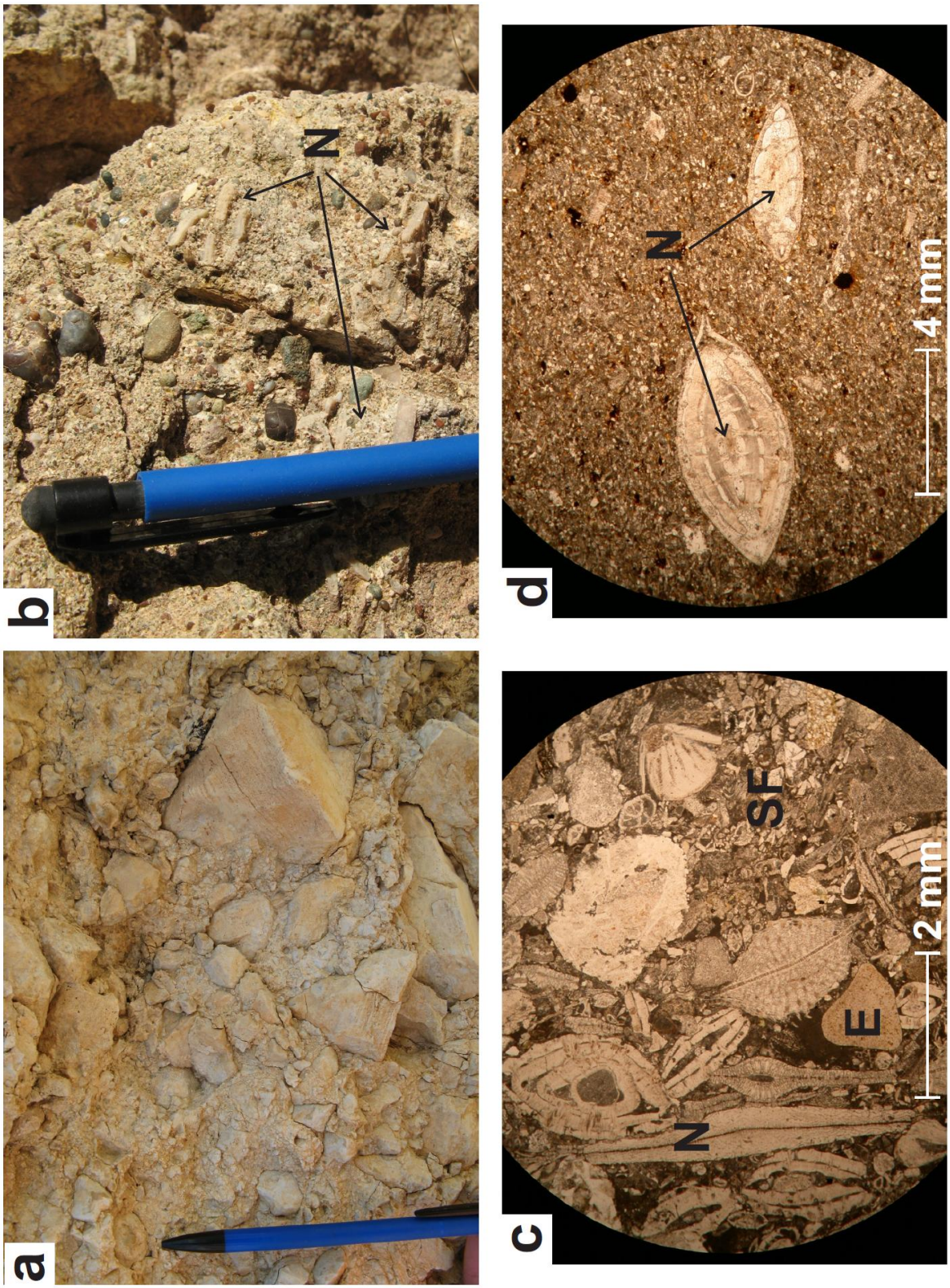

Figure 2.27. Field photograph and photomicrographs. a, basal breccia near Asar Tepe, at the base of the Korgantepe Formation; b, Pebbly, coarse sandstone of the Korgantepe Formation, rich in fossils including *Nummulites* sp.; c & d, Plane-polarised light (PPL) images showing the diverse fossil assemblage and large benthic Foraminifera, *Nummulites* sp. in the Korgantepe Formation.

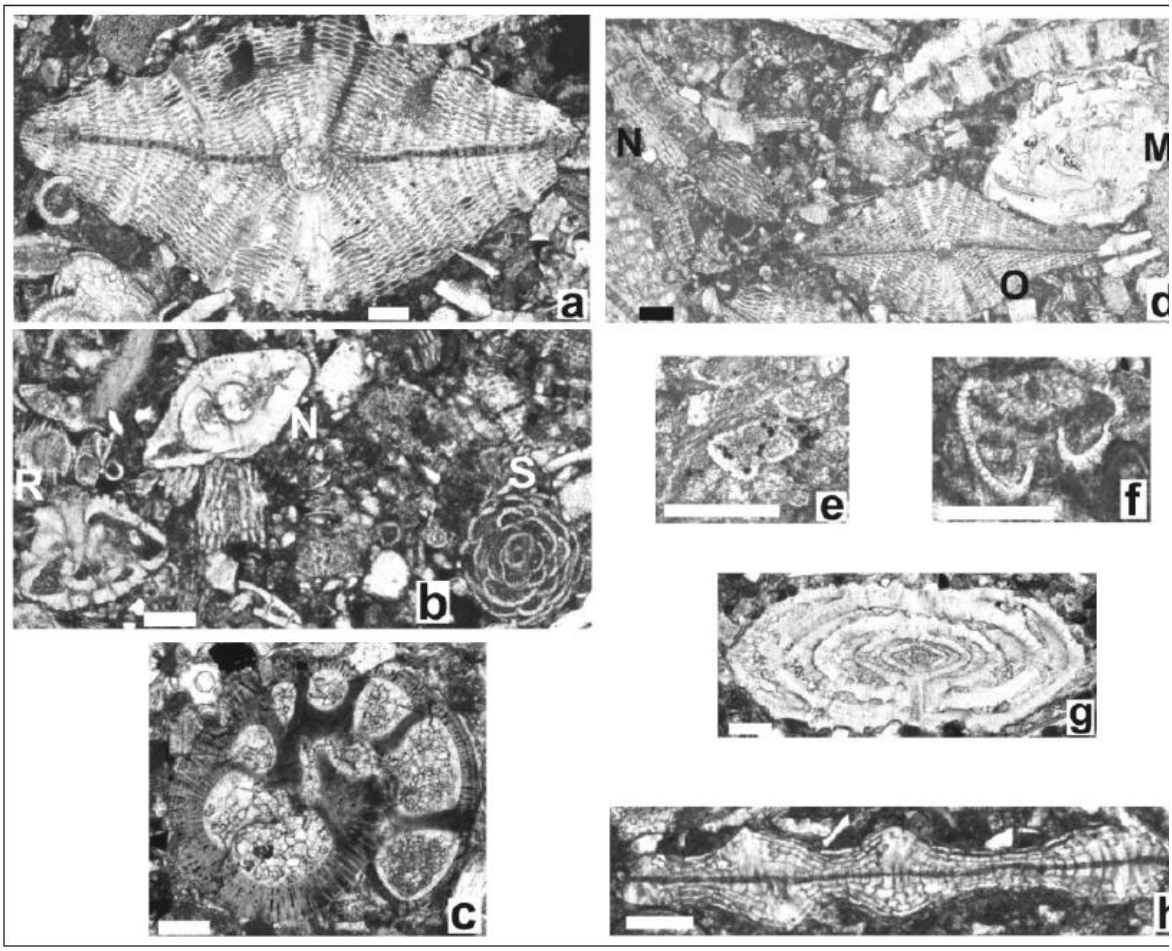

Figure 2.28. Thin-section microphotographs of selected benthic and planktonic foraminifera from the Korgantepe Formation; a. *Discocyclina* cf. *scalaris*, sample MB09-B96; b. *Neorotalia vienotti* (R), *Nummulites millecaput* (N), *Sphaerogypsina globula* (S), sample MB09-B59; c. *Gyroidinella magna*, sample MB09-B73; d. *Orbitoclypeus* cf. *ramaraoi ramaraoi* (O), *Nummulites millecaput* (M), *Nemkovella* sp. (N), sample MB10-2; e. *Igorina broedermanni*, sample MB09-B121; f. *Acarinina bulbrooki*, MB09-B59; g. *Nummulites* cf. *hormoensis*, sample MB09-B77; h. *Asterocyclina* sp., sample MB09-B59. Scale bars 100 µm.

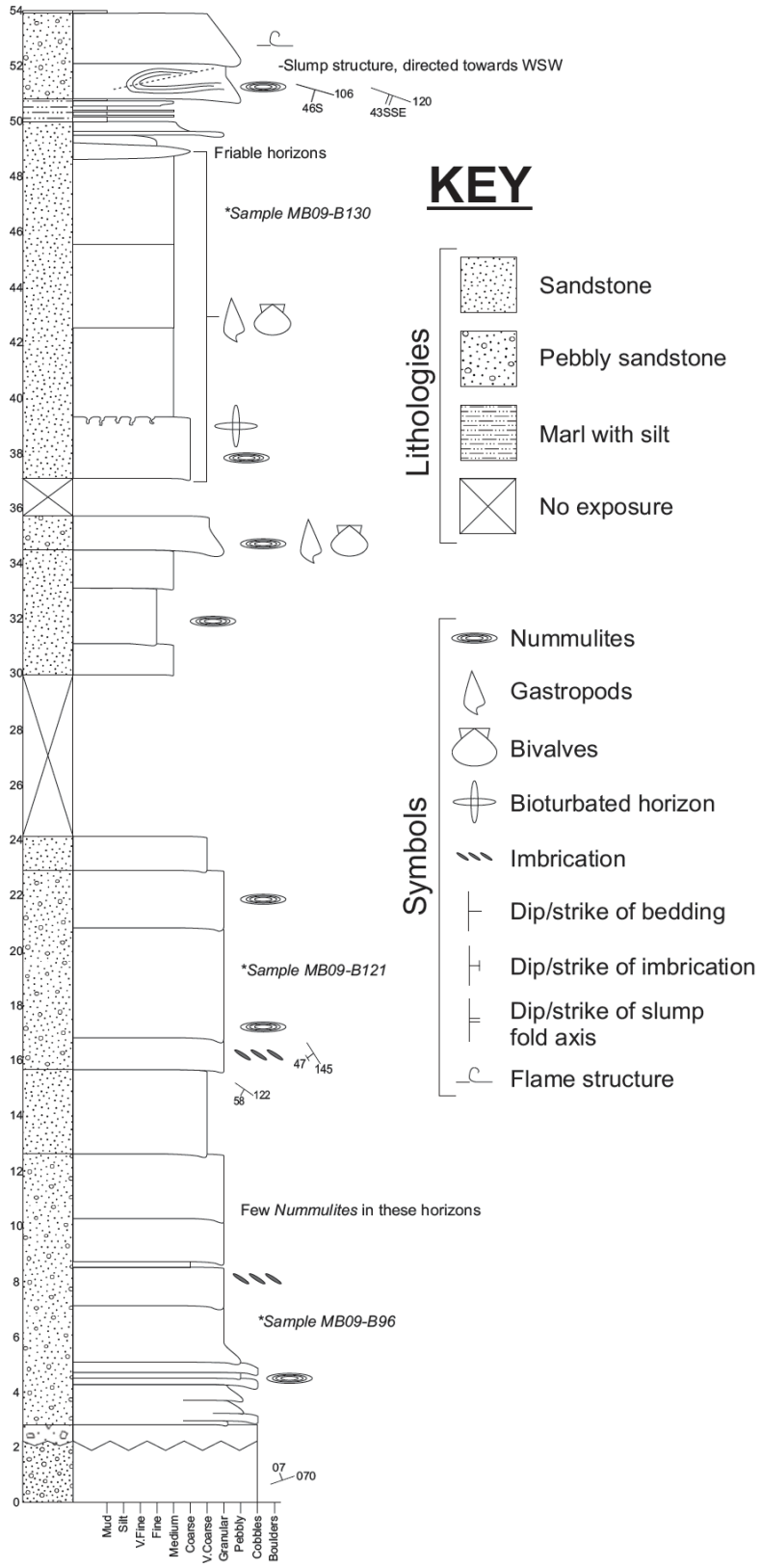

Figure 2.29. Logged succession of the Korgantepe Formation. The formation unconformably overlies the Ulupınar Formation. The formation is predominantly composed of alternating sandstones and is faunally diverse. Note the slump fold at ~51 m (location e on Fig 2.25).

The Korgantepe Formation is thinner (<11 m) in the northwest of the basin, north of Darende (Çukurkaya area), where it is exposed within a N-S- trending valley. The sandstones there are texturally mature, ranging from fine, to medium, to coarse-grained, with minor pebbly horizons (Fig. 2.26c). There is relatively less siltstone in the northwest of the basin where the sandstones pass over ~5 m into marls of the Yenice Formation.

In the west of the basin, the Korgantepe Formation reaches ~20 m and comprises coarse to pebbly *Nummulites* sp. rich sandstones at the base followed by finer sandstone and sandstone-siltstone interbeds which become dominated by marls before passing into the Yenice Formation (Fig. 2.30).

In the northeast of the basin (Karakayalar area, Fig. 2.26d and locality d on Fig. 2.25) the Korgantepe Formation is thicker (up to 64 m) beginning with thinly bedded siltstone-calcarenite alternations. The calcarenites contain abundant *Nummulites* sp., gastropods and bivalves. Sedimentary structures include vertical burrows and dewatering structures such as flame casts and dish and pillar structures. The Korgantepe Formation in this area includes ~220 m of volcanic rocks, defined as the Karakayalar Member (see below).

The higher levels of the Korgantepe Formation in the Karakayalar area begin with a laterally discontinuous conglomerate layer (1-2 m thick). This contains well-rounded, cobble-sized clasts composed of basalt, set in a matrix that was derived from underlying volcanogenic rocks. The matrix of the conglomerate contains abundant *Nummulites* sp. Massive, amalgamated, faunally diverse and bioturbated calcarenites alternate with thick fissile siltstones in the uppermost part of the Formation in the area.

Boundaries: The lower boundary of the Korgantepe Formation is an angular unconformity above the Cretaceous facies. In northern areas of the basin the discordance ranges from ~5-10^{o}. In southern areas (e.g. Yenice) an angular discordance is locally apparent, which ranges up to ~ 45^{o}. The upper boundary is gradational with the Yenice Formation (below) in all areas.

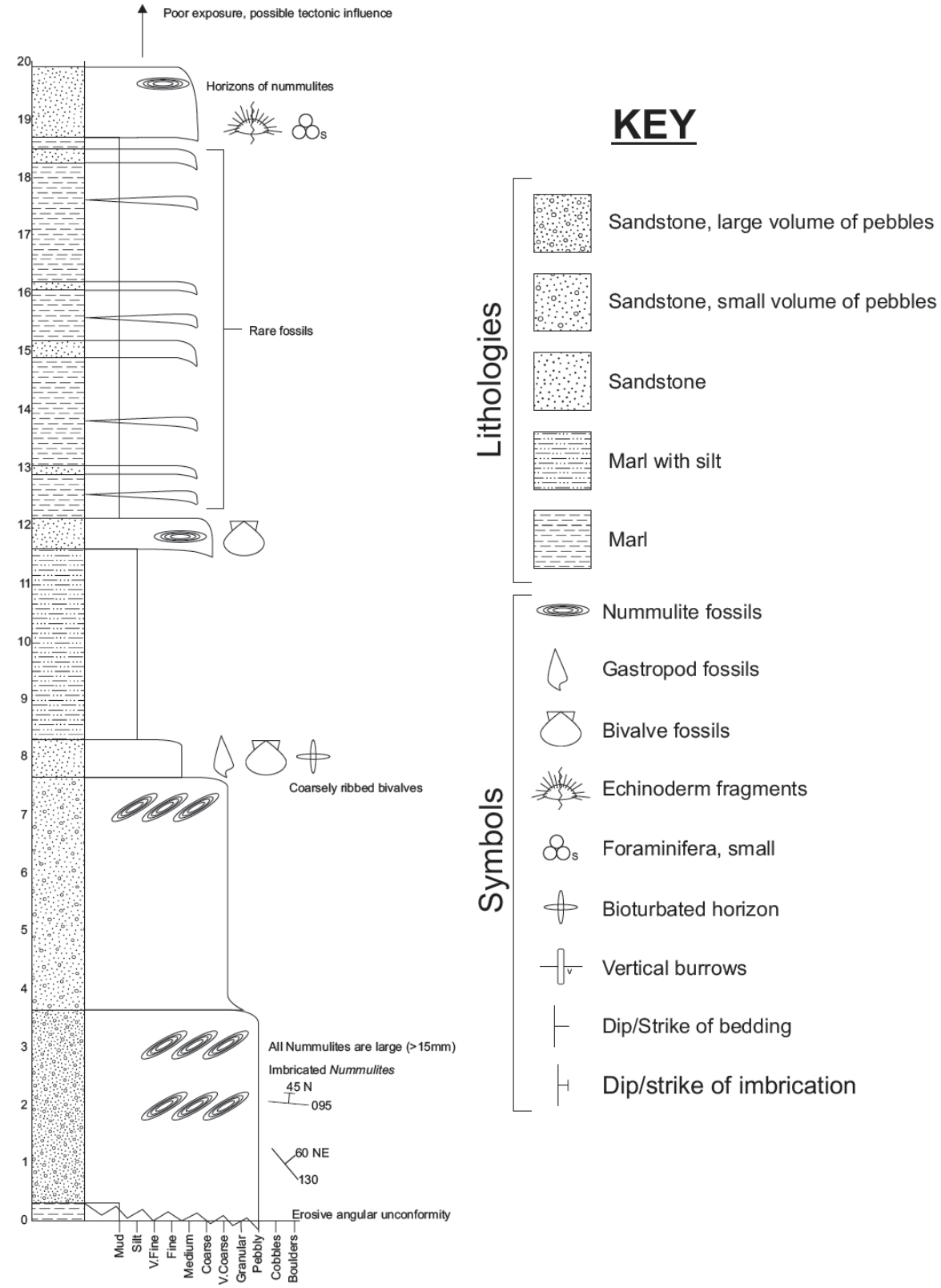

Figure 2.30. Logged section of the Korgantepe Formation (location f on Fig. 2.25). The formation unconformably overlies the Ulupınar Formation. Here the formation is composed of a sandstone-rich lower part, overlain by sandstone-siltstone and sandstone-marl alternations.

Thickness and extent: The Korgantepe Formation is well exposed around the southern periphery of the Darende Basin. The thickness of the formation ranges from ~20 m in the south to ~64 m in the northern part of the basin. The formation is laterally discontinuous and poorly represented in the basin.

Age: The Korgantepe Formation is dated as Ilerdian-Lutetian (Early-Middle Eocene) based on foraminiferal analysis (Table 2.3, Fig. 2.28).

Korgantepe Formation (Ilerdian to early Priabonian)			
Samples	**Benthic Foraminifera (BF)**	**Planktic Foraminifera (PF)**	**Age**
MB09-B 121	***Nummulites* cf. *formosus***, *Idalina sinjarica*, Miliolidae		Ilerdian
MB08-82, MB09-B59, MB09-B61, MB09-B96, MB10-2	***Assilina* cf. *exponens***, *Assilina* sp., *Asterigerina rotula*, *Asterocyclina stella taramellii*, *Asterocyclina* sp., *Chapmanina* sp., *Discocyclina archiaci bartholomei*, *Discocyclina* cf. *scalaris*, *Eorupertia* sp., ***Fabiania cassis***, *Gypsina marianensis*, *Gyroidinella magna*, *Idalina sinjarica*, *Medocia blayensis*, *Neorotalia vienotti*, ***Nummulites* cf. *uranensis***, *Nummulites incrassatus*, ***Nummulites millecaput***, *Nummulites* sp., *Operculina* sp., *Lenticulina* sp., *Linderina* sp., *Orbitoclypeus* cf. *ramaraoi ramaraoi*, ***Orbitoclypeus varians roberti***, *Sphaerogypsina anatolica*, *Sphaerogypsina globula*.	***Acarinina bullbrooki***, *Acarinina* cf. *primitiva*, *Chiloguembelina* sp., *Globigerinatheka* sp., *Subbotina* sp.	Lutetian

Table 2.3. Micropalaeontology results from the Korgantepe Formation. Fossils marked in bold are diagnostic.

2.4.5.2 Interpretation of the Early-Middle Eocene shallow-marine clastics (Korgantepe Formation)

Eustatic sea level rose throughout the Ypresian (Early Eocene) (Miller *et al.* 2005). However, the oldest Eocene sediments dated during this study (Korgantepe Formation) are of Ilerdian (Early-Middle Eocene) age (Table 2.3), a time when eustatic sea level was apparently lower than during the preceding Ypresian Stage (Fig. 2.5). The benthic fossil assemblages and reworked nature of the sandstones in the Korgantepe Formation indicate a high-energy shoreface, to shallow-marine setting. Erosion of topographic highs to the south of the Darende Basin is likely to have supplied ophiolite-related clastic material, as indicated by the local NW-directed palaeocurrents. However, the composition of the conglomerates was probably determined by the lithology of the surrounding topographic highs. The angularity of the clasts in the localised basal breccias suggests rapid erosion of

an irregular topography that was created during the Paleocene phase of subaerial exposure. This was probably caused by penecontemporaneous faulting (although no direct evidence was observed).

2.4.5.3 Middle Eocene Volcanism (Karakayalar Member)

Name: The name is derived from a hamlet built on the lavas in the northeast part of the Darende Basin (Fig. 2.25).

Type locality: The type section of the Karakayalar Member, Previously only described by Akkuş (1971), lies within the largest and best-exposed outcrop of the volcanogenic rocks in the northeast of the basin around Karakayalar. Good exposures occur at the base of a NW-SE striking ridge (Korgan Tepe; Fig 2.31).

Lithology: The Karakayalar Member is typically composed of highly weathered volcanic rocks that are green to grey in the lower part and dark grey in the upper part. The lithology is mainly clinopyroxene-phyric and plagioclase-phyric (Fig. 2.32a) lava breccia, together with matrix-supported volcanogenic debris flows. Rare, metre-scale blocks of fragmented pillow lava occur within the lava breccias over a vertical interval of ~30 m from the base of the unit (Fig. 2.32b). Up-section, the block size decreases to large cobbles composed of basalt, set within well-bedded, lenticular, predominantly matrix-supported volcaniclastic sediments (Fig 2.32c).

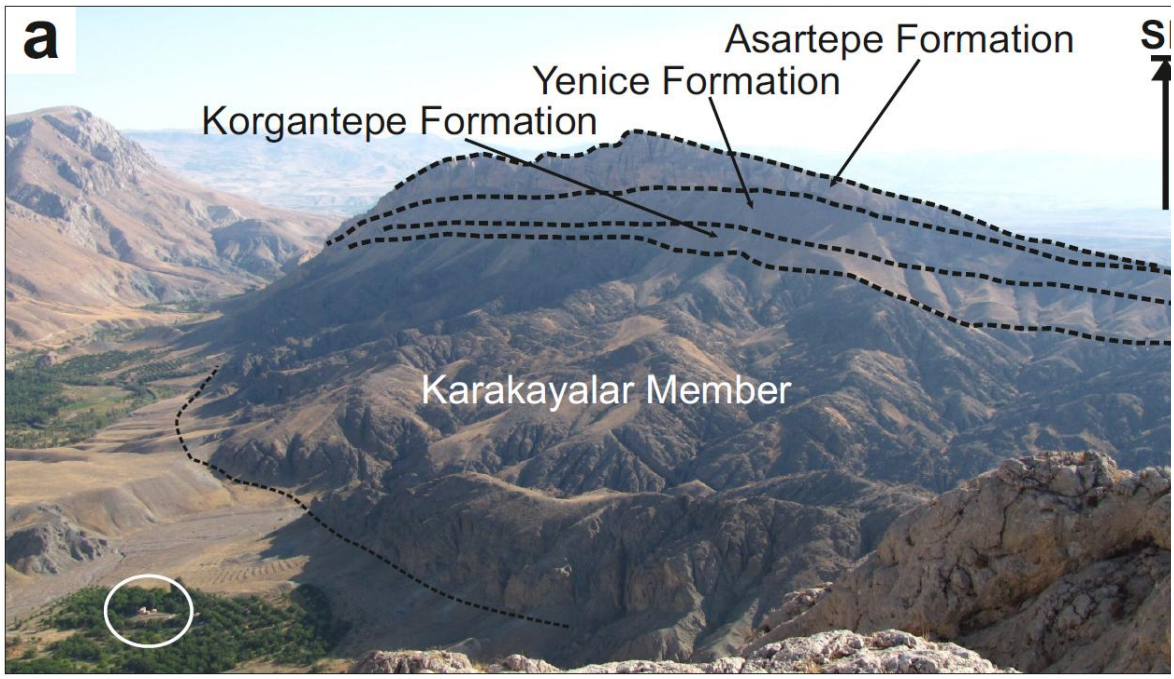

Figure 2.31. Field photograph (taken from location Ka on Fig. 2.25) showing Middle Eocene volcanic rocks (Karakayalar Member) and overlying sedimentary lithologies in the type area. House and trees for scale in lower left (circled).

Boundaries: The lower boundary of the Karakayalar Member is tectonic. The upper boundary is conformable with the Korgantepe Formation (above). The volcanic rocks appear to have erupted during the deposition of the Korgantepe Formation. A basal conglomerate layer with *Nummulites* sp. in the matrix and clasts entirely composed of basalt is commonly found stratigraphically above the lavas (see 2.4.5.1 for description). The conglomerate rapidly grades into shallow-marine *Nummulitic* sandstone with siltstone, marl and limestone interbeds.

Thickness and extent: The Karakayalar Member has a maximum thickness of 300m and a minimum thickness of 150m towards the margins of the unit. The unit occurs in localised areas of the Darende Basin, Karakayalar being by far the biggest and best exposed. The extent of the unit in the Karakayalar region can easily be distinguished from satellite images due to the marked contrast between the dark green-grey of the lavas and the pale brown-cream colour of the surrounding sedimentary lithologies (Fig. 2.33). Similar volcanogenic rocks occur elsewhere (e.g. south of Hisarcık; location Kb on Fig. 2.25; see Fig. 2.32d), where they are thinner (<100m) and located between the top of the Korgantepe Formation and the base of the overlying Yenice Formation. Submarine pillow lavas, lava flows and volcaniclastic debris flows predominate there.

Age: The volcanogenic Karakayalar Member is dated as Ilerdian-Lutetian (Early-Middle Eocene) owing to its stratigraphic position in the lower part of the well dated Korgantepe Formation.

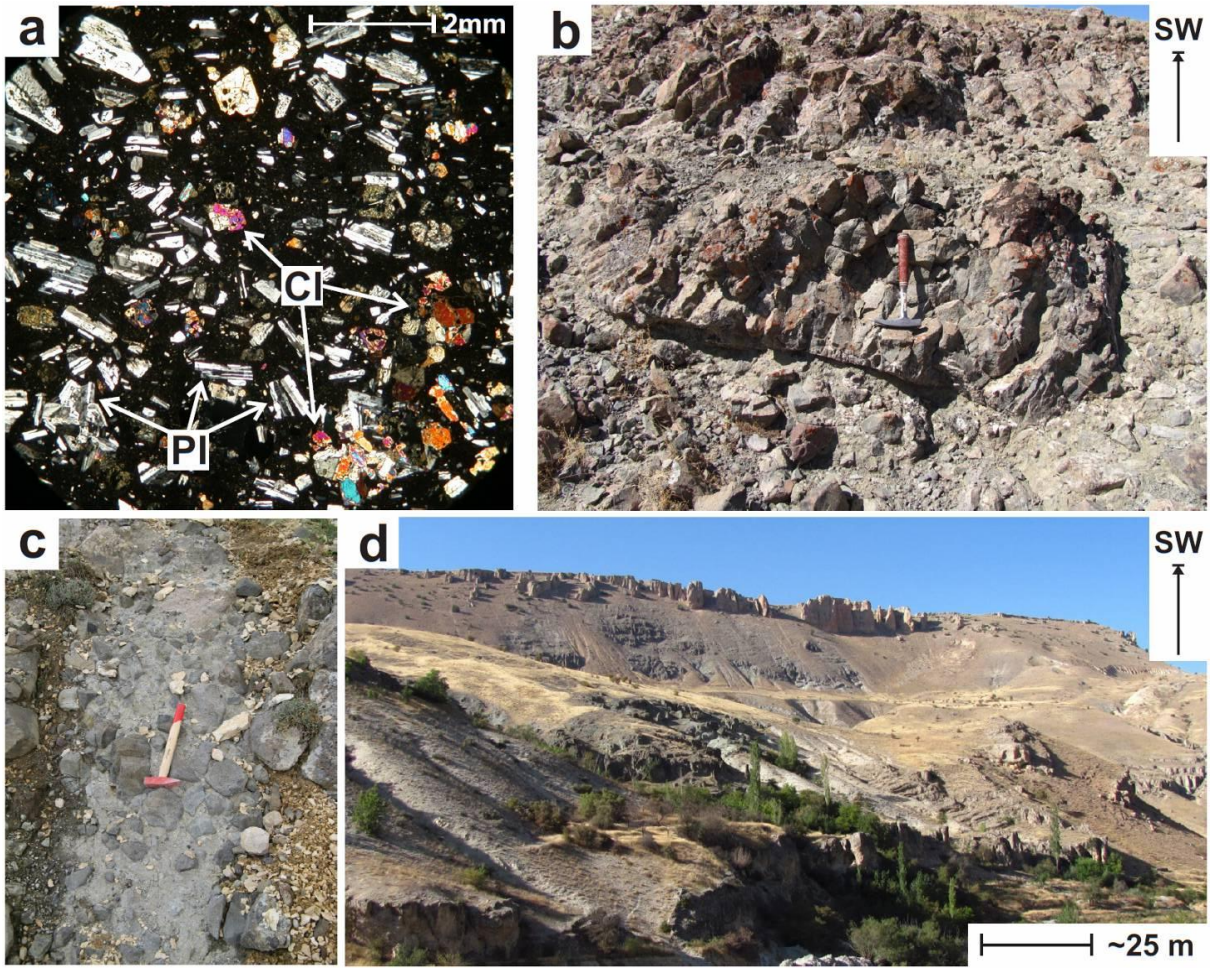

Figure 2.32. Photomicrograph and field photographs. a, Photomicrograph (crossed polars) of a typical Karakayalar Member lava breccia clast showing plagioclase and clinopyroxene phenocrysts set in a fine-grained matrix; b, Photograph showing the outline of a pillow of basalt near the base of the sequence; c, Typical outcrop of sub-rounded lava debris flow deposit; d, Photograph of lavas outcropping near Hisarcık (taken from location Kb on Fig 2.25). Light grey in middle ground is marl of the Yenice Formation (see below); dark grey above is Karakayalar Member basalt which is overlain by brown, horizontally bedded limestones of the Asartepe Formation on the skyline.

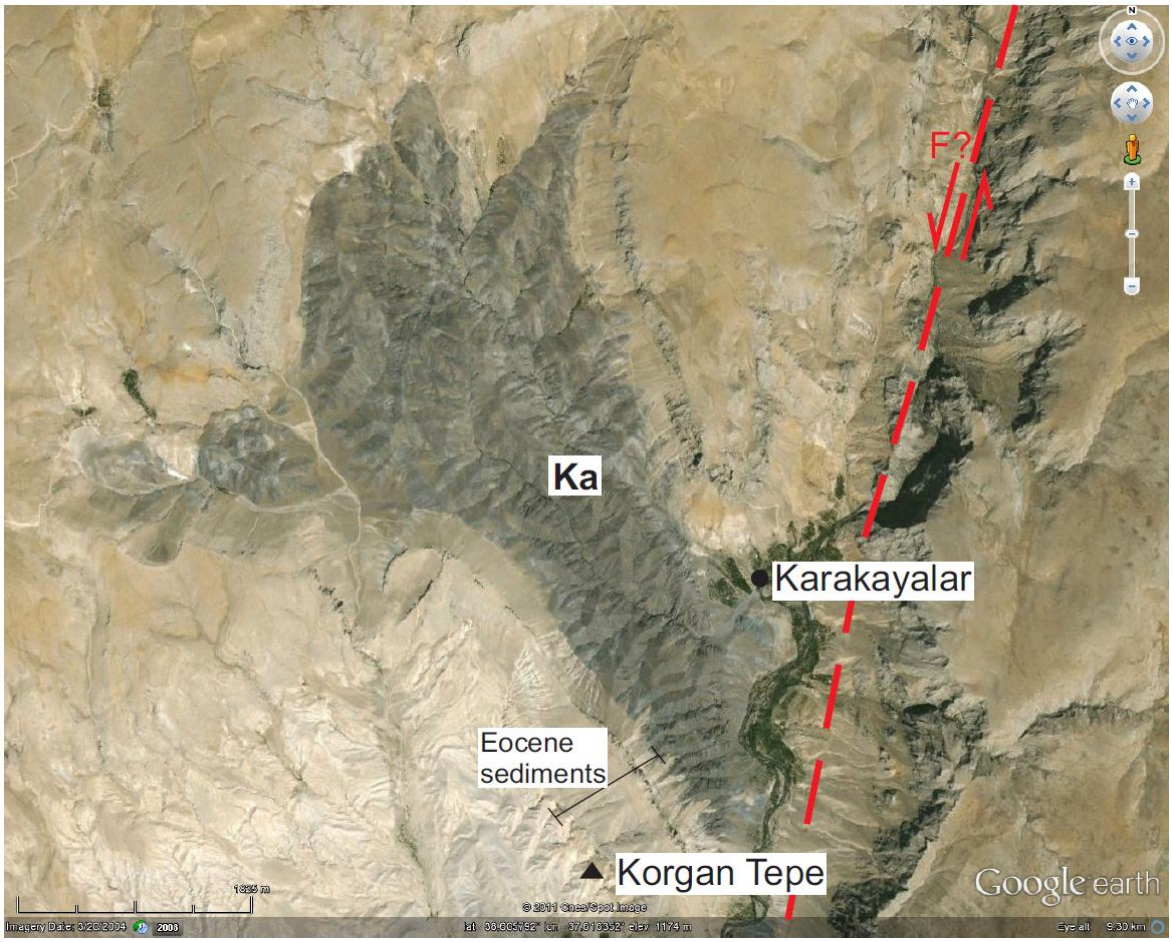

Figure 2.33. Google Earth satellite image of the Karakayalar Member. The extent of the lava is clearly defined due to the colour contrast between the dark grey of the lava and the white-to-buff colour of the surrounding sediment. A high angle NNE-SSW striking sinistral strike-slip fault (red dashed line) occurs on the eastern flank of the lava which also juxtaposes Eocene sediments with Mesozoic limestones of the Geniz Formation.

2.4.5.4 Geochemistry

To help determine the volcanic affinities and possible tectonic setting of eruption, relatively unaltered basic volcanic rocks from different parts of the sequence at the Karakayalar Member type section were chemically analysed for major and trace elements by X-ray fluorescence (XRF), using the method specified by Fitton *et al.* (1998). The complete results are given in Table 2.4. The rocks are classified as andesite by plotting on a Total Alkalis versus Silica (TAS) rock classification diagram (Fig. 2.34). Data from the Karakayalar region, as well as from the Hisarcık area to the east of the basin, have been plotted together and show good correlation which indicates that the two outcrops could share a geochemically similar parent magma. A 'spider' plot of major- and trace-element data, normalised to mid-ocean ridge basalt (MORB) (Fig. 2.35), shows a marked relative

enrichment of Large Ion Lithophile Elements (LILE) compared to High Field Strength Elements (HFSE). LILE enrichment is indicative of partial melting of a mantle source either in a rift-related or an ocean island setting (Pearce l982, l983, l996; Pearce *et al.* 1984). Given the continental association, a rift-related setting is inferred in this case. In addition, the relative depletion of Nb suggests the involvement of a subduction zone component (Pearce 1996; Baier *et al.* 2008). This subduction zone signature could in principle have been contemporaneous (Eocene) or inherited from some earlier subduction in the region (e.g. Late Cretaceous). A similar relative Nb depletion has been noted in the Middle Paleocene-Middle Eocene within-plate-type basalts of the Ulukişla Basin to the west of the study area (Clark & Robertson 2002).

Sample	MB08-111	MB09-D13	MB09-D16	MB10-8a	MB10-8b	MB10-9	MB10-26a	MB10-26b
latitude	38.61022	38.59807	38.59384	38.60533	38.60533	38.60533	38.44945	38.44945
longitude	37.59862	37.62409	37.62419	37.63103	37.63103	37.63103	37.71190	37.71190
Majors								
SiO_2	59.72	58.26	61.51	58.95	59.00	58.22	57.64	57.81
Al_2O_3	17.18	18.37	18.81	17.03	17.06	16.91	17.73	17.75
Fe_2O_3	6.14	6.19	4.84	5.47	5.32	5.41	6.10	5.86
MgO	3.96	3.50	1.83	3.37	3.30	3.97	4.14	3.90
CaO	5.91	7.63	6.61	6.87	6.79	7.19	7.51	7.73
Na_2O	3.36	3.87	3.68	3.24	3.26	3.73	3.43	3.34
K_2O	2.48	0.98	1.77	1.34	1.34	1.35	1.23	1.28
TiO_2	0.83	0.91	0.73	0.66	0.64	0.67	0.80	0.76
MnO	0.11	0.10	0.04	0.07	0.07	0.09	0.11	0.10
P_2O_5	0.31	0.18	0.18	0.13	0.13	0.13	0.16	0.15
LOI	1.30	1.71	3.02	2.46	2.41	1.73	0.98	1.29
Total	99.55	99.55	99.53	99.60	99.34	99.40	99.82	99.97
Total - LOI	98.25	97.84	96.51	97.14	96.93	97.67	98.84	98.68
Minors								
Zn	71.20	54.00	43.40	59.00	64.80	47.50	47.30	48.40
Cu	21.30	31.30	12.40	38.50	34.30	16.60	14.90	21.90
Ni	32.90	13.30	6.60	32.20	35.10	36.80	36.40	33.50
Cr	57.00	20.30	4.90	127.90	135.10	138.40	133.70	128.60
V	122.40	202.50	177.00	170.20	175.50	202.20	200.30	171.30
Ba	472.20	376.40	427.00	392.80	390.80	392.90	391.60	388.00
Sc	16.70	25.80	17.10	25.20	25.20	21.70	21.50	23.70
La	39.60	18.50	24.70	19.40	22.60	22.00	21.70	20.60
Ce	67.90	40.20	51.00	41.20	44.80	40.90	41.00	41.80
Nd	29.10	21.10	23.60	18.90	19.40	17.50	18.30	17.90
U_2	3.70	2.10	1.80	1.50	1.30	1.50	1.80	1.70
Th	12.10	7.80	8.80	6.40	6.50	7.40	7.50	7.10
Pb	14.00	5.90	5.90	5.60	5.90	6.40	6.30	6.60
Nb	23.40	11.70	12.00	10.20	10.50	10.40	10.40	10.40
Zr	216.00	158.50	163.30	137.30	139.00	141.70	142.60	140.20
Y	26.20	26.50	24.70	23.30	23.90	22.90	22.50	22.90
Sr	338.80	336.20	306.30	315.90	302.30	279.30	278.10	268.00
Rb	79.40	36.60	60.80	47.30	48.40	52.40	52.60	51.80

Table 2.4. Raw data (majors recalculated for LOI) for the Karakayalar samples.

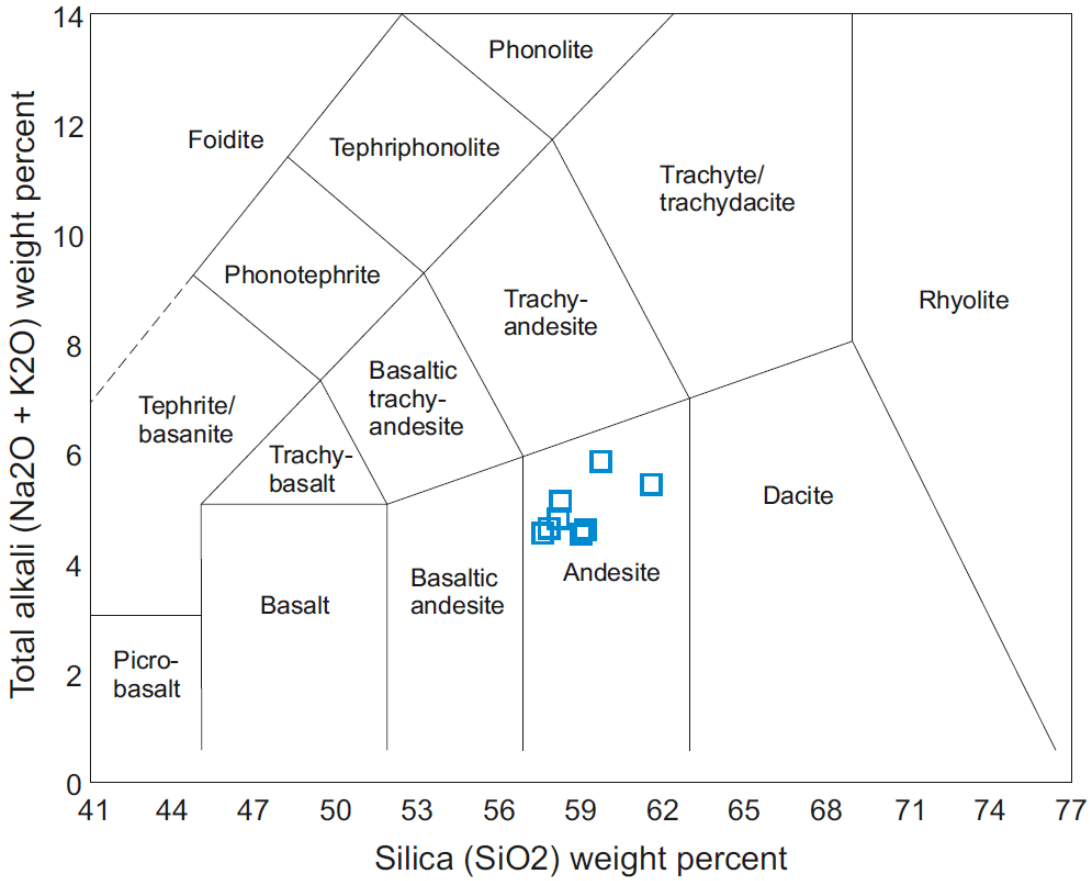

Figure 2.34. Total alkali vs. Silica plot for the volcanic rocks of the Karakayalar Member. All samples plot within the andesite field. See Table 2.4 for the complete analyses and the text for explanation.

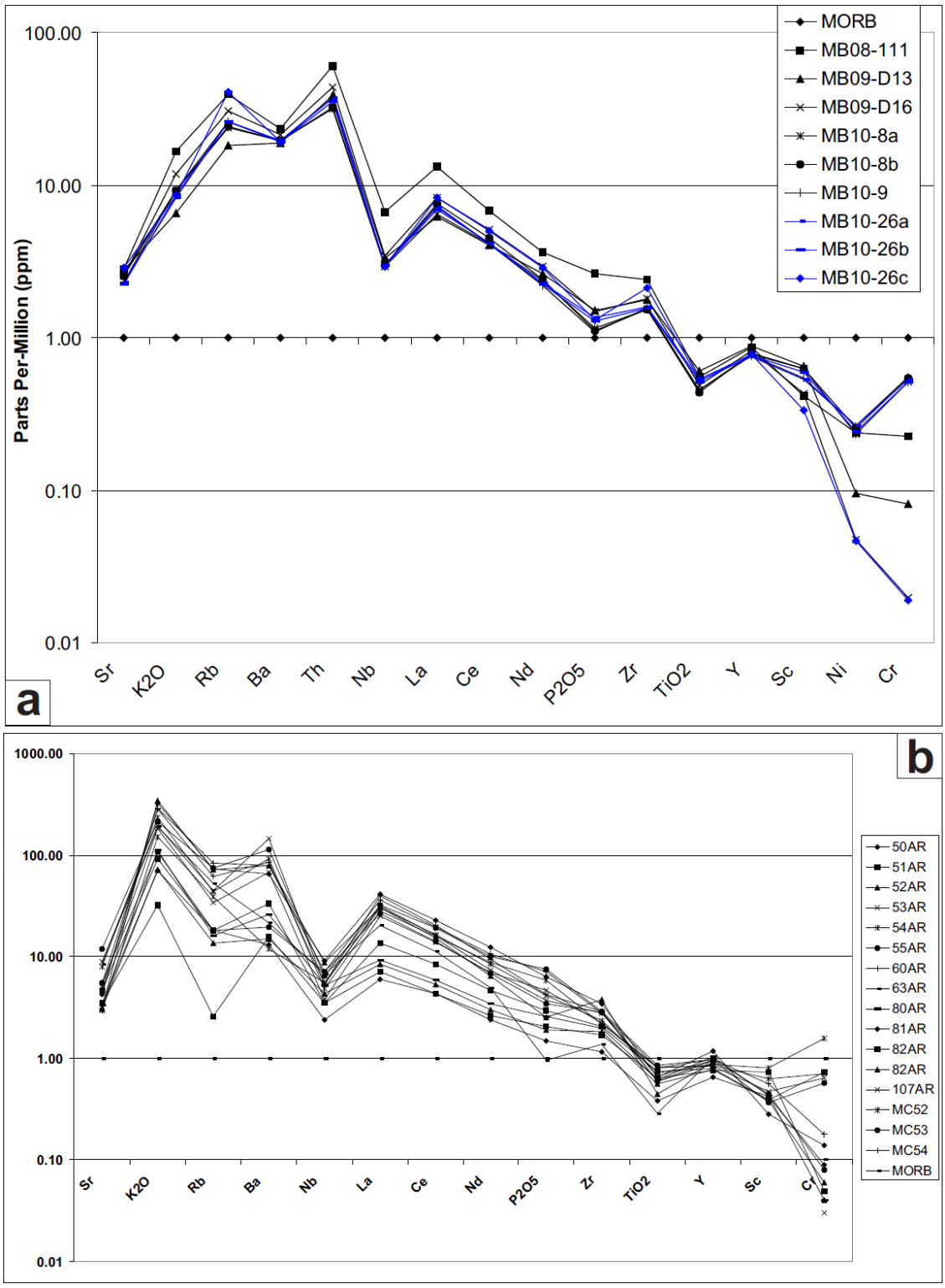

Figure 2.35. a, MORB-normalised spider diagram for volcanic rocks of the Karakayalar Member (from Pearce l982 and Saunders & Tarney 1984). These are generally 'enriched' in Large Ion Lithophile elements compared to MORB. A relative Nb negative anomaly is also present. Blue lines represent analyses from the eastern part of the basin, near Hisarcık. See Table 2.4 for the complete analyses and the text for explanation; b, MORB-normalised spider diagram for the Eocene volcanic rocks of the Ulukışla Basin from Clark & Robertson (2002). Note the geochemical similarity of the two volcanic suites.

2.4.5.5 Interpretation of the Middle Eocene Volcanism (Karakayalar Member)

The Mid-Eocene volcanism (Karakayalar Member) began in a submarine setting, as suggested by the shallow-marine benthic fauna beneath (although the lower contact is tectonic). Occasional pillow lavas indicate subaqueous eruption (Fig 2.32b). The volcanic pile became emergent as evidenced by the vesicular nature of the lava and the presence of rounded, spalled clasts. The majority of the outcrop is defined by volcaniclastic debris flows in a slope setting. Overlying conglomerates with well-rounded basalt clasts and numerous large foraminifera may indicate a marine transgression sourcing material previously rounded in a fluvial system.

2.4.5.6 Middle Eocene marine carbonates (Yenice Formation)

Name: Derived from the village Yenice on the SW margin of the Darende Basin.

Type locality: Numerous sections can be observed in the valley to the SE of Yenice.

Lithology: The Yenice Formation is mainly composed of light grey marls, alternating between laminated fissile marls and bedded non-fissile marls (beds <10 cm-50 cm thick). Abundant planktic foraminifera and fine grained cubic to hexagonal pyrite grains occur throughout. Slump folds and rafted blocks occur in the lower part of the formation in the south of the basin. Thin interbeds (<5 cm) of fine to medium grained, light brown calcarenite are widespread in the Yenice and Çukurkaya areas (Figs. 2.36 a & b). The calcarenite beds are texturally immature, composed of reworked carbonate and ophiolite-related grains. The beds are typically normally graded and erosive-based, with grooves indicating palaeoflow to the northwest.

A thicker sequence (up to 80 m) of well bedded, light brown erosive based calcarenite is exposed in the upper part of the formation around the Yenice type section area (Fig. 2.36b & Fig. 2.37 ~20–94 m). The calcarenites are again texturally immature and composed of reworked carbonate and ophiolite-related grains. Calcarenite beds are frequently normally graded, with parallel lamination and other sedimentary structures,

including marl rip-up clasts, graded bed tops, flute casts and grooves (e.g. Fig. 2.36b ~90–120 m, Fig. 2.37 ~20–94 m and Fig. 2.38 ~12.5–19.5 m). These sedimentary structures together are indicative of the B-E divisions of turbidity current deposits (Bouma 1962). The calcarenites at Yenice, specifically, contain abundant benthic foraminifera (Fig. 2.39), together with echinoid, coralline algae and bryozoan fragments and also sparse planktic foraminifera, bioturbated horizons and well-preserved trace fossils including *Thalassinoides.*

Boundaries: The lower boundary is conformable on the Korgantepe Formation. In the Yenice type section area, lithic sandstones and siltstones of the Korgantepe Formation grade into marls of the Yenice Formation over a vertical distance of approximately 5-10 m. In the north of the basin, for example the Karakayalar area, the boundary is again gradational with the underlying Korgantepe Formation.

Thickness and extent: In the type section (at Yenice) the Yenice Formation is up to 350 m thick. The calcarenite package in the upper part of the Yenice Formation in the type section is 30-80 m thick, as shown in Figure 2.36b. The calcarenite package transgresses marls with an erosional contact (Fig. 2.40) and then pinches out laterally to the northwest and southeast of Yenice (over <10 km, e.g. Fig. 2.38 ~12.5–19.5 m). As a result, the calcarenite unit is absent 4.2 km to the southeast, at Asartepe (Fig. 2.36c). Furthermore, the marls of the Yenice Formation are less than 100 m thick at the Asartepe type section. In the north of the basin the Yenice Formation is approximately 75 m thick at Çukurkaya (Fig. 2.36a) but ~45 m thick near Karakayalar (Fig. 2.36d) and also in the eastern parts of the basin.

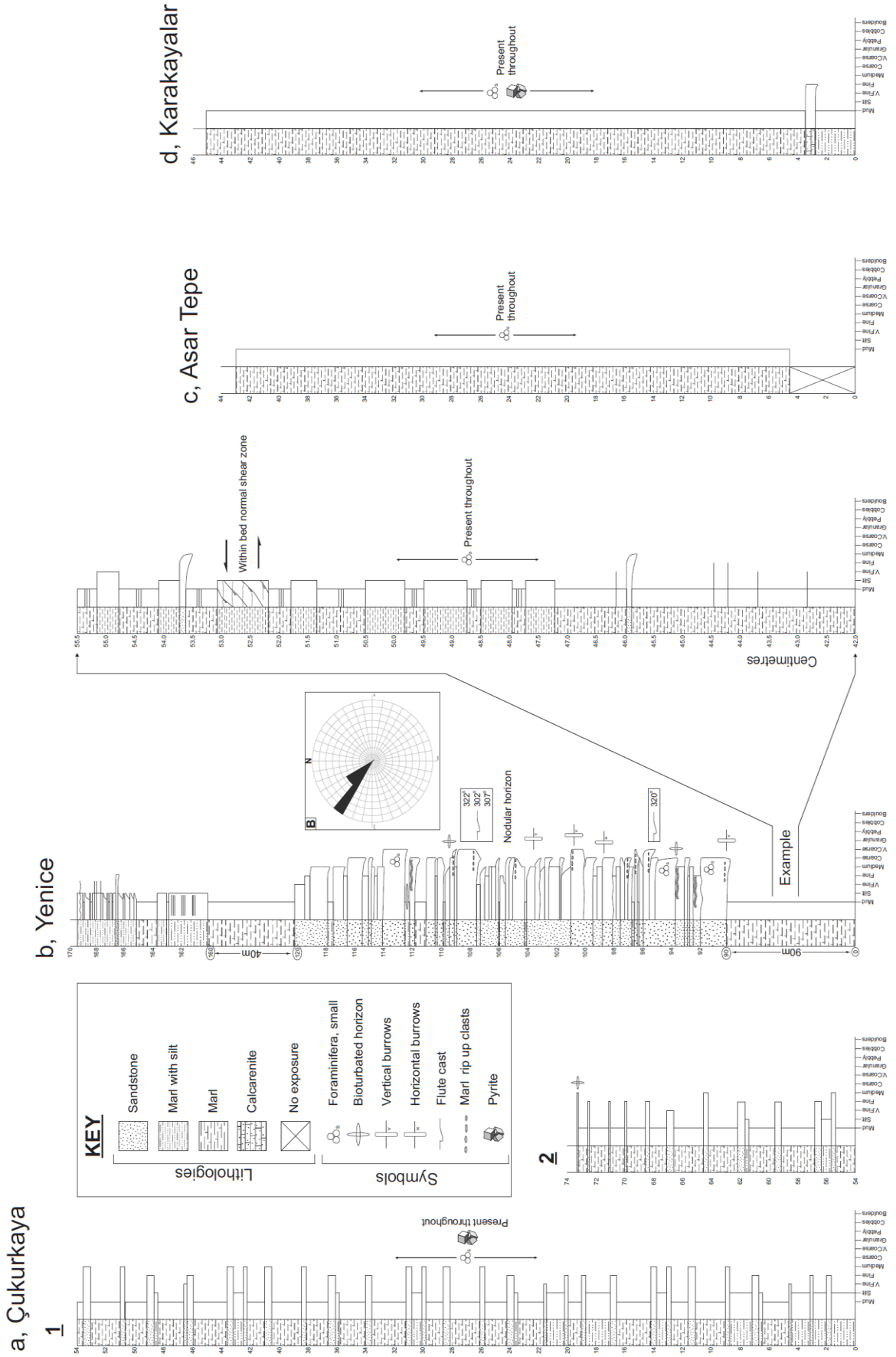
a, Çukurkaya
1
2
b, Yenice
c, Asar Tepe
d, Karakayalar
KEY
Lithologies
Sandstone
Marl with silt
Marl
Calcarenite
No exposure
Symbols
Foraminifera, small
Bioturbated horizon
Vertical burrows
Horizontal burrows
Flute cast
Marl rip up clasts
Pyrite
Present throughout
Within bed normal shear zone
Nodular horizon
322°
302°
307°
320°
Example
40m
90m
Centimetres
Mud
Silt
V.Fine
Fine
Medium
Coarse
V.Coarse
Granular
Pebbly
Cobbles
Boulders

Figure 2.36. Measured successions of the Yenice Formation as logged at: Çukurkaya, Yenice, Asar Tepe & Karakayalar (locations c, b, a & d, respectively on Fig. 2.25). Note the calcarenite turbidites (~30 m thick) within marls in the Yenice type section (not seen elsewhere). The rose diagram shows palaeocurrent data from the calcarenites that indicate flow to the northwest.

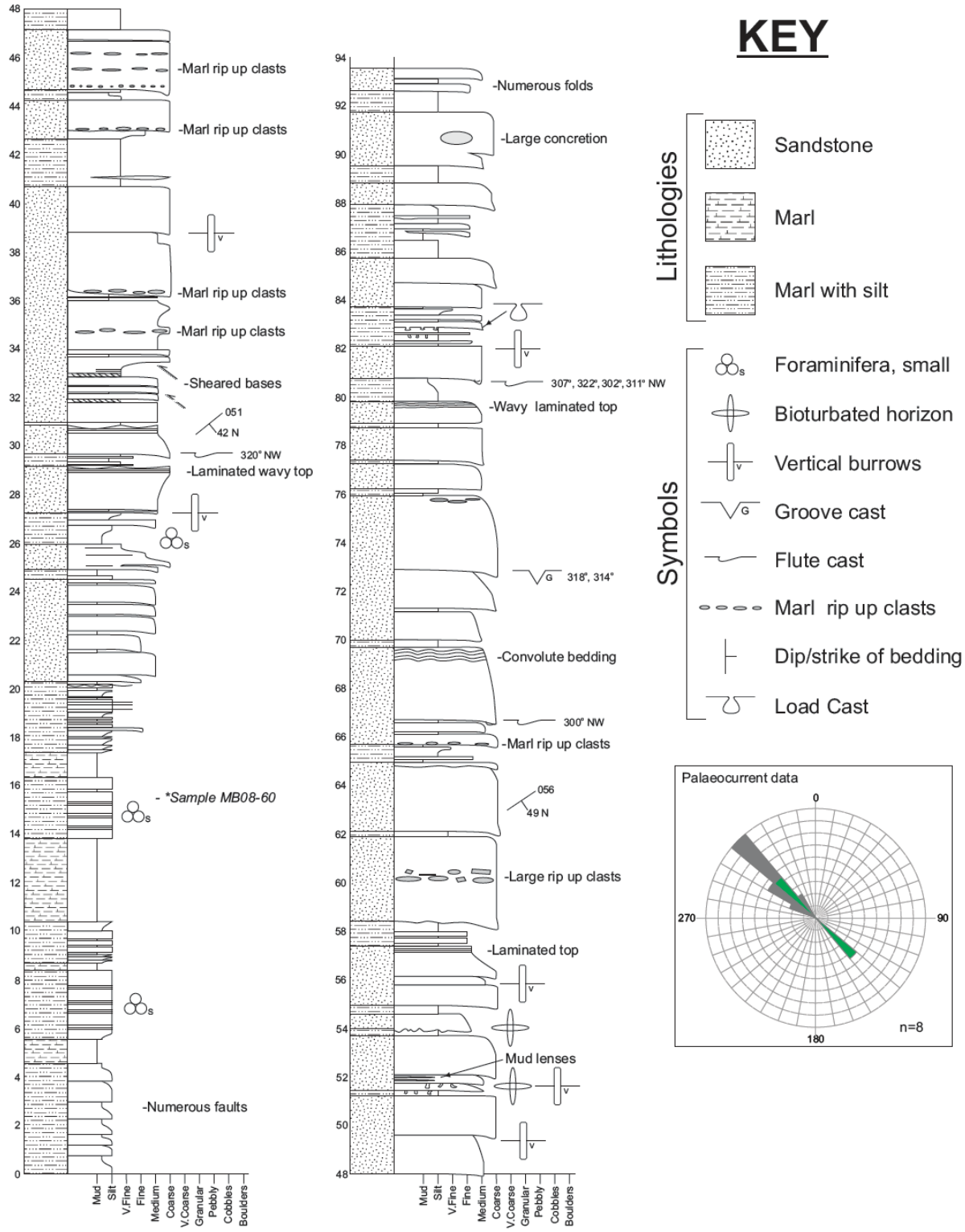

Figure 2.37. Logged succession of the Yenice Formation and Yenice Member (location g on Fig. 2.25). Sandstones predominate throughout the logged section although the facies varies considerably up section. Palaeocurrents taken from the turbidites trend northwestwards (green indicates bidirectional currents taken from groove casts; all other measurements are from flute casts).

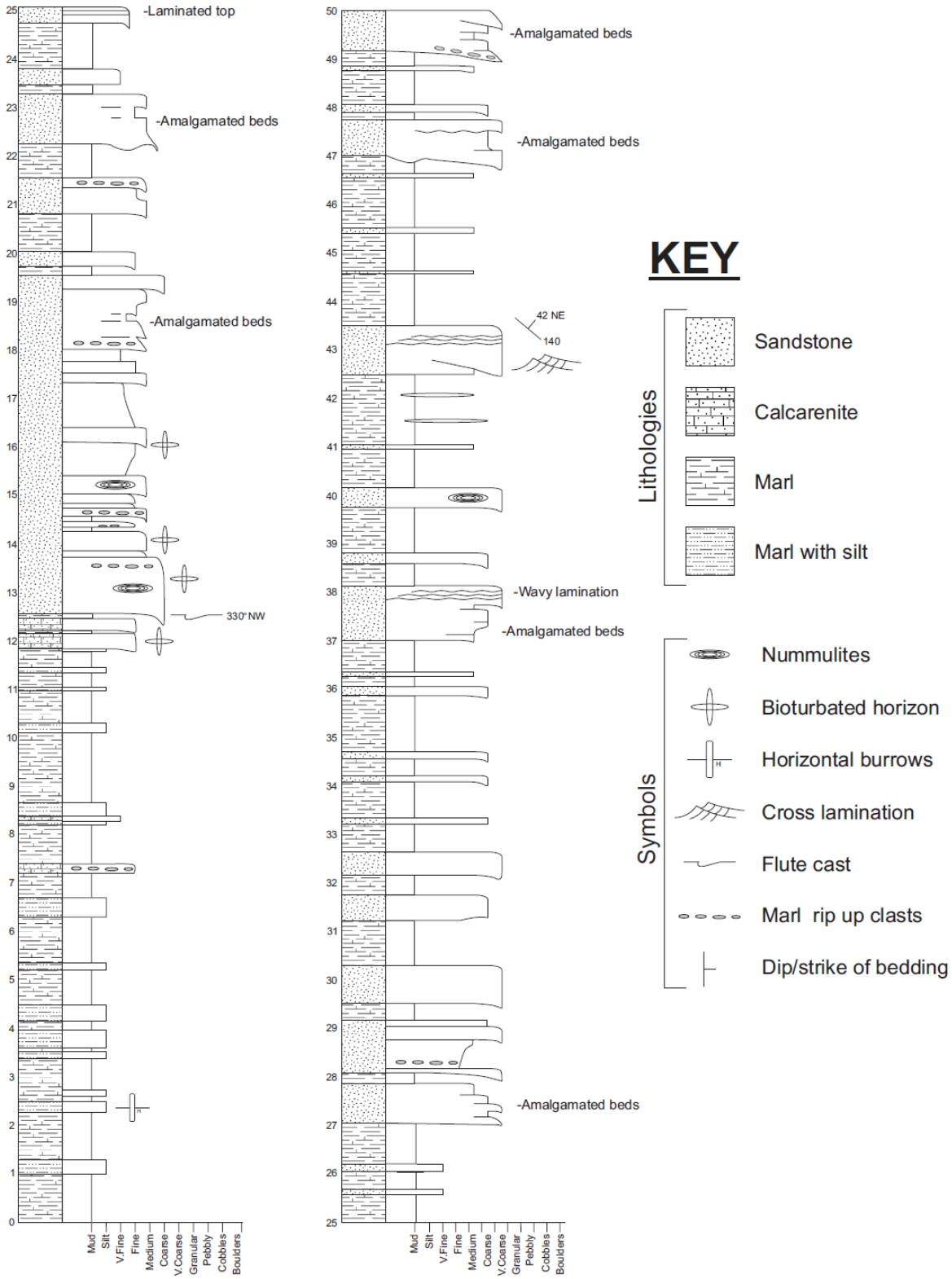

Figure 2.38. Logged section of the Yenice Formation and the Yenice Member (location f on Fig. 2.25). This sequence mainly comprises marls with thin interbeds of sandstone interpreted as thin turbidite deposits. Note the thin succession of sandstone turbidite deposits between ~12.5–19.5, interpreted as the Yenice Member. The member is much thinner here than in the Yenice type section area.

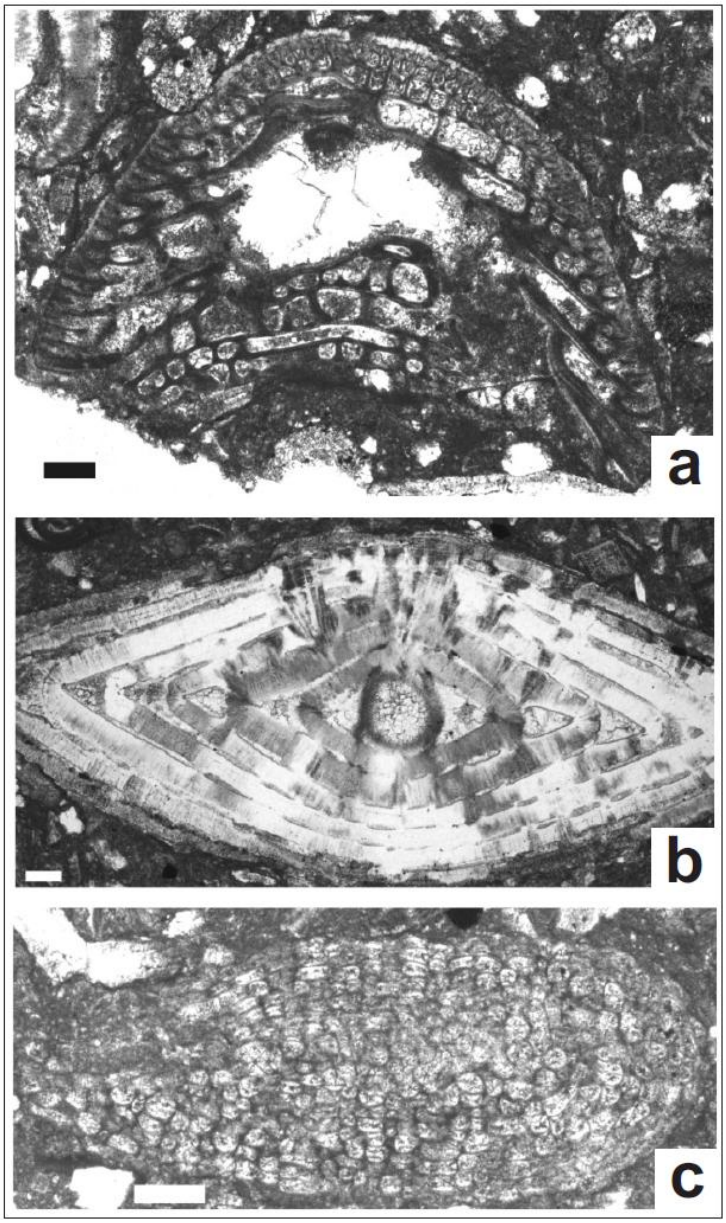

Figure 2.39. Thin-section microphotographs of selected benthic and planktonic foraminifera from the Yenice Formation; a. *Fabiania cassis*, sample MB10-12; b. *Nummulites* cf. *uranensis*, sample MB10-12, c. *Gypsina marianensis*, sample MB10-12. Scale bars 100 µm.

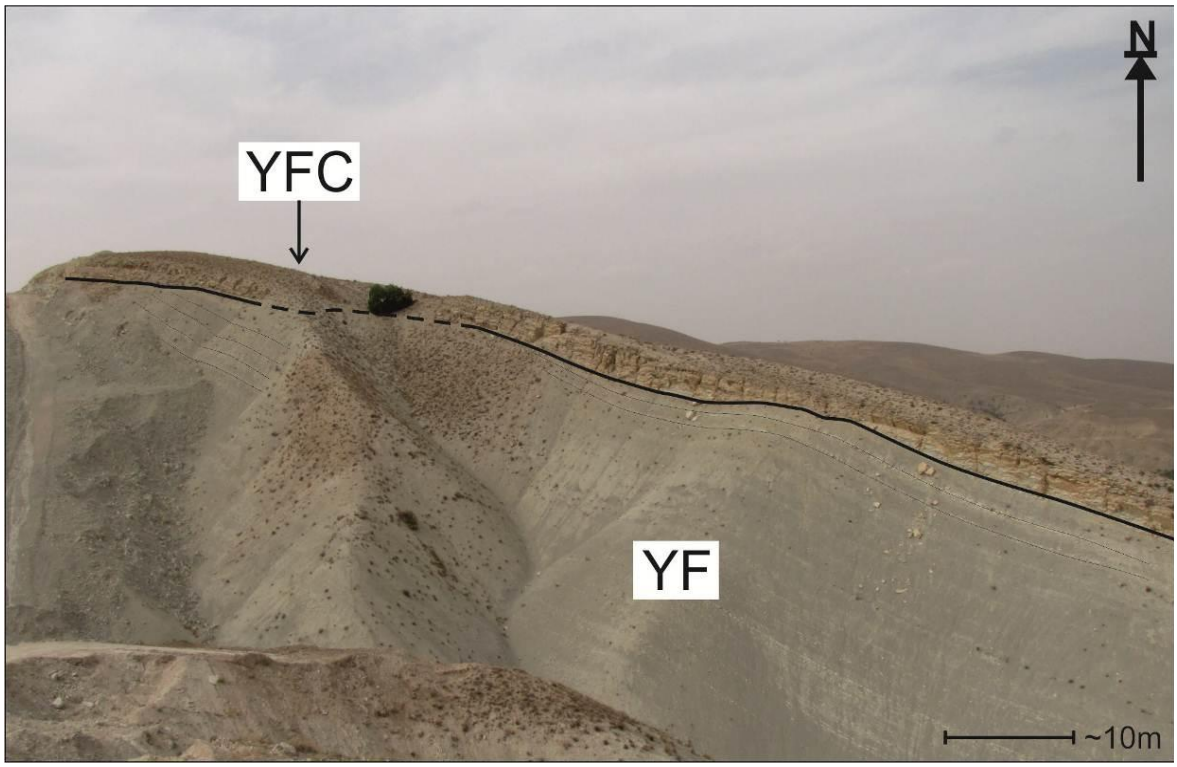

Figure 2.40. Field photograph showing calcarenite of the Yenice Formation (YFC) overlying marls of the Yenice Formation (YF) with an erosive contact. Picture taken from location Yc on Fig. 2.25.

Age: The fossil assemblage within the calcarenites and the planktonic foraminifera within the marls of the Yenice Formation (Table 2.5, Fig. 2.39) are dated as Lutetian.

Yenice Formation (Ilerdian-Lutetian)

Samples	Benthic Foraminifera (BF)	Planktic Foraminifera (PF)	Age
MB09-B52, MB08-101	***Chrysalidina* aff. *floridana***, *Idalina sinjarica*, *Orbitoclypeus* cf. *ramaraoi*, *Orbitoclypeus* cf. *ramaraoi crimensis*, ***Periloculina* cf. *slovenica***, *Amphistegina* sp., *Asterocyclina* sp., *Assilina* sp.,*Discocyclina* sp., *Pfendericonus* sp., *Spirolina* sp., *Valvulina* sp., Miliolidae		Early Eocene (Ilerdian)
MB08-60, MB09-B105, MB10-12, MB09-B84, MB10-5	*Amphistegina* sp., *Assilina* sp., *Asterigerina rotula*, *Asterocyclina* sp., *Discocyclina* sp., ***Fabiania cassis***, *Gypsina marianensis*, *Gyroidinella magna*, *Idalina sinjarica*, ***Nummulites* cf. *uranensis***, *Operculina* sp.	***Acarinina bullbrooki***, ***Acarinina topilensis***, *Catpsydrax* sp., *Chiloguembelina* sp., *Globigerinatheka* sp., *Igorina* cf. *broedermanni*, *Morozovella* sp., *Pseudohastigerina* sp., *Subbotina* sp., *Turborotalia* sp.	Lutetian

Table 2.5. Micropalaeontology results from the Yenice Formation. Fossils highlighted in bold are age-diagnostic.

2.4.5.7 Interpretation of the Middle Eocene marine carbonates (Yenice Formation)

The Mid-Eocene Yenice Formation represents continued transgression and deepening of the Darende Basin. Field relationships indicate that the Korgantepe Formation is overlain by hemipelagic marls of the Yenice Formation (see below). However, analysis of microfossils (mainly Foraminifera, Table 2.5; Fig. 2.39) indicates that the Korgantepe and Yenice Formations were deposited more or less contemporaneously. It seems likely that the shallow-marine conditions which promoted the deposition of the Korgantepe Formation persisted at the basin margins whereas deeper marine marls were deposited within the subsiding basin depocentre (Fig. 2.41). Furthermore, the shallow-marine basin-margin sediments (marginal carbonate shelf?) were probably the source region for the thin calcarenite turbidite deposits in addition to the more substantial calcarenite package in the Yenice area. The basin hinterland in the south is likely to have been uplifted and eroding while the basin margin subsided triggering carbonate production.

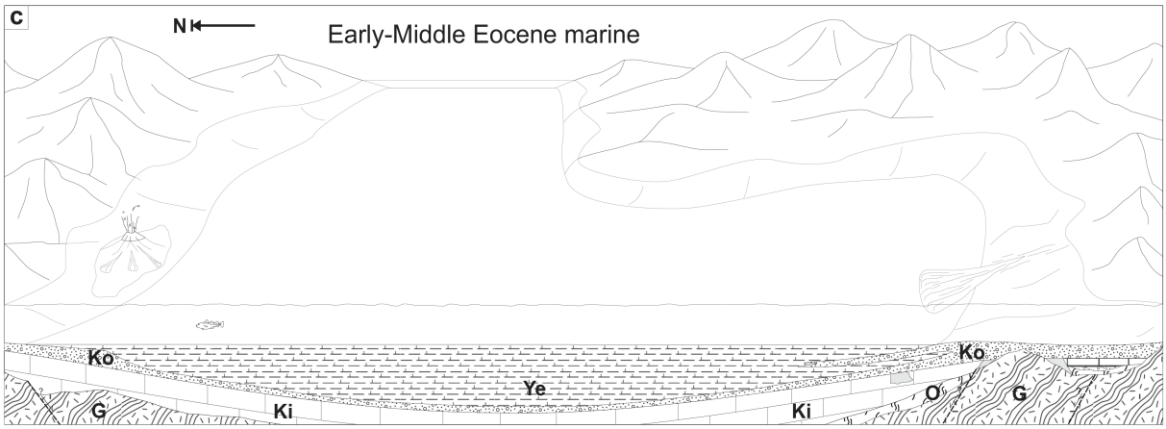

Figure 2.41. Lutetian shallow-marine transgression onto Paleocene unconformity (Korgantepe and Yenice Formations), together with localised alkaline volcanism and northward directed turbidity flows. Kı, Kırankaya Formation; To, Tohma Member; G, Geniz Formation; O, Hocalikova ophiolite Formation; Ul, Ulupınar Formation; Ko, Korgantepe Formation; Ye, Yenice Formation.

2.4.5.8 Middle Eocene shallow-marine carbonates (Asartepe Formation)

Name: Derived from a mountain (Asar Tepe) which means ‘Hanging Mountain’.

Type locality: Asar Tepe is situated approximately 4 km southeast of Yenice. The mountain is well seen to west of the D300 highway, south of Aşağıulupınar (Fig. 2.42).

Lithology: The Asartepe Formation is dominated by medium-to-thick bedded (10-30 cm thick), white to buff coloured fossiliferous limestones, alternating with medium-to-thick bedded (10-30 cm), medium-to-coarse grained calcarenites and medium bedded (~15 cm) finely crystalline limestones (Fig. 2.43a-d). The lower part of the formation is mainly calcarenite containing grains composed of ophiolite-related lithologies and carbonate grains, some of which are likely to be reworked from underlying, older sediments. The calcarenites are also distinguished by intensely bioturbated horizons and sedimentary flow structures including flute and groove casts, marl rip-up clasts and occasional cross lamination. Dish and pillar structures and flame casts were also observed. The middle-to-upper part of the Formation is predominantly biomicritic limestone, as exposed in the eastern part of the basin. Syn-sedimentary deformation was observed near the northern margin of the basin, where a package of limestone beds thickens by ~20% into an inferred syn-sedimentary fault zone.

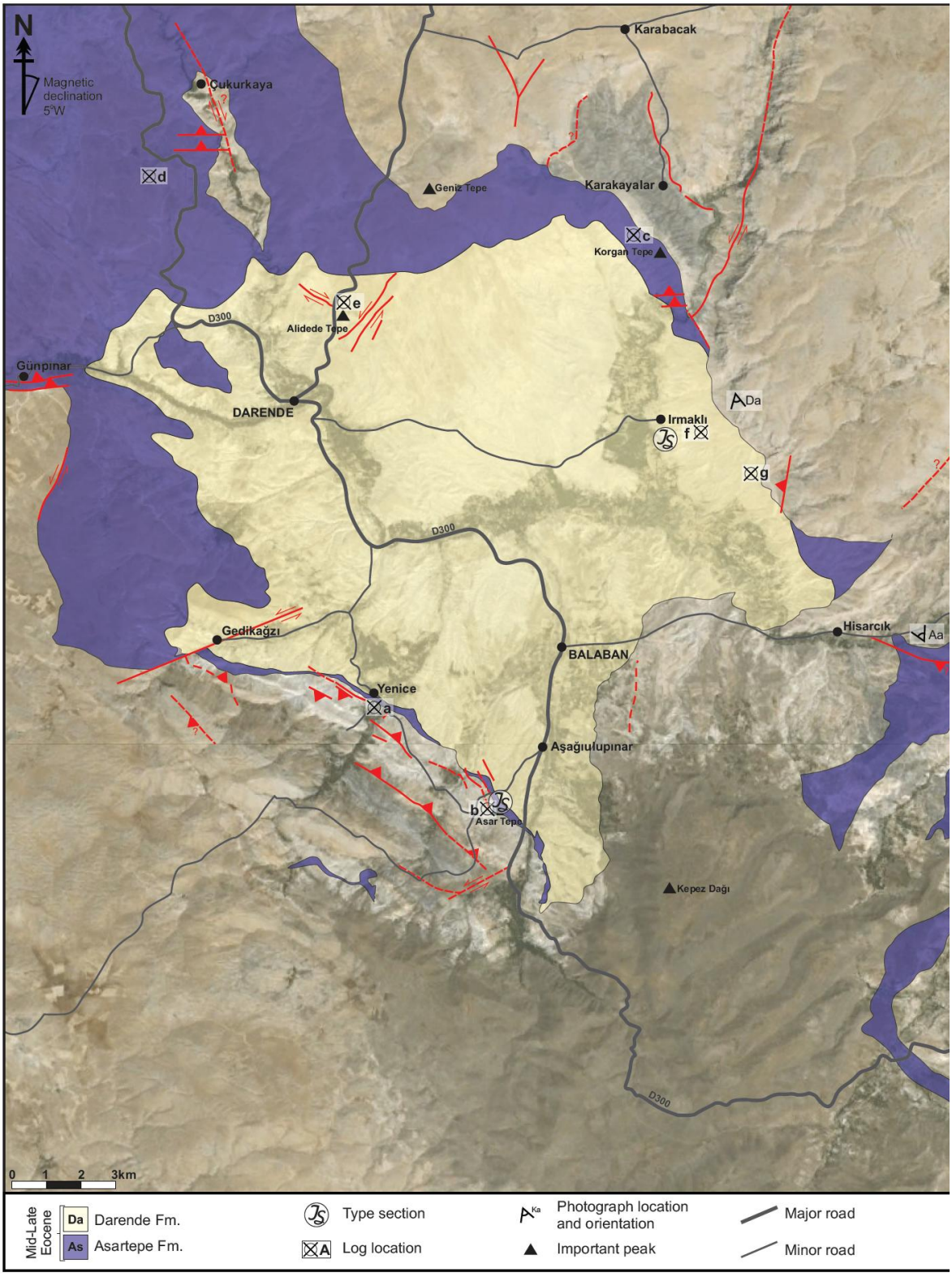

Figure 2.42. Simplified geological map showing the extent of the Asartepe and Darende Formations draped over a satellite image of the Darende Basin. Also shown are logged section locations together with the location and approximate bearings of landscape photographs.

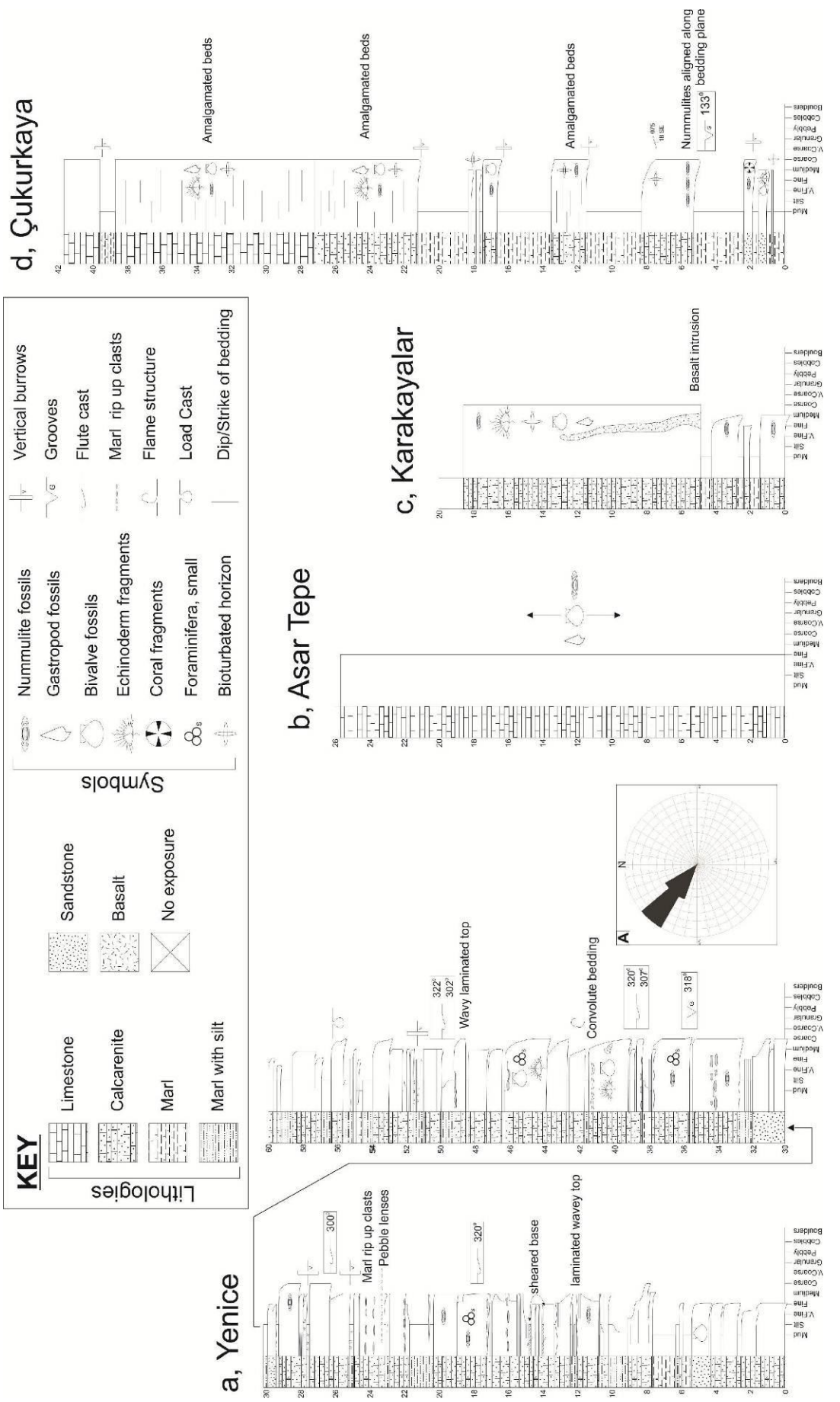
KEY
Lithologies
Limestone
Calcarenite
Marl
Marl with silt
Sandstone
Basalt
No exposure
Symbols
Nummulite fossils
Gastropod fossils
Bivalve fossils
Echinoderm fragments
Coral fragments
Foraminifera, small
Bioturbated horizon
Vertical burrows
Grooves
Flute cast
Marl rip up clasts
Flame structure
Load Cast
Dip/Strike of bedding
a, Yenice
Marl rip up clasts
Pebble lenses
sheared base
laminated wavey top
b, Asar Tepe
Wavy laminated top
Convolute bedding
c, Karakayalar
Basalt intrusion
d, Çukurkaya
Amalgamated beds
Amalgamated beds
Amalgamated beds
Nummulites aligned along bedding plane
Mud
Silt
V.Fine
Fine
Medium
Coarse
V.Coarse
Granular
Pebbly
Cobbles
Boulders

Figure 2.43. Measured sequences of the Asartepe Formation as logged at, a, Yenice; b, Asar Tepe; c, Karakayalar; d, Çukurkaya (Fig. 2.42 locations a-d respectively). The rose diagram shows palaeocurrent data from the Yenice that indicate flow towards the northwest.

The Asartepe Formation is faunally diverse, with microfossils including *Nummulites* sp., *Alveolina* sp., *Discocyclina* sp. and milliolids (Fig. 2.44). The macrofauna include gastropods, bivalves and fragmented echinoids (*e.g.* spines and tests) as well as intact echinoid tests, plus common coral and red algae in the higher levels (Fig. 2.45). Fish spine ossicles and a crab test were also observed.

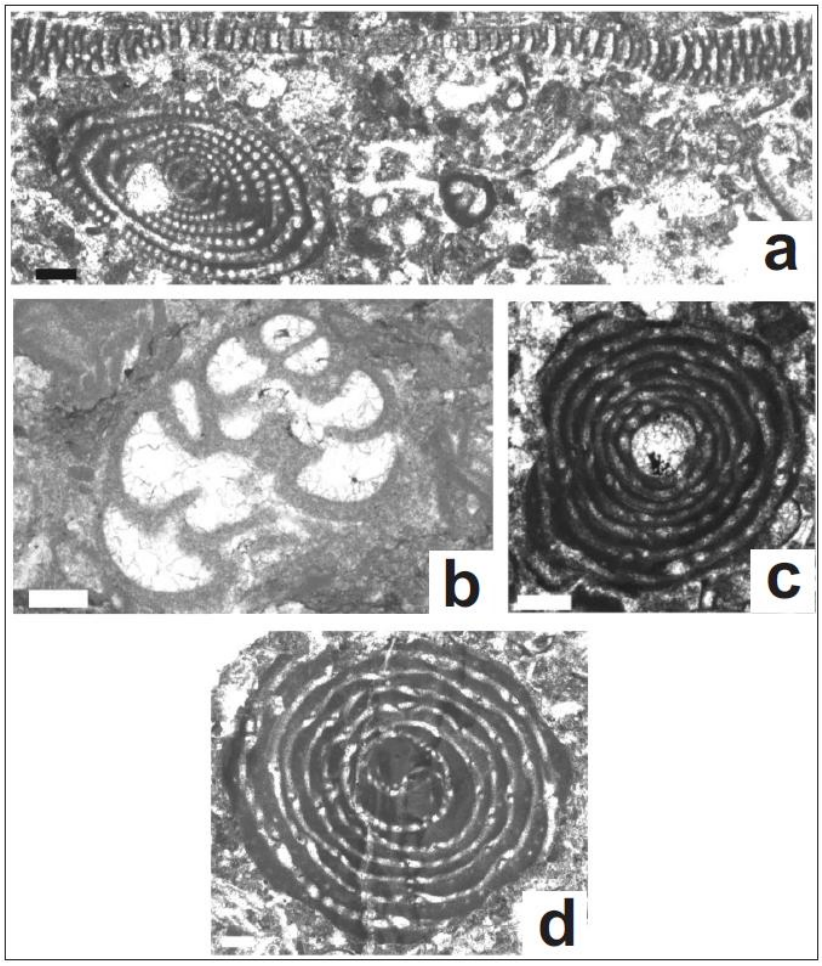

Figure 2.44. Thin-section microphotographs of selected benthic and planktonic foraminifera from the Asartepe Formation; l. *Chrysalidina* cf. *floridana*, sample MB08-66; m. *Orbitolites complanatus* (top), *Alveolina* (*Glomalveolina*) *subtilis* (lower left), sample MB09-B131; n. *Alveolina* (*Glomalveolina*) *levis*, sample MB09-B131; o. *Alveolina* (*Alveolina*) *aragonensis*, sample MB09-B131. Scale bars 100 µm.

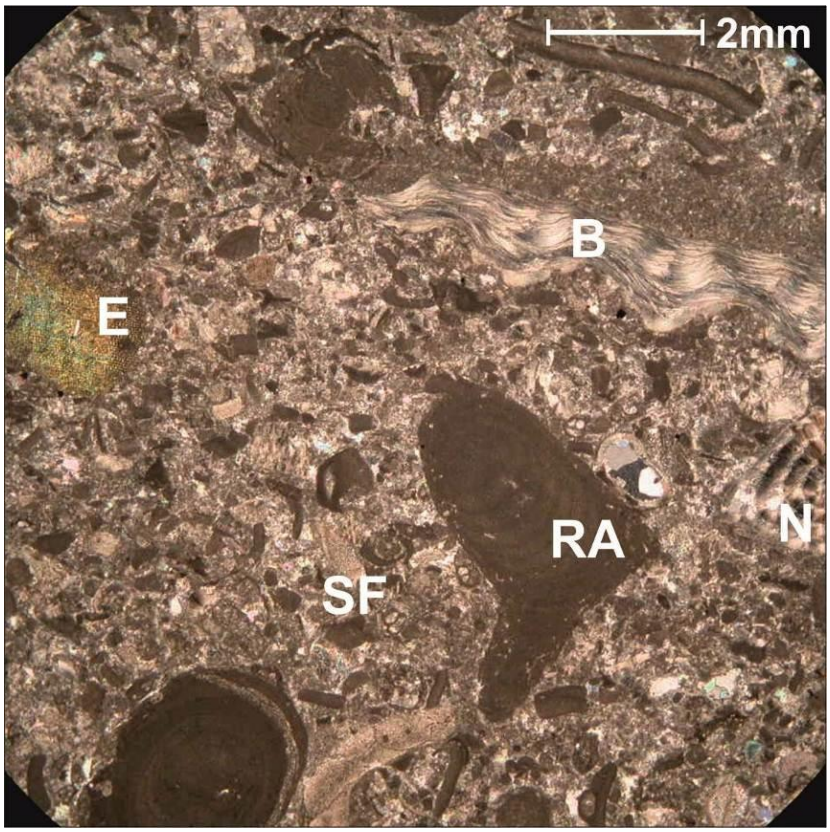

Figure 2.45. Photomicrograph (crossed-polars) showing the bioclastic nature of the Asartepe Formation (E, echinoderm fragment; B, brachiopod fragment; SF, small foraminifera; RA, red algae; N, *Nummulites* sp.).

A sinuous, sub-vertical feeder dyke (~50 cm wide by ~10 m long) was observed passing through the Yenice Formation, extending upwards and terminating within the Asartepe Formation (Fig. 2.43c). This dyke is composed of fine-grained basalt with clinopyroxene and sparse plagioclase feldspar phenocrysts.

Boundaries: In most areas of the Darende Basin the Asartepe Formation begins with a sharp, conformable contact with the marls of the Yenice Formation. However, the Formation unconformably overlies Mesozoic platform carbonates in the northwest, southeast and particularly the east of the basin (e.g. east of Irmaklı, Fig. 2.46). The upper contact of the Formation is generally not well exposed. However, in the north of the basin the upper contact is marked by an abrupt change to the overlying Darende Formation.

Thickness and extent: The Formation ranges in thickness from 30-80m in the south of the basin (Fig. 2.43a & b), thickening to ~120 m towards the northern margin of the basin, at Karakayalar (Fig 2.43c). However, it is thickest (~180 m) to the north of the Darende

Basin, north of Çukurkaya (Fig. 2.43d) and in the east of the basin, where it directly overlies Mesozoic carbonate platform limestones (Genız Formation).

This formation is one of the most widely represented throughout the basin and together with the carbonate platform limestone forms topographic highs due to its resistance to weathering and erosion.

Age: The predominantly benthic faunal assemblage is dated as Lutetian-Bartonian (Late Eocene) (Table 2.6, Fig. 2.44).

Figure 2.46. Limestones of the Asartepe Formation (AF) unconformably overlying Mesozoic limestones of the Geniz Formation (GF) (blocked out white area is unrelated foreground). Photograph taken from location Aa on Fig. 2.40.

Asartepe Formation (Ilerdian to early Priabonian)

Samples	Benthic Foraminifera (BF)	Planktic Foraminifera (PF)	Age
MB08-117, MB08-120, MB08-122, MB08-123, MB09-B130, MB09-B131	*Asterigerina rotula*, ***Alveolina* (*Alveolina*) *aragonensis***, ***Alveolina* cf. *cuspidata***, ***Alveolina* (*Glomalveolina*) *levis***, ***Alveolina* (*Glomalveolina*) *subtilis***, ***Chrysalidina* cf. *floridana***, ***Fabularia* cf. *donatae***, ***Periloculina* cf. *slovenica***, *Idalina sinjarica*, *Gyroidinella magna*, ***Lockhartia* cf. *conditi***, *Medocia blayensis*, ***Nummulites* cf. *formosus***, ***Orbitolites complanatus***, *Alveolina* sp., *Assilina* sp., *Chrysalidina* sp., *Discocyclina* sp., *Fabiania* sp., *Ophthalmidium* sp., *Orbitolites* sp., *Periloculina* sp., *Pfendericonus* sp.,*Planorbulina* sp., *Pyrgo* sp., *Rotalia* sp., *Quinqueloculia* sp., *Spirolina* sp., *Triloculina* sp., *Valvulina* sp., Miliolidae		Early Eocen (Ilerdian)
MB08-80, MB08-86, MB08-92, MB08-94, MB08-95, MB09-B48, MB09-B49, MB09-B67	*Asterigerina rotula*, ***Assilina* cf. *exponens***, ***Assilina* cf. *praespira***, ***Assilina* cf. *tenuimarginata***, ***Fabiania cassis***, *Gyroidinella magna*, *Gypsina* cf. *marianensis*, ***Halkyardia* cf. *bikiniensis***, *Idalina sinjarica*, ***Discocyclina* cf. *archiaci bartholomei***, *Medocia* cf. *blayensis*, *Neorotalia vienotti*, ***Nummulites* cf. *uranensis***, ***Peneroplis* cf. *planatus***, ***Sphaerogypsina globula***, ***Sphaerogypsina anatolica***, *Nummulites* sp., *Amphistegina* sp., *Anomalina* sp., *Asterocyclina* sp., *Assilina* sp., *Discocyclina* sp., *Gypsina* sp., *Linderin* a sp., *Nummulites* sp., *Orbitoclypeus* sp., *Planorbulina* sp., *Periloculina* sp., *Pseudonummoloculina* sp.	*Globigerinatheka* sp., *Igorina* sp., *Morozovella* sp., *Pseudohastigerina* sp., *Subbotina* sp.	Lutetian
MB08-66, MB08-119, MB09-B91	*Asterigerina rotula*, ***Austrotrillina* cf. *striata***, ***Eoannulaira eocenica***, *Idalina sinjarica*, *Gypsina linearis*, *Gypsina marianensis*, ***Chapmanina gassinensis***, ***Malatyna anatolica***, *Neorotalia vienotti*, ***Nummulites* cf. *hormoensis***, ***Nummulites* cf. *incrassatus***, ***Nummulites* cf. *striatus***, ***Nummulites fabianii***, ***Orbitolites* cf. *minimus***, ***Spiroclypeus sirotti***, *Anomalina* sp., *Linderina* sp., *Nephrolepidina* sp., *Operculina* sp., *Praebullalveolina* sp., *Praerhapydionina* sp.		Late Bartonian-Early Priabonian

Table 2.6. Micropalaeontological results from the Asartepe Formation. Fossils highlighted in bold are age-diagnostic.

2.4.5.8 Interpretation of the Middle Eocene shallow-marine carbonates (Asartepe Formation)

The conformably overlying shallow-marine limestones of the Asartepe Formation record progressive shallowing of the basin during the Late Lutetian. Clastic sediments continued to be derived from the ophiolite-related mélange, either directly, or by reworking of pre-existing sediments containing this material (i.e. Ulupınar and Korgantepe Formations).

The marked sediment thickness changes in the vicinity of faults are interpreted as the result of high-angle growth faulting. The continued transgression of the Mesozoic platform carbonate 'basement' (Fig. 2.46) indicates broadening of the basin to form a regional-scale transgressive unit (Fig. 2.47). In the NE and E of the basin the basal beds are draped over a relict palaeotopography which probably remained since the Late Cretaceous or was created by erosion and/or faulting during latest Cretaceous to Mid Eocene time (*i.e.* represent by the Paleocene unconformity).

The Asartepe Formation extends northwards, breaching the basin margins as defined by the earlier Eocene and Cretaceous sediments. The formation thickens northwards and potentially merges with limestones of similar age and lithology around Gürün ~30 km northwest of Darende (Robertson *et al.* in press). Similar Eocene-aged limestones crop out in canyons ~40 km east of Darende and join up with outcrop of Eocene limestones in the Hekimhan area, to the northeast of Darende.

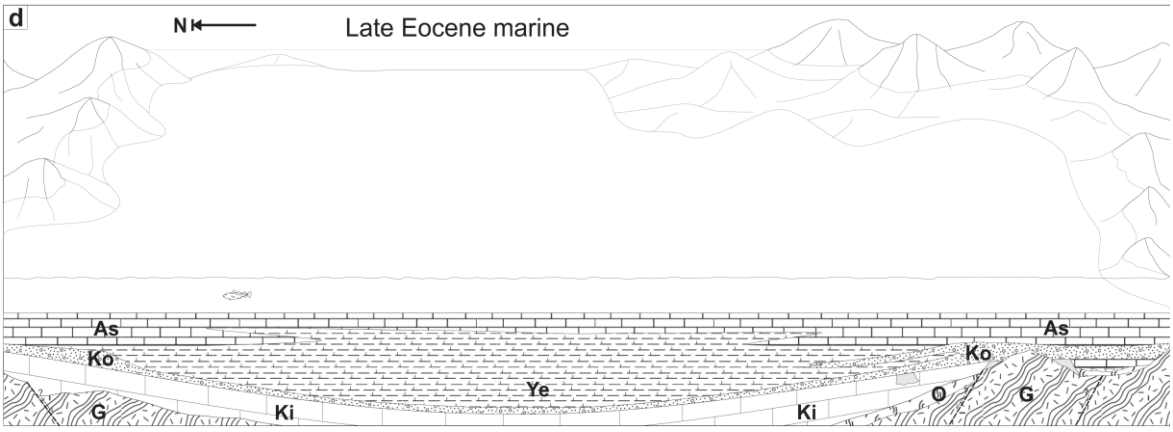

Figure 2.47. Late Lutetian shallow-marine limestones of the Asartepe Formation onlapping Mesozoic limestones. The limestones filled and breached the basin margins to the north and west to connect with regional equivalents. Kı, Kırankaya Formation; To, Tohma Member; G, Geniz Formation; O, Hocalikova Formation; Ul, Ulupınar Formation; Ko, Korgantepe Formation; Ye, Yenice Formation; As, Asartepe Formation.

2.4.5.9 Late-Eocene shallow-marine regressive facies (Darende Formation)

Name: Derived from the town of Darende which this formation surrounds.

Type locality: The lower part of the Darende Formation is best observed at Alidede Tepe on the road leading NNE out of Darende (locality e on Fig. 2.42). The upper part of the formation is best observed in the badlands topography in the area directly east of Darende around a village called Irmaklı.

Lithology: The Darende Formation comprises alternations of fine-to coarse-grained sandstones, siltstones, limestones and marls, with subordinate conglomerates in the lower part of the succession (*e.g.* at Alidede Tepe; *e.g.* 84-129 m, Fig. 2.48). Millimetre-scale gypsum laminations are widespread within the marls (Fig. 2.48 a[1]). Sandstones lower in the succession are faunally diverse with benthic foraminifera (Fig. 2.49), echinoid debris (tests and spine fragments), bivalves (*e.g.* oysters up to 10 cm across), gastropods, coral fragments and algal rhodoliths (Fig. 2.50). Organic matter, including wood fragments and leaves is also present (Fig. 2.51 ~3.5 m). Many limestone beds in the northeast of the basin contain stringers of black chert nodules (Fig 2.51 ~4.5–10 m), similar to many formations of similar age throughout the Eastern Mediterranean (*e.g.* Robertson 1977). Palaeocurrent measurements taken from a combination of current lineation, ripples,

groove and flute casts indicate palaeoflow towards the northwest (Fig. 2.48). Desiccation cracks are rarely present on the surfaces of mudstone beds. The upper part of the succession is dominated by thick marl/gypsum alternations, with subordinate sandstone and siltstone interbeds. Gypsum layers, 1-50 cm thick, occur throughout the marls at irregular intervals. These marls are cut by numerous veins and fractures, some of which are filled with coarse selenitic gypsum.

Boundaries: The Darende Formation is conformable on the Asartepe Formation in the south of the basin. However, it unconformably overlies the Mesozoic platform carbonates along the northeastern basin margin, to the east of Irmaklı (Fig. 2.52).

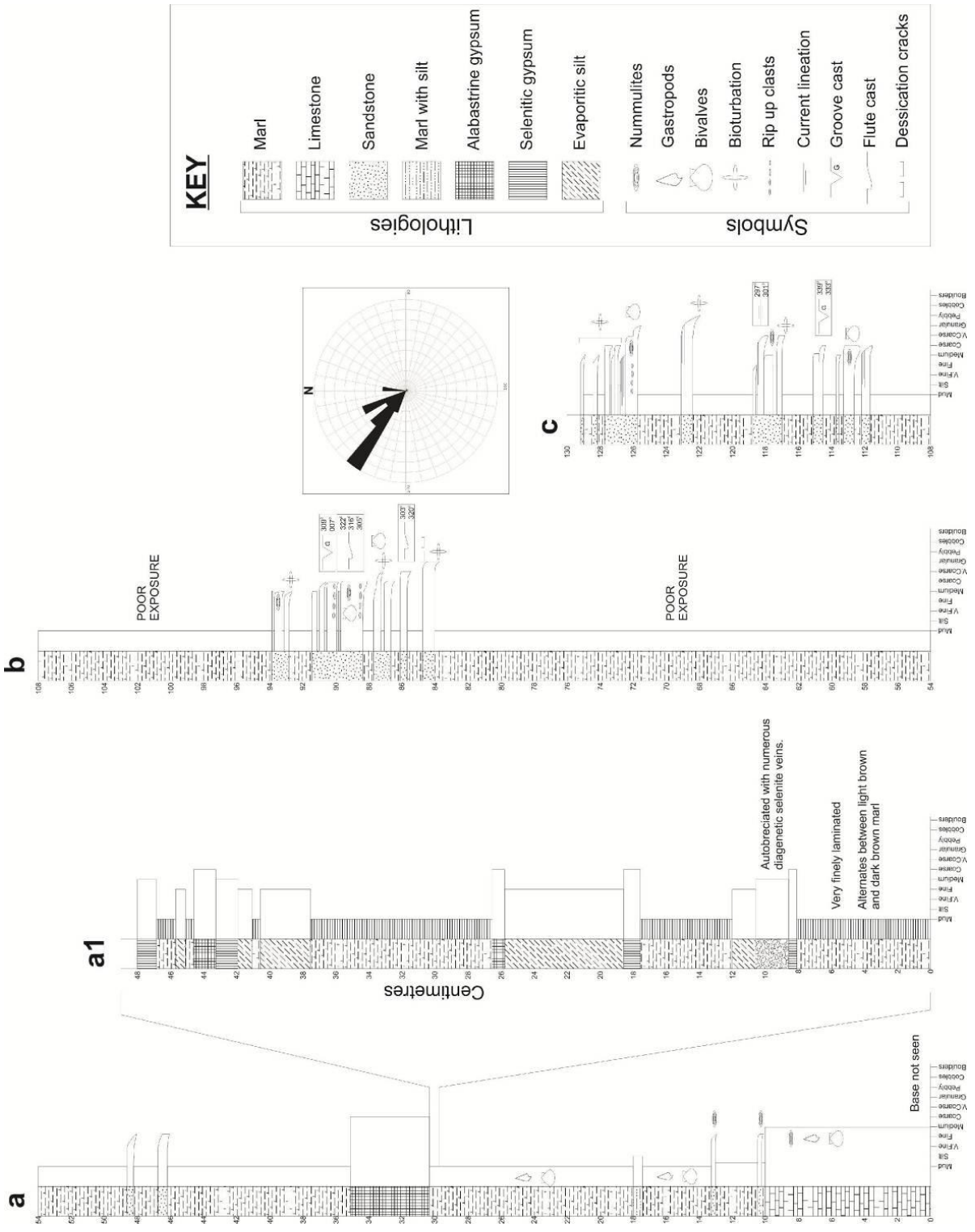

Figure 2.48. Measured succession of the Darende Formation as logged at Alidede Tepe (location e on Fig. 2.40). a[1] is a representative centimetre-scale log of evaporitic marls. The Rose diagram shows palaeocurrent data from flute casts found in sandstone beds that indicate flow to the northwest.

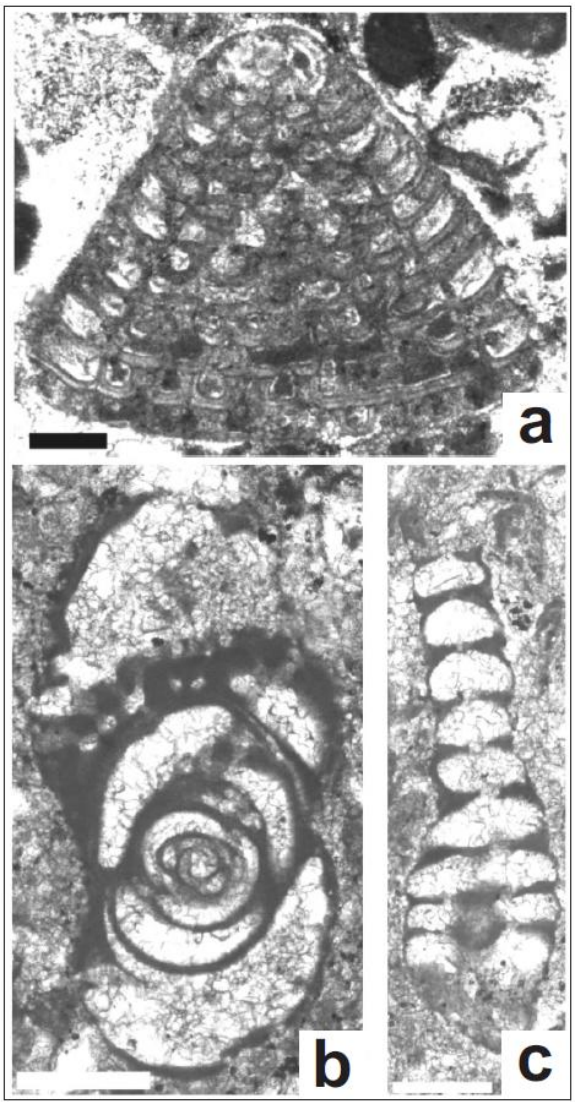

Figure 2.49. Thin-section microphotographs of selected benthic and planktonic foraminifera from the Darende Formation; p. *Chapmanina gassinensis*, sample MB09-B34; q. *Austrotrillina* cf. *striata*, sample MB09-B26; r. *Malatyna* sp., sample MB09-B26. Scale bars 100 µm.

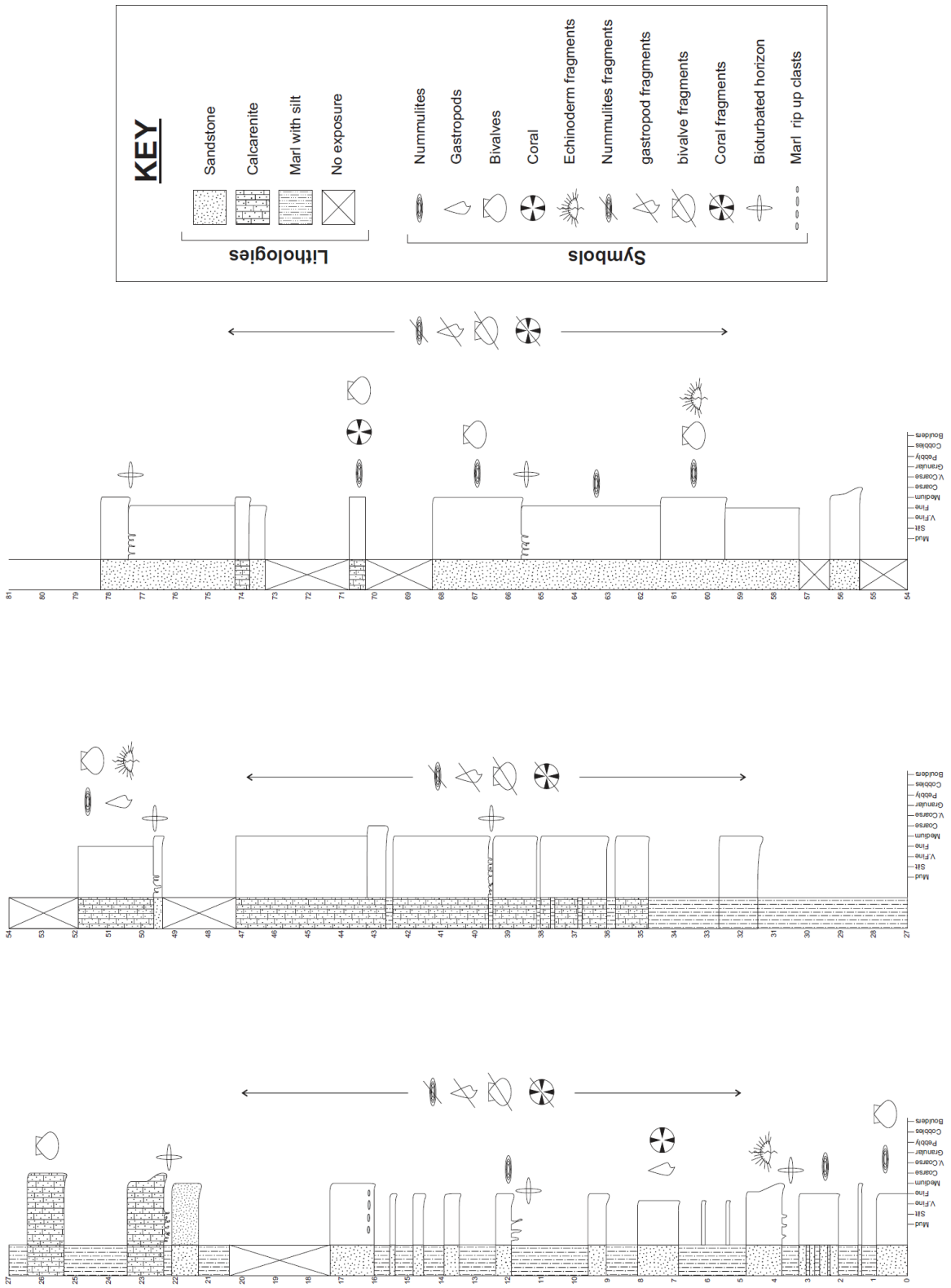

Figure 2.50. Measured succession of the Darende Formation (location f on Fig. 2.40). The formation alternates between marl and thick sandstones which are faunally diverse.

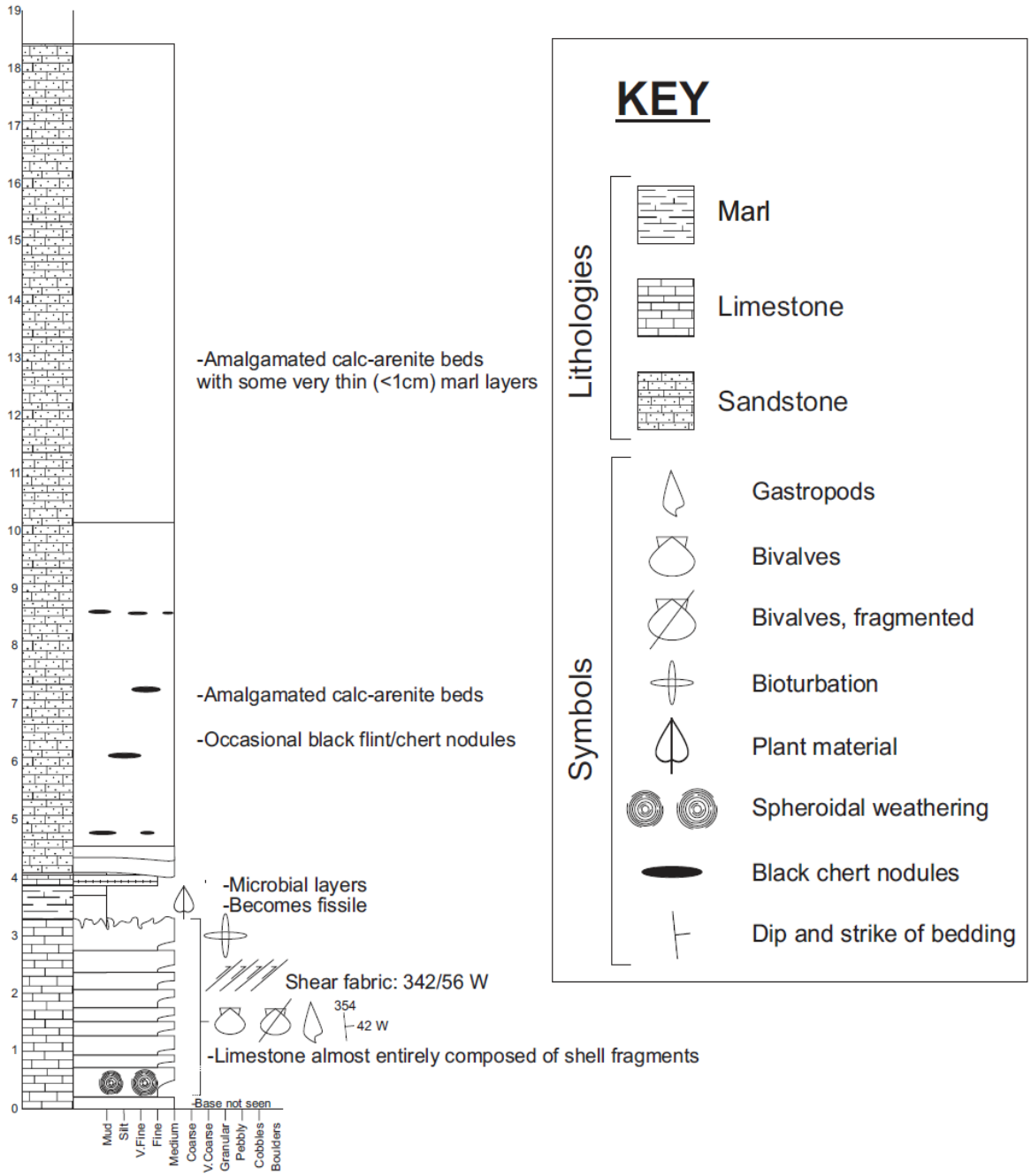

Figure 2.51. Measured succession of the Darende Formation (location g on Fig. 2.40). This section was measured through limestone and calcarenite. The limestones are biolithic. Marl interbeds are commonly sheared. Wood and leaf fragments as well as chert nodules were observed in this succession.

Figure 2.52. Mixed lithologies of the Darende Formation (DF) unconformably onlapping limestones of the Mesozoic Geniz Formation (GF) towards the north. Picture taken from location Da on Fig. 2.40.

Thickness and extent: The Darende Formation is widespread in the field area and mainly outcrops in the topographically lower badlands topography to the south and east of Darende and north of Balaban. The strata on the northern margin of the basin dip towards the south, whereas the strata to the south of the basin dip towards the north, preserving a bowl-shaped structure. The lower part of the Darende Formation is up to 160 m thick. The upper part of the sequence is almost as thick again (~150 m), giving a total thickness of ~300 m.

Age: The faunal assemblage of the Darende Formation indicates a Late-Barthonian to Early-Priabonian age (Table 2.7, Fig. 2.49).

Darende Formation (late Bartonian- early Priabonian)			
Samples	**Benthic Foraminifera (BF)**	**Planktic Foraminifera (PF)**	**Age**
MB09-B23, MB09-B25, MB09-B26, MB09-B34, MB09-B73, MB09-B77	***Austrotillina* cf. *striata*, *Nummulites* cf. *incrassatus*, *Nummulites cf. striatus, Nummulites cf. hormoensis, Baculogypsinoides* cf. *tetraedra*, *Chapmanina gassinensis*, *Giyroidinella magna*, *Gypsina* cf. *marianensis, Idalina sinjarica, Medocia blayensis, Sphaerogypsina globula, Fabiania* sp., *Heterostegina* sp., *Ophthalmidium* sp., *Orbitolites* sp., Operculina sp., *Peneroplis* sp., *Praerhapydionina* sp., *Malatyna* sp., *Valvulina* sp., Miliolidae**	-	Late Bartonian-Early Priabonian

Table 2.7. Micropalaeontology results from the Darende Formation. Fossils highlighted in bold are characteristic of the age.

2.4.5.10 Interpretation of the Late Eocene shallow-marine regressive facies (Darende Formation)

Deposition culminated in the shallow-marine, to restricted evaporitic sediments of the Darende Formation (Fig. 2.53). This formation also unconformably onlaps the Mesozoic limestones around the basin margins (Fig. 2.52). The intercalations of shallow-marine and gypsum-rich sediments suggest marked fluctuations in salinity caused by opening and closure of a marine gateway. Desiccation cracks and the presence of potentially fluvial derived conglomerates indicate intermittent emergence of parts, or all, of the basin. Overall, the basin went through several stages of restriction, emergence and replenishment before finally becoming emergent during the Priabonian (Late Eocene), probably as a result of sediment infill, eustatic sea level fall (Miller *et al.* 1995), or regional uplift.

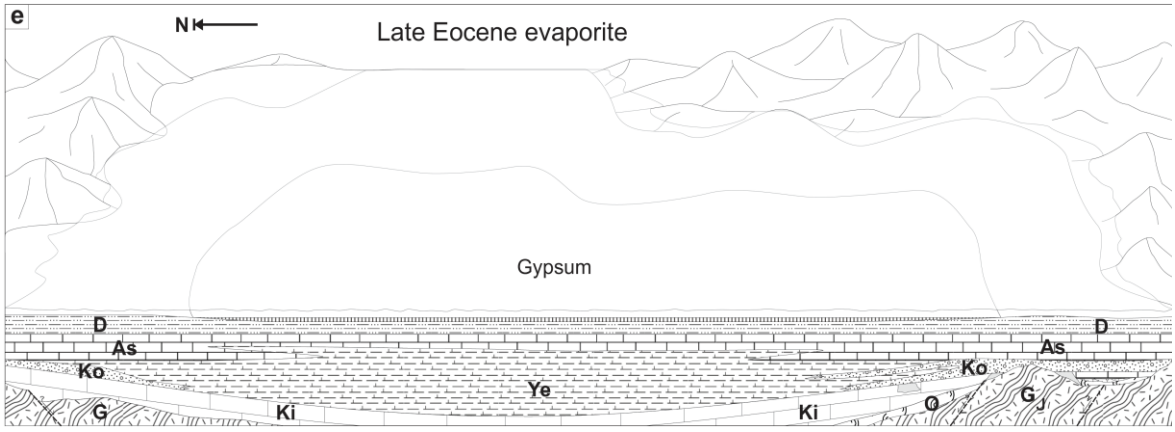

Figure 2.53. Early Priabonian shallow-marine restriction and emergence of the basin (Darende Formation). Kı, Kırankaya Formation; To, Tohma Member; G, Geniz Formation; O, Hocalikova ophiolite Formation; Ul, Ulupınar Formation; Ko, Korgantepe Formation; Ye, Yenice Formation; As, Asartepe Formation; D, Darende Formation.

2.4.6 Post Eocene

2.4.6.1 Tahtalı Formation

Name: *Unknown*

Type locality: The southeasternmost part of the Darende Basin (Fig. 2.54).

Lithology: The Tahtalı Formation begins with horizontally bedded, undeformed, weakly lithified light grey, to brown fossiliferous marls. Numerous intraclasts of well-lithified shelly limestone are present. The upper part of the marine intercalation is made of light-brown limestone with abundant macrofossils (*e.g.* both disarticulated and articulated bivalves, gastropods, coral (*favosites*, Fig. 2.55a) and echinoid fragments). In eastern parts of the basin, south of Hisarcık, the limestones are bored by molluscs (Fig 2.55b). Some horizons contain well-preserved large bivalves (*e.g.* oysters). This outcrop is characterised by metre-scale foresets (Fig 2.55c), locally directed westwards.

Boundaries: In the western and southeastern areas of the basin the Miocene carbonates onlap folded and faulted Eocene lithologies. The upper boundary forms a shallow-angle unconformity overlain by Miocene subaerial basalts.

Thickness and extent: The weakly lithified lower part of the Formation is ~ 15 m thick whereas the overlying lithified brown limestone is ~10 m thick, as measured in the southeast of the field area.

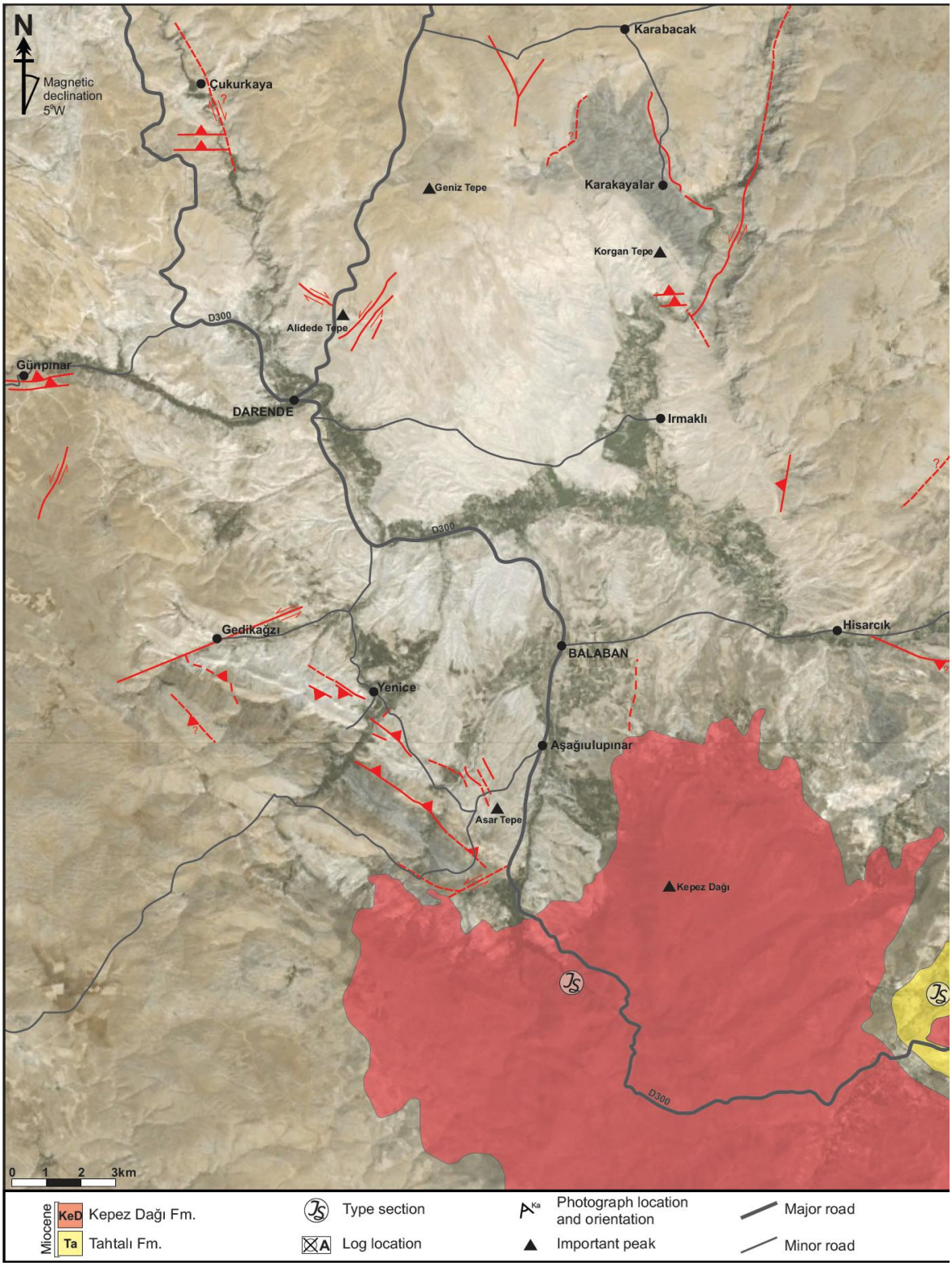

Figure 2.54. Simplified geological map showing the extent of the Tahtalı and Kepez Dağı Formations draped onto a satellite image of the Darende Basin. Also shown are type section location areas.

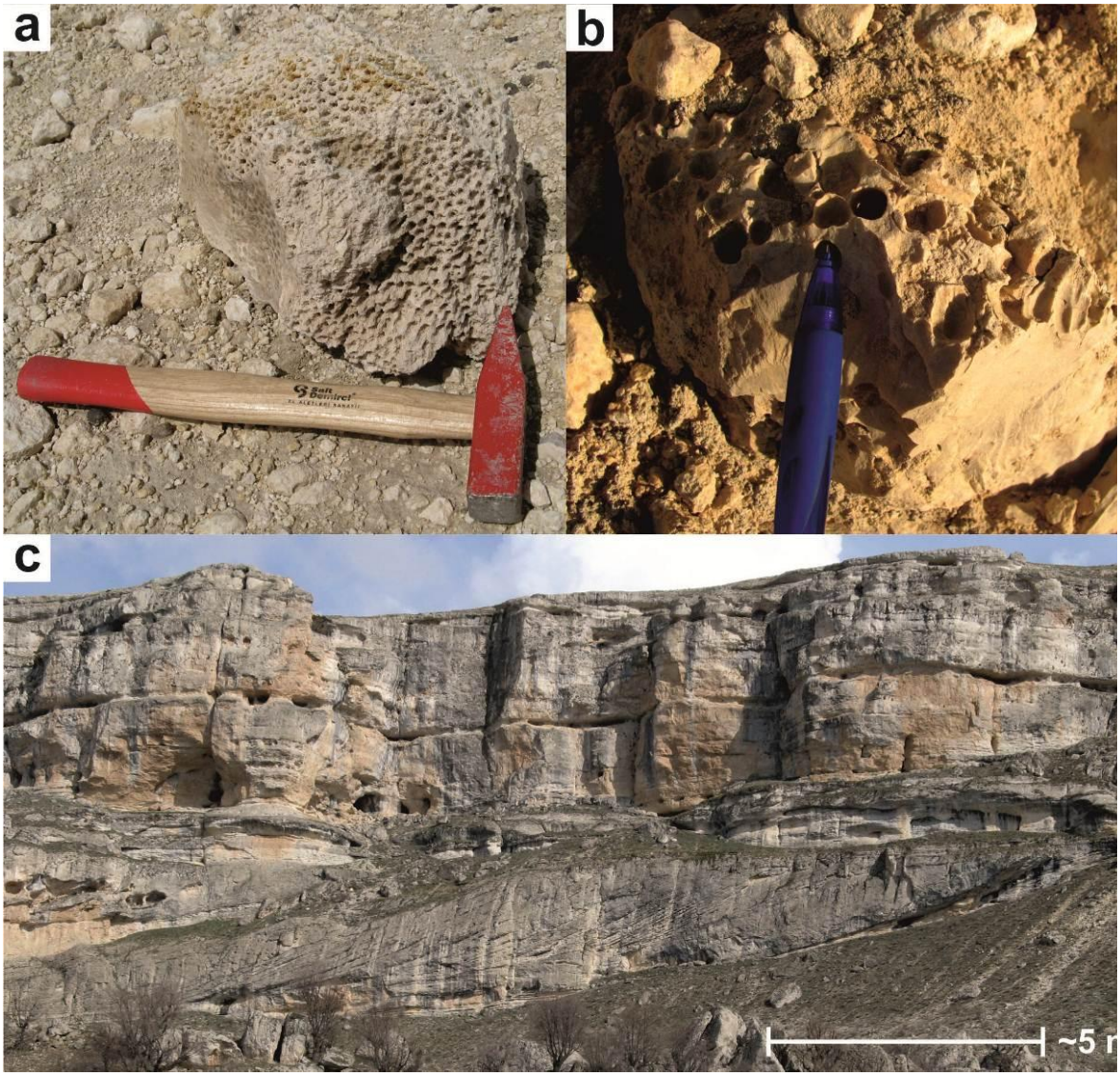

Figure 2.55. Field photographs; a, Large *Favosites*-type coral; b, Circular borings probably created by molluscs in limestones; c, Foresets trending ~ westwards within the Tahtalı Formation. All field localities are from the eastern part of the field area, south of Hisarcık.

2.4.6.2 Interpretation of the Miocene Tahtalı Formation

A short-lived marine transgression deposited faunally diverse marl and carbonate facies. This formation overlies partially deformed and tilted Eocene sediments. However, the Tahtalı Formation is relatively undeformed and remains sub-horizontal indicating that any collision related compression was largely complete before the onset of deposition. Furthermore, it implies the postponement of regional uplift until after the Mid-Miocene.

Comparable Miocene shallow-marine sediments are seen in several other basins throughout central Turkey (Türkmen *et al.* 2007; Hüsing *et al.* 2009).

2.4.6.3 Kepez Formation

Name: Name taken from Kepez Dağı (which means 'Black Mountain') to the southeast of Balaban (Kepez Dağı Formation of Akkuş 1971).

Type locality: The Kepez Dağı Formation is best observed around Kepez Dağı, to the south of the field area.

Lithology: The Kepez Dağı Formation is composed of a thick sequence (~1000 m) of clinopyroxene-and feldspar-phyric basaltic lava flows and associated volcanogenic debris-flows, individually up to 10 m thick (Fig 2.56). The debris flows contain sub-angular clasts of basalt. Crosscutting sills up to 5 m thick were also observed and display columnar jointing. Bright orange and red tuffs are also associated with this formation.

Figure 2.56. Field photograph from the south of the Darende Basin showing layered subaerially erupted basaltic lava flows.

Boundaries: The lower boundary forms a low-angle unconformity over the Miocene Tahtalı Formation. The upper boundary is not well exposed in the field area.

Thickness and extent: The Kepez Dağı Formation is up to 1000 m thick and covers an area ~ 400 km^2, including a large portion of the south and southeast of the Darende Basin. Basalts of similar age are widespread throughout eastern Anatolia (Arger *et al.* 2000; Demir *et al.* 2009; Ekici *et al.* 2009). The lithologically similar Yamadağ Formation is believed to be an eastward extension of the Kepez Formation.

Age: This volcanic unit and its lithological equivalent (Yamadağ Formation) within the Hekimhan Basin to the east (Arger *et al.* 2000; Kürüm *et al.* 2008; Demir *et al.* 2009) have been radiometrically dated as Middle Miocene, 15.8 +/- 0.2 Ma using the $^{40}Ar/^{39}Ar$ method (Kürüm *et al.* 2008).

2.4.6.4 Interpretation of the Kepez Formation

The lava flows erupted in a subaerial setting and were partially reworked by fluvial and gravity processes to form volcanogenic debris flows. Regionally similar Miocene-aged basaltic lavas were identified by Kürüm *et al.* (2008) (e.g. Arapkir, Inle and Adamkıran).

2.4.6.5 Çaybaşı Formation

Name: Given by Akkuş 1971

Type locality: Around Günpınar (not mapped during this study).

Lithology: Predominantly composed of well-rounded, clast-supported conglomerates with lenticular bedding geometries (Fig 2.57a). Clasts are composed of a mixture of the underlying facies including ophiolite-related lithologies and various limestones, including *Nummulitic* limestone clasts. Associated sandstones and palaeosols with well-developed caliche were also observed. In some areas (*e.g.* around Günpınar and to the north of Hisarcık) tufa deposits have formed with well-preserved vertical tubular structures (Fig. 2.57b).

Boundaries: Lower boundaries form unconformities over underlying formations.

Thickness and extent: The conglomerates and sandstones are up to 12 m thick, as measured at Günpınar. The Tufa is up to ~5 m thick as observed north of Hisarcık.

Age: Pliocene to Quaternary.

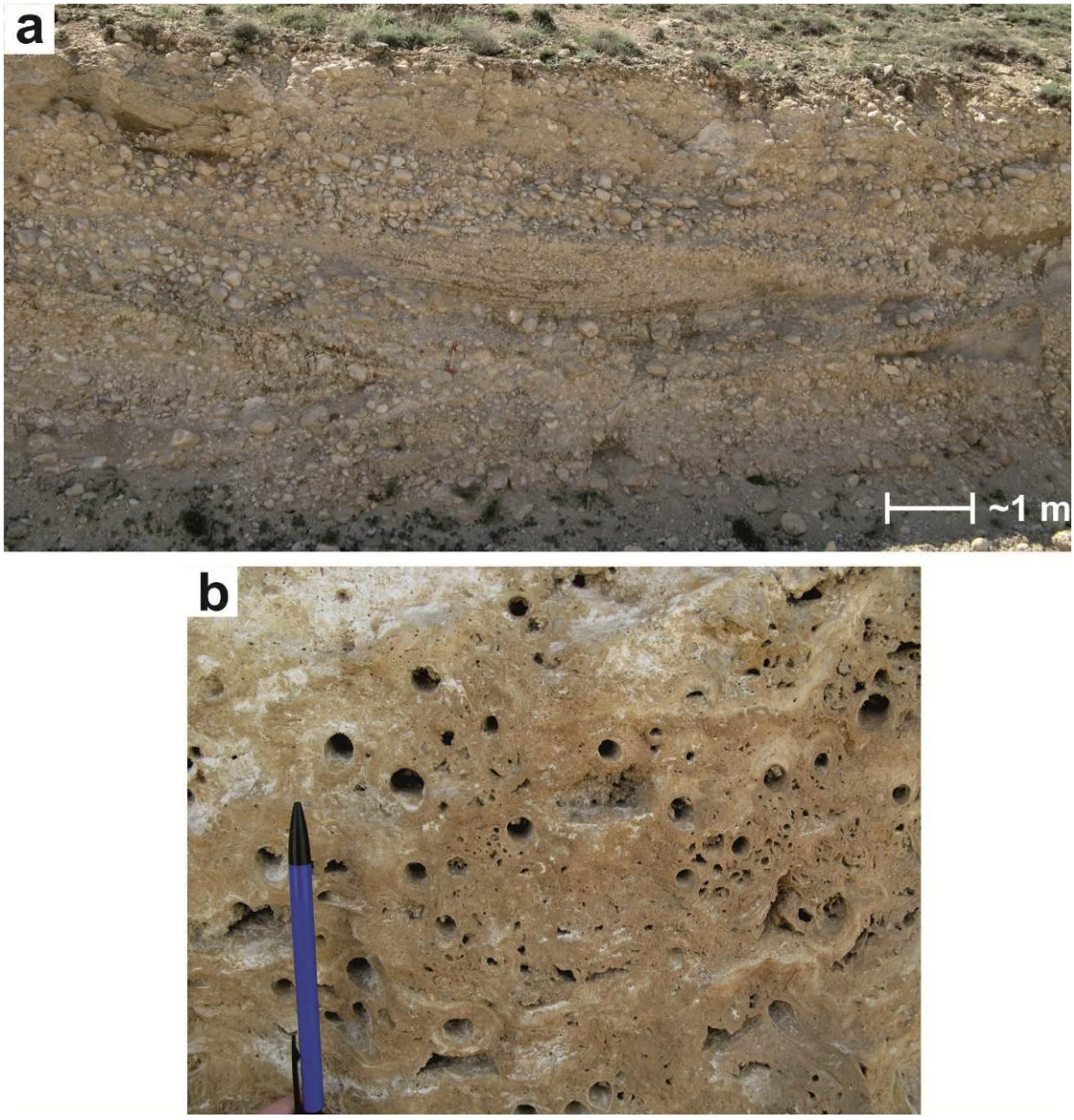

Figure 2.57. Field photographs; a, lenticular, inverse graded conglomerates and sandstones indicating fluvial deposition of reworked basin lithologies; b, tubular structures in tufa deposits.

2.4.6.6 Interpretation of the Çaybaşı Formation

The Çaybaşı Formation represents an entirely non-marine succession from the Pliocene to the Quaternary and present day. It includes fluvially deposited conglomerates and sandstones as well as fresh-water derived tufa deposits.The modern river system may have exploited long lived tectonic weaknesses because many of the fluvial conglomerates are cut into by the modern river system to form ‘terraces’. The tufa deposits indicate periods of cool, flowing fresh water (*e.g.* lakes) where the tubular structures formed around the remains of plant matter (*e.g.* reeds; Pedley 1990; Glover & Robertson 2003).

2.5 STRUCTURAL DEVELOPMENT OF THE DARENDE BASIN

2.5.1 Introduction

Previous work on the structural development of the Darende Basin is limited. Akkuş (1971) reported a range of structures including extensional, compressional and strike-slip fault zones, as well as folds throughout the basin. An attempt was made to categorise the phases of deformation in terms of timing (e.g. Hercynian, Vorgosau, Laramian and Pyrenean). However, these classifications are out of date and were largely unsupported by structural analysis. Other workers (e.g. Gürbüz & Gül 2005) did not conduct structural analysis of the basin.

In order to establish the deformation history, a range of fault planes, fold axial planes and, where present, kinematic indicators (e.g. slickensides, fault steps & shear fabrics) were measured in the field and processed using TectonicsFP (Ortner *et al.* 2002), Steronet7 (Allmendinger 2011) or FaultKin5.2 (Allmendinger 1992; 1995). The aim was to determine the orientation patterns and palaeostress for each of the deformation phases.

The remainder of this chapter will focus on the field description and analysis of the deformation affecting the Darende Basin and draws on sedimentary as well as volcanic evidence to further elucidate the structural history.

2.5.2 Extensional features

2.5.2.1 Extension within Mesozoic rocks

Several high-angle, sinuous, normal fault zones were observed within the Mesozoic limestones of the Geniz Formation. No significant fault scarps are associated with these faults, as is normally the case with strike-slip and oblique faults (see below). The sinuosity of the fault zones could have been caused by reactivation during subsequent phases of deformation, although no cross cutting fault relationships were observed. Extensional faults with a similar orientation were observed within the overlying ophiolitic mélange. In contrast, normal faults were rarely seen in the Maastrichtian-aged sediments. Figure 2.58a shows a possible syn-sedimentary fault zone within Maastrichtian-aged limestones of the Kırankaya Formation. It shows offset of approximately 1 m of two, relatively thickly-bedded limestone beds which are overlain by undeformed, thinly-bedded limestone and red mudstone layers. Some rare examples of normal faults affecting the Ulupınar Formation are shown in Figure 2.58b, although their age cannot be constrained.

Structural evidence for any deformation during the Maastrichtian is sparse. This could be due to reactivation and overprinting by Eocene-aged extension and later compression and strike-slip. Cross cutting relationships are rare. A further problem was the limited outcrop area of Maastrichtian rocks (see map).

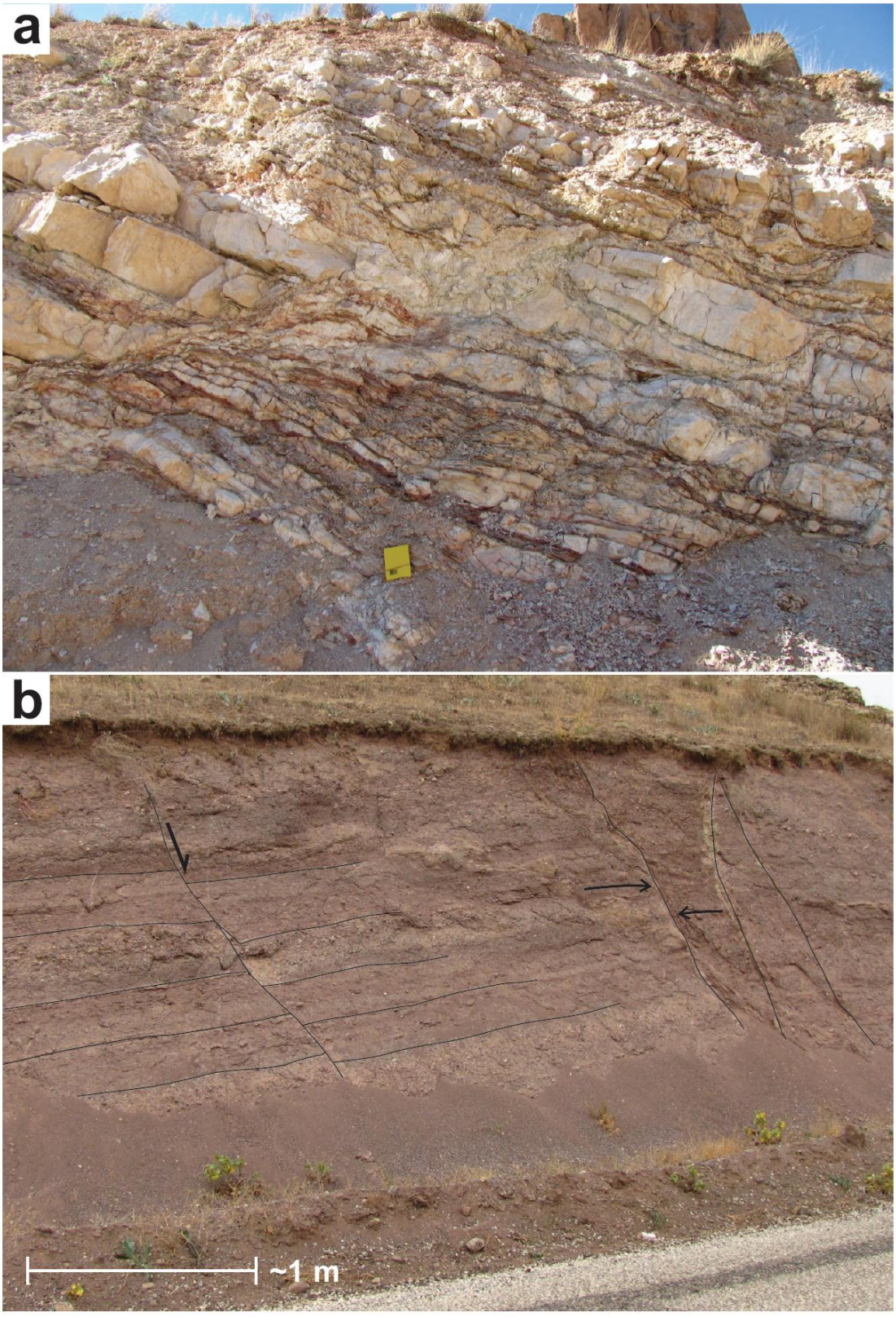

Figure 2.58 Field photographs showing: a, Syn-sedimentary deformation or possibly just extension within limestones and mudstones of the Kırankaya Formation (notebook for scale); b, Extensional faults in the Ulupinar Formation.

2.5.2.2 Extension within Eocene rocks

Numerous normal fault zones were observed within the Eocene facies. The majority of these faults are relatively small in scale (e.g. Fig. 2.59) and may be used as reliable tools for unravelling the structural history of the basin.

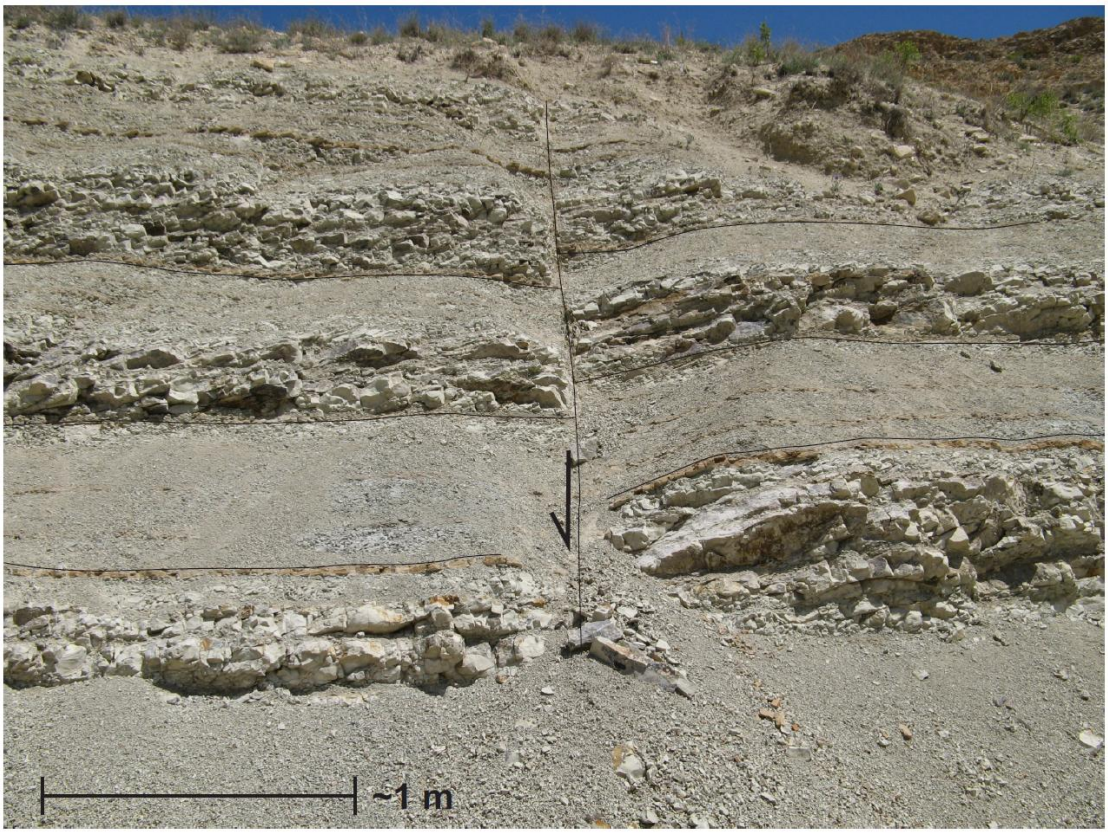

Figure 2.59. Field photograph showing a typical example of a small, vertical, extensional fault in Eocene marls (Yenice Formation).

Evidence of extension is interpreted from coeval 'secondary' structures that were formed as a result of tectonic processes, such as syn-sedimentary deformation.

Marls within the lower part of the Yenice Formation in the south of the basin near the Yenice type section, were affected by syn-depositional deformation. Throughout the lower part of the sequence small-scale slump folds (<1 m amplitude) have affected marl packages <10 cm thick and large-scale slumps (>1 m amplitude) have affected marl packages several metres thick (Fig. 2.60). Sections of isolated, competent calcarenite beds were frequently observed to have slipped over less competent marl and are termed 'rafted blocks'. Some of the rafted blocks have stacked up against each other forming a pseudo

imbrication structure. No preferred orientation could be established from the slump folds. Above ~50 m vertically the marls are parallel bedded and undeformed (see upper part of Fig. 2.60a).

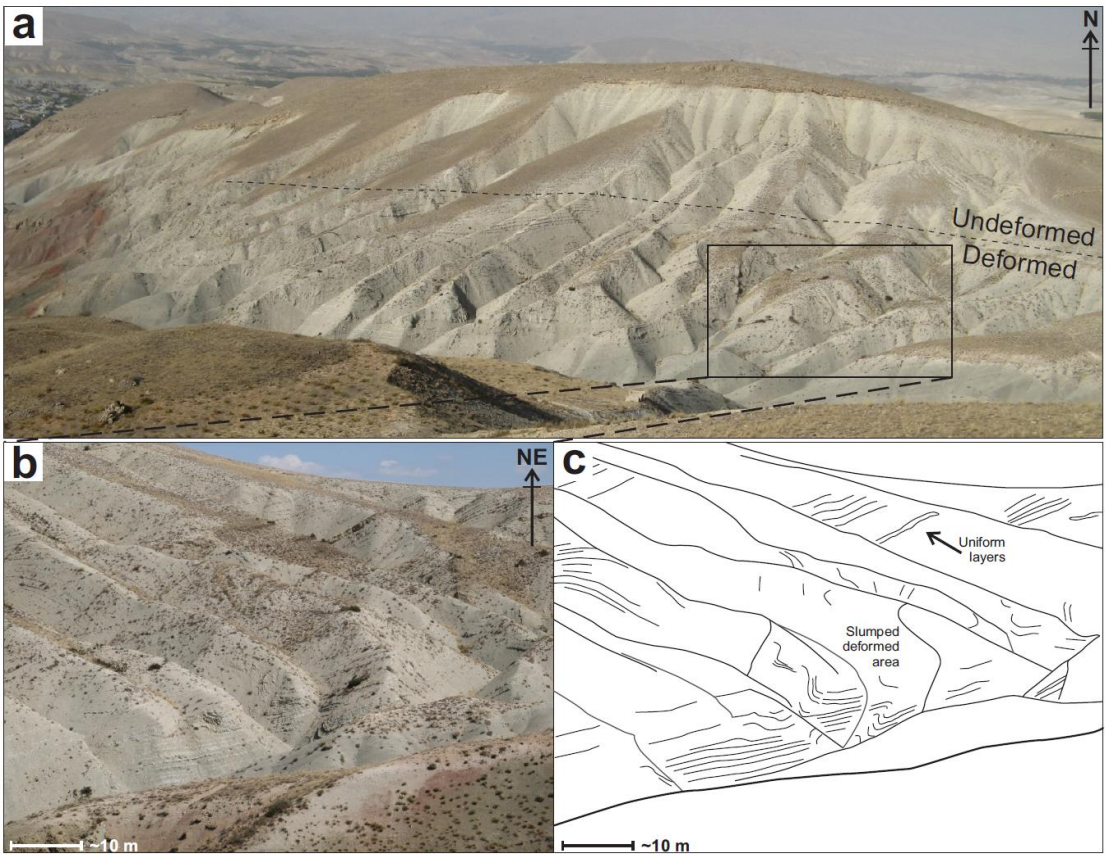

Figure 2.60. Field photographs showing; a, Yenice Formation marls (light grey) on hillside, overlain by calcarenites (brown) outcropping near the ridge line. Note that the lower part of the sequence appears to be chaotic, whilst the upper part remains relatively undeformed; b, Closer view of section highlighted in a; c, Line drawing of b, indicating syn-sedimentary deformation.

An intraformational unconformity was observed in the Yenice Formation where marls have been eroded and disconformably overlain by calcarenite. This could be related to slight tectonic tilting or highly erosive-based sediment flows (Fig. 2.61). The erosive features were not traceable across the entire basin but were observed locally in different parts of the basin indicating that they may be linked to a basin-wide event rather than localised erosive sediment flows.

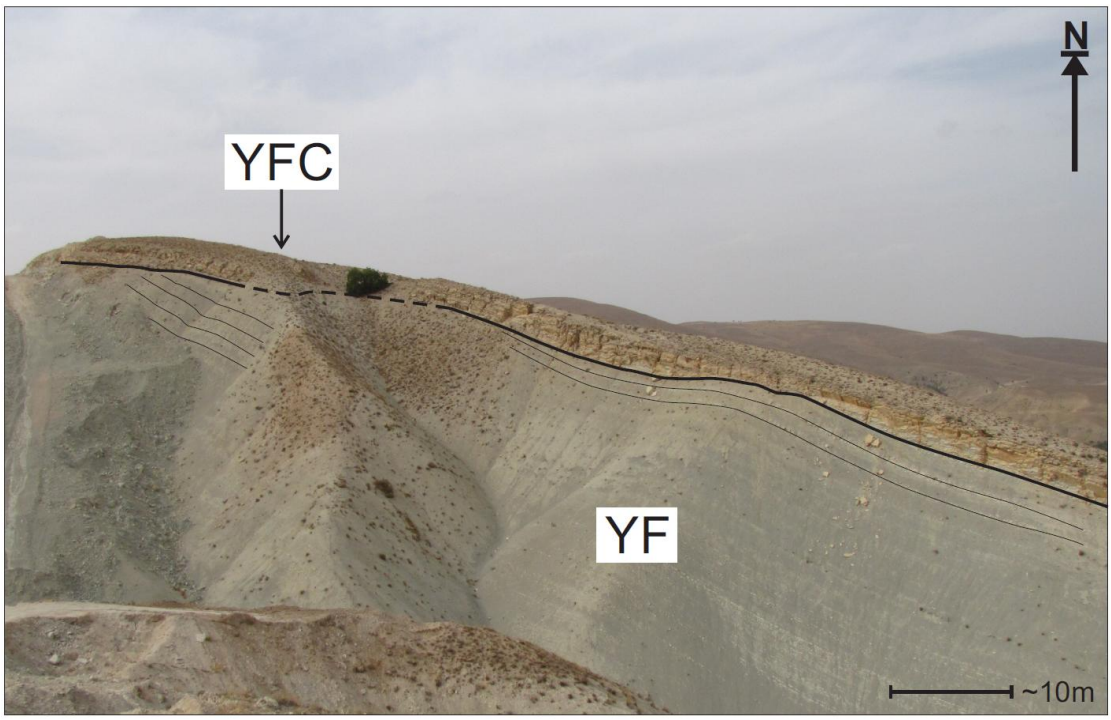

Figure 2.61. Field photograph highlighting a possible internal unconformity and the erosive based nature of the Yenice Calcarenites.

A single syn-sedimentary fault was observed in limestone of the Asartepe Formation in the Karakayalar area, towards the north of the basin (Fig. 2.62). However, the area has been affected by fault reactivation during later stages of deformation (see below) which tends to obscure such features.

Figure 2.62. Field photograph showing a wedge-shaped limestone package within the Eocene-aged Asartepe Formation, potentially indicating syn-sedimentary extensional faulting. However, the fault zone itself is buried by scree and the area has probably experienced fault reactivation.

2.5.3 Compressional features

The basin has a bowl-shaped structure which was possibly generated by compression of the basin-fill by the rigid indenters of the Mesozoic carbonate platform highs situated to the northeast and southwest of the basin. The stereonets in Figure 2.63 a & b show the orientation of sedimentary beds unaffected by deformation in both the northern and southern parts of the basin. These show that the strata in the south of the basin dip ~northeast whereas the strata in the north of the basin dip ~southwest. This reflects regional-scale warping about a NW-SE axis, although sediment compaction could also have played a role.

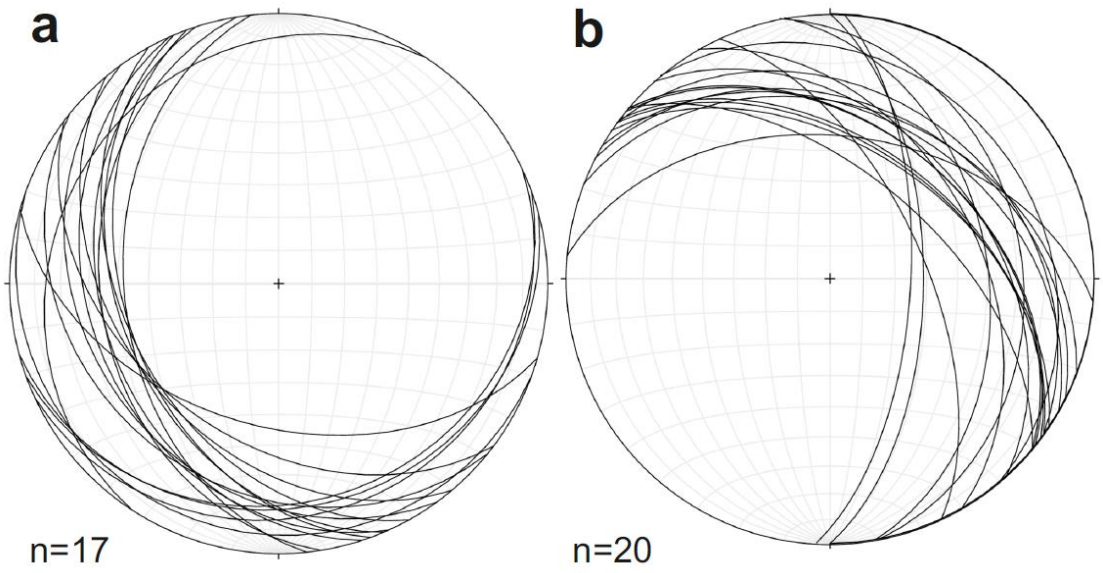

Figure 2.63. Stereonets showing great circles of, a, Bedding measurements taken from undeformed beds along the southwestern margin of the basin, and; b, Bedding measurements taken from undeformed beds along the northeastern margin of the basin.

2.5.3.1 Folding

Folding has affected the Mesozoic formations (i.e. Geniz, Hocalikova, Ulupinar, Tohma and Kirankaya) and the Eocene formations (i.e. Korgantepe, Yenice, Asartepe and Darende) formations to some extent. For example ~10 m-wavelength cylindrical folds were observed in the Darende Formation in the badlands topography to the east of Darende (centre of the basin). However, most of the folding is concentrated towards the

basin margins. There are three notable areas of folding around the basin margins: 1) The northeastern margin where the Darende Formation (the only formation locally exposed) is affected by tight folds ~5 m in amplitude with axial planes inclined 20-45^{o} to the north (Fig 2.64a); 2) The western basin margin where the Asartepe Formation is affected by thrusting and large-scale folding (amplitude >25 m; Fig 2.64b) and the Darende Formation is heavily folded, with fold wavelengths ranging from 1 to 10 m (Fig 2.64c). The fold hinges are locally marked by linear, extensional faults up to 5 m in length, typically with 20 cm offsets; 3) The southern basin margin which is affected by large-scale folding with amplitudes of tens of metres (Fig. 2.64d), together with small-scale symmetrical open folds with amplitudes of <1 m both, probably caused by the northward thrusting of Mesozoic limestone.

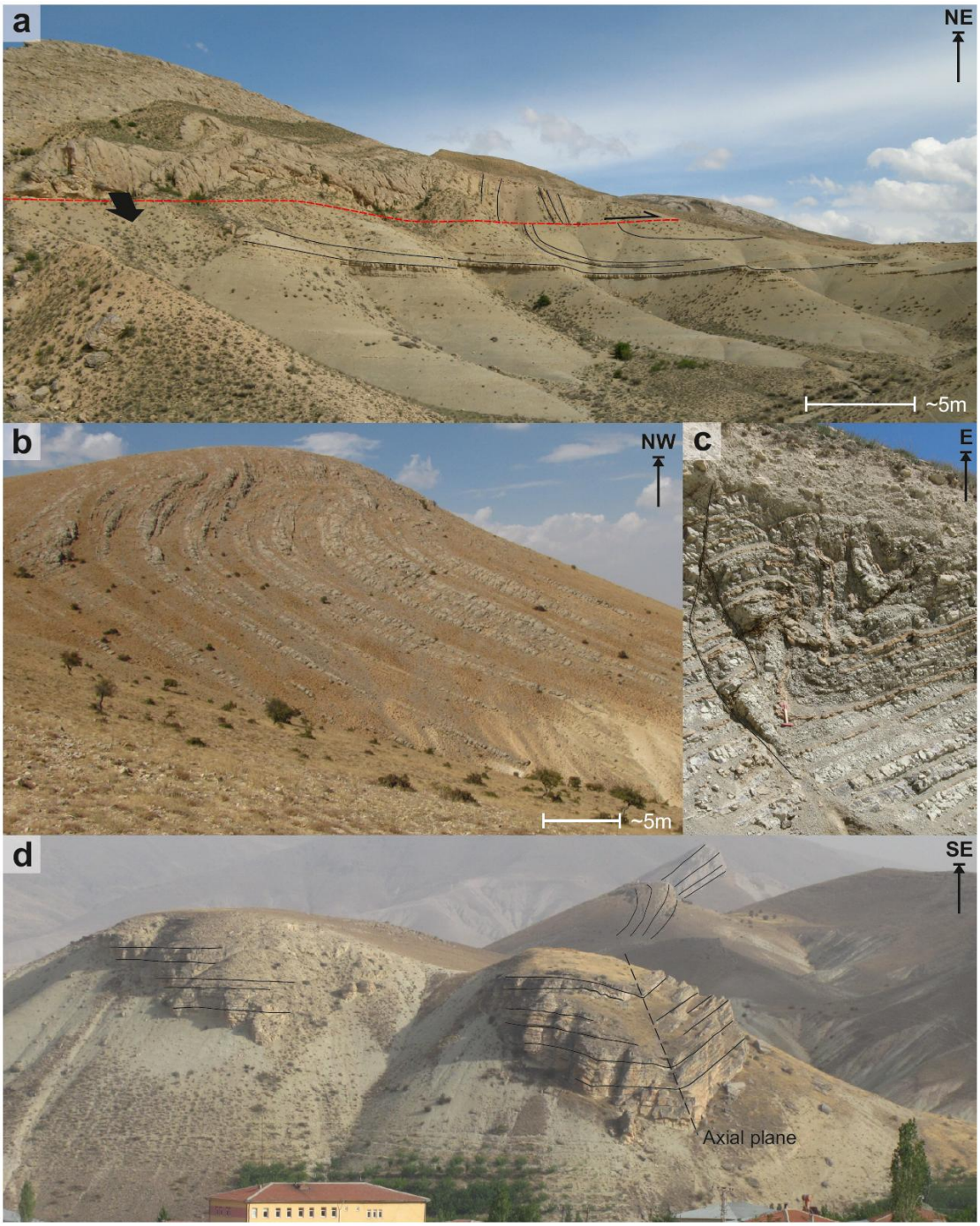

Figure 2.64. Field photographs showing; a, Tight folds within the Darende Formation in the north of the field area which have been affected by later low-angle thrusting; b, Long-wavelength open fold in the south of the field area deforming limestones of the Asartepe Formation; c, Small closed, plunging Z-fold in marls of the Yenice Formation; d, Very long-wavelength open fold affecting Eocene rocks along large parts of the southern basin margin.

Outcrop-scale folds permit direct measurement of axial planes in the field. Figure 2.65 shows great circles of inclined axial planes, taken from a range of localities throughout the Darende Basin. Anticlines (Fig. 2.65a) and synclines (Fig. 2.65b) both show a clustering of E-W orientated great circles which can be explained by ~N-S shortening. The great circles highlighted in blue are clustered in a N-S orientation and indicate E-W compression. These measurements were taken from the western basin margin where some impingement of the Mesozoic carbonate platform may have affected the basin-margin sediments. These faults may thus be localised and may not fit with the structural evolution of the basin. A series of plunging anticlines (Fig. 2.65c) and synclines (Fig. 2.65d) were also measured. The fold axial planes are orientated ~E-W and plunge westwards.

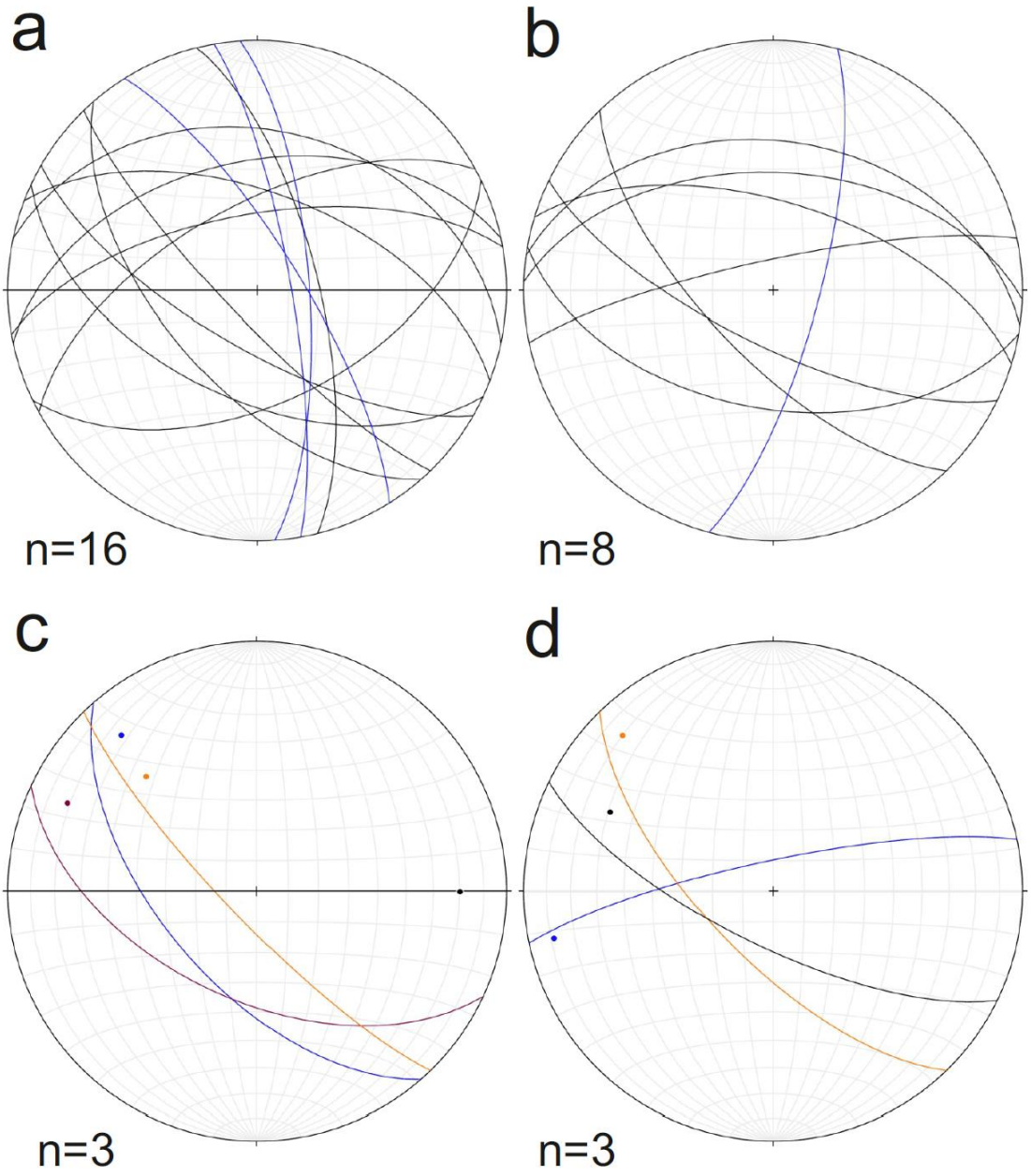

Figure 2.65. Stereonets showing: a, Great circles and poles representing the fold axial planes of anticlines; b, Great circles and poles representing the fold axial planes of synclines; c, Great circles representing axial planes and the trend and plunge of hinge lines of three anticlines; d, Great circles representing axial planes and the trend and plunge of hinge lines of three synclines.

Folds which formed as a result of the propagation of a thrust fault (thrust tip fold) and are subsequently cut through by the thrust (breached thrust propagation folds) were observed in thick limestone sequences of the Asartepe Formation in the northern part of the basin (Fig. 2.66).

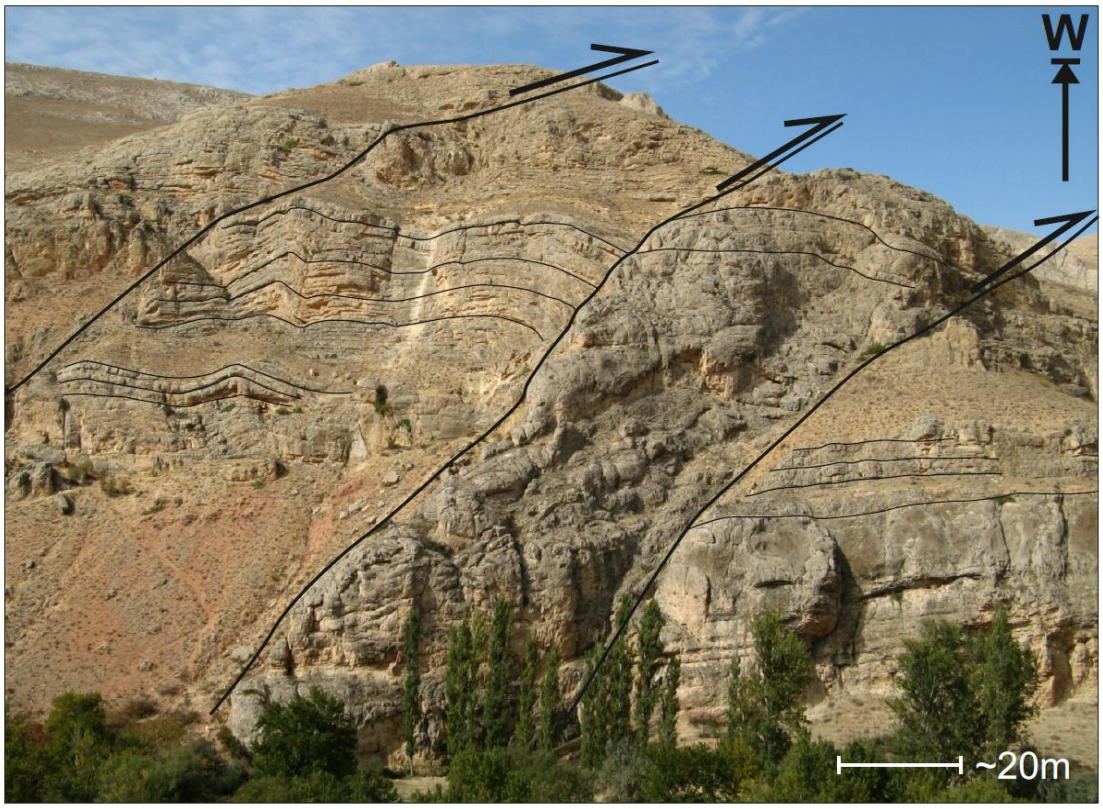

Figure 2.66. Annotated field photograph showing thrust faults and breached thrust-propagation folds in Eocene limestones of the Asartepe Formation.

Figure 2.67 shows asymmetrical chevron folds (~metre scale wavelengths) within a large-scale anticlinal structure (~100 m wavelength) that deformed the Mesozoic limestones of the Geniz Formation, ~10 km to the east of the field area.

Figure 2.67. Field photograph showing asymmetrical chevron folds within a larger scale anticline that deforms limestones of the Geniz Formation.

2.5.3.2 Reverse faulting

Compressional faults are widespread. Mesozoic limestones in the southwest, directly south of Yenice, are thrust northwards onto the latest Cretaceous mélange, marked by sinuous low-angle thrusts with well developed shear fabrics. A road-cut to the east of the basin exposes a thrust zone which has emplaced limestones of the Geniz Formation northwards onto a sliver of intensely sheared ophiolitic mélange. Within the Çukurkaya valley to the north of Darende, limestones of the Asartepe Formation are affected by at least three north-verging sinuous thrusts, with displacements of at least 10 m. Facies change and thickness variations (e.g. from massive to bedded limestones) enabled fault zone displacement to be estimated for some fault zones, as these changes could be traced across fault zones (i.e. piercing points, Fig. 2.66). Two *en-echelon* low-angle thrusts occur together with decametre-scale folds, along the poorly exposed western margin of

the basin, near Günpınar. The lower thrust fault has emplaced a slice of Eocene limestone of the Asartepe Formation northwards onto Upper Eocene marls and sandstones of the Darende Formation. The higher thrust has emplaced a slice of Mesozoic limestone northwards over Eocene sediments. Cataclastic fault breccias, up to ~25 cm thick, are present along the two major fault planes. In the east of the basin, conglomerates of the Ulupınar Formation are thrust northwestwards over ophiolitic mélange and a Maastrichtian patch reef (Tohma Member). Observations of slickensides and fault steps confirm that the faulting is compressional.

Forty three thrust faults of various dimensions were measured in the field. The dip directions of all the fault zones were plotted on a Rose diagram (Fig. 2.68a) and indicate a strong N-S orientation of dip direction. Fig. 2.68b shows the fault planes plotted as great circles on a stereonet and indicate an E-W orientation for the fault zones. The poles to the fault zones (Fig. 2.68c) and a contour plot of the poles (Fig. 2.68d) suggest a strong clustering in the N-NE (indicating faults inclined to the south) and S-SW (indicating faults inclined to the north). This clustering is indicative of ~N-S shortening.

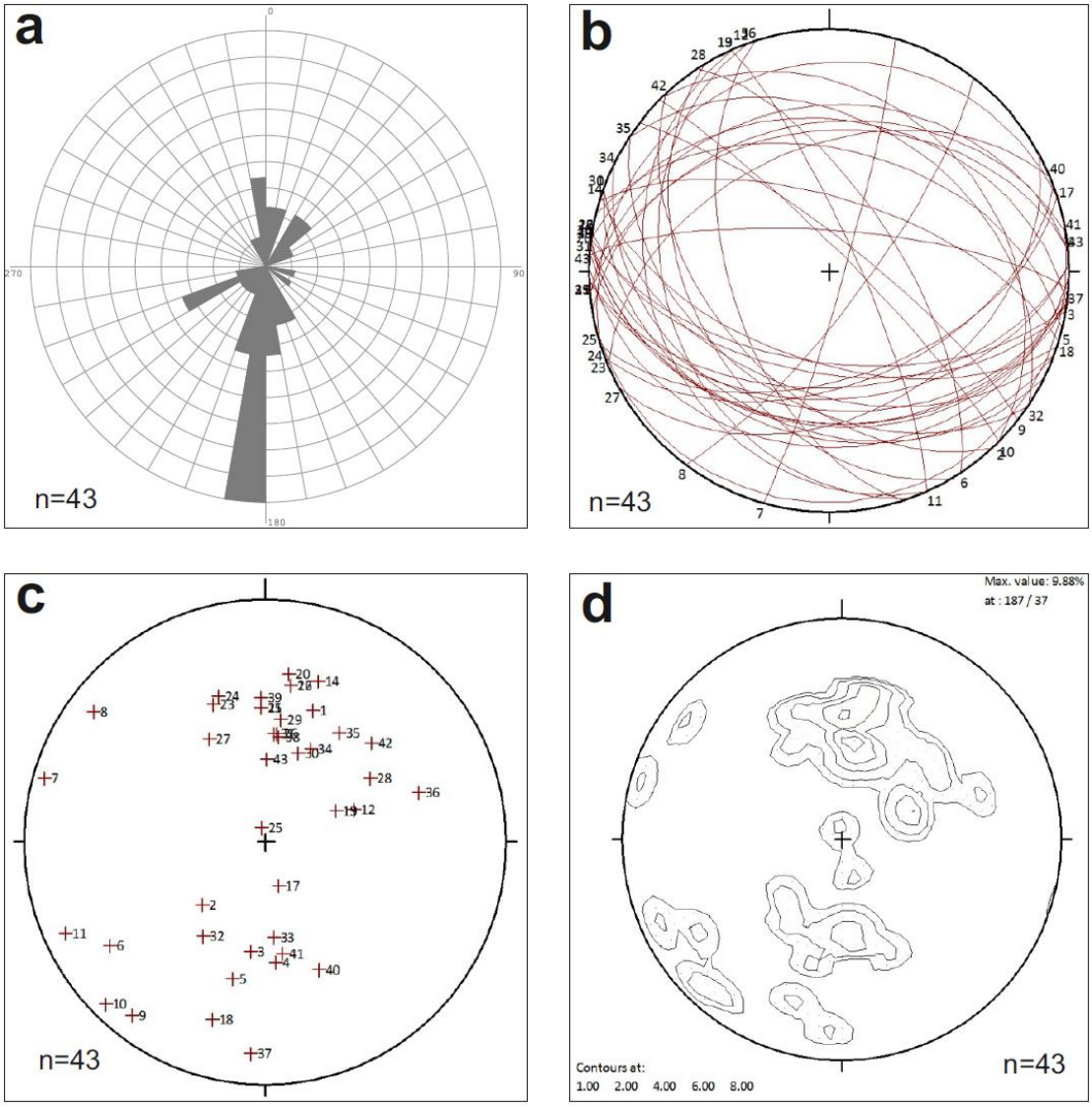

Figure 2.68. a, Rose diagram showing the dip directions of all of the thrusts in the Darende Basin; b, Stereonet showing great circles of all of the thrust planes; c, Stereonet showing poles to thrust planes; d, Contour plot of poles to thrust planes indicating a clustering of poles in the north and south.

Of the 43 thrust faults measured in the field, 12 were observed with slickensides and other associated kinematic information (e.g. fault steps) indicative of offset direction.

A rose diagram showing the dip direction (azimuth) together with the plunge of the slickensides associated with the 12 fault zones indicates that most of the faults moved either to the NE or the SW (Fig. 2.69a). Plotting the fault zones and kinematic data on an Angelier diagram (Angelier 1994; Fig. 2.69b) implies a ~NE-SW direction of shorting. A single fault measured in the field as compressional plots as an oblique sinistral fault in

Stereonet5.2. This unresolved fault zone could have been incorrectly measured in the field or may belong to a separate phase of deformation.

The fault-plane solutions shown in Fig 2.69c are indicative of slip along a fault where P & T represent the axes of maximum shortening and extension, respectively. The B axis is located at the intersection of the fault plane and auxiliary planes. The P-, B- and T- axes are assumed to be approximately parallel to the principal stress orientations σ1, σ2 and σ3, respectively. Furthermore, the clustering indicates a homogenous data set. The probability that the faults comprising the homogenous data set occurred in the same palaeostress regime can be calculated (R). TectonicsFP contains a useful function which automatically calculates R for each of the P-, B- and T- axes. For example, the mean vector of the principal compressional stress (P-axis, σ1) is orientated 037/03 with 65% confidence calculated using R probability. The mean vector of the principal extensional stress direction (T-axis, σ3) is orientated ~NW-SE with 66% confidence. When the potentially dubious sinistral strike-slip fault is discounted the confidence of the principal compressional and extensional stress orientations increases to 73% and 76%, respectively.

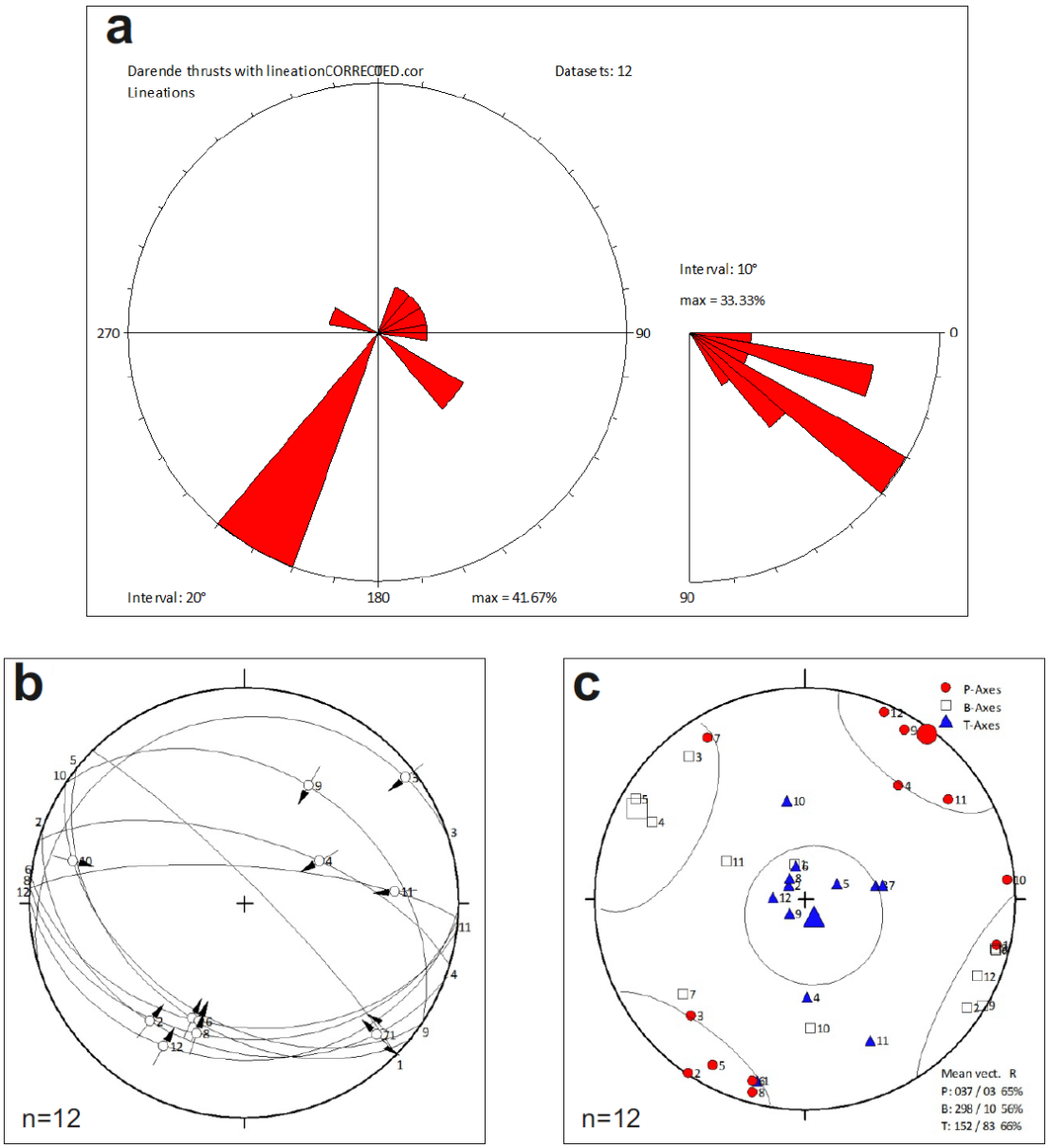

Figure 2.69. a, Rose diagram showing the dip direction (and dip angles) of the 12 thrust planes with associated kinematic information; b, Angelier plot of the thrust planes with movement directions; c, P-, B- and T-axes calculated from the fault plane solutions together with mean vector and R* (see text for discussion).

Compression-related shear fabrics (e.g. CS type fabric) are associated with some thrust zones. Fig. 2.70 shows 4 thrust faults (solid lines) with associated shear fabric orientations (dashed lines). Two of the fault zones trend ~E-W and two trend ~NW-SE. However, all of the associated shear fabric orientations trend ~E-W. This indicates that the two fault zones, which trend ~NW-SE, are likely to be oblique-slip compressional faults, i.e. 'transpressional'. This could be the result of reactivation along favourably orientated, pre-existing (Late Cretaceous or Early-Mid Eocene) extensional faults.

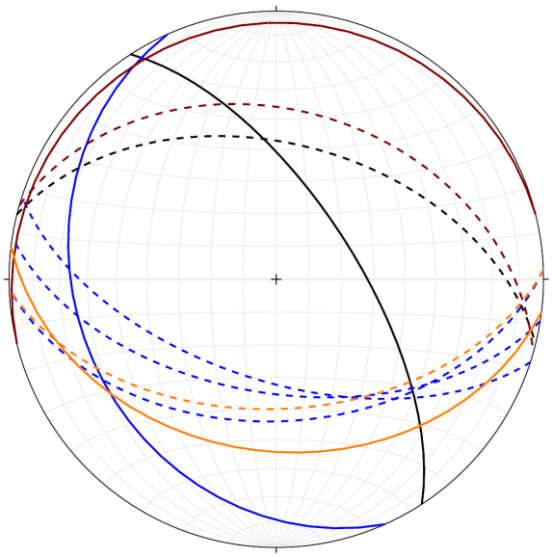

Figure 2.70. Stereonet showing 4 fault planes (solid lines) with associated shear fabrics (dashed lines).

Along the western margin and atop ridges to the east of the Darende Basin, horizontally-bedded, Middle Miocene limestones (Tahtalı Formation) unconformably overlie the Eocene formations. The Tahtalı Formation is affected by neotectonic (i.e. Miocene–recent) strike-slip faulting but is unaffected by the extension and compressional phases.

2.5.4 Strike-slip faulting

Numerous strike-slip faults were observed in the Darende Basin and are associated with neotectonic deformation. Most of the neotectonic strike-slip faults were observed in transverse vertical sections (e.g. in valleys and canyons). It was, therefore, difficult to evaluate lateral offsets. Fault cores are generally absent as usually only one slip surface remains as a fault scarp.

Kinematic data (e.g. slickensides) were frequently observed on exposed fault scarps. Fifty eight fault planes identified as strike-slip faults were measured across the Darende Basin (Fig. 2.71 a-d). Of these, 25 display slickensides with kinematic orientations sufficient to delineate offset direction (i.e. sinistral vs. dextral). However, no patterns were observed when both sinistral and dextral faults were plotted together (Fig. 2.71 e & f).

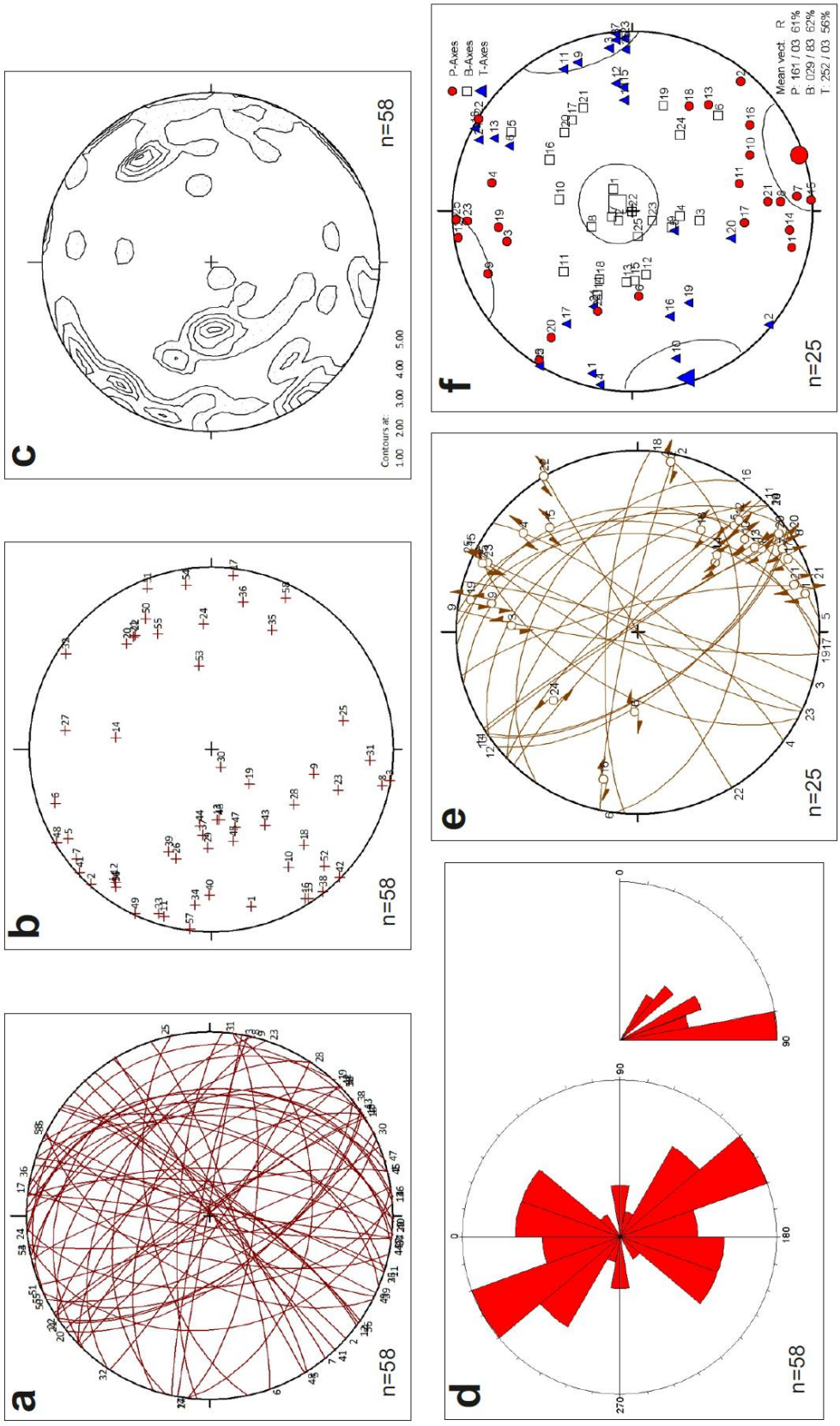

Figure 2.71. a, Stereonet showing great circles of all strike-slip faults in the Darende Basin; b, Stereonet showing poles of strike-slip fault planes; c, Contour plot of 2.67b; d, Bidirectional rose diagram of all strike slip faults; e, Angelier plot showing great circles of strike-slip fault planes with associated kinematic features (slickensides), and; f, P-, B- and T-axes fault plane solutions

together with mean vector and R* calculation.

13 strike-slip faults displayed slickensides which indicate a dextral sense of movement (Fig 2.72 a & b).

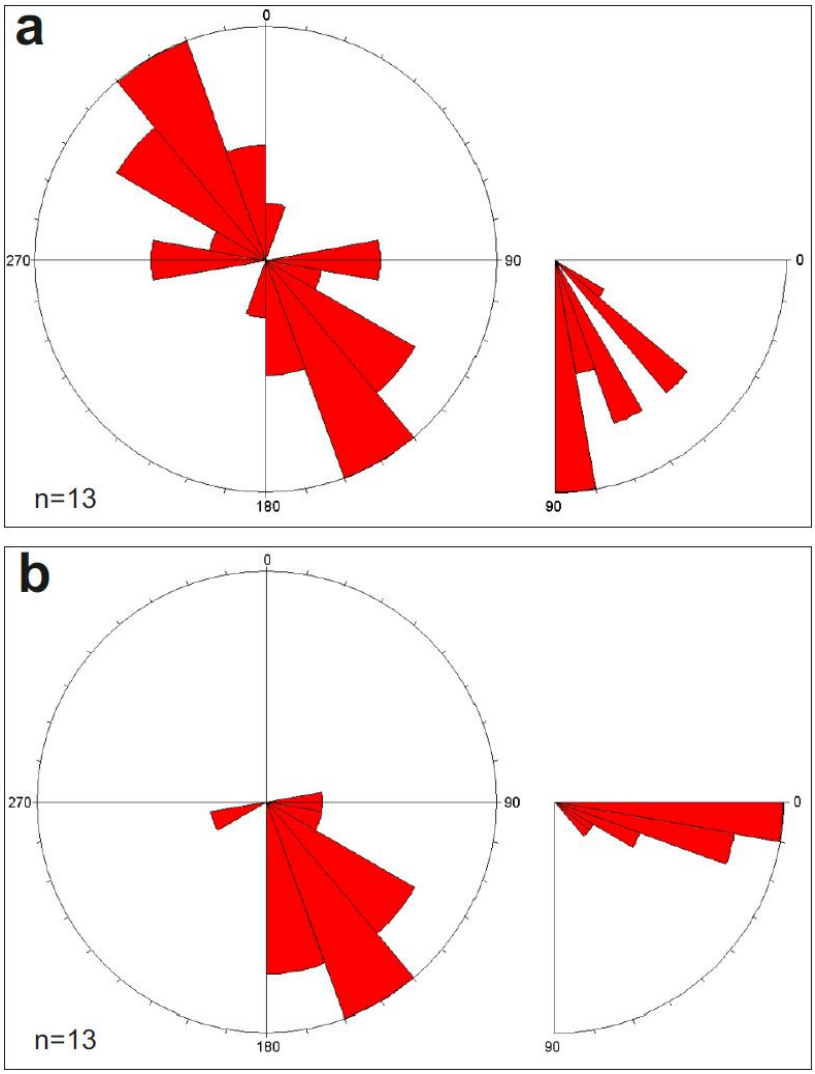

Figure 2.72. a, Bidirectional rose diagram of all dextral strike-slip faults with associated kinematic features, and; b, Azimuth and plunge of slickensides associated with these dextral strike-slip faults.

An Angelier plot (Fig 2.73a) for the data suggests an approximate NW-SE trend. The P-axis is orientated at 187/17 (R=64%), the B-axis at 008/74 (R=65%) and the T-axis at 098/06 (R=64%) which supports a NW-SE orientation as the P and T-axes (which are ~parallel with σ1 and σ3) are ~ horizontal, whereas the B-axis (~parallel with σ2) is ~vertical (Fig. 2.73b).

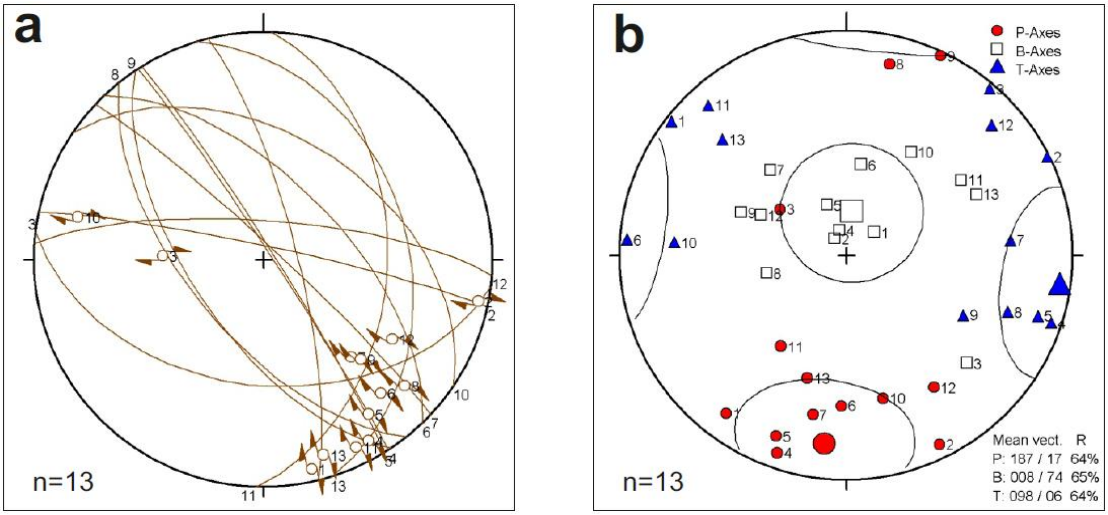

Figure 2.73. a, Angelier plot showing great circles of dextral strike-slip fault planes together with offset direction (predominantly orientated NW-SE), and; b, P-, B- and T-axes calculations together with mean vector and R*.

Twelve strike-slip faults display slickensides which indicate a sinistral sense of movement (Fig 2.74 a & b).

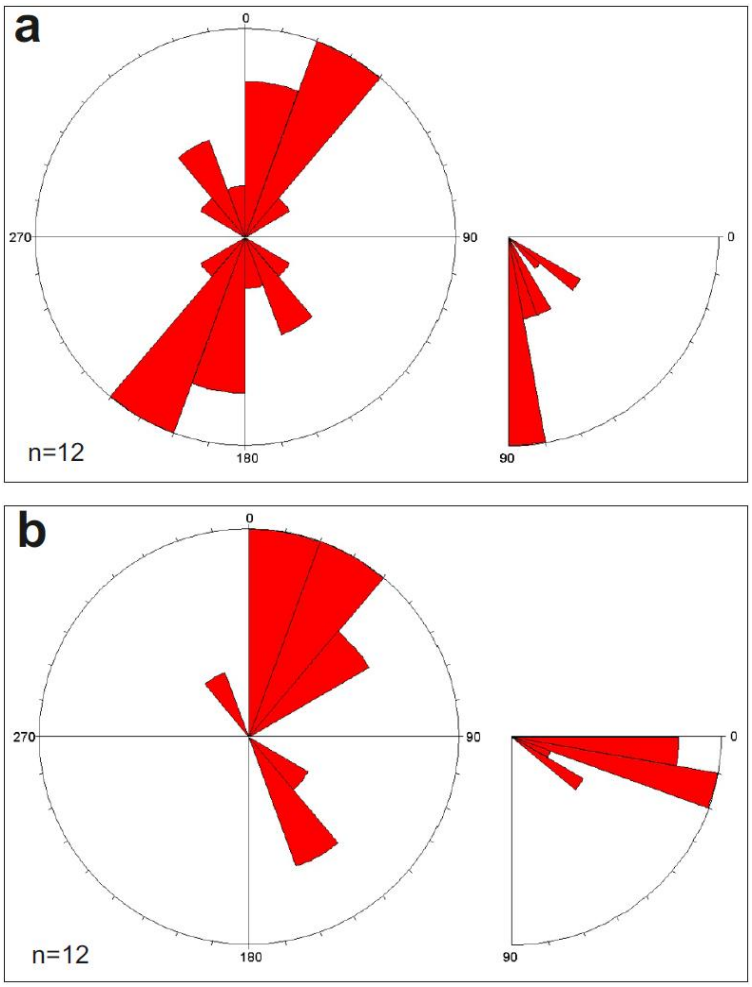

Figure 2.74. a, Bidirectional rose diagram of all sinistral strike-slip faults with associated kinematic features, and; b, Azimuth and plunge of slickensides associated with these sinistral strike-slip faults.

An Angelier plot (Fig 2.75a) for the data suggests an approximate NE-SW trend. The P-axis is orientated at 355/11 (R=65%), the B-axis at 129/84 (R=64%) and the T-axis at 267/08 (R=52%) which supports a NE-SW orientation as the P and T-axes (which are ~parallel with σ1 and σ3) are ~ horizontal whereas the B-axis (~parallel with σ2) is ~vertical (Fig. 2.75b).

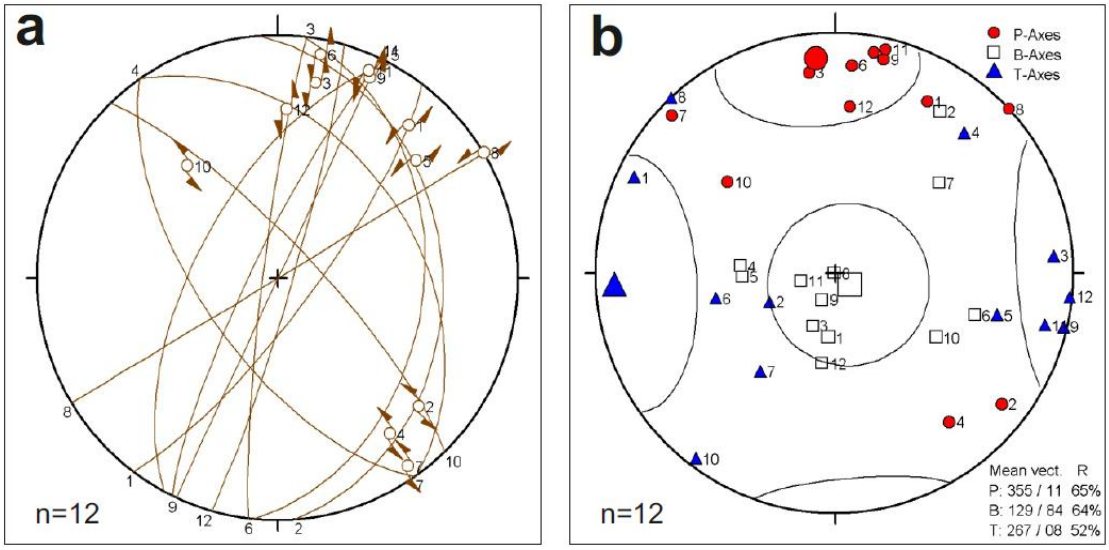

Figure 2.75. a, Angelier plot showing great circles of sinistral strike-slip fault planes together with offset direction (predominantly orientated NE-SW); b, P-, B- and T-axes calculations together with mean vector and R*.

Figure 2.76 shows slickensides crosscutting an earlier set of slickensides which is interpreted as evidence for structural reactivation of fault planes during successive deformation phases.

Figure 2.76. Photograph showing a high-angle fault plane with a set of slickensides dipping towards the SE (oblique dextral), overprinted by a set of slickensides dipping towards the NW (unresolved).

2.5.5 Interpretation of structural data

During this study the deformation affecting the region has been divided into 4 main phases: 1) Late Cretaceous (Maastrichtian) extension; 2) Early Eocene (Ilerdian-Lutetian) extension; 3) Late Eocene-Oligocene compression, and; 4) Miocene to Recent strike-slip.

Normal faults were observed within the Mesozoic Geniz and Hocalikova Formations. However, relatively few normal faults were observed in the Maastrichtian basin sediments, which could indicate that an extensional phase could have initiated the basin, but ceased prior to the onset of Maastrichtian sedimentation. The Maastrichtian sediments are relatively thin compared with, for example, the Hekimhan Basin where there is much evidence of extension (chapter 3). Eustatic sea level fell throughout the Maastrichtian (Miller *et al.* 2005) making it unfeasible for sedimentation in the Darende Basin to be solely controlled by eustacy. A shallow-angle unconformity exists between the Maastrichtian sediments and the overlying Eocene sediments. However, in places the unconformity is high-angle and is best explained by block rotations (extension) of Maastrichtian sediments prior to the onset of Eocene sedimentation. Localised extensional faults within Mesozoic rocks and possible syn-sedimentary faulting fit well with a regional interpretation of extension-controlled basin formation during the Maastrichtian (post-ophiolitic mélange emplacement) which has been well documented in other Late Cretaceous-Paleogene basins in Turkey, e.g. the Ulukışla Basin (Nairn *et al.* in press) and the Hekimhan Basin (see chapter 3).

Evidence for extension during the Eocene is more compelling. A syn-sedimentary fault zone was observed in limestones of the Asartepe Formation although few other age-constrained extensional fault zones were observed in the field. However, numerous slump folds and an intraformational unconformity were also observed in Eocene marls at the base of the Yenice Formation. These are interpreted to be the result of syn-sedimentary extension of the Darende Basin. The Karakayalar Member (composed of alkali basalts and volcaniclastic material) is interpreted to have erupted during the Early Eocene in a rift-related setting based on geochemical analysis (see Chapter 2.4.5.4) and, therefore, provides further evidence for extension during this time.

The timing and direction of compression is well constrained in the Darende Basin. Folding and faulting affects both Eocene and Mesozoic rocks. Fold axes and thrust fault orientations measured from all strata in the Darende Basin predominantly trend E-W to NW-SE, respectively indicating ~N-S orientated compression. Folds and thrusts affect all of the Eocene and Maastrichtian-aged sediments. Additionally, the ophiolitic mélange may have acted as a décollement surface during the compression. Deformed Eocene formations are overlain by undeformed, horizontally bedded Middle Miocene shallow-marine sediments indicating that compression must have occurred during the latest Eocene to Oligocene and must have ceased prior to the the Middle Miocene. However, folding may predate thrust faulting in the basin as none of the compressive faults are themselves folded. In contrast, in the north of the basin, thrust propagation folds have been breached by thrust faults. Deformation of the Tauride carbonate platform has been dated as Eocene in the Gürün area (Robertson *et al.* in press) to the north of the field area and it is likely that the folding and thrusting seen in the Darende Basin is of similar age.

Strike-slip faulting affected all of the formations in the Darende Basin. The majority of the sinistral strike-slip faults are orientated NE-SW, sub-parallel to the sinistral Malatya-Ovacık fault zone (Kaymakcı *et al.* 2006) and Göksu fault zone (Kozlu *et al.* 1990). The Malatya-Ovacık and Göksu fault zones are themselves sub-parallel with the East Anatolian Fault Zone (EAFZ,) and could represent major intracontinental splay faults of the dextral North Anatolian Fault Zone (NAFZ) (Koçyiğit & Beyhan 1998). The majority of the dextral fault zones are orientated ~NW-SE, sub-parallel with the dextral NAFZ. Sinistral movement along the EAFZ and dextral movement along the NAFZ accommodate the (current) westward escape of Anatolia and Turkey (Westaway *et al.* 2008). The sinistral and dextral faults affecting the Darende Basin may, in principal, have occurred during different deformation phases. Some evidence of reactivation was observed in the field which supports this. However, the NW-SE trending dextral and NE-SW trending sinistral faults in the Darende Basin fit well with the westward tectonic escape model (Piper *et al.* 2010). Furthermore, the Darende Basin may represent an intracontinental relay or strain transfer zone, although a detailed interpretation lies beyond the scope of this thesis.

2.6 BASIN DEVELOPMENT

The stratigraphically lowest unit in the Darende Basin, the Geniz Formation, is interpreted as part of the regional Jurassic-Cretaceous Tauride carbonate platform. This developed after Triassic rifting during a phase of passive margin subsidence of the Tauride-Anatolide microcontinent bordering Neotethys (Demirtaşlı *et al.* l984; Perincek & Kozlu l984; Özgül l996 Taslı *et al.* 2006; Robertson *et al.* in press).

The overlying ophiolite-related mélange (Hocalikova Formation) was formed by a combination of tectonic and sedimentary processes, although the local outcrop is too small to permit detailed interpretation. Elsewhere in the region similar mélange was emplaced onto the northern margin of the Tauride platform in the Gürün area, northwest of the Darende Basin during Campanian-Maastrichtian time (Perinçek & Kozlu, l984; Robertson *et al.* in press). The lithologies were accreted above a northward-dipping subduction zone within the Inner Tauride ocean and then emplaced southwards onto the Tauride carbonate platform during latest Cretaceous time (Robertson *et al.* in press). The ophiolitic rocks themselves are likely to have formed in a supra-subduction zone setting, probably related to the subduction of the Inner Tauride ocean (Görür *et al.* 1984), as inferred for other ophiolites overlying the Tauride-Anatolide microcontinent (Robertson, 2002, 2006; Parlak *et al.* 2000, 2004, 2009).

2.6.1 Latest Cretaceous

Erosion of the Mesozoic carbonate platform and the poorly consolidated ophiolite-related mélange was followed by deposition of the Maastrichtian reddish, non-marine sediments (Ulupınar Formation). Fluvial deposition in a braided system is indicated by the erosive, channelised and cross-bedded nature of many of the beds, coupled with the ubiquitous clast rounding. Local changes in sediment thickness reflect deposition over a variable palaeotopography including ‘highs’ and ‘lows’ (Fig. 2.58). Deposition was initiated in the south of the basin in topographic depressions created by erosion or faulting. Once filled, an unconstrained braided fluvial system prograded generally northwards across the basin. Similar red continental clastic sediments accumulated in the east of the basin (Hisarcık area), where palaeocurrents trend westwards.

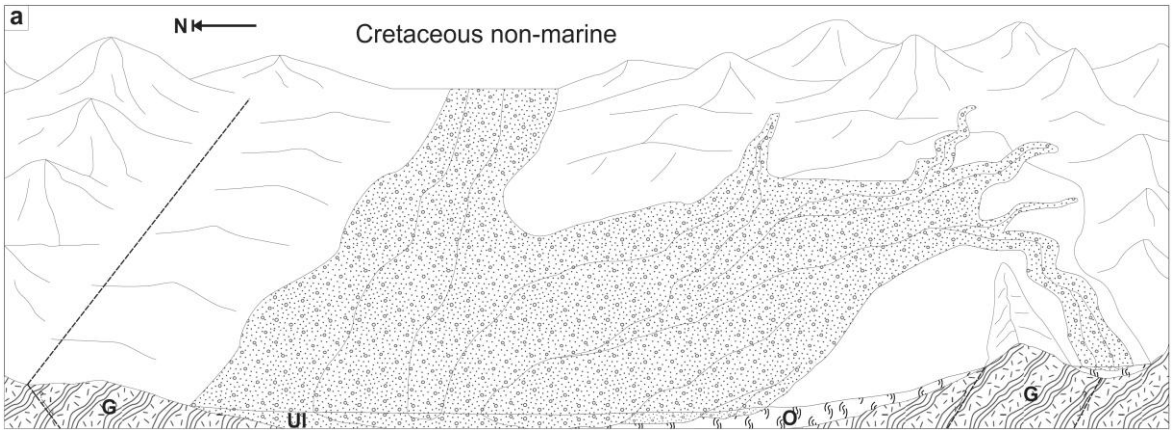

Figure 2.58. Palaeogeographic reconstruction of the latest Cretaceous (Maastrichtian) clastic deposition (Ulupınar Formation). G, Geniz Formation; O, Hocalikova ophiolite Formation; Ul, Ulupınar Formation.

The subsequent marine transgression during the Maastrichtian was characterised by the development of the rudist-rich patch reefs (Tohma Member) on elongate topographic highs (Fig. 2.59). The rudist reefs nucleated on relatively immobile non-marine clastic sediments and then grew on top of each other to form mounds. Rudist bivalves as a whole flourished in tropical waters, before becoming extinct at the Cretaceous-Tertiary boundary (Steuber & Loser 2000).

The relatively thin variable facies near the margin of the basin (Kırankaya Formation), including bird's-eye texture, pedogenesis, palaeosols and caliche formed a very shallow-marine to evaporitic environment, followed by emergence.

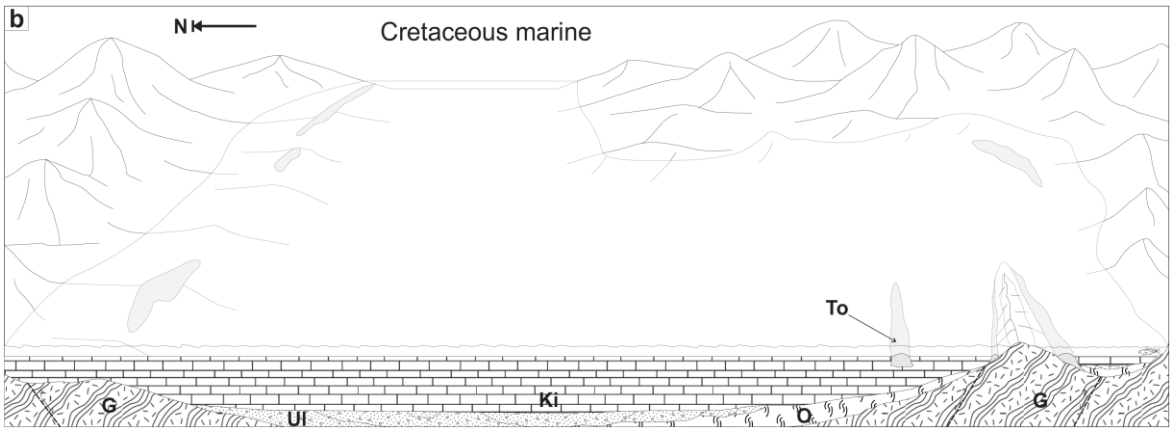

Figure 2.59. Palaeogeographic reconstruction of the latest Cretaceous (Maastrichtian) marine Kırankaya Formation and Tohma Member deposition. Kı, Kırankaya Formation; To, Tohma Member; G, Geniz Formation; O, Hocalikova ophiolite Formation; Ul, Ulupınar Formation.

2.6.2 Palaeocene-Early Eocene emergence

The basin appears to have remained emergent throughout Paleocene-Early Eocene time. A less likely alternative is that sediments of this age range were deposited but then completely eroded. The implied hiatus contrasts with some other basins in central Anatolia that include Paleocene sediments, namely the Ulukışla, Kırıkkale, Tuz Gölü, Çankırı and Sivas basins (Nairn *et al.* in press). The absence of Paleocene deposition in the Darende Basin could be explained by sedimentary infill of the shallow Late Maastrichtian basin, coupled with eustatic regression (Miller *et al.* 2005). However, tectonics must also have played a role because in some locations the Maastrichtian sediments were tilted by up to ~40^{o} prior to the deposition of the overlying Middle Eocene facies (Fig. 2.23).

2.6.3 Middle Eocene transgression

Eustatic sea level rose throughout the Ypresian (Early Eocene) (Miller *et al.* 2005). However, the oldest Eocene sediments dated during this study (Korgantepe Formation) are of Lutetian (Middle Eocene) age (Fig. 2.5), a time when eustatic sea level was apparently lower than during the preceding Ypresian Stage. The benthic fossil assemblages and reworked nature of the sandstones in the Lutetian formation indicate a high-energy shoreface, to shallow-marine setting. Erosion of topographic highs to the south of the Darende Basin is likely to have supplied ophiolite-related clastic material, as indicated by the local NW-directed palaeocurrents. The angularity of the clasts in the local basal breccias suggests rapid erosion of an irregular topography. This was probably caused by penecontemporaneous faulting.

The Mid-Eocene volcanism (Karakayalar Member) began in a submarine setting, as suggested by the shallow-marine benthic fauna beneath. Occasional pillow lavas also indicate subaqueous eruption. The volcanic pile emerged in the northeast of the area, giving rise to volcaniclastic debris flows in a slope setting. Overlying conglomerates with well-rounded basalt clasts and numerous large foraminifera reflect fluvial reworking of pre-existing marine material (Fig. 2.60).

The Mid-Eocene Yenice Formation represents continued transgression and deepening of the Darende Basin. The biostratigraphical evidence suggests that the shallow-marine Korgantepe Formation and the deeper-marine Yenice Formation are likely to be contemporaneous, although not exposed together. Northward-flowing turbidity currents introduced sands derived from the ophiolite-related 'basement', although this sediment did not reach the northernmost parts of the basin. In addition, northwesterly-flowing turbidity currents carried bioclastic carbonates from a marginal carbonate shelf (Fig. 2.60). The basin hinterland in the south is likely to have been uplifted and eroded while the basin margins subsided stimulating carbonate production.

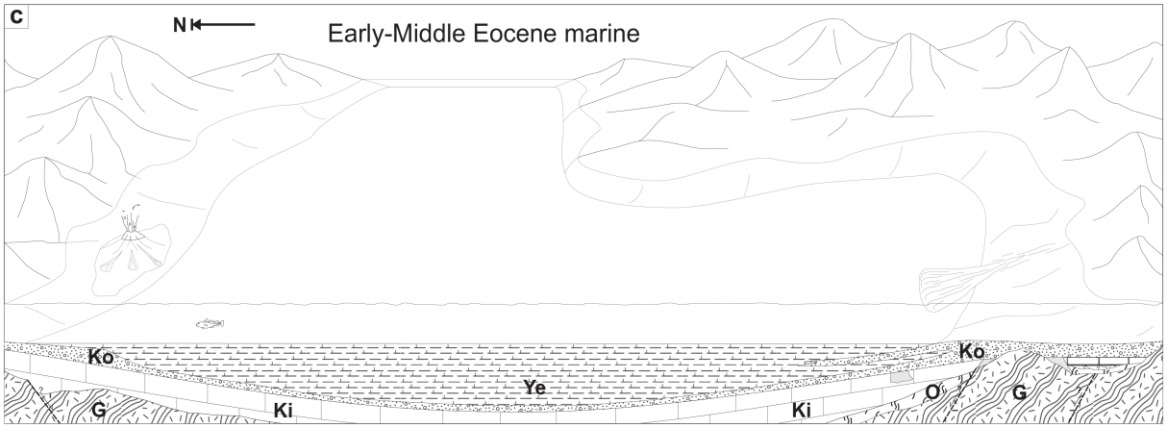

Figure 2.60. Lutetian shallow-marine transgression onto Paleocene unconformity (Korgantepe and Yenice Formations), together with localised alkaline volcanism and northward directed turbidity flows. Kı, Kırankaya Formation; To, Tohma Member; G, Geniz Formation; O, Hocalikova ophiolite Formation; Ul, Ulupınar Formation; Ko, Korgantepe Formation; Ye, Yenice Formation.

2.6.4 Late Eocene shallow-marine carbonates

The conformably overlying shallow-marine limestones (Asartepe Formation; Fig. 2.61) record progressive shallowing of the basin during the Late Lutetian. Clastic sediments continued to be derived from the ophiolite-related mélange, either directly, or by cannibalisation of pre-existing sediments containing this material (i.e. Ulupınar and Korgantepe Formations).

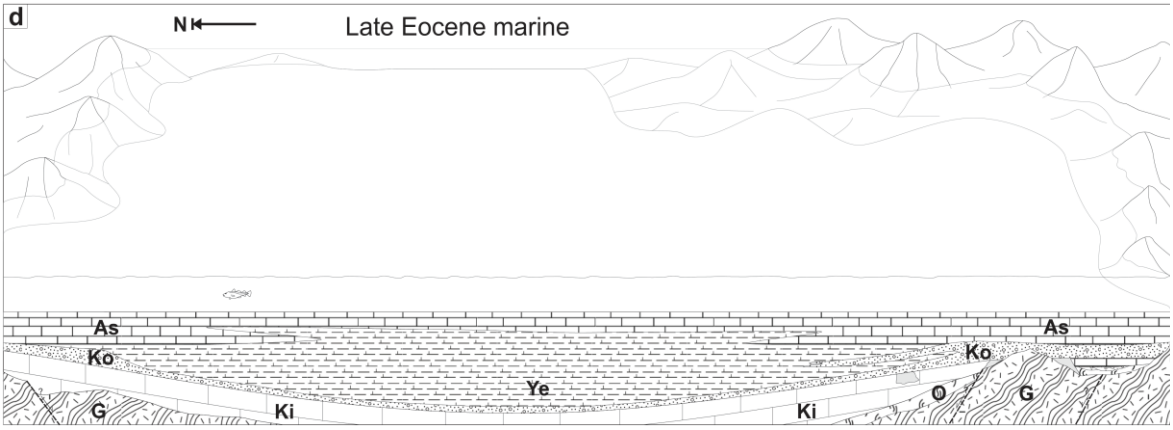

Figure 2.61. Late Lutetian shallow-marine limestones of the Asartepe Formation onlapping Mesozoic limestones. The limestones filled and breached the basin margins to the north and west to connect with regional equivalents. Kı, Kırankaya Formation; To, Tohma Member; G, Geniz Formation; O, Hocalikova Formation; Ul, Ulupınar Formation; Ko, Korgantepe Formation; Ye, Yenice Formation; As, Asartepe Formation.

The marked sediment thickness changes in the vicinity of faults are interpreted as high-angle growth faults. The continued transgression of the Mesozoic platform carbonate 'basement' (Fig. 2.46) indicates broadening of the basin to form a regional-scale transgressive unit (Fig. 2.62). Deposition culminated in shallow-marine, to restricted evaporitic sedimentation (Darende Formation; Fig. 2.5) which also unconformably onlaps the Mesozoic limestones around the basin margins. The intercalations of shallow-marine and gypsum-rich sediments suggest marked fluctuations in salinity caused by opening and closure of a marine gateway.

Final basin emergence took place during the Priabonian (Late Eocene), probably as a result of sediment infill, eustatic sea level fall (Miller *et al.* 1995), or regional uplift. The Darende Basin remained emergent throughout Oligocene-Early Miocene time when fluvial sediments were deposited. Middle Miocene transgression is reflected by the westward progradation of shallow-marine bioclastic sand waves.

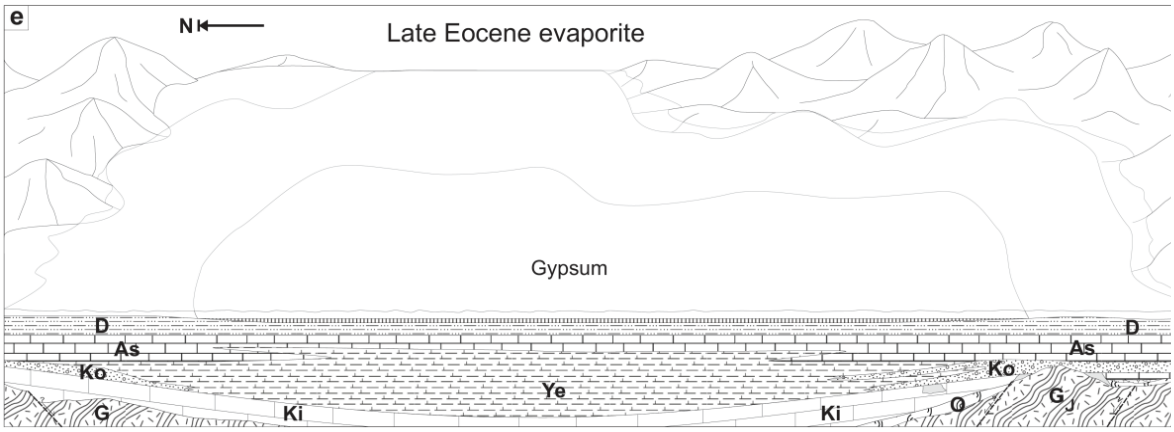

Figure 2.62. Early Priabonian shallow-marine restriction and emergence of the basin (Darende Formation). Kı, Kırankaya Formation; To, Tohma Member; G, Geniz Formation; O, Hocalikova ophiolite Formation; Ul, Ulupınar Formation; Ko, Korgantepe Formation; Ye, Yenice Formation; As, Asartepe Formation; D, Darende Formation.

Chapter 3: The Hekimhan Basin

Chapter 3. Revised stratigraphy, lithological description and interpretation of the Hekimhan Basin

3.1 INTRODUCTION

This chapter focuses on a complete geological analysis and interpretation of the Hekimhan Basin. The Hekimhan Basin is a composite basin recording two separate stages of tectonic development, first during the latest Cretaceous (Maastrichtian) and then during the Eocene (Lutetian-Priabonian). Maastrichtian strata were deposited under an extensional tectonic regime, following ophiolitic mélange emplacement, whereas the Eocene strata reflect a syn-collisional tectonic setting. Post-Eocene deposits are represented by subaerial clastic sedimentation, followed by a Miocene short-lived marine transgression, and a culmination in Pliocene subaerial volcanism. The Hekimhan Basin was chosen for this study because comparatively little work has been carried out on sedimentary-tectonic basins of Central Eastern Anatolian in this critical tectonic location. These basins highlight the later stages of continental collision in the Tethyan region.

Geographically, the Hekimhan Basin is located in central eastern Turkey ~80 km N of the city of Malatya (Fig. 3.1) The basin is located on the Tauride-Anatolide micro-continental unit, to the east of the Niğde-Kırşehir Massif and to the south of the Izmir-Ankara-Erzincan Suture Zone (Fig. 3.2), which marks the remnants of the Izmir-Ankara-Erzincan ocean which closed during Late Cretaceous-Late Eocene times (see chapter 1; Şengor & Yılmaz 1981; Robertson & Dixon 1984). The Hekimhan Basin occupies an area of ~1000 km^2 making it comparitively small compared with some other Upper Mesozoic-Cenozoic basins in central Turkey (*e.g.* Çankırı Basin, see e.g. Nairn *et al.* in press).

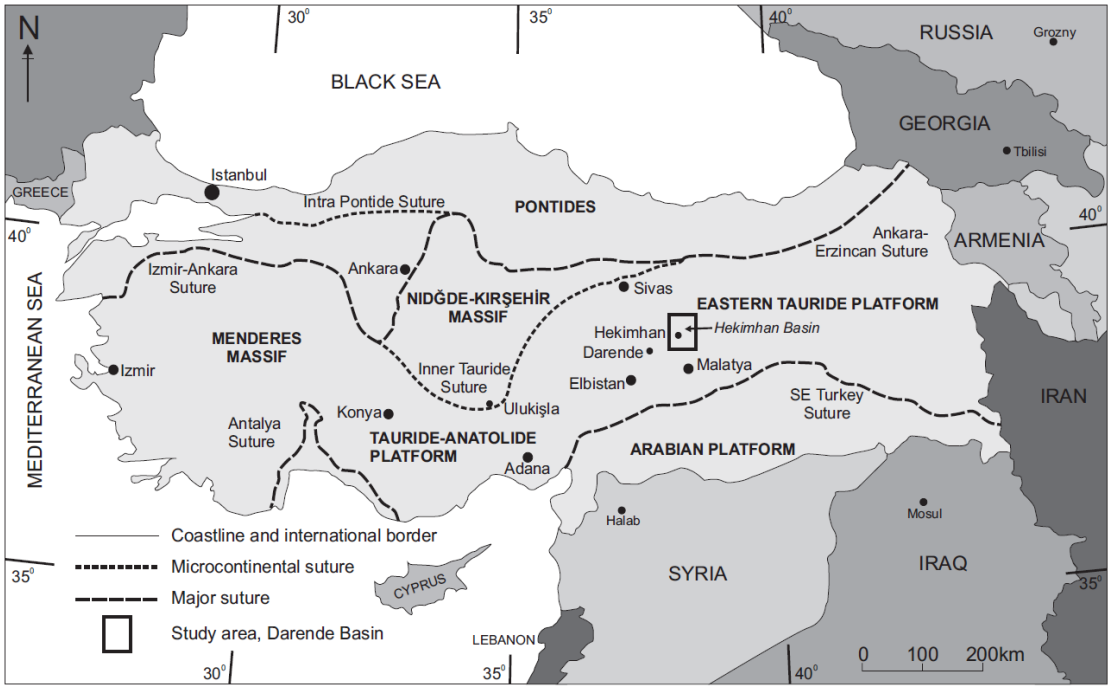

Figure 3.1. Location map and outline of the tectonic suture zones of mainland Turkey (modified from Clark & Robertson 2002). The Hekimhan Basin in central eastern Anatolia is marked by a rectangle.

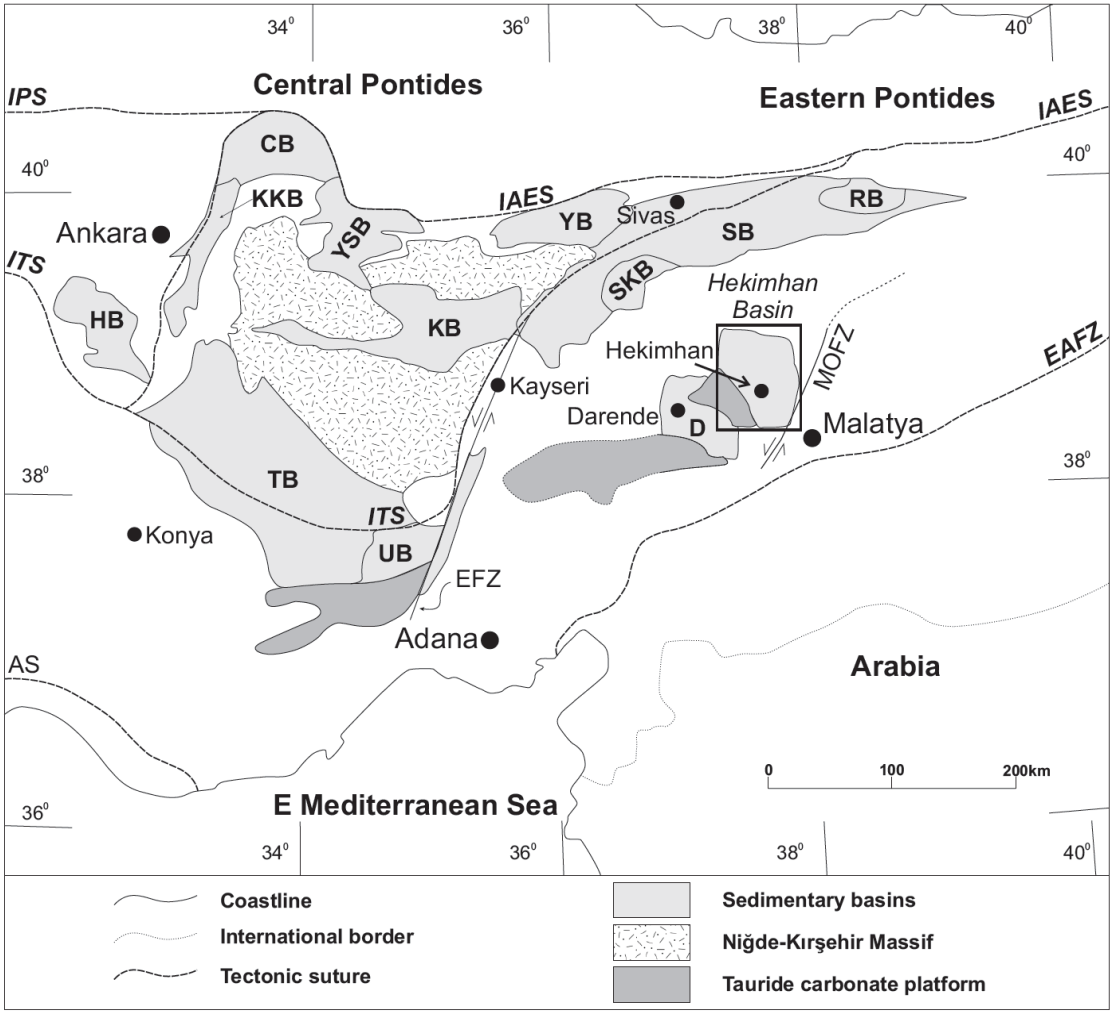

Figure 3.2. Regional outline map showing the major suture zones and fault zones (IPS, Intra Pontide Suture; ITS, Inner Tauride Suture; AS, Antalya Suture; IAES, İzmir-Ankara-Erzincan Suture; EAFZ, East Anatolian Fault Zone; MOFZ, Malatya-Ovacık Fault Zone; EFZ, Ecemiş Fault Zone) and the major sedimentary basins (HB, Haymana Basin; KKB, Kırıkkale Basin; CB, Çankırı Basin; YSB, Yozgat-Sorgun Basin; KB, Kızılırmak Basin; YB, Yıldızeli Basin; SKB, Şarkışla Basin; SB, Sivas Basin; RB, Refahiye Basin; TB, Tuzgölü Basin; UB, Ulukışla Basin; D, Darende Basin) in Central Eastern Anatolia. Study area shown by black rectangle. Modified from Görür et al. (1998).

3.2 AIMS

The objective of this chapter is to discuss new sedimentary, stratigraphic, palaeontological, geochemical and structural data gathered during the course of this study. This detailed, multidisciplinary approach has hitherto not been undertaken for the Hekimhan Basin. The geological map of the Hekimhan Basin utilises a combination of regional 1:500,000-scale geological maps compiled by General Directorate of Mineral Research and Exploration (MTA) (2002), together with detailed remapping of key field localities. A previous contribution of a small part of the centre of the basin has been assimilated and edited (*Gürer 1994*). Mapping was enhanced and boundaries ratified by utilisation of Digital Elevation Models (DEM) and projection software (ArcGIS and Google Earth) in a combined approach at remapping the Hekimhan Basin in its entirety for the first time (Fig.3.3).

The basin includes Mid-Eocene (Lutetian) lavas that are apparently unique to the Central Anatolian basins which span the Izmir-Ankara-Erzincan suture zone. Eocene lavas are not normally found so far south and are, therefore, poorly represented in the literature. The geochemistry of these lavas has been undertaken for the first time here.

Figure 3.3. (Below) Geological map of the Hekimhan Basin region. Modified and partially re-mapped during this study after Gürer (1994).

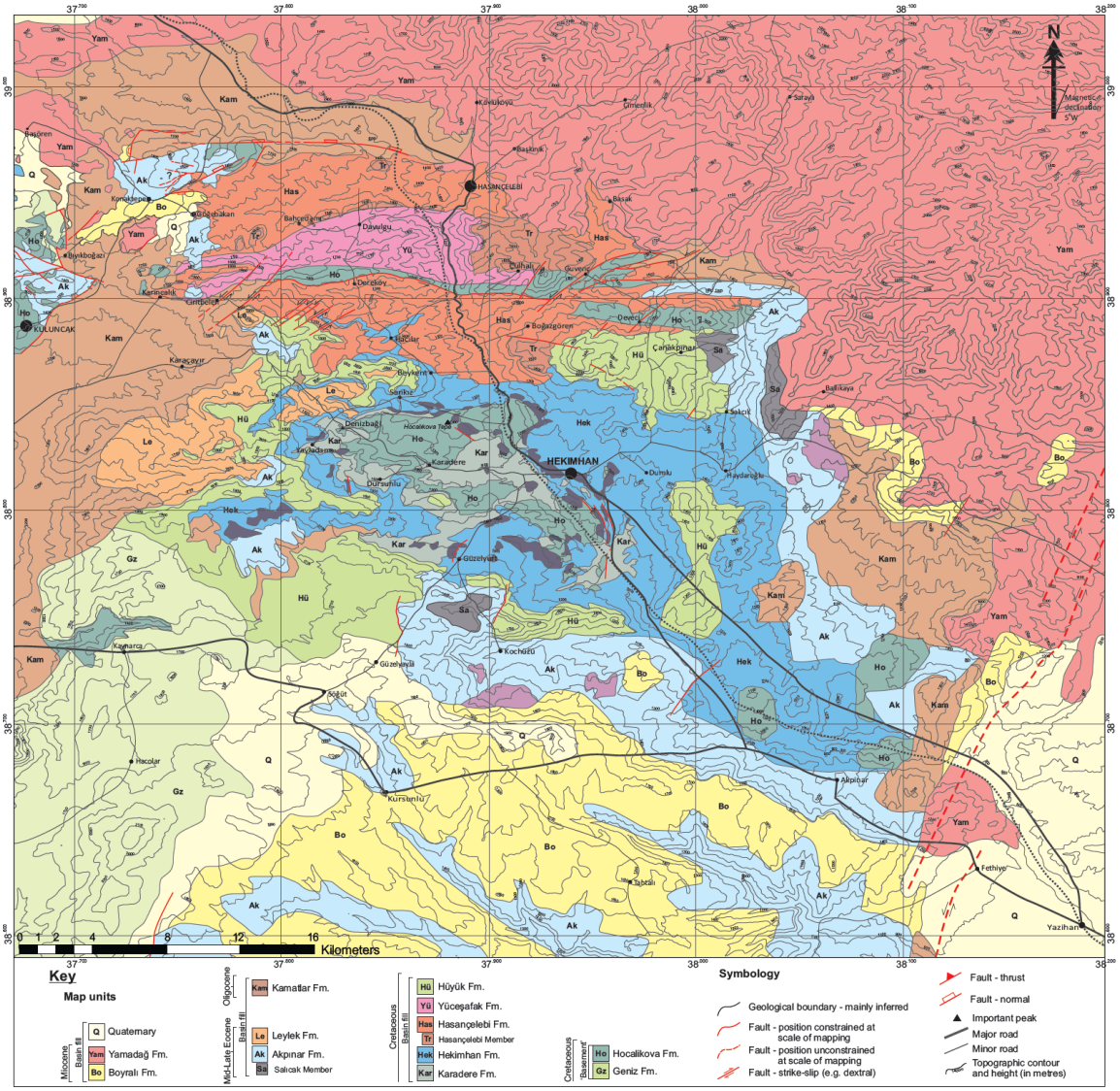
HEKIMHAN
KULUNCAK
HASANÇELEBİ
Kovuklıoyu
Çimenlik
Sarayı
Başkınık
Başak
Davelgu
Bulhalı
Güvenç
Dereböv
Karaçayır
Boğazgören
Çanakpınar
Salıcık
Dumlu
Güzelyayla
Kocharlı
Kurşunlu
Akpınar
Fethiye
Yazıhan
Tahtalı
Kaharca
Hacılar
Karadere
Denizbağı
Hocalıkova Tepe
Kayadaşı
Dursunlu
Beyköprü
Sarıhıdır
Karamanlık
Gümpelek
Büyükboğazı
Bahçedüzü
Konakpınar
Ballıkaya
Aydanlık
Kılıçlar
Beyören
Magnetic declination 5°W
0 1 2 4 8 12 16 Kilometers
Key
Map units
Miocene Basin fill
Q Quaternary
Yam Yamadağ Fm.
Bo Boyralı Fm.
Oligocene
Mid-Late Eocene Basin fill
Kam Kamatlar Fm.
Le Leylek Fm.
Ak Akpınar Fm.
Sa Salıcak Member
Cretaceous Basin fill
Hü Hüyük Fm.
Yü Yüceşafak Fm.
Has Hasançelebi Fm.
Tr Hasançelebi Member
Hek Hekimhan Fm.
Kar Karadere Fm.
Cretaceous Basement
Ho Hocalikova Fm.
Gz Geniz Fm.
Symbology
Geological boundary - mainly inferred
Fault - position constrained at scale of mapping
Fault - position unconstrained at scale of mapping
Fault - strike-slip (e.g. dextral)
Fault - thrust
Fault - normal
Important peak
Major road
Minor road
Topographic contour and height (in metres)

3.3 PREVIOUS WORK

The Hekimhan Basin was initially investigated by the Turkish General Directorate of Mineral Research and Exploration (MTA) during the regional geological mapping of Turkey (~1936). The first detailed geological study was conducted by Ayan (1961). The Hekimhan area was found to host several natural mineral resources leading to diverse elements of the Hekimhan area being studied in detail. Yilmaz *et al.* (1993) conducted a basin-wide field and geochemical study on the Cretaceous and Cenozoic igneous rocks. Özdemir & Tunç (1993) conducted a palaeontological analysis and established a basic stratigraphic nomenclature. A complete study of the Cretaceous to Miocene stratigraphy, volcanism and magmatism of the Hekimhan basin, together with the first attempt to understand the geodynamic evolution of the basin was undertaken by Gürer (1994) (Fig. 3.4). The investigation concluded that the Hekimhan Basin developed as a back-arc basin. This interpretation was supported by an investigation into the Hasançelebi magmatism (northern part of Hekimhan Basin) (Gürer 1996). Further research included an investigation of clay mineral genesis within Cretaceous-Cenozoic sediments from the breakdown of ophiolitic rocks (Yalçın & Bozkaya 1995; Yalçın, Bozkaya & Hozatlıoğlu 2009); an investigation into the origin of iron deposits in the Hasançelebi area (Stendal *et al.* 1995; Uçurum *et al.* 1996), and a new discovery of the Cretaceous/Cenozoic (KT) boundary within evaporitic rocks (Yalçın & Bozkaya 1996). More recent studies have included; the geochemical analysis of Cenozoic evaporites from the Hekimhan Basin as part of a regional investigation (Palmer *et al.* 2004); the petrography and geochemistry of Cretaceous-Eocene alkali magmatism (Özgenç & İlbeyli 2008); the palaeontology of Foraminifera and rudist bivalves (Çaglar & Önal 2009); ophiolite-associated ore mineralogy and geochemistry (Marschik *et al.* 2008; Yalçin *et al.* 2009); the geochemistry and isotopic dating of Miocene volcanism as part of a regional investigation (Kürüm *et al.* 2009; Gürsoy *et al.* 2011); the isotopic analysis of copper and gold bearing iron-oxide deposits resulting from the intrusion and associated hydrothermal alteration of a syenite batholith (Kuşcu *et al.* 2011).

The research carried out as part of this project (Fig. 3.4) builds on and substantially added to the pioneering work of Gürer (1994) and others.

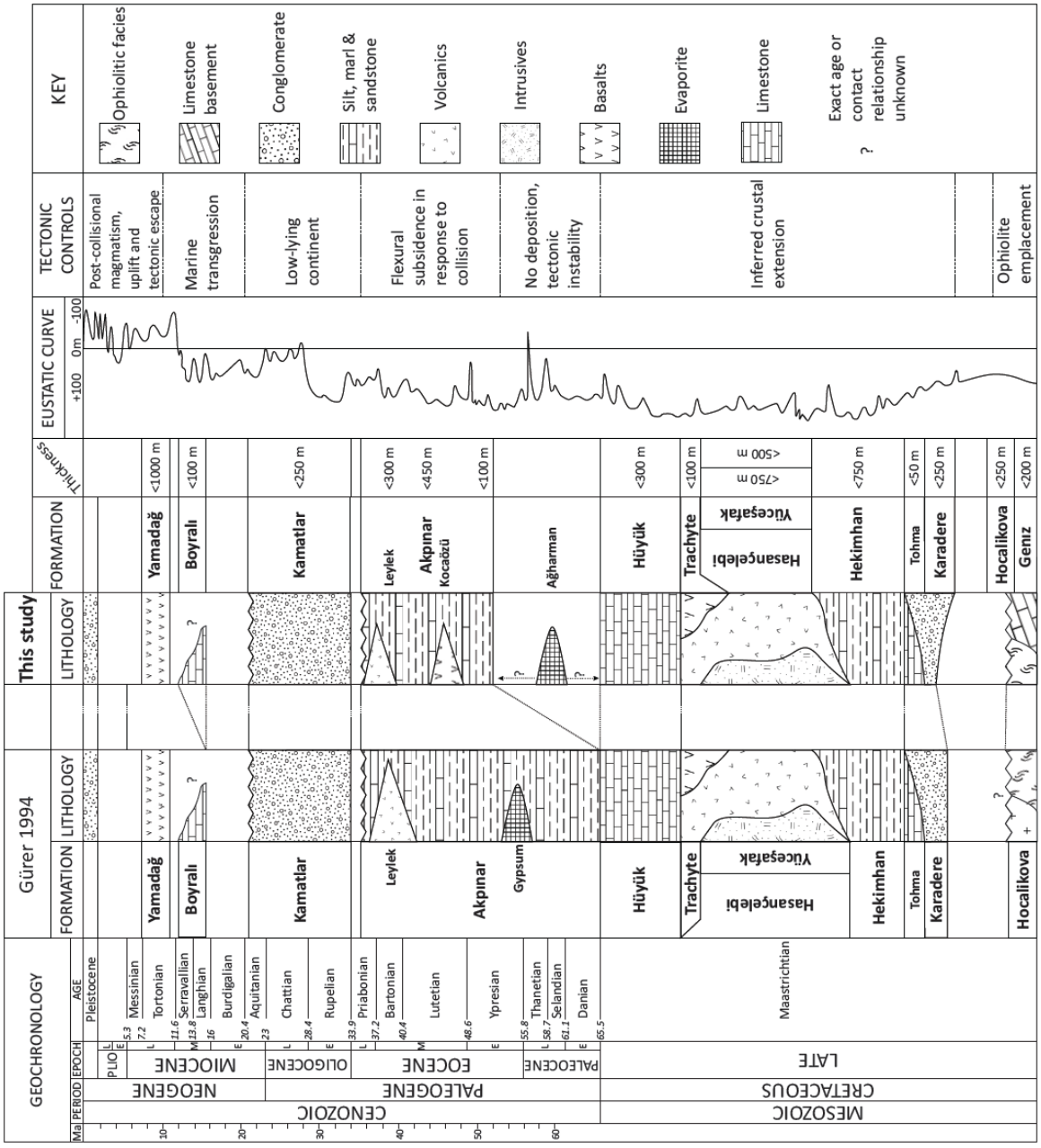

Figure 3.4. Previous and revised stratigraphic nomenclatures of the Hekimhan Basin. The most complete work by Gürer (1994) is shown here. The revision (this study) takes account of improved knowledge of the Mesozoic carbonate platform and emplaced ophiolite-related mélange (Robertson *et al.* in press), the dating of microfossils during this work and also of recent radiometric dating of Miocene volcanic rocks (Gürsoy *et al.* 2011). A global eustatic sea level curve (Miller *et al.* 2005) is included on the right to aid discussion of the controls of sediment deposition (i.e. tectonics versus sea level change). The main inferred controls of deposition are also summarised.

3.4 STRATIGRAPHY

In this section, new stratigraphic, sedimentary and volcanic data are presented based on measured stratigraphic logs, new field-mapping and the geochemical, petrological and palaeontological study of rock samples collected in the field. New lithofacies analysis is presented here and defined in terms of grain size, bed thickness, sedimentary structures and lithology. The stratigraphic units are described here in geochronological order.

3.4.1 Mesozoic 'Basement'

3.4.1.*1* Mesozoic Bolkar Carbonate Platform (Geniz Formation)

Name: No formal stratigraphic name for this formation was found in the literature. It has therefore been named the Geniz Formation in order to preserve stratigraphic continuity with the adjacent Darende Basin.

Type locality: Within the valleys surrounding Hacolar (Fig. 3.5).

Lithology: The Geniz Formation is mainly composed of white to buff, well-bedded (typically ~50 cm thick), hard, microcrystalline limestone (diagenetically recrystallised) with a sugary texture, locally interbedded with minor, thin marls. It is typically fractured, faulted, folded with metre scale brecciated areas containing abundant calcite filled geoid deposits. Fragmented macro and microfossils can be seen as etchings on weathered surfaces, although it was not possible to establish dates from these.

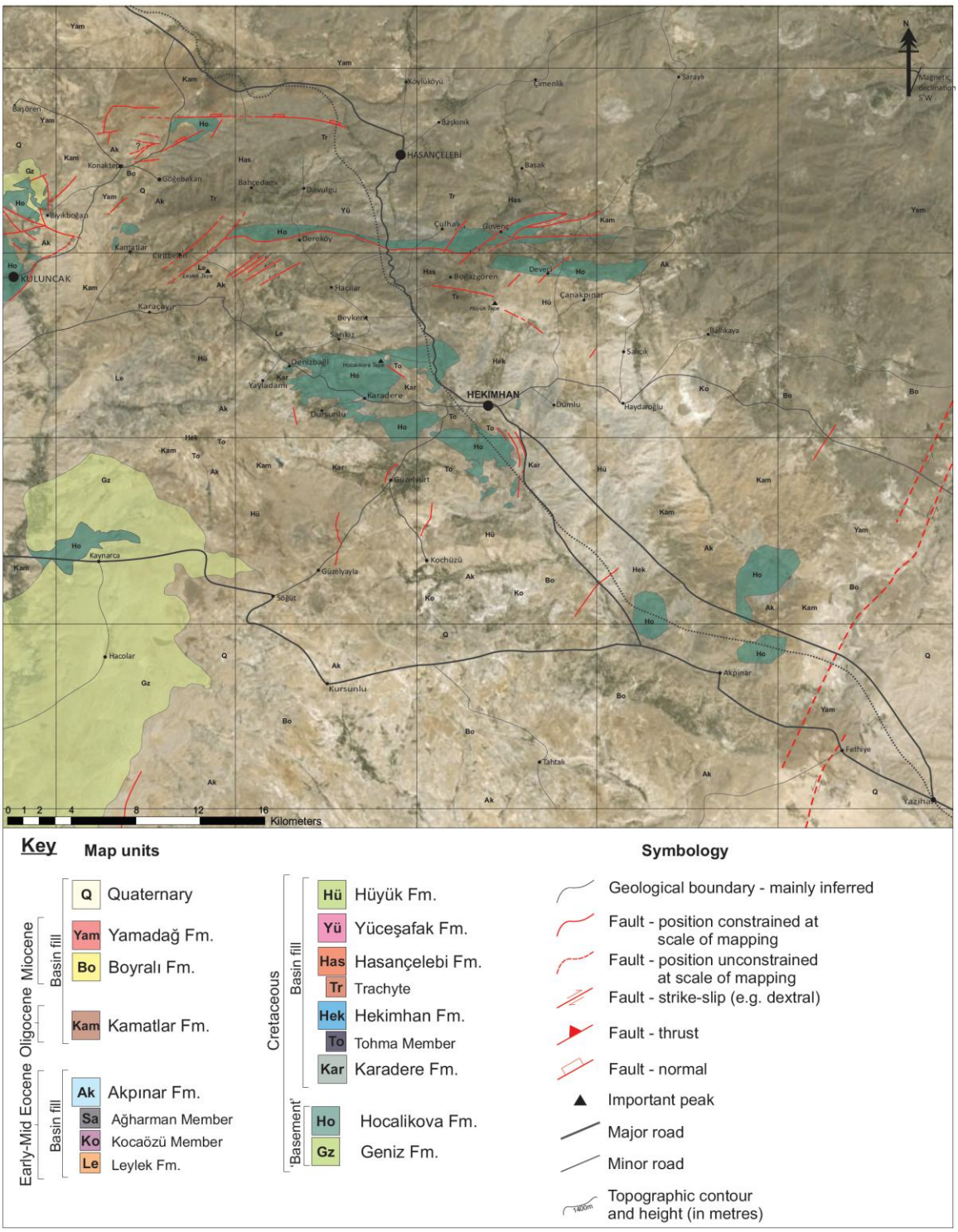

Figure 3.5. Simplified geological map showing the extent of the Geniz and Hocalikova Formations draped over a satellite image of the Hekimhan Basin.

Boundaries: The basal contact is not observed in the field area. The formation is believed to overlie Triassic sediments to the south of Pınarbaşı (approximately 135 km SE of the Hekimhan basin (Akkuş, 1971). The upper contact is not well exposed in the field area.

To the SW of the basin, ophiolite mélange is thrust above and, in turn, overthrust by the Geniz Formation.

Thickness and extent: The Geniz Formation is underrepresented in the Hekimhan Basin compared to the Darende Basin. The formation is only exposed to the southwest of the field area (see map) around the village of Hacolar. Outcrops were observed in high plataeu areas, often richly farmed (leading to poor, discontinuous exposures), where the maximum observable thickness is ~300 m. Elsewhere, the equivalent of the Geniz Formation, known regionally as the Tauride Carbonate Platform, is typically up to several kilometres thick (e.g. Perınçek & Kozlu l984). For example, shallow-water carbonates overlie Triassic sediments to the south of Pınarbaşı (~100 km west of the Darende Basin), where they exceed 1000 m in thickness (Akkuş 1971). A borehole to the NW of the field area is recorded as reaching 2090 m within neritic carbonates before terminating (Akkuş 1971; Table 2.1, exact location unspecified). The Geniz Formation is well exposed and well represented in and around the field area. Similar limestone outcrops ~90 km NW of Hekimhan, near Gürün, and are believed to be a structural extension of the regional Tauride carbonate platform 'basement' unit. However, this part of the platform was detached and is likely to be a regional-scale allochthonous thrust sheet (Robertson *et al.* in press).

Age: The age of the Geniz Formation is Mesozoic and it is believed to have been deposited from the Late Jurassic to Mid-Late Cretaceous basin on Foraminifera (Akkuş, 1971, Perincek & Kozlu l984, Robertson *et al.* in press).

3.4.1.2 Interpretation of the Mesozoic Platform Limestones (Geniz Formation)

The limestones of the Geniz Formation represent long-term (Jurassic-Cretaceous) deposition on a carbonate shelf platform. Features such as calcite filled geoid deposits within fractured areas are interpreted as collapse structures associated with fluid flow. The Mesozoic Bolkar carbonate platform which formed from the Late Jurassic to Mid-Late Cretaceous (Akkuş 1971; Tasli et al. 2006; Robertson *et al.* in press) in the Hekimhan Basin is an extension of the Geniz Formation which outcrops extensively in

the Darende Basin (Booth *et al.* in press; Gürbüz & Gül 2005) and underlies much of Central Anatolia (Robertson *et al.* in press). The Geniz Formation is interpreted as part of the regional Eastern Tauride carbonate platform. The Taurides are traditionally divided into three contiguous parts, the Western Taurides (Collins & Robertson 1998; Okay *et al.* 2001), the Central Taurides (Özgül l984, l997; Göncüoğlu *et al.* 2003; Mackintosh & Robertson 2009) and the Eastern Taurides (Perincek & Kozlu l984, Robertson *et al*. in press). The Eastern Taurides, east of the ~NE-SW striking Neotectonic Ecemiş fault zone (Fig. 3.2) developed after Triassic rifting during a phase of passive margin subsidence of the Tauride-Anatolide microcontinent bordering Neotethys (Demirtaşlı *et al.* l984; Perincek & Kozlu l984; Özgül l996 Taslı *et al.* 2006; Robertson *et al.* in press).

3.4.1.3 Upper Cretaceous ophiolitic mélange (Hocalikova Formation)

Name: Introduced by Gürer (1994). Possibly derived from a mountain ~2 km NW of Karadere (Hocalikova Tepe). The ophiolitic mélange in the Darende Basin is also termed the Hocalikova Formation.

Type locality: Good exposures of ophiolitic mélange can be found to the NW of Karadere. Detached blocks of ultramafic material are well exposed in the mountains surrounding Dereköy.

Lithology: The ophiolitic mélange in the Hekimhan Basin can be divided into two distinct units; first, sheared sedimentary mélange (see Raymond l984 for definition of mélange) and, secondly, massive debris flow mélange. The sheared sedimentary mélange outcrops in the central and southern parts of the basin, notably around the town of Hekimhan. The sheared sedimentary mélange (Fig 3.6a) is composed of ophiolite-derived clasts ranging from granular, to pebbly, to very large blocks up to tens of metres in diameter, termed olistoliths. The clasts and blocks are dominated by highly altered gabbro, pillow basalt (Fig. 3.6b), serpentinised ultramafic rocks including harzburgite, dunite and wherlite, red radiolarian chert and neretic limestone, typically set in a dark grey, clay-rich, sheared sandy matrix. Sheared, dark grey, matrix-supported conglomerates and sandstones composed of sub-rounded granule-to cobble-sized clasts of ophiolite-related lithologies,

set in a clay-rich matrix are also typically associated with the sedimentary mélange. This mélange is very susceptible to erosion owing to the broken nature of the deposit.

The massive debris flow mélange is mainly exposed along an E-W orientated tectonic lineament towards the north of the basin, ~ 5 km south of Hasançelebi. There, the mélange contains intact blocks composed of serpentinised harzburgite (Fig 3.6c) (commonly enriched with chromite and bronzite), dunite, wherlite, pyroxenite, tonalite and plagiogranite together with less altered massive gabbro. These blocks are juxtaposed at all levels by high angle fault zones. However, it was not possible to gauge a sense or scale of movement along these faults. Doleritic and gabbroic dykes were frequently observed and often rodingitised. Listvenite veins (secondary silica) were also observed in ultra-basic lithologies. In one section to the southeast of the basin, sheared serpentinite with isolated doleritic dykes is overlain by a thin sequence (< 30 m) of red radiolarite ribbon chert (Fig. 3.6d).

Boundaries: The lower boundary of the sedimentary mélange is an unconformable contact above the Geniz limestone Formation, which is often affected by post-emplacement tectonics. However, this boundary was only seen in the far west of the basin, ~ 9 km south of Kuluncak. The upper boundary forms an unconformity onto which Maastrichtian aged clastics and marine limestones were deposited (see below). The massive debris flow mélange was tectonically emplaced via a network of E-W orientated, predominantly sinistral, strike-slip faults. However, the kinematics may only have preserved the most recent movement event.

Thickness and extent: The sedimentary mélange covers much of the Hekimhan Basin, especially towards the centre and south of the basin. However, the lower boundary was only seen in extreme western parts of the basin making stratigraphic thickness difficult to estimate. Within the centre of the basin the ophiolite outcrops reach ~100 m. The locally and tectonically exposed massive debris flow mélange reaches ~400 m in thickness at outcrop ~5 km south of Hasançelebi. Due to the tectonic emplacement of this unit it was not possible to estimate stratigraphic thickness.

Age: Both parts of the Hocalikova ophiolitic mélange form part of a regional-scale supra-subduction zone (SSZ) type ophiolite which is believed to have been obducted onto the

Mesozoic Tauride carbonate platform during the Late Cretaceous (Parlak *et al.* 2000; 2004; Robertson *et al.* 2009; in press).

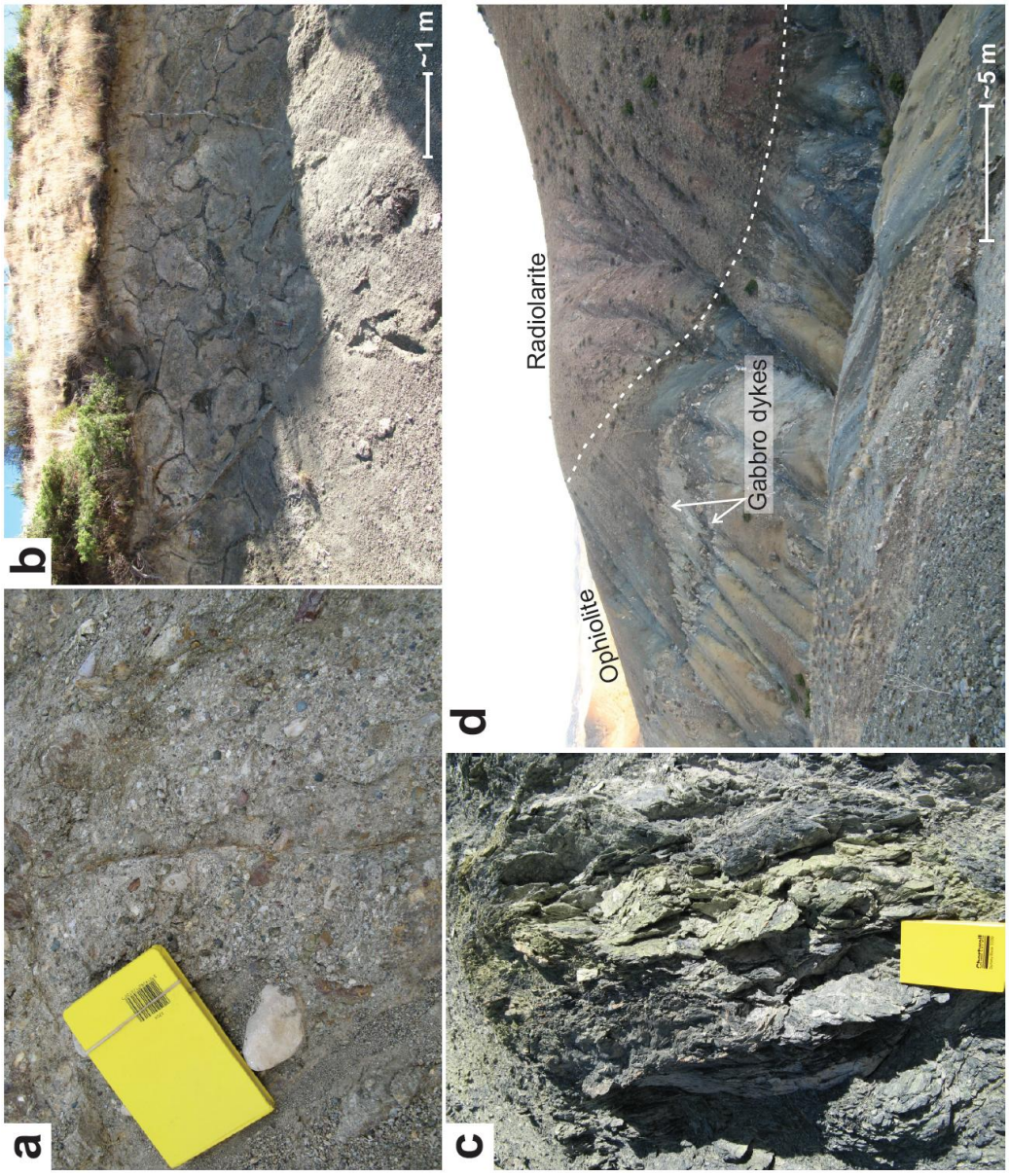

Figure 3.6. Field photographs showing, a, granular to pebbly sheared sedimentary ophiolitic mélange; b, hydrothermally altered ophiolitic pillow lava olistolith; c, serpentinised harzburgite; d, ophiolitic material cross cut by gabbroic dykes and overlain by red radiolarian chert.

3.4.1.4 Interpretation of the Upper Cretaceous ophiolitic mélange (Hocalikova Formation)

The ophiolite-related mélange (Hocalikova Formation) was formed by a combination of tectonic and sedimentary processes. The sheared sedimentary mélange likely represents emplacement and accretion of an ophiolite which was broken apart and dissected as it was obducted. The massive debris flow mélange represents a tectonic mélange where lower crustal and mantle rocks were tectonically juxtaposed and obducted.

Rodingitisation commonly occurs during metasomatism of basic to intermediate dykes within ultramafic rocks. During rodingitisation, silica is leached out of host minerals leading to the formation of serpentinite veins (*Hatzipanagiotou et al.* 2003).

Listvenitisation concentrates silica as well as carbonates from host rocks into listvenite bearing veins (Buısson & Le Blanc 1986).

Elsewhere in the region (e.g. in the Gürün area, ~60 km E of Hekimhan) similar mélange was emplaced onto the northern margin of the Tauride platform during Campanian-Maastrichtian time (Perinçek & Kozlu, l984; Robertson *et al.* in press). The lithologies are interpreted to have accreted above a northward-dipping subduction zone within Neotethys and then emplaced southwards onto the Tauride carbonate platform during latest Cretaceous time (Robertson *et al.* in press). The ophiolitic rocks themselves are likely to have formed in a supra-subduction zone setting, probably the Inner Tauride ocean (Görür *et al.* 1984), as inferred for other ophiolites overlying the Tauride-Anatolide microcontinent (Robertson, 2002, 2006; Parlak *et al.* 2000, 2004, 2009).

3.4.1.5 Ophiolite Geochemistry

Samples of basalt from the ophiolitic melange (Hocalikova Formation) were collected for X-Ray Fluorescence (XRF) analysis. It is important to note that the basalts are a component of the oceanic crust which was broken up and emplaced as ophiolitic mélange and as such, do not represent the geochemistry of the ophiolite proper. Figure 3.7 shows four samples normalised to Mid Ocean Ridge Basalt (MORB). The samples (MB08-1, MB08-127, MB09-33 and MB10-116) show enrichment of Large Ion Lithophile

Elements (LILE's) Sr–Ba and the Light Rare Earth Elements (LREE's) La–Ce. The High Field Strength Elements (HFSE's) Nb, Zr and Ti are slightly enriched but much less so than the LILE's and LREE's. Metal elements (e.g. Cr and Ni) on the right hand side of the graph are depleted. This pattern is related to the nature of the parental magma (Pearce 1982). Many of the elements in the plot are incompatible with a basaltic magma which crystallises olivine, plagioclase and clinopyroxene. However, Sr is compatible with plagioclase and Cr is compatible with mafic minerals. As a result the elements situated on the left hand side of the plot (LILE's and LREE's) become enriched during fractional crystallisation (Pearce 1982). The High Field Strength Elements (HFSE's) Nb, Zr, and Ti are slightly enriched with respect to MORB but significantly less enriched than the LILE's and LREE's. Most notably Nb, which appears to have a slight negative trend. Lesser enrichment of Nb compared with LILE's and LREE's can be attributed to a mantle source influenced by a subduction zone component (Pearce *et al.* 1990; Keskin *et al.* 1998; Dilek & Furnes 2009). LILE's and LREE's are mobile elements that are easily transported in aqueous fluids which are driven off subducted oceanic crust and associated sediments. In this way, they are concentrated in magmas which are generated above subduction zones. Nb is comparatively immobile in aqueous fluids and thus enrichment does not occur (Pearce 1982; Baier *et al.* 2008). The four samples in Figure 3.7 are especially depleted in Ni and Cr. However, the source of this assumed subduction zone component is not resolved here (discussed further in chapter 4).

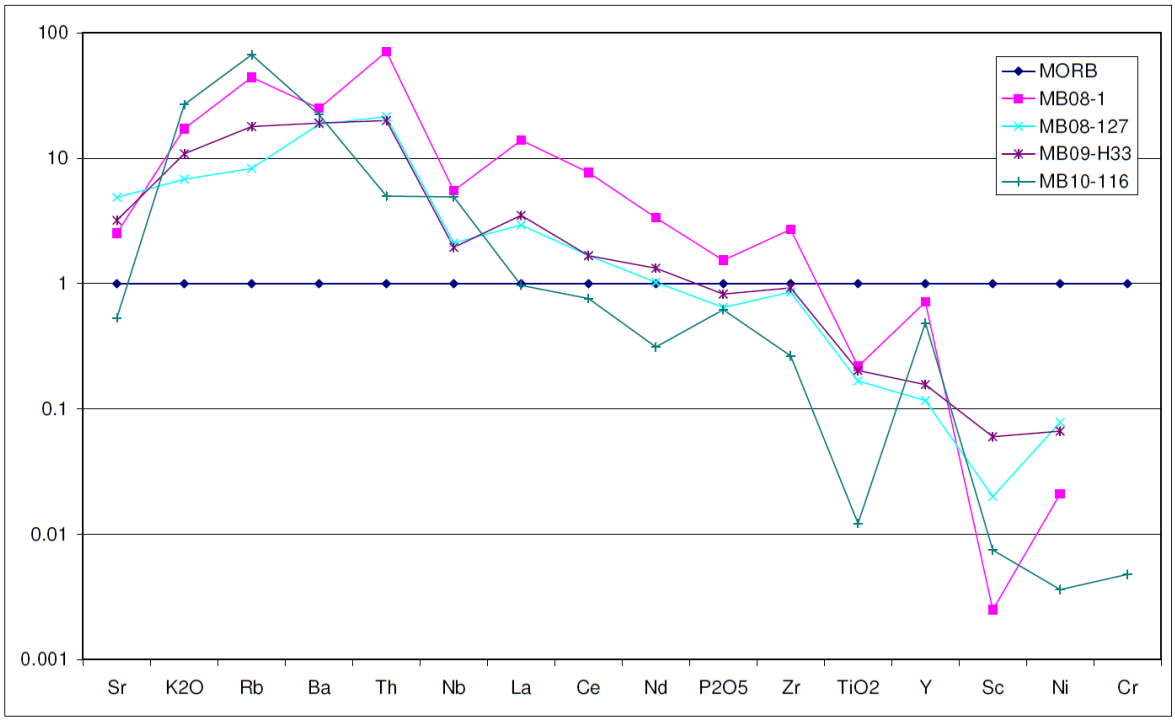

Figure 3.7. Spider diagram showing the geochemistry of basaltic clasts from the ophiolitic mélange (Hocalikova Formation) normalised to MORB (MORB data from Pearce 1982 and Saunders & Tarney 1984). Note negative Nb anomaly. Samples MB08-5 and MB09-56 are likely to be hydrothermally altered or weathered.

3.4.2 Maastrichtian sediments, volcanism and magmatism

Sedimentation in the Hekimhan Basin, as defined here, began during the Maastrichtian with the deposition of red conglomerates, sandstones and mudstones, termed the Karadere Formation. The formation consists of dark red conglomerates, sandstones and mudstones. The formation is unfossiliferous but is inferred to be of Maastrichtian age owing to its position between the Campanian-Maastrichtian ophiolite-related mélange, below (Perinçek& Kozlu l984; Robertson *et al.* in press) and overlying marine carbonates that are dated as Maastrichtian. These sediments are dominated by light grey marls, termed the Hekimhan Formation. The formation includes distinctive carbonate build-ups rich in rudist bivalves that are distinguished as the Tohma Member. The Hasançelbi Formation is an important, extensive, basic volcanic event which occurred, stratigraphically in the upper part of the Hekimhan Formation and is localised to the south of Hasançelbi. An E-W orientated, elongate, alkali syenite body (~ 15x 7 km) was intruded into the volcanics in the latest Cretaceous (Yüceşafak Member). A thick sequence of buff-coloured fossiliferous limestone overlies these sequences, termed the Hüyük Formation. The upper Cretaceous sediments and volcanics unconformably overlie the Hocalikova ophiolitic mélange.

3.4.2.1 Maastrichtian non-marine clastics (Karadere Formation)

Name: Introduced by Gürer (1994). Presumably named after the village of Karadere (Gürer, 1994) ~5 km west of Hekimhan (Fig. 3.8).

Type locality: Within valleys ~ 1 km SW of Hekimhan.

Lithology: The Karadere Formation has a distinctive dark red to dark brown colour. It is generally composed of poorly sorted, texturally immature, fine-to-granular erosive-based, often lenticular sandstones and pebbly conglomerates exhibiting a general fining-upwards trend (Fig. 3.9a). The beds range in thickness from 30-80cm. Sandstones are typically cross-bedded and show imbrication with palaeocurrents in the type section, directed to the ~W (Fig. 3.10). The clasts are predominantly sub-rounded to rounded, particularly the larger clasts. The beds are predominantly composed of altered basalt derived from the underlying ophiolite and other ophiolitic lithologies including radiolarite, chert, gabbro

and serpentinised ultramafic rocks (Fig. 3.9b). There is also a small component (<5%) of Mesozoic neritic limestone. Manganese-coated clasts are common and not limited to modern weathering, as excavated clasts were also coated. Finer-grained sandstone beds contain placer deposits with concentrations of dark minerals, possibly chromite (which is mined locally) or magnetite (Fig. 3.9c). A single surface with mud cracks was observed near the type section area. Further west (<1 km south of Sarıkız) the colour of the Karadere Formation alternates between dark grey and red due to the addition of decimetre thick, red mudstone packages. Syn-sedimentary extensional faulting was also observed in this area.

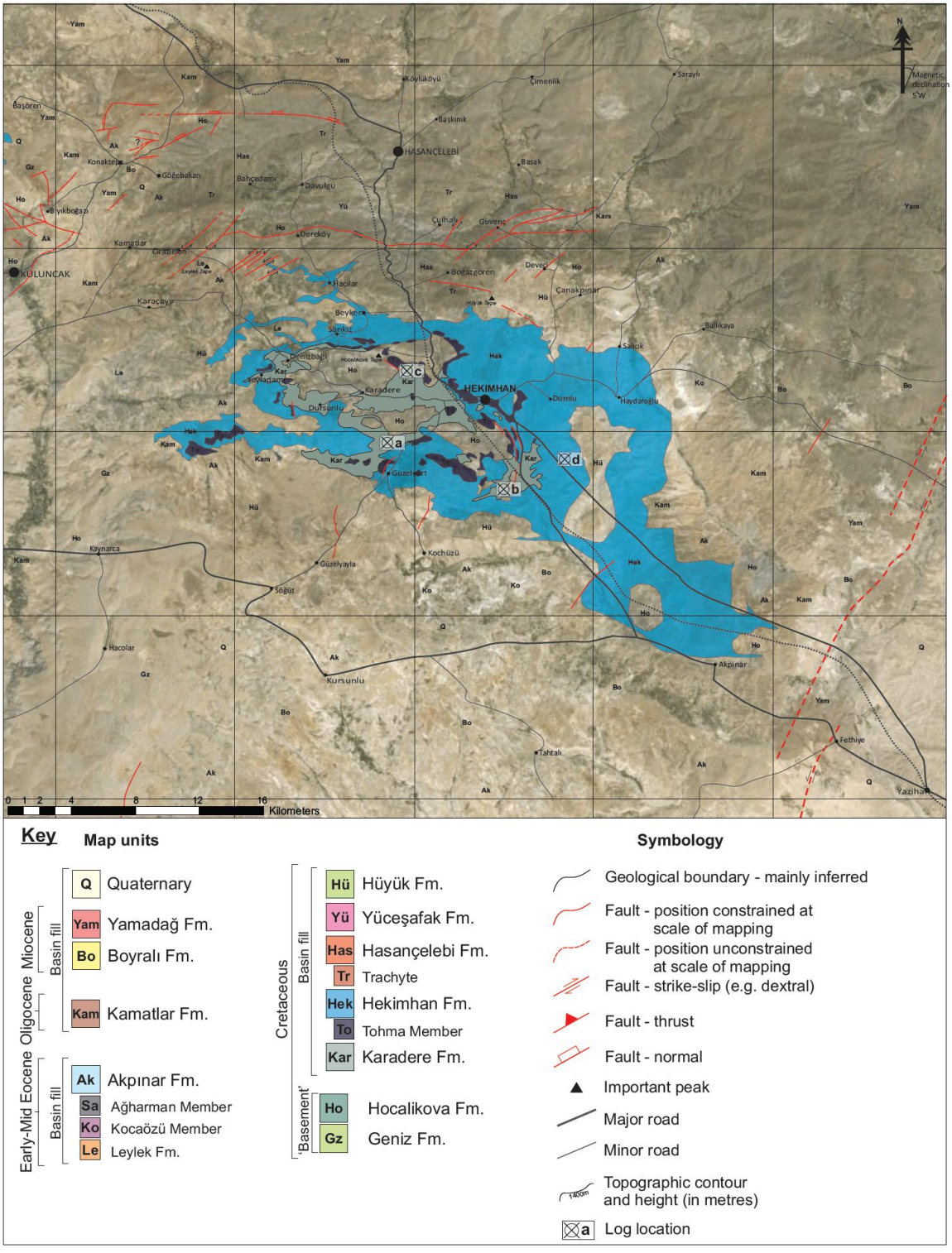

Figure 3.8. Simplified geological map showing the extent of the Karadere and Hekimhan Formations as well as the Tohma Member draped over a satellite image of the Hekimhan Basin. Also shown are logged section locations.

Boundaries: The lower boundary forms an unconformable contact over the ophiolitic mélange and displays varying degrees of angular discordance along the contact. The

upper boundary is represented by a marine transgression which deposited rudist-bearing Tohma Member limestones or Hekimhan Formation marls on top of the conglomerates (e.g. 81–103 m on Fig. 3.10).

Thickness and extent: The formation is exposed extensively in lowlands to the south and west of Hekimhan (Fig. 3.8). The formation reaches a maximum thickness of ~200 m at the type section. However, considerable lateral thickness and lithological variations occur throughout the basin. For example, the central part of the basin is mainly represented by sandstone and conglomerate alternations (e.g. Fig. 3.10 and 3.11) whereas the western areas are mainly represented by red mudstone with minor conglomerates (e.g. Fig. 3.12).

Age: The Karadere Formation is unfossiliferous but is dated based on its stratigraphic position between the ophiolite-related mélange below, that was regionally emplaced during latest Cretaceous (Campanian-Maastrichtian) time (Perınçek& Kozlu l984; Robertson *et al.* in press), and the overlying marls of the Hekimhan Formation and also the Tohma Member which are dated as Maastrichtian.

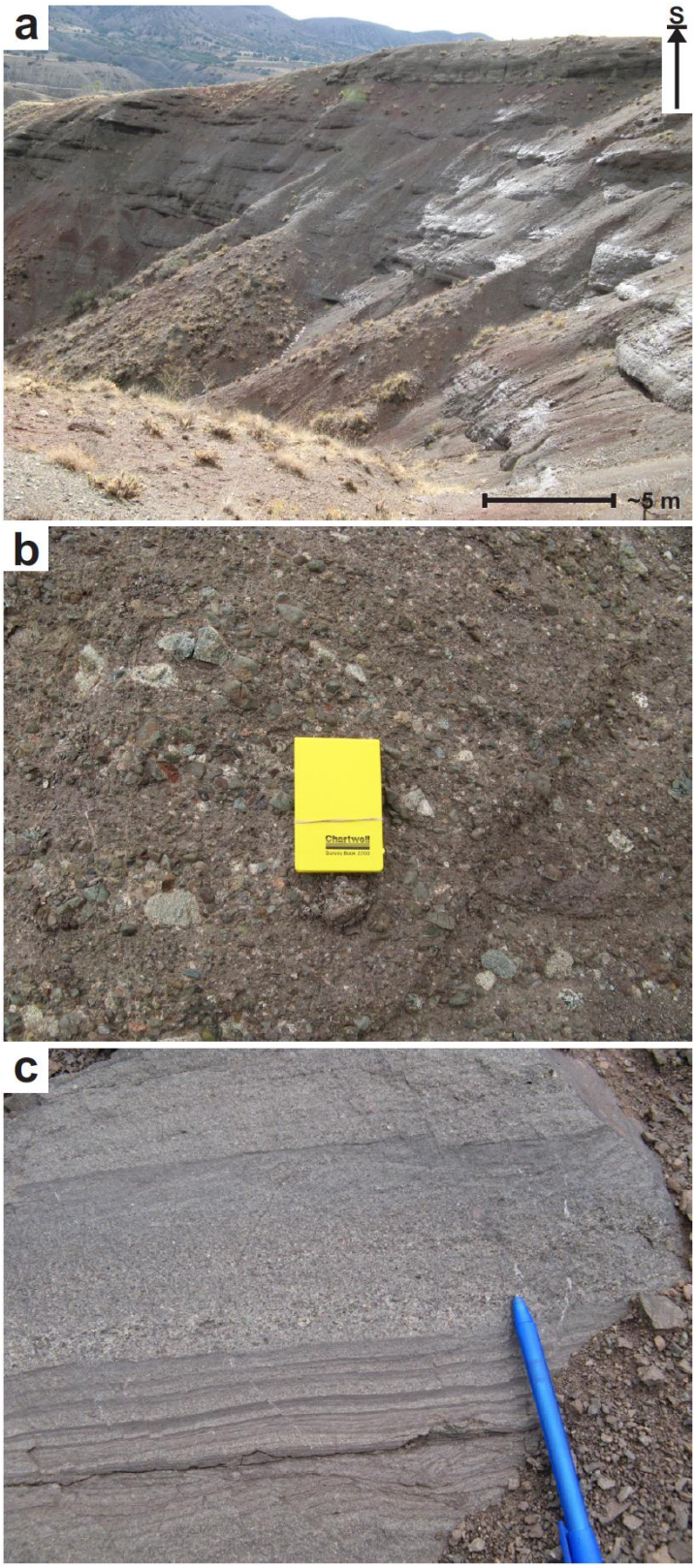

Figure 3.9. Field photographs of the Karadere Formation showing, a, dark red, lenticular bedded sandstones; b, closer view showing the immature, sub-rounded nature of the Karadere Formation conglomeratic beds; c, normally-graded granular to-medium grained sandstones in the upper part with poorly developed cross lamination and placer deposits in the lower part.

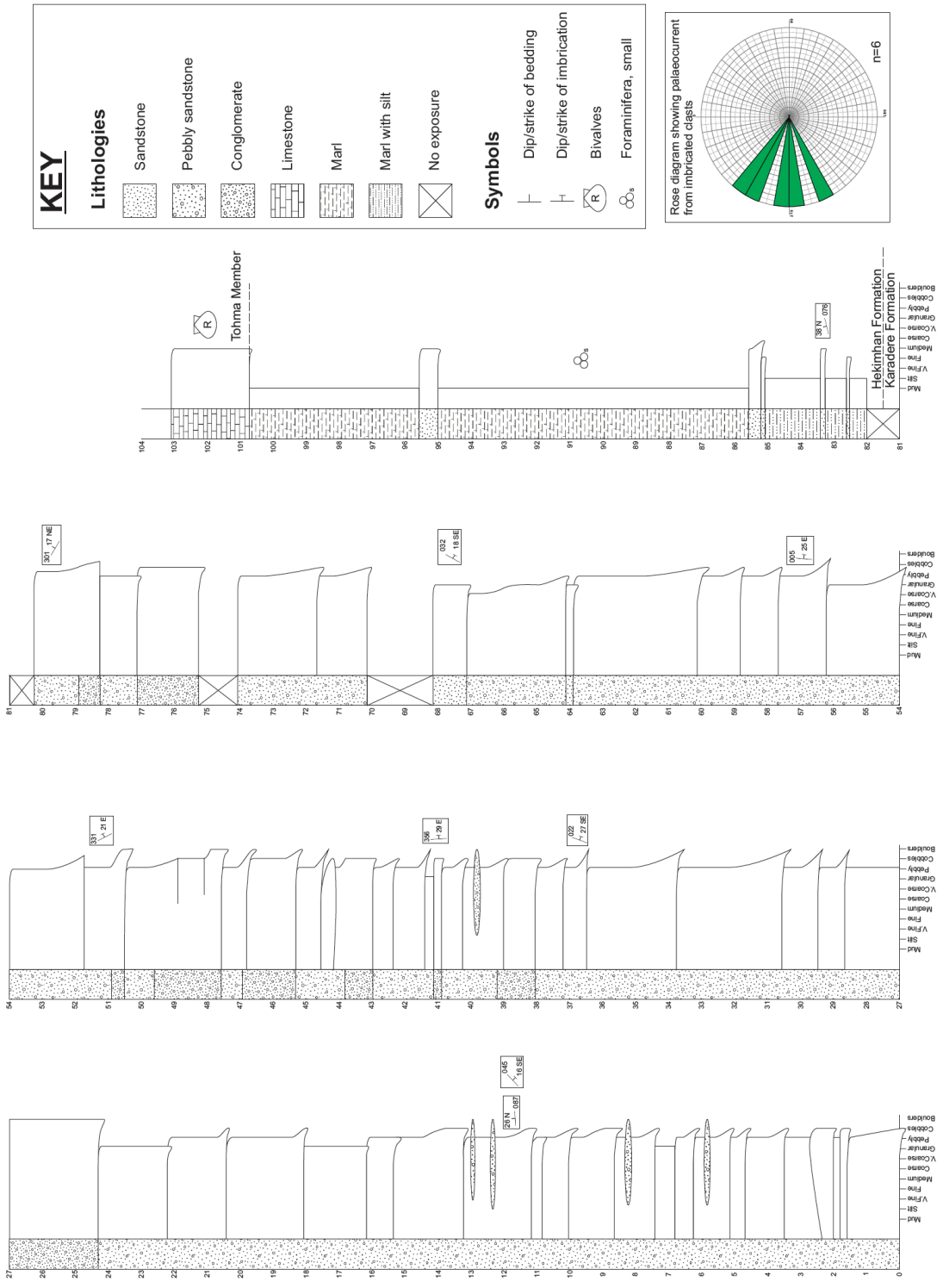

Figure 3.10. Measured sequence of part of the Karadere Formation, as logged at locality 'a' on the simplified geological map (Fig. 3.8).

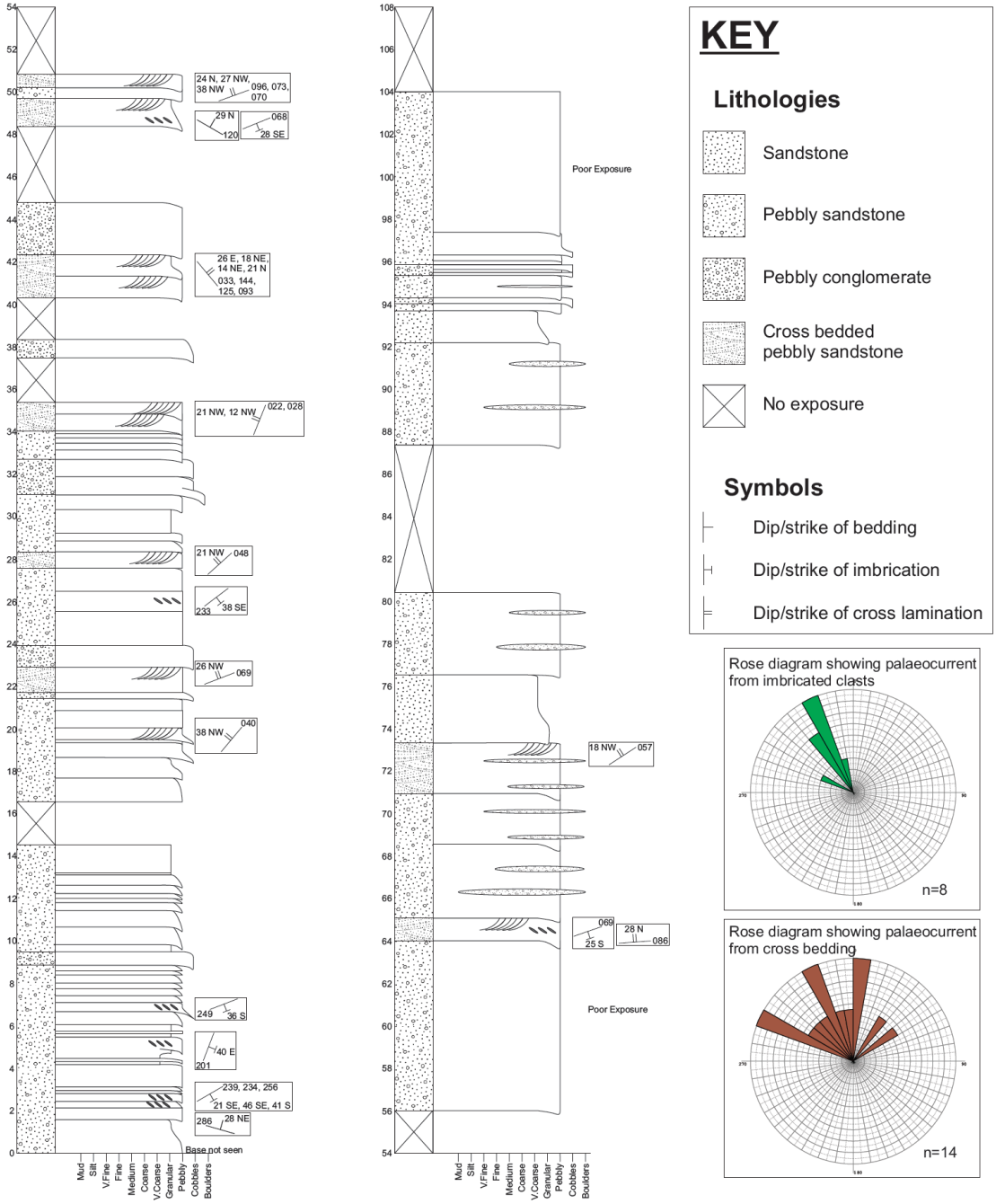

Figure 3.11. Measured sequence of part of the Karadere Formation, as logged at locality 'b' on the simplified geological map (Fig. 3.8).

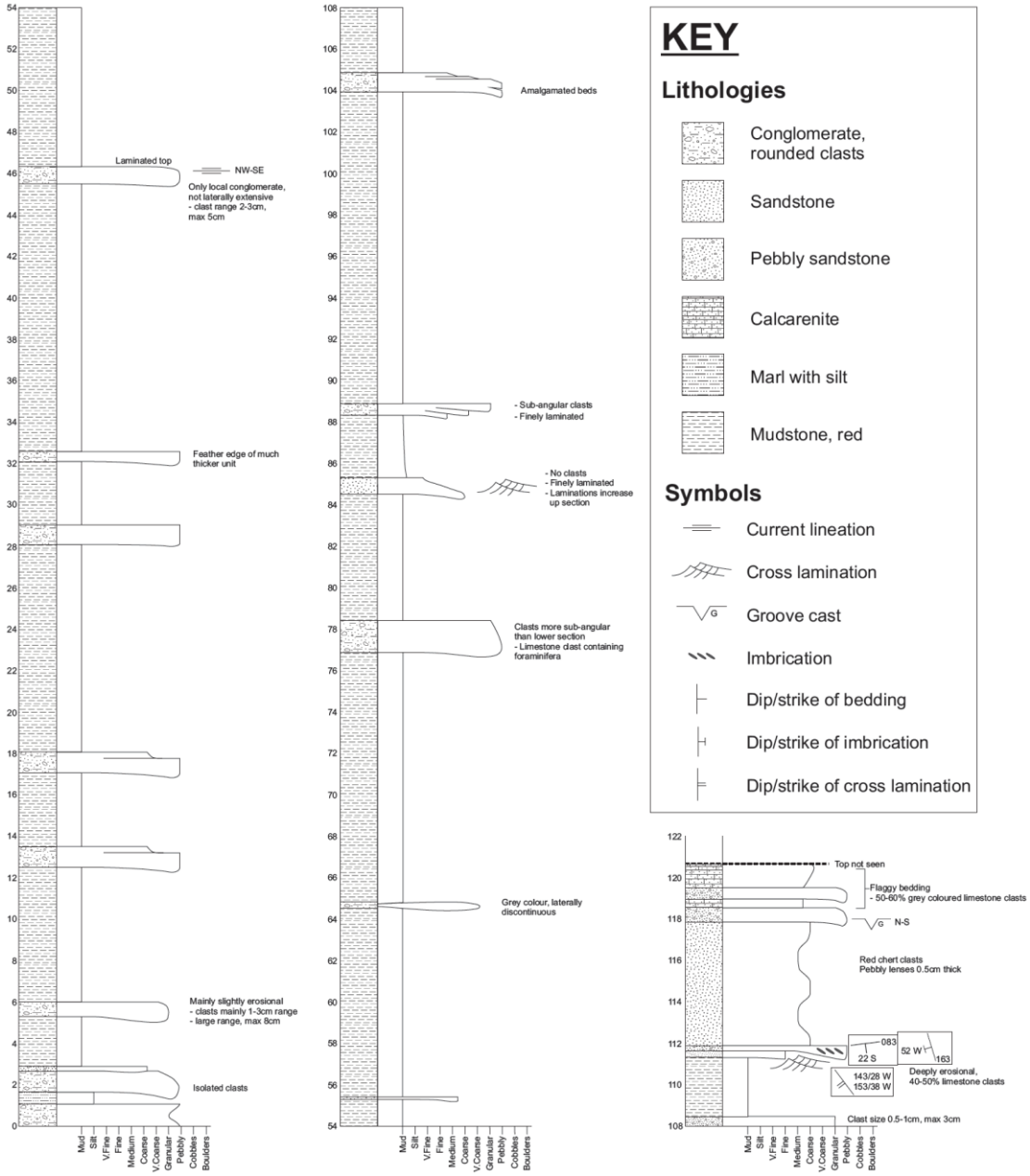

Figure 3.12. Measured sequence of part of the Karadere Formation, as logged at locality 'c' on the simplified geological map (Fig. 3.8).

3.4.2.2 Interpretation of the Maastrichtian non-marine clastics (Karadere Formation)

The Karadere Formation is interpreted as non-marine, mainly due to a lack of fossils. The red colour of the rocks and the presence of manganese coated clasts additionally suggest an arid environment. Furthermore, a fluvial depositional-system is interpreted from the rounded clasts and the erosive based, cross-bedded and imbricated nature of the sandstone

beds. Figure 3.13 shows that lateral changes in thickness reflect its deposition in palaeotopographic valleys that remained after ophiolite emplacement and subsequent erosion.

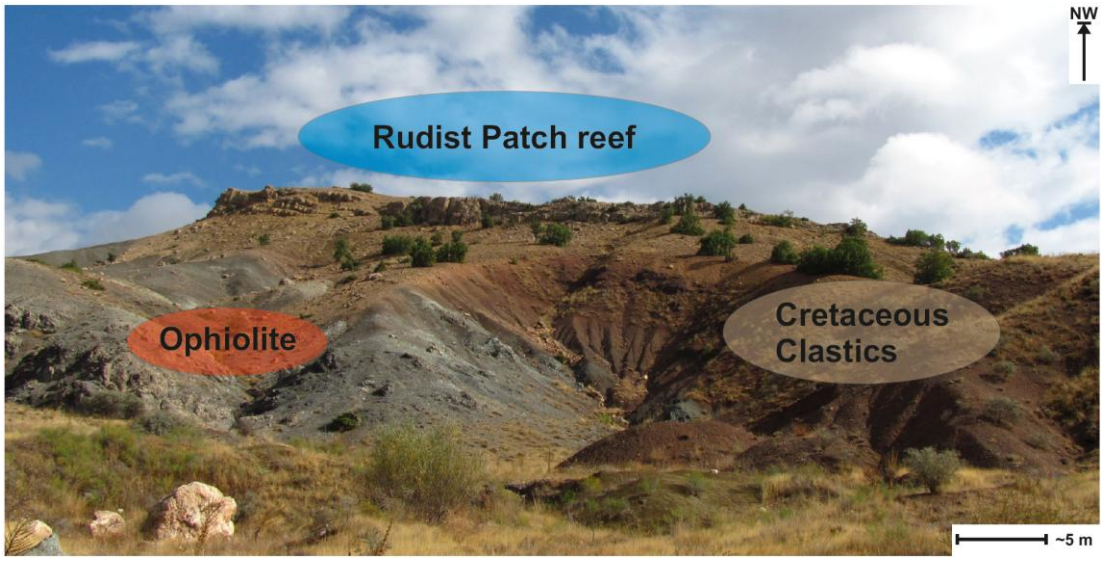

Figure 3.13. Photograph showing red continental clastics of the Karadere Formation onlapping ophiolitic mélange. Both of which are unconformably overlain by a rudist bearing patch reef of the Tohma Member.

3.4.2.3 Rudist bearing patch reefs (Tohma Member)

Name: This unit is named the Tohma Member in both the Hekimhan and Darende Basins. The name is probably derived from the Tohma River which flows from west to east across the Darende Basin.

Type locality: A NW-SE striking ridge line ~ 4 km NW of Hekimhan.

Lithology: The Member is characterised by an abundance of rudist bivalves (Fig. 3.14a) (e.g. Steuber & Löser 2000; Özer *et al.* 2009). Many of the hand specimens are of the species *Hippurites* sp. (Özer 1988; Steuber 2002). The rudists range in size from <5 cm to 30 cm (Fig. 3.14b) and occur in great abundance within poorly lithified silty to micritic limestone. Rudist assemblage consists chiefly of two species *Miseia bilacunosa* Özer and *M. hekimhanensis* Karacabey Öztemür (Çaglar & Önal 2009). The associated macrofauna include gastropods and other bivalves. The shells of the rudist bivalves are made of calcite and consequently have a high preservation potential. However, portions of the

inside of the test were made of aragonite and have subsequently recrystallised to calcite spar (Falini *et al.* 1996; Steuber 1999). The morphology of the rudist-bearing reefs are well preserved such that in situ reef structures can be seen to pass laterally into broken talus material. Occasional thin (<20 cm thick) debris flows concentrated with small and broken rudist bivalves were observed within marls of the Hekimhan Formation.

Boundaries: The lower boundaries of the Tohma Member are unconformable. The unit is either found directly overlying ophiolitic lithologies or the Karadere Formation. The upper boundaries are usually transitional with marls of the Hekimhan Formation.

Thickness and extent: The rudist-rich units commonly form elongate, ridge-like outcrops, ranging from <10 m long x <2 m wide, to >150 m long x 40 m wide, and are up to 30 m high. The size and abundance of rudists decrease in outcrops containing relatively high proportions of terrigenous clastic material compared to carbonate material.

Age: Rudist bivalves existed throughout the Jurassic and Cretaceous and were particularly widespread during the Maastrichtian. Many of the rudists found in the Tohma Member are characteristic of the Maastrichtian (Steuber & Löser 2000).

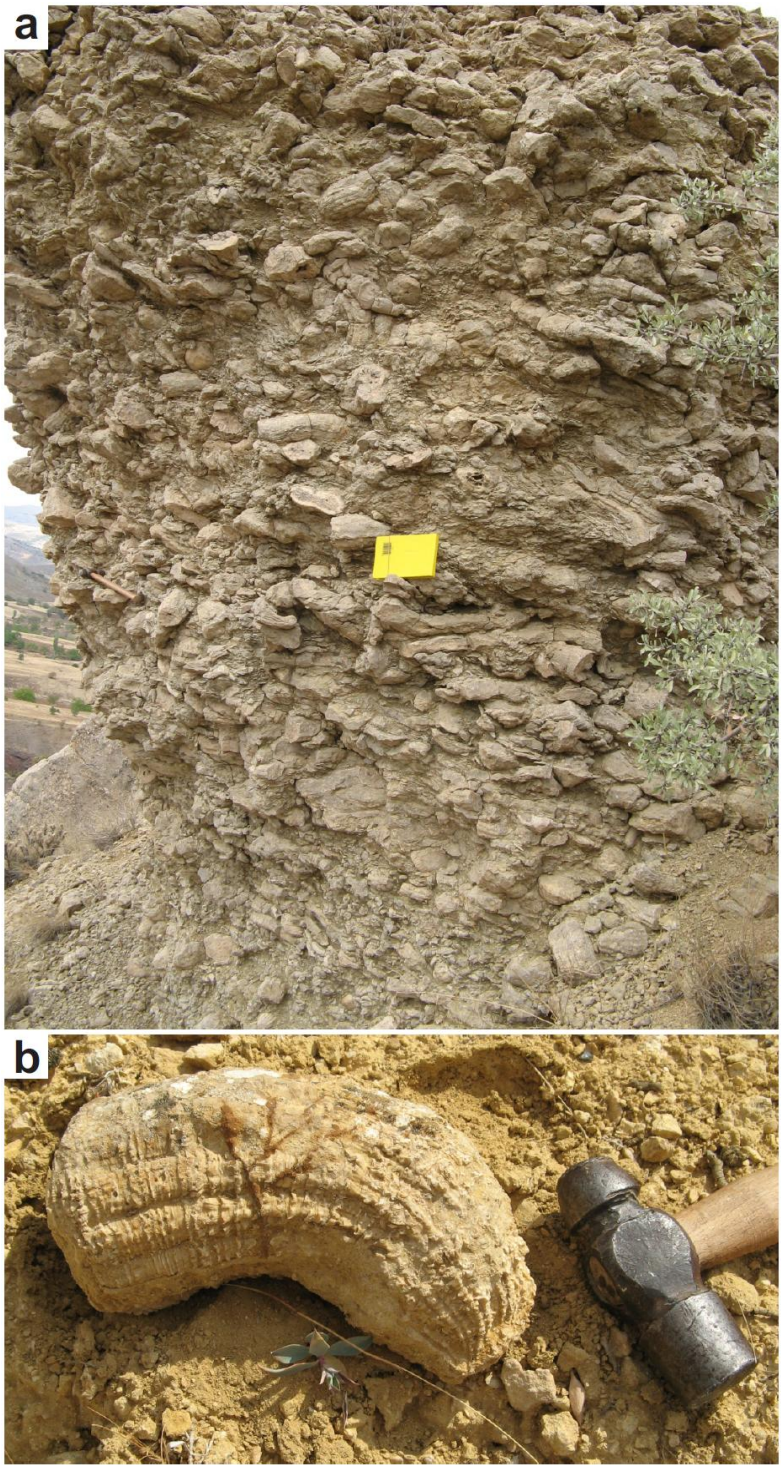

Figure 3.14. Photographs showing; a, rudist-bearing patch reef. Rudist bivalves would have grown curving upwards, note that the rudists are now horizontally orientated; b, typical example of rudist bivalve.

3.4.2.4 Interpretation of the rudist bearing patch reefs (Tohma Member)

Rudist-bearing carbonate sequences are common in the Neotethyan realm (and are an important hydrocarbon reservoir rock for the Eastern Mediterranean region) (Demirel &

Kozlu 1997; Sarı & Özer 2009). Rudist bivalves as a whole flourished in shallow-marine, tropical waters with low siliciclastic input, in similar conditions to modern tropical corals, before becoming extinct at the Cretaceous-Cenozoic boundary (Steuber & Löser 2000; Stössel & Bernoulli 2000). The marine transgression during the Maastrichtian in the Hekimhan Basin was characterised by the development of rudist-rich patch reefs on elongate topographic highs. The rudist reefs nucleated on relatively immobile non-marine clastic sediments of the Karadere Formation or the ophiolitic mélange of the Hocalikova Formation. These sessile, epibenthic rudists grew on top of each other to form mounds and acted as reef bafflers, trapping sediment and other organisms between there shells as they grew. As the reefs matured, reef talus material was transported and deposited down slope forming minor debris flows preserved within the Hekimhan Formation.

3.4.2.5 Maastrichtian transgressive marine marls (Hekimhan Formation)

Name: Introduced by Gürer (1994). Probably derived from the town of Hekimhan.

Type section: ~8 km SSE of Hekimhan where a section up to 400 m thick is well exposed on the eastern flank of the valley.

Lithology: The majority of the Hekimhan Formation consists of light grey, laminated marls interbedded with minor calcarenite beds. The marls vary on a decimetre scale from finely laminated fissile, to less fissile, thickly laminated marl. This is most notable in exposures to the east of the basin. Light brown to cream calcarenite deposits range in thickness from a few centimetres up to ~1 m (e.g. Fig. 3.15) and range in grain size from fine (calcilutite) to very coarse (calcirudite). They are mainly composed of reworked carbonate grains and fossil fragments with minor terrigenous quartz, plagioclase and other, mainly mafic minerals. Marl rip-up clasts and flute and groove casts were observed at the base of some calcarenite beds. Graded beds, laminated tops and occasional ripple lamination were also observed. Numerous pelagic Foraminifera were observed in the marls. Benthic Foraminifera, together with fragmented bivalves, gastropods, echinoids and corals, were observed within calcarenite beds. Rare whole *Gryphea* (up to 8 cm in length) were also observed. Thalassinoides, Skolithos and Zoophycos trace fossils were

also commonly observed (Fig. 3.16). Locally, vertical burrows show diagenetic glauconite.

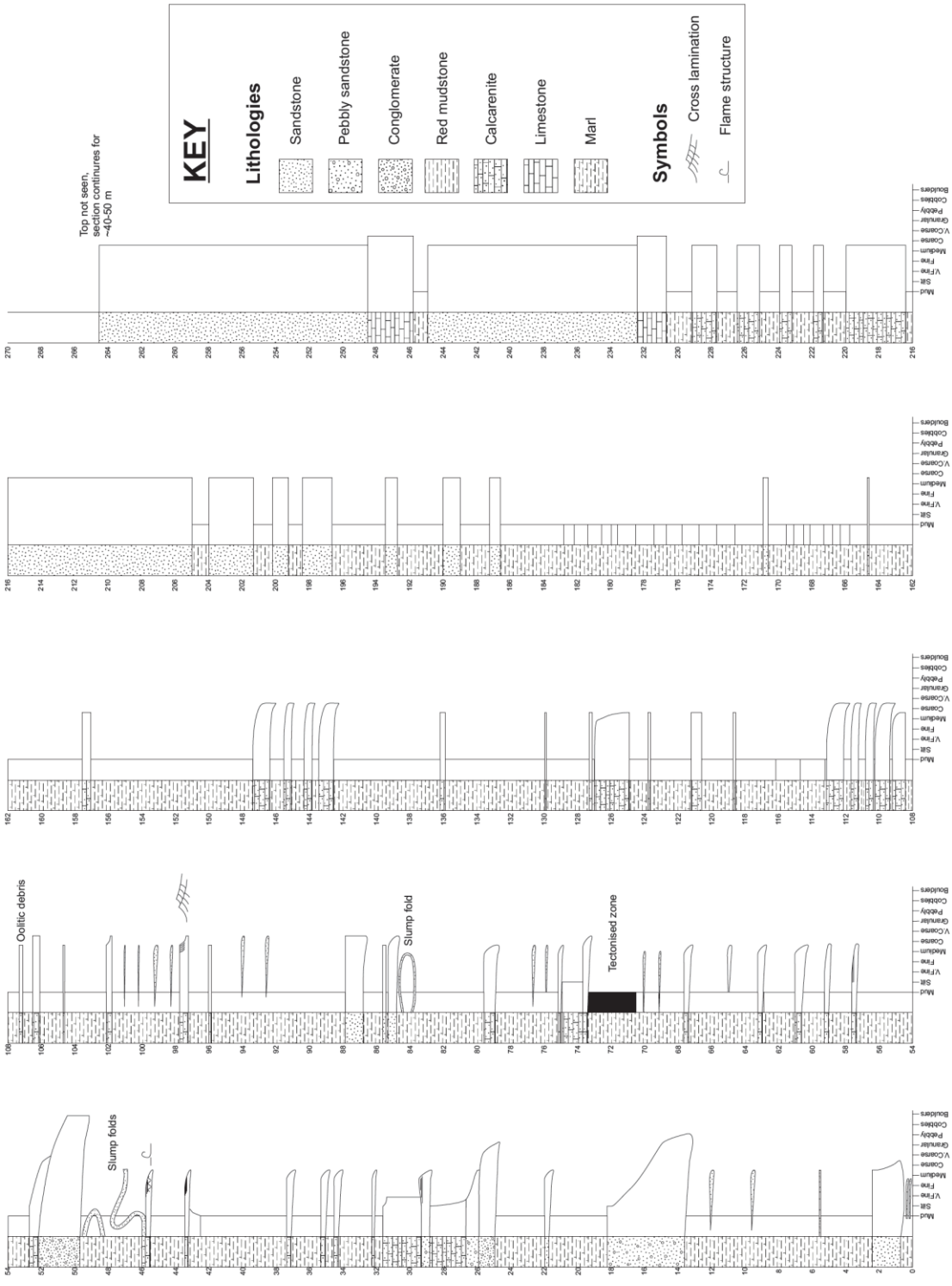

Figure 3.15. Measured sequence of part of the Hekimhan Formation, as logged at locality 'd' on the simplified geological map (Fig. 3.8).

Figure 3.16. Collection of commonly preserved trace fossils within a calcarenite bed from the Hekimhan Formation. The trace fossils include Thalassinoides and Skolithos. Pencil for scale

Locally, dark-grey conglomerates with a medium to coarse-grained sandstone matrix and clasts up to cobble size, composed of ophiolite-related lithologies were observed at the base of the formation (Fig. 3.17a). Where present the conglomerates are less than 5 m thick and often pass into ~25 m of dark-grey to-black, laminated, fissile mudstone with subordinate, thin (<10 cm) ungraded, pebbly sandstone beds. Partially pyritised, disarticulated casts of large (up to ~20 cm across), thickly-ribbed bivalves are common in the mudstones (Fig. 3.17b). Shallow-angle, internal unconformities are common within the black mudstone and sandstone intercalations.

Localised, laterally discontinuous units, ~50 cm thick, are almost entirely composed of fragments of small rudist bivalves were observed within marls of the Hekimhan Formation (Fig. 3.17c).

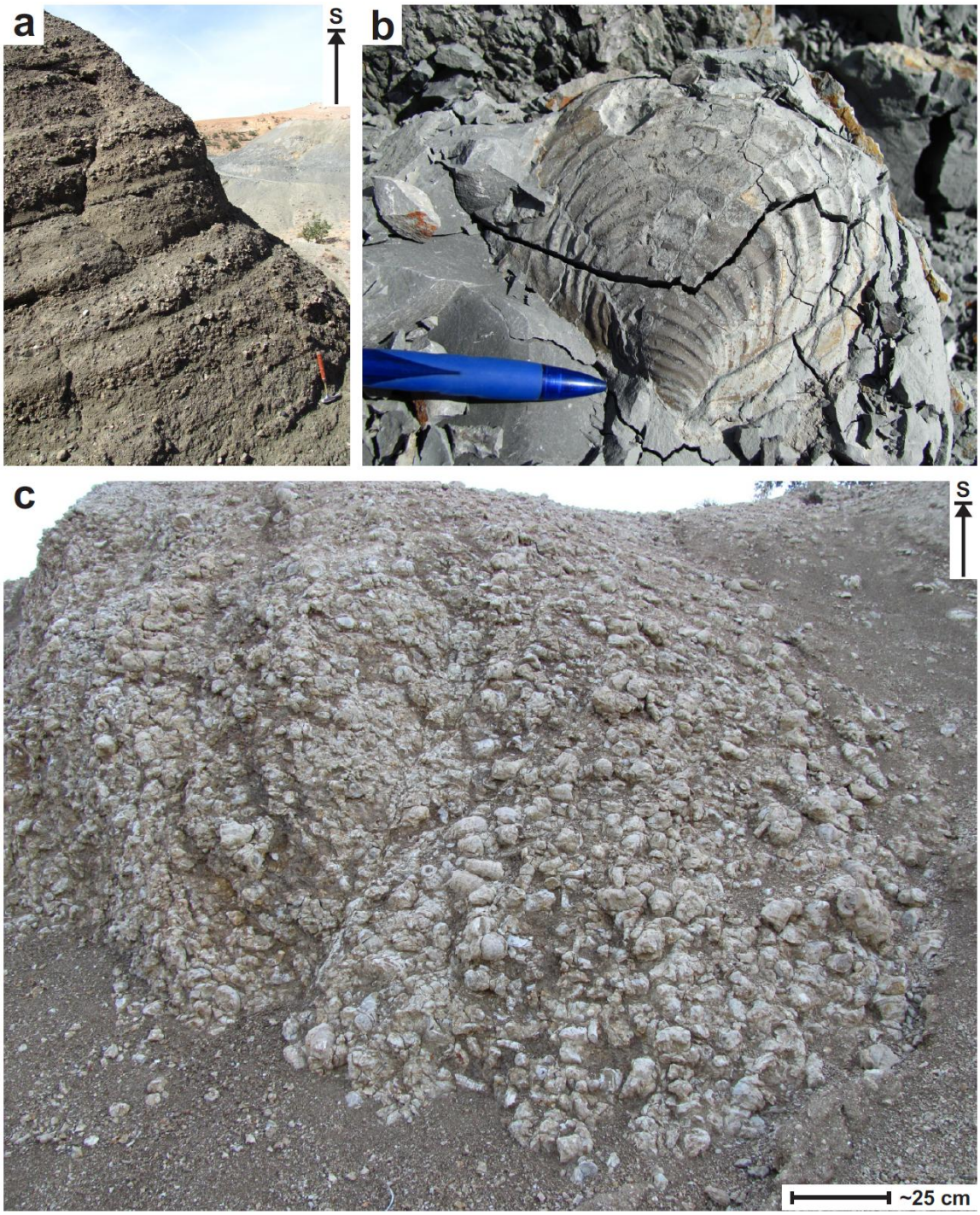

Figure 3.17. Field photographs of the Hekimhan Formation showing; a, dark grey, ophiolite-derived, sandy conglomerates (hammer for scale in lower right); b, Thickly ribbed, disarticulated and partially-pyritised bivalve within dark calcareous mudstone (pencil for scale); c, dark calcareous marl and conglomerate composed entirely of fragmented rudist bivalves.

Localised deposits of medium to pebbly calcarenite situated towards the top of the Hekimhan Formation contain important, mobile, Fungid corals (Fig. 3.18). The Fungid corals are well preserved. However, no preferred orientation of the fossils was observed within the sediment.

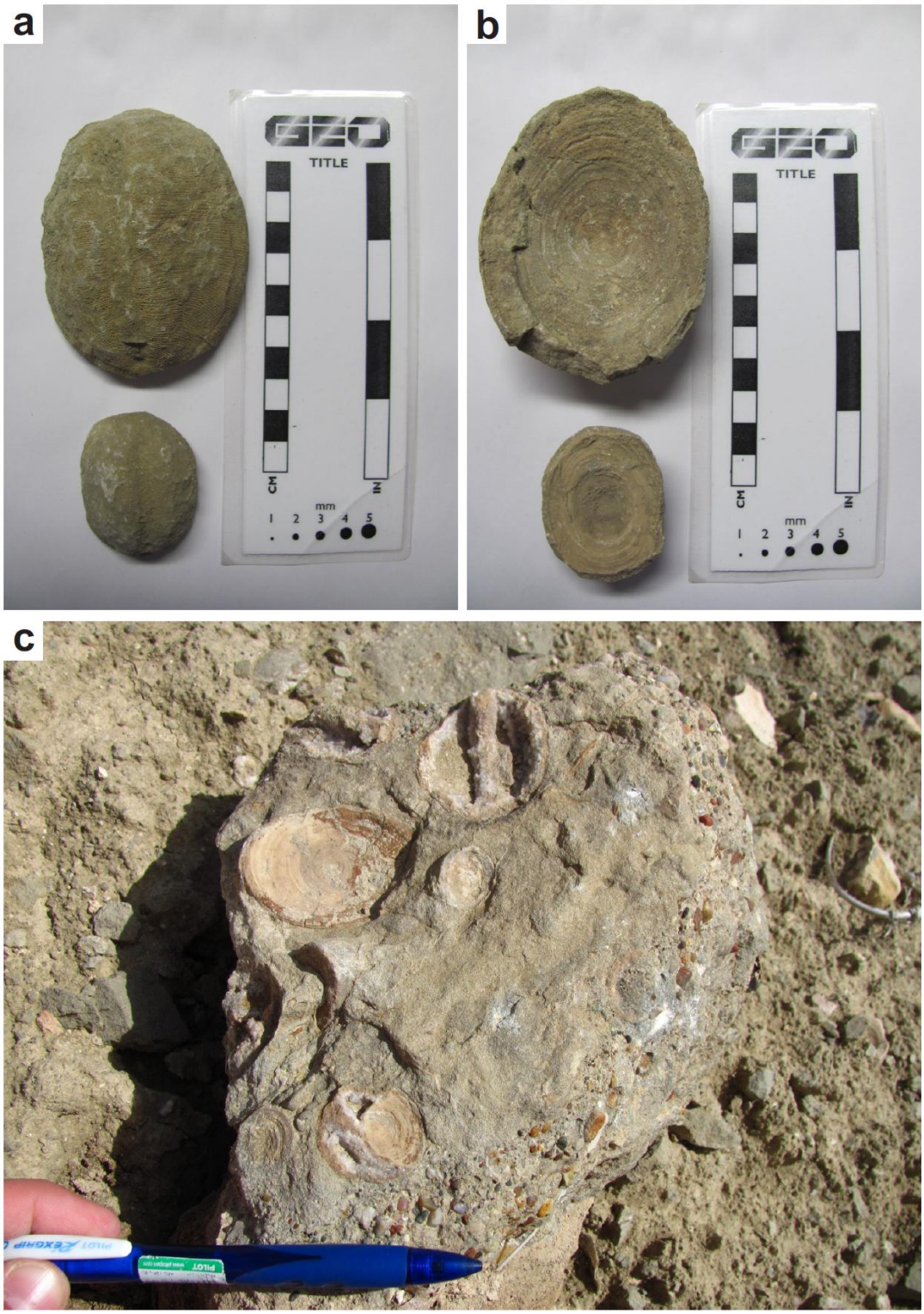

Figure 3.18. Photographs showing; a, top side of two Fungid corals with fine 'ribs' crossing the fossil in an E-W orientation. Notice the bilateral symmetry; b, underside of the same two Fungid corals with fine radial features; c, Examples of Fungid corals in a loose block composed of coarse sandstone and pebbly conglomerate (pencil for scale).

Syn-sedimentary slump folds and blocks have slipped down slope over weaker marl (rafted blocks) and stacked up on top of each other (imbricated blocks) are common in marl and calcarenite alternations in outcrops to the south of the field area (**e.g. ~46–50 m on Fig. 3.15**).

Boundaries: Usually, the base of the Hekimhan Formation is conformable above the Karadere Formation. However, the lower boundary is often influenced by the presence of a relict palaeotopography left over from the emplacement of the ophiolitic mélange. Therefore, the formation locally overlies the Karadere Formation (as well as the Tohma Member and Hocalikova Formation) above a shallow-angle unconformity.

The upper boundary is a sharp, conformable contact with massive limestones of the Hüyük Formation. However, the Hekimhan Formation is syn-depositional with volcanics of the Hasançelbi Formation towards the centre and north of the basin.

Thickness and extent: The Hekimhan Formation is well represented, with exposures around a large area in the centre of the basin (around the town of Hekimhan). The thickness varies from the north (where it is deposited alongside Hasançelebi volcanics, see below) to the south where it reaches a maximum thickness of ~750m. Localised lithological variations also occur around the Hekimhan Basin.

Age: The Hekimhan Formation is Maastrichtian in age based on the identification of Foraminifera and the presence of isolated rudist bivalves (Table 3.1). These ages are consistent with those recorded by other workers (Gürer 1994; Çalgar and Önal 2009).

Hekimhan Formation (Maastrichtian)

Samples	Rock type	Benthic Formanifera (BF)	Planktic Foraminifera (PF)	Other	Age
MB08-3	micrite	-	*Rugoglobigerina rugosa*, *Globotruncanita conica*, *Globotruncana arca*, *Pithonella ovalis*	-	Late Maastrichtian
MB08-27	micrite	-	*Globotruncanita stuartiformis*, *Contusotruncana* sp., *Rugoglobigerina* sp., *Heterohelix* sp., *Archaeoglobigerina* sp.	-	Maastrichtian
MB08-41	micrite	-	*Rugoglobigerina rugosa*, *Globotruncana ventricosa*, *Pseudotextularia* sp.	-	Maastrichtian
MB08-156	sandy limestone	*Sirtina orbitoidiformis*, *Pseudovalvulineria clementiana*, *Orbitoides* sp., *Lepidorbitoides* sp.	*Globotruncanita* sp., Pithonella ovalis, Calcisphaerula inniminata	Rudist, coralline algae	Late Maastrichtian
MB09-H47	marly limestone	*Pseudovalvulineria clementiana*	*Rugoglobigerina macrocephala*, *Globotruncanita* sp., *Pseudotextularia* sp., *Pithonella ovalis*	-	Late Maastrichtian

Table 3.1. Table showing the results of palaeontological analysis of samples from the Hekimhan Formation (courtesy of N Inan & K Taslı).

3.4.2.6 Interpretation of the Maastrichtian transgressive marine marls (Hekimhan Formation)

The Hekimhan Formation represents a major marine transgression within the Hekimhan Basin. This is evidenced by the change from continental fluvial red beds of the Karadere Formation to the faunally diverse marl and calcarenite alternations seen in the Hekimhan Formation. The marls are rich in pelagic Foraminifera, whilst the calcarenites are characterised by an abundance of benthic Foraminifera and fragmented bivalve, gastropod, echinoid and coral fossils. Graded beds, laminated tops and occasional ripple lamination, observed within the calcarenites, are typical features of the Bouma sequence (Bouma 1962). These calcarenites are likely to have been transported downslope as high density gravity flows from a shelf-like environment based on the presence of the fragmented benthic fossil assemblage. Calcareous marl forms the majority of the sediment in the Hekimhan Formation and represents the 'background' sedimentation. The localised black calcareous mudstones are likely to be sapropels, perhaps formed in isolated, relatively anoxic, palaeotopographic depressions. Anoxic is evidenced by the pyrite replacement of organic material. The ungraded, pebbly sandstone units,

predominantly composed of ophiolitic material, located within the sapropels are likely to represent debris flows. Similarly, the thin, laterally discontinuous units composed of fragmented rudist bivalves are interpreted as representing reef talus debris flows that were transported into deeper parts of the basin from Tohma Member patch reefs.

In northern parts of the basin the Hekimhan Formation is syn-depositional with the Hasançelebi Formation. The majority of the sediment associated with the Hasançelebi Formation is volcaniclastic and derived internally. However, localised pillow and lava flows were observed with inter-lava marl sediment which contained pelagic Foraminifera that were dated as Maastrichtian (Table 3.1).

Vertical burrows within bioturbated calcarenites are locally replaced by glauconite. Glauconite forms as an early diagenetic replacement mineral and is influenced by the decaying process of organic matter degraded by bacteria in marine animal shells. Glauconite is a characteristic diagenetic mineral in environments with slow accumulation rates and is typical of transgressive shelf/slope settings (Odin 1988).

Fungid corals enjoy similar living conditions to modern tropical corals (shallow-marine, nutrient rich, well oxygenated water within the photic-zone) (Matthai 1948). The Fungid corals observed in the Hekimhan Formation occur in abundance and are randomly orientated within localised deposits of medium to pebbly calcarenite. The Fungid corals may represent a death assemblage as the fossils are predominantly intact but show no preferred orientation within the coarse sediment. The Fungid-bearing calcarenite deposits are interpreted as mass flow deposits which cemented the corals into the matrix. These flows may have been initiated by storm events or mass wasting up slope.

3.4.2.7 Maastrichtian volcanism (Hasançelebi Formation)

Name: Introduced by Gürer (1994). Probably derived from the town of Hasançelebi to the north of the field area (Fig. 3.19).

Type section: Numerous road sections ~3 km east of Hacılar.

Lithology: The Hasançelebi Formation is composed of an amalgamation of extrusive and intrusive volcanic rocks and associated volcanogenic sediments.

The extrusive volcanic rocks consist of basaltic pillow lavas, lava flows and lava breccias (Fig. 3.20a). Individual pillows range in size from <half a metre up to ~1 m in scale (Fig. 3.20b). Rare elongate bolsters and lava tubes were also observed in the pillow lava sequences. Basaltic lava flows ranging in thickness from ~10 cm up to ~60 cm were observed at varying intervals within the Hasançelebi Formation (e.g. Fig. 3.21). Lava breccia is the most represented component of the Hasançelebi Formation (Fig. 3.20c and Fig. 3.22). The breccia is angular with clasts ranging from pebble to cobble-size. Commonly the pillow basalts and lava flows grade laterally into the lava breccia along the same stratigraphic horizon. The basalts are clinopyroxene and plagioclase phyric, set within a fine-grained matrix of clinopyroxene and plagioclase (Fig. 3.20d). Plagioclase phenocrysts within lava flows are often platy and aligned parallel to the boundaries of the flow unit (Fig. 3.20e). Lath shaped plagioclase forming the matrix also flow around phenocrysts (Fig. 3.20d).

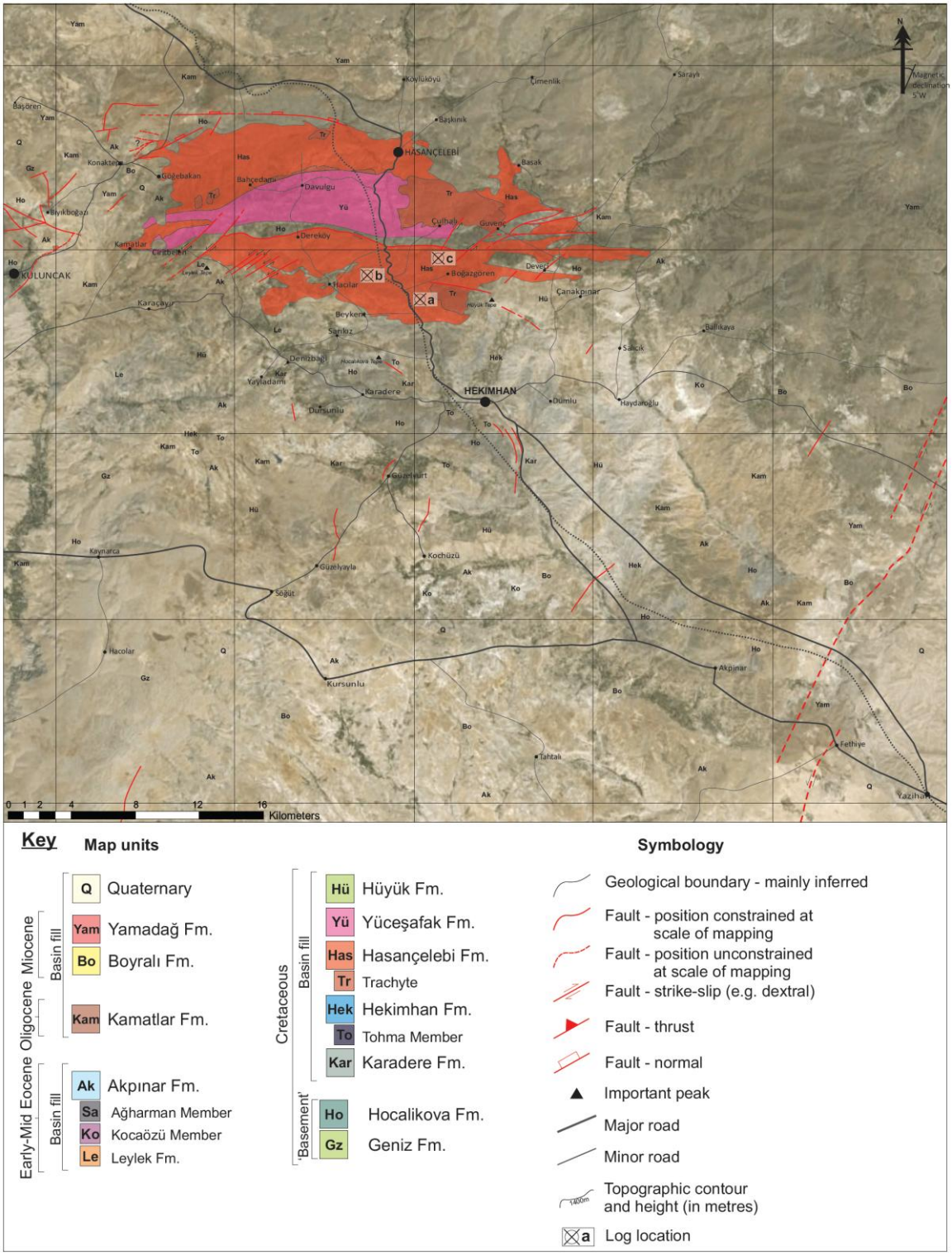

Figure 3.19. Simplified geological map showing the extent of the Hasançelbi and Yuceşafak Formations as well as the localised trachyte outcrops draped over a satellite image of the Hekimhan Basin. Also shown are logged section locations.

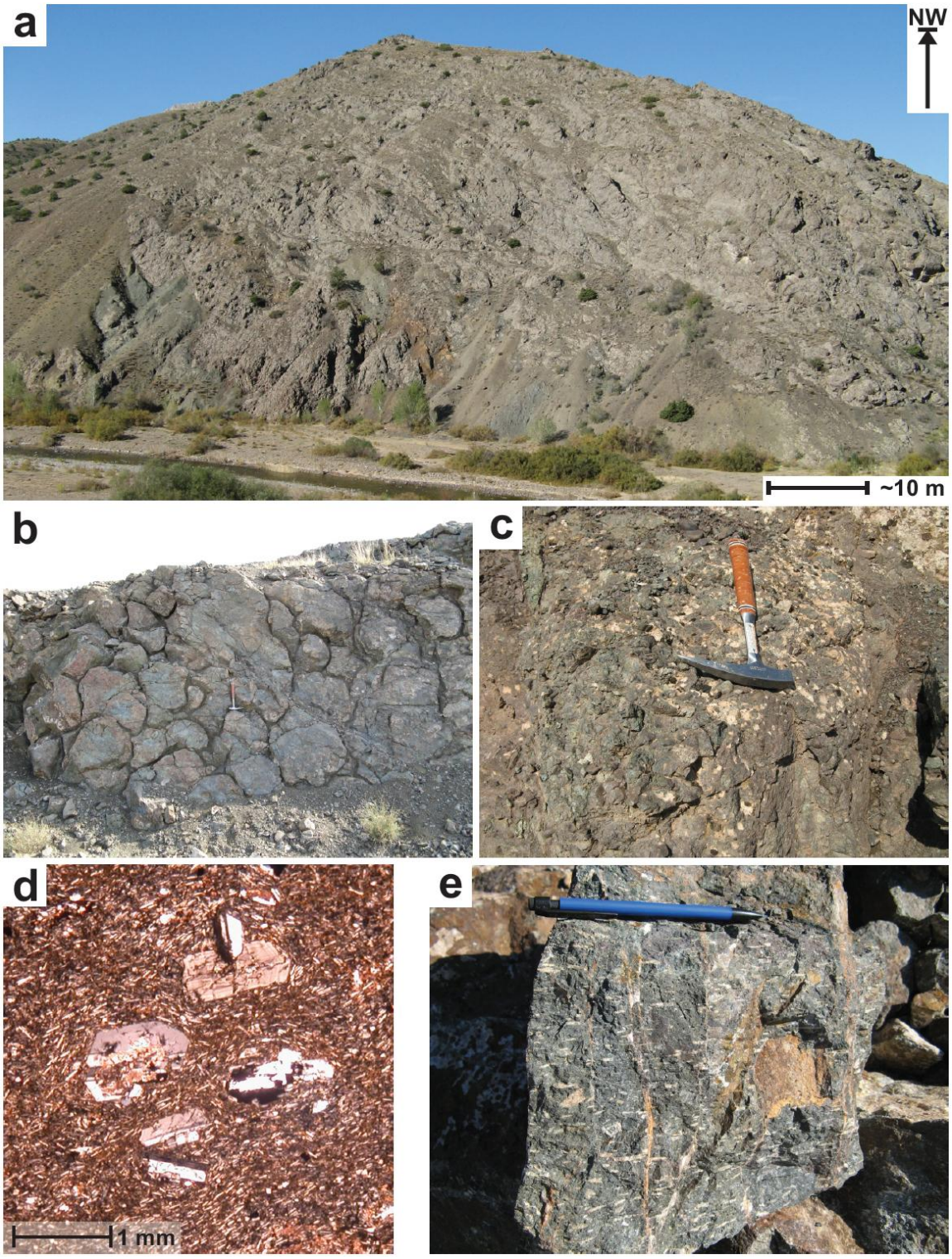

Figure 3.20. Field photographs showing, a, typical outcrop of the Hasançelebi Formation where lava flows, pillow lavas and lava breccias alternate stratigraphically and laterally; b, road section through pillow lava sequence; c, close up view of lava breccia (hammer for scale in b and c); d, Tabular plagioclase phenocrysts with lath shaped matrix plagioclase flowing around them; e, block from a lava flow showing the alignment of white, elongate plagioclase minerals (~ aligned with pencil).

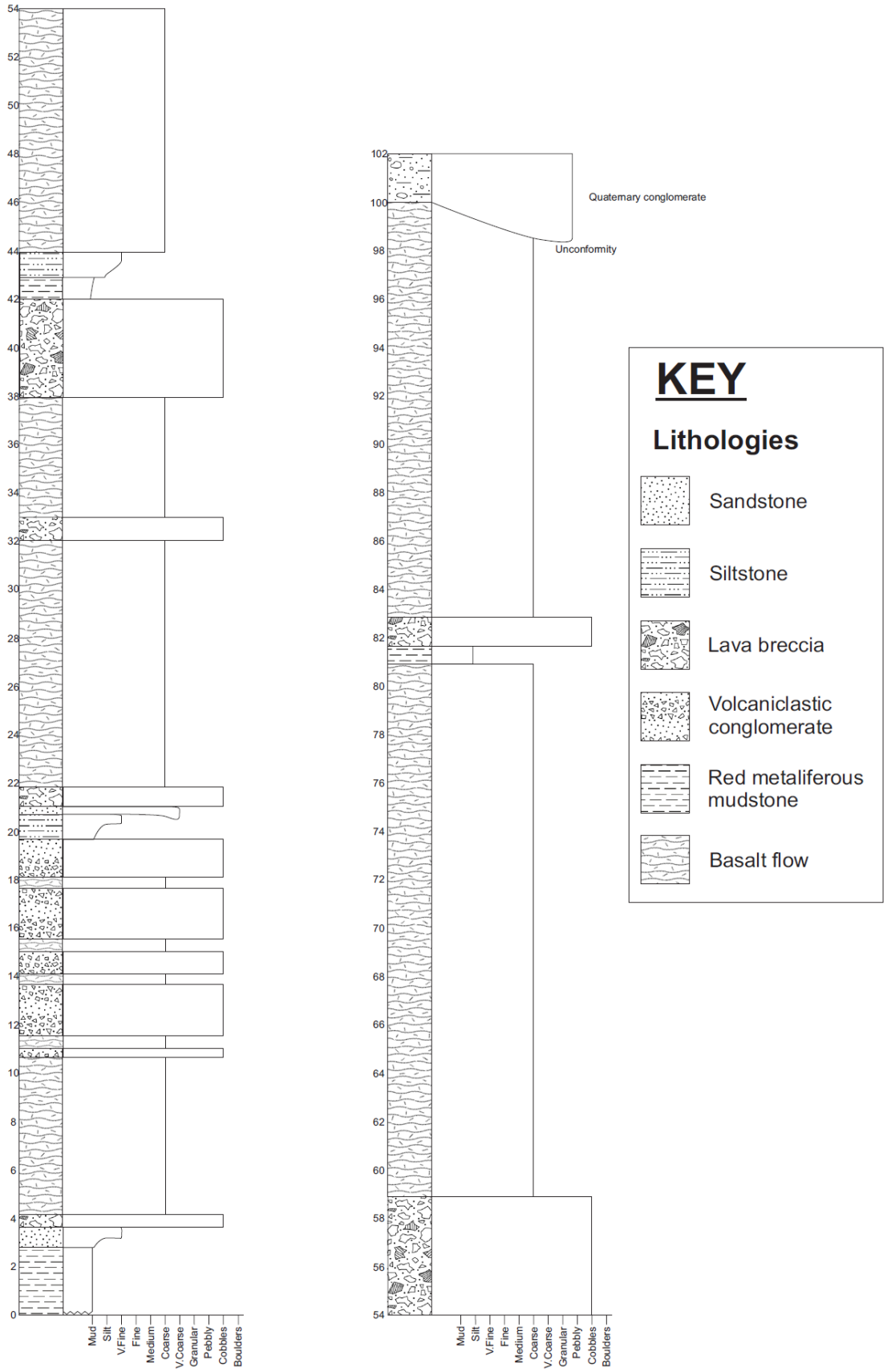

Figure 3.21. Measured sequence of part of the Hasançelebi Formation taken from locality 'a' on the simplified geological map (Fig. 3.19).

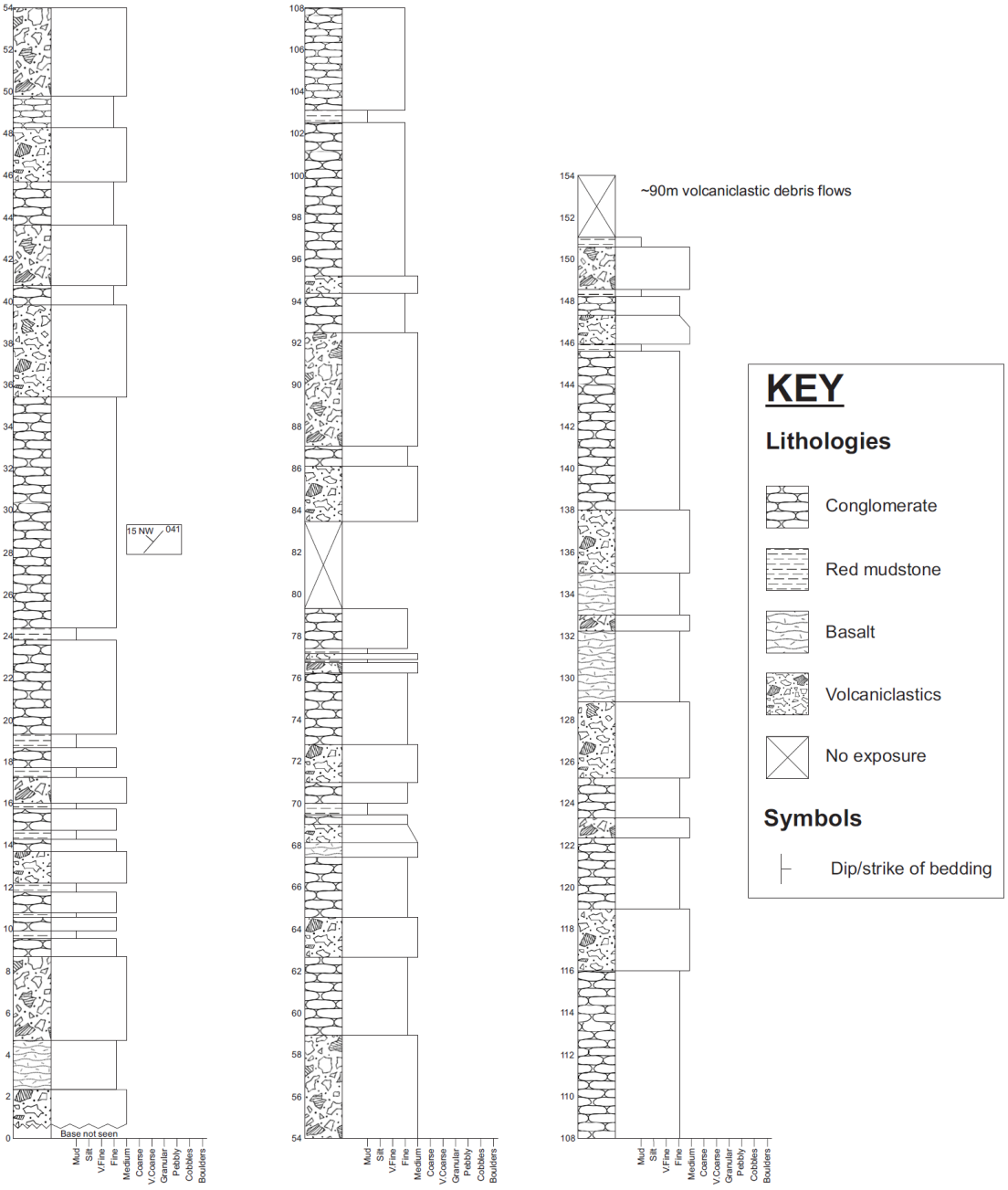

Figure 3.22. Measured sequence of part of the Hasançelebi Formation taken from locality 'b' on the simplified geological map (Fig. 3.19).

The intrusive rocks are composed of fine to medium grained basalt, forming dykes which crosscut Hasançelebi Formation lavas as well as Hekimhan Formation sediments in the vicinity of the Hasançelebi Formation (Fig. 3.23a). The dykes range in width from centimetre-scale 'dyklets' attached to wider primary dykes. Primary dykes can be up to 1 m thick. Dykes within sedimentary material commonly have well developed chilled and baked margins, typically centimetres wide. Dykes within volcanic Hasançelebi Formation rocks have thin chilled and baked margins, typically millimetres wide (Fig. 3.23b).

A sequence of pale, altered lava (?trachyte) is exposed to the west of Hüyük Tepe. The mineralogy of the unit is almost entirely altered. However, some relatively unaltered samples were sectioned and an example is shown in Figure 3.24 Trachyte is the extrusive equivelant of syenite (which was also observed in the field area, see Chapter 3.4.2.10).

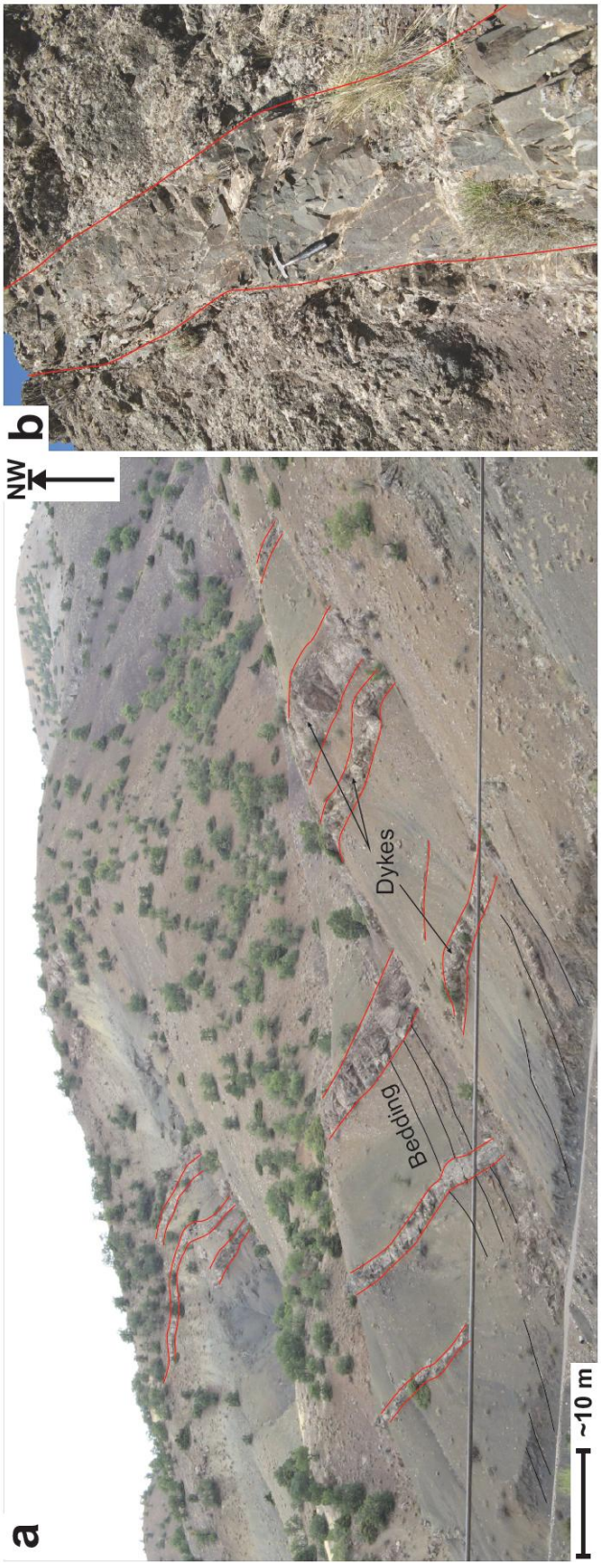

Figure 3.23. Field photographs showing; a, Hekimhan Formation sediments in the central part of the basin to the south of the Hasançelebi Formation. Sinuous dykes of various widths penetrate the sediments here approximately perpendicular to the regional bedding. These dykes have well developed chilled and baked margins; b, dyke cross cutting Hasançelebi Formation lavas with poorly developed chilled and baked margins (hammer for scale in centre).

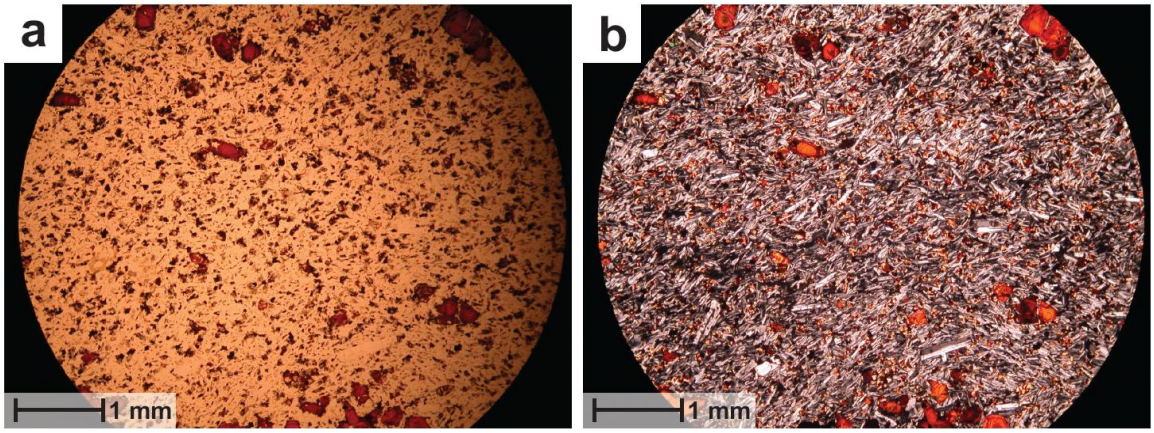

Figure 3.24. a, PPL image of altered trachyte; b, XPL image of altered trachyte showing randomly orientated plagioclase crystals and undistinguished orange mineral which is probably a clay mineral.

Volcaniclastic sediments including; mudstone, sandstone, conglomerate and tuff deposits form a significant component of the Hasançelebi Formation. The mudstone is red, unfossiliferous and finely laminated. It usually occurs as thin packages between pillow lavas, lava flows or other associated volcaniclastic sediments. The mudstone is enriched in metalliferous elements including manganese. Marble-sized manganese concretions are common in the mudstone and often weather out of road sections (Fig. 3.25a). Where lava has directly interacted with unlithified, wet sediment, pieces of the volcanic material have mixed and been incorporated into the sediment to form peperite structures (Fig. 3.25b). The dark-grey to dark-red sandstones are coarse grained, angular and texturally immature. Sandstone beds are often graded with laminated tops (Fig. 3.25c). They are composed of mafic minerals and volcanic glass (hyaloclastite). The most abundant volcaniclastic sediments are dark grey conglomerates composed of angular, usually cobble-sized clasts set in a coarse, sandy matrix (Fig. 3.25d). The clasts and matrix are composed almost entirely of basalt. To the north of Hasançelebi, light grey, fine grained tuff deposits interbedded with graded volcaniclastic sandstones were observed (Fig. 3.25e). Syn-sedimentary deformation (primarily slump folds) is common within the volcaniclastic sediments throughout the Hasançelebi Formation (e.g. ~150–158 m on Fig. 3.26).

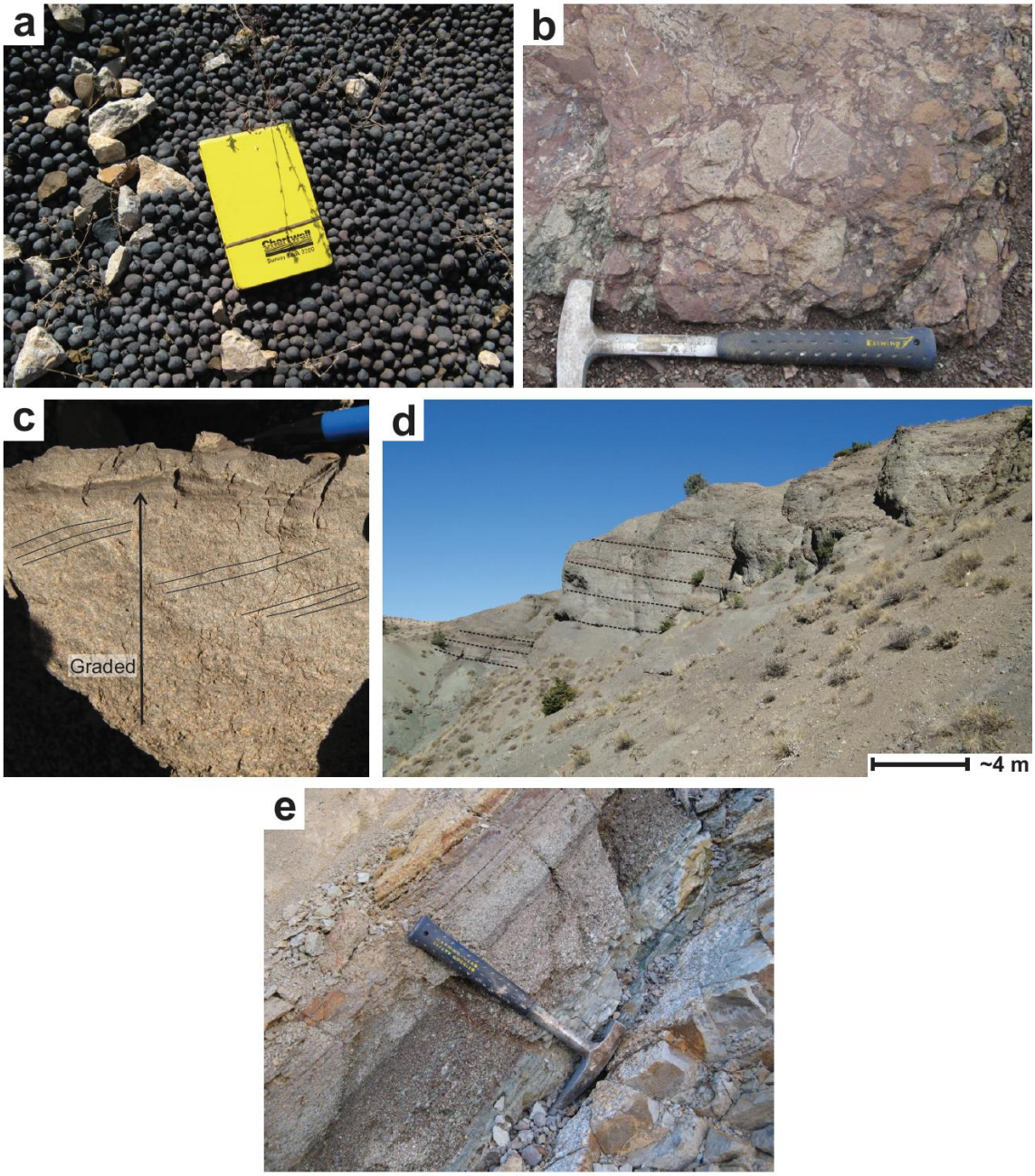

Figure 3.25. Field photographs showing; a, marble sized manganese concretions eroded out of volcaniclastic mudstone; b, pepperite structures; c, graded volcaniclastic sandstone with poorly developed cross lamination and laminated top (pencil for scale in upper right); d, sequence of volcaniclastic debris flows; e, light grey tuff overlain by graded volcaniclastic sandstone.

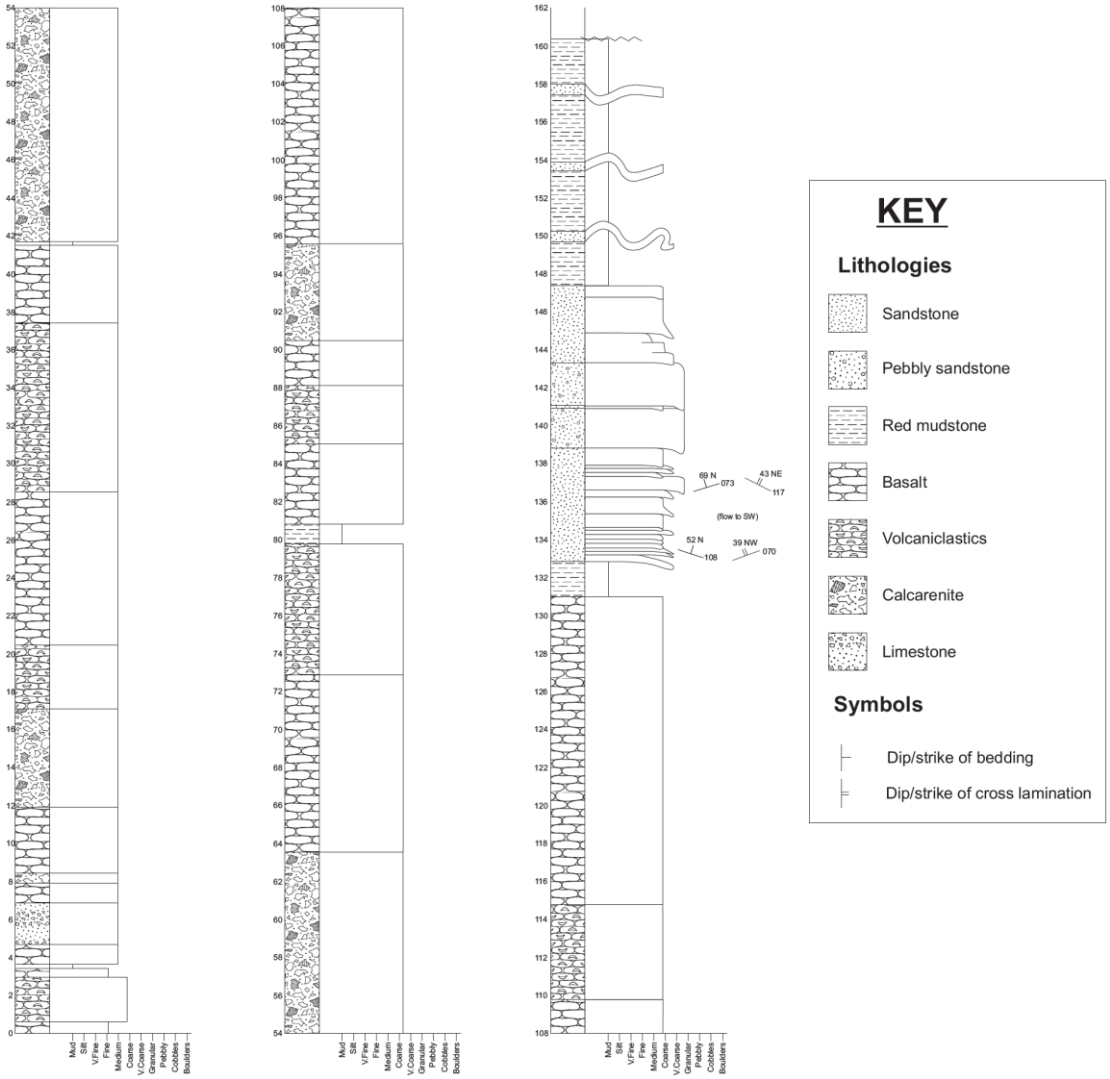

Figure 3.26. Measured sequence of part of the Hasançelebi Formation taken from locality 'c' on the simplified geological map (Fig. 3.21).

Hydrothermal alteration is common in the Hasançelebi Formation. Localised fracture networks with metalliferous mineralisation (e.g. malachite and azurite) were observed in some of the lavas (Fig. 3.27a & b). The plagioclase and clinopyroxene basalts have been mineralogically altered in areas affected by hydrothermal processes (discussed further in 3.4.2.8 Hasançelebi Formation geochemistry). Localised, vertical, hydrothermally altered zones were observed within marl and limestone alternations (Hekimhan Formation) near Hacılar. These areas were characterised by light brown, heavily fractured sediments with manganese mineralisation commonly observed along fracture planes (Fig. 3.27c).

Figure 3.27. Field photographs showing; a, azurite and minor malachite mineralisation; b, malachite mineralisation; c, fractured and altered carbonate sediments with manganese mineralisation on major fracture planes. Hammer for scale in all pictures.

Boundaries: A stratigraphic lower boundary was not observed in the field. However, sediments identified as belonging to the Hekimhan Formation were interleaved with Hasançelebi Formation lavas in many areas. A stratigraphic upper contact was not observed in the field area. However, a tectonic contact between the Hasançelebi Formation and limestones of the Hüyük Formation was observed ~1 km east of Boğazgören. The ?trachyte sequence is topographically higher than the Hasançelebi Formation lavas. However, no stratigraphic relationships could be observed in the field.

Thickness and extent: The Hasançelebi Formation is well exposed and well represented in the Hekimhan Basin. An east-west orientated sequence, ~12 km across, outcrops around, and to the west of, Hasançelebi. A second, better exposed, outcrop ~15 km across is situated half way between Hasançelebi and Hekimhan and is partially exposed by tectonic lineaments along the northern margin.

Overall, the Hasançelebi Formation reaches a total thickness of ~750 m. The formation is composed of alternations of pillow lava, lava flows, lava breccias and associated volcaniclastic sediments. The thickness of the individual components ranges from individual flows or beds to packages up to ~25 m thick. Lava breccias were also observed as lateral extensions of lava flows. The volcaniclastic sediments vary in thickness laterally. For example, red metalliferous mudstone often occurs as isolated pods which appear to fill depressions (i.e. the undulating surfaces of pillow lava beds).

Age: Mid-Late Maastrichtian based on the palaeontology of pelagic Foraminifera from interbedded marls.

3.4.2.8 Geochemistry of the Maastrichtian volcanism (Hasançelebi Formation)

The Hasançelebi Formation represents extensive volcanism related to the formation of the Hekimhan Basin. The geochemistry of the volcanic rocks sheds light upon the tectonic history of the region. Twenty five samples of volcanic rocks and six samples of volcaniclastic sediment from the Hasançelebi Formation were analysed using X-Ray Fluorescence (XRF).

The samples were screened to remove those which have undergone a large degree of alteration in order to obtain the best quality data for interpretation. Two separate screening criteria were utilised in order to establish samples which could safely be used. Both criteria utilise SiO_2, MgO and CaO. The first pass was a bulk analysis where the combined values of MgO+CaO must lie between 12 and 22 wt. % and SiO_2 values must lie between 42 and 56 wt. % (Pearce & Cann 1973). This method determined that 8 out of the 25 samples were eligible for further geochemical analysis. The second method involved ascertaining whether three individual criteria were met. These were; SiO2 >43% and <56%, MgO <4%, CaO >5% and <15%. This resulted in 8 usable samples out of 25, 5 of which were different to the 8 which passed the initial method. For the purposes of this study, the 8 samples which survived the first method as well as the additional 5 from the second method were utilised for geochemical interpretation. In addition, samples which passed 2 out of the 3 criteria in the second method were also carried forward.

However, these last were flagged during the geochemical analysis should any discrepancies arise during the interpretation (see Table 3.2).

Sample	SiO2	MgO	CaO	MgO + CaO	MgO+CaO >12 and <22 and SiO2 >42 and <56	SiO2 >43% and <56%	MgO <4%	CaO >5% and <15%
MB08-8	55.08	2.95	9.27	12.22	OK	OK	OK	OK
MB08-18	42.47	12.05	26.15	38.20	Altered	Altered	Altered	Altered
MB08-20	49.99	6.08	10.04	16.11	OK	OK	Altered	OK
MB08-140	50.60	5.89	9.91	15.80	OK	OK	Altered	OK
MB08-183	46.35	6.50	19.34	25.84	Altered	OK	Altered	Altered
MB08-223	51.64	4.47	7.84	12.31	OK	OK	Altered	OK
MB08-224	56.12	3.30	7.34	10.63	Altered	Altered	OK	OK
MB08-225	49.96	12.94	26.93	39.87	Altered	OK	Altered	Altered
MB08-227	48.28	7.13	6.14	13.27	OK	OK	Altered	OK
MB08-228	58.05	2.93	6.00	8.92	Altered	Altered	OK	OK
MB08-232	53.84	1.34	5.85	7.19	Altered	OK	OK	OK
MB09-H36	51.60	8.02	9.22	17.24	OK	OK	Altered	OK
MB09-H93	53.98	3.32	11.63	14.95	OK	OK	OK	OK
MB08-131	53.51	2.43	7.89	10.33	Altered	OK	OK	OK
MB08-132	54.61	1.88	4.75	6.63	Altered	OK	OK	Altered
MB08-135	53.40	2.98	7.66	10.64	Altered	OK	OK	OK
MB08-200	59.52	1.29	6.87	8.16	Altered	Altered	OK	OK
MB08-203	53.90	2.00	8.12	10.12	Altered	OK	OK	OK
MB08-204	64.81	2.60	7.55	10.15	Altered	Altered	OK	OK
MB09-D27	54.32	3.01	6.63	9.64	Altered	OK	OK	OK
MB10-48	51.99	3.49	12.09	15.58	OK	OK	OK	OK
MB10-110a	57.80	4.65	5.49	10.14	Altered	Altered	Altered	OK
MB10-110b	58.42	4.74	4.78	9.52	Altered	Altered	Altered	Altered
MB10-111a	59.07	4.29	7.66	11.95	Altered	Altered	Altered	OK
MB10-111b	58.30	4.99	8.53	13.51	Altered	Altered	Altered	OK

Table 3.2. Filtering parameters for volcanic rocks from the Hasançelebi Formation. The first method (bulk method) accepted 8 samples for further analysis (highlighted in yellow). The second method (individual criteria method) accepted 8 samples, some of which were different from the first method (highlighted in green). However, samples which failed only one parameter of the second method were also accepted for further analysis (highlighted in blue), albeit with caution. All samples are calculated on a volatile free basis (recalculated for LOI).

Loss on ignition (LOI) was high in some of the rocks and is indicative of post-emplacement alteration. Samples with high LOI (>8%, 3 samples: MB09-H36, MB09-H93 and MB09-D27) were flagged, in order to be removed at a later stage if problematic. LOI results were within a normal range in general (~3-6%). However, the samples were recalculated on a volatile-free basis to reduce the effect of LOI on the geochemical analyses. Values of TiO_2 were also recalculated to Ti ppm for use in some tectonic discrimination diagrams (below).

A volcanic rock classification diagram utilising total alkalis ($Na_2O + K_2O$) versus Silica (SiO_2) (Le Maitre *et al.* 2002) is shown in Figure 3.28. This shows that the majority of the rocks sampled from the Hasançelebi Formation plot in and around the basaltic-trachyandesite, trachy-andesite, andesite, basaltic andesite and basalt fields.

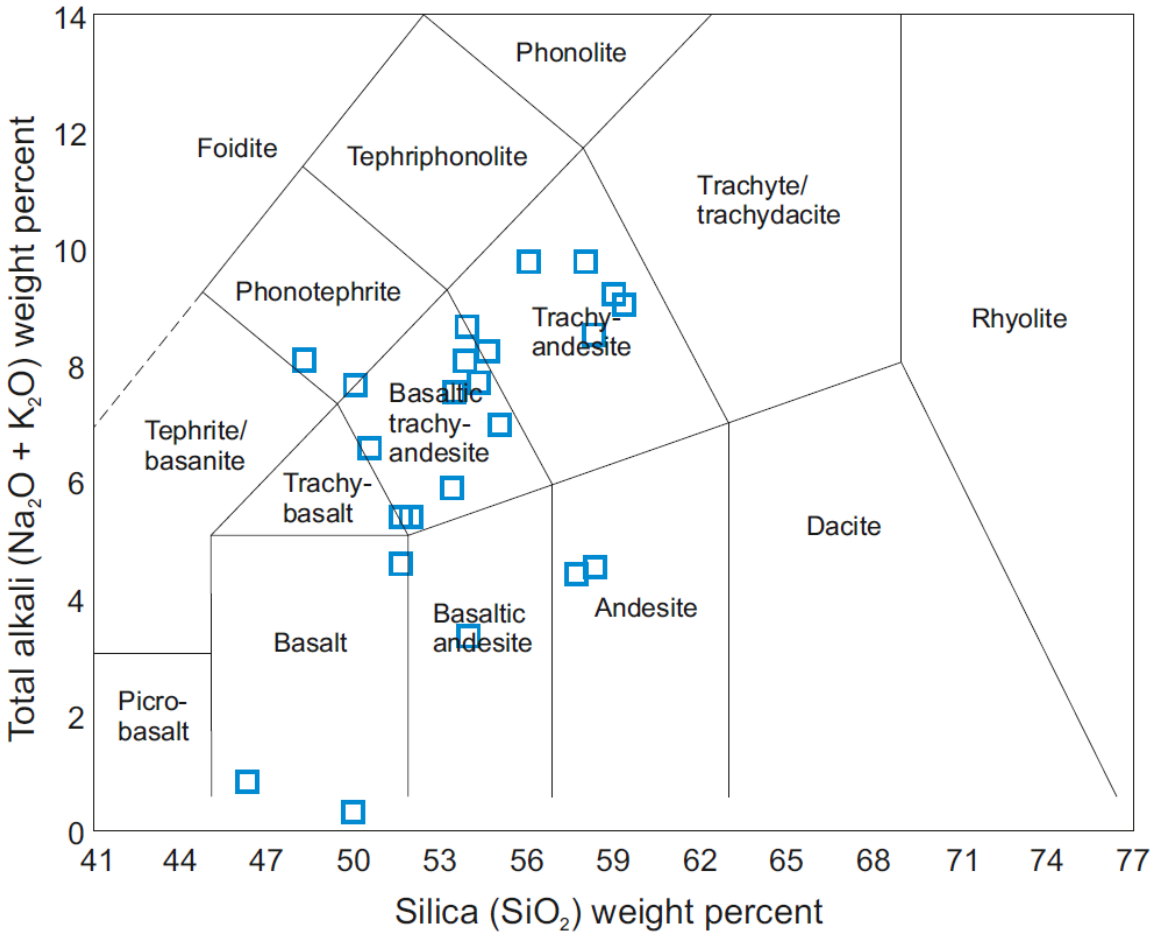

Figure 3.28. Volcanic rock classification diagram utilising total alkalis ($Na_2O + K_2O$) versus Silica (SiO_2) (Le Maitre *et al.* 2002).

Tectonic discrimination diagrams can also be used to ascertain a likely geological setting for the volcanic rocks. However, given the general nature of the volcanic rocks of the Hasançelebi Formation (i.e. subduction zone influenced), care must be taken when utilising these diagrams.

The first tectonic discrimination diagram utilises Zr and Ti (ppm) on a logarithmic plot to distinguish between volcanic-arc, within-plate and MORB affinities (Fig. 3.29). This shows that the majority of the Hasançelebi Formation volcanic rocks plot in the within-plate field albeit with a large scatter.

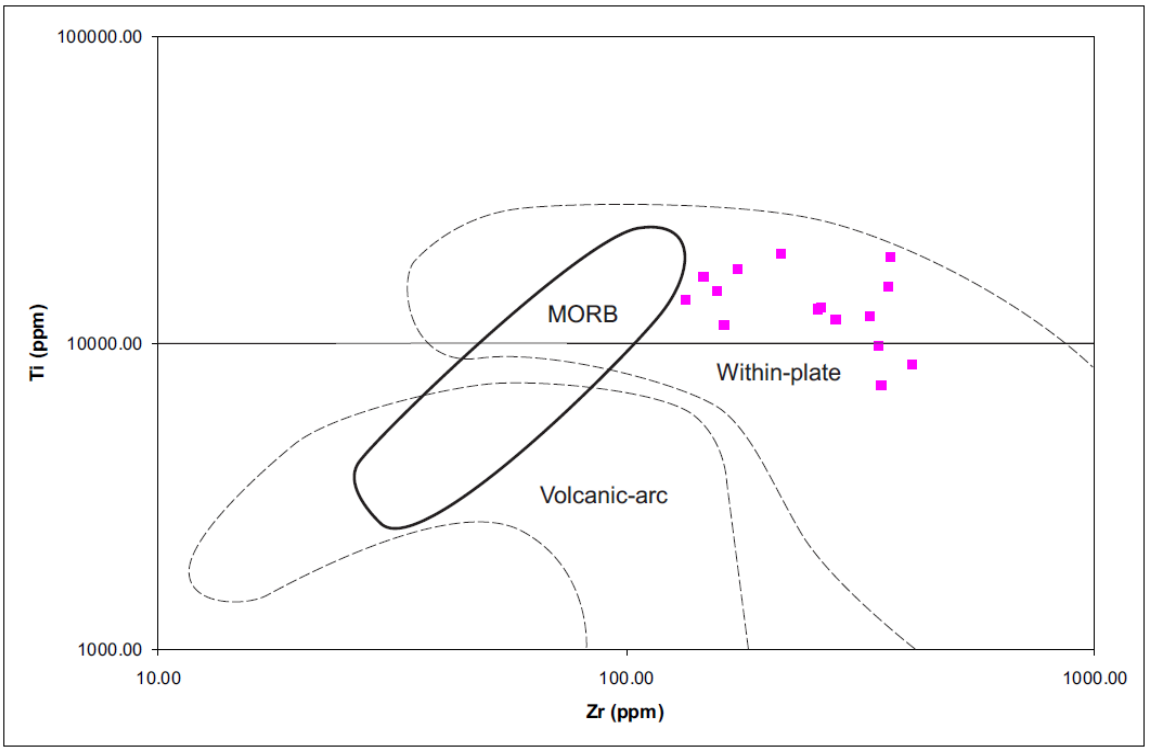

Figure 3.29. Discrimination diagram for Hasançelebi Formation basalts based upon Ti-Zr variations (after Pearce & Cann 1973).

The Zr/Y-Zr discrimination diagram can be used to determine whether basalts have an ocean-island, MORB or within-plate affinity (Pearce & Norry 1979). Figure 3.30 shows a Zr/Y-Zr discrimination diagram for basalts from the Hasançelebi Formation. The plot indicates that the majority of the samples have a within-plate affinity.

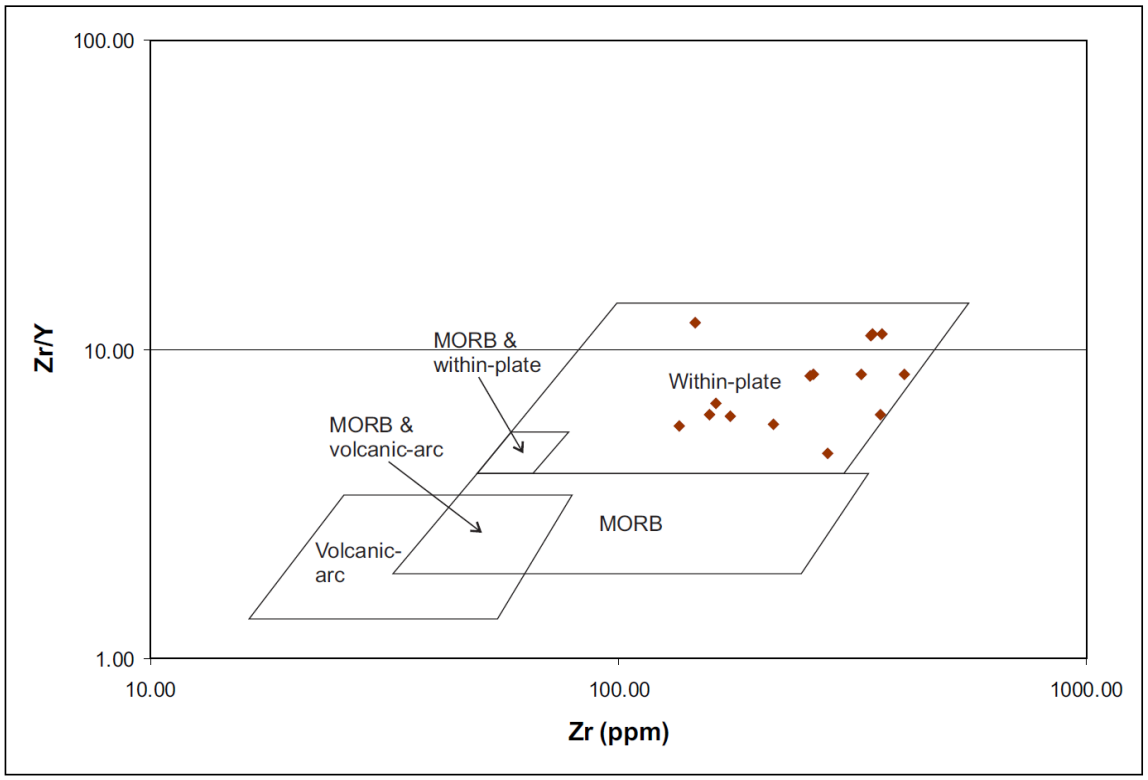

Figure 3.30. Discrimination diagram based upon Zr/Y-Zr variations. Basalts from the Hasançelebi Formation mainly plot in the within-plate field, albeit with a large scatter. The plot has a logarithmic scale (after Pearce & Norry 1979).

The Ti/Y-Nb/Y plot can be used to determine the tectonic affinity of basaltic rocks as well as to differentiate between tholeiitic, transitional and alkaline. Figure 3.31 shows a Ti/Y-Nb/Y discrimination plot which shows the affinity of basaltic rocks from the Hasançelebi Formation mainly plot in the within-plate field and are either transitional or alkaline in nature. The scatter within the data set could be a result of Nb. As discussed earlier, Nb may not be a reliable element for basalts influenced by subduction zone processes.

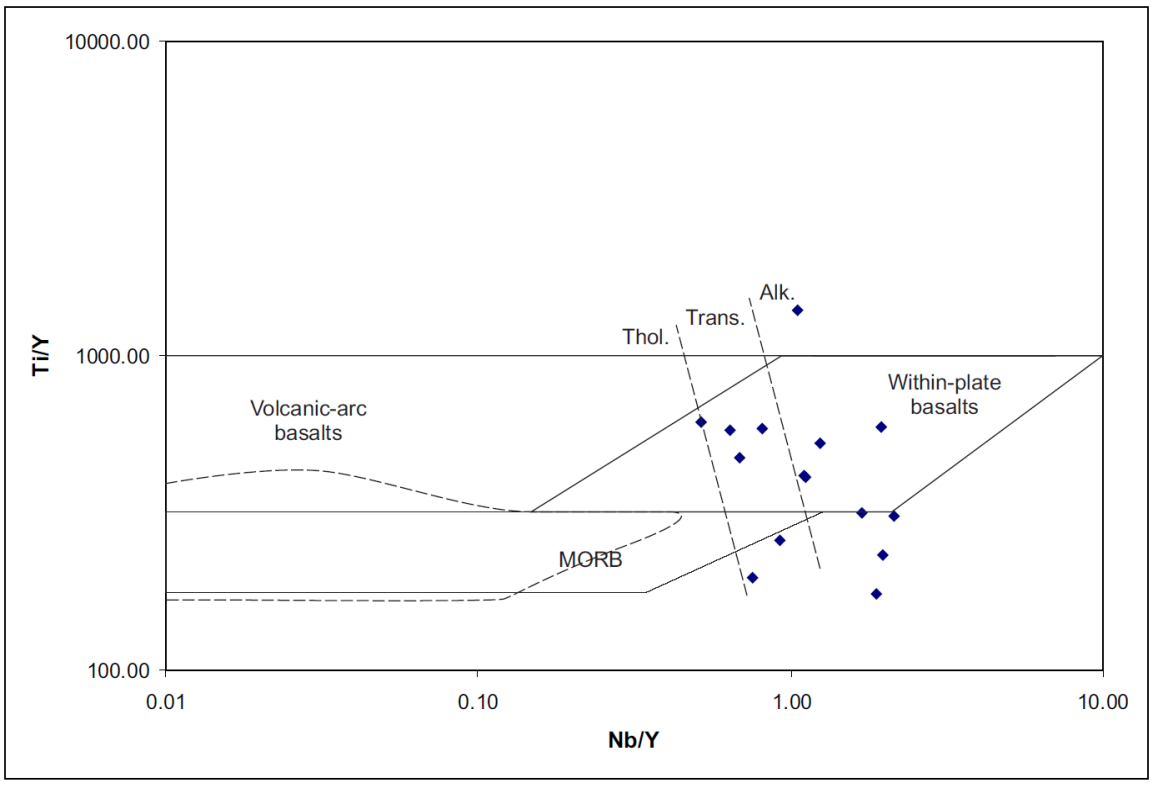

Figure 3.31. Ti/Y-Nb/Y discrimination diagram for the Hasançelebi Formation volcanic rocks. The samples mainly lie within the within-plate basalts field and are transitional-alkaline in nature (after Pearce 1982). The scatter could be a result of Nb.

Normalised multi-element diagrams ('spider diagrams') are based upon a grouping of elements that are incompatible with respect to typical mantle mineralogy. The samples of basalt from the Hasançelebi Formation were normalised to Mid Ocean Ridge Basalt (MORB). Figure 3.32 shows that the volcanic rocks from the Hasançelebi Formation resemble the geochemical characteristics of Within-Plate Basalts (WPB). The normalising data used are from Pearce (1982) and Saunders & Tarney (1984).

The multi-element 'spider' plot (Fig. 3.32) shows an enrichment of the Large Ion Lithophile Elements (LILE's) Sr–Ba and the Light Rare Earth Elements (LREE's) La–Ce. The High Field Strength Elements (HFSE's) Nb, Zr and Ti are slightly enriched but much less so than the LILE's and LREE's. HFSEs on the right hand side of the plot are relatively depleted. This pattern is related to the source of the parental magma (Pearce 1982). Many of the elements in the plot are incompatible with a basaltic magma which crystallises olivine, plagioclase and clinopyroxene. However, Sr is compatible with plagioclase and Cr is compatible with mafic minerals. As a result the elements situated on the left-hand side of the plot (LILE's and LREE's) become enriched during fractional

crystallisation (Pearce 1982). The High Field Strength Elements (HFSE's) Nb, Zr, and Ti are slightly enriched with respect to MORB but significantly less enriched than the LILE's and LREE's. Notably Nb, exhibits a slight negative anomaly. Lesser enrichment of Nb compared with LILE's and LREE's can probably be attributed to a mantle source influenced by a subduction zone component (Pearce *et al.* 1990; Keskin *et al.* 1998; Dilek & Furnes 2009). LILE's and LREE's are mobile elements that are easily transported in aqueous fluids which are driven off subducted oceanic crust and associated sediments. In this way, they are concentrated in magmas which are generated above subduction zones. Nb is comparatively immobile in aqueous fluids and thus enrichment does not occur (Pearce 1982; Baier *et al.* 2008).

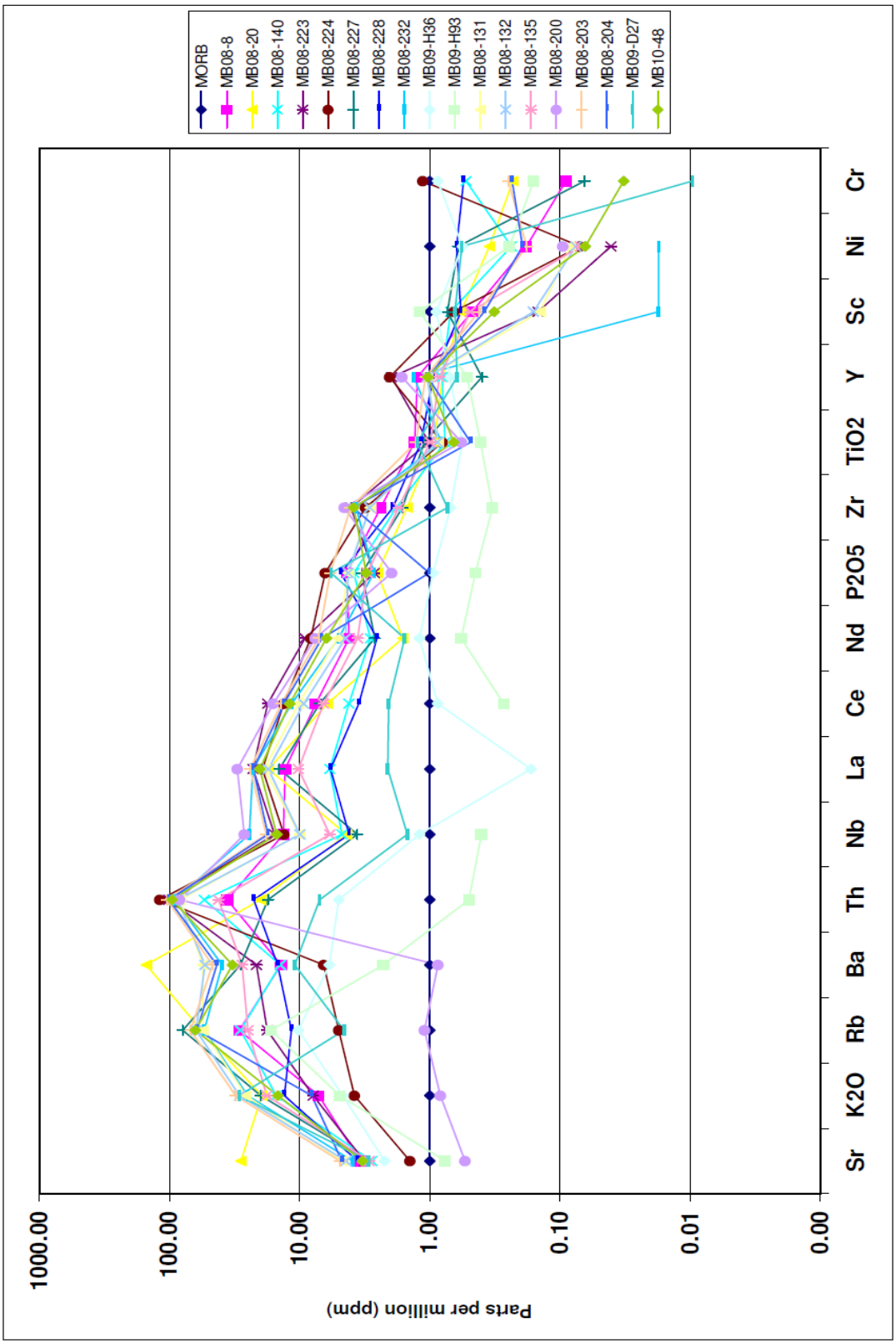

Figure 3.32. Spider diagram of basic volcanic rocks from the Hasançelebi Formation normalised to MORB (MORB data from Pearce 1982 and Saunders & Tarney 1984).

Three anomalous samples were identified from the 'spider' diagram in Figure 3.32 (MB08-200, MB09-H36 and MB09-H93). These samples were normalised to a typical volcanic arc signature. Two of these samples (H36 and H93) show a volcanic arc affinity. However, this could be a result of re-melting of already depleted mantle lithosphere and does not necessarily indicate a coeval arc setting, as described below, especially given the small number of samples. Sample MB08-200 is likely to be highly altered or weathered. These samples correlate with the anomalous samples shown in Figure 3.28 (crosses inside boxes), and have been removed from further consideration.

Metasomatic processes and also the assimilation of crustal rocks have been shown to influence enrichment of Nb (Pearce & Cann 1973; Keskin *et al.* 1998; 2001). Therefore, Nb has to be used with some caution when interpreting a subduction-influenced signature. However, all of the samples analysed from the Hasançelebi Formation exhibit a negative Nb anomaly and it is likely that this was caused by a subduction-influenced source. Similar Nb anomalies attributed to a subduction influenced magma source have been reported from other tectonic-sedimentary basins in Central Anatolia, including the Ulukışla Basin (Clark & Robertson 2002, 2005) and the Çankırı Basin (Nairn *et al.* in press).

As noted above the negative Nb anomaly observed in the Hasançelebi Formation volcanic rocks is believed to be inherited from an earlier phase of subduction and not representative of a contemporaneous subduction zone and related volcanic arc. The evidence for this includes:

- The tectonostratigraphy of the Hekimhan Basin is not suggestive of a subduction zone origin. There is no evidence of typical arc-like rocks in the basin or its vicinity (e.g. andesite, tuff).
- The basin is characterised by subsidence and collapse rather than compression and related arc magmatism (see structure section, chapter 3.5).
- The main geochemical aspects of the Hasançelebi Formation volcanics as well as the plutonic Yuceşafak Member (see below) are indicative of a within-plate setting.

In light of the above points the subduction zone signature is believed to be inherited from a subduction zone that was active in the area prior to the formation of the Hekimhan Basin. For example, partial melting of a mantle source where Nb was preferentially depleted (as at a subduction zone) and was then subsequently re-melted, or otherwise included in a later partial melt. This process would overprint the chemical signature of the later melt with an inherited Nb anomaly. The genesis and location of this inferred subduction zone is likely to involve the destruction of the Inner Tauride Ocean during the late Cretaceous; this is discussed in detail in chapter 4.

3.4.2.9 Geochemistry of the Maastrichtian inter-lava sediments (Hasançelebi Formation)

Six samples of inter-lava volcaniclastic sediment were also analysed by XRF. The sediments are composed of red metalliferous mudstone occurring in thin layers (usually <10 cm thick) between lava flows.

In general, Al and Ti are assumed to be derived from a terriginous source while heavy and metalliferous elements (e.g. Fe, Mn, Ba, Cu, Ni and Cr) are assumed to be derived from a volcanic or hydrothermal source (Turekian & Wedepohl 1961). Figure 3.33 shows a ternary plot of Al plotted against Fe and Mn. Al ranges from ~40–70%, Fe from ~20–60% and Mn from ~0–10%. The volcaniclastic sediments are, therefore, enriched in Fe. However, Mn is low. This is attributed to diagenetic remobilisation of Mn into the observed Mn-rich concretions. In essence, the Mn was present within the sediments but has been diagenetically concentrated into the concretions (Fig. 3.25a).

The volcaniclastic material analysed shows enrichment of Fe relative to Al and Mn. The trend observed in Figure 3.33 is typical of sediments associated with submarine volcanism, for example the Upper Jurassic-Lower Cretaceous deep sea sediments in Antalya, Turkey and the deep sea sediments associated with ophiolitic rocks within the Upper Cretaceous Troodos Arakapas transform fault zone, Cyprus (Robertson & Boyle 1983).

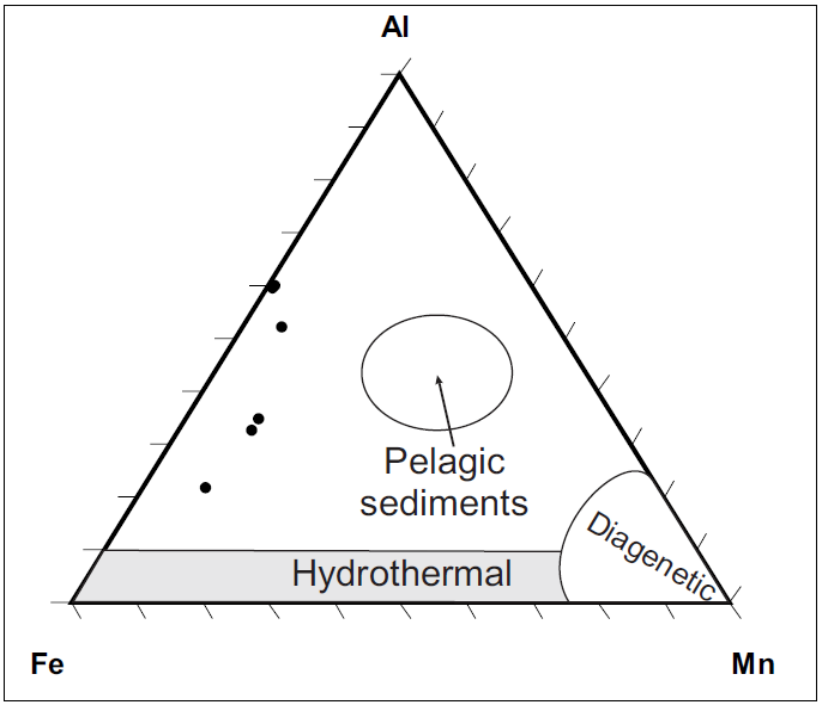

Figure 3.33. Ternary plot of Al, Fe and Mn calculated as a percentage. The plot shows a general enrichment of Fe relative to Al, but little Mn.

A number of bivariate plots are shown in Figure 3.34 in order to establish the relative contribution of terriginous material versus volcanic-derived material in the Hasançelebi Formation metalliferous sediments. An inverse linear trend is apparent in Figure 3.34a which indicates that an increasing amount of Fe coincides with decreasing Al. This trend is mirrored in the Ti versus Fe plot (Fig. 3.34b). Positive linear trends are apparent when Cr is plotted against Al (Fig. 3.34c) and Ti (Fig. 3.34d).

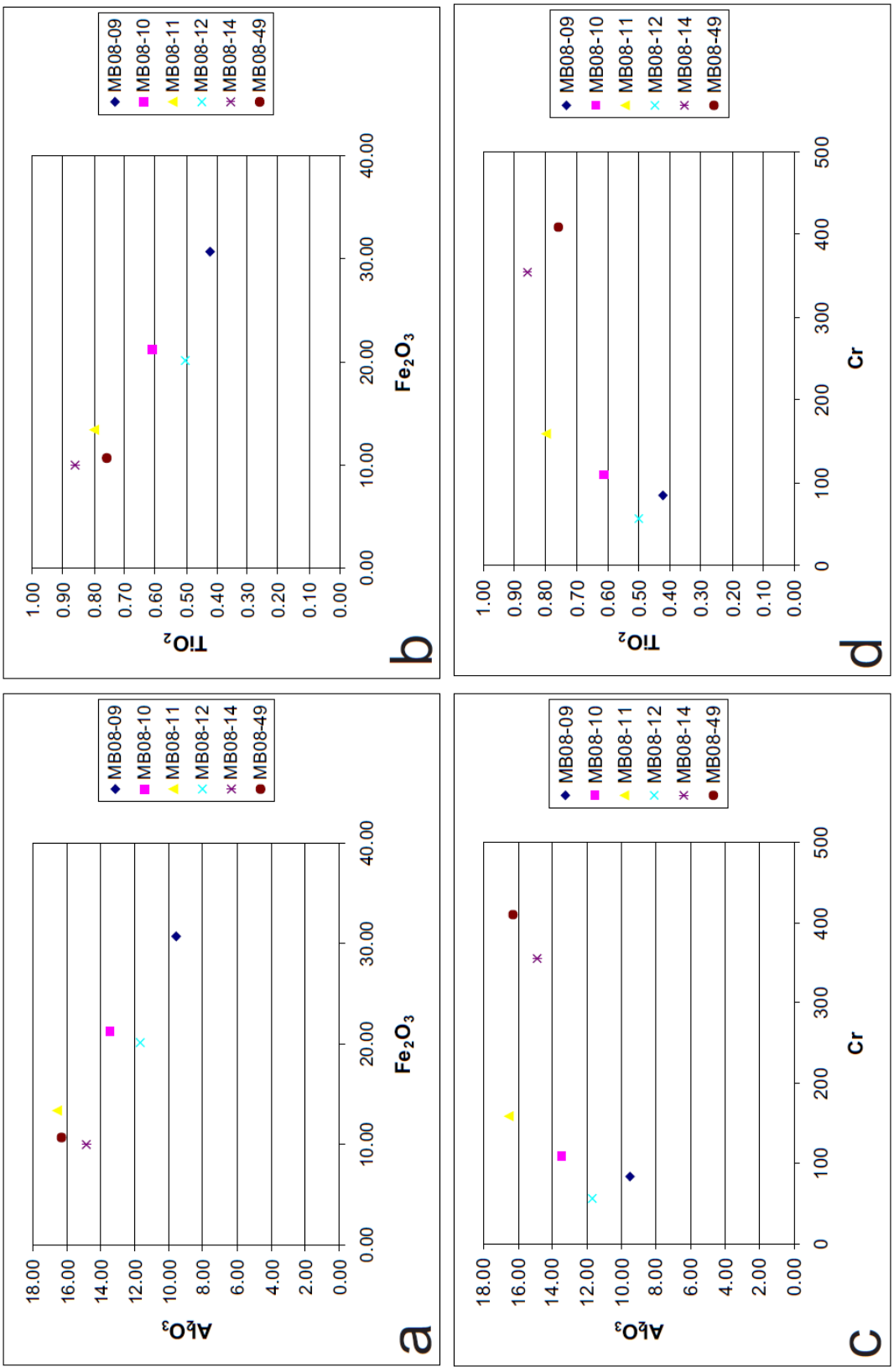

Figure 3.34. Bivariate plots showing; a, Al versus Fe; b, Ti versus Fe; c, Al versus Cr, and; d, Ti versus Cr.

Figure 3.35 is a plot of Al against Ti and shows a positive linear trend.

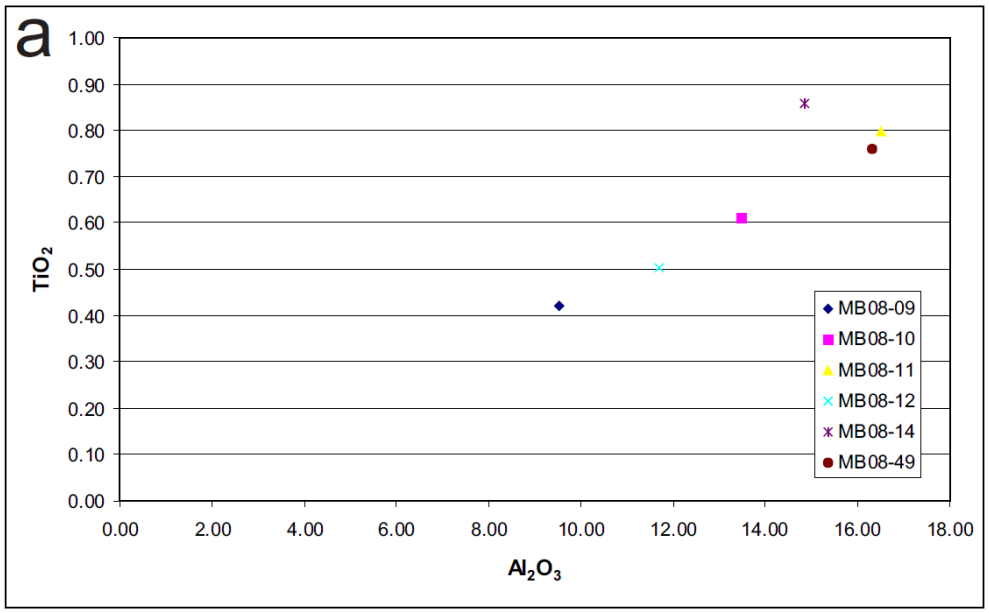

Figure 3.35. Bivariate plot showing a positive linear trend between Al and Ti.

Shale-normalised spider plots show which elements are enriched and depleted relative to a typical terrigenous shale. Figure 3.36 shows the Hasançelebi Formation sediments normalised to average upper continental crust (McLennan *et al.* 2006). The plot indicates that the sediments are enriched in the metals V, Cr, Ni and Pb and depleted in Rb, Zr, Nb, Ba and Th. This trend indicates that the sediments are not simply of terrigenous origin.

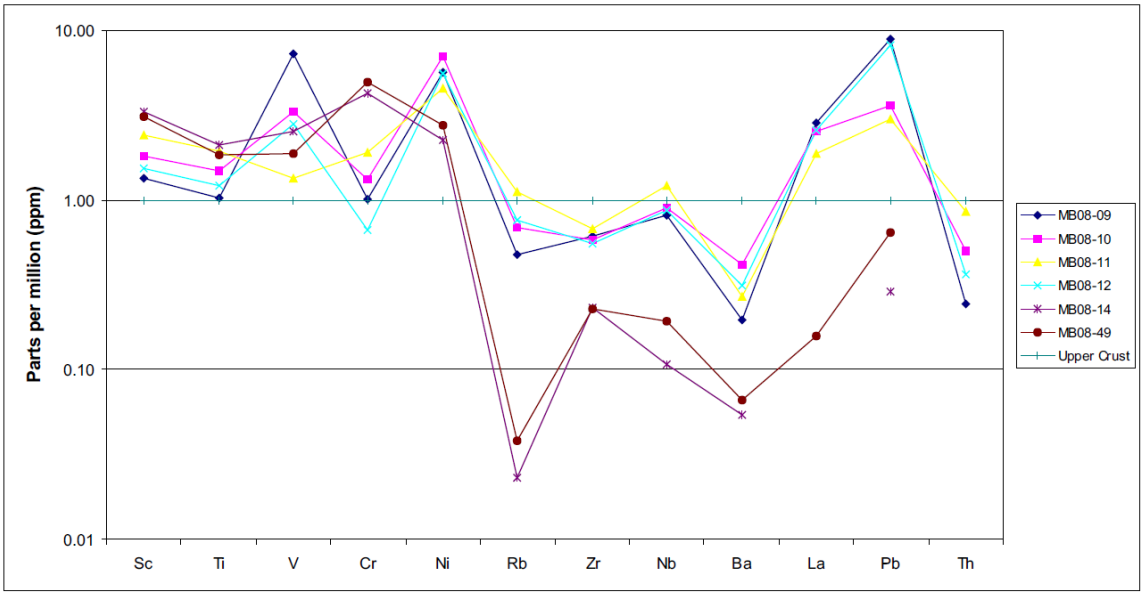

Figure 3.36. Spider plot of the Hasançelebi Formation volcaniclastic sediments normalised to average upper continental crust (data from McLennan *et al.* 2006).

Figure 3.37 shows the Hasançelebi Formation sediments normalised to an average basalt sample from the Hasançelebi Formation. The plot shows that the sediments are enriched in the metals V, Cr and Ni (however, Ti is depleted) and depleted in Rb-Ba relative to the basalt sample. This trend indicates that the sediments are not simply derived from adjacent volcanic rocks (e.g. Hasançelebi Formation).

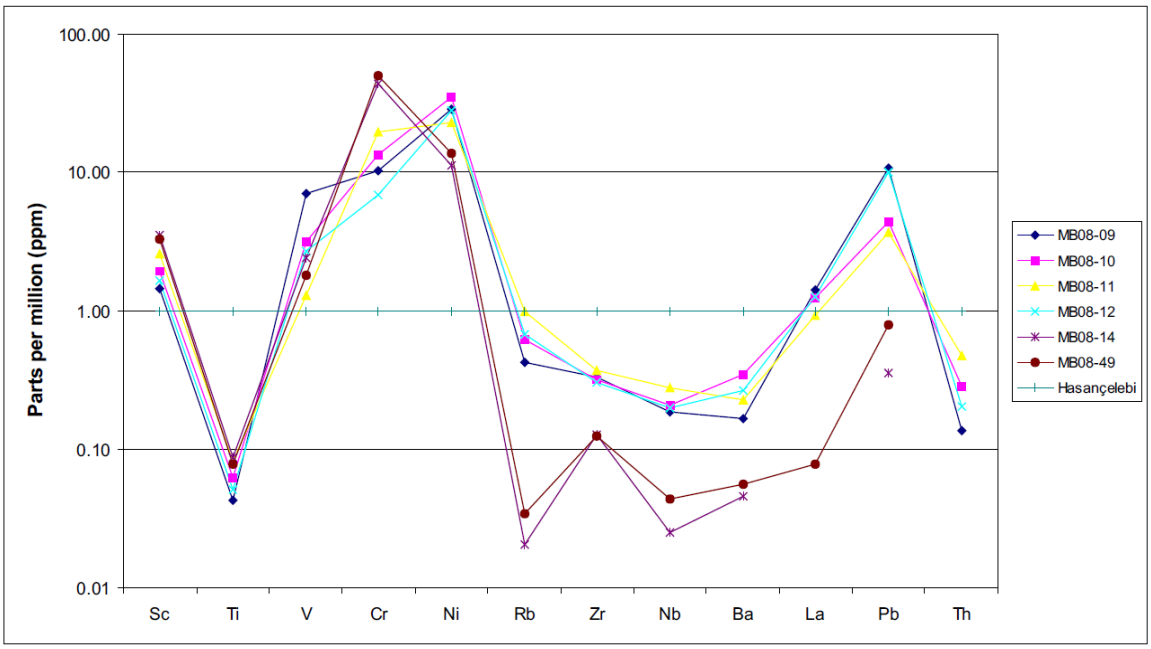

Figure 3.37. Spider plot of the Hasançelebi Formation volcaniclastic sediments normalised to an average sample of basaltic material from the Hasançelebi Formation.

3.4.2.10 Interpretation of the Maastrichtian volcanism and inter-lava sediments (Hasançelebi Formation)

The lavas of the Hasançelebi Formation formed in a submarine environment, in several hundred metres of water, as suggested by the presence of planktic Foraminifera in interbedded sediments, pillow lavas, hyaloclastite, pepperite structures and volcaniclastic sediments (i.e. mudstone).

The Hasançelebi Formation volcanic rocks are attributed to the eruption of the lavas into the deepest part of the Hekimhan Basin. This is evidenced by the intercalated nature of the ~750 m Hekimhan Formation with the ~750 m thick Hasançelebi Formation. Furthermore, limestones of the Hüyük Formation (see below) at Hüyük Tepe generally thicken towards the NW in the direction of the Hasançelebi Formation potentially indicating a slope, deepening to the NW.

In summary, the geochemistry of the Hasançelebi Formation lavas indicates that the rocks are typical within-plate basalts showing marked enrichment in immobile incompatibles relative to MORB and a range of compatible elements (e.g. Cr and Ni), generally less enriched than MORB. The results imply that the rocks are moderately evolved as a result of minor fractional crystallisation of a parent basalt. The volcanic rocks could be derived from small melt fractions of a subduction-influenced mantle source or a mixture of a small melt fractionated from a normal mantle source plus a component of subduction-related basic melts from an earlier episode. Additionally, the Hasançelebi Formation was likely deposited in an extensional environment as evidenced by the large volume of lava breccia and associated volcaniclastic debris flow material (i.e. filling of accommodation space).

The relative Nb depletion is interpreted to be a SSZ signature and is likely inherited from the northward subduction of Neotethyan oceanic crust during the Cretaceous. This tectonic setting is discussed in detail in Chapter 4.

The interlava sediments within the Hasançelebi Formation are enriched in metals. It has been shown from linear trends in Figures 3.34a & b that sediments with relatively higher proportions of Fe correspond with lower proportions of Al and Ti, which indicates

that at least some of the Fe was likely derived from a hydrothermal source. Black smokers were the likely source of the Fe entering the water column and from there, in to the sediments (Cann & Gillis 2004). Figures 3.34c & d shows that increasing proportions of Cr correspond to increasing Al and Ti, indicating a detrital origin for the Cr. Figures 3.35 & 3.36 show that Cr, together with V and Ni are enriched in the sediments relative to both average continental crust and average Hasançelebi Formation basalt suggesting that V, Cr and Ni are derived from a detrital source which is not the Hasançelebi Formation. Ultramafic rocks, specifically, are enriched in Cr and Ni and thus it is likely that these elements were contributed by erosion of the Late Cretaceous ophiolite-related rocks that underlie the Hekimhan Basin in some areas. Therefore, these inter-lava sediments were likely formed from a complex mix of detrital (volcanic and terrigenous), ophiolitic and hydrothermal components, which is common in some other volcano-sedimentary oceanic basins, for example the Woodlark Basin (Robertson & Sharp 2002).

3.4.2.11 Maastrichtian Magmatism (Yüceşafak Member)

Name: Introduced by Gürer (1994). Unknown origin.

Type section: To the west of the highway ~3 km SE of Davulgu.

Lithology: The Yüceşafak Member is predominantly composed of white, coarse grained, holocrystalline, alkali feldspar-bearing syenite. Compositionally the rock is up to 90% orthoclase feldspar with minor hornblende, quartz and biotite (e.g. Fig. 3.38a & b). Small amounts of olivine are also present in thin section. However, in many areas the ferromagnesian minerals have been altered by hydrothermal, metasomatic or weathering processes. In some areas the syenite appears dark-green to dark-grey with a granitoid appearance. This is attributed to the addition of nepheline and the absence of quartz. Radial crystal patterns are common within the Yüceşafak Member (Fig. 3.39a and b).

Locally, the syenite is altered and appears rubbly, weak and easily fragmented. This is usually in the vicinity of thin, sinuous, mafic dyke intrusions. The mafic dykes have themselves been heavily altered and appear loose and fragmented. Sulphide mineralisation, including; malachite, azurite and chalcanthite is common within these

dykes (Fig. 3.39c and d). Isolated enclaves of mafic material and pegmatitic syenite veins were also observed.

The northeastern part of the syenite body is characterised by large quantities of heavily altered intrusions. Many of the dykes appear green and are rich in coarse crystals (up to 2 cm across) of biotite mica as well as pyrite and chalcopyrite. An individual, isolated carbonatite dyke was also observed.

Boundaries: The southern boundary of the member forms an intrusive contact with ophiolitic mélange of the Hocalikova Formation (Fig. 3.39e). The northern margin is less clear as no field relationships were found. However, it appears that the Yüceşafak Member intruded lavas of the Hasançelebi Formation.

Thickness and extent: The Yüceşafak Member forms an E-W trending body only exposed to the south of Hasançelebi and around Davulgu. The maximum thickness exposed in the field is ~300 m. However, the base of the member was not seen.

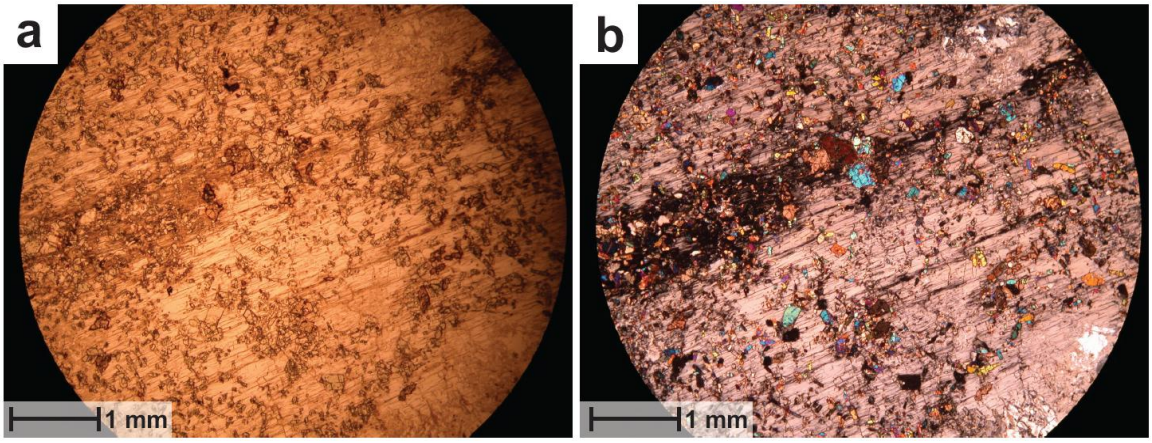

Figure 3.38. a, PPL image of alkali syenite; b, XPL image of alkali syenite. Minor amounts of clinopyroxene and olivine are also present.

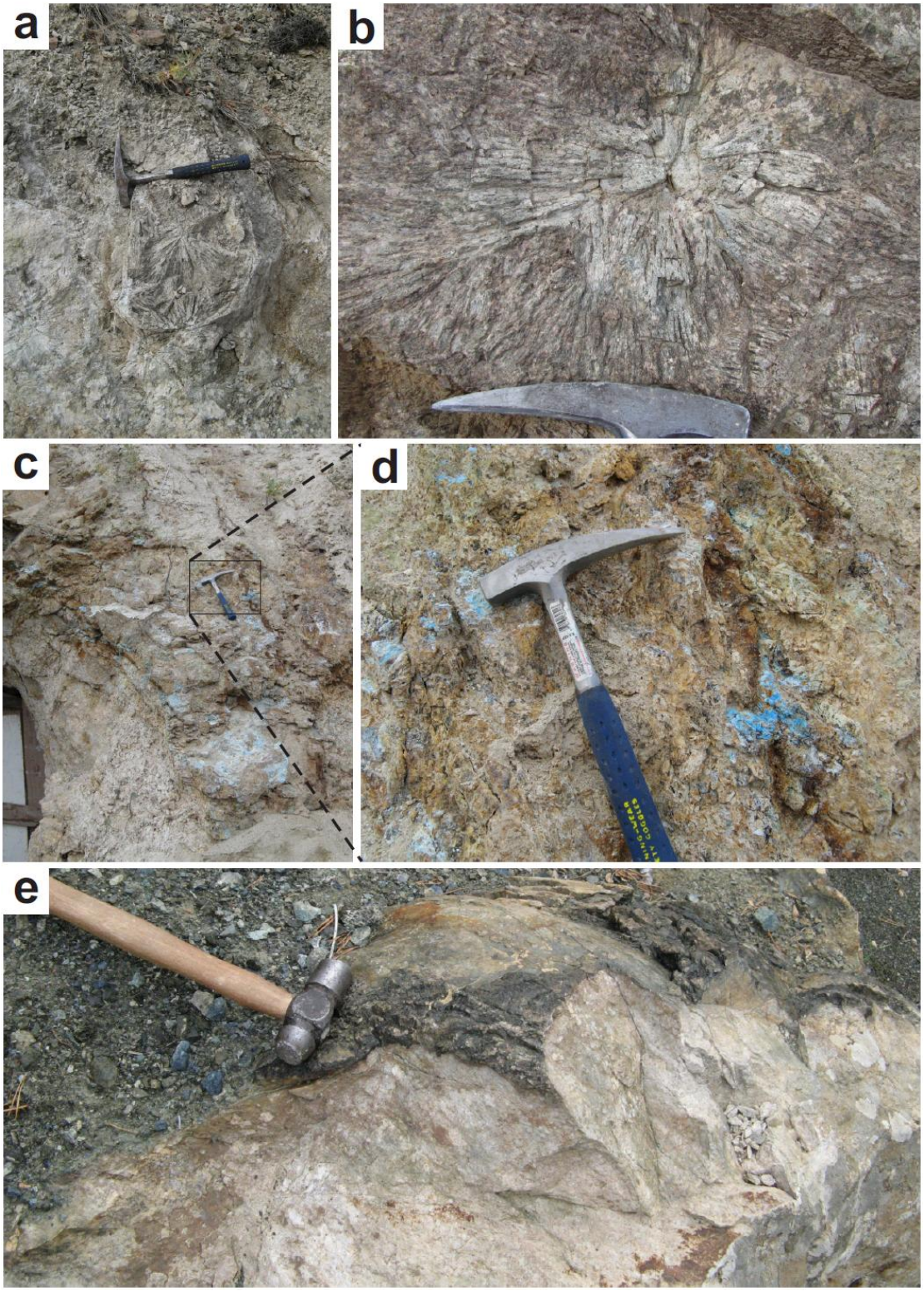

Figure 3.39. Field photographs showing; a, radiating crystals in syenite; b, closer view of radiating crystal structure; c, sulphide mineralisation within mafic dykes intruded into syenite; d, closer view of sulphide mineralisation (primarily azurite and chalcanthite); e, baked margin contact between syenite intrusion and ophiolite related mélange material. Hammers for scale.

Age: Geochronological analysis was not conducted as part of this study. However, $^{40}Ar/^{39}Ar$ age determinations from biotite veins cutting the syenite body have recorded

ages of 73.43±0.41, 74.92±0.39 and 73.12±0.75 Ma (Marschik *et al.* 2008). $^{40}Ar/^{39}Ar$ age determinations from K-feldspar within syenite pegmatite porphyry intrusions suggest ages of 71.3±0.3 Ma (Kuşcu *et al.* 2011). These ages record the minimum age for intrusions within the syenite pluton. Therefore, the Yüceşafak Member itself must have an intrusive age of at least 74.92±0.39 Ma (Campanian).

However, a single $^{40}Ar/^{39}Ar$ age determination by Leo *et al.* (1973) yielded an age of 65.2±1.6 Ma (late Maastrichtian). This age fits with field relationships where syenite has intruded both the Hocalikova and Hasançelebi Formations.

3.4.2.12 Geochemistry of the Maastrichtian Magmatism (Yüceşafak Member)

Four samples of plutonic material from the Yüceşafak Member were collected and analysed using XRF. Figure 3.40 indicates that three samples are syenite-syeno-diorite and one is granite-grano-diorite.

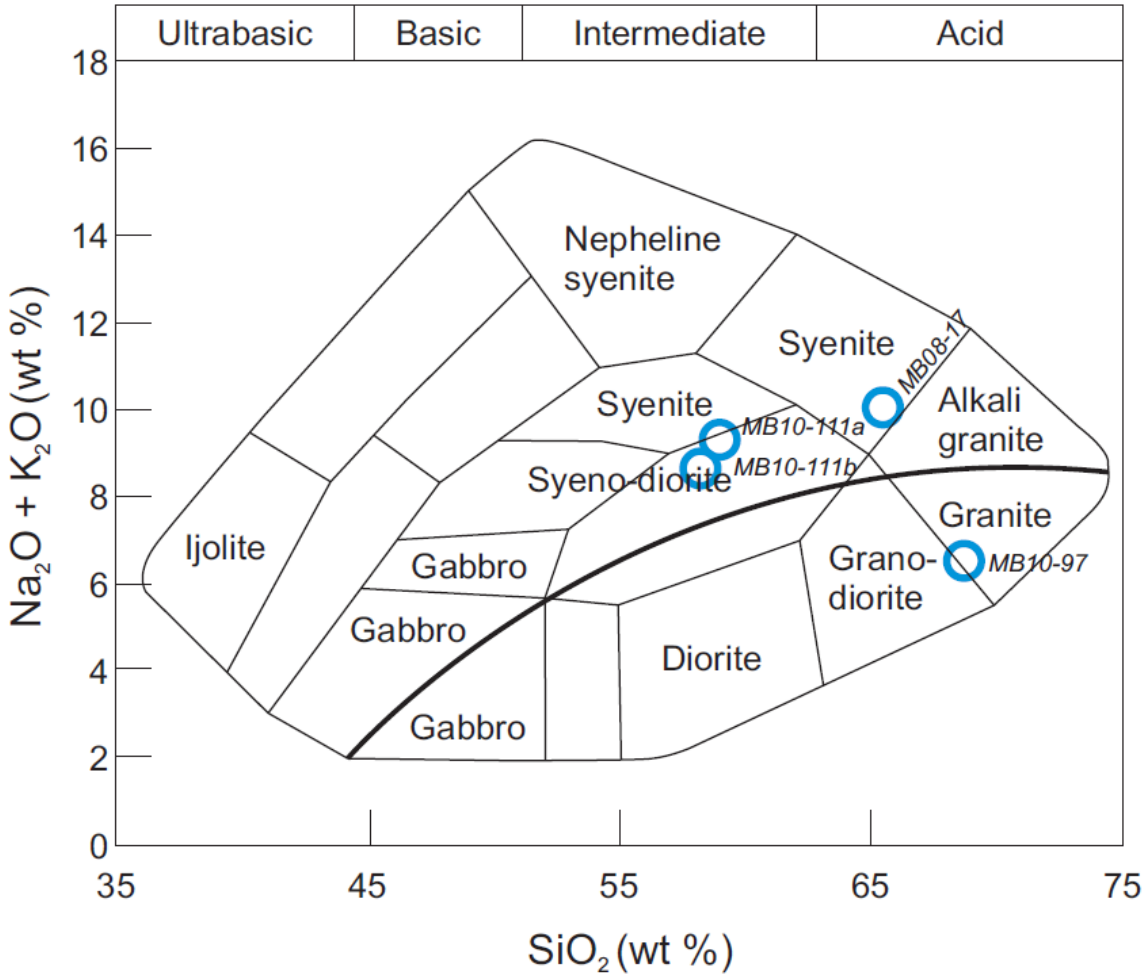

Figure 3.40. A plutonic TAS diagram for four samples of the Yüceşafak Member (after Cox *et al.* 1979, adapted by Wilson 1989). The curved solid line subdivides the alkalic from subalkalic rocks.

3.4.2.13 Interpretation of the Maastrichtian Magmatism (Yüceşafak Member)

Gürer (1996) suggests that the Yüceşafak Member formed in a back-arc tectonic setting and that the Hekimhan Basin represents a back-arc basin. However, this interpretation is inconsistent with the tectono-stratigraphy of the Hekimhan Basin. The geological and geochemical evidence points to the alkaline magmatism of the Yüceşafak Member being emplaced in a within-plate environment.

Age ranges from geochronological studies range from ~74–65 Ma (Leo *et al.* 1973; Marschik *et al.* 2008; Kuşcu *et al.* 2011). However, field relationships indicate that syenitic dykes have intruded elements of the Hocalikova and Hasançelebi Formations and must therefore be younger than these units. The Hasançelebi Formation has been dated as late Maastrichtian by planktic Foraminifera within marl interbeds. Fine-grained mafic

dykes, which are intensely hydrothermally altered, were observed in the Yüceşafak Member, although it was unclear if these dykes are related to the Hasançelebi Formation, or later Eocene volcanism. The emplacement of Yüceşafak Member was likely fault controlled due to the extensional nature of the Hekimhan Basin during the Maastrichtian. The Yüceşafak Member is characterised by a high degree of hydrothermal and metasomatic alteration, particularly the northern and eastern exposures. Some of the fault zones may have acted as conduits for these alteration fluids. Syenite is often seen as the plutonic equivalent of trachyte (MacKenzie *et al.* 1997), which has also been observed in the Hekimhan Basin. Although not exposed together, they may be genetically linked.

3.4.2.14 Maastrichtian shallow-marine transgressive carbonates (Hüyük Formation)

Name: Introduced by Gürer (1994). Probably derived from Hüyük Tepe situated to the NNE of Hekimhan (Fig. 3.41).

Type section: The south side of Hüyük Tepe.

Lithology: The Hüyük Formation is composed of fossiliferous calcarenites interbedded with thin marls in the lower part which rapidly give way to fossiliferous, crystalline limestones up section (Fig. 3.42a). At the type section at Hüyük Tepe, the limestone beds dip slightly ($<10^0$) to the SE but appear to thicken towards the NW. The uppermost part of the formation is composed of medium-bedded limestones which are typically algal laminated. Tepee-type dewatering structures where also observed in some horizons within this upper part of the formation (Fig. 3.42b). Typical fossils include benthic and planktic Foraminifera as well as echinoid, coraline algae and rudist fragments. Upper parts of the Hüyük Formation are dolomitised. Locally, the top ~2 m of the formation is heavily fractured, dissolved and calcified (Fig. 3.42c and d).

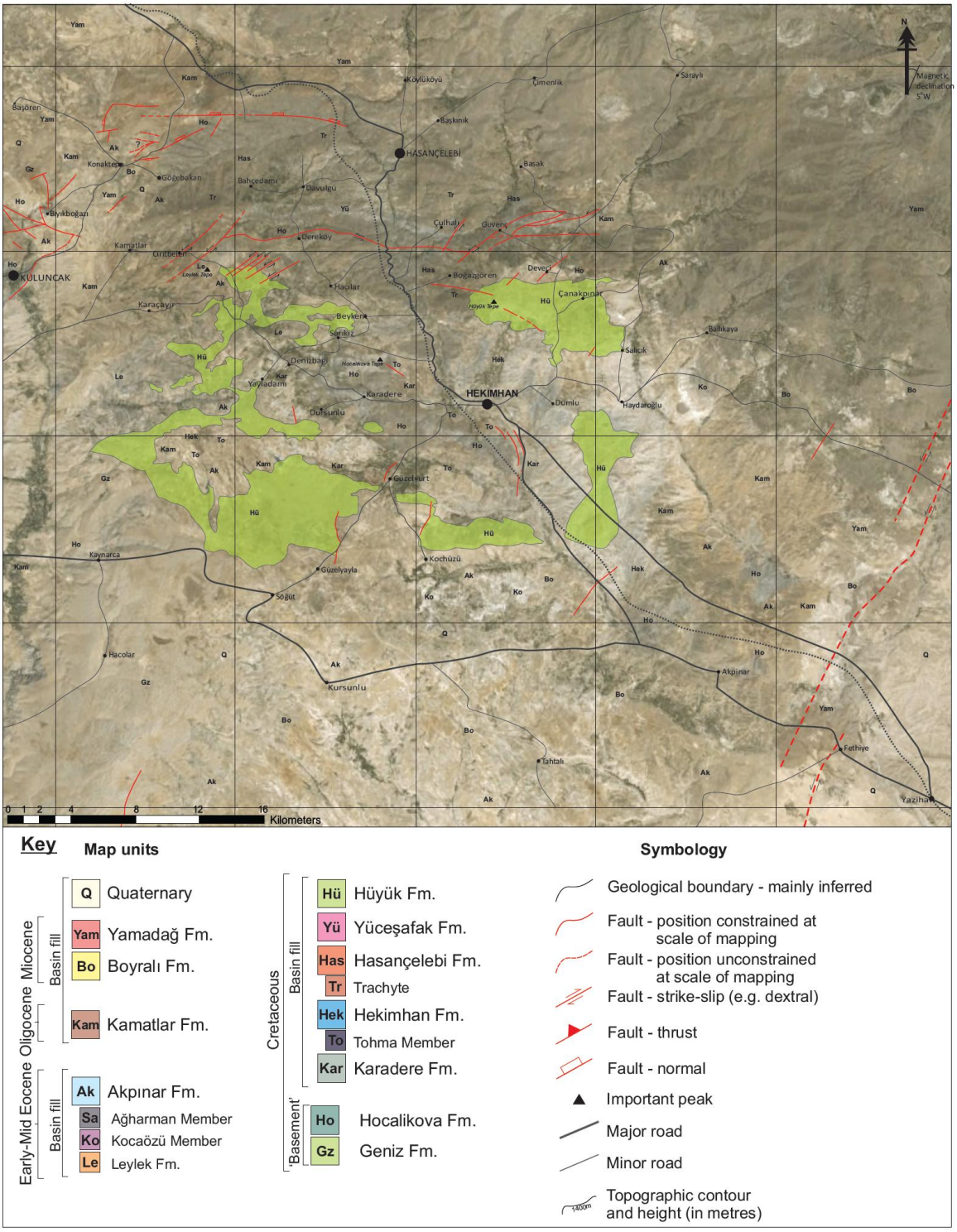

Figure 3.41. Simplified geological map showing the extent of the Hüyük Formation draped over a satellite image of the Hekimhan Basin.

Boundaries: The lower boundary is conformable on the Hekimhan Formation. A stratigraphic contact over the Hasançelebi Formation was not observed. However, a tectonic contact between the Hasançelebi Formation and limestones of the Hüyük

Formation was observed to the north of Hüyük Tepe. The upper boundary is represented by a basin-wide shallow-angle unconformity, in places characterised by thick limestone karst surfaces.

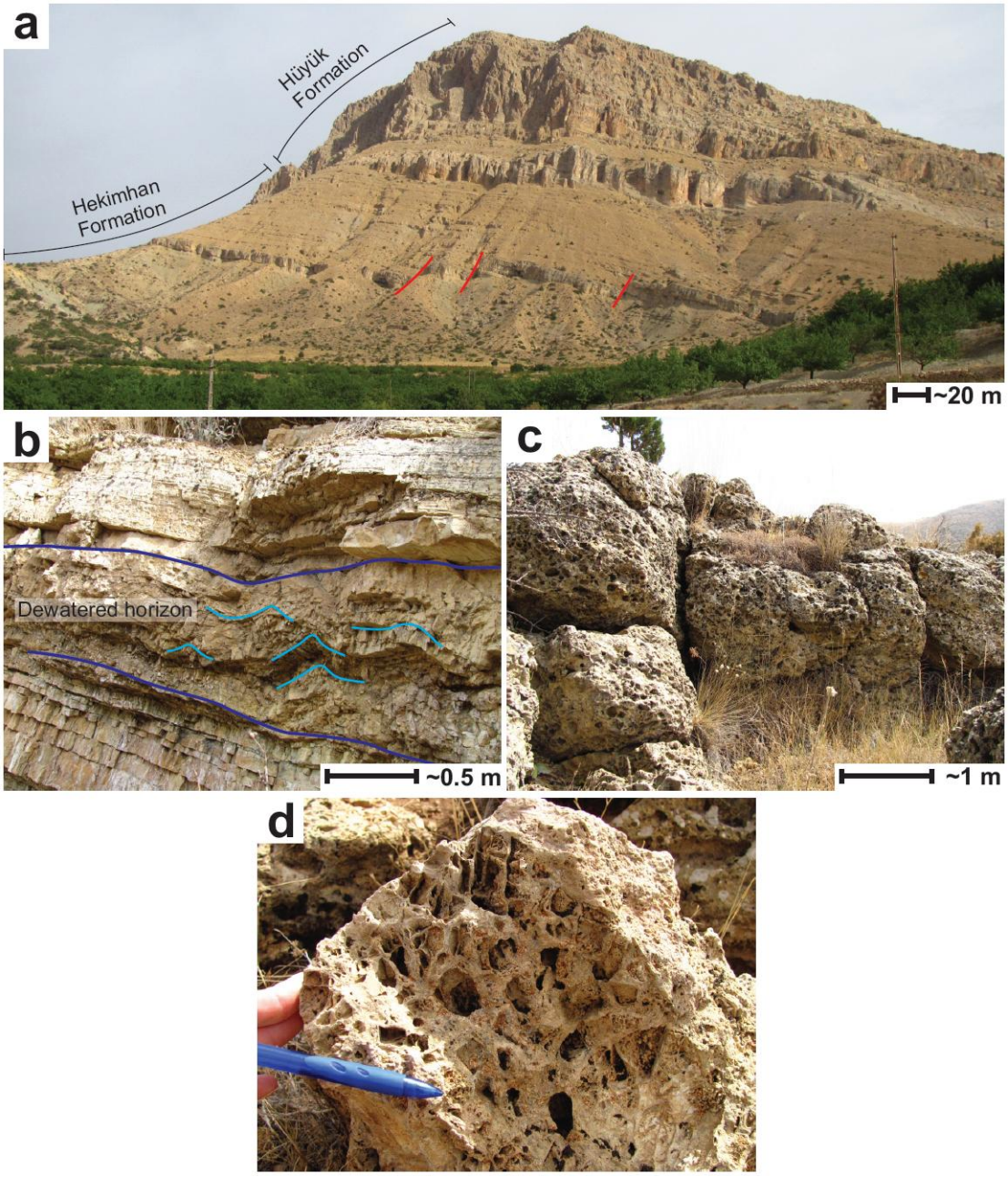

Figure 3.42. Photographs showing; a, upper part of the Hekimhan Formation and the conformably overlying limestones of the Hüyük Formation; b, upper part of the Hüyük Formation showing medium bedded microbial laminated limestones with dewatered horizons; c, karstic surface at the top of the Hüyük Formation; d, closer view of the karstified limestone.

Thickness and extent: The Hüyük Formation is well represented around the centre of the basin. The maximum thickness of the formation is ~300 m. However, this is only

observed at Hüyük Tepe and the E-W trending ridgeline to the north of Kocaözü. In other areas the formation is much reduced.

Age: Maastrichtian based on dating of benthic and pelagic Foraminifera (Table 3.3).

Hekimhan Formation (Maastrichtian)

Samples	Rock type	Benthic Formanifera (BF)	Planktic Foraminifera (PF)	Other	Age
MB08-45	sparry limestone	*Sivasella monolateralis*, *Orbitoides* sp., *Anomalina* sp.	-	Rudist, echinoderm, coralline alga	Late Maastrichtian
MB08-151	limestone	*Mississippina binkhorsti*, *Orbitoides* sp., *Anomalina* sp.	-	Rudist, echinoderm, coralline alga	Maastrichtian
MB08-160	limestone	*Sirtina orbitoidiformis*, *Pseudovalvulineria clementiana*, *Chrysalidina* sp., *Lepidorbitoides* sp.	*Rugoglobigerina rugosa*, *Globotruncana falsostuarti*, Globotruncanita sp.	-	Late Maastrichtian
MB08-217	limestone	-	-	Rudist	Late Cretaceous
MB08-235	limestone	*Sirtina orbitoidiformis*	-	Rudist	Late Maastrichtian
MB09-H52		*Orbitoides* sp.	-	-	Campanian-Maastrichtian
MB09-H91	limestone	*Sirtina orbitoidiformis*, *Siderolites* sp., *Eponides* sp.	*Rugoglobigerina* sp., Globotruncana sp., Pithonella ovalis	Coralline alga, echinoderm, bryozoa	Late Maastrichtian
MB10-52	limestone beneath leylek	*Orbitoides media*	-	Rudist	Late Maastrichtian
MB10-115	limestone below evaporite	*Pseudovalvulineria clementiana*	*Rugoglobigerina hexacamerata*, *Globotruncana falsostuarti*, *Globotruncanella havanensis*, *Heterohelix* sp., *Pithonella ovalis*	-	Late Maastrichtian

Table 3.3. Table showing the palaeontological analysis of samples of Hüyük Formation limestone (courtesy of N Inan & K Taslı).

3.4.2.15 Interpretation of the Maastrichtian shallow-marine transgressive carbonates (Hüyük Formation)

The Hüyük Formation is formed from limestone and interbedded marls which contain planktic Foraminifera indicating a relatively deep water depth. Calcarenite beds become more common up section and contain benthic foraminifera. Little syn-sedimentary deformation is aparant in the Hüyük Formation compared with the underlying Hekimhan Formation indicating a change from extension to a more stable tectonic environment. The formation represents a progressively shallowing basin and reflects filling of

accommodation space probably as a result of the cessation of extension. Although, eustatic sea level fall cannot be ruled out. The formation varies in thickness across the basin. Exposures to the south and NE of Hekimhan appear to thicken northwards and northwestwards respectively, towards the inferred basin depocentre. The localised fractured and recemented horizons capping the sequence are interpreted as palaeokarstic surfaces and reflect subaerial exposure, weathering and erosion.

3.4.3 Paleocene–Eocene sediments and volcanic rocks

Sedimentation resumed in the Early Eocene with the accumulation of the Akpınar Formation. The formation consists of mixed lithologies including sandstones and Nummulitic limestones at the base, through a major sequence of marl and interbedded Nummulitic calcarenites in the middle and upper part. The Kocaözü Member is composed of isolated patches (100x100 m) of extrusive basalts erupted simultaneously with the deposition of Akpınar Formation marls within southern and eastern parts of the Hekimhan Basin. The andesitic Leylek Member outcrops exclusively in western parts of the Hekimhan Basin within the upper part of the Akpınar Formation.

3.4.3.1 Paleocene–Eocene evaporites (Ağharman Member)

Name: Introduced by Gürer (1994). Unknown origin.

Type section: The type section is situated ~1.5 km NW of Salıcık within an area which is heavily mined for evaporite deposits (Fig. 3.43).

Lithology: The member is characterised by alterations of three main lithologies: 1) light-grey, evaporitic marl (individual beds up to 50 cm); 2) massive, white, alabastrine gypsum beds (individual beds up to 1 m), and; 3) subordinate, red, very-fine, silty mudstone (individual beds are usually less than 10 cm) (Fig. 3.44a). The alabastrine gypsum is finely laminated and the laminations frequently appear wavy and brown stained. The gypsum has a marine origin (Palmer *et al.* 2004). Some horizons of the evaporite are folded with no discernable deformation pattern (i.e. chaotic) (Fig. 3.44b). This is especially evident within outcrops to the north of Kocaözü. Tepee structures were observed in some of the alabastrine gypsum layers (Fig. 3.44c). The red, silty mudstone

contains dark red, concentric, oval structures, up to 5 cm across in long axis (Fig. 3.44d). A typical sequence of the Ağharman Member begins with ~10 cm of evaporitic marl abruptly overlain by ~50 cm of wavy laminated alabastrine gypsum, which is in turn abruptly overlain by ~10 cm of red mudstone. Isolated beds of nodular 'chicken wire' structure gypsum were also observed. Diagenetic selenite veins have penetrated all parts of the sequence.

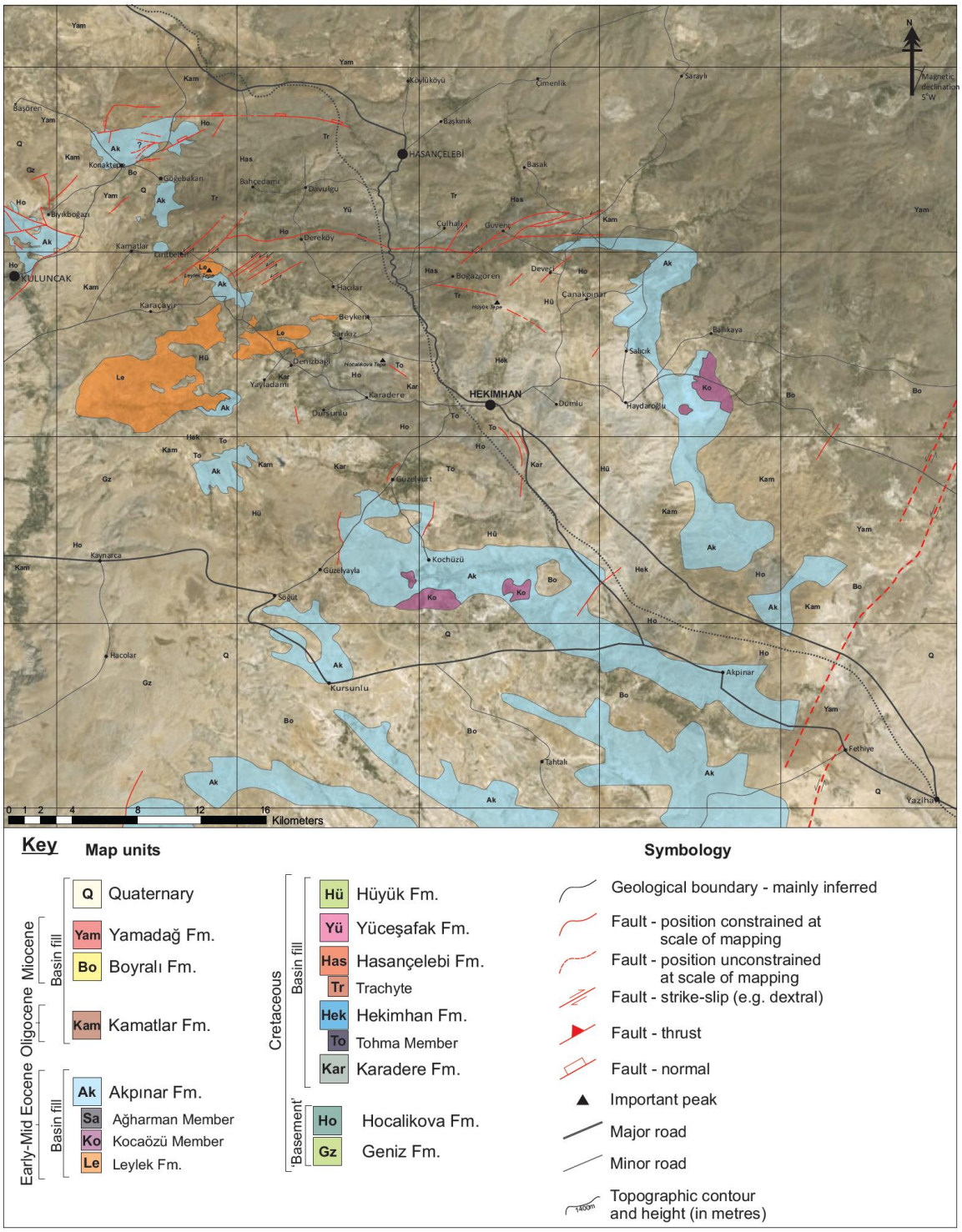

Key

Map units

Basin fill
- Q Quaternary
- Yam Yamadağ Fm.
- Bo Boyralı Fm.
- Kam Kamatlar Fm.

Early-Mid Eocene Oligocene Miocene
Basin fill
- Ak Akpınar Fm.
  - Sa Ağharman Member
  - Ko Kocaözü Member
  - Le Leylek Fm.

Cretaceous
Basin fill
- Hü Hüyük Fm.
- Yü Yüceşafak Fm.
- Has Hasançelebi Fm.
- Tr Trachyte
- Hek Hekimhan Fm.
- To Tohma Member
- Kar Karadere Fm.

Basement
- Ho Hocalikova Fm.
- Gz Geniz Fm.

Symbology
- Geological boundary - mainly inferred
- Fault - position constrained at scale of mapping
- Fault - position unconstrained at scale of mapping
- Fault - strike-slip (e.g. dextral)
- Fault - thrust
- Fault - normal
- Important peak
- Major road
- Minor road
- Topographic contour and height (in metres)

Figure 3.43. Simplified geological map showing the extent of the Akpınar Formation, together with the Kocaözü and Leylek Members, draped over a satellite image of the Hekimhan Basin.

Boundaries: No lower contact was established in the field due to the presence of farmland. However, the lower boundary appears to be above the karstic surface at the top of the Hüyük Formation. The upper boundary forms an unconformity with the lower part of the Akpınar Formation to the east of Salıcık.

Thickness and extent: The Ağharman Member is only locally exposed within the Hekimhan Basin (see map). The thickness of the units varies considerably. The maximum thickness is ~100 m in the area being mined to the NW of Salıcık. However, evaporites exposed to the east of Hüyük Tepe reach a maximum thickness of ~15 m before terminating. Similarly, evaporites exposed in the mountains to the north of Kocaözü reach a maximum thickness of ~15 m.

Age: The age of the Ağharman Member remains unclear. Palaeontological dating was attempted. However, no Foraminifera were found within the interbedded marls. Yalcın and Bozkaya (1996) indicate the existence of the Cretaceous-Cenozoic (KT) boundary within marine evaporites in the Hekimhan Basin. It is unclear precisely where they found this boundary. The boundary was positioned via geochemical analysis which determined a decrease in calcite content and an increase in the proportion of smectites and K-feldspar through the boundary layer as well as an increase in the amounts of some transition elements and HFSEs.

From field relationships, there are three possible ages for the Ağharman Member; 1) the member overlies emergent limestones of the Hüyük Formation and may, therefore, be related to the emmergence event. However, no other Cretaceous-aged evaporites have been discovered in Central Anatolia.; 2) it may have been deposited during the Paleocene. However, no other sediments of Paleocene age have been recorded in the Hekimhan or the adjacent Darende Basins; 3) deposition may have been during the early Eocene, prior to the onset of a full marine transgression.

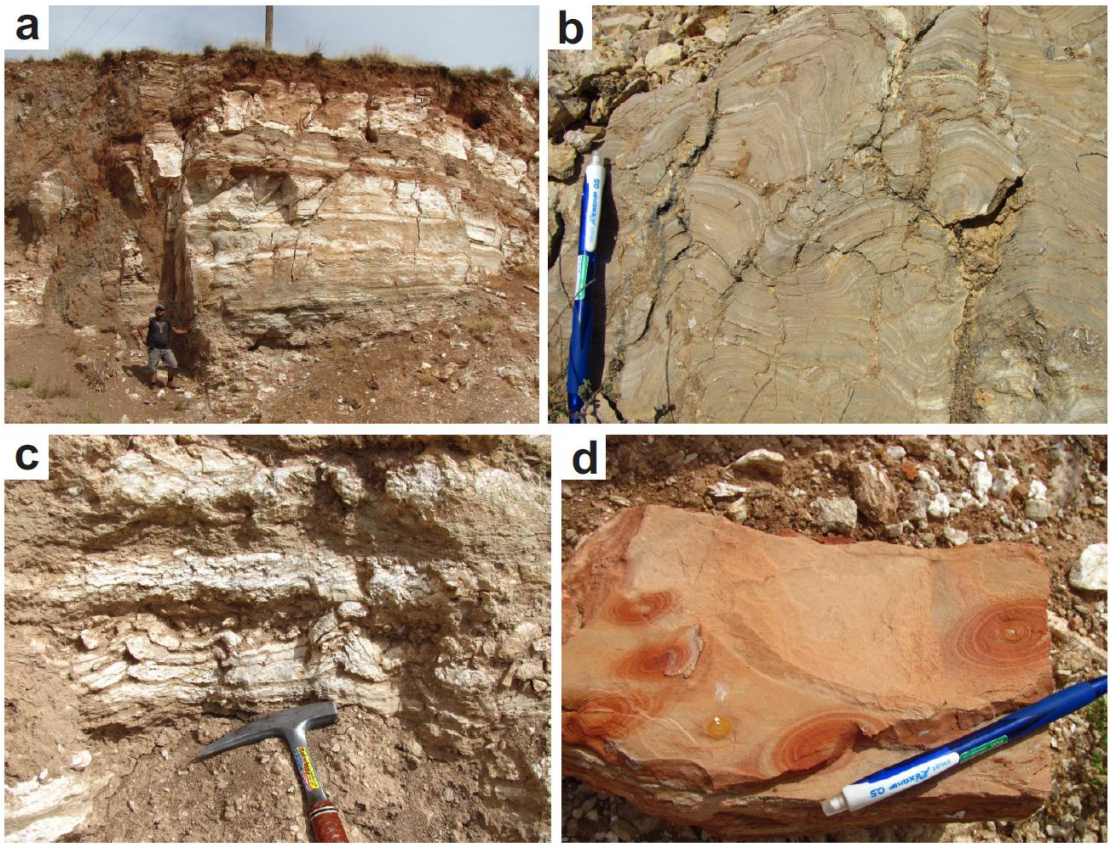

Figure 3.44. Field photographs showing; a, outcrop of Ağharman Member evaporites to the east of Hüyük Tepe (person for scale); b, chaotic bedding within alabastrine gypsum north of Kocaözü; c, Tepee structures within alabastrine gypsum layers; d, red, concentric rings in red silty mudstone.

3.4.3.2 Interpretation of the Paleocene–Eocene evaporites (Ağharman Member)

The Ağharman Member was deposited in a restricted shallow-marine environment (Palmer *et al.* 2004). The marl-evaporite-mudstone sequence may represent progressive evaporation of a water body, emergence and then a recharge event. The tepee-like structures are interpreted as water escape structures and, together with the chaotic bedding within the gypsum layers, may indicate a syn-tectonic environment of deposition. However, these structures may have similarly formed during burial and compaction or massive dewatering and dissolution of evaporitic layers. Nodular gypsum horizons are indicative of sabkah deposits in a coastal plane setting (Shearman 1997). The red concentric rings are interpreted as liesegang rings, or oxidation rings.

The localised outcrops and thickness variations between the outcrops is attributed to deposition in isolated palaeogeographically confined 'sub-basins'.

The Ağharman Member is unlikely to have been deposited during the Maastrichtian as this was a time of globally high CO_2 and a tropical climate (Hay 2008) meaning that conditions would be unsuitable for evaporite formation (e.g. Keller *et al.* 2002). No Paleocene rocks have been discovered in the Hekimhan or adjacent Darende Basins. It therefore seems unlikely that the evaporites are Paleocene-aged. The evaporites have a marine origin (Palmer *et al.* 2004). Marine sedimentation did not occur until the Eocene. Therefore, a minor, Paleocene-aged transgression and subsequent regression would be required to begin forming the evaporites, which seems unlikely. An early Eocene-age for the formation of the Ağharman Member evaporites is favoured here because: 1) the early Eocene rocks lie in stratigraphic continuity above the evaporites, and; 2) early Eocene-aged evaporites have been well documented across Central Anatolia (e.g. Clark & Robertson 2005; Gündogan *et al.* 2005).

3.4.3.3 Eocene transgressive sediments (Akpınar Formation)

Name: Introduced by Gürer (1994). Presumably named after the village called Akpınar to the SE of the Hekimhan Basin.

Type section: Around the village of Kocaözü.

Lithology: The Akpınar Formation varies considerably within the Hekimhan Basin. To the southeast of the basin, around Akpınar, the base of the formation is represented by red conglomerates, sandstones and mudstones interbedded with white, sandy, unfossiliferous limestones (Fig. 3.45a). The clasts within the conglomerate are sub rounded, up to cobble grade and predominantly composed of white unfossiliferous limestone. The base of the limestone beds are often transitional with the red beds whereas the tops often form sharp contacts with the red beds. The conglomerates and sandstones are typically lenticular and laterally discontinuous. They often appear weakly deformed. This sequence is overlain by undeformed marl and calcarenite intercalations and then massive limestones (Fig. 3.45b). The calcarenites and limestones contain abundant *Nummulites* sp.

To the east of Haydaroğlu, the sequence of red clastic rocks and white limestones is again present. However, the overlying marl and calcarenite sequence is much thicker and contains an important unit of localised basaltic volcanism (discussed below). Slump folds within the marls are also present in this area.

To the south of Hekimhan, around Kocaözü, the red clastic sequence is absent. Instead, intercalations of marl and calcarenite (and localised basalt) pass directly into massive Nummulitic limestones. Here, the marls have been deformed, whilst limestone beds have been faulted but are internally unaffected (Fig. 3.45c). The massive limestones near the top of the formation are predominantly composed of recrystallised carbonate. Fossils including *Nummulites* sp. and other benthic Foraminifera, mollusc and echinoid fragments are only recorded as etchings on weathered surfaces (Fig. 3.45d). Above the limestones, a sequence of silty marls interbedded with fine-grained calcarenite contains asymmetrical ripples and organic matter such as leaves (Fig. 3.45e). The sequence then passes into evaporite deposits consisting mainly of alabastrine gypsum. Localised

volcaniclastic sandstone and tuff deposits were observed within this part of the formation. The tuffs are light brown and very fine-grained. The sandstones are dark-grey to dark-brown, predominantly medium-grained, sub-angular, relatively structureless and mainly composed of mafic minerals (Fig. 3.45f).

To the south of the basin, a thin sequence of marl passes into massive Nummulities-bearing calcarenite and limestone beds exposed in vast canyons.

Western areas of the basin are characterised by a much thinner sequence overall. Marls are intruded by thick, columnar jointed dykes of the Leylek Formation (discussed below) and limestones contain abundant build ups of echinoid spines (Fig. 3.45g) as well as isolated, in situ, colonial corals (Fig. 3.45h).

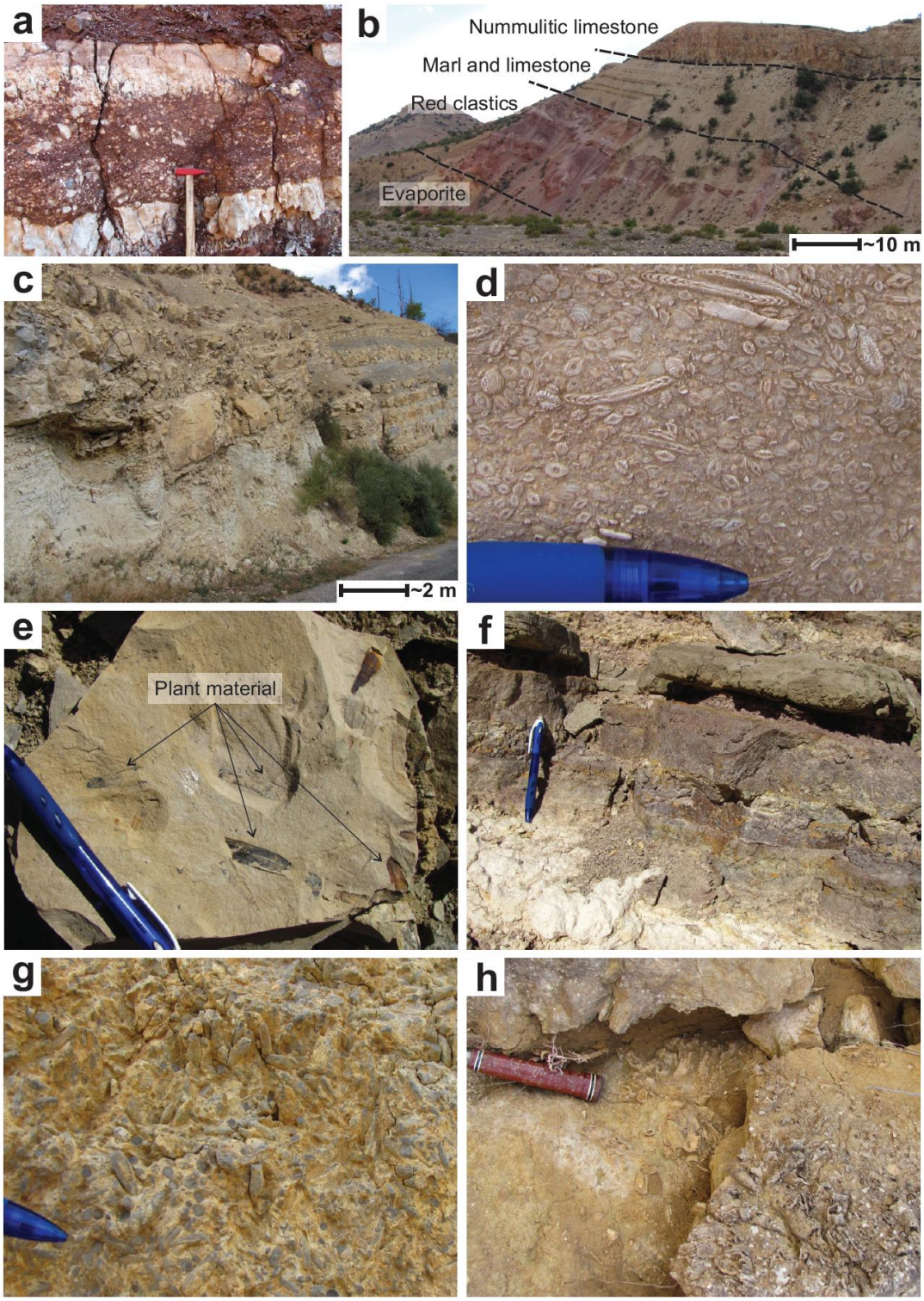

Figure 3.45.Photographs showing; a, red conglomerate with limestone clasts interbedded with white unfossiliferous limestone beds; b, lower part of the Akpınar Formation from the SE of the basin; c, folded and sheared marls overlain by massive, block faulted limestone beds; d, *Nummulites* Sp. etchings on a weathered surface of recrystalised limestone; e, plant debris from the upper part of the Akpınar Formation; f, volcaniclastic sandstone deposits from the upper part of the Akpınar Formation; g, abundant echinoid spines and fragments from the western part of the basin; h, in situ colonial corals. Hammer for scale in a and h pencil for scale in d, e, f and g.

Boundaries: The lower boundary of the Akpınar Formation was not directly observed in the field area. However, the formation overlies either the Maastrichtian Hüyük Formation limestones or the Ağharman Member evaporites. The upper boundary forms an unconformity overlain by Oligocene clastics of the Kamatlar Formation. A thrust contact between red beds in the lower part of the formation and marls from higher up in the formation was observed near Salıcık (Fig. 3.46).

Figure 3.46. Photograph showing a high angle thrust contact between red clastics at the base of the Akpınar Formation (left), overlying marls and limestones in the upper part of the Akpınar Formation (right).

Thickness and extent: The Akpınar Formation outcrops extensively in the Hekimhan Basin, although the lithology varies considerably across the basin. The formation has a maximum thickness of ~450 m. However, a complete stratigraphic section was not observed in the field. The lower red clastic component, where present, reaches ~30 m. The interbedded marl and calcarenite component varies from <10 m in the south and southeast of the basin to ~300 m in eastern parts of the basin. Massive limestones in the east of the basin reach ~100 m and are capped by organic-rich marl and evaporite sequences ~50 m thick. In the south of the basin the massive limestones reach ~200 m although a complete sequence was not observed. It was not possible to establish a total thickness for the Akpınar Formation in the west of the basin due to the intrusive and extrusive andesitic Leylek Member interval.

Age: The Akpınar Formation has been dated using Foraminifera as Early to Middle Eocene (Lutetian) (Table 3.4).

Akpınar Formation (Eocene)

Samples	Rock Type	Benthic Formanifera (BF)	Planktic Foraminifera (PF)	Other	Age
MB08-32		*Idalina sinjarica*, *Periloculina slovenica*, *Chrysalidina* aff. *floridana*, *Spirolina* sp., *Pfendericonus* sp.	-	-	Late Paleocene
MB08-60	micrite	-	*Acarinina* sp., *Pseudohastigerina* sp.	-	Eocene
MB10-38	nummulitic sandstone	*Nummulites* cf. *striatus*, *Assilina* cf. *praespira*, *Neorotalia vienotti*, *Assilina* cf. *prisca*, *Sphaerogypsina globula*	-	-	Mid Eocene (Lutetian)
MB10-66	nummulitic limestone	*Idalina sinjarica*, *Alveolina* cf. *aragonensis*, *Chrysalidina* cf. *floridana*, *Alveolina* cf. *cuspidata*, *Periloculina* cf. *slovenica*, *Pfendericonus* sp.	-	-	Early Eocene (Ilerdian)
MB10-69	nummulitic calcarenite	*Asterigerina rotula*, *Neorotalia vienotti*, *Discocyclina* cf. *scalaris*, *Assilina* cf. *praespira*, *Orbitoclypeus* cf. *ramaraoi ramaraoi*, *Nummulites millecaput*, *Nummulites* cf. *striatus*, *Operculina* sp.	*Acarinina bullbrooki*, *Igorina broedermani*, *Globigerinatheka* sp., *Subbotina* sp.	-	Mid Eocene (Lutetian)
MB10-80	nummulitic limestone	*Nummmuites* cf. *minervensis*, *Alveolina* cf. *aragonensis*, *Lockhartia haimei*, *Orbitolites* sp.	*Morozovella* sp., *Chiloguembelina* sp.	-	Early Eocene (Ilerdian)
MB10-83	nummulitic limestone	*Orbitolites complanatus*, *Nummulites* cf. *minervensis*, *Alveolina* cf. *ellipsoidalis, Alveolina pasticillata, Alveolina* (*Glomalveolina*) *levis*, *Opertorbitolites* cf. *latimarginalis*, *Idalina sinjarica*	-	Dasycladacea, echinoderm	Early Eocene (Ilerdian)
MB10-87	nummulitic limestone	*Alveolina* (*Glomalveolina*) *lepidula*, *Chrysalidina* cf. *floridana*, *Medocia blayensis*, *Idalina sinjarica*, *Orbitolites* sp.	Indet. planktic foraminifers	echinoderm	Early Eocene (Ilerdian)
MB10-113	nummulitic limestone	*Nummulites* cf. *striatus*, *Assilina* cf. *spira*, *Medocia blayensis*, *Gyroidinella magna*, *Neorotalia vienotti*, *Ranikothalia* sp., *Orbitolites* sp.,	*Globigerinatheka* sp.	-	Mid Eocene (Lutetian)
MB10-114	nummulitic limestone on top of red facies	*Alveolina* (*Glomalveolina*) sp., *Orbitolites* sp.	Indet. planktic foraminifers	echinoderm	Latest Paleocene to Mid Eocene
MB10-122	nummulitic limestone beneath Kochüzü Fm.	*Alveolina* (*Glomalveolina*) *lepidula*, *Alveolina* (*Glomalveolina*) *subtilis*, *Fabularia* cf. *donatae*, *Orbitolites* sp., *Lockhartia* sp.	-	-	Early Eocene

Table 3.4. Table showing the palaeontological analysis of samples of Akpınar Formation limestone (courtesy of N Inan & K Taslı).

3.4.3.4 Interpretation of the Eocene transgressive sediments (Akpınar Formation)

The basal part of the Akpınar Formation consists of red clastics and white limestones which are interpreted as continental and lacustrine deposits respectively. These units have not been dated and may represent part of a Paleocene or early Eocene sequence. They are overlain by marine marls and Nummulitic limestones representing a marine transgression initiated in the Early Eocene. Localised basaltic volcanism (Kocaözü Member) erupted within the marls. Later andesitic volcanism (Leylek Member) erupted in the upper part of the Akpınar Formation. The formation is capped by shallow-marine facies which contain organic matter and finally by evaporitic beds. This sequence is interpreted as a shallow-marine sea which shallowed before becoming emergent.

The Akpınar Formation may have been deposited in a syn-tectonic environment as evidenced by localised slump folds and the extension-related basic volcanism (see below).

3.4.3.5 Eocene basaltic volcanism (Kocaözü Member)

Name: Previously unrecognised. The name that has been given here is the nearest village to the type section.

Type section: ~1.5 km SSW of Kocaözü.

Lithology: The Kocaözü Member is composed of plagioclase and clinopyroxene phyric basalt (Fig. 3.47a & b). The basalts have a weakly defined pillow structure. The base of the member is well exposed SSW of Kocaözü where well preserved lava-sediment interaction structures were observed including ‘load balls’ of lava (Fig. 3.47c). The member outcrops ~1.5 km north and also to the NW of Haydaroğlu where small pillow basalts are better defined (Fig. 3.47d). There, the basalts are overlain by a thin sequence of localised, dark-grey, volcaniclastic conglomerate.

Boundaries: The Kocaözü Member outcrops entirely within marls of the Akpınar Formation.

Thickness and extent: The Kocaözü Member outcrops in relatively small, localised areas to the south and the east of Hekimhan. The member reaches a maximum thickness of ~30 m at outcrop.

Age: The Kocaözü Member is dated as Early–Middle Eocene based on palaeontological dating of the Akpınar Formation which the member outcrops within (Table 3.4).

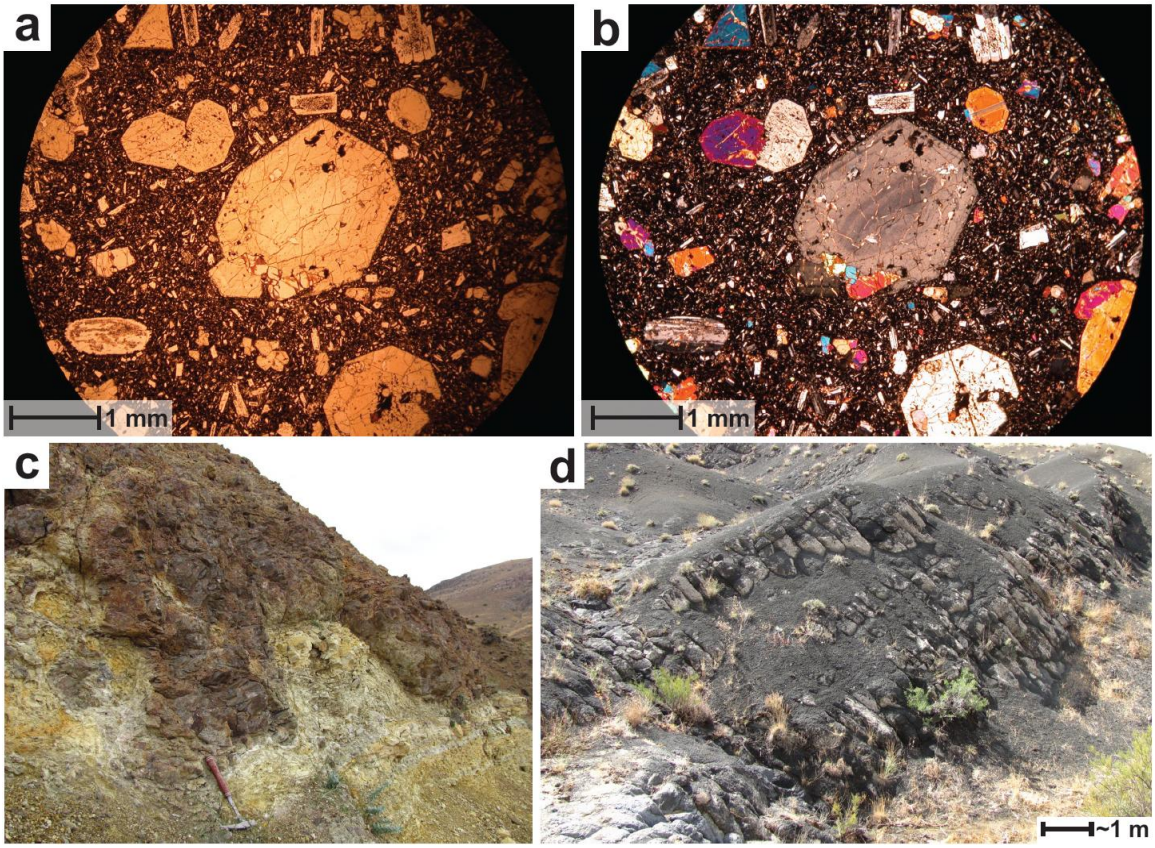

Figure 3.47. Photographs showing; a & b, PPL (a) and XPL (b) images of euhedral plagioclase and pyroxene phenocrysts in a fine grained, plagioclase dominated matrix. The pyroxene phenocrysts commonly show oscillatory zonation. The plagioclase phenocrysts are commonly partially resorbed; c, lava sediment interaction near Kocaözü; d, well developed, small pillow basalts near Haydaroğlu.

3.4.3.6 Geochemistry of the Eocene basaltic volcanism (Kocaözü Member)

Six samples of the Kocaözü volcanic member were collected in the field, three from the east of Haydaroğlu and three from the south of Kocaözü. A volcanic classification diagram (TAS diagram) displaying the 6 Kocaözü Member samples is shown in Figure 3.48. The samples show a relatively small scatter on the diagram with two samples plotting within the ‘basalt’ field and the rest within the ‘andesite-basalt’ field. The lavas

were erupted into wet, hemi-pelagic marl (indicated by planktonic Foraminifera within the marl). Lava-sediment interaction is widespread. Load casts of hot lava penetrated down into the wet hemi-pelagic marl forming hyaloclastite and peperite structures. The marl adjacent to the lava is hydrothermally altered. Outcrops of Kocaözü Member basalt are often very weathered, probably as a result of the highly porous marl medium which the unit was located in. Every effort was made to collect the freshest samples possible. However, some amount of alteration cannot be ruled out.

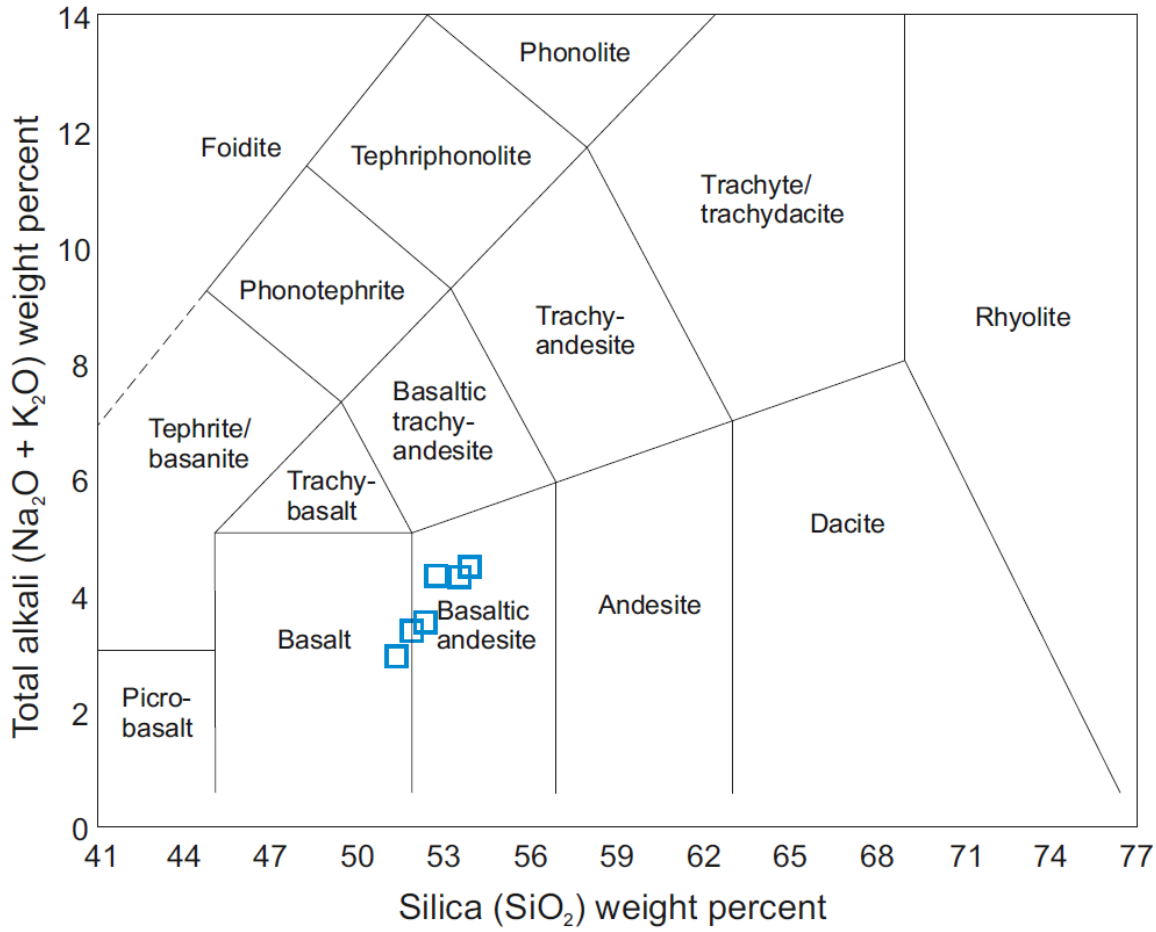

Figure 3.48. Total Alkali Silica (TAS) diagram for samples from the Kocaözü Member.

Figure 3.49 shows a spider diagram of the samples from the Kocaözü Member. The rocks are enriched in LILE's and LREE's and relatively depleted in HFSE's and heavy metal elements (Ni and Cr). There is an apparent negative Nb anomaly (similar to the Hasançelebi Formation) which was attributed to a subduction zone influenced source.

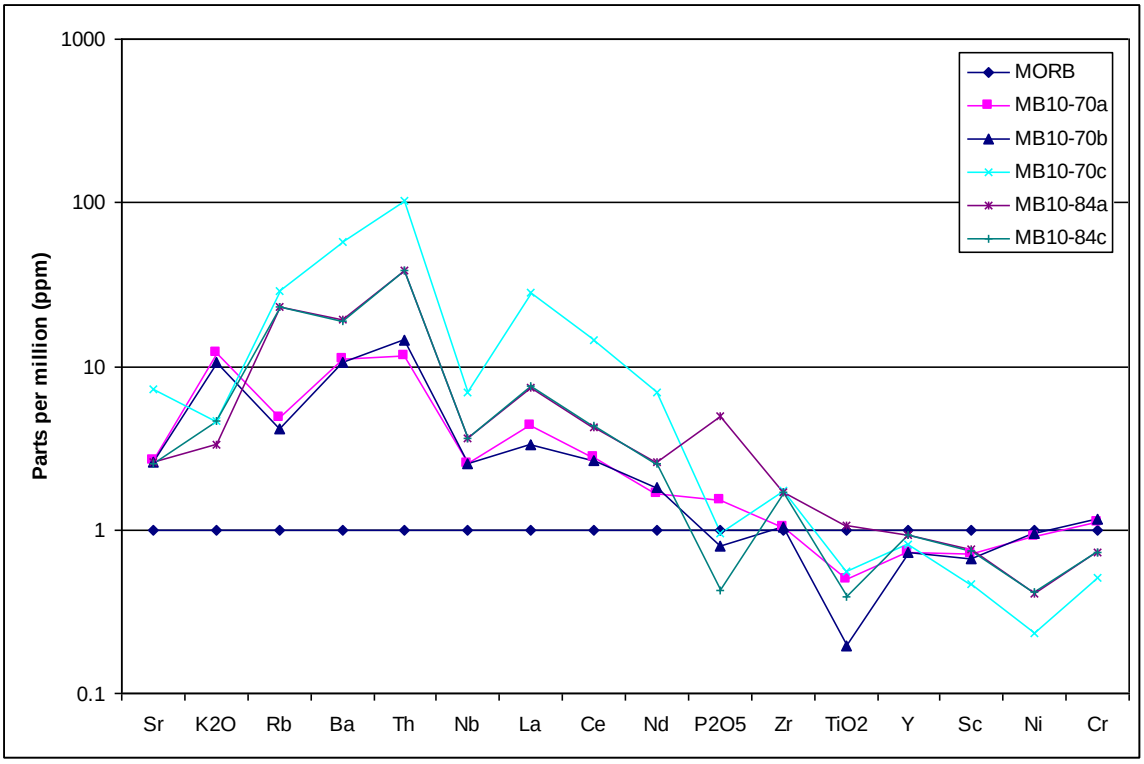

Figure 3.49. Spider diagram of volcanic rocks from the Kocaözü Member normalised to MORB (MORB data from Pearce 1982 and Saunders & Tarney 1984).

Figure 3.50 shows a series of tectonic discrimination diagrams. Figure 3.50a is a tectonic discrimination plot which utilises Zr and Ti (ppm) on a logarithmic plot to distinguish between volcanic-arc, within-plate and MORB affinities. It shows that most of the samples plot within or close to the within-plate field with one sample plotting within the volcanic-arc field. Figure 3.50b is a diagram based on Zr/Y-Zr variations and shows that all of the samples plot within the within-plate field (only 3 points are visible because geochemical analyses are very similar for 3 of the samples).

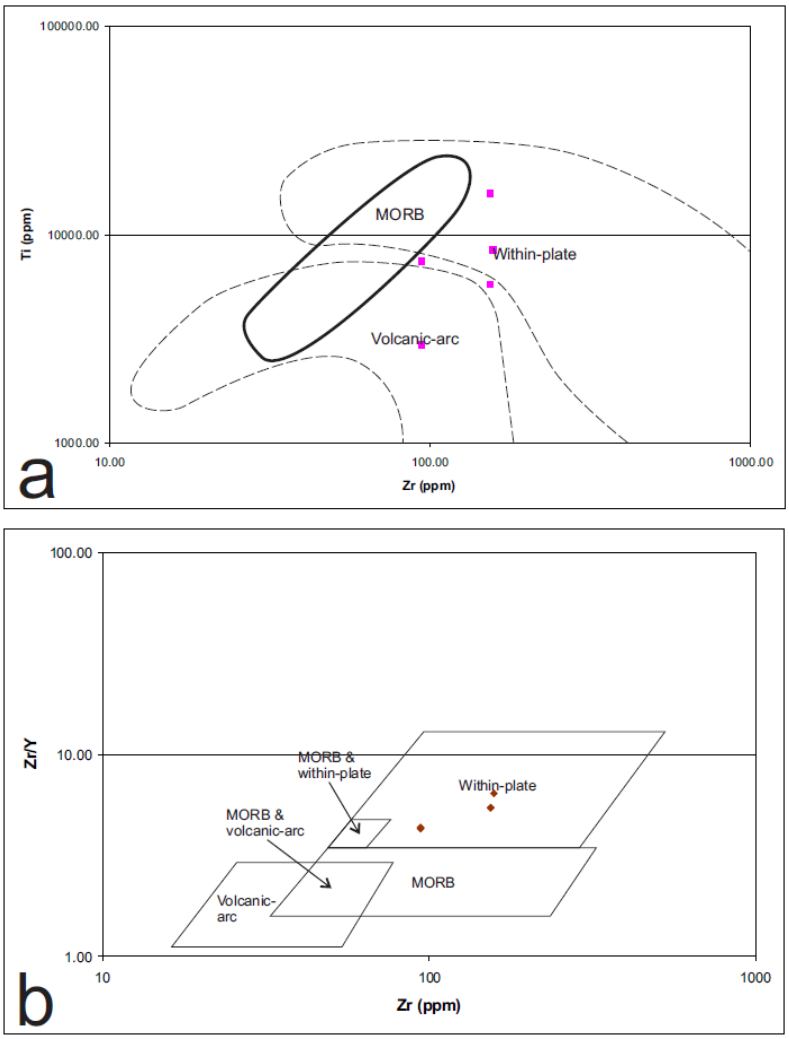

Figure 3.50. Discrimination diagrams for the Kocaözü Member samples based upon; a, Ti-Zr variations (after Pearce & Cann 1973); b, Zr/Y-Zr variations (after Pearce & Norry 1979).

In summary, the geochemistry indicates that the Kocaözü Member erupted in a within-plate environment.

3.4.3.7 Interpretation of the Eocene basaltic volcanism (Kocaözü Member)

The Kocaözü Member was erupted in a submarine setting within several hundred metres of water as evidence by the presence of pillow lavas, the stratigraphic position within planktic Foraminifera-bearing hemi-pelagic marl and the lava-sediment interaction structures. The eruptions produced small scale volcanic piles which may have been fault controlled. However, little evidence for faulting (other than minor slumping within marls of the Akpınar Formation) exists in the field area. The volcanism occurred within the same time frame to and is mineralogically (and geochemically) similar to the Karakayalar Member volcanism within the Darende Basin, but on a smaller scale.

3.4.3.8 Eocene andesitic volcanism (Leylek Member)

Name: Given by Gürer (1994). The name presumably derives from Leylek Tepe.

Type section: Leylek Tepe.

Lithology: The Leylek Member is characterised by andesitic composition volcanism and associated intrusions. The andesite is medium-grained, composed primarily of plagioclase, clinopyroxene (orthopyroxene is also present) and minor hornblende (Fig. 3.51). Accessory magnetite was also observed. The andesite contains lath-shaped plagioclase phenocrysts and is often vesicular. The andesite at Leylek Tepe is either massive and structureless, or roughly arranged into beds ~50 cm thick. Thin andesitic dyklets were often observed penetrating the massive and bedded andesite (Fig. 3.52a).

Intrusive sills with an andesitic composition (but not vesicular) were observed in formations surrounding Leylek Tepe. The sills are typically sinuous and up to 5 m thick (Fig. 3.52b). They commonly display well-formed columnar jointing (Fig. 3.52c).

Sediments, including volcaniclastic sediment, were observed within the vicinity of Leylek Tepe, stratigraphically below, and above the volcanic pile. Nummulites-bearing limestones appear to dip beneath Leylek Tepe on the south side of the mountain. Sequences of dark grey, coarse-grained, sandstone (Fig. 3.52d) interbedded with diagenetic chert horizons (Fig. 3.52e) and occasional light brown limestones onlap the volcanic pile on the eastern side of Leylek Tepe. The limestones contain rare, small bivalves and gastropods. Dewatering structures were commonly observed within the sandstones. Debris flows to the north of Leylek Tepe contain sub-rounded cobble sized clasts of vesicular andesite.

Boundaries: A normal lower stratigraphic boundary was not observed in the field. However, it appears that Nummulites-bearing limestones dip below the andesitic volcanic pile at Leylek Tepe. The volcanic pile is overlain by marine sediments and volcaniclastic sediments. However, there are no age constraints on these sediments. Oligocene-aged, red, continental clastics (Kamatlar Formation) overlie the volcanic pile to the south of Leylek Tepe above an angular, erosive unconformity (Fig. 3.52f).

Thickness and extent: The Leylek Member outcrops exclusively to the WNW of Hekimhan and reaches a maximum thickness of ~300 m.

Age: The Leylek Member is interpreted as being erupted during the Late Eocene due to its stratigraphic position above Nummulitic limestone and below Oligocene-aged clastics. This fits well with $^{40}Ar/^{39}Ar$ K-feldspar geochronology conducted by Kuşcu *et al.* (2007) which yielded an age of 34.4 Ma ±1.1.

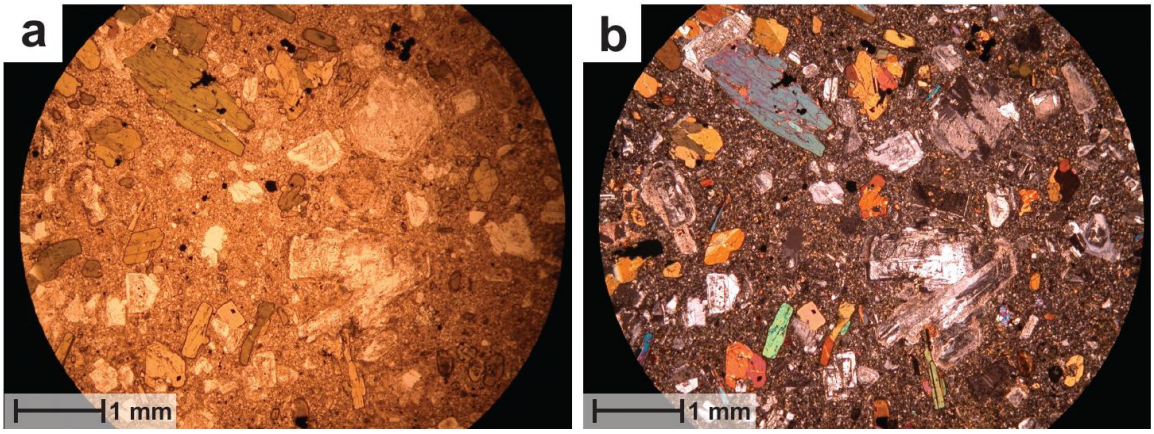

Figure 3.51. PPL (a) and XPL (b) images of andesite from the Leylek Member. Resorbed plagioclase phenocrysts can be identified as well as clino- and orthopyroxene phenocrysts.

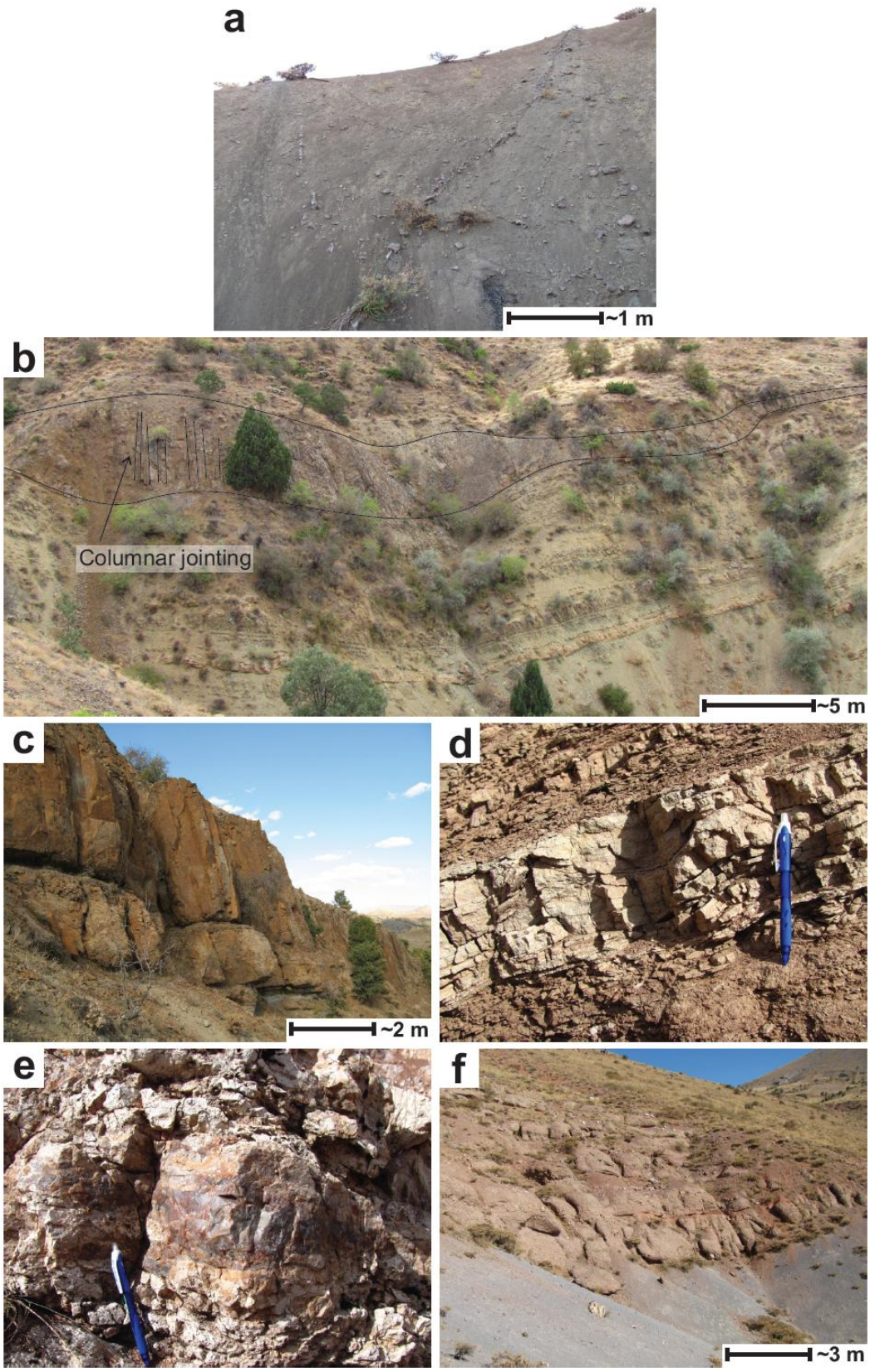

Figure 3.52. Photographs showing; a, dyklets within massive andesite; b, sinuous, columnar jointed andesite sill within the Hekimhan Formation; c, columnar jointed sill; d, volcaniclastic sandstone with dewatering structures; e, chert horizons in tuff deposits; f, Kamatlar Formation continental conglomerates unconformably and erosively overlying massive andesite of the Leylek Formation.

3.4.3.9 Geochemistry of the Eocene Andesitic volcanism (Leylek Member)

Four samples of the Leylek Member were analysed using XRF. Figure 3.53 shows the samples plotted on a Total Alkali versus Silica (TAS) volcanic classification diagram. The results are significantly scattered across the diagram and plot in andesite, trachy-andesite and rhyolite. All of these samples are therefore intermediate to evolved.

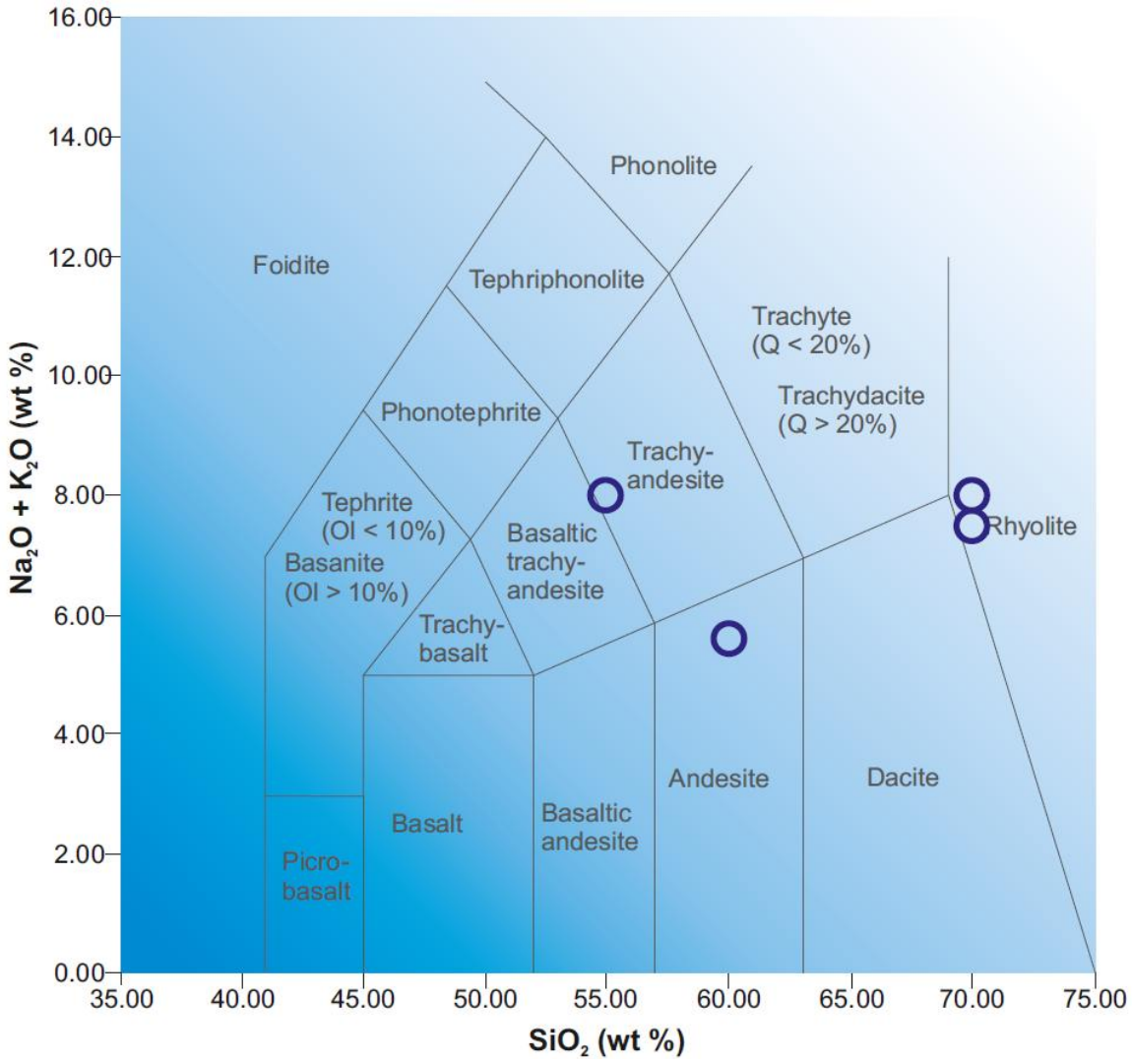

Figure 3.53. TAS diagram for the Leylek Member volcanic samples after Le Maitre *et al.* (1989). Q = normative quartz; Ol = normative olivine.

3.4.3.10 Interpretation of the Eocene Andesitic volcanism (Leylek Member)

$^{40}Ar/^{39}Ar$ K-feldspar geochronology of the Leylek Member by Kuşcu *et al.* (2007) yielded an age of 34.4 Ma ±1.1 which is consistent with field observations. The member is underlain and overlain by Nummulites-bearing limestones and interbedded

volcaniclastic sediments. The volcaniclastics were likely derived locally. The Leylek Member was emplaced in a sub-marine setting as indicated by the presence of marine sediments stratigraphically below and above the unit. Interbedded chert horizons represent diagenetic remobilisation of silica which was probably indirectly sourced from the Leylek Member, which contains 55–70% silica (Fig. 3.53).

The Leylek Member could have been ponded and fractionated at depth from an earlier basic magma. A degree of melting and assimilation of the continental crust is also likely as indicated by the high silica content. The Leylek Member probably represents post-collisional magmatism.

3.4.4 Post Eocene

3.4.4.1 Oligocene continental sediments (Kamatlar Formation)

Name: Introduced by Gürer (1994). Presumably derived from the village of Kamatlar which this formation surrounds (Fig. 3.54).

Type section: The relatively flat land to the south of Kamatlar.

Lithology: The Kamatlar Formation is composed of red sandstones and pebble to cobble-grade conglomerates (e.g. Fig. 3.55). The matrix and clasts are sub-rounded, poorly sorted and texturally immature. They are composed of limestone (some clasts containing *Nummulites* sp.) and volcanic clasts including; basalt, gabbro, trachyte, serpentinised ultramafics as well as rare syenite. Beds are typically decimetres thick and lenticular with erosive bases. The majority of the beds are matrix supported. However, some horizons are clast supported and weakly inverse graded (Fig. 3.56a). Structures include cross lamination, cross bedding, imbrication and massive groove casts (Fig 3.56b). Gürer (1994) reported findings of pollen spores (*Polyporopollenites undulosos* and *Periporopollenites multiporatus*) within sandstones of the Kamatlar Formation.

Boundaries: The Kamatlar Formation overlies underlying formations (e.g. Hasançelbi, Akpınar and Leylek) above an erosive, angular unconformity across the Hekimhan Basin. The formation is unconformably overlain by Miocene limestones (Boyralı Formation).

Thickness and extent: The Kamatlar Formation is up to 250 m thick. It mainly outcrops to the west and NW of the Hekimhan Basin as well as some isolated areas to the east.

Age: No body fossils were observed in the Kamatlar Formation. The formation is stratigraphically above the Eocene aged Akpınar Formation and below the Miocene aged Boyralı Formation giving an approximate Oligocene age.

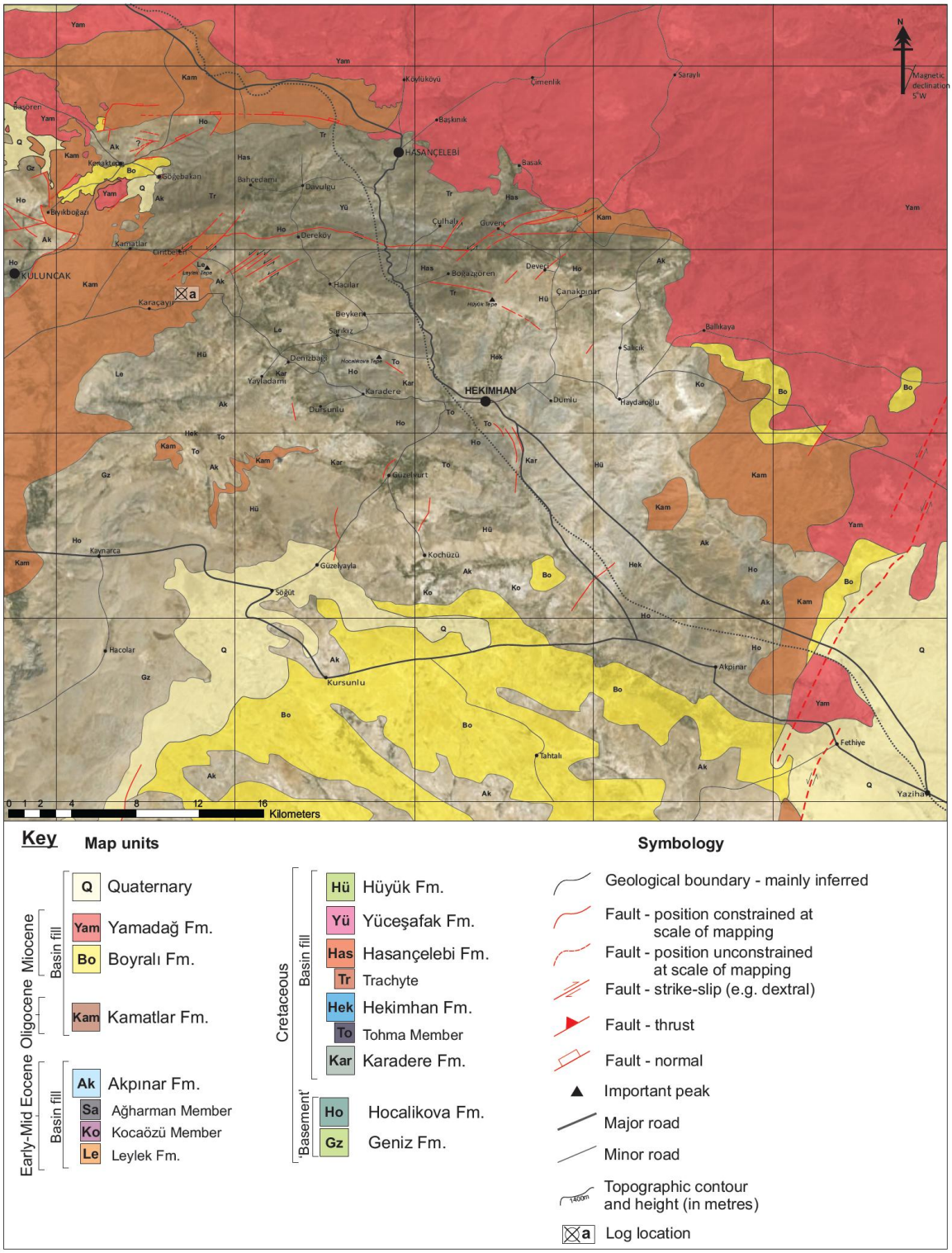

Figure 3.54. Simplified geological map showing the extent of the Kamatlar, Boyralı, Yamadağ and Quaternary Formations draped over a satellite image of the Hekimhan Basin. Also shown is the location of a logged section of the Kamatlar Formation.

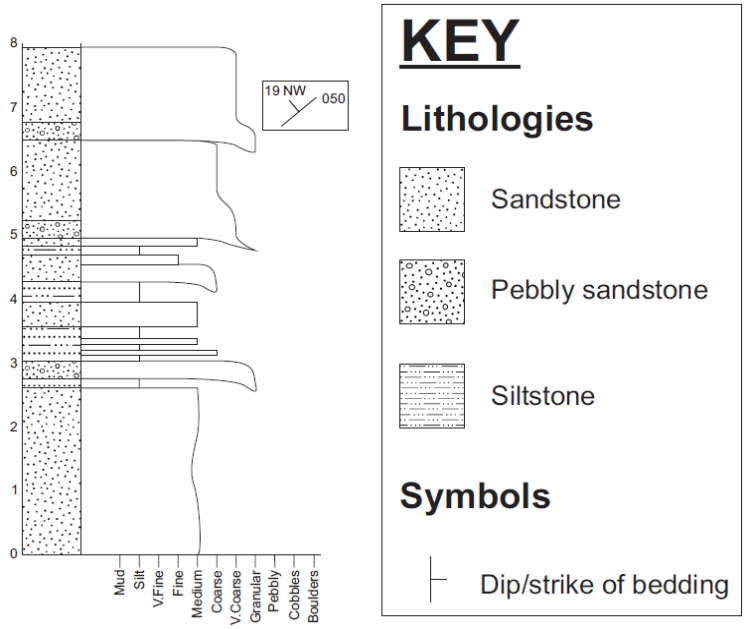

Figure 3.55. Measured sequence of part of the Kamatlar Formation taken from location 'a' on the simplified geological map (Fig. 3.37).

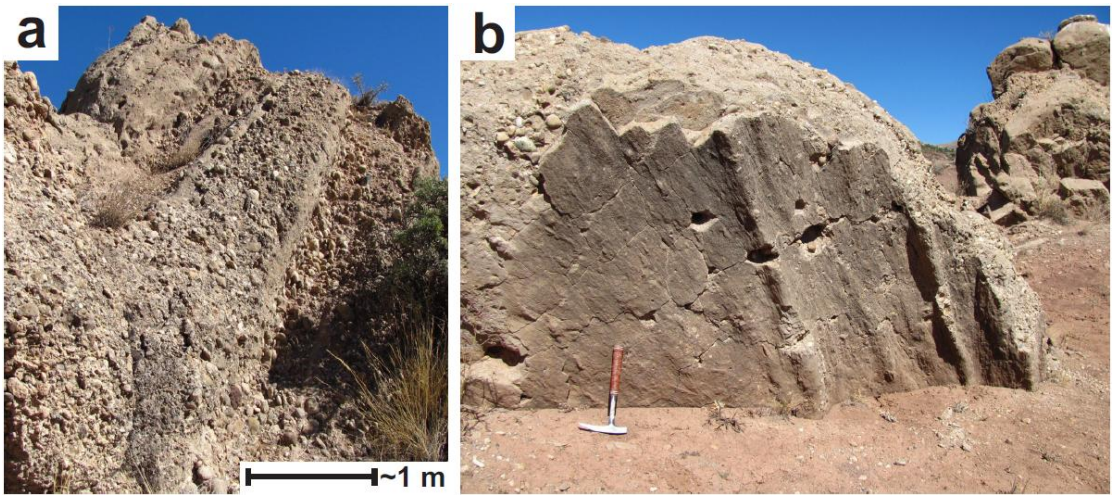

Figure 3.56. Photographs showing; a, weakly inverse graded, clast supported, cobble-grade conglomerates interbedded with red, pebbly sandstone; b, massive groove cast structures on the base of a pebbly sandstone bed.

3.4.4.2 Interpretation of the Oligocene continental sediments (Kamatlar Formation)

The sandstones and conglomerates of the Kamatlar Formation source rocks from the stratigraphically lower formations. For example, Nummulitic limestone clasts are likely derived from the Akpınar Formation, Rudist-bearing limestone clasts are likely derived from the Tohma Member and basalt clasts could be derived from the Kocaözü, Hasançelebi or Hocalikova Formations. Serpentinised ultramafic, doleritic and gabbroic clasts are derived from the Hocalikova Formation.

The rounded nature of the clasts and the lenticular erosive based nature of the beds, coupled with the sedimentary structures (groove casts and cross bedding) indicates a fluvial environment of deposition. The red nature of the beds may indicate an arid continental palaeoenvironment. Pollen spores and the lack of marine body fossils supports a non-marine setting. The weakly inverse-graded, clast supported conglomeratic units are interpreted as debris-flow deposits and may represent individual flooding events (e.g. lahar or similar).

3.4.4.3 Miocene transgressive carbonates (Boyralı Formation)

Name: Introduced by Gürer (1994). Unknown origin.

Type section: To the south of Kursunlu in the south of the Hekimhan Basin.

Lithology: The Boyralı Formation is composed of a lower part of sandy marl with matrix supported pebble and cobble-grade beds and an upper part composed of faunally diverse massive limestone. Cemented horizons of large oysters are common in the lower part. Large-scale forsets were observed within the limestones in the upper part (Fig. 3.57). The limestone beds are rich in bivalves and gastropods and bored surfaces are common. The Miocene exposures are sub-horizontally bedded and relatively undeformed throughout the Hekimhan Basin.

Boundaries: The lower boundary forms an angular unconformity with Eocene limestones (Akpınar Formation) in the south of the basin and a shallower angle unconformity with Oligocene clastics (Kamatlar Formation) in other areas in the basin.

Figure 3.57. Photograph showing forsets prograding ~southwestwards within limestones of the Boyralı Formation.

Thickness and extent: The formation is most extensive in the plateau and canyon topography in the south of the basin. Isolated exposures were observed in the NW and east of the basin. The Boyralı Formation reaches a total maximum thickness of 100 m in the south of the basin, around the type section area. The formation is much thinner (up to 25 m) in the isolated exposures to the NW and east of the basin.

Age: The Boyralı Formation was dated by Gürer (1994) as Miocene based on microfossil analysis (Table 3.5).

Fossil name	Type	Age range
Miogypsina irregularis (Michelotti)	Benthic Foram	Miocene
Miogypsina grandipustulus Cole	Benthic Foram	Miocene
Amphistegina cf. lessoni D'Orbigny	Benthic Foram	Miocene
Pararotalia sp.	Benthic Foram	Miocene-recent
Miliolidae	Benthic Foram	Cretaceous-recent
Litholhamnium sp.	Calcareous Algae	Miocene-recent

Table 3.5. Microfossil assemblage found in the Boyralı Formation. Data from Gürer (1994).

3.4.4.4 Interpretation of the Miocene transgressive carbonates (Boyralı Formation)

A short-lived marine transgression deposited faunally diverse marl and shallow-marine carbonate facies. This formation overlies partially deformed and tilted Eocene and Oligocene sediments. However, the Boyralı Formation is relatively undeformed and remains sub-horizontal indicating that any collision related compression was largely complete before the onset of deposition. Furthermore, it implies the postponement of regional uplift until after the Mid-Miocene (see structure section, Chapter 3.5). Comparable Miocene shallow-marine sediments are seen in several other basins throughout central Turkey (Türkmen *et al.* 2007; Hüsing *et al.* 2009).

3.4.4.5 Pliocene subaerial volcanism (Yamadağ Formation)

Name: Introduced by Gürer (1994). Unknown origin.

Type section: Saraylı in the NE of the Hekimhan Basin.

Lithology: The Yamadağ Formation is composed of a thick sequence of clinopyroxene- and feldspar-phyric basaltic lava flows (Fig. 3.58a) and associated volcanogenic debris-flows, individually up to 10 m thick. The debris flows contain sub-angular clasts of basalt (Fig. 3.58b). Crosscutting sills up to 15 m thick were also observed and often display columnar jointing. Bright orange and red tuffs are also associated with this formation. The tuffs contain large angular clasts of volcaniclastic material (Fig. 3.58c). 'Fairy chimney' weathering is well developed in this formation.

Boundaries: No stratigraphic boundaries were observed during this study although the formation is believed to overlie limestones of the Boyralı Formation.

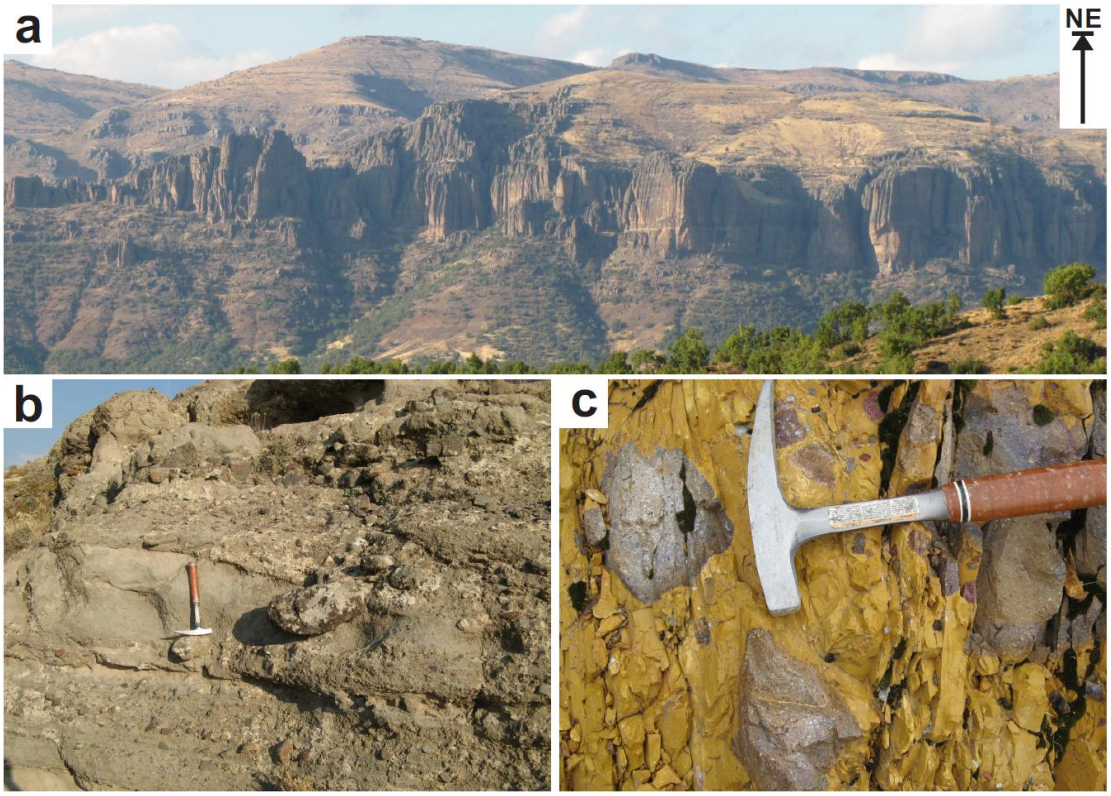

Figure 3.58. Photographs showing; a, thick lava flows and 'fairy chimney' weathering of the Yamadağ Formation (field of view ~500 m); b, volcaniclastic sediments associated with the Yamadağ Formation; c, bright yellow tuff and angular volcaniclastic clasts. Hammer for scale in b and c.

Thickness and extent: The Boyralı Formation is up to 1000 m thick and covers a large area of central Anatolia as shown in Figure 3.59. Basalts of similar age are widespread throughout eastern Anatolia (Arger *et al.* 2000; Demir *et al.* 2009; Ekici *et al.* 2009). The lithologically similar Kepez Dağı Formation (within the Darende Basin) is believed to be a westward extension of the Yamadağ Formation.

Age: The Yamadağ Formation was dated by Gürsoy *et al.* (2011) as being Middle Miocene, the bulk of the volcanic activity having taken place between ~15–13.5Ma.

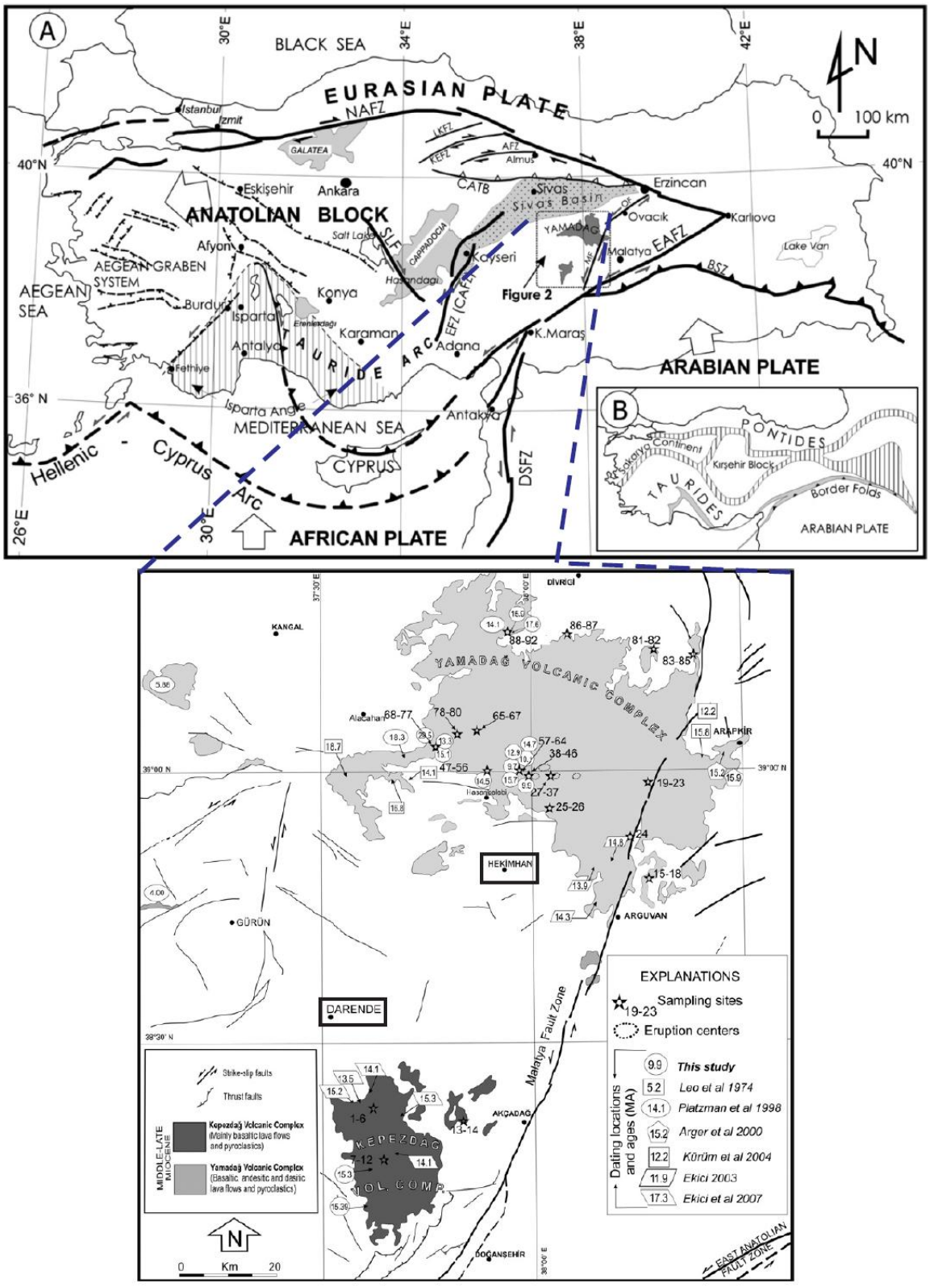

Figure 3.59. Outline map showing the extent of the Yamadağ Formation within Turkey as a whole and within the Malatya region of central eastern Turkey. Taken from Gürsoy *et al.* (2011).

3.4.4.6 Interpretation of the Pliocene subaerial volcanism (Yamadağ Formation)

The lava flows erupted in a subaerial setting and were partially reworked by fluvial and gravity processes to form volcanogenic debris flows. Regionally similar Miocene-aged basaltic lavas were identified by Kürüm *et al.* (2008) (e.g. Arapkir, Inle and Adamkıran).

3.5 Structural development of the Hekimhan Basin

3.5.1 Introduction

Previous work on the structural development of the Hekimhan Basin is limited. Much of the research involving the Hekimhan Basin has revolved around isolated aspects. For example, Yalçın & Bozkaya (1995) investigated the mineralogy and alteration of part of the ophiolite sequence, Yildiz & Özdemir (1999) investigated a small part of the Hekimhan Formation and Ozgenc & Ilbeyli (2009) investigated the geochemistry and suggested a potential genesis of the alkaline magmatism (Yüceşafak Member) (see chapter 3.3 for detailed previous work). Gürer (1994) proposed the first, and only, tectonic evolution models for the Hekimhan Basin based on field studies of the sedimentary, volcanic and magmatic rocks. However, no structural data was presented.

More recently, Kaymakci *et al.* (2006) proposed a three stage deformation history for the Malatya-Ovacık fault zone located within the Malatya Basin (~35 km east of the Hekimhan Basin). Stage 1 is characterised by NW-SE directed extension during the Early-Middle Miocene, stage 2 is characterised by WNW-ESE directed compression operating from the Late Miocene to Middle Pliocene, and, stage 3 is characterised by strike-slip tectonics active from the Late Pliocene to recent. However, Kuşcu *et al.* (2011) researched the mineralogy and geochronology of the mineralisation associated with the Yüceşafak Member in the Hekimhan Basin. They conclude that the magmatism was emplaced under an extension stress regime during the Late Cretaceous and have confusingly referenced Kaymakci *et al.* (2006) as evidence for this Cretaceous extension. However, Kaymakci *et al.* (2006) only report the structural history of the Malatya Basin which begins in the Early Miocene.

The structural data presented here is the first comprehensive study which is integrated with a complete analysis of the sedimentary and igneous rocks in the Hekimhan Basin in order to fully understand the tectonic evolution. In order to establish the deformation history, a range of fault planes, fold axial planes and, where present, kinematic indicators (e.g. slickensides, fault steps & shear fabrics) were measured in the field and processed using TectonicsFP (Ortner *et al.* 2002), Steronet7 (Allmendinger

2011) or FaultKin5.2 (Allmendinger 1992; 1995). The aim was to determine the orientation patterns and palaeostress for each of the deformation phases.

The majority of the deformation features observed within the Hekimhan Basin are faults, particularly strike-slip faults. Few folds exist in the basin compared to the Darende Basin.

The remainder of this chapter will focus on the description of deformation and the analysis of the deformation affecting the Hekimhan Basin. The interpretation of deformation draws heavily on sedimentary as well as volcanic evidence to further elucidate the structural history.

3.5.2 Extensional features

No extensional structures were observed within the Mesozoic Geniz Formation. This is mainly due to the small, localised nature of the outcrops within the Hekimhan Basin. Numerous fault and shear planes were observed within the serpentinised tectonic mélange (Hocalikova Formation). However, serpentinite is easily deformed making the interpretation of structures within this unit unreliable.

Numerous, small-scale extensional faults (typically <5 m in length, <5 cm width at outcrop, with displacements typically <20 cm) were observed within the Maastrichtian-aged Karadere and Hekimhan Formations. A stereonet of faults observed within these formations is shown in Figure 3.60 and indicates that the majority of the fault zones are orientated E-W with displacements towards the N or S. Comparatively few faults were observed within the Hasançelebi Formation and Yüceşafak Member.

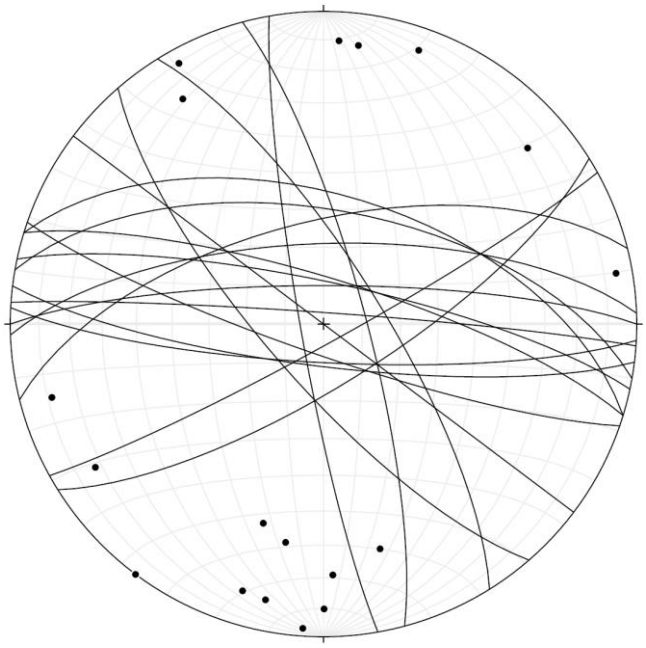

Figure 3.60. Equal area stereonet showing great circles and poles to planes of extensional fault planes observed within the Karadere and Hekimhan Formations (n=18).

Much of the evidence for extension within the Maastrichtian-aged rocks is derived from features observed within sedimentary rocks. Syn-sedimentary faulting has produced wedge shaped sedimentary packages. Figure 3.61a shows en-echelon normal faulting associated with wedge-shaped buff coloured sandstone packages set within black

mudstone in the lower part of the Hekimhan Formation. Figure 3.61b shows a single wedge-shaped package of grey pebbly sandstone set within red pebbly sandstone of the Karadere Formation. The fault is probably located beneath the road. In both of these figures, the wedge-shaped sandstone packages thicken towards the north.

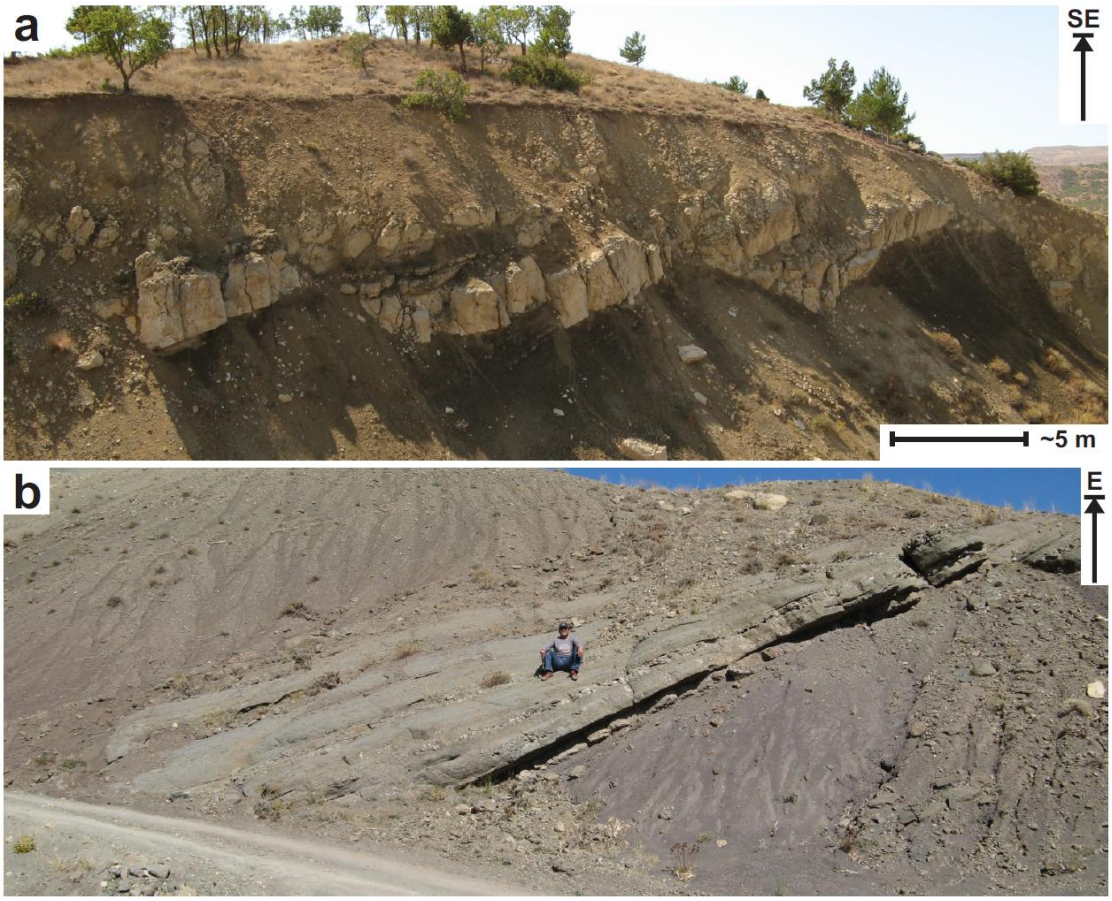

Figure 3.61. Field photographs showing: a, Normal faults associated with wedge shaped sandstone packages in the lower part of the Hekimhan Formation; b, Wedge shape package of grey pebbly sandstone within red pebbly sandstone. The fault is unfortunately located beneath the road. Person for scale.

Internal unconformities are common in the Hekimhan Formation. Several of which are marked in figure 3.62 within sapropelic mudstone in the lower part of the Hekimhan Formation.

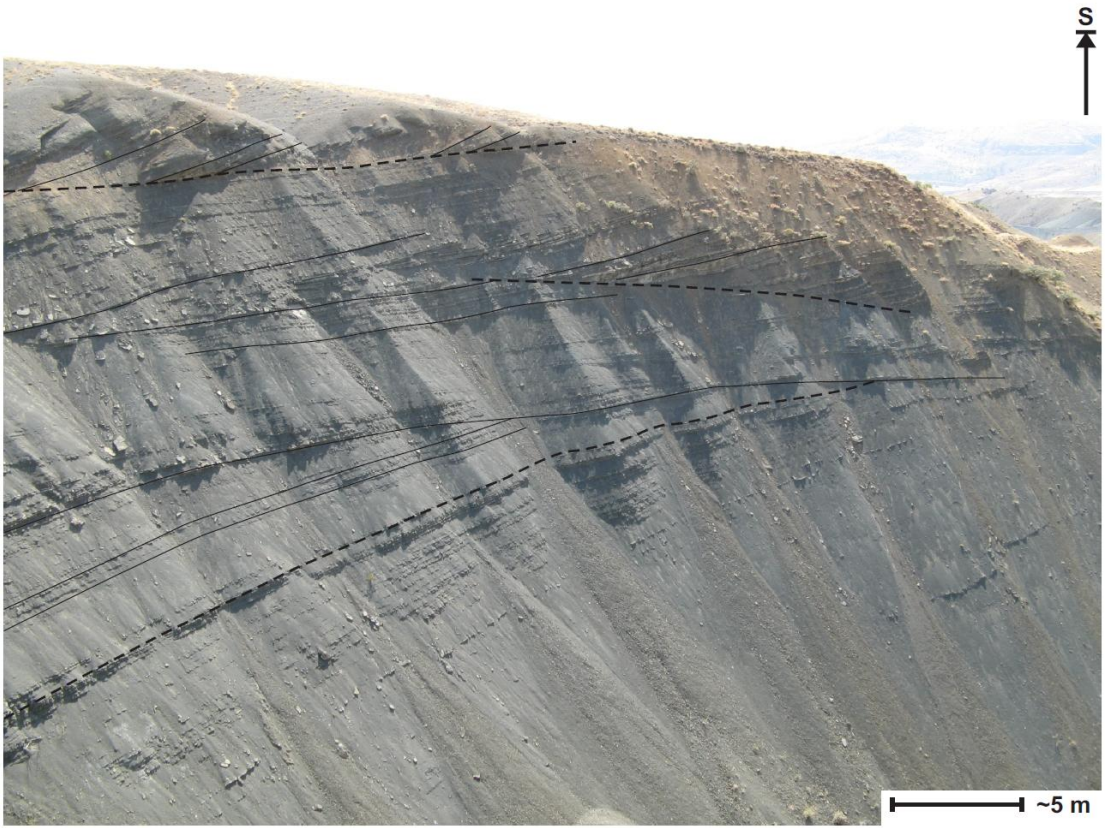

Figure 3.62. Black sapropelic mudstone in the lower part of the Hekimhan Formation with several internal unconformities (marked by dashed lines).

Slump folds were frequently observed in the Hekimhan Formation. Typically, competent beds of calcarenite have slipped over less competent hemipelagic marl. Isolated, 'rafted blocks' of calcarenite were observed within deformed marl (Fig. 3.63a), some of which were stacked up, forming a pseudo-imbriccation (Fig. 3.63b).

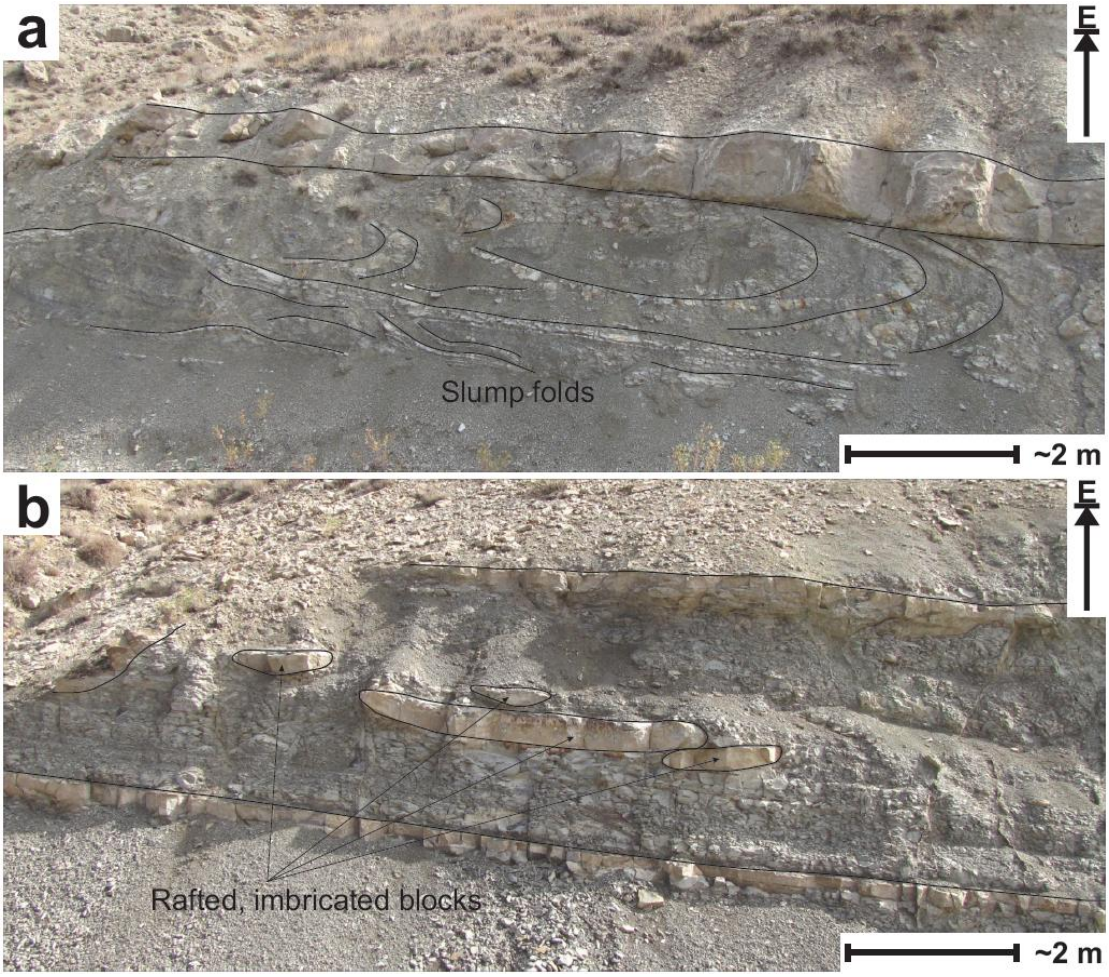

Figure 3.63. Photographs showing; a, slump folds within marl layers overlain by a relatively undeformed calcarenite bed; and; b, rafted and imbricated blocks of competent (lithified) calcarenite within marl.

A stereonet of a collection of slump axial planes is shown in Figure 3.64. The slump fold axes all dip to the south. However, the geometry of a slump fold is such that if the axial plane of the slump fold dips to the south, the movement direction will be northwards. Hence, the green arrow shows the approximate down-slope movement direction of slump folds measured within the Hekimhan Formation.

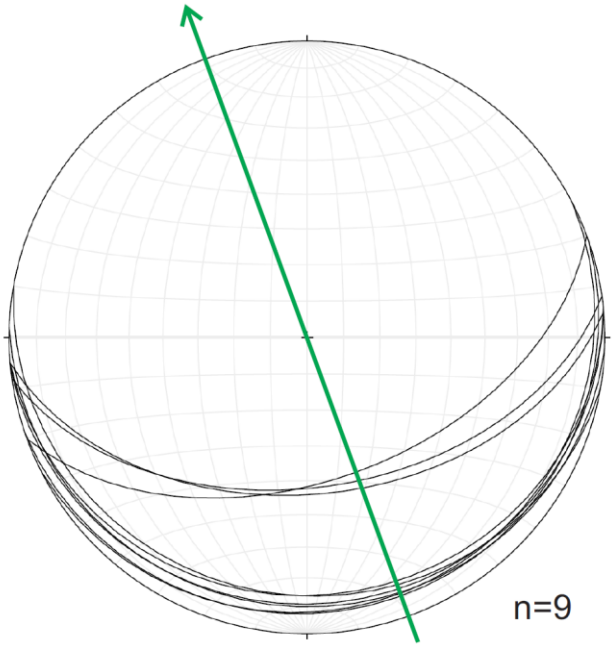

Figure 3.64. Stereonet showing great circles of slump fold axial planes. Green arrow indicates down-slope movement direction of the slumped material (n=9).

Deformed strata situated stratigraphically higher up in the Hekimhan Formation are overlain by undeformed beds (Fig. 3.65).

Figure 3.65. Field photograph of the Hekimhan Formation showing syn-sedimentary deformation (below the dashed line) overlain by undeformed beds. The massive unit in the upper right is Hüyük Formation limestone. Alastair Robertson for scale in centre.

Little evidence for extension was observed in the field within the Eocene-aged Akpınar Formation. A series of small normal faults were observed in the east and the south of the basin. These faults were generally less than 5 m in length with fault cores less than 2 cm wide and displacements less than 10 cm. Figure 3.66 shows that the majority of these fault zones are E-W orientated and dip towards the north.

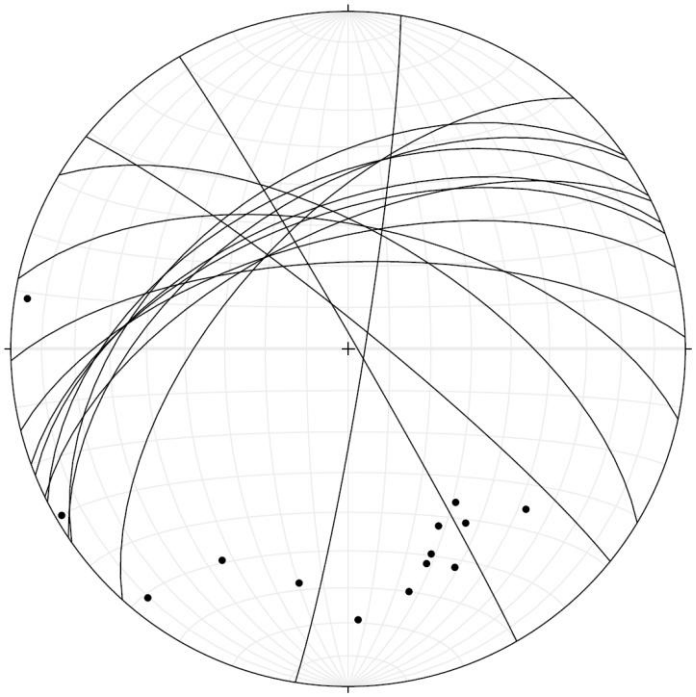

Figure 3.66. Equal area stereonet showing great circles and poles to planes of extensional fault zones observed within the Akpınar Formation (n=14).

3.5.3 Compressional features

3.5.3.1 Folding

No significant folds were observed in the Cretaceous-aged rocks in the Hekimhan Basin. An isolated box fold was observed within volcaniclastic sediments of the Hasançelebi Formation (Fig. 3.67a). However, it remains unclear whether this fold formed as a direct result of a basin-wide compressional event or a localised event related to the emplacement of lava and dykes.

Minor folds were associated with Eocene-aged rocks. An isolated recumbent S-fold was observed within marls of the Akpınar Formation in the east of the basin (Fig

3.67b). It was unclear whether beds above and below this fold were similarly affected. Folds were observed within sandy-marls in the Akpınar Formation around Kocöazü in the south of the basin (Fig. 3.67c). The folds appear to be associated with compressional faulting. Overlying limestone beds are unaffected.

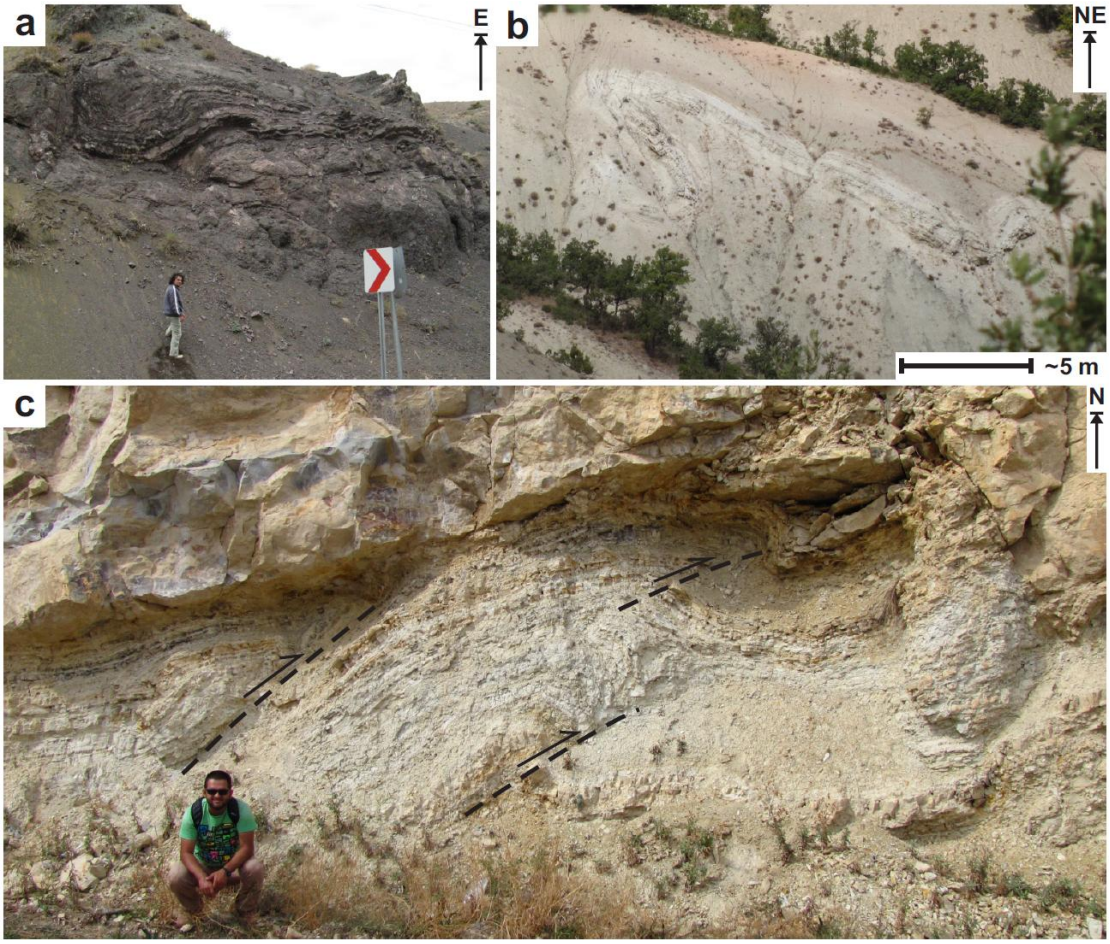

Figure 3.67. Field photographs showing: a, Box fold within volcaniclastic sediments of the Hasançelebi Formation (person for scale); b, Recumbent S-fold in marls of the Akpınar Formation; c, Folds associated with small faults (marked by dashed lines) within the Akpınar Formation (person for scale).

3.5.3.2 Reverse faulting

Compressional faults are widespread in the Hekimhan Basin. They were observed in Maastrichtian through to Oligocene-aged rocks but not within Miocene-aged rocks. Slices of Mesozoic limestone (Geniz Formation) are thrust with ophiolitic material (Hocalikova Formation) in the far SW of the basin. Thrusts planes were often eroded, typically several hundred metres long, low-angle, straight with fault cores not more than 20 cm thick. It was not possible to establish any displacement from these faults. Many of the larger-scale fault zones in the Hekimhan Basin are associated with the ophiolitic Hocalikova Formation. In the SE of the basin ophiolitic material (with an in situ block of unconformably overlying Tohma Member limestone) has been thrust northwards over red sandstones and conglomerates of the Karadere Formation above an ~45^{o} straight fault zone (Fig 3.68a). In the centre of the basin, pillow lavas and lava flows of the Hasançelebi Formation have been thrust northwards over the Hocalikova ophiolite above a high-angle thrust zone (Fig. 3.68b). However, limited kinematic features indicate that this fault zone may have undergone a degree of (more recent) sinistral strike-slip movement. In the centre of the basin (~2 km SW of Hüyük Tepe) heavily altered Hasançelebi Formation rocks have been thrust southwards over a low-angle sinuous thrust fault above Hocalikova Formation ophiolitic rocks (Fig. 3.68c). The fault core forms a shear zone ~2 m thick. However, kinematic indicators were difficult to establish. Thrust faults were also observed within Eocene-aged rocks. In the east of the basin (~4 km south of Salıcak) red continental and white lacustrine rocks from the lower part of the Akpınar Formation have been thrust southwards over marl and limestone alternations of the upper part of the Akpınar Formation above a high angle reverse fault (Fig. 3.68d).

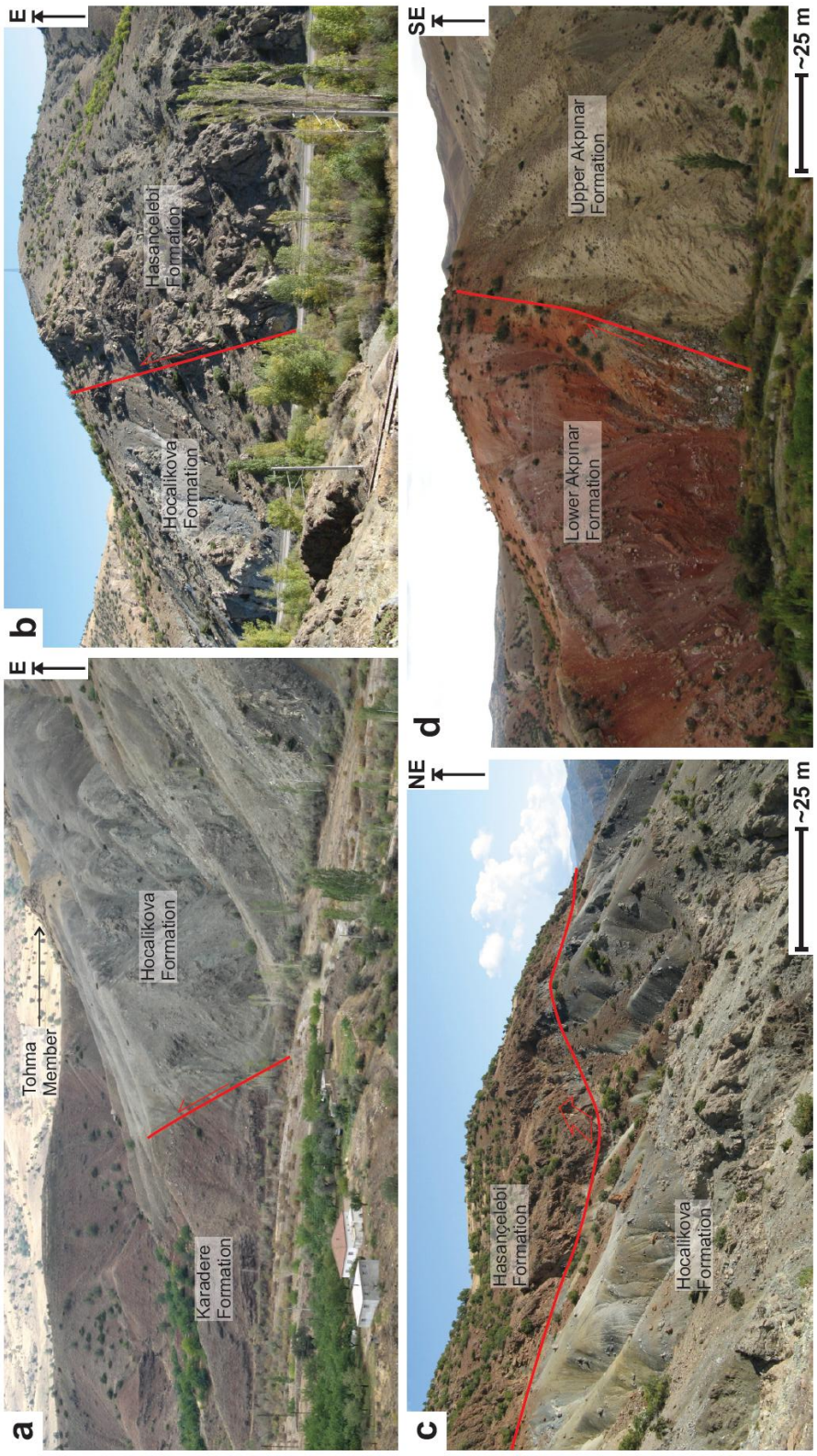

Figure 3.68. Field photographs showing: a, Ophiolitic rocks of the Hocalikova Formation thrust northwards over the Karadere Formation. Notice the in situ block of Tohma limestone. House for scale; b, Hasançelebi Formation rocks thrust northwards over rocks of the Hocalikova Formation. Pylon for scale; c, Hasançelebi Formation rocks thrust southwards over rocks of the Hocalikova Formation; d, Rocks from the lower part of the Akpınar Formation thrust southwards over rocks from the upper part of the Akpınar Formation.

Twenty four thrust faults of various dimensions were measured in the field. The dip directions of all the fault zones are plotted on a Rose diagram (Fig. 3.69a) and indicate a strong N-S orientation of dip direction. Fig. 3.69b shows the fault planes plotted as great circles and poles to planes on a stereonet and indicate an E-W orientation of the fault zones. The plots suggest a strong clustering in the N (indicating faults inclined to the south) and S-SW (indicating faults inclined to the north). This clustering is indicative of ~N-S shortening.

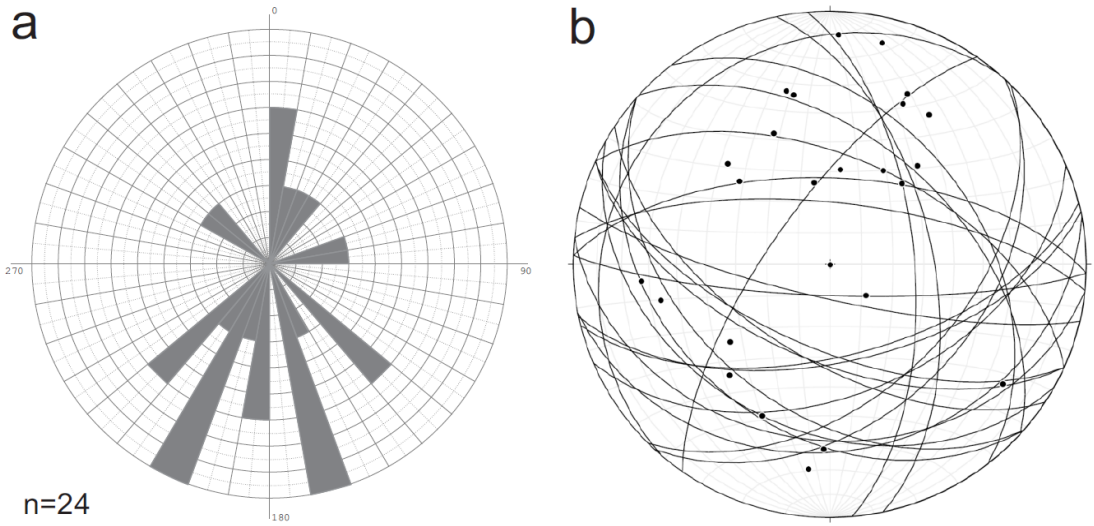

Figure 3.69. a, Rose diagram showing the dip directions of all of the thrusts in the Hekimhan Basin; b, Equal area stereonet showing great circles and poles to planes of thrust fault planes observed within the Hekimhan Basin (n=24).

Insufficient kinematic information was associated with thrust faults in the Hekimhan Basin, limiting further structural analysis.

3.5.4 Strike-slip faulting

Numerous strike-slip faults were observed in the Hekimhan Basin and are associated with neotectonic deformation. Most of the neotectonic strike-slip faults were observed in transverse vertical sections (e.g. in valleys and canyons). It was, therefore, difficult to evaluate lateral offsets. Typically, fault cores are absent (with some noted exceptions) as usually only one slip surface remains as a fault scarp. However, a series of sub-parallel, E-W trending, dextral strike-slip faults were identified by the offset of Tohma Member limestones which were cut by the fault zones (Fig. 3.70a). Strike-slip faults in the Hekimhan Basin usually have a compressional or tensional component. Approximately 2 km north of Hüyük Tepe, a strike-slip fault zone juxtaposes volcanic rocks of the Hasançelebi Formation with limestones of the Hüyük Formation along a highly transpressional fault zone (Fig. 3.70b). A christmas tree like structure has formed adjacent to the slip planes and pencil cleavage has developed in the surrounding limestones (Fig. 3.70c). The Malatya-Ovacik fault zone is an important NE-SW trending, neotectonic, sinistral strike-slip fault which cuts the field area off in the eastern part. Figure 3.70d is believed to be the Malatya-Ovacik fault zone (or a sub-parallel splay of the fault zone).

Kinematic data (e.g. slickensides) were frequently observed on exposed fault scarps (Fig 3.70e). Forty two fault planes identified as strike-slip faults were measured across the Hekimhan Basin (Fig. 3.71a-d). Of these, twenty display slickensides with kinematic orientations sufficient to delineate offset direction (i.e. sinistral vs. dextral). However, no patterns were observed when both sinistral and dextral faults were plotted together (Fig. 3.71e & f).

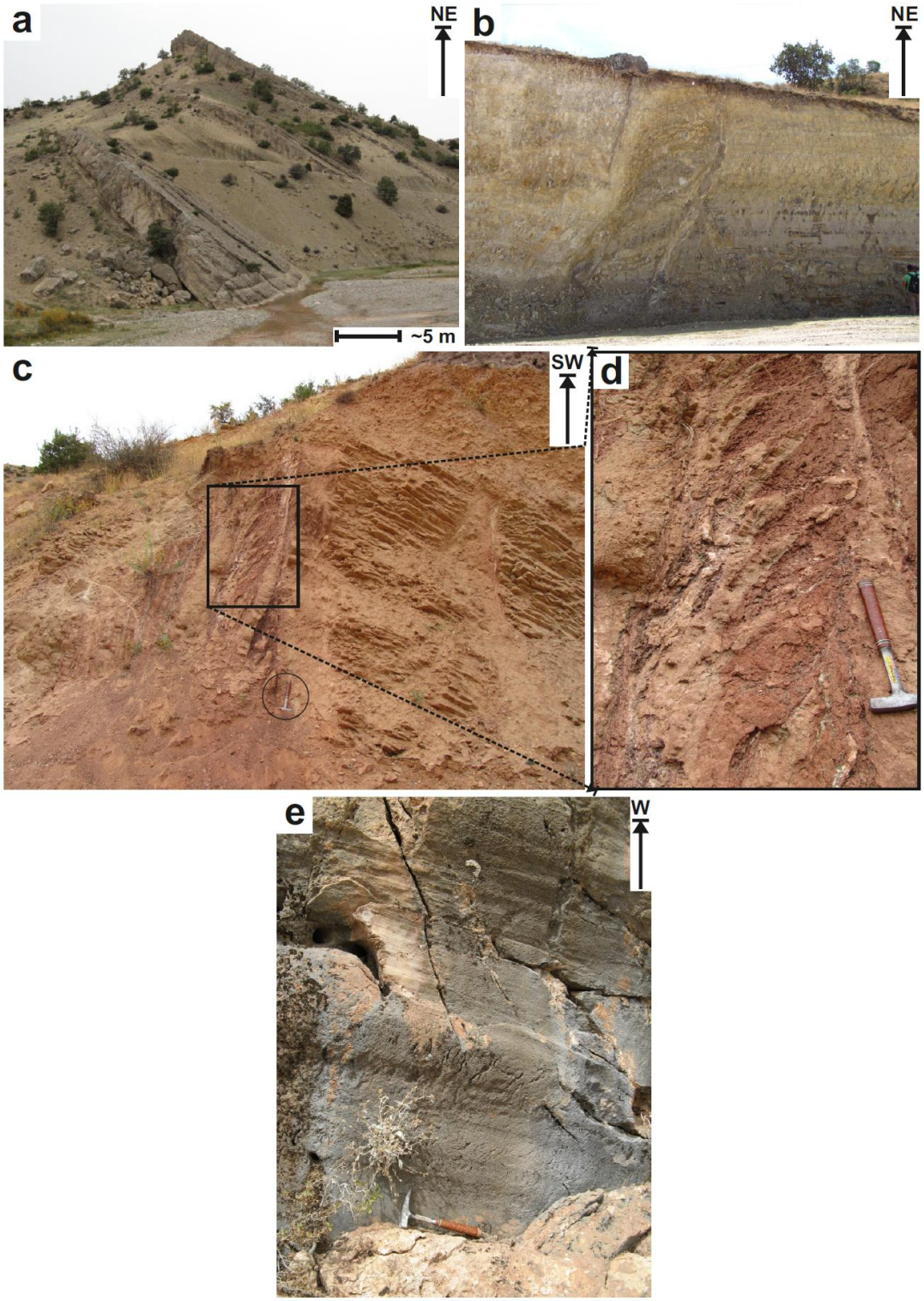

Figure 3.70. Field photographs showing: a, Tohma Member rudist patch reefs offset by high-angle, en-echelon, dextral fault zones; b, High-angle sinistral strike-slip zone, potentially the Malatya-Ovacık fault zone (person for scale, far right); c, Transpressional fault zone with christmas tree strucure in the fault core and pressure solution cleavage in the adjacent limestone; d, Close up view of the christmas tree structure; e, Well developed slickenlines on an exposed strike-slip fault scarp. Hammers for scale in c-e.

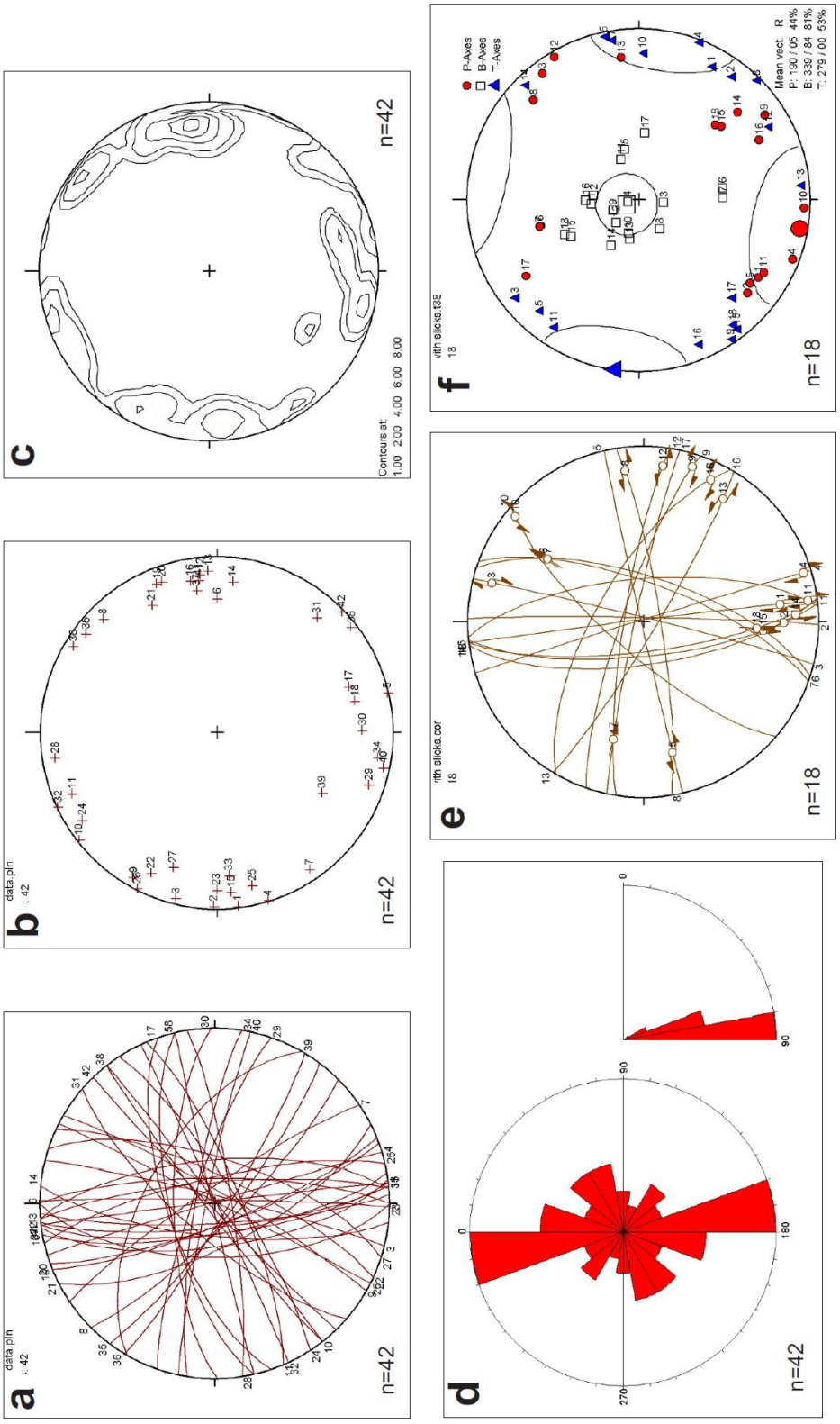

Figure 3.71. a, Stereonet showing great circles of all strike-slip faults in the Hekimhan Basin; b, Stereonet showing poles of strike-slip fault planes; c, Contour plot of b; d, Bidirectional rose diagram of all strike slip faults; e, Angelier plot showing great circles of strike-slip fault planes with associated kinematic features (slickensides), and; f, P-, B- and T-axes fault plane solutions together with mean vector and R* calculation.

Eight strike-slip faults displayed slickensides which indicate a dextral sense of movement (Fig 3.72 a & b). An Angelier plot (Fig 3.72c) for the data suggests two trends;

~N-S and another ~NW-SE. The P-axis is orientated at 165/07 (R=61%), the B-axis at 030/78 (R=91%) and the T-axis at 255/08 (R=66%) which supports an ~N-S fault zone orientation as the P and T-axes (which are ~parallel with σ1 and σ3) are orientated ~horizontally and perpendicular to each other, whereas the B-axis (~parallel with σ2) is ~vertical (Fig. 3.72d).

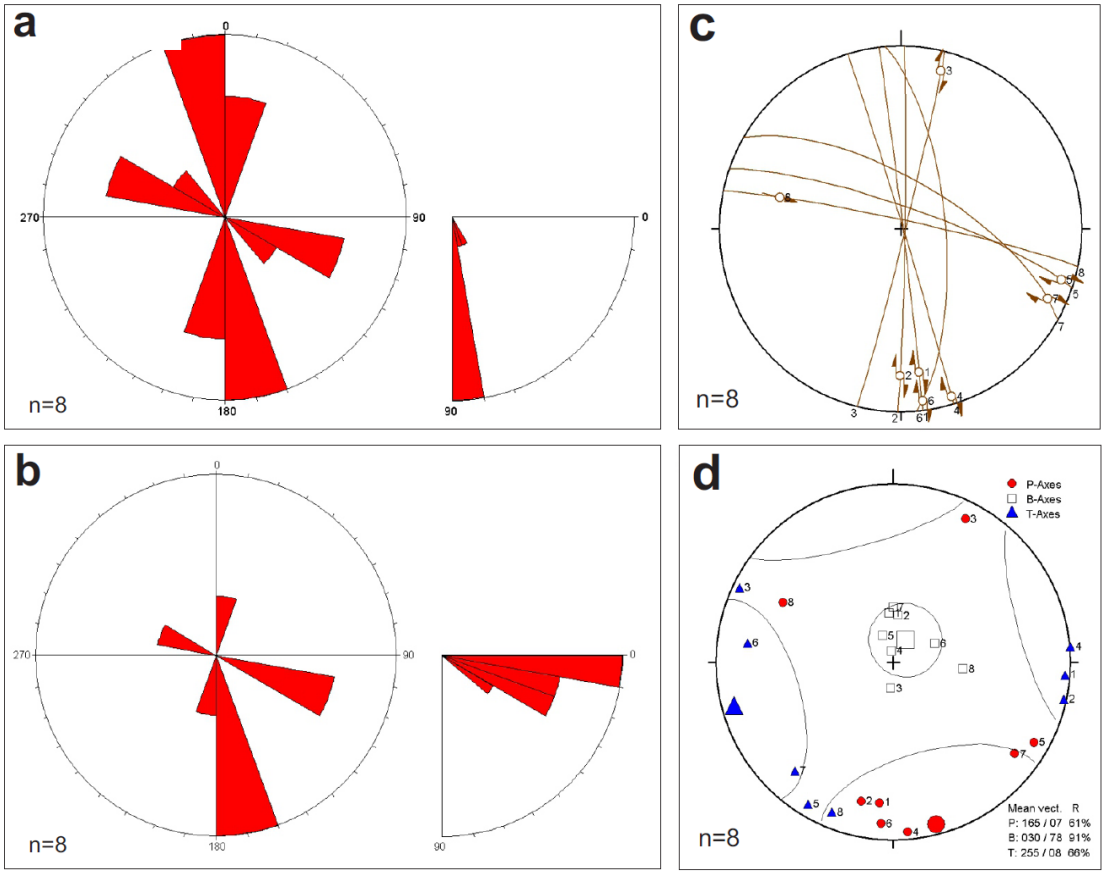

Figure 3.72. a, Bidirectional rose diagram of all dextral strike-slip faults with associated kinematic features; b, Azimuth and plunge of slickensides associated with these dextral strike-slip faults; c, Angelier plot showing great circles of dextral strike-slip fault planes together with offset direction, and; d, P-, B- and T-axes calculations together with mean vector and R*.

Ten strike-slip faults display slickensides which indicate a sinistral sense of movement (Fig 3.73 a & b). An Angelier plot is shown in Figure 3.73c which shows an approximate N-S trend for 5 of the fault zones. The P-, B- and T- axes indicate a NE-SW fault plane orientation resulting from a NW-SE trending σ1 (P-axis). The P-axis is orientated at 139/03 (R=37%), the B-axis at 282/84 (R=77%) and the T-axis at 055/02 (R=39%). However, the R values indicate an unreliable probability of a relationship trend for this data set (Fig. 3.73d).

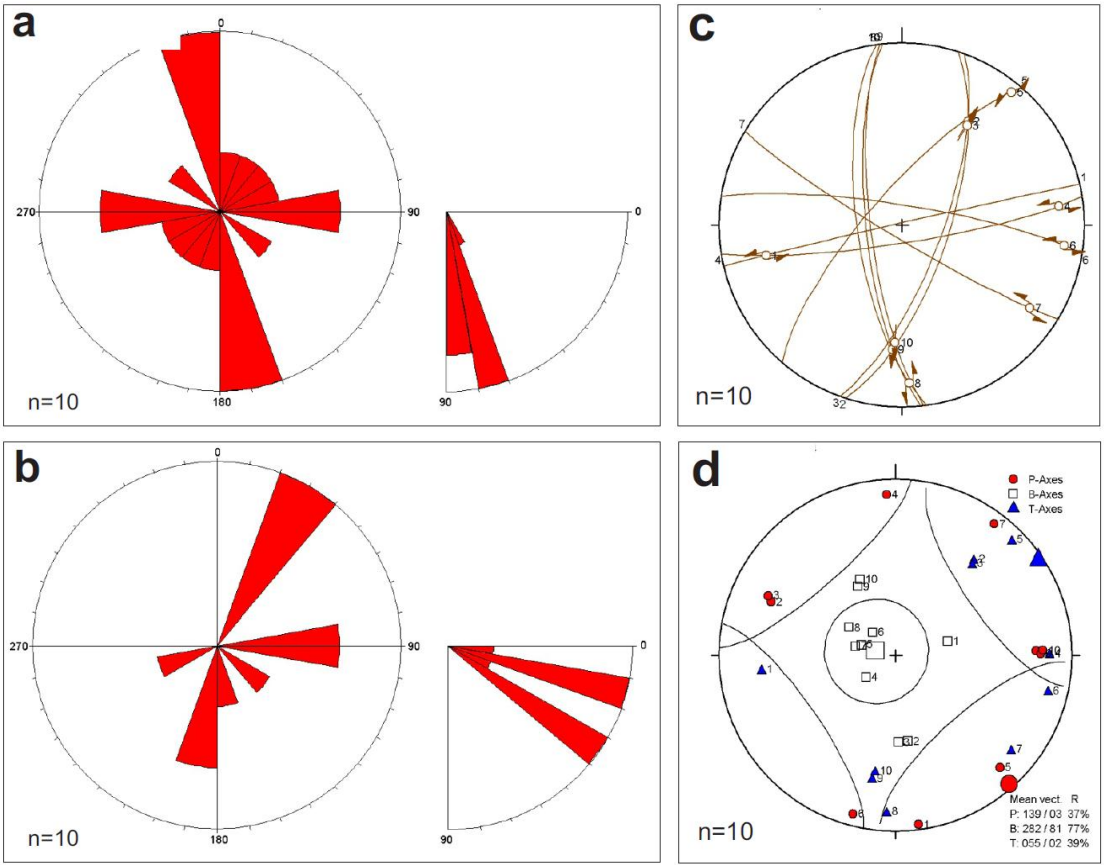

Figure 3.73. Bidirectional rose diagram of all sinistral strike-slip faults with associated kinematic features; b, Azimuth and plunge of slickensides associated with these sinistral strike-slip faults; c, Angelier plot showing great circles of sinistral strike-slip fault planes together with offset direction; b, P-, B- and T-axes calculations together with mean vector and R*.

3.5.5 Interpretation of structural data

An interpretation of the structural history of the Hekimhan Basin is complicated by the number of deformation phases which have affected it. Evidence for extension, compression and strike-slip deformation has been presented.

Normal faulting was observed in the Maastrichtian aged rocks, especially the Karadere Formation. Although only a relatively small data set of 18 fault zones were measured, the majority of these indicate an E-W orientation, resulting from N-S directed extension. Compelling evidence for extension was observed in the sedimentary and volcanic rocks within the Hekimhan Basin. Wedge-shaped conglomerate and sandstone packages within the Karadere Formation indicate syn-sedimentary extensional deformation. Numerous slump folds were observed within marls and interbedded calcarenite deposits in the Hekimhan Formation. They were observed to the south of the Hasançelebi Formation outcrop (southern part of the basin) and are all directed ~northwards indicating that the basin depocentre was located to the north of this point. Furthermore, sapropelic marls within the Hekimhan Formation (deposited synchronously with the Hasançelebi Formation) are present in the centre of the basin (around the town of Hekimhan) and are absent in the south of the basin. The sapropelic marls are assumed to have been deposited in deeper water than hemi-pelagic marl indicating that deeper parts of the basin are situated towards the north of Hekimhan. Few extensional faults were observed within the Hasançelebi Formation. However, the volcanism has been shown to have a within-plate affinity (Chapter 3.4.2.8) and is, therefore, likely to have been erupted in an extensional setting. It, therefore, seems reasonable to conclude that the Hasançelebi Formation erupted in the deepest part of the basin (the basin depocentre). The basin depocentre is commonly associated with the highest degree of extension. The presence of syn-sedimentary deformation and internal unconformities within the Hekimhan Formation also indicates an evolving tectonic environment. Figure 3.65 shows deformed hemi-pelagic strata in the Hekimhan Formation overlain by undeformed beds of the uppermost part of the Hekimhan Formation and then shallow-marine limestones of the Hüyük Formation. The change from deformed to undisturbed beds likely represents the cessation, or pausing, of extension in the Maastrichtian. The cessation, or pausing, of tectonic extension coincides with a facies change from hemi-pelagic marl to shallow-

marine limestone deposition which may indicate the reduction of accommodation space promoting the deposition of shallow-marine facies. An apparent lack of extensional faults within the Hasançelebi Formation was attributed to the exploitation of extensional features by dykes.

Extensional faults were observed in the Eocene-aged Akpınar Formatıon. However, the majority of the Akpınar Formatıon is represented by undeformed, bedded and laminated marl alternations punctuated by thin calcarenites and bookended by packages of shallow-marine nummulitic limestones. Localised, within-plate basalts (Kocaözü Member) were erupted synchronously with marls of the Akpınar Formatıon and indicate an extensional setting during the Eocene.

Compressional features, mainly faults, were observed in Cretaceous-Oligocene-aged rocks within the Hekimhan Basin. Folding was limited throughout the Hekimhan Basin. Figure 3.67a & b show isolated folds which could be attributed to dyke emplacement and slupming respectively. Figure 3.67c shows folding within Eocene-aged marls related to reverse faults. Not enough fold structures were observed in the field to make a reliable contribution to the structural evolution of the Hekimhan Basin. Localised tilting (up to ~40^{o}) of the stratigraphy has occured in parts of the basin but is attributed to block faulting rather than large-scale folding. Faults range from a few centimetres to hundreds of metres in length. Limited kinematic indicators were associated with the thrusts faults, meaing detailed structural analysis is limited. Many of the major thrusts were directly associated with the ophiolitic mélange (Hocalikova Formation). Some of the strain caused by compression of the Hekimhan Basin may have been taken up by movement along, and deformation of, the ophiolitic mélange which acted as a décollement surface. Slip along distinct décollement surfaces, causing block faulting, may help to explain the general lack of folding in the Hekimhan Basin. The majority of the kinematic information was derived from piercing points as few structural kinematic indicators (i.e. slickensides) were observed on the thrust faults. Most of the compressional faults are orientated ~E-W (Fig. 3.69) indicating a N-S direction of shortening which fits well with other basins in the region. The Darende Basin underwent N-S shortening during the Eocene (Chapter 2.5.3). Furthermore, deformation of the Tauride carbonate platform has been dated as Eocene in the Gürün area (Robertson *et al.* in press) to the west of the

field area and it is likely that the folding and thrusting seen in the Hekimhan Basin is of similar age.

Compressional faults were observed in Maastrichtian–Oligocene aged strata but not within Miocene-aged strata indicating that compressional deformation had ceased prior to the deposition of the Miocene-aged Boyralı Formation

Strike-slip faulting affected all of the formations in the Hekimhan Basin. However, unlike the Darende Basin, no discernable deformation patterns could be established from fault analysis. This may be due, in part, to the small dataset of faults associated with kinematic indicators. Another possibility is that the strike-slip faults in the Hekimhan Basin have reactivated previously extensional or compressional fault zones, especially those which are associated with the structurally weak ophiolitic mélange components. In this respect, neotectonic fault orientation is not totally constrained by the strike-slip stress regime.

In summary, from analysis of all available structural information from the Hekimhan Basin and comparison with the Darende Basin and other regional counterparts; the Hekimhan Basin evolved under 4 structurally controlled regimes: 1) Extension during the Late Cretaceous; 2) Further extension during the Eocene; 3) Mid-Late Eocene to Oligocene compression, and; 4) Neotectonic strike-slip deformation.

3.6 BASIN DEVELOPMENT

The stratigraphically lowest unit, and most poorly represented in the Hekimhan Basin, the Jurassic-Cretaceous carbonate platform (Geniz Formation), is interpreted as part of the regional Tauride carbonate platform. This developed after Triassic rifting during a phase of passive margin subsidence of the Tauride-Anatolide microcontinent bordering Neotethys (Demirtaşlı *et al.* l984; Perincek & Kozlu l984; Özgül l996 Taslı *et al.* 2006; Robertson *et al.* in press).

The overlying ophiolite-related mélange (Hocalikova Formation) was formed by a combination of tectonic and sedimentary processes. The tectonic mélange is formed of large blocks (typically hundreds of metres in scale), termed olistoliths, which were sheared and faulted into place. The blocks are commonly composed of ultramafic mantle or lower crustal lithologies, including, harzburgite, dunite and wherlite which are typically serpentinised as well as gabbro and plagiogranite. However, the contacts of the tectonic mélange are commonly deformed by high-angle, neotectonic faults. The sedimentary mélange consists of conglomerates formed from smaller olistoliths (tens of metres in scale) and clasts of the aforementioned ophiolite-related lithologies, together with intermediate and basic igneous lithologies (commonly dolerite and basalt), typically set in a sheared serpentinised muddy-sandy matrix. The conglomerates were emplaced as massive debris flows on to the Tauride carbonate platform.

Elsewhere in the region similar sedimentary mélange was emplaced onto the northern margin of the Tauride platform in the Gürün area, west of the Hekimhan Basin during Campanian-Maastrichtian time (Perinçek & Kozlu, l984; Robertson *et al.* in press). The lithologies were accreted above a northward-dipping subduction zone within Neotethys and then emplaced southwards onto the Tauride carbonate platform during latest Cretaceous time (Robertson *et al.* in press). The ophiolitic rocks themselves are likely to have formed in a supra-subduction zone setting, probably the Inner Tauride ocean (Görür *et al.* 1984), as inferred for other ophiolites overlying the Tauride-Anatolide microcontinent (Robertson, 2002, 2006; Parlak *et al.* 2000, 2004, 2009).

3.6.1 Latest Cretaceous

The first sediments to be deposited in the Hekimhan Basin were reddish-brown, non-marine sandstones and pebbly sandstones (Karadere Formation). The ophiolitic mélange (Hocalikova Formation) formed a widespread source for the sedimentary material. The sediments were deposited in a braided fluvial system as indicated by the erosive, channelised and cross-bedded nature of many of the beds, coupled with clast imbrication and the ubiquitous clast rounding. Local changes in sediment thickness mainly reflect deposition over a variable palaeotopography including 'highs' and 'lows' as well as localised syn-sedimentary faulting interpreted from wedge-shaped beds. Palaeocurrents measured from the south of the basin are directed ~northwards and westwards, probably influenced by the relict palaeotopography resulting from subaerial erosion of the emplaced ophiolitic mélange.

The subsequent marine transgression during the Maastrichtian was characterised by the development of rudist-rich patch reefs (Tohma Member) on elongate topographic highs. The rudist reefs nucleated on both the Hocalikova and Karadere Formations and then grew on top of each other to form elongate mounds which probably acted as marginal, fringing reef systems. Rudist bivalves as a whole flourished in tropical waters, before becoming extinct at the Cretaceous-Tertiary boundary (Steuber & Loser 2000).

The continuing marine transgression resulted in the deposition of hemi-pelagic marls (Hekimhan Formation) in most parts of the basin. Towards the centre of the basin the marls are black, and contain large, partially pyritised bivalves. They are interpreted as sapropelic horizons which likely formed in isolated, palaeotopographic depressions. The sapropels are common in central and northern exposures which are believed to be the deepest part of the basin (i.e. around the town of Hasançelebi). Black, pebbly conglomerates composed of material shed from the ophiolite mélange ponded in these depressions. Debris flows consisting almost entirely of rudist bivalve fragments were observed within the hemi-pelagic marls. Together, these debris flows may indicate that the marine sedimentation in the Hekimhan Basin was influenced by active tectonics. Further evidence of tectonics is indicated by the large degree of syn-sedimentary deformation within the Maastrichtian marls and the interbedded calcarenite deposits. Most of the slump axial folds were measured in the south of the basin and these indicate a

northward direction of movement, implying that the basin deepened towards the north (at least locally). As well as the sedimentary evidence for active tectonics, volcanism, with a geochemical within-plate affinity, is interpreted to have been emplaced in an extensional setting. The evidence as a whole indicates that the basin is likely to have evolved in an extensional setting during the Maastrichtian.

The timing of emplacement of the Hasançelebi Formation is well constrained as Maastrichtian from palaeontological analysis of marls interleaved with lava flows. The marls are thought to be time and facies equivalents of the Hekimhan Formation implying that the Hekimhan and Hasançelebi Formations deposited synchronously.

It was not possible to establish a genetic link between the alkaline, within-plate type volcanism (Hasançelebi Formation) and the alkaline syenite pluton (Yüceşafak Member) during this study. The Yüceşafak Member has been the subject of three limited investigations. Yilmaz *et al.* (1993) and Ozgenc & Ilbeyli (2009) report an unsubstantiated Paleocene-age for the Yüceşafak Member (described as syenite-mozonite), which they termed the Hasançelebi pluton. These authors classified the Yüceşafak Member as an alkaline oversaturated subtype of the cafemic association (i.e. mantle derived source) with a felsic I-type character which indicates a within-plate affinity. Kuşcu *et al.* (2011) conducted $^{40}Ar/^{39}Ar$ and U-Pb geochronology on hydrothermally altered intrusions in the Hasançelebi area and identified four separate phases of alteration ranging from ~74-68 Ma. The second phase of alteration formed at about 71.3 Ma and is spatially and temporally associated with syenite porphyry and microsyenite porphyry intrusions. These ages imply that the Yüceşafak Member was intruded prior to the latest Campanian. However, a single $^{40}Ar/^{39}Ar$ age determination by Leo *et al.* (1973) yielded an age of 65.2±1.6 Ma. This latter fits with field observations made during the course of this study whereby isolated syenitic dykes were observed cutting volcanic rocks of the Hasançelebi Formation. As mentioned above, the Hasançelebi Formation is believed to have erupted during the Maastrichtian. The Yüceşafak Member must, therefore, be younger in order to crosscut the volcanic rocks of the Hasançelebi Formation.

Figure 3.65 shows marls and interbedded calcarenites deformed under a syn-sedimentary extensional-regime overlain by ~10 m of undeformed rock of the same

lithology, and in turn followed by an abrupt contact with shallow-marine limestones of the Hüyük Formation. This boundary is interpreted as a hiatus or cessation in extension. A reduction in extension within the basin would have resulted in a net reduction of accommodation space, promoting the deposition of shallow-marine facies. Alternatively, the cessation of extension coincided with a global eustatic regression (with or without an accommodation space control) which culminated in the emergence of the Hekimhan Basin in the latest Maastrichtian and resulted in the formation of localised karstified surfaces.

3.6.2 Paleocene

Localised evaporites of variable thickness were observed in the Hekimhan Basin. It was not possible to establish an absolute age of deposition from field observations and the unit could not be dated during this study. Yalcın & Bozkaya (1996) reported the discovery of the Cretaceous/Tertiary boundary within marine evaporitic facies in the Hekimhan Basin, although the evidence for this is unclear. On the other hand, Palmer *et al.* (2004) report a Paleocene-age for the evaporitic facies based on the comparison of $\delta^{34}S$–$\delta^{18}O_{sulphate}$ with historical samples. However, the history of seawater $\delta^{18}O_{sulphate}$ values is less well defined than for S and Sr, hence these results may not be reliable. A limestone karst surface requires subaerial exposure and an amount of time to form, suggesting that an unconformity is likely to exist between the top of the Hüyük Formation and the evaporite deposits, although this could not be seen in the field. The geochemistry of the evaporites points towards a marine origin (Palmer *et al.* 2004). Therefore, the evaporites cannot be explained by evaporation of restricted lacustrine lakes. A substantial eustatic sea level rise is reported during the Late Paleocene (Miller *et al.* 2005). A minor marine transgression in the Hekimhan Basin could have ponded water in isolated palaeogeographic depressions promoting evaporite formation. A late Paleocene–Early Eocene age rather than Late Cretaceous or Early–Mid Paleocene age of the evaporites is therefore preferred.

A basin-wide, shallow-angle ($<5^{o}$) unconformity followed during the remainder of the Paleocene in some parts of the basin. However, this contact was rarely observed in the field. In other areas, red continental mudstone, sandstone and conglomerates alternate with white lacustrine limestones. The implied hiatus or the deposition of isolated marine

evaporites or variable continental facies contrasts with other basins in central Anatolia that include Paleocene sediments, namely the Ulukışla, Kırıkkale, Tuz Gölü, Çankırı and Sivas basins where relatively deep-marine mudstone and turbidite intercalations were deposited (Nairn *et al.* in press). The variable associations seen the Hekimhan Basin may be a result of sedimentary infill of the shallow-marine Late Maastrichtian basin, coupled with eustatic regression (Miller *et al.* 2005). However, tectonics may also have played a role.

3.6.3 Eocene

The variable Paleocene deposits of the Hekimhan Basin abruptly pass into sandy Nummulites-rich limestones recording a relatively rapid, basin-wide marine transgression (Akpınar Formation). The middle part of the Akpınar Formation is represented by hemi-pelagic marl indicating the continued deepening of the Eocene-aged basin. Localised pillow lavas (Kocaözü Member) with a geochemical within-plate affinity erupted onto the marls on the sea floor probably in an extensional environment. Localised andesitic-dacitic volcanism (Leylek Member) occurred in the western parts of the Hekimhan Basin within the upper part of the Akpınar Formation. In the central and eastern parts of the basin, the upper part of the Akpınar Formation is represented by thin sequences (<50 m) of shallow-marine Nummulites-rich limestone. In the south of the basin the sequences are much thicker (up to 200 m). Both instances record a change from hemi-pelagic to shallow-marine deposition during Middle-Late Eocene time. Localised evaporites inter-bedded with shallow-marine limestones, rich in organic matter (e.g. leaves), record fluctuating salinity in a restricted basin. The basin became emergent towards the end of the Eocene probably as a result of sediment infill, eustatic sea level fall (Miller *et al.* 1995), or regional uplift.

3.6.4 Post-Eocene

Post-Eocene deposition is reflected by extensive, Oligocene-aged, red continental fluvial sandstone and conglomerate accumulations (Kamatlar Formation) which source all the underlying formations of the Hekimhan Basin. These are overlain by Middle Miocene, thin (<50 m total), shallow-marine facies including bioclastic limestones with Gilbert-

type foresets (Boyralı Formation) which prograde generally south-westwards. The shallow-marine facies record a minor marine transgression which indicates that uplift must have been postponed until after the Middle Miocene. The basin is capped by thick sequences (up to 1000 m) of basic volcanics interpreted as subaerial lava flows and associated volcaniclastic sediments (Yamadağ Formation). The lavas are interpreted as post collisional. The transgressive sediments and subaerial volcanism are unaffected by extension and compression but are affected by neotectonic strike-slip faults.

Chapter 4: Discussion

Chapter 4. Comparison and discussion

4.1 INTRODUCTION

Turkey provides an exceptional natural laboratory in which to study all aspects of the geotectonic history of an ancient continental collision zone as noted in the thesis introduction. It is widely accepted that Turkey formed from the amalgamation of several discrete microcontinents associated with the subduction and suturing of oceanic lithosphere which lead to the formation of subduction-accretion complexes, emplaced ophiolites, magmatic and volcanic arcs and multiple tectono-sedimentary basins.

The Late Mesozoic-Early Cenozoic geohistory of the Eastern Mediterranean can be summarised as follows: After Palaeotethys reached its maximum extent during the Triassic and began subducting northwards (beneath Laurasia), new oceanic crust (the Neotethys) was formed by rifting of a passive northern margin of the Gondwana supercontinent to the south (Robertson & Dixon 1984; Şengör *et al.* 1984; Stampfli 2000; Stampfli & Borel 2002; Chan *et al.* 2008; Mackintosh & Robertson 2009). The Neotethys oceanic lithosphere then began to subduct northwards under the Eurasian (Pontide) active margin during the Late Mesozoic-Early Cenozoic (Şengör & Yilmaz 1981; Rice *et al.* 2006; Ustaömer & Robertson 1997; 2010). A second northward directed intra-oceanic subduction zone may have developed to the south of the Niğde-Kırşehir Massif (Görür *et al.* 1984). Supra-subduction zone-type ophiolites generated above these subduction zones were emplaced during the Late Cretaceous prior to collision and suturing of the oceanic basins (Robertson *et al.* 2009). However, elements of the ocean remained open until the Middle Eocene after which regional suture tightening tectonics took place (Jaffey & Robertson 2001; Göğuş & Pysklywec 2008).

Sedimentary basins that developed during regional plate convergence provide a record of the timing, evolution and processes active during these incipient stages of collision. The Central Anatolian sedimentary basins in Turkey are especially important as they help to elucidate a regionally complex geohistory. For example, the Kırıkkale and the Tuz Gölü Basins to the NW and W of the Niğde-Kırşehir Massif were developed on a variable assemblage of accretionary and ophiolitic material emplaced onto elements of the northern margin of the Niğde-Kırşehir Massif (Nairn *et al.* in press). In contrast, in the

south and east, the Late Cretaceous-Late Eocene Ulukışla Basin (Clark & Robertson 2002) and the Sivas Basin (Kavak *et al.* 1997; Yılmaz & Yılmaz 2006) developed after ophiolites were emplaced onto the northern margin of the Tauride microcontinent (Fig. 4.1).

The Darende and Hekimhan Basins in Central Eastern Turkey (Fig. 4.1) are envisaged to have developed after Neotethyan supra-subduction zone-type ophiolites were emplaced southwards onto the northern margin of the Tauride microcontinent during the latest Cretaceous (Parlak *et al.* in press) and then evolved in two separate stages. The first, during the Late Cretaceous, was related to the closure of an Inner Tauride Ocean. The second, during the Eocene, was involved with the collision of the Tauride microcontinent with Eurasia to the north. Previous work on these basins (e.g. Akkuş 1971; Gürer 1994; Gürüz & Gül 2005) has been restricted to localised sedimentary and stratigraphic analysis or, in the case of the Hekimhan Basin, mineral exploration. The Darende and Hekimhan Basins were selected for this study because they provide a unique opportunity to investigate the processes related to the collision and suturing of microcontinents in the Eastern Mediterranean and remain remarkably well preserved and exposed. They may also help to elucidate the eastwards extent of the Niğde-Kırşehir Massif.

A complete description, analysis and interpretation for each of the Darende and Hekimhan Basins, based on new sedimentary, stratigraphic, structural, geochemical and palaeontological data, has been provided in Chapters 2 and 3. The purpose of this chapter is first to compare and contrast aspects of the development of the Darende and Hekimhan Basins directly, and with other Central Anatolian sedimentary basins and, secondly, to compare existing tectonic evolution models and, where appropriate, present a new tectonic model based on the evidence gathered during this study.

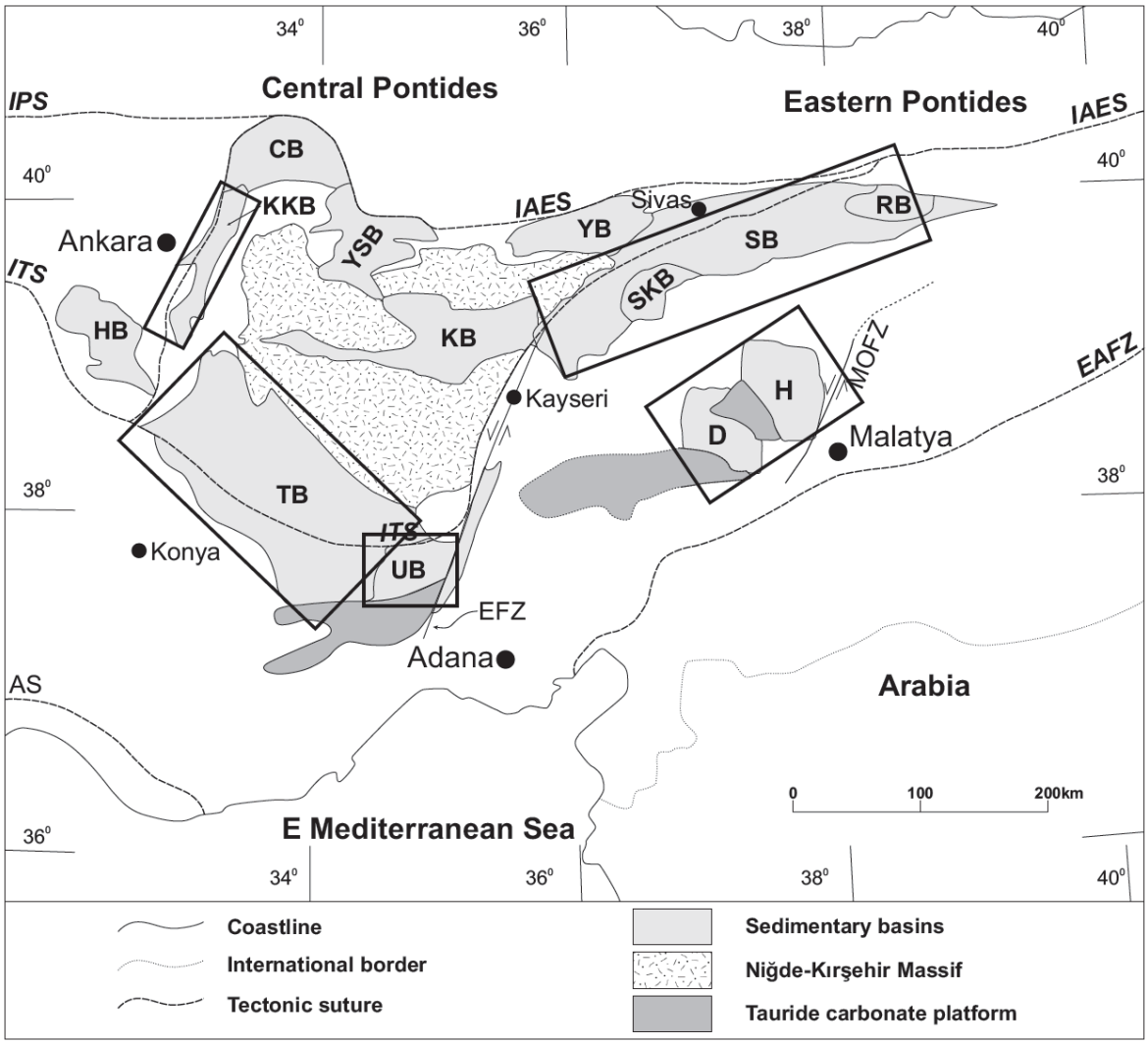

Figure 4.1. Regional outline map of Central Eastern Anatolia showing the extent of the Niğde-Kırşehir Massif and some key sedimentary-tectonic basins surrounding it denoted by the black rectangles (KKB, Kırıkkale Basin; TB, Tuzgölü Basin; UB, Ulukışla Basin; SB, Sivas Basin; D, Darende Basin; H, Hekimhan Basin), as well as the major suture zones and fault zones (IPS, Intra Pontide Suture; ITS, Inner Tauride Suture; AS, Antalya Suture; IAES, İzmir-Ankara-Erzincan Suture; EAFZ, East Anatolian Fault Zone; MOFZ, Malatya-Ovacık Fault Zone; EFZ, Ecemiş Fault Zone). Other sedimentary basins are also highlighted (HB, Haymana Basin; CB, Çankırı Basin; YSB, Yozgat-Sorgun Basin; KB, Kızılırmak Basin; YB, Yıldızeli Basin; SKB, Şarkışla Basin; RB, Refahiye Basin). Modified from Görür *et al.* (1998). See text for explanation.

4.2 COMPARISON OF THE DARENDE AND HEKIMHAN BASINS

Complete descriptions, analyses and interpretations of the Darende and Hekimhan Basins are provided in Chapters 2 and 3, respectively. Here, the stratigraphy and structure of the basins are compared and contrasted in geochronological order (Fig. 4.2) in terms of a unified evolutionary model.

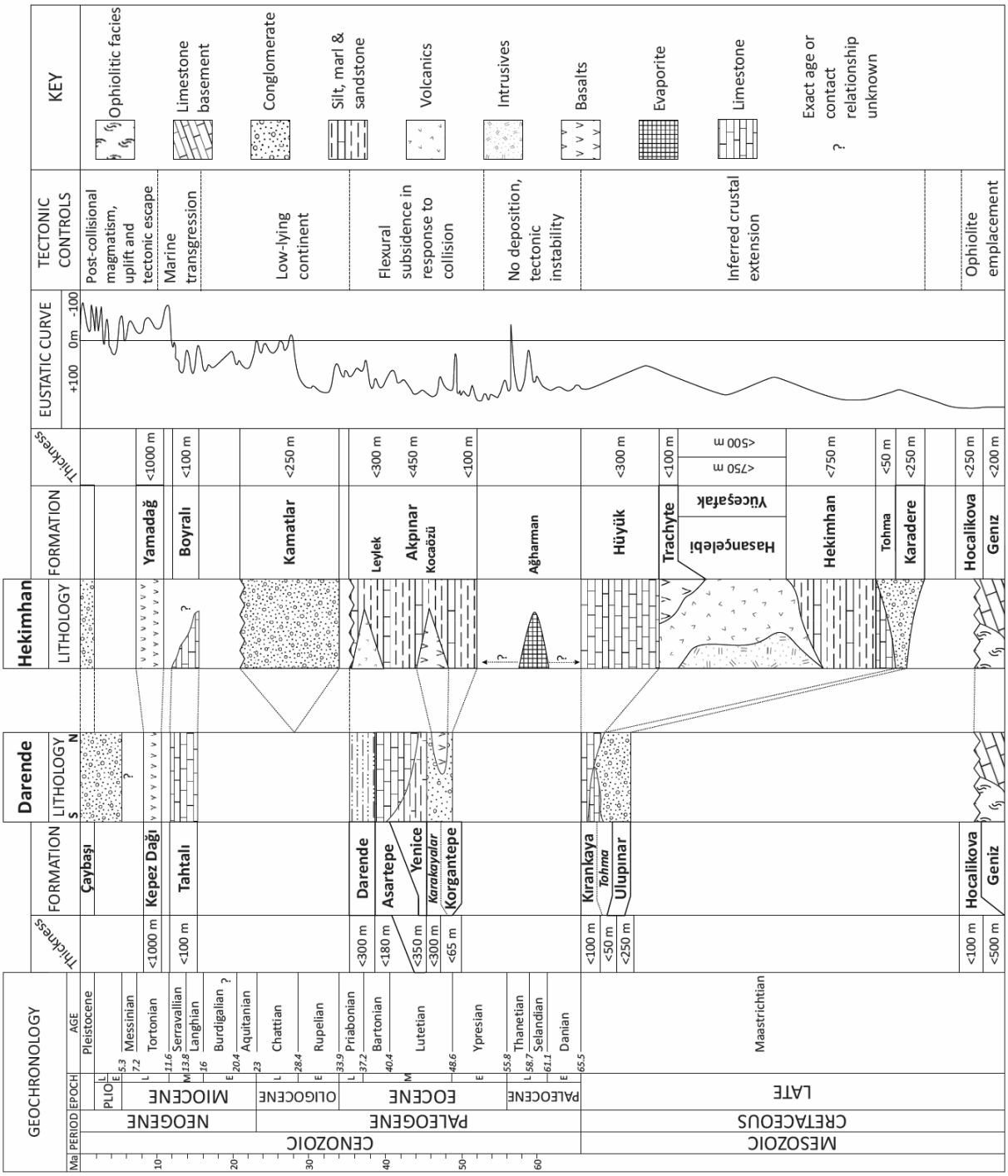

Figure 4.2. Revised stratigraphic successions for the Darende and Hekimhan Basins. The revisions take account of improved knowledge of the Mesozoic carbonate platform and emplaced ophiolite-related mélange (Robertson *et al.* in press), the dating of microfossils during this work and also of recent radiometric dating of Miocene volcanic rocks (Gürsoy *et al.* 2011). A global eustatic sea level curve (Miller *et al.* 2005) is included on the right to aid discussion. The main inferred controls of deposition are also summarised. Note: The Maastrichtian is not drawn to the same scale as the Cenozoic.

4.2.1 Maastrichtian

The Darende and Hekimhan Basins are both constructed on elements of the Jurassic-Cretaceous Tauride carbonate platform (Geniz Formation). In the Darende Basin several hundred metres of carbonate platform material is extensively exposed in the NE and SW of the basin, whereas only small elements are exposed in the SW of the Hekimhan Basin. Regionally the platform is several hundred to several thousand metres thick, for example the Gürun Basin, situated to the north of the Darende Basin. There, the platform rocks have been thrust southwards to form structurally allochthonous units probably during the Late Cretaceous (Robertson *et al.* in press). Several slivers of ophiolite-related mélange were exposed along low angle fault zones within the platform rocks in the Darende and Hekimhan Basins. It is, therefore, inferred that the carbonate platform 'basement' rocks of the Darende and Hekimhan Basins formed similar allochthonous thrust units.

Ophiolites were emplaced in both the Darende and Hekimhan Basins during the Upper Cretaceous (Hocalikova Formation). Exposures of ophiolite in the Darende Basin are limited to the basin margins and are commonly structurally exposed. The ophiolite-related mélange outcrops in the Darende Basin probably formed in an oceanic foredeep by mixing of oceanic sediment with terrigenous material shed from parts of the over-riding ophiolite. These were then emplaced primarily as sedimentary debris flows that were tectonised to form the sheared sedimentary mélange. Ophiolite-related rocks are more widely exposed in the Hekimhan Basin. Ophiolite-related blocks several hundred metres across commonly composed of serpentinised harzburgite and dunite were exposed and juxtaposed with other ophiolite-related lithologies via high-angle fault zones. The ophiolite-related lithologies formed an important source material for the overlying basin sediments.

Sedimentation in both basins began during the Maastrichtian with the deposition of non-marine, red clastics termed the Ulupınar Formation in the Darende Basin and the Karadere Formation in the Hekimhan Basin. The formations are of similar thickness in both basins. They are also stratigraphically similar, being formed of alternations of cross-bedded sandstones and pebbly, often imbricated sandstones, interpreted as braided river deposits, together with beds of red mudstone, interpreted as overbank deposits. Compositionally, both formations are texturally immature, with poorly sorted and sub-

angular to sub-rounded clasts. However, a greater percentage of the clasts from the Ulupınar Formation (Darende Basin) were derived from the Mesozoic platform carbonates (Geniz Formation) compared to the Karadere Formation (Hekimhan Basin) which has a higher percentage of ophiolite-related lithologies (e.g. serpentinised ultramafics, gabbro and basalt). This could reflect the variable catchment areas available as a source for these formations (i.e. more carbonate platform exposed in the Darende Basin resulting in a greater proportion of carbonate clasts). This difference is also reflected in the colour of the formations. From a distance the Ulupınar Formation is pinky-red whereas the Karadere Formation is dark red-brown. Considerable lateral thickness variations are apparent in both of the formations which reflects deposition onto a palaeotopographically complex terrain left over after rapid uplift and erosion of the carbonate platform and emplaced ophiolite-related units.

The evolution of the Darende and Hekimhan Basins diverges significantly during the Maastrichtian after the deposition of the non-marine clastics. A transgression occured in both basins, indicated in some areas by the development of fringing, rudist-bearing patch reefs (Tohma Member), variably deposited on either ophiolitic material or Maastrichtian clastics. Marine sediments were deposited synchronously with patch reefs in some areas, represented by the Kırankaya Formation in the Darende Basin and the Hekimhan Formation in the Hekimhan Basin. The transgression was poorly developed and probably short lived in the south of the Darende Basin amounting to <30 m in stratigraphic thickness. Towards the north and east of the basin the Kırankaya Formation is better developed with up to 100 m of shallow-marine limestones. A genetic link to a part of the Hekimhan Basin could have existed at this time. However, it was not possible to confirm this in the field as the area between the two basins is covered by Eocene limestones. In the Hekimhan Basin, the Hekimhan Formation comprises up to 750 m of hemipelagic marl, calcarenite turbidites and isolated sapropels, that were deposited during an extensional tectonic regime. Extension is highlighted by the presence of syn-sedimentary extensional faults coupled with numerous slumped horizons and debris flow units. These facies suggest that the Hekimhan Basin was significantly deeper than the Darende Basin at this time. The eruption of the volcanics of the Hasançelebi Formation was synchronous with deposits of the marls of the Hekimhan Formation during the Maastrichtian. This is indicated by palaeontological analyses of pelagic Foraminifera within marl horizons that are interbedded with lava flows and breccia. The Hasançelebi

Formation is variably made up of pillow basalts, lava flows, lava breccias and associated volcaniclastic material. The basalt has a within-plate geochemical signature and erupted via extensional tectonics into the basin depocentre (the deepest part of the Maastrichtian-aged basin) probably under several hundred metres of water (Pickering *et al.* 1989). As indicated by the apparent ratio of planktic to benthic Foraminifera within the Hekimhan Formation. For comparison, shallow-marine limestones in the Darende Basin were probably deposited in tens of metres of water (Nichols 1999). As indicated by the algal laminated limestone beds. $^{40}Ar/^{39}Ar$ age determinations of the syenite pluton in the Hekimhan Basin (Yüceşafak Member) from biotite in altered veins and syenite pegmatite porphyry intrusions yielded ages ranging from 74–65 Ma (Leo *et al.* 1973; Marschik *et al.* 2008; Kuşcu *et al.* 2011**)**. It is likely that the Yüceşafak Member intruded the Hasançelebi Formation during the late Maastrichtian owing to the exposed intrusive field relationships. The volcanic and magmatic rocks are overlain by a sequence of undeformed hemi-pelagic marls, followed by shallow-marine limestones (the Hüyük Formation), up to 300 m thick. These sediments record a basin-wide regression which could have been induced by a cessation of active extension (suggested by the undeformed nature of the beds). Localised palaeokarstic surfaces developed on the top of the limestones indicate a period of subaerial exposure, erosion and unconformity. In the Darende Basin, the Late Maastrichtian Kırankaya Formation became evaporitic towards the top, as indicated by the presence of bird's-eye structure and autobrecciated horizons, and eventually became emergent, represented by an unconformity. Both basins are interpreted to have evolved during active extension.

A similar Maastrichtian-aged sequence of channelised non-marine clastic rocks overlain by shallow-marine bioclastic limestones has been reported from the Ulukışla Basin (Clark & Robertson 2002), to the SW of the Darende Basin. In contrast, deposition is continuous into the Paleocene, whereas both the Darende and Hekimhan Basins became emergent at the end of the Maastrichtian. No marine sedimentation is recorded in the Sivas Basin to the north of the Darende and Hekimhan Basins during the Maastrichtian (Dirik *et al.* 1999; Yılmaz & Yılmaz 2004; 2006).

4.2.2 Paleocene

The Paleocene is represented in the Darende Basin by a period of localised faulting which induced block rotations, as is especially evident in the south of the basin where a relatively high-angle (40^o) unconformity is present in some places between the Maastrichtian and Eocene facies. Localised unconformities in the Hekimhan Basin reach a maximum of 5^o of angularity. This unconformity is in marked contrast to some of the other Central Anatolian sedimentary basins, for example the Ulukışla Basin where deep-marine marls and clastic turbidites were deposited during the Paleocene (Clark & Robertson 2002).

4.2.3 Eocene

Sedimentation in the Hekimhan Basin resumed during the Early Eocene (Ypresian) with the deposition of localised evaporites (Ağharman Member) followed by localised deposition of non-marine clastic and lacustrine rocks (however, this sequence could be of late Paleocene age). This was followed by a transgression depositing Nummulites-bearing shallow-marine limestone, then hemi-pelagic marl (Akpınar Formation). Within the marl, localised within-plate-type basalts (Kocaözü Member) were erupted. The Eocene succession in the Darende Basin is very similar. The succession begins with shallow-marine to shoreface clastic deposits with localised basal breccias representing the initial flooding surface (Korgantepe Formation). These sediments were interupted by localised within-plate-type basaltic eruptions (Karakayalar Member), that are petrologically and geochemically similar to those in the Hekimhan Basin, and are then overlain by hemi-pelagic marls (Yenice Formation). Furthermore, the Middle Eocene basaltic volcanism observed in the Darende and Hekimhan Basins is geochemically similar to other, Eocene-aged volcanic deposits in Central, Northern and Eastern Turkey (Keskin et al. 2008; Clark & Robertson 2005,) as well as volcanic rocks in Northern Iran and Azerbaijan (Vincent et al. 2005). Shallow-marine, faunally diverse, Nummulitic limestones (Asartepe Formation) were followed by mixed evaporitic facies (Darende Formation) completing the Eocene sequence in the Darende Basin. A similar succession was observed in the Hekimhan Basin where Late Eocene-aged shallow-marine limestones pass into evaporitic facies (top of the Akpınar Formation). However, they are interupted by localised andesitic-dacitic-type volcanic eruptions mainly in the west of the Hekimhan Basin.

The Eocene sequence in the Darende Basin is interpreted to have evolved during active extension as evidenced by intensive syn-sedimentary deformation in the hemi-pelagic marls (Yenice Formation), as well as rare syn-sedimentary faulting. However, evidence for Eocene extension is scarce in the Hekimhan Basin.

Eocene sedimentation in the Sivas Basin began in the Lutetian (Middle Eocene) with shallow-marine clastic and limestone rocks interbedded with localised basalt and geochemically and geochronologically unnassociated andesitic volcanism. The Hekimhan Basin is capped by mixed evaporites (Yılmaz & Yılmaz 2006), which is very similar to that observed in the Darende and Hekimhan Basins. A somewhat similar sequence was observed in the Ulukışla Basin, except that the facies were predominantly deposited in a deeper-marine environment than the Darende and Hekimhan Basins (Clark & Robertson 2002; 2005).

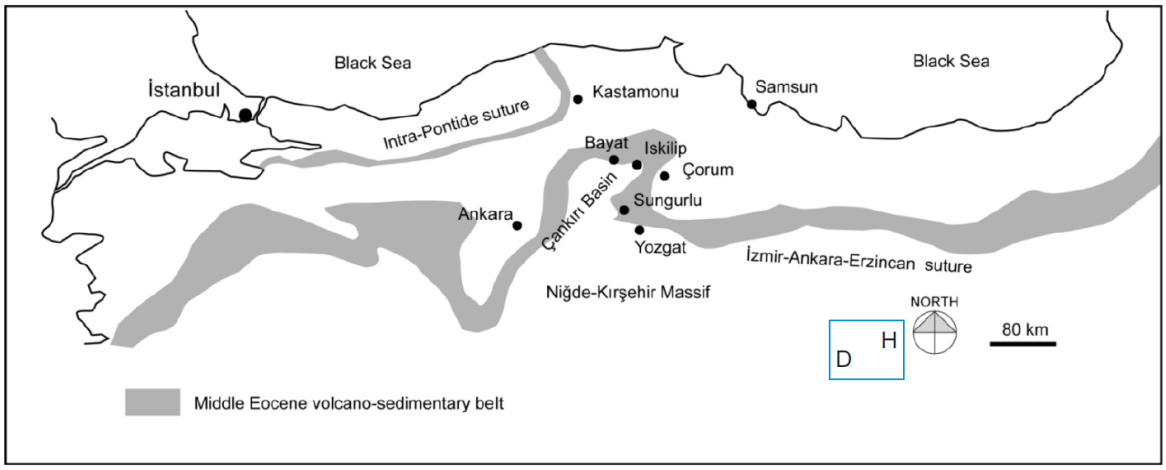

Figure 4.3. Sketch map of Turkey showing the distribution of the Middle Eocene volcano-sedimentary belt. Blue box and D and H represent the approximate location of the Darende and Hekimhan Basins. From Nairn in press (modified from Keskin *et al.* 2008).

4.2.4 Post Eocene

The Oligocene is represented in the Hekimhan Basin by non-marine, red, channelised clastic rocks (Kamatlar Formation), interpreted as braided river deposits. No equivalent facies were observed in the Darende Basin. Non-marine clastic rocks were also observed in the Sivas and Ulukışla Basins. However, deep-marine sedimentation prevailed in the Elazığ Basin (located to the east of the Darende Basin) until the Late Oligocene (Aksoy *et al.* 2005; Hüsing *et al.* 2009). The Darende and Hekimhan Basins experienced a Miocene-

aged minor marine transgression (Tahtalı and Boyralı Formations respectively), depositing bioclastic siltstones and faunally diverse limestones which are common in other sedimentary basins across Central Eastern Turkey (e.g. Harzhauser *et al.* 2002; Sancay *et al.* 2006). Thick sequences (up to 1000 m) of subaerial basalt erupted in the Darende and Hekimhan Basins (Kepez Dağı and Yamadağ Formations, respectively) during the Mid-Late Miocene. Similar basalts are widely exposed in Central and Eastern Turkey (e.g. Keskin *et al.* 1998; Ekici *et al.* 2009; Shabanian *et al.* 2012).

4.3 EXISTING REGIONAL TECTONIC MODELS

As noted in the thesis introduction, there are two 'end-member' models for the tectonic evolution of Central and Eastern Turkey. In one model, the Niğde-Kırşehir Massif represents a promontory of a single Tauride microcontinent, with a single Northern Neotethys Ocean to the north (Göncüoğlu *et al.* l996-l997). Oceanic lithosphere was consumed northwards beneath the Eurasian margin via a single subduction zone. Ophiolites were emplaced southwards for several hundred kilometres. Intra-continental sedimentary basins developed on the emplaced ophiolites (Gürer & Aldanmaz 2002). In this model, there is no distinction between the Upper Cretaceous-Upper Eocene tectono-sedimentary basins situated to the north and west of the Niğde-Kırşehir Massif (e.g. the Tuz Gölü and Kırıkkale Basins; Nairn *et al.* in press) and those to the east and south of the Niğde-Kırşehir Massif (e.g. the Sivas, Ulukışla, Darende and Hekimhan Basins).

In the second model, the Niğde-Kırşehir Massif formed a microcontinent which had previously rifted off the northern margin of Gondwana (Mackintosh & Robertson 2009) and divided the Northern Neotethys Ocean into the Inner Tauride Ocean (between the Niğde-Kırşehir Massif and the Tauride microcontinent) to the south, and the İzmir-Ankara-Erzincan Ocean (separating the Niğde-Kırşehir Massif from the Pontide [Eurasian] margin) to the north (Görür *et al.* l984; Dilek & Whitney, 2000; Clark & Robertson 2002; Robertson *et al.* 2009; Pourteau *et al.* 2010). Accretionary forearc/syn-collisional-type sedimentary basins developed in response to active northwards dipping subduction zones which generated supra-subduction zone ophiolites (Görür *et al.* 1984; Koçyiğit 1991; Görür *et al.* 1998; Robertson *et al.* 2009).

4.4 DEVELOPMENT OF THE DARENDE AND HEKIMHAN BASINS

4.4.1. Regional context

This section is an attempt to define the regional tectonic setting in which the Darende and Hekimhan Basins evolved. It is important to note that the models presented here rely on the existence of the Inner Tauride Ocean. The following evidence supports the existence of the Inner-Tauride Ocean:

- The northern part of the Tauride microcontinent (the Anatolide part) located between the unmetamorphosed Mesozoic Tauride platform to the south and the Niğde-Kırşehir Massif to the north has undergone HP/LT metamorphism (Candan *et al.* 2005; Robertson *et al*. 2009; Pourteau *et al*. 2010). The HP/LT rocks have been shown to extend into the Eastern Taurides, as far as the Kayseri area (Oberhansli *et al.* 2010). The HP/LT metamorphism is inferred to relate to subduction of the northern margin of the Tauride microcontinent during the latest Cretaceous (Dilek & Whitney 2000; Okay et al. 2001; Robertson *et al*. 2010; Pourteau *et al.* 2010). In contrast, the Niğde-Kırşehir Massif shows no evidence of comparable HP/LT metamorphism (Whitney & Dilek, 1998; Whitney *et al*. 2001). The Niğde-Kırşehir Massif experienced maximum metamorphic conditions of 5-6 kbar and >700^{o}C (Amphibolite facies; Whitney & Dilek 1998). This contrasting, but juxtaposed, metamorphic grade suggests a contrasting tectonic setting; e.g. a separate microcontinent.

- The timing of high-grade metamorphism in the Niğde-Kırşehir Massif is documented as Late Cretaceous (84.1 ± 0.8 Ma). This age is at least 50 Ma older than Alpine amphibolite facies metamorphism in the Menderes Massif in western Turkey. A model reconstructing the Niğde-Kırşehir Massif as a promontory of the Tauride microcontinent cannot explain such a large time difference within a small region (Whitney & Hamilton 2004; Pourteau *et al.* 2010).

- Ophiolite-related rocks have been located as far south as near Mersin (Parlak & Robertson 2004). If the Niğde-Kırşehir Massif represented a promontory of the

Tauride microcontinent then ophiolites must have been generated above a single subduction zone situated to the north. Therefore, the ophiolites at Mersin, for example, are required to have been transported in excess of 500 km across the Niğde-Kırşehir Massif, which seems unfeasible (Andrew & Robertson 2002).

- The Niğde-Kırşehir Massif and the overlying ophiolite-related material are intruded by a series of Upper Cretaceous plutons of mainly granitic, granodioritic, monzonitic and syenitic composition. The intrusives have been dated by a range of methods as ~74-92 Ma (Whitney *et al.* 2003; Ilbeyli *et al.* 2004; Köksal *et al.* 2004; Kadıoğlu *et al.* 2003). Some workers consider the magmatism as reflecting a syn- to post-collisional setting, which was generated during crustal thickening, following a period of Late Cretaceous continental collision related to the collision of the Niğde-Kırşehir Massif and the Pontide margin to the north (Boztuğ 1998; Düzgören-Aydin *et al.* 2001; Köksal *et al.* 2004; Ilbeyli 2005; Köksal *et al.* 2008; Boztuğ *et al.* 2009; Ilbeyli & Kibici 2009). For others, the magmatism is related to the subduction of Inner Tauride oceanic lithosphere beneath the Niğde-Kırşehir Massif (Görür *et al.* 1984; Kadıoğlu *et al.* 2006; Robertson *et al.* 2009). This is supported by recent studies which indicate that no significant collision-related deformation occurred in the Kırıkkale Basin until Late Paleocene-Eocene time (Nairn 2010). Furthermore, geochemical analysis of granites in the Kırıkkale Basin indicate a close association with arc magmatism and metasomatised mantle, consistent with emplacement in a subduction zone setting (Nairn 2010).

In light of the above evidence, a tectonic model for the evolution of the Darende and Hekimhan Basins need to include two north-dipping subduction zones, one to the north of the Niğde-Kırşehir Massif (dipping beneath the Pontides) and one to the south (dipping beneath the Niğde-Kırşehir Massif). The northern and southern subduction zones correlate with the closure and suturing of the Izmir-Ankara-Erzincan Ocean and the Inner-Tauride Ocean, respectively (Fig. 4.4).

4.4.2 Evolution of the Darende and Hekimhan Basins

The Tauride microcontinent rifted from the northern margin of Gondwana during the Mid-Late Triassic. Then, during the Mesozoic, two Neotethyan oceanic basins are likely

to have existed in the region, namely the Inner Tauride ocean to the south and the İzmir-Ankara-Erzincan ocean to the north (Görür *et al.* l984; Robertson & Dixon l984; Ricou l996; Dilek & Whitney 2000; Robertson *et al.* 2009; Pourteau *et al.* 2010). The oceans were separated by the Niğde-Kırşehir microcontinent (Fig. 4.4). North-dipping subduction zones are inferred to have existed, both to the north and the south of the Niğde-Kırşehir microcontinent (Robertson *et al.* 2009; Nairn *et al.* in press). It has been shown from the Gürun Basin, situated to the north of the Darende Basin, that carbonate platform rocks associated with the Tauride microcontinent have been thrust southwards to form structurally allochthonous units, probably during the Late Cretaceous (Robertson *et al.* in press). To the west of the field areas, the leading edge of the Tauride plate subducted northwards underneath the Niğde-Kırşehir Massif. It is unclear how far east the wedge-shaped Niğde-Kırşehir Massif extends. However, it seems reasonable that parts of the Niğde-Kırşehir Massif structurally underlie the platform rocks in the field areas, particularly the Darende Basin which is located closer to the Niğde-Kırşehir Massif. Since no evidence of the Niğde-Kırşehir Massif was observed at outcrop during this study, it is assumed that the Darende and Hekimhan basins developed on the northern margin of the Tauride microcontinent. However, the evolution of the Darende and Hekimhan Basins was heavily influenced by the close proximity of the Niğde-Kırşehir Massif (Fig 4.4).

The leading edge of the Tauride microcontinent is characterised by carbonate platform sequences (e.g. Geniz Formation) which were deposited throughout the Mesozoic. Collision of the passive oceanic margin with an intra-oceanic subduction zone instigated the collapse and drowning of the platform. A regional-scale ophiolite formed above a north-dipping intra-oceanic subduction zone associated with the closure of the Inner Tauride Ocean during Upper Cretaceous time (~ 90 Ma; Robertson *et al.* 2009; in press). In adjacent field areas (e.g. Pınarbaşı, Divriği), metamorphic soles, locally with 'enriched' (seamount type) volcanism, formed in response to accretion (and underplating) of oceanic crust to the leading edge of supra-subduction oceanic crust (Parlak *et al.* 2000; 2006; Vergili & Parlak 2005).

The ophiolitic mélanges formed by accretion to the base of the over-riding ophiolite by a combination of tectonic and sedimentary processes. The advancing oceanic plate caused down-flexure of the Tauride margin, which submerged to form a Late Cretaceous (Campanian-Maastrichtian) foredeep in which the ophiolite-related mélanges

formed. The subduction trench then collided with the drowned passive margin. The mud-matrix mélange formed when oceanic material mixed with the terrigenous sediments prior to and during overthrusting by the accretionary wedge. The ophiolites and mélanges were then emplaced onto the northern margin of the Tauride platform during latest Cretaceous time (Fig. 4.4; e.g. Karsantı-Pozantı [Alihoca] and Pınarbaşı mélanges [Parlak *et al.* 2000; 2006; Vergili & Parlak 2005]). Ophiolite emplacement corresponded to the cessation of active subduction. This intra-oceanic subduction zone is an eastward extension of an inferred subduction zone dipping northwards beneath the Niğde-Kırşehir microcontinent. As a result, the ophiolites underlying the Darende and Hekimhan Basins share a similar age and emplacement history to those underlying the Ulukışla Basin, to the south of the Niğde-Kırşehir microcontinent (Clark & Robertson 2002; 2005). Trench-margin collision ended by Late Maastrichtian time and instigated the development of sedimentary basins on the emplaced ophiolites and ophiolite-related mélanges.

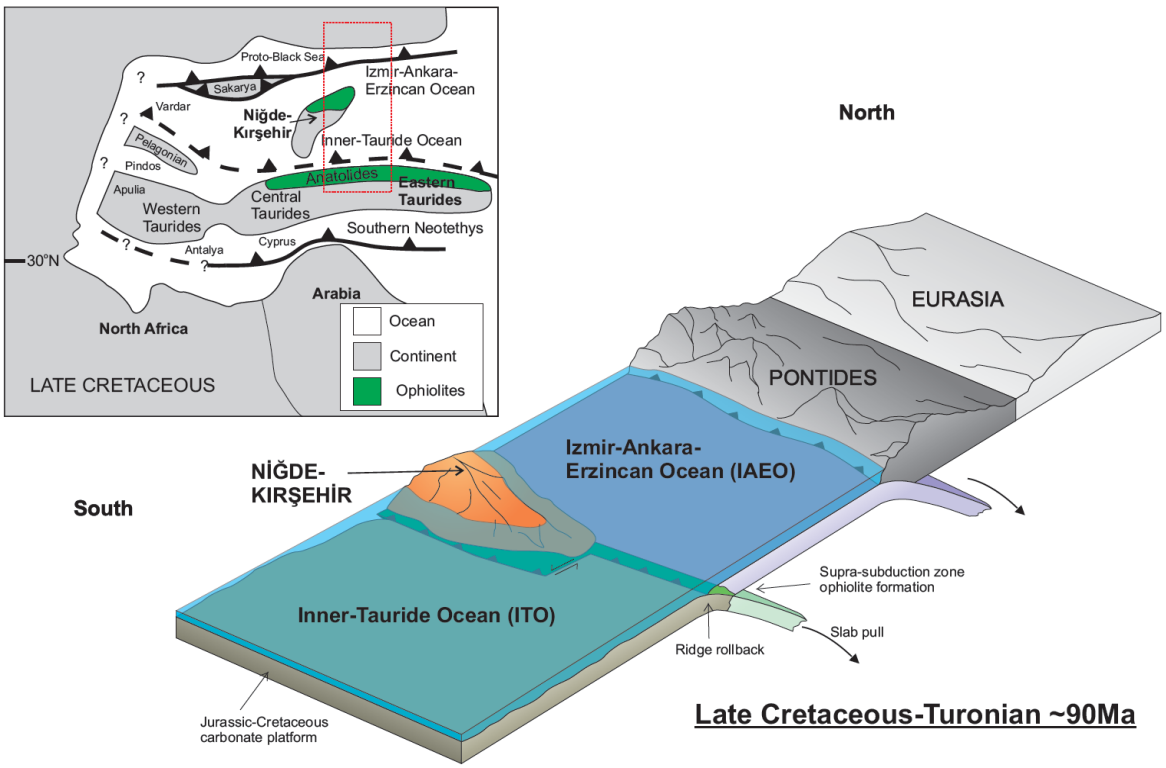

Figure 4.4. Regional palaeogeographic and plate tectonic reconstruction for the Late Cretaceous. Sketch map indicates the approximate location of microcontinents within the wider Tethys Ocean (modified from Robertson *et al.* 2009). Dashed red box on the sketch map indicates the approximate extent of the tectonic block diagrams (in this figure, and those that follow).

The Darende and Hekimhan Basins developed shortly after the ophiolites were emplaced (i.e. Late Maastrichtian). Sedimentation took place in a subaerial setting

initially (Ulupınar and Karadere Formations). This was likely to be an isostatic response to the cessation of subduction. Active extension instigated the marine transgressions in both basins, as indicated by the shallow-marine limestones of the Darende Basin (Kırankaya Formation) and the shallow-to deep-marine sedimentats in the Hekimhan Basin (Hekimhan Formation). Extension is evidenced by syn-sedimentary faulting and deformation (slump folds), debris flows and internal unconformities. In the Hekimhan Basin, up to 1000 m of subaqueous, extension-related, within-plate volcanism (Hasaçelebi Formation) was erupted near the (infered) basin depocentre along with the intrusion of a post-collisional syenite pluton (Yüceşafak Member). Extension and transgression within the Darende and Hekimhan Basins was possibly related to isostatic compensation and on-going slab-pull resulting from the northward subduction of remaining Neotethyan oceanic lithosphere beneath the Eurasian margin to the north (Fig. 4.5). The variation in the stratigraphy between the Darende and Hekimhan Basins at this time (i.e. shallow-to deep-marine sedimentation, volcanism and magmatism in an extension dominated environment in the Hekimhan Basin, versus shallow-marine sedimentation in a mildly extensional environment in the Darende Basin) could reflect the nature of the underlying 'basement' of the basins. The Darende Basin is situated close to the Niğde-Kırşehir Massif which could have acted against far field extension generated by the subduction of the Izmir-Ankara-Erzincan Ocean to the north (affectively residing in a 'strain shadow'). In contrast, the Hekimhan Basin was situated futher east and away from the Niğde-Kırşehir Massif, and could thus have been more susceptable to far-field extension. However, the Izmir-Ankara-Erzincan Ocean is thought to have remained open until the Late Paleocene to Early Eocene in the Eastern Taurides. The ocean could have still been extensive during the Maastrichtian, hence the northern subduction zone could have been situated well to the north of the Darende and Hekimhan Basins at this time.

The tectonic development of the Ulukışla Basin was characterised by Paleocene–Eocene alkaline volcanism that can be explained by similar regional crustal extension or transtension (Clark & Robertson 2002; 2005). Similar extension-related features are also known from the Sivas basin (A. Poisson personal communication 2012). The whole of the northern margin of the Tauride platform was therefore affected by crustal extension during latest Cretaceous time.

The inferred extensional setting can usefully be compared with northeastern Oman where the Upper Cretaceous Semail ophiolite was emplaced onto the Arabian continental margin (Robertson & Searle l990). The platform was then dissected into extension-controlled basins during latest Cretaceous time. Non-marine clastic sediments are overlain by Maastrichtian rudist-rich, shallow-marine carbonates, in places associated with alkaline volcanic rocks (Filbrandt *et al.* 1990; Shelton 1990).

Alternatively, the large volume of serpentinised ophiolite-related material in the Hekimhan Basin (compared to Darende Basin), could have acted as décollement horizons, potentially reactivating thrusts which originally emplaced the ophiolites into extensional faults. This could have generated an extensional setting which allowed for the accumulation of the Hekimhan Basin sediments, volcanism and magmatism. However, detachment faults could similarly have developed with the carbonate platform rocks or along the platform basement margin.

The Niğde-Kırşehir microcontinent has recently been subdivided into three crustal units, which can be restored as a single elongate NE–SW trending microcontinent during the Cretaceous (Lefebvre *et al.* 2012). Collision of this microcontinent with the Pontide margin to the north began in the Late Cretaceous and initiated the block rotations that culminated in the present triangular geometry of the Niğde-Kırşehir Massif. The collision of the Niğde-Kırşehir microcontinent with the Pontide margin caused the oroclinal bending of the Eurasian continental margin, as demonstrated by palaeomagnetic data (Meijers *et al.* 2010). Taken together, the collision-induced block rotations and oroclinal bending suggest that Late Cretaceous–Paleocene deformation was concentrated on the Niğde-Kırşehir microcontinent and surrounding areas. However, the İzmir-Ankara-Erzincan ocean was not completely closed, both to the west and to the east of the Niğde-Kırşehir microcontinent until Late Paleocene–Early Eocene time. Collision was, therefore, progressive and diachronous.

In the light of the above comparisons, we infer that the Darende and Hekimhan Basins were initiated soon after the Maastrichtian ophiolite and mélange emplacement, in response to SW-NE crustal extension and that this caused subsidence and block faulting (e.g. as evidenced along the southwest margin of the Darende Basin). The likely driving mechanism is seen as regional slab pull resulting from northward subduction of the

remaining İzmir-Ankara-Erzincan ocean, beneath the Pontide active margin to the north (Fig. 4.5).

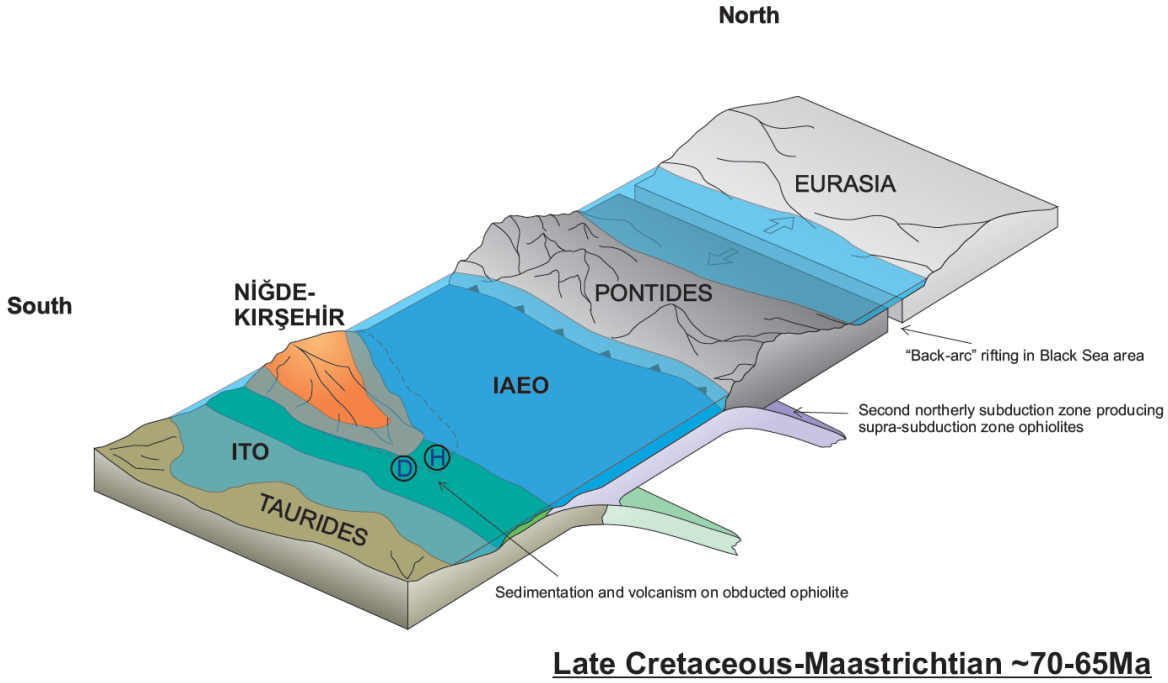

Figure 4.5. Regional palaeogeographic and plate tectonic reconstruction for the Late Cretaceous depicting the closure of the Inner Tauride Ocean to the south of the Niğde-Kırşehir Massif. This lead to the emplacement of ophiolites and related mélanges along the northern margin of the Tauride microcontinent during northwards subduction. The Darende and Hekimhan Basins (D and H) developed shortly afterwards on the emplaced ophiolites in an extensional setting, possibly related to isostatic compensation and on-going slab-pull during northward subduction of the remaining Neotethyan oceanic lithosphere to the north.

The Darende and Hekimhan Basins both shallowed and became emergent at the end of the Cretaceous. The Paleocene was characterised by localised high-angle unconformities caused by fault-block rotations in the Darende Basin and a low-angle basin-wide unconformity in the Hekimhan Basin. No rocks of Paleocene-age have been recorded in either basin. Crustal thickening in response to suture tightening of the former Inner-Tauride Ocean is not envisaged as a mechanism for uplifting the Darende and Hekimhan Basins at the end of the Cretaceous and through the Paleocene. This is due to the presence of Paleocene-aged deep-marine sedimentary successions and within-plate volcanism observed in the Ulukışla Basin to the south of the Niğde-Kırşehir Massif which forms a regional extensional setting. Emergence of the Darende and Hekimhan Basins was possibly controlled by regional flexural uplift as the down-going plate to the north approached the subduction zone, which could have generated a flexural fore-bulge

affecting the down-going plate, as the Taurides began to collide with the Pontides, and was possibly also influenced by eustatic sea-level change (Fig. 4.6).

The geology of the Eastern Pontides is interpreted in terms of closure of the İzmir-Ankara-Erzincan ocean and the collision of the Tauride continental block with Eurasia during Paleocene-Eocene time (Okay & Şahintürk 1997). An unbroken Campanian-Lower Eocene sedimentary succession in the Erzincan area is interpreted as sedimentation in a forearc setting, which was terminated by collision during or soon after the Early Eocene (Rice *et al.* 2006, 2009). Strong deformation took place throughout the eastern Pontides during the Eocene (Okay & Şahintürk 1997; Rice *et al.* 2006, 2009; Ustaömer & Robertson 2010).

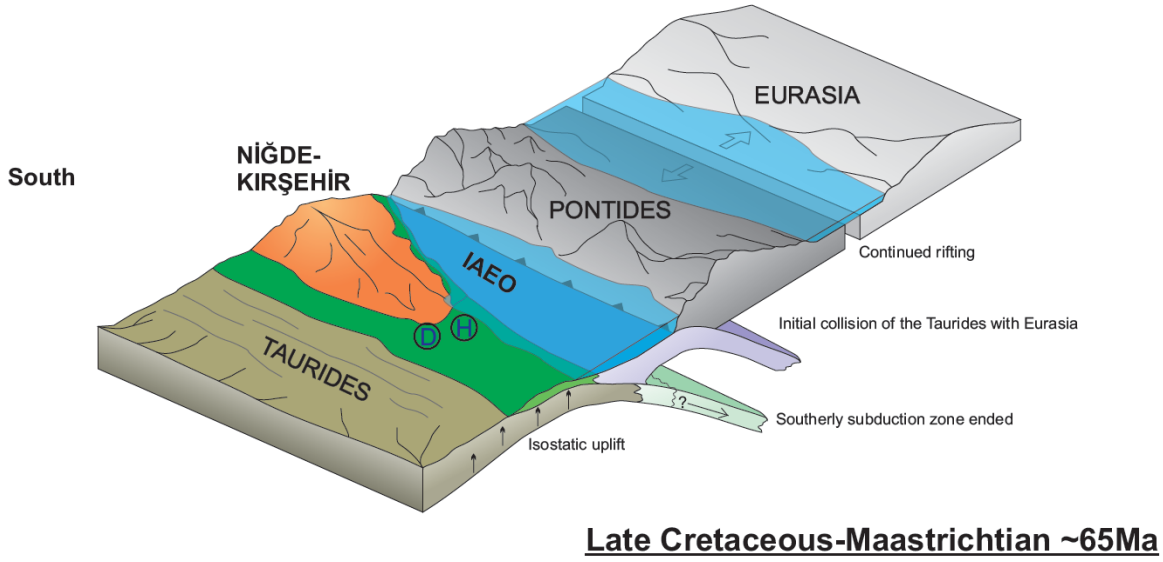

Figure 4.6. Regional palaeogeographic and plate tectonic reconstruction for the latest Cretaceous depicting the suturing of the Inner-Tauride Ocean and the closure of the Izmir-Ankara-Erzincan Ocean. Emergence of the Darende and Hekimhan Basins (D and H) in the latest Cretaceous was possibly controlled by regional flexural uplift as the down-going plate approached the subduction zone to the north (and was possibly also influenced by eustatic sea-level change).

Eocene turbiditic sediments accumulated on the Gürün platform, part of the Tauride carbonate platform that is exposed to the northwest of the Darende Basin (Perinçek & Kozlu 1984; Robertson *et al.* in press). These sediments are explained by flexural subsidence and the formation of a foreland basin related to the collision in the Pontides. A flexural foreland basin developed across the Taurides as a whole during Early–Mid Eocene, as seen in the Geyik Dağ of the central Taurides (Özgül 1997; Mackintosh & Robertson in press). Therefore, the Middle Eocene regional transgression of the Darende and Hekimhan Basins and adjacent areas could reflect collision-related

flexural subsidence (Fig. 4.7). The basins are envisaged as underfilled depocentres that were isolated from direct input of clastic sediment from the suture zone to the north.
The localised Mid-Eocene alkaline volcanism within the Darende and Hekimhan Basins is likely to have been triggered by extension associated with regional-scale collision-related subsidence. Post-collisional slab break-off has been inferred as the trigger for Mid-Eocene volcanism triggered in the central Pontides (Keskin *et al.* 2008). However, the Darende and Hekimhan Eocene volcanic rocks are situated on the Mesozoic Tauride-Anatolide block ~160 km south of the İzmir-Ankara-Erzincan suture zone and are compositionally dissimilar (alkaline rather than adakitic or calc-alkaline). Furthermore, the Mid-Eocene volcanism predates the Neogene post-collisional volcanism of eastern Anatolia (Pearce *et al.* 1990; Kuşçu *et al.* 2010). However, the volcanism could have resulted from regional back-arc style extension related to the subduction of the Southern Neotethyan oceanic crust, which is thought to have a high roll-back velocity associated with it (Vincent et al. 2005). The decrease or end of volcanism during the Late Eocene may, therefore, be attributed to the initial collision of Arabia with Eurasia at this time (Hempton, 1987; Yilmaz, 1993; Robertson, 2000; Clark & Robertson, 2005). However, the onset of collision remains contentious throughout the Africa-Arabia tectonic setting.

The localised andesitic-dacitic volcanism in the Hekimhan Basin could have a post collisional origin, similar to the Pontides to the north. Adakitic rocks have been observed in the Pontides and have been related to melting of a subducting plate during the later stages of subduction (Eyuboglu *et al.* 2012). They have also been inferred to relate to slab break-off (Eyuboglu *et al* 2011). However, they may also be generated by melting of a subducting slab or ridge, low pressure fractional crystallisation of amphibole-bearing basalts, high pressure fractional crystallisation or melting of metamorphosed basalts within the lower crust or melting of the lower mafic crust (Zellmer *et al.* 1996; Castillo 2006).

In an alternative scenario, the Eocene time intervals of the Darende and Hekimhan Basins may have developed as part of a regionally extensive back-arc basin system associated with the northward subduction of South Neotethyan oceanic crust. Many workers have identified extensive outcrops of Eocene-aged basic to intermediate-composition volcanic rocks covering parts of Turkey, Armenia, Azerbaijan and Northern Iran (e.g. Vincent *et al.* 2005; Omrani *et al.* 2008; Allen 2009). For example Keskin *et al.* (2008) identified

numerous Eocene-aged basalts throughout Central Turkey. Additional outcrops exist in southern areas of Turkey, including, and not limited to, the Ulukışla Basin (Clark & Robertson 2002; 2005), the Berit area (Robertson *et al.* 2006), the Maden Complex (Aktaş & Robertson 1984; Yiğitbaş & Yılmaz 1996) as well as the basins studied during this work (Darende and Hekimhan Basins). In Azerbaijan, Eocene-aged volcanics are interleaved with shallow-marine sedimentation in less than 200 m water depth (Vincent *et al.* 2005). The Eocene in Central Iran is represented by mixed successions of limestone and clastic sediments interbedded with basic volcanic rocks. These facies often terminate in a Late Eocene regionally extensive angular unconformity.

The Maden Complex, situated ~200 km SSE of the Hekimhan Basin, refers to a volcanosedimentary succession of Middle Eocene age composed of transgressive limestones and mainly basaltic volcanism (Robertson *et al.* 2012). The basin began by rifting within a basement composed of metamorphosed ophiolite associations and the metamorphic massifs during the Early Eocene. Rifting was accompanied by alkaline volcanism in the early stages. The lavas are associated with successions of continental to shallow-marine clastic rocks. The basal clastic units grade into pelagic sedimentary rocks including red limestone, shale, mudstone, and radiolarite. The pelagic successions were accompanied by transitional and MORB-type basaltic lavas (Aktaş & Robertson 1984; Yiğitbaş & Yılmaz 1996). This stratigraphy is typical of the early stages of rifting related to back-arc extension (Martinez *et al.* 1995). The basin was terminated in the Middle to Late Eocene when extension switched to compression and a series of southward directed nappes moved over the Maden complex (Yiğitbaş & Yılmaz 1996).

Many of the Middle Eocene volcanic rocks in Turkey, Iran and adjacent countries are interbedded with marine limestones or turbidites, implying that extension took place within crust of normal thickness or that was partially thinned. Similarities between Central Iran, the Zagros region and Central Eastern Turkey (i.e. Darende and Hekimhan Basins) include an Eocene shallow-marine stratigraphy coupled with extension-related volcanism which terminate in a Late Eocene angular unconformity onto which either shallow-marine calcareous or terrestrial clastic rocks were deposited. This unconformity is interpreted by some workers as reflecting the initial collision of Arabia and Eurasia (e.g. Allen & Armstrong 2008; Agard *et al.* 2011). Allen & Armstrong (2008) argue for a synchronous collisional front stretching from Anatolia through to the Persian Gulf during

this time which is then followed in all areas by Oligocene to Early Miocene thrusting. Furthermore, Agard *et al.* (2011) attribute the Late Eocene volcanism to slab break-off followed by renewed and vigorous subduction of the South Neotethyan oceanic crust resulting in an extensional environment in the overriding Eurasian plate. This extension could, in principal, have provided the accomodation space for the Eocene intervals of the Darende and Hekimhan Basins to form in the Anatolian region. A problem with this model is that the onset of collision throughout the Eastern Mediterranean region is often thought to be diachronous (e.g. Robertson *et al.* 2012). Agard *et al.* (2011) also attribute the Late Eocene unconformity events in Iran to a pre-collisional, regional-scale flexural forebulge. In addition, some of the volcanic rocks in northern Turkey are clearly related to closure (and possibly slab brak-off) within the suture zone of the İzmir-Ankara-Erzincan ocean well to the North of and unrelated to the South Neotethys. Furthermore, most workers currently working in SE Turkey accept the evidence that the Southern Neotethys closed in the Early Miocene (Okay *et al.* 2010). By now the geology of Turkey is generally more fully documented than comparable areas of Iran and it is possible that interpretations of Iranian geology have not fully taken account of more northerly oceanic basins similar to the İzmir-Ankara-Erzincan ocean in Turkey. Nevertheless, it is accepted here that the Eocene history of the two basins researched for this thesis could well have been influenced by back-arc extension. On the other hand the Early-Mid Eocene is the accepted time of final closure of the İzmir-Ankara-Erzincan ocean which affected the whole of the Pontide and the Tauride realm. It is therefore likely the two sets of processes interacted, namely final closure of the northerly basin and back-arc extension behind the southerly basin in ways that are not yet fully understood.

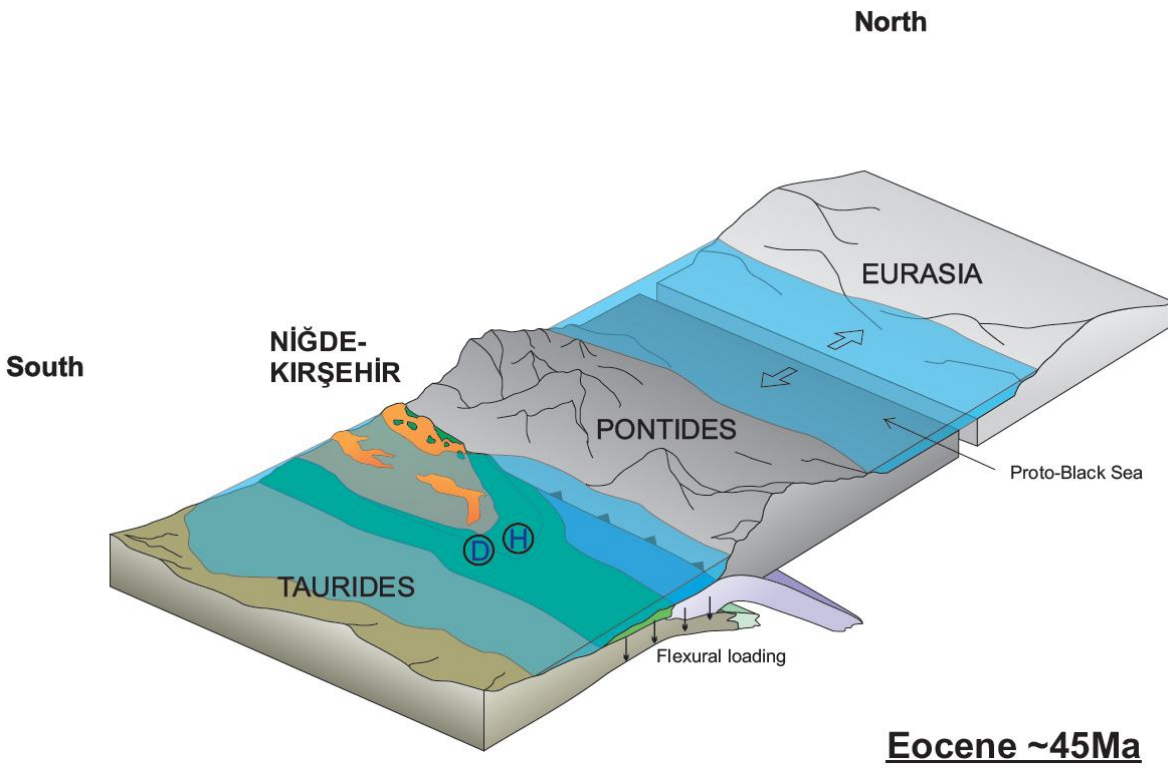

Figure 4.7. Regional palaeogeographic and plate tectonic reconstruction of the Middle Eocene showing active sedimentation in the Darende and Hekimhan Basins (D and H) in a subsiding setting related to flexural loading of the over-riding Eurasian margin.

Sedimentation in the Darende and Hekimhan Basins ended during the Late Eocene (Priabonian). Shallow-marine sediments and evaporite sequences indicate progressive shallowing and isolation of the basins followed eventually by emergence. In contrast to areas further west (e.g. Ulukışla Basin) and north (Pontides), that were strongly affected by thrusting and folding, the Eocene deformation affecting the Darende Basin and the Hekimhan Basin was mainly restricted to folding and minor thrusting. The folding and faulting seen within the Darende and Hekimhan Basins took place after the Late Eocene deposition, but prior to the deposition of the sub-horizontal (undeformed) Mid-Miocene transgressive limestones. Pre-existing extension-related faults around the margins of the Darende Basin are likely to have been stratigraphically inverted to form thrusts and folds during latest Eocene time (syn–post Priabonian). This can be seen as a late-stage collisional effect (i.e. suture tightening). Uplift to form the Anatolian plateau took place from the Middle Miocene onwards related to Arabia-Eurasia collision (e.g. Ballato *et al.* 2010; Schildgen *et al.* 2012). The location of the Darende and Hekimhan Basins along the northern margin of the Tauride-Anatolide continental block ~160 km south of the Pontide suture zone and 170 km east of the Niğde-Kırşehir continental unit

(Fig. 4.8) appears to have shielded the basin from strong deformation within a regional "strain shadow".

The strike-slip fault which cuts the Darende Basin along the southwest margin and the Malatya-Ovacik Fault Zone (Westaway & Arger 2001; Kaymakcı *et al.* 2006) cutting the eastern margin of the Hekimhan Basin may link up with the Göksu Fault Zone, which extends to the Mediterranean Sea south of Adana (Kozlu *et al.* 1990; Robertson *et al.* in press). The strike-slip faulting is generally linked to the westward 'tectonic escape' of Anatolia towards the Aegean Sea (Şengör *et al.* 1985; Allen *et al.* 2006; Piper *et al.* 2010; Gürsoy *et al.* 2011).

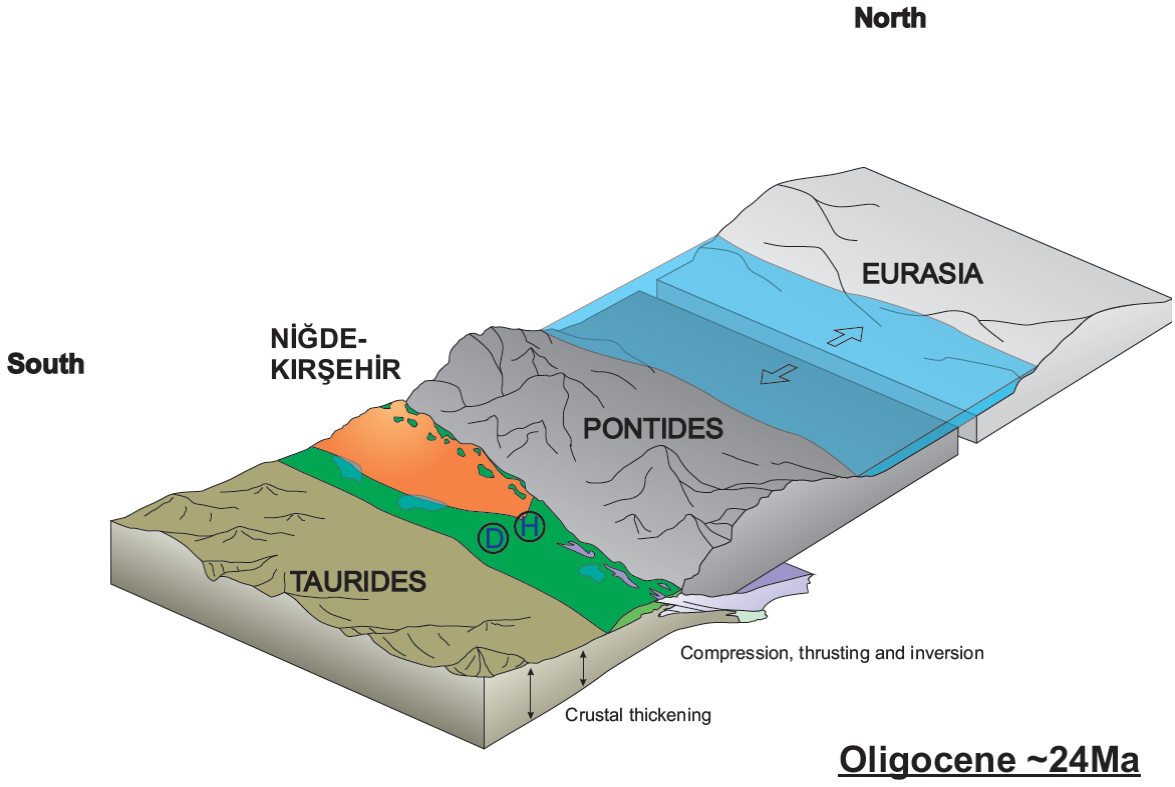

Figure 4.8. Regional palaeogeographic and plate tectonic reconstruction for the Oligocene showing subaerial exposure of the Darende and Hekimhan Basins (D and H). Mid-Late Eocene 'hard collision' resulted in regional uplift, progressive isolation and subaerial exposure of the basins. Suture tightening and compression, during the Late Eocene-Miocene, resulted in reactivation of pre-existing extensional faults and terminated marine sedimentation.

Chapter 5: Conclusions

Chapter 5. Conclusions

The stratigraphy of the Darende and Hekimhan Basins has been significantly revised, both in terms of lithostratigraphy and biostratigraphy. Sedimentological work has characterised the basin history in terms of facies and facies relationships. The revised stratigraphic scheme takes into account sedimentological data combined with structural data that were used together to construct a relatively simple evolution of the basins. Geochemistry of the volcanic and magmatic suites in the Darende and Hekimhan Basins was carried out using XRF and this was crucial in developing the geohistories of the basins.

The latest Cretaceous-Late Eocene development of the Darende and Hekimhan Basins occurred in two main phases:

- The first phase of basin development took place during the Late Maastrichtian, following ophiolite and accretionary melange emplacement and subaerial exposure. Continental clastic sedimentation began in topographic depressions during the Late Maastrichtian. A marine transgression instigated rudist patch reefs and a microbial (algal) carbonate shelf in different areas in the Darende Basin. In contrast, hemi-pelagic marl and coeval basaltic volcanism followed by shallow-marine limestone were deposited in the Hekimhan Basin.
- The transgression is mainly explained by extension-related subsidence. This was possibly activated by slab-pull towards the Pontide subduction zone, as remnant oceanic crust was subducted northwards beneath Eurasia. Extension was less dominant in the Darende Basin, possibly due to its location further south on the Tauride microcontinental margin.
- The absence of Paleocene sediments in the Darende and Hekimhan Basins can be explained by collision related up-flexure.
- After a hiatus and tilting of <5° sedimentation resumed during Middle Eocene time, preceded by faulting and strong stratal rotation in parts of the Darende Basin.

- The second phase of basin development during the Mid- to Late Eocene can be explained by flexural subsidence related to the collision of the Taurides with Eurasia in the Pontides to the north. On the other hand it may also be influenced by back-arc extension related to subduction of the S Neotethys (or a combination of both). Subsidence and related fault reactivation created an underfilled foreland basin, with sediment input from surrounding areas. Widespread marine transgression resulted in the deposition of hemi-pelagic marls and redeposited carbonates. Small volumes of extension-related alkaline volcanic rocks erupted in shallow-marine to subaerial settings. The Darende and Hekimhan Basins culminated in Upper Eocene mixed shallow-marine and evaporitic sediments. Open folding and localised thrusting (fault reactivation and inversion) reflect late-stage suture tightening, probably during latest Eocene time.
- Post-collisional uplift was delayed until after local Mid-Miocene shallow-water carbonate deposition within parts of the basins. Neogene, strike-slip faulting affected the Darende Basin and in places defined its western margin.

References

References

AGARD, P., OMRANI, J., JOLIVET, L., WHITECHURCH, H., VRIELYNCK, B., SPAKMAN, W., MONIE, P., MEYER, B. & WORTEL, R. 2011. Zagros orogeny: a subduction-dominated process. *Geological Magazine,* **148**, 692-725.

AKKUŞ, M. F. 1970. The lithostratigraphic units in Darende-Balaban Basin (Malatya, ESE Anatolia) and new information about the age of the gypsum formation. *Mineral Research and Exploration Institute of Turkey (MTA) Bulletin,* **75**, 1-14 [in Turkish with English abstract].

AKKUŞ, M. F. 1971. The geologic and stratigraphical research of Darende-Balaban Basin (Malatya ESE Anatolia). *Mineral Research and Exploration Institute of Turkey (MTA) Bulletin,* **76**, 1-60.

AKSOY, E., TÜRKMEN, İ. & TURAN, M. 2005. Tectonics and sedimentation in convergent margin basins: an example from the Tertiary Elazığ Basin, Eastern Turkey. *Journal of Asian Earth Sciences*, **25**, 459–472.

AKTAŞ, G. & ROBERTSON, A. H. F. 1984. The Maden Complex, SE Turkey: evolution of a Neotethyan active margin. *In*: DIXON, J. E. & ROBERTSON, A. H. F. (eds.) *The Geological Evolution of the Eastern Mediterranean*. The Geological Society, London, Special Publications, **17**, 375-402.

AKYÜREK, B., BILGINER, E., AKBAŞ, B., HEPŞEN, N., PEHLIVAN, Ş., SUNU, O., SOYSAL, Y., DAĞER, Z., ÇATAL, E., SÖZERI, Z., YILDIRIM, H. & HAKYEMEZ, Y. 1984. The geology of the Ankara-Elmadağ-Kalecik region. *Jeoloji Mühendisliği Dergisi*, **20**, 31-46.

AKYÜREK, B., ÖZATA, A., TOPRAK, S., AFŞIN, Ö., ÇETIN, N. İ., SAN, B. T., AYDIN, A., ÇIPLAK, R. & YIĞIT, E. 2001. Kırıkkale-Kalecik (Ankara) Arasının. *Jeolojisi. MTA Report No. 10407*.

ALLEN, M. B. 2009. Discussion on the Eocene bimodal Piranshahr Massif of the Sanadaj-Sirjan Zone, West Iran: a marker of the end of collision in the Zagros orogen. *Journal of the Geologcial Society, London,* **166**, 981-982.

ALLEN, M. B., WALKER, R., JACKSON, J. A., BLANC, E. J. P., TALEBIAN, M. & GHASSEMI, M. 2006. Contrasting styles of convergence in the Arabia-Eurasia collision: why escape tectonics does not occur in Iran. *In:* DILEK, Y. & PAVLIDES, S. (eds)

Postcollisional Tectonics and Magmatism in the Mediterranean Region and Asia. Geological Society of America, Special Papers, **409**, 579–589.

ALLEN, M. B. & ARMSTRONG, H. A. 2008. Arabia-Eurasia collision and the forcing of mid-Cenozoic global cooling. *Palaeogeography, Palaeoclimatology, Palaeoecology*, **265**, 52-58.

ALLMENDINGER, R. W. (2011) Stereonet 7 for Windows [Online]. Available from: http://www.geo.cornell.edu/geology/faculty/RWA/programs/stereonet-7-for-windows.html

ALLMENDINGER, R. W. 1995. STERONET Version 4.9, computer program user's manual, 45 p.

ALLMENDINGER, R. W., MARRETT, R. A. & CLADOUHOS, T. 1992. FaultKin Version 3.25, computer program and user's manual, 26 p.

ALPASLAN, M., FREI, R., BOZTUĞ, D., KURT, M. A. & TEMEL, A. 2004. Geochemical and Pb–Sr–Nd isotopic constraints for an enriched-mantle source for the late cretaceous to early tertiary volcanism in the Çamardı-Ulukışla basin Niğde province, central Anatolia, Turkey. *International Geology Revivew*, **46**, 1022–1041.

ALPASLAN, M., BOZTUĞ, D., FREI, R., TEMEL, A. & KURT, M. A. 2006. Geochemical and Pb-Sr-Nd isotopic composition of the ultrapotassic volcanic rocks from the extension related Çamardı-Ulukışla basin, Niğde Province, Central Anatolia, Turkey. *Journal of Asian Earth Sciences*, **27**, 613-627.

ALTAY, T., KARAKAYA, M.Ç. & MURAT, A. 2010. Mineralogy and Geochemistry of the Neogene Lacustrine Sediments of Bor-Ulukışla Basin (Niğde, Turkey). *Goldschmidt Conference Abstracts 2010*, **1**, 37-44.

ANDREW, T. & ROBERTSON, A. H. F. 2002. The Beysehir-Hoyran-Hadim Nappes: genesis and emplacement of Mesozoic marginal and oceanic units of the northern Neotethys in southern Turkey. *Journal of the Geological Society*, **159**, 529-543.

ANGELIER, J. 1979. Determination of the mean principal directions of stresses for a given fault population. *Tectonophysics*, **56**, T17-T26.

ANGELIER, J. 1994. Fault slip analysis and palaeostress reconstruction. *In:* HANCOCK, P. L. (ed) *Continental deformation.* Pergamon Press, Oxford, 53–100.

ANONYMOUS. 1972. Penrose field conference on ophiolites. *Geotimes*, **17**, 24–25.

ARGER, J., MİTCHELL, J. & WESTAWAY, R. W. C. 2000. Neogene and Quaternary volcanism of southeastern Turkey. *In:* BOZKURT, E., WİNCHESTER, J. A. & PİPER, J.

D. A. (eds) *Tectonics and Magmatism in Turkey and the Surrounding Area.* The Geological Society, London, Special Publications, **173**, 459-487.

ARIKAN, Y. 1975. The geology and petroleum prospects of the Tuzgölü Basin. *Maden Tetkik ve Arama Bulletin,* **85**, 17-38 [in Turkish with English abstract].

ARSLAN, M., TÜYSÜZ, N., KORKMAZ, S. & KURT, H. 1997. Geochemistry and petrogenesis of the eastern Pontide volcanic rocks, Northeast Turkey. *Chemie der Erde,* **57**, 157–187.

ARSLAN, M. & ASLAN, Z. 2006. Mineralogy, petrography and whole-rock geochemistry of the Tertiary granitic intrusions in the Eastern Pontides, Turkey. *Journal of Asian Earth Sciences*, **27**, 177–193.

ATABEY, E., GÖNCÜOĞLU, M. C. & TURHAN, N. 1990. Turkish geological map series. No. 33, Section J19. Maden Tekik ve Arama Genel Müdürlüğü (General Directorate of Mineral Research and Exploration Ankara).

AYAN, T. 1961, Detailed geology and petroleum potential of the Hekimhan-Ebreme region (north of Malatya). MTA Rep., **4186** (unpublished), Ankara [in Turkish].

AYDEMIR, A. 2008. Hydrocarbon potential of the Tuzgolu (Salt Lake) Basin, Central Anatolia, Turkey: A comparison of geophysical investigation results with the geochemical data. *Journal of Petroleum Science and Engineering*, **61**, 33-47.

---, 2009. Tectonic investigation of Central Anatolia, Turkey, using geophysical data. *Journal of Applied Geophysics*, **68**, 321-334.

AYDEMIR, A. & ATEŞ, A. 2005. Preliminary evaluation of Central Anatolian basins in Turkey using the gravity & magnetic data. *Journal of the Balkan Geophysical Society*, **8**, 7-19.

---, 2006. Structural interpretation of the Tüzgölu and Haymana Basins, Central Anatolia, Turkey, using seismic, gravity and aeromagnetic data. *Earth Planets Space*, **58**, 951-961.

BAIER, J., AUDÉTAT, A. & KEPPLER, H. 2008. The origin of the negative niobium tantalum anomaly in subduction zone magmas. *Earth and Planetary Science Letters,* **267**, 290-300.

BALLATO, P., UBA, C. E., LANDGRAF, A., STRECKER, M. R., SUDO, M., STOCKLI, D. F., FRIEDRICH, A. TABATABAEI, S. H. 2010. Arabia-Eurasia continental collision: Insights from late Tertiary foreland-basin evolution in the Alborz Mountains,

northern Iran *Geological Society of America Bulletin, B30091.1, first published on October 28, 2010, doi:10.1130/B30091.1*

BAYKAL, F. 1965. Malatya-Darende-Gürün bölgesindeki yeşil sahrelerle sediment kayaçlar arasındaki ilişki. *Maden Tetkik ve Arama* Report, **1257** (unpublished) [in Turkish].

BÉDARD, J. H. 1999. Petrogenesis of boninites from the Betts Cove ophiolite, Newfoundland, Canada: identification of subducted source components. *Journal of Petrology,* **40**, 1853–1889.

BERNOULLI, D. & JENKYNS, H. C. 2009. Ophiolites in ocean-continent transitions: from the Steinmann Trinity to sea-floor spreading. *Comptes Rendus Geoscience,* **341**, 363–381.

BLUMENTHAL, M. 1956. Yüksek Bolkardağin Kuzey Kenari Bögelerinin ve Bati Uzantilarinin Jeolojisi: MTA. Yay. Seri. D., Jeol. Hrt. Mat. 7.

BOSWORTH, W., EL-HAWAT, A. S., HELGESON, D. E. & BURKE, K. 2008. Cyrenaican "shock absorber" and associated inversion strain shadow in the collision of northeast Africa. *Geology,* **36**, 695-698.

BOUMA, A. H. 1962. *Sedimentology of some Flysch Deposits: A Graphic Approach to Facies Interpretation.* Elsevier, Amsterdam. 168 pp.

BOZTUĞ, D. 1998. Post–Collisional Central Anatolian Alkaline Plutonism, Turkey. *Turkish Journal of Earth Sciences,* **7**, 145-165.

BOZTUĞ, D., HARLAVAN, Y., AREHART, G. B., SATIR, M. & AVCI, N. 2007. K-Ar age, whole-rock and isotope geochemistry of A-type granitoids in the Divriği-Sivas region, eastern-central Anatolia, Turkey. *Lithos,* **97**, 193–218.

BOZTUĞ, D., TEMİZ, H., JONCKHEERE, R. & RATSCHBACHER, L. 2008a. Punctuated exhumation and foreland basin formation and infilling in (circum)-Central Anatolia (Turkey) associated with the Neotethyan closure. *Turkish Journal of Earth Sciences,* **17**, 673-684.

BOZTUĞ, D. & HARLAVAN, Y. 2008b. K–Ar ages of granitoids unravel the stages of Neo-Tethyan convergence in the eastern Pontides and central Anatolia, Turkey. *International Journal of Earth Sciences,* **97**, 585-599.

BOZTUĞ, D., JONCKHEERE, R. C., HEIZLER, M., RATSCHBACHER, L., HARLAVAN, Y. & TICHMIROVA, M. 2009. Timing of post-obduction granitoids from intrusion through cooling to exhumation in central Anatolia, Turkey. *Tectonophysics,* **473**, 223-233.

BUISSON, G. & LE BLANC, M. 1986. Gold-bearing listvenites (carbonatised ultramafic rocks) from ophiolite complexes. *In:* GALLAGHER, M. J., IXER, R. J., NEARY, C. R. & PRITCHARD, H. M. (eds) *Metallogeny of basic and ultrabasic rocks.* Institution of Mining and Metallurgy, 121-131.

BULLARD, E. C., EVERETT, J. E. & SMITH, A. G. 1965. Fit of continents around the Atlantic. *In:* BLACKETT, P. M. S., BULLARD, E. C. & RUCORN, S. A. (eds) *A Symposium on Continental Drift.* Philosophical Transactions of the Royal Society of London, Series A, **258**, 41-75.

BURKE, K. 1988. Tectonic evolution of the Caribbean. *Annual Review of Earth and Planetary Sciences*, **16**, 201-230.

ÇAGLAR, M. & ÖNAL, M. 2009. Systematic palaeontology, biostratigraphy, palaeobiogeography of *Loftusia* (foraminifera) and *Rudist* assemblages in a regressive sequence in the Hekimhan-Malatya area (Eastern Anatolia) Turkey. *Journal of the Geological Society of India*, **74**, 329-342.

ÇAMUR, M. Z., GÜVEN, İ. H. & ER, M. 1996. Geochemical characteristics of the eastern Pontide volcanics: an example of multiple volcanic cycles in arc evolution. *Turkish Journal of Earth Sciences*, **5**, 123–144.

ÇEMEN, I., GÖNCÜOĞLU, M. C. & DIRIK, K. 1999. Structural Evolution of the Tuzgölü Basin in Central Anatolia, Turkey. *Journal of Geology*, **107**, 693-706.

ÇEVIKBAŞ A. & ÖZUNTALI, Ö. 1991. Ore deposits in the Ulukışla¸ amardi (Niğde) Basin. Jeoloji Mühendisliği, **39**, 22–40 [in Turkish with English abstract].

ÇINKU, M. C., HİSARLI, M., HELLER, F., ORBAY, N. & USTAÖMER, T. 2011. Middle Eocene palaeomagnetic data from the eastern Sakarya Zone and the Central Pontides: Implications for the tectonic evolution of north central Anatolia. *Tectonics*, **30**, 1-19.

CANDAN, O., ÇETINKAPLAN, M., OBERHÄNSLI, R., RIMMELÉ, G. & AKAL, C. 2005. Alpine high-P/low-T metamorphism of the Afyon Zone and implications for the metamorphic evolution of Western Anatolia, Turkey. *Lithos*, **84**, 102-124.

CANN, J. & GILLIS, K. 2004. Hydrothermal insights from the Troodos ophiolite, Cyprus. *In:* DAVIES, E. E. & ELDERFIELD, H. (eds) *Hydrogeology of the Oceanic Lithosphere*. Cambridge University Press, 274–310.

CASTILLO, P. R. 2006. An overview of adakites petrogenesis. *Chinese Science Bulletin*, **51**, 257–268.

CATER, J. M. L., HANNA, S. S., RIES, A. C. & TURNER, P. 1991. Tertiary evolution of the Sivas Basin, central Turkey. Tectonophysics, 195, 29-46. CHARLTON, T. R. 2000. Tertiary evolution of the Eastern Indonesia Collision Complex. *Journal of Asian Earth Sciences,* **18**, 603-631.

CHAN, G. H. N., MALPAS, J., XENOPHONTOS, C. & LO, C. H. 2008. Magmatism associated with Gondwanaland rifting and Neo-Tethyan oceanic basin development: evidence from the Mamonia Complex, SW Cyprus. *Journal of the Geological Society, London,* **165**, 699-709.

CLARK, M. 2002. The latest Cretaceous–Early Tertiary Ulukışla Basin, S Turkey: sedimentation and tectonics of an evolving Tethyan suture zone. Unpublished PhD thesis, University of Edinburgh, Edinburgh, UK.

CLARK, M. & ROBERTSON, A. H. F. 2002. The role of the Early Tertiary Ulukışla Basin, southern Turkey, in suturing of the Mesozoic Tethys ocean. *Journal of the Geological Society, London,* **159**, 673-690.

CLARK, M. & ROBERTSON, A. H. F. 2005. Uppermost Cretaceous-Lower Tertiary Ulukışla Basin, south-central Turkey: sedimentary evolution of part of a unified basin complex within an evolving Neotethyan suture zone. *Sedimentary Geology,* **173**, 15-51.

COLE, M. R. & ARMENTROUT, J. M. 1979. Neogene palaeogeography of the western United States. *In:* ARMENTROUT, J. M., COLE, M. R. & TERBEST, H. JR. (eds) *Cenozoic Paleogeography of the Western United States*. Pacific Section, Society of Economic Paleontologists and Mineralogists, Pacific Coast Paleogeography Symposium, **3**, 297-324.

COLEMAN, R. G. & LANPHERE, M. A. 1971. Distribution and age of high-grade blueschists, associated eclogites, and amphibolites from Oregon and California. *Geological Society of America Bulletin,* **82**, 2397–2412.

COLLINS, A. & ROBERTSON, A. H. F. 1998. Processes of Late Cretaceous to Late Miocene episodic thrust-sheet translation in the Lycian Taurides, southwestern Turkey. *Journal of the Geological Society, London,* **155**, 759-772.

COX, K. G., BELL, J. D. & PANKHURST, R. J. 1979. The interpretation of igneous rocks. *George, Allen and Unwin, London.*

DELIBAŞ, O. & GENÇ, Y.,2004. Origin and Formation Processes of Iron, Copper-Molybdenum and Lead Mineralisations of Karacaali (Kırıkkale) Magmatic Complex. *Türkiye Jeoloji Kurumu Bülteni*, **47**, 47-60.

DELLALOĞLU, A. & AKSU, R. 1984. Haymana - Tuz Gölü Kaya Stratigrfi Birimleri. *TPAO Report* No. **2006**.

DEMİR, T., SEYREK, A., GUILLOU, H., SCAILLET, S., WESTAWAY, R. & BRIDGLAND, D. 2009. Preservation by basalt of a staircase of latest Pliocene terraces of the River Murat in eastern Turkey: Evidence for rapid uplift of the eastern Anatolian Plateau. *Global and Planetary Change*, **68**, 254-269.

DEMIREL, I. H. & KOZLU, H. 1997. Evaluation of burial history, thermal maturity and source-rock assessment of the Upper Paleozoic succession of the eastern Taurus region, southern Turkey. *Marine and Petroleum Geology,* **14**, 867-877.

DEMIRTAŞLI, E., BILGIN, A. Z., ERENLER, W., ISIKLAR, S., SANLI, D. Y., SELIM, M. & TURHAN, N. 1975. Geology of the Bolkar Mountains. *In:* ALPAN, S. (ed) *Congress of Earth Sciences 50th Year of the Republic, Mineral Research and Exploration Institute of Turkey (MTA)*. Special Publication, Ankara, pp. 42– 57.

DEMİRTAŞLI, E., TURHAN, N., BİLGİN, A. Z. & SELİM, M. 1984. Geology of the Bolkar Mountains. *In:* TEKELI, O. & GÖNCÜOĞLU, M. C. (eds) *Geology of the Taurus Belt.* Proceedings of the International Symposium on the Geology of the Taurus Belt, Ankara, Turkey. Mineral Resources and Exploration Institute of Turkey, 12-141.

DERCOURT, J., ZONENSHAIN, L. -P., RICOU, L. E., KAZMIN, V. G., LE PICHON, X., KNIPPER, A. L., GRANDJACQUET, C., SBORTSHIKOV, I. M., GEYSSANT, J., LEPVRIER, C., PECHIERSKY, D. H., BOULIN, J., SIBUET, J. C., SAVOSTIN, L. A., SOROKHTIN, O., WESTPHAL, M., BAZHENOV, M. L., LAUER, J. P. & BIJUDUVAL, B. 1986. Geological evolution of the Tethys belt from the Atlantic to the Pamirs since the Lias. *Tectonophysics,* **123**, 241-315.

DERCOURT, J., GAETANI, M., VRIELYNCK, B., BARRIER, E., BIJU-DUVAL, B., BRUNET, M. F., CADET, J. P., CRASQUIN, S. & SANDULESCU, M. 2000. Atlas Peri-Tethys, palaeogeographical maps. *Commission de la Carte Géologique du Monde/Commission for the Geologic Map of the World, Paris, Explanatory Notes, 269 p.*

DERMAN, A. S., ROJAY, B., GÜNEY, H. & YILDIZ, M. 2000. New sedimentological data on the evolution of Şereflikoçhisar-Aksaray fault zone. *In:* Haymana-Tuzgölü-Ulukışla Basins Workshop. *TAPG Special Publication,* **5**, 47-70.

DEWEY, J. F. & BIRD, J. M. 1970. Mountain belts and the new global tectonics. *Journal of Geophysical Research,* **75**, 2625–2647.

DEWEY, J. F. & BIRD, J. M. 1971. Origin and emplacement of the ophiolite suite: Appalachian ophiolites in Newfoundland. *Journal of Geophysical Research,* **76**, 3179–3206.

DEWEY, J.F., CANDE, S. & PITMAN III, W.C. 1989. Tectonic evolution of the Indian/Eurasia Collision Zone. *Eclogae geologicae Helvetiae,* **82**, 717–734.

DICKINSON, W. R. & SHEELY, D. R. 1979. Structure and stratigraphy of forearc regions. *American Association of Petroleum Geologists Bulletin,* **63**, 2-31.

DILEK, Y. & WHITNEY, D. L. 2000. Cenozoic crustal evolution in Central Anatolia: extension, magmatism and landscape development. *In:* PANAYIDES, I., XENOPHONTOS, C. & MALPAS, J. (eds) *Proceedings of the Third International Congress on the Geology of the Eastern Mediterranean*, Geological Survey Department, September 1998. Nicosia-Cyprus, 183–192.

DİLEK, Y. & FURNES, H. 2009. Structure and geochemistry of Tethyan ophiolites and their petrogenesis in subduction rollback systems. *Lithos,* **113**, 1-20.

DİLEK, Y. & FURNES, H. 2011. Ophiolite genesis and global tectonics: Geochemical and tectonic fingerprinting of ancient oceanic lithosphere. *Geological Society of America Bulletin,* **123**, 387–411.

DİRİK, K., GÖNCÜOĞLU, M. C. & KOZLU, H. 1999. Stratigraphy and pre-Miocene tectonic evolution of the southwestern part of the Sivas Basin, Central Anatolia, Turkey. *Geological Journal,* **34**, 303-319.

DÖNMEZ, M., AKÇAY, A. E., KARA, H., YERGÖK, A. F. & ESENTÜRK, K. 2008. Türkiye Jeoloji haritalari No.90 Kırşehir - İ30 Paftasi, 1:100 000. Maden Tektik ve Arama Genel Müdürlüğü (General Directorate of Mineral Research and Exploration), Ankarapp

DÜZGÖREN-AYDIN, N. S., MALPAS, J., GÖNCÜOĞLU, M. C. & ERLER, A. 2001. A Review of Magmatism in Central Anatolia during the Mesozoic Post-Collisional Period. *International Geology Review,* **43**, 695-710.

EKİCİ, T., ALPASLAN, M., PARLAK, O. & UÇURUM, A. 2009. Geochemistry of the Middle Miocene collision-related Yamadağı (Eastern Anatolia) calc-alkaline volcanics, Turkey. *Turkish Journal of Earth Sciences,* **18**, 511-528.

EYÜBOĞLU, Y., DILEK, Y., BOZKURT, E., BEKTAS, O., ROJAY, B. & SEN, C. 2010. Structure and geochemistry of an Alaskan-type ultramafic-mafic complex in the Eastern Pontides, NE Turkey. *Gondwana Research*, **18**, 230-252.

EYÜBOĞLU, Y., CHUNG, S-L., SANTOSH, M., DUDAS, F. O. & AKARYALI, E. 2011. Transition from shoshonitic to adakitic magmatism in the eastern Pontides, NE Turkey: Implications for slab window melting. *Gondwana Research*, **19**, 413–429.

EYÜBOĞLU, Y., SANTOSH, M., KEEWOOK, Y., BEKTAŞ, O. & KWON, S. 2012. Discovery of Miocene adakitic dacite from the Eastern Pontides Belt (NE Turkey) and a revised geodynamic model for the late Cenozoic evolution of the Eastern Mediterranean region. *Lithos*, **146-147**, 218–232.

FALINI, G., ALBECK, S. & ADDADI, L. 1996. Control of aragonite or calcite polymorphism by mollusc shell macromolecules. *Science*, **271**, 67-69.

FAYON, A. K., WHITNEY, D. L., TEYSSIER, C., GARVER, J. I. & DILEK, Y. 2001. Effects of plate convergence obliquity on timing and mechanisms of exhumation of a mid-crustal terrain, the Central Anatolian Crystalline Complex. *Earth and Planetary Science Letters*, **192**, 191-205.

FILBRANDT, S. C., NOLAN, S. C. & RIES, A. C. 1990. Late Cretaceous and early Tertiary evolution of the Jebel Ja'alan and adjacent areas, NE Oman. *In:* ROBERTSON, A. H. F., SEARLE, M. P. & RİES, S. C. (eds) *The Geology and Tectonics of the Oman Region*, The Geological Society, London, Special Publication, **49**, 697-714.

FITTON , J. G., SAUNDERS, A. D., LARSEN, L. M., HARDARSON, B. S. & NORRY, M. J. 1998. Volcanic rocks froms the southeast Greenland margin at 63^0N: composition, petrogenesis and mantle sources. *In:* SAUNDERS, A. D., LARSEN, H. C. & WİSE, S. W., JR. (eds) *Proceedings of the Ocean Drilling Program, Scientific Results,* **152**. Ocean Drilling Program, TX, 331-350.

FLOYD, P. A., GÖNCÜOĞLU, M. C., WINCHESTER, J. A. & YALINIZ, M. K. 2000. Geochemical Character and Tectonic Environment of Neotethyan Ophiolitic Fragments and Metabasites in the Central Anatolian Crystalline Complex, Turkey. *In:* BOZKURT, E., WINCHESTER, J. A. & PIPER, J. D. A. (eds) *Tectonics and*

Magmatism in Turkey and the Surrounding Area. Geological Society, London, Special Publications, **173**, 183-202.

FRIEDMANN, S. J. & BURBANK, D. W. 1995. Rift basins and supra-detachment basins: Intracontinental extensional end-members. *Basin Research*, **7**, 109-127.

GATTINGER, T. E. 1958. Vorbericht über die Revisionsarbeiten des Jahres 1957-M. 1:100,000 im Raume Malatya-Elazığ. *Maden Tetkik ve Arama* **2997** (unpublished) [in German].

GENÇ, Y. & YÜRÜR, M. T. Coeval extension and compression in Late Mesozoic-Recent thin-skinned extensional tectonics in central Anatolia, Turkey. *Journal of Structural Geology*, **32**, 623-640.

GLENNIE, K. W., HUGHES CLARKE, M. W. & BOEUF, W. G. A., PILAAR, W. F. H. & REINHARDT, B. M. 1990. Inter-relationship of Makran-Oman Mountains belts of convergence. *In:* ROBERTSON, A. H. F., SEARLE, M. P. & RIES, A. C. (eds) *The Geology and Tectonics of the Oman Region.* Geological Society, London, Special Publications, **49**, 773-786.

GLOVER, C. & ROBERTSON, A. H. F. 2003. Origin of tufa (cool-water carbonate) and related terraces in the Antalya area, SW Turkey. *Geological Journal*, **38**, 329–358.

GÖĞUŞ, O. H. & PYSKLYWEC, R. N. 2008. Mantle lithosphere delamination driving uplift and synconvergent extension in eastern Anatolia. *Geology*, **36**, 723-726.

GÖNCÜOĞLU , M. C., DIRIK, K. & KOZLU, H. 1996–1997. Pre-alpine and alpine terranes in Turkey: explanatory notes to the terrane map of Turkey. *Annalles Géologiques des Pays Héllenique*, **37**, 1–3.

GÖNCÜOĞLU, M. C. 1986. Geochronological data from the southernmost part of the Central Anatolian Massif. *Maden Tetkik ve Arama Bulletin*, **105-106**, 111-124.

GÖNCÜOĞLU, M. C., ERLER, A., TOPRAK, V., OLGUN, E., YALINIZ, M. K. & KUŞCU, I. 1991. Geology of the western part of the Central Anatolian Massif. *Türkiye Petrolleri Anonim Ortaklığı Rapor No*. *2909.*

GÖNCÜOĞLU, M. C., YALINIZ, K. M. & TEKIN, U. K. 2006. Geochemistry, tectono-magmatic discrimination and radiolarian ages of basic extrusives from the İzmir-Ankara suture belt (NW Turkey): time constraints for the Neotethyan evolution. *Ofioliti*, **31**, 25-38.

GÖRÜR, N. & DERMAN, S. 1978. Tuz Gölü-Haymana havzasının stratigrafik ve tektonik analizi. *Unpublished TPAO Report, No.1514.*

GÖRÜR, N., OKTAY, F. Y., SEYMEN, I., & ŞENGÖR, A. M. C. 1984. Palaeotectonic evolution of the Tuzgölü basin complex, Central Turkey: sedimentary record of a Neo-Tethyan closure. *In*: DIXON, J. E. & ROBERTSON, A. H. F. (eds.) *The Geological Evolution of the Eastern Mediterranean*. The Geological Society, London, Special Publications, **17**, 467-482.

GÖRÜR, N., TÜYSÜZ, O. & ŞENGÖR, A. M. C. 1998. Tectonic evolution of the Central Anatolian basins. *International Geology Review,* **9**, 832-850.

GÖRÜR, N. & TÜYSÜZ, O. 2001. Cretaceous to Miocene palaeogeographic evolution of Turkey: implications for hydrocarbon potential. *Journal of Petroleum Geology,* **24**, 119-146.

GRADSTEIN, F. M., OGG, J. G., SMITH, A. G. & AL, E. 2004. A Geologic Time Scale. *Cambridge University Press*, pp.

GÜNDOGAN, İ., ÖNAL, M. & DEPÇİ, T. 2005. Sedimentology, petrography and diagenesis of Eocene-Oligocene evaporites: the Tuzhisar Formation, SW Sivas Basin, Turkey. *Journal of Asian Earth Sciences,* **25**, 791-803.

GÜRBÜZ, K. & GÜL, M. 2005. Evolution of and factors controlling Eocene Sedimentation in the Darende-Balaban Basin, Malatya (Eastern Turkey). *Turkish Journal of Earth Sciences,* **14**, 311-335.

GÜRER, Ö. F. 1994. Upper Cretaceous stratigraphy of Hekimhan-Hasançelebi region and the basin evolution. *Geological Bulletin of Turkey,* **37**, 135-148.

GÜRER, Ö. F. 1996. Geological position and the genesis of Hasançelebi alkaline magmatism at [*sic*] the Eastern Taurides (NW Malatya). *Turkish Journal of Earth Sciences,* **5**, 71-88.

GÜRER, Ö. F. & ALDANMAZ, E. 2002. Origin of the Upper Cretaceous-Tertiary sedimentary basins within the Tauride-Anatolide platform in Turkey. *Geology Magazine,* **139**, 191-197.

GÜRSOY, H., PIPER, J. D. A., TATAR, O. & TEMIZ, H. 1997. A palaeomagnetic study of the Sivas Basin, central Turkey: Crustal deformation during lateral extrusion of the Anatolian Block. *Tectonophysics,* **271**, 89-105.

GÜRSOY, H., TATAR, O., PIPER, J. D. A., KOÇBULUT, F., AKPINAR, Z., HUANG, B., ROBERTS, A. P. & MESCİ, B. L. 2011. Palaeomagnetic study of the Kepezdağ and Yamadağ volcanic complexes, central Turkey: Neogene tectonic escape and block definition in the central-east Anatolides. *Journal of Geodynamics,* **51**, 308-326.

HARZHAUSER, M., PILLER, W. E. & STEININGER, F. F. 2002. Circum-Mediterranean Oligo-Miocene biostratigraphic evolution – the gastropods' point of view. *Paleogeography, Paleoclimatology, Paleoecology*, **183**, 103–133.

HATZIPANAGIOTOU, K., TSIKOURAS, B., MIGIROS, G., GARTZOS, E. & SERELIS, K. 2003. Origin of rodingites in ultramafic rocks from Lesvos Island (NE Aegean, Greece). *Ofioliti,* **28**, 13-23.

HAY, W. W. 2008. Evolving ideas about the Cretaceous climate and ocean circulation. *Cretaceous Research,* **29**, 725-753.

Hempton, M.R. 1987. Constraints on Arabian plate motion and extensional history of the Red Sea: Tectonics, **6**, 687–705.

HINSCHBERGER, F., MALOD, J.-A., RÉHAULT, J.-P., VILLENEUVE, M., ROYER, J.-Y. & BURHANUDDIN, S. 2005. Late Cenozoic geodynamic evolution of Eastern Indonesia. *Tectonophysics,* **404**, 91-118.

HÜSİNG, S. K., ZACHARİASSE, W-J., VAN HİNSBERGEN, D. J. J., KRİJGSMAN, W., INCEÖZ, M., HARZHAUSER, M., MANDİC, O. & KROH, A. 2009. Oligocene-Miocene basin evolution in SE Anatolia, Turkey: constraints on the closure of the eastern Tethys gateway. *In*: VAN HINSBERGEN, D. J. J., EDWARDS, M. A. & GOVERS, R. (eds) *Collision and Collapse at the Africa–Arabia–Eurasia Subduction Zone.* The Geological Society, London, Special Publications, **311**, 107–132.

ILBEYLI, N. 2005. Mineralogical–geochemical constraints on intrusives in central Anatolia, Turkey: tectono-magmatic evolution and characteristics of mantle source. *Geological Magazine,* **142**, 187-207.

ILBEYLI, N., PEARCE, J. A., THIRLWALL, M. F. & MITCHELL, J. G. 2004. Petrogenesis of collision-related plutonics in Central Anatolia, Turkey. *Lithos*, **72**, 163-182.

ILBEYLI, N. & KIBICI, Y. 2009. Collision-related granite magma genesis, potential sources and tectono-magmatic evolution: comparison between central, northwestern and western Anatolia (Turkey). *International Geology Review*, **51-3**, 252-278.

JAMES, D. E. 1971. Plate tectonic model for the evolution of the Central Andes. *Geological Society of America, Bulletin,* **82**, 3325-3346.

JAFFEY, M & ROBERTSON, A. H. F. 2001. New sedimentological and structural data from the Eçemiş Fault Zone, southern Turkey: implications for its timing and offset and the Cenozoic tectonic escape of Anatolia. *Journal of the Geological Society, London,* **18**, 367-378.

KADIOĞLU, Y. K., DILEK, Y., GÜLEÇ, N. & FOLAND, K. A. 2003. Tectonomagmatic Evolution of Bimodal Plutons in the Central Anatolian Crystalline Complex, Turkey. *The Journal of Geology*, **111**, 671-690.

KADIOĞLU, Y. K., DILEK, Y. & FOLAND, K. A. 2006. Slab break-off and syncollisional origin of the Late Cretaceous magmatism in the Central Anatolian crystalline complex, Turkey *Postcollisional tectonics and magmatism in the Mediterranean region and Asia*. Geological Society of America Special Paper, **409**, 381-415.

KALELIOĞLU, O., ZORLU, K., KURT, M. A., GUL, M. & GULER, C. 2009. Delineating compositionally different dykes in the Ulukışla Basin (Central Anatolia, Turkey) using computer-enhanced multi-spectral remote sensing data. *International Journal of Remote Sensing,* **30**, 2997-3011.

KAVAK, K., POISSON, A. & GUEZOU, J. 1997. Tectonostratigraphy of the Southern Sivas Tertiary Basin (Central Turkey) and Comparison with Landsat MSS Imagery. *International Geology Review*, **39**, 353 - 364.

KAYGUSUZ, A., ARSLAN, M., SIEBEL, W. & ŞEN, C. 2011. Geochemical and Sr-Nd isotopic characteristics of post-collisional calc-alkaline volcanics in the Eastern Pontides (NE Turkey). *Turkish Journal of Earth Sciences,* **20**, 137-159.

KAYMAKCI, N., WHITE, S. H. & VAN DIJK, P. M. 2000. Paleostress inversion in a multiphase deformed area: Kinematic and structural evolution of the Çankırı Basin (central Turkey), part 1. *In:* Bozkurt, E., Winchester, J. A. & and Piper, J. D. A. (eds) *Tectonics and Magmatism in Turkey and the Surrounding Area*. The Geological Society, London, Special Publication, **173**, 445–473.

KAYMAKCI, N., DUERMEIJER, C. E., LANGEREIS, C., WHITE, S. H. &. VAN DIJK, P. M. 2003a. Palaeomagnetic evolution of the Çankırı basin (central Anatolia, Turkey): Implications for oroclinal bending due to indentation. *Geological Magazine,* **140**, 343–355.

KAYMAKCI, N., WHITE, S. H. & VANDIJK, P. M. 2003b. Kinematic and structural development of the Çankiri Basin (Central Anatolia, Turkey): a paleostress inversion study. *Tectonophysics,* **364**, 85-113.

KAYMAKCI, N., İNCEÖZ, M. & ERETPINAR, P. 2006. 3D-Architecture and Neogene Evolution of the Malatya Basin: Inferences for the kinematics of the Malatya and Ovacik Fault Zones. *Turkish Journal of Earth Sciences,* **15**, 123–154.

KAYMAKCI, N., ÖZÇELİK, Y., WHITE, S. H. & VAN DIJK, P. M. 2009. Tectono-stratigraphy of the Çankırı Basin: Late Cretaceous to early Miocene evolution of the Neotethyan Suture Zone in Turkey. *In:* VAN HINSBERGEN, D. J. J., EDWARDS, M. A. & GOVERS, R. (eds) *Collision and Collapse at the Africa–Arabia–Eurasia Subduction Zone.* The Geological Society, London, Special Publications, **311**, 67–106.

KAYSERI, M. S. & AKGÜN, F. 2008. Palynostratigraphy, palaeovegetational and palaeoclimatic investigation on the Miocene deposits in Central Anatolia (Çorum and Sivas Basin). *Turkish Journal of Earth Sciences,* **17**, 361-403.

KAZMIN, V. G. & TIKHONOVA, N. F. 2006. Evolution of early Mesozoic back-arc basins in the Black Sea-Caucasus segment of a Tethyan active margin. *In:* ROBERTSON, A. H. F. & MOUNTRAKIS, M. (eds) *Tectonic Development of the Eastern Mediterranean Region*. Geological Society, London, Special Publications, **260**, 179-200.

KEAREY, P., KLEPEIS, K. A. & VINE, F. J. 2009. Global Tectonics (3rd. ed). *Chichester, Wiley*.

KELLER, G., & ADATTE, T., BURNS, S. J. & TANTAWY, A. A. 2002. High-stress paleoenvironment during the late Maastrichtian to early Paleocene in Central Egypt. *Palaeogeography, Palaeoclimatology, Palaeoecology,* **187**, 35-60.

KELLING, G., ROBERTSON, A. H. F. & VAN BUCHEM, F. 2005. Cenozoic sedimentary basins of southern Turkey: an introduction. *Sedimentary Geology,* **173**, 1-14.

KESKIN, M., PEARCE, J. A. & MITCHELL, J. G. 1998. Volcano-stratigraphy and geochemistry of collision-related volcanism on the Erzurum-Kars Plateau, northeastern Turkey. *Jounral of Volcanology and Geothermal Research*, **85**, 355-404.

KESKİN, M. 2003. Magma generation by slab steepening and breakoff beneath a subduction-accretion complex: An alternative model for collision-related volcanism in Eastern Anatolia, Turkey. *Geophysical Research Letters*, **30**, 8046.

KESKİN, M., GENÇ, Ş. C. & TÜYSÜZ, O. 2008. Petrology and geochemistry of post-collisional Middle Eocene volcanic units in North-Central Turkey: Evidence for magma generation by slab break off following the closure of the Northern Neotethys Ocean. *Lithos,* **104**, 267-305.

KOÇYIĞIT, A. 1991. An example of an accretionary forearc basin from northern central Anatolia and its implications for the history of subduction of Neo-Tethys in Turkey. *Geological Society of America Bulletin*, **103**, 22-36.

KÖKSAL, S., ROMER, R. L., GÖNCÜOĞLU, M. C. & TOKSOY-KÖKSAL, F. 2004. Timing of postcollisional H-type to A-type granitic magmatism: U–Pb titanite ages from the Alpine central Anatolian granitoids (Turkey). *International Journal of Earth Sciences*, **93**, 974-989.

KÖKSAL, S., GÖNCÜOĞLU, M. C., TOKSOY-KÖKSAL, F., MÖLLER, A. & KEMNITZ, H. 2008. Zircon typologies and internal structures as petrogenetic indicators in contrasting granitoids types from central Anatolia, Turkey. *Mineralogy and Petrology*, **93**, 185-211.

KURT, M. A., ALPASLAN, M., GÖNCÜOĞLU, M. C. & TEMEL, A. 2008. Geochemistry of late stage medium to high-K calc-alkaline and shoshonitic dykes in the Ulukışla Basin (Central Anatolia, Turkey): petrogenesis and tectonic setting. *Geochemistry International*, **46**, 1145-1163.

KURTMAN, F. (1961). Geologie des Gebietes zwischen Sivas und Divriği sowie Bemerkungen über die Gipsserie. *Maden Tetkik ve Arama Bulletin* **56** [in German].

KÜRÜM, S., ÖNAL, A., BOZTUĞ, D., SPELL, T. & ARSLAN, M. 2008. $^{40}Ar/^{39}Ar$ age and geochemistry of the post-collisional Miocene Yamadağ volcanics in the Arapkir area (Malatya Province), eastern Anatolia, Turkey. *Journal of Asian Earth Sciences*, **33**, 229–251.

KUŞCU, I., GENÇALIOGLU KUSCU, G., MEINERT, L. D. & FLOYD, P. A. 2002. Tectonic setting and petrogenesis of the Çelebi granitoid, (KIrIkkale-Turkey) and comparison with world skarn granitoids. *Journal of Geochemical Exploration*, **76**, 175-194.

KUŞCU, I., YILMAZER, E., DEMİRELA, G., GÜLEÇ, N., KUŞCU, G., KAYMAKCI, N., GÖKÇE, H., ŞALIS¸, B., AND MARSCHİK, R. 2007. Hasançelebi-Hekimhan (Malatya) Bölgeleri emiroksit Yataklarının Demir Oksit-Bakır-Altın (DOBA) Yatakları Açısından I·ncelenmesi ve Bakır-Altın Potansiyellerinin Aras¸tırılması: *TÜBI·TAK Project-ÇAYDAG 103Y023, 190* [in Turkish with English abstract].

KUŞCU, I., KUŞCU, G. G., TOSDAL, R. M., ULRICH, T. D. & FRIEDMAN, R. 2010. Magmatism in the southeastern Anatolian orogenic belt: transition from arc to post-collisional setting in an evolving orogen. *In:* SOSSON, M., KAYMAKCI, N., STEPHENSON, R. A., BERGERAT, F. & STAROSTENKO, V. (eds) *Sedimentary Basin tectonics from the Black Sea and Caucasus to the Arabian Platform.* The Geological Society, London, Special Publications, **340**, 437–460.

KUŞCU, İ., YILMAZER, E., GÜLEÇ, N., BAYIR, S., DEMIRELA, G., KUŞCU, G. G., KURU, G. S. KAYMAKŞI, N. 2011. U-Pb and ^{40}Ar-^{39}Ar Geochronology and isotopic constraints on the genesis of copper-gold-bearing iron oxide deposits in the Hasançelebi district, Eastern Turkey. *Economic Geology,* **106**, 261–288.

KUTLUAY, A., DİRİK, K., CİNER, A. & BERTOTTİ, G. 2010. 3D architecture and Miocene evolution of the Tuz Gölü Basin in Central Anatolian plateau, Turkey. *EGU General Assembly, Vienna, p.15042.*

LE MAITRE, R. W., BATEMAN, P., DUDEK, A., KELLER, J., LAMEYRE LE BAS, M. J., SABİNE, P. A., SCHMİD, R., SORENSEN, H., STRECKEİSEN, A., WOOLLEY, A. R. & ZANETTİN, B. 1989. A classification of igneous rocks and glossary of terms. *Blackwell, Oxford.*

LE MAITRE, R. W., STRECKEISEN, A., ZANETTIN, B., LE BAS, M. J., BONIN, B., BATEMAN, P., BELLIENI, G., DUDEK, A., EFREMOVA, S., KELLER, J., LAMERE, J., SABINE, P. A., SCHMID, R., SORENSEN, H. & WOOLEY, A. R. 2002. Igneous Rocks: A Classification and Glossary of Terms, Recommendations of the International Union of Geological Sciences, Subcommission of the Systematics of Igneous Rocks. *Cambridge University Press.*

LEFEBVRE, C. 2011. Unpublished PhD Thesis. The tectonics of the Central Anatolian Crystalline Complex: a structural, metamorphic and palaeomagnetic study. The University of Utrecht, Netherlands.

LEO, G. W., MARVIN, R. F. & MEHNERT, H. H. 1974. Geologic framework of the Kuluncak-Sofular area, East-Central Turkey, and K-Ar ages of igneous rocks. *Geological Society of America Bulletin,* **85**, 1785–1788.

LIPPARD, S. J., SHELTON, A. W. & GASS, I. G. l986. The Ophiolite of Northern Oman. *Geological Society of London, Memoir,* **11**.

MACKENZIE, W. S., DONALDSON, C. H. & GUILFORD, C. 1997. *Atlas of Igneous Rocks and their Tectures*. 7th edition. Addison Wesley Longman Limited, Essex.

MACKINTOSH, P. W., 2008. Unpublished PhD thesis. Tectonic-sedimentary evolution of the northern margin of Gondwana during Late Palaeozoic – Early Cenozoic time in the Eastern Mediterranean region: evidence from the Central Taurus Mountains, Turkey. University of Edinburgh, UK.

MACKINTOSH, P. W. & ROBERTSON, A. H. F. 2009. Structural and sedimentary evidence from the northern margin of the Tauride platform in south central Turkey used to

test alternative models of Tethys during Early Mesozoic time. *Tectonophysics*, **473**, 149-172.

MACKINTOSH, P. W. & ROBERTSON, A. H. F. 2012. Late Devonian-Late Triassic sedimentary development of the central Taurides, S Turkey: implications for the northern margin of Gondwana. *Gondwana Research,* **21-4**, 1089-1114.

MACKINTOSH, P. W. & ROBERTSON, A. H. F. Sedimentary and structural evidence for a two-phase Upper Cretaceous and Paleogene emplacement of the Tauride thrust sheets in central southern Turkey. *Geological Society, London, Special Publication.* In press.

MANN, A., HANNA, S. S. & NOLAN, S. C. 1990. The post-Campanian tectonic evolution of the Central Oman Mountains: Tertiary extension of the Eastern Arabian Margin. *In*: ROBERTSON, A. H. F., SEARLE, M. P. AND RIES, A. C. (eds) *The Geology and Tectonics of the Oman Region*. The Geological Society, London, Special Publication, **49**, 549-563.

MARSCHIK, T., SPIKINGS, R. & KUŞCU, İ. 2008. Geochronology and stable isotope signature of alteration related to hydrothermal magnetite ores in Central Anatolia, Turkey. *Mineralium Deposita,* **43**, 111–124.

MARTINEZ, F., FRYER, P., BAKER, N. A. & YAMAZAKI, T. 1995. Evolution of backarc rifting: Mariana Trough. *Journal of Geophysical Research,* **100**, 3807-3827.

MATTHAI, G. 1948. On the mode of growth of the skeleton in Fungid Corals. *Philosophical Transactions of the Royal Society of London,* **233**, 177-195.

MCLENNAN, S. M., ROSS TAYLOR, S. & HEMMING, S. R. 2006. Composition, differentiation, and evolution of continental crust: constraints from sedimentary rocks and heat flow. *In:* BROWN, M. & RUSHMER, T. (eds) *Evolution and differentiation of the continental crust.* Cambridge University Press, 92–134.

MEIJERS, M. J. M., KAYMAKCI, N., VAN HINSBERGEN, D. J. J., LANGEREIS, C. G., STEPHENSON, R. A. & HIPPOLYTE, J-C. 2010. Late Cretaceous to Paleocene oroclinal bending in the central Pontides (Turkey). *Tectonics,* **29**, TC4016.

MESCHEDE, M. & FRISCH, W. 1998. A plate tectonic model for the Mesozoic and Early Cenozoic history of the Caribbean plate. *Tectonophysics,* **296**, 269-291.

MILLER, K. G., KOMINZ, M. A., BROWNING, J. V., WRIGHT, J. D., MOUNTAIN, G. S.,KATZ, M. E., SUGARMAN, P. J., CRAMER, B, S., CHRISTIE-BLICK, N. & PEKAR, S. F. 2005. The Phanerozoic Record of Global Sea-Level Change, *Science,* **25**, 1293–1298.

MILSOM, J. 2001. Subduction in Eastern Indonesia: how many slabs? *Tectonophysics,* **338**, 167-178.

MILSOM, J., BARRETTO, J., AGUDA, N., BRINGAS, D., HO, R. & AITCHISON, J. 2009. The gravity fields of Palawan and New Caledonia insights into the subsurface geometries of ophiolites. *Journal of the Geological Society, London,* **166**, 985–988.

MOIX, P., BECCALETTO, L., KOZUR, H. W., HOCHARD, C., ROSSELET, F., & STAMPFLI, G. M., 2008. A new classification of the Turkish terranes and sutures and its implication for the palaeotectonic history of the region. *Tectonophysics*, 451, 7-39.

MTA. 2001. 1:500 000, Geological Map of Turkey, Ankara-Turkey.

NAIRN, S. P. 2010. Unpublished PhD thesis. Testing alternative models of continental collision in Central Turkey by a study of the sedimentology, provenance and tectonic setting of Late Cretaceous–Early Cenozoic syn-tectonic sedimentary basins. University of Edinburgh, UK.

NAIRN, S. P, ROBERTSON, A. H. F., ÜNLÜGENÇ, U. C., İNAN, N & TASLI, K. Tectonostratigraphic evolution of the Upper Cretaceous–Cenozoic central Anatolian basins: an integrated model of diachronous ocean basin closure and continental collision. *Geological Society, London, Special Publications, **372**, in press.*

NAZİK, A. 1993. Micropalaeontological (ostracoda and foraminifera) investigation of Tertiary sequence of Darende Basin. *Geological Society of Turkey Bulletin,* **36**, 13-36 [in Turkish with English abstract].

NICHOLS, G., 1999. *Sedimentology and Stratigraphy*. Blackwell Science Ltd, Cambridge. pp

NILSEN, T. H. & MCKEE, E. H. 1979. Paleogene palaeogeography of the western United States. *In:* ARMENTROUT, J. M., COLE, M. R. & TERBEST, H. JR. (eds) *Cenozoic Paleogeography of the Western United States.* Pacific Section, Society of Economic Paleontologists and Mineralogists. Pacific Coast Paleogeography Symposium, **3**, 257-276.

NORMAN, T. N. 1972. Ankara Yahşihan bölgesinde Üst Kretase-Alt Terisyer istifinin stratigrafisi. *Geological Society of Turkey Bulletin* **15**, 180-276 [in Turkish].

---, 1973a. Ankara Yahşıhan bölgesinde Üst Kretase-Alt Tersiyer sadimentasyonu. *Bulletin of the Geological Society of Turkey*, **16**, 41-66 [in Turkish].

---, 1973b. Ankara Yahşıhan bölgesinin Eosen'den sonraki tektonik gelişmesi. *Bulletin of the Geological Society of Turkey*, **16**, 67-81 [in Turkish].

OBERHANSLI, R., POURTEAU, A., CANDAN, O, ÇETINKAPLAN, M. & BOUSQUET, R. 2010. Peritethyan high pressure belts. *7th International Symposium on Eastern Mediterranean Geology, 18-22 October 2010, University of Çukurova, Adana, Turkey, p. 2.*

ODIN, G.S. 1988. Green marine clays. *Development in sedimentology*, **45**. Elsevier, Amsterdam.

OCAKOĞLU, F. 2001. Repetitive subtidal-to-coastal sabkha cycles from a Lower-Middle Miocene marine sequence, Eastern Sivas Basin. *Turkish Journal of Earth Sciences,* **10**, 17-34.

OKTAY, F. Y. 1973. Sedimentary and tectonic history of the Ulukışla area, southern Turkey. Unpublished PhD Thesis, University of London, 414 pp.

OKTAY, F. Y. 1982. Ulukışla ve everesinin stratigrafisi ve jeolojik evrimi. Bulletin of the Geological Society of Turkey, **25**, 15– 23.

OKAY, A. I. & ŞAHINTÜRK, Ö. 1997. Geology of the Eastern Pontides. *In:* ROBINSON, A.G. (ed) *Regional and Petroleum Geology of the Black Sea and Surrounding Region.* American Association of Petroleum Geologists Memoir, **68**, 291-311.

OKAY, A. I. & TÜYSÜZ, O. 1999. Tethyan sutures of Northern Turkey. *In:* DURAND, B., JOLIVET, L., HORVÁRTH, F. & SÉRANNE, M. (eds) *The Mediterranean Basins: Tertiary Extension within the Alpine Orogen.* The Geological Society, London, Special Publications, **156**, 475–515.

OKAY A. I., TANSEL, I. & TÜYSÜZ, O. 2001. Obduction, subduction and collision as reflected in the Upper Cretaceous-Lower Eocene sedimentary record of western Turkey. *Geological Magazine* **138**, 117-142.

OKAY, A. I. & GÖNCÜOĞLU, M. C. 2004. The Karakaya Complex: A Review of Data and Concepts. *Turkish Journal of Earth Sciences,* **13**, 75-95.

OKAY, A. I. & SATIR, M., 2006. Geochronology of Eocene plutonism and metamorphism in northwest Turkey: evidence for a possible magmatic arc. *Geodinamica Acta*, **19**, 251-266.

OKAY, A, I., ZATTIN, M. & CAVAZZA, W. 2010. Apatite fission-track data for the Miocene Arabia-Eurasia collision. *Geology*, **38,** 35-38.

ONAL, K. M., BUYUKSARAC, A., AYDEMIR, A. & ATES, A. 2008. Investigation of the deep structure of the Sivas Basin (innereast Anatolia, Turkey) with geophysical methods. *Tectonophysics*, **460**, 186-197.

ORTNER, H., REITER, F. & ACS, P., 2002. Easy handling of tectonic data: the programs TectonicVB for Mac and TectonicsFP for Windows(TM). *Computers & Geosciences,* **28**, 1193-1200.

ÖZDEMİR, Z. & TUNÇ, M. 1993. Palaeontologic and stratigraphic features of Upper Cretaceous units in the vicinity of Hekimhan (Malatya). *Geological Bulletin of Turkey,* **36**, 131-144 [in Turkish with English abstract].

ÖZER, S. 1988. The paleontology and biogeography of the pironaean (Rudist) species from the Central-East-Southeast Anatolia and Kocaeli Peninsula. *Türkiye Jeoloji Bülteni,* **31**, 47-58.

ÖZER, S., MERİÇ, E., GÖRMÜŞ, M. & KANBUR, S. 2009. Biogeographic distribution of rudists and benthic foraminifera: An approach to Campanian-Maastrichtian Palaeobiogeography of Turkey. *Geobios,* **42**, 623-638.

ÖZGENÇ, I. & İLBEYLİ, N. 2009. Geochemical constraints on pertogenesis of Late Cretaceous alkaline magmatism in east-central Anatolia (Hasançelebi-Basören, Malatya), Turkey. *Mineralogy & Petrology,* **95**, 71-85.

ÖZGÜL, N. 1997. Stratigraphy of the tectono-stratigraphic units in the region Bozkır-Hadim-Taşkent (northern central Taurides). *Maden Tetkik ve Arama Bulletin,* **119,** 113-174 [in Turkish].

PAMLER, M. R., HELVACÍ, C. & FALLICK, A. E. 2004. Sulphur, sulphate oxygen and strontium, isotope composition of Cenozoic Turkish evaporates. *Chemical Geology*, **209**, 341-356.

PARLAK, O., HOECK, V. & DELALOYE, M. 2000. Suprasubduction zone origin of the Pozantı-Karsantı ophiolite (southern Turkey) deduced from whole-rock and mineral chemistry of the gabbroic cumulates. *In:* BOZKURT, E., WINCHESTER J. A., PIPER J. D. A. (eds) *Tectonics and Magmatism in Turkey and the Surrounding Area*. Geological Society, London, Special Publications, **173**, 219–234.

PARLAK, O. & ROBERTSON, A. H. F. 2004. The ophiolite-related Mersin Melange, southern Turkey: its role in the tectonic-sedimentary setting of Tethys in the Eastern Mediterranean region. *Geological Magazine,* **141**, 257-286.

PARLAK, O., HÖCK, V., KOZLU, H. & DELALOYE, M. 2004. Oceanic crust generation in an island arc tectonic setting, SE Anatolian orogenic belt (Turkey). *Geological Magazine,* **141**, 583-603.

PARLAK. O., YILMAZ, H., BOZTUĞ, D. 2006. Origin and significance of the metamorphic sole of the Divriği Ophiolite (Sivas, Turkey): evidence for slab break-off prior to ophiolite emplacement. *Turkish Journal of Earth Sciences*, **15**, 25-45.

PARLAK, O., RIZAOĞLU, T., BAĞCI, U., KARAOĞLAN, F. & HÖCK, V. 2009. Tectonic significance of the geochemistry and petrology of ophiolites in southeast Anatolia, Turkey. *Tectonophysics*, **473**, 173-187.

PARLAK, O., KARAOĞLAN, F., RIZAOĞLU, T., NURLU, N., BAĞCI, U., HÖCK, V., ÖNAL, A., KÜRÜM, S. & TOPAK, Y. 2012. Petrology of the Ispendere (Malatya) ophiolite from Southeast Anatolia: implications for the Late Mesozoic evolution of the southern Neotethyan Ocean. *In review.*

PEARCE, J. A. & CANN, J. R. 1973. Tectonic setting of basic volcanic rocks determined using trace element analysis. *Earth and Planetary Science Letters*, **19**, 290–300.

PEARCE, J. A. & NORRY, M. J. 1979. Petrogenetic implications of Ti, Zr, Y and Nb variations in volcanic rocks. *Contributions to Mineralogy and Petrology*, **69**, 33–47.

PEARCE, J. A. 1982. Trace element characteristics of lavas from destructive plate boundaries. *In:* THORPE, R. S. (ed) *Andesites.* Wiley, Chichester, 525-548.

PEARCE, J. A. 1983. Role of the sub-continental lithosphere in magma genesis at active continental margins. *In:* HAWKESWORTH, C. J. & NORRY, M. J. (eds) *Continental Basalts and Mantle Xenoliths.* Shiva, Nantwich, 230-249.

PEARCE, J. A., 1996. A user's guide to basalt discrimination diagrams. *In:* D.A. WYMAN (ed) *Trace element geochemistry of volcanic rocks: Applications for massive sulphide exploration*. Geological Association of Canada, Short Course Notes, **12**, 79-113.

PEARCE, J. A., BENDER, J. F., DE LONG, S. E., KIDD, W. S. F., LOW, P. J., GÜNER, Y., SAROGLU, F., YILMAZ, Y., MOORBATH, S. & MITCHELL, J. G. 1990. Genesis of collision volcanism in Eastern Anatolia, Turkey. *Journal of Volcanology and Geothermal Research*, **44**, 189-229.

PEARCE, J. A., LIPPARD, S. J. & ROBERTS, S. 1984. Characteristics and tectonic significance of supra-subduction zone ophiolites. *In:* KOKELAAR, B. P. & HOWELLS, M. F. (eds) *Marginal Basin Geology: Volcanic and Associated Sedimentary and Tectonic Processes in Modern and Ancient Marginal Basins.* The Geological Society, London, Special Publications, **16**, 77-89.

PEDLEY, H. M. 1990. Classification and environmental models of cool freshwater tufas. *Sedimentary Geology*, **68**, 143–154.

PERİNÇEK, D. & KOZLU, H. 1984. Stratigraphy and structural relations of the units in the Afşin-Elbistan-Doğanşehir region (Eastern Taurus). *In:* TEKELI, O. & GÖNCÜOĞLU, M. C. (eds.) *Geology of the Taurus Belt*. Proceedings of the International Symposium on the Geology of the Taurus Belt, MTA, Turkey, 182-198.

PICCARDO, G. B., VANNUCCI, R. & GUARNIERI, L. 2009, Evolution of the lithospheric mantle in an extensional setting: Insights from ophiolitic peridotites. *Lithos*, **1**, 81–87.

PICKERING, K. T., HISCOTT, R. N. & HEIN, F. J. 1989. *Deep marine environments, clastic sedimentation and tectonics*. Unwin Hyman London. 416 pp

POURTEAU, A., CANDAN, O. & OBERHÄNSLI, R. 2010. High-Pressure metasediments in central Turkey: constraints on the Neotethyan closure history. *Tectonics*, **29**, 18pp.

RAMOS, V. A. & KAY, S. M. 2006. Overview and tectonic evolution of the southern Central Andes of Mendoza and Neuqúen (35^{o}–39^{o}S latitude). *In:* KAY, S. M. & RAMOS, V. A. (eds) *Evolution of an Andean margin: A tectonic and magmatic view from the Andes to the Neuqúen Basin (35^{o}–39^{o}S latitude)*. Geological Society of America, Special Paper, **407**, 1-17.

RAMPONE, E., ROMAIRONE, A., ABOUCHAMI, W., PICCARDO, G. B. & HOFMANN, A. W. 2005. Chronology, petrology, and isotope geochemistry of the Erro-Tobbio peridotites (Ligurian Alps, Italy): Records of late Palaeo zoic lithospheric extension. *Journal of Petrology*, **46**, 799–827.

RAWLING, T. J. & LISTER, G. S. 1999. Oscillating modes of orogeny in the Southwest Pacific and the tectonic evolution of New Caledonia. *In:* RING, U., BRANDON, M. T., LISTER, G. S. & WILLETT, S. D. (eds) *Exhumation Process: Normal Faulting, Ductile Flow and Erosion.* The Geological Society, London, Special Publications, **154**, 109–127.

RAYMOND, L.A. 1984. Classification of mélanges. *In:* RAYMOND, L. A. (ed) *Mélanges: Their nature, origin, and significance*. Geological Society of America Special Paper, **198**, 7-20.

RICE, S. P. 2005. Unpublished PhD Thesis. The role of an Upper Cretaceous volcanic arc and related units in tectonic assembly of the Tethyan suture zone, Central and Eastern Pontides, North Turkey. The University of Edinburgh, UK.

RICE, S. P., ROBERTSON, A. H. F. & USTAÖMER, T. 2006. Late Cretaceous-Early Cenozoic tectonic evolution of the Eurasian active margin in the Central and Eastern Pontides, northern Turkey. *In:* ROBERTSON, A. H. F. & MOUNTRAKIS, D. (eds) *Tectonic Development of the Eastern Mediterranean Region*. The Geological Society, London, Special Publications, **260**, 413-445.

RICE, S., ROBERTSON, A. H. F., USTAÖMER, T., N. İNAN & K. TASLI, K. 2009. Late Cretaceous-Early Eocene tectonic development of the Tethyan suture zone in the Erzincan area, Eastern Pontides, Turkey. *Geological Magazine*, **46**, 567-590.

RICOU, L.-E. l996. The plate tectonic history of the past Tethys ocean. *In:* NAIRN, A. E. M., RICOU, L. E., VRIELINCK, B. & DERCOURT, J. (eds) The Ocean Basins and Margins, **8**, The Tethys Ocean, Plenum Press, New York & London 3-70.

RIGO DE RIGHI, M. & CORTESINI, A. 1959. Regional studies of the Central Anatolian basin, *Progress Report. Unpubl. Petro Isleri rep.*, no. **11**.

ROBERTSON, A. H. F. 1977. The origin and diagenesis of cherts from Cyprus. *Sedimentology*, **24**, 11–30.

ROBERTSON, A. H. F. 1989. Palaeoceanography and tectonic setting of the Jurassic Coast Range ophiolite, Central California: Evidence from the extrusive rocks and the volcaniclastic sediment cover. *Marine & Petroleum Geology*, **6**, 194–220.

ROBERTSON, A. H. F. l994. Role of the tectonic facies concept in orogenic analysis and its application to Tethys in the Eastern Mediterranean region. *Earth-Science Reviews*, **37**, 139-213.

ROBERTSON, A. H. F. 2002. Overview of the genesis and emplacement of Mesozoic ophiolites in the Eastern Mediterranean Tethyan region. *Lithos*, **65**, 1-67.

ROBERTSON, A. H. F. 2004. Development of concepts concerning the genesis and emplacement of Tethyan ophiolites in the Eastern Mediterranean and Oman regions. *Earth-Science Reviews*, **66**, 331-387.

ROBERTSON, A. H. F. 2006. Contrasting modes of ophiolite emplacement in the Eastern Mediterranean region. *In:* GEE, D. G. & STEPHENSON, R. A. (eds) 2006. *European Lithosphere Dynamics*. The Geological Society, London, Memoirs, **32**, 235–261.

ROBERTSON, A. H. F. & BOYLE, J. F. 1983. Tectonic setting and origin of metalliferous sediments in the Mesozoic Tethys Ocean. *In:* RONA, P. A., BOSTROM, K., LAUBIER, L. & SMITH, K. L. JR. (eds). *Hydrothermal Processes of Seafloor Spreading Centres.* Plenum, New York, 595-663.

ROBERTSON, A. H. F. & DIXON, J.E. 1984. Introduction: aspects of the geological evolution of the Eastern Mediterranean. *In*: DIXON, J.E., ROBERTSON, A.H.F. (eds) *Geological Evolution of the Eastern Mediterranean*, The Geological Society, London, Special Publication, **17**, 1-74.

ROBERTSON, A. H. F. & SEARLE, M. P. l990. The northern Oman Tethyan continental margin: stratigraphy, structure, concepts and controversies. *In*: ROBERTSON, A. H. F., SEARLE, M. P. AND RIES, A. C. (eds) *The Geology and Tectonics of the Oman Region*. The Geological Society, London, Special Publication, **49**, 3-25.

ROBERTSON, A. H. F., CLIFT, P. D., DEGNAN, P. J. & JONES, G. 1991. Palaeogeographic and palaeotectonic evolution of the Eastern Mediterranean Neotethys. *Palaeogeography, Palaeoclimatology, Palaeoecology*, **87**, 289-343.

ROBERTSON, A. H. F. & XENOPHONTOS, C. 1993. Development of concepts concerning the Troodos ophiolite and adjacent units in Cyprus. *In:* PRICHARD, H. M., ALABASTER, T., HARRIS, N. B. & NEARY, C. R. (eds) *Magmatic Processes and Plate Tectonics.* Geological Society, London, Special Publication, **76**, 85–119.

ROBERTSON, A. H. F. & SHARP, T. R. 2002. Geochemical and mineralogical evidence for the provenance of mixed volcanogenic/terrigenous hemipelagic sediments in the Pliocene-Pleistocene Woodlark backarc rift basin, Southwest Pacific: Ocean Drilling Program Leg 180. *Proceedings of the Ocean Drilling Program, Scientific Results*, **80**, 1-53.

ROBERTSON, A. H. F. & USTAÖMER, T. 2004. Tectonic evolution of the Intra-Pontide suture zone in the Armutlu Peninsula, NW Turkey. *Tectonophysics*, **381**, 175-209.

ROBERTSON, A. H. F., USTAÖMER, T., PARLAK, O., ÜNLÜGENÇ, U. C., TAŞLI, K. & İNAN, N. 2006. The Berit transect of the Tauride thrust belt, S Turkey: Late Cretaceous-Early Cenozoic accretionary/collisional processes related to closure of the Southern Neotethys. *Journal of Asian Earth Sciences*, **27**, 108-145.

ROBERTSON, A. H. F., PARLAK, O. & USTAÖMER, T. 2009. Melange genesis and ophiolite emplacement related to subduction of the northern margin of the Tauride Anatolide continent, central and eastern Turkey. *In:* VAN HINSBERGEN, D. J. J., EDWARDS, M. A. & GOVERS, R. (eds) *Collision and Collapse at the Africa-Arabia-Eurasia Subduction Zone.* The Geological Society, London, Special Publications, **311**, 9-66.

ROBERTSON, A H. F., PARLAK, O., METIN, Y., VERGILI, O., TASLI. K., INAN, N. & SOYCAN, H. 2012. Late Palaeozoic-Cenozoic tectonic development of carbonate platform,

margin and oceanic units in the Eastern Taurides, Turkey. *The Geological Society, London, Special Publications,* **372**, *in press.*

ROBERTSON, A. H. F., PARLAK, O. & USTAÖMER, T. 2012. Overview of the Palaeozoic-Neogene evolution of Neotethys in the Eastern Mediterranean region (southern Turkey, Cyprus, Syria). *Petroleum Geoscience,* **18**, 381-404.

ROBINSON, A. G., BANKS, C. J., RUTHERFORD, M. M. & HIRST, J. P. P. 1995. Stratigraphic and structural development of the Eastern Pontides, Turkey. *Journal of the Geological Society,* **152**, 861-872.

SANCAY, R. H., BATI, Z., ISIK, U., KIRICI, S. & AKCA, N. 2006. Palynomorph, Foraminifera, and Calcareous Nannoplankton Biostratigraphy of Oligo-Miocene Sediments in the Mus¸ Basin, Eastern Anatolia, Turkey. *Turkish Journal of Earth Sciences*, **15**, 259–319.

SARI, B. & ÖZER, S., 2009. Upper Cretaceous rudist biostratigraphy of the Bey DaglarI Carbonate Platform, Western Taurides, SW Turkey. *Geobios,* **42**, 359-380.

SAUNDERS, A. D. & TARNEY, J. 1984. Geochemical characteristics of basaltic volcanism within back-arc basins. *In:* KOKELAAR, B. P. & HOWELLS, M. F. (eds) *Marginal Basin Geology: Volcanic and Associated Sedimentary and Tectonic Processes in Modern and Ancient Marginal Basins.* The Geological Society, London, Special Publications, **16**, 59-76.

SEYMEN, I. 1981. Stratigraphy and metamorphism of the Kırşehir Massif around Kaman (Kırşehir - Turkey). *Bulletin of the Geological Society of Turkey*, **24**, 7-14.

ŞENALP, M. 1979. Turbidites, olistostrome and olistoliths of Eocene age in the Sungurlu region of the Çankırı-Çorum basin. *Maden Tetkik ve Arama Bulletin,* **73**, 27-55 [in Turkish with English abstract].

ŞENALP, M. 1981. Sedimentological Sstudies of the continental Fformations around the region of Çankırı-Çorum Basin. *Turkish Geological Society Bulletin,* **24**, 65-74. [in Turkish with English abstract].

ŞENGÖR, A.M.C. & YILMAZ, Y.1981. Tethyan evolution of Turkey: a plate tectonic approach, *Tectonophysics*, **75**, 81-241.

ŞENGÖR, A. M. C., YILMAZ, Y. & SUNGURLU, O. 1984. Tectonics of the Mediterranean Cimmerides: nature and evolution of the western termination of Palaeo-Tethys. *In:* ROBERTSON, A. H. F. & DIXON, J. E. (eds) *The Geological Evolution of the Eastern Mediterranean.* Geological Society, London, Special Publications, **17**, 77-112.

ŞENGÖR, A. M. C., GÖRÜR, N. & ŞAROĞLU. F. 1985. Strike-slip deformation basin formation and sedimentation. *Society of Economic Palaeontolgists and Mineralogists, Special Publication*, **37**, 227-264.

SHABANIAN, E., ACOCELLA, V., GEONCADA, A., GHASEMI, H. & BELLIER, O. 2012. Structural control on volcanism in intraplate post collisional settings: Late Cenozoic to Quaternary examples of Iran and Eastern Turkey. *Tectonics*, **31**, TC3013.

SHEARMAN, D. J. 1997. Evaporite Sediments and Rocks: The Calcium Sulphate and Halite Facies. *Chapman & Hall.*

SHELTON, A. W. 1990. The interpretation of gravity data in Oman: constraints on the ophiolite emplacement mechanism. *In*: ROBERTSON, A. H. F., SEARLE, M. P. & RIES, A. C. (eds) *The Geology and Tectonics of the Oman Region*. The Geological Society, London, Special Publications, **49**, 459-471.

SPERNER, B., RATSCHBACHER, L. & OTT, R. 1993. Fault-striae analysis: A turbo pascal program package for graphical presentation and reduced stress tensor calculation. *Computers & Geosciences*, **19**, 1361-1388.

STAMPFLI, G. M. 2000. Tethyan oceans. *In:* BOZKURT, E., WINCHESTER, J. A., & PIPER, J. D. A. (eds) *Tectonics and Magmatism in Turkey and the Surrounding Area*. Geological Society, London, Special Publications, **173**, 1-23.

STAMPFLI, G. M. & BOREL, G. D. 2002. A plate tectonic model for the Paleozoic and Mesozoic constrained by dynamic plate boundaries and restored synthetic oceanic isochrons. *Earth and Planetary Science Letters,* **196**, 17-33.

STCHEPINSKY, V. 1944. Rapport sur la geologie et les resources minerals de la region de Malatya sud. *Maden Tetkik ve Arama Bulletin,* **1491** (unpublished), Ankara.

STENDAL, H., ÜNLÜ, T. & KONNERUP-MADSEN, J. 1995. Geological setting of iron deposits of Hekimhan province, Malatya, Central Anatolia, Turkey. *Transactions of the Institution of Mining and Mineralisation,* **104**, 46-54.

STERN, R. J. & BLOOMER, S. H. 1992. Subduction zone infancy: Examples from the Eocene Izu-Bonin-Mariana and Jurassic California arcs. *Geological Society of America Bulletin,* **12,** 1621-1636.

STERN, R. J. 2010. The anatomy and ontogeny of modern intra-oceanic arc systems. *In:* KUSKY, T. M., ZHAI, M. –G. & XIAO, W. (eds) *The Evolving Continents: Understanding Processes of Continental Growth.* The Geological Society, London, Special Publications, **338**, 7-34.

STEUBER, T. & LÖSER, H. 2000. Species richness and abundance patterns of Tethyan Cretaceous rudist bivalves (Mollusca: Hippuritacea) in the central-eastern Mediterranean and Middle East, analysed from a palaeontological database. *Palaeogeography, Palaeoclimatology, Palaeoecology*, **162**, 75-104.

STEUBER, T. 1999. Isotopic and chemical intra-shell variations in low-Mg calcite of rudist bivalves (Mollusca-Hippuritacea): disequilibrium fractionations and late Cretaceous seasonality. *International Journal of Earth Sciences*, **88**, 551-570.

STEUBER, T. 2002. Plate tectonic control on the evolution of Cretaceous platform carbonate production. *Geology*, **30**, 259-262.

STÖSSEL, I. AND BERNOULLI, D. 2000. Rudist lithosome development on the Maiella Carbonate Platform margin. In: Insalco, E., Skelton, P. W., and Palmer, T. J. (Eds.) *Carbonate Platform Systems: Components and Interactions*. Geological Society, London, Special Publications, **178**, 177-190

TAKANASHI, N., KODAIRA, S., KLEMPERER, S. L., TATSUMI, Y., KANEDA, Y. & SUYEHIRO, K. 2007. Crustal structure and evolution of the Mariana intra-oceanic island arc. *Geology*, **35**, 203-206.

TASLI, K., ÖZER, E. & KOÇ, H. 2006. Benthic foraminiferal assemblages of the Cretaceous platform carbonate succession in the Yavca area (Bolkar Mountains, S Turkey): biostratigraphy and palaeoenvironments. *Geobios*, **39**, 521-533.

TEKIN, E., AYYILDIZ, T., GÜNDOGAN, I. & ORTI, F. 2007. Modern halolites (halite oolites) in the Tuz Gölü, Turkey. *Sedimentary Geology*, **195**, 101-112.

TEMIZ, H. 2004. The role of thrust ramp reactivation in pull-apart mechanism of the Erzincan basin, North Anatolian Fault Zone, Turkey. *Geodinamica Acta*, **17-3**, 219-228.

TEMIZEL, I., ARSLAN, M., RUFFET, G. & PEUCAT, J. J. 2012. Petrochemistry, geochronology and Sr–Nd isotopic systematics of the Tertiary collisional and post-collisional volcanic rocks from the Ulubey (Ordu) area, eastern Pontide, NE Turkey: Implications for extension-related origin and mantle source characteristics. *Lithos*, **128**, 126-147.

TOPUZ, G., ALTHERR, R., SATIR, M., & SCHWARZ, W. H. 2004. Low-grade metamorphic rocks from the Pulur complex, NE Turkey: implications for the pre-Liassic evolution of the Eastern Pontides. *International Journal of Earth Sciences*, **93**, 72–91.

TOPUZ, G., OKAY, A. I., ALTHERR, R., SCHWARZ, W. H., SIEBEL, W., ZACK, T., SATIR, M. & ŞEN, C. 2011. Post-collisional adakite-like magmatism in the Ağvanis Massif and implications for the evolution of the Eocene magmatism in the Eastern Pontides (NE Turkey). *Lithos,* **125**, 131-150.

TURNER, F. J. 1953. Nature and dynamic interpretation of deformation lamellae in calcite of three marbles. *American Journal of Science*, **251**, 276-298.

TUREKIAN, K. K. & WEDEPOHL, K. H. 1961. Distribution of the elements in some major units of the Earth's crust. *Geological Society of America, Bulletin*, **72**, 175-192.

TÜRKMEN, İ., AKSOY, E. & TAŞGIN, C. K. 2007. Alluvial and lacustrine facies in an extensional basin: The Miocene of Malatya Basin, eastern Turkey. *Journal of Asian Earth Sciences*, **30**, 181-198.

TÜYSÜZ, O. 1990. Tectonic evolution of a part of the Tethyian orogenic collage: the Kargi Massif, Northern Turkey. *Tectonics,* **9**, 141-160.

UÇURUM, A., LARSON, L. T. & BOZTUĞ, D. 1996. Geology, geochemistry and petrology of the alkaline subvolcanic trachyte-hosted iron deposit in the Karakuz area, northwestern Hekimhan-Malatya, Turkey. *International Geology Review,* **38**, 995-1005.

UĞURTAŞ, G. 1975. Geophysical interpretation of part of the Tuz Gölü Basin. *Maden Tektik ve Arama Dergisi,* **85**, 38-45.

USTAÖMER, T. & ROBERTSON, A. H. F. 1997. Tectonicsedimentary evolution of the North Tethyan margin in the Central Pontides of Northern Turkey. *In:* ROBINSON, A. G. (ed) *Regional and Petroleum Geology of the Black Sea and Surrounding region*, AAPG Memoir no. **86,** 255–290.

USTAÖMER, T. & ROBERTSON, A. H. F. 2010. Late Palaeozoic-Early Cenozoic tectonic development of the Eastern Pontides (Artvin area), Turkey: stages of closure of Tethys along the southern margin of Eurasia. *In:* SOSSON, M., KAYMAKCI, N., STEPHENSON, R. R., BERGERAT, F. & STAROSTENKO, V. (eds) *Sedimentary Basin Tectonics from the Black Sea and Caucasus to the Arabian Platform.* The Geological Society, London, Special Publications, **340**, 281-327.

VERGİLİ, Ö. & PARLAK, O. 2005. Geochemistry and tectonic setting of metamorphic sole rocks and mafic dikes from the Pınarbaşı (Kayseri) ophiolite, Central Anatolia. *Ofioliti,* **30**, 37–52.

VINCENT, S. J., ALLEN, M. B., ISMAIL-ZADEH, A. D., FLECKER, R., FOLAND, K. A. & SIMMONS, M. D. Insights from the Talysh of Azerbaijan into the Paleogene evolution of the South Caspian region. *GSA Bulletin,* **117**, 1513-1533.

WAKABAYASHI, J. 1992. Nappes, tectonics of oblique plate convergence, and metamorphic evolution related to 140 million years of continuous subduction, Franciscan Complex, California. *Journal of Geology,* **100**, 19-40.

WAKABAYASHI, J. & DILEK, Y. 2000. Spatial and temporal relations between ophiolites and their subophiolitic soles: a test of models of forearc ophiolite genesis. *In:* DILEK, Y., MOORES, E. M., ELTHON, D. & NICOLAS, A. (eds) *Ophiolites and Oceanic Crust: New Insights from Field Studies and the Ocean Drilling Program*. Geological Society of America, Special Papers, **349**, 53-64.

WAKABAYASHI, J. & DILEK, Y. 2003. What constitutes 'emplacement' of an ophiolite?: Mechanisms and relationship to subduction initiation and formation of metamorphic soles. *In:* DILEK, Y. & ROBINSON, P. T. (eds) *Ophiolites in Earth History*. The Geological Society, London, Special Publications, **218**, 427-447.

WARBURTON, J., BURNHILL, T. J., GRAHAM, R. H. & ISAAC, K. P. 1990. The evolution of the Oman Mountains Foreland Basin. *In*: ROBERTSON, A. H. F., SEARLE, M. P. AND RIES, A. C. (eds) *The Geology and Tectonics of the Oman Region*. The Geological Society, London, Special Publication, **49**, 419-427.

WESTAWAY, R. & ARGER, J. Kinematics of the Malatya-Ovacik Fault Zone, *Geodinamica Acta,* **14**, 103–131.

WHATTAM, S. A. & STERN, R. J. 2011. The 'subduction initiation rule': a key for linking ophiolites, intra-oceanic forearcs, and subduction initiation. *Contributions to Mineralogy and Petrology,* **162**, 1031–1045.

WHITNEY, D. L. & DILEK, Y. 1998. Metamorphism during Alpine Crustal Thickening and Extension in Central Anatolia, Turkey: the Niğde Metamorphic Core Complex. *Journal of Petrology,* **39**, 1385-1403.

WHITNEY, D. L., TEYSSIER, C., DILEK, Y. & FAYON, A. K. 2001. Metamorphism of the Central Anatolian Crystalline Complex, Turkey: influence of orogen-normal collision vs. wrench dominated tectonics on P-T-t paths. *Journal of metamorphic geology,* **19**, 411-432.

WHITNEY, D. L., TEYSSIER, C., FAYON, A. K., HAMILTON, M. A. & HEIZLER, M. 2003. Tectonic controls on metamorphism, partial melting, and intrusion: timing and

duration of regional metamorphism and magmatism in the Niğde Massif, Turkey. *Tectonophysics*, **376**, 37-60.

WHITNEY, D. L. & HAMILTON, M. A. 2004. Timing of high-grade metamorphism in central Turkey and the assembly of Anatolia. *Journal of the Geological Society, London*, **161**, 823-828.

WILSON, M. 1966. Did the Atlantic close and then re-open? *Nature*, **211**, 676-681.

WILSON, M. 1989. Igneous petrogenesis. Unwin Hyman, London.

WINCHESTER, J. A. & FLOYD, P. A. 1977. Geochemical discrimination of different magma series and their differentiation products using immobile elements. *Chemical Geology*, **20**, 325-343.

WIRTZ, D. 1955. Bericht über die geolgischen Aufnahmen im Gebiet von Malatya und der Tohmasuyu-Depression. *Turkish Geological Society Bulletin*, **2364** (unpublished).

YALÇIN, H. & BOZKAYA, Ö. 1995. Sepiolite-palygorskite from the Hekimhan region (Turkey). *Clays & Minerals*, **43**, 705-717.

YALÇIN, H. & BOZKAYA, Ö. 1996. A new discovery of the Cretaceous/Tertiary boundary from the Tethyan Belt, Hekimhan Basin, Turkey: mineralogical and geochemical evidence. *International Geology Review*,**38**, 759-767.

YALÇIN, H., BOZKAYA, Ö. & Hozatlıoğlu, D. 2009. Cretaceous serpentinite-hosted phlogopite occurrences in Malatya-Kuluncak area, Turkey. *Proceedings of 14th National Clay Symposium (Turkey)*, pp. 174-192.

YALINIZ, M. K., FLOYD, P. A. & GÖNCÜOĞLU, M. C. 1996. Supra-subduction zone ophiolites of Central Anatolia; geochemical evidence from the Sarikaraman Ophiolite, Aksaray, Turkey. *Mineralogical Magazine*, **60**, 697-710.

YALINIZ, K. M., FLOYD, P. A. & GÖNCÜOĞLU, M. C.,2000. Geochemistry of Volcanic Rocks from the Çiçekdağ, Ophiolite, Central Anatolia, Turkey, and Their Inferred Tectonic Setting within the Northern Branch of the Neotethyan Ocean. *In:* BOZKURT, E., WINCHESTER, J. A. & PIPER, J. D. A. (eds) *Tectonics and Magmatism in Turkey and the Surrounding Area*. Geological Society, London, Special Publications, **173**, 203-218.

YAZGAN, E. & CHESSEX, R. 1991. Geology and tectonic evolution of the southeastern Taurides in the region of Malatya. *Turkish Association of Petroleum Geologists Bulletin*, **3**, 11-42.

YIĞITBAŞ, E. & YILMAZ, Y. 1996. New evidence and solution to the Maden complex controversy of the Southeast Anatolian orogenic belt (Turkey). *Geol Rundsch,* **85**, 250-263.

YILMAZ, Y. 1993, New evidence and model on the evolution of the southeast Anatolian orogen. *Geological Society of America Bulletin*, **105**, 251-271.

YILMAZ, A. & YILMAZ, H. 2004. Geology and structural evolution of the Divriği-Sivas region. *Geological Bulletin of Turkey,* **47**, 14-15.

YILMAZ, A. & YILMAZ, H. 2006. Characteristic features and structural evolution of a post collisional basin: The Sivas Basin, Central Anatolia, Turkey. *Journal of Asian Earth Sciences,* **27**, 16.

YILMAZ, S., BOZTU, D. & ÖZTÜRK, A. 1993. Geological setting, petrographic and geochemical characteristics of the Cretaceous and Tertiary igneous rocks in the Hekimhan- Hasançelebi area, northwest Malatya, Turkey. *Geological Journal,* **28**, 383-398.

YILMAZ, Y., TÜYSĞZ, O., YIĞITBAŞ, E., CAN GENÇ, Ş. & ŞENGÖR, A. M. 1997. Geology and tectonic evolution of the Pontides. *In:* ROBINSON, A. G. (ed) *Regional and Petroleum Geology of the Black Sea and Surrounding Region*. American Association of Petroleum Geologists, Memoirs **68**, 183-226.

YIN, A. 2006. Cenozoic tectonic evolution of the Himalayan orogen as constrained by along-strike variation of structural geometry, exhumation history, and foreland sedimentation. *Earth-Science Reviews,* **76**, 1–131.

ZELLER, G. F., LIZUKA, Y., MIYOSHI, M., TAMURA, Y. & TATSUMI, Y. 2012. Lower crustal H_2O controls on the formation of adakitic melts. *Geology,* **40**, 487–490.

ZORLU, K., INAN, S., GÜL, M., INAN, N., KURT, M. A. & ALPASLAN, M. 2011. Geological evolution of the Ulukışla Basin (Late Cretaceous-Eocene) Central Anatolia, Turkey. *Bulletin of the Earth Sciences Application and Research Centre of Hacettepe University*, **32**, 151-170.

Appendices

Appendix 1: X-Ray Fluorescence methodology and data

Whole rock X-Ray Fluorescence (XRF) geochemical analysis was carried out on 66 rock samples at the University of Edinburgh, School of Geosciences. The method used is that described by Fitton *et al.* (1998). A brief description is outlined below.

Weathered edges and vein material were removed from the samples. Rock samples weighing approximately 200g were crushed using a tungsten carbide jaw crusher. Larger samples were used for coarser grained material in order to reduce the risk of biased results due to phenocryst content. Then, approximately 50 g of material was ground to a fine-grained uniform powder in a tungsten carbide grinding mill for ~3 minutes. The powder was dried in an oven at ~80^{o}C for 24 hours.

For major element analysis, small quantities of powder were fired in platinum crucibles in a furnace at 1100^{o}C. A calculated weight of lithium flux powder was then added to the fired samples before being ignited in the furnace again. The resultant melt was pressed into glass discs. The samples were analysed using standard procedures on a Panalytical PW2404 wavelength-dispersive sequential X-Ray spectrometer at the University of Edinburgh, School of Geosciences.

For trace element analysis, powder was mixed with a PVA based binding agent and pressed in to pellets with a hydraulic press. The pellets were analysed using the aforementioned spectrometer.

The XRF data from the Darende Basin is presented here first, followed by the Hekimhan Basin. Samples have been split into there respective formations and presented in geochronological order.

Table 1.1. Whole rock major oxide (wt. %) and trace element (ppm) abundances determined by XRF of samples from the Karakayalar Member in the Darende Basin.

	Karakayalar Member								
Sample	MB08-111	MB09-D13	MB09-D16	MB10-8a	MB10-8b	MB10-9	MB10-26a	MB10-26b	MB10-26c
Rock type	Basalt	Basalt	Basalt	Basalt	Basalt	Basalt	Basalt	Basalt	Basalt
Location	MB08-15.2	MB09-2.4	MB09-3.3	MB10-3.1	MB10-3.1	MB10-3.1	MB10-7.4	MB10-7.4	MB10-7.4
latitude	38.6102	38.5981	38.5938	38.6053	38.6053	38.6053	38.4494	38.4494	38.4494
longitude	37.5986	37.6241	37.6242	37.6310	37.6310	37.6310	37.7119	37.7119	37.7119
Majors (wt %)									
SiO_2	59.72	58.26	61.51	58.95	59.00	58.22	57.64	57.81	57.56
Al_2O_3	17.18	18.37	18.81	17.03	17.06	16.91	17.73	17.75	17.68
Fe_2O_3	6.14	6.19	4.84	5.47	5.32	5.41	6.10	5.86	6.05
MgO	3.96	3.50	1.83	3.37	3.30	3.97	4.14	3.90	4.17
CaO	5.91	7.63	6.61	6.87	6.79	7.19	7.51	7.73	7.42
Na_2O	3.36	3.87	3.68	3.24	3.26	3.73	3.43	3.34	3.31
K_2O	2.48	0.98	1.77	1.34	1.34	1.35	1.23	1.28	1.27
TiO_2	0.83	0.91	0.73	0.66	0.64	0.67	0.80	0.76	0.78
MnO	0.11	0.10	0.04	0.07	0.07	0.09	0.11	0.10	0.10
P_2O_5	0.31	0.18	0.18	0.13	0.13	0.13	0.16	0.15	0.16
LOI	1.30	1.71	3.02	2.46	2.41	1.73	0.98	1.29	1.03
Total	99.55	99.55	99.53	99.60	99.34	99.40	99.82	99.97	99.52
Total - LOI	98.25	97.84	96.51	97.14	96.93	97.67	98.84	98.68	98.49
Trace elements (ppm)									
Zn	71.20	54.00	43.40	59.00	64.80	47.50	47.30	48.40	58.30
Cu	21.30	31.30	12.40	38.50	34.30	16.60	14.90	21.90	12.70
Ni	32.90	13.30	6.60	32.20	35.10	36.80	36.40	33.50	6.40
Cr	57.00	20.30	4.90	127.90	135.10	138.40	133.70	128.60	4.80
V	122.40	202.50	177.00	170.20	175.50	202.20	200.30	171.30	118.90
Ba	472.20	376.40	427.00	392.80	390.80	392.90	391.60	388.00	387.70
Sc	16.70	25.80	17.10	25.20	25.20	21.70	21.50	23.70	13.50
La	39.60	18.50	24.70	19.40	22.60	22.00	21.70	20.60	25.00
Ce	67.90	40.20	51.00	41.20	44.80	40.90	41.00	41.80	50.30
Nd	29.10	21.10	23.60	18.90	19.40	17.50	18.30	17.90	23.20
U_2	3.70	2.10	1.80	1.50	1.30	1.50	1.80	1.70	n.d
Th	12.10	7.80	8.80	6.40	6.50	7.40	7.50	7.10	n.d
Pb	14.00	5.90	5.90	5.60	5.90	6.40	6.30	6.60	n.d
Nb	23.40	11.70	12.00	10.20	10.50	10.40	10.40	10.40	10.20
Zr	216.00	158.50	163.30	137.30	139.00	141.70	142.60	140.20	190.80
Y	26.20	26.50	24.70	23.30	23.90	22.90	22.50	22.90	23.30
Sr	338.80	336.20	306.30	315.90	302.30	279.30	278.10	268.00	347.40
Rb	79.40	36.60	60.80	47.30	48.40	52.40	52.60	51.80	81.50

Table 1.2. Whole rock major oxide (wt. %) and trace element (ppm) abundances determined by XRF of samples from the Hocalikova Formation in the Hekimhan Basin.

Hocalikova Formation						
Sample	**MB08-1**	**MB08-5**	**MB08-127**	**MB09-H33**	**MB09-H56**	**MB10-116**
Rock type	Dacite	Gabbro	Rhyo-dacite	Rhyo-dacite	ex-Gabbro	Plagiogranite
Location	MB08-5.3	MB08-5.6	MB08-17.1	MB09-8.3	MB09-10.2	MB10-22.3
latitude	38.7943	38.7990	38.8042	38.7861	38.8988	38.7515
longitude	37.8985	37.9214	37.9135	37.8256	37.9195	38.1157
Majors (wt %)						
SiO_2	66.645	47.715	72.032	70.617	52.873	75.07
Al_2O_3	17.398	16.056	16.014	16.734	18.064	14.94
Fe_2O_3	3.920	4.355	1.163	1.582	9.576	0.65
MgO	0.579	12.599	0.408	1.255	5.152	0.14
CaO	4.313	18.223	3.733	4.661	4.656	0.73
Na_2O	3.962	0.784	5.294	3.100	6.820	4.28
K_2O	2.583	0.051	1.020	1.630	0.505	4.03
TiO_2	0.328	0.125	0.251	0.304	1.591	0.02
MnO	0.088	0.084	0.008	0.018	0.160	0.06
P_2O_5	0.184	0.008	0.078	0.099	0.602	0.07
LOI	2.68	2.94	1.32	4.38	4.92	0.79
Total	99.36	99.84	99.36	99.50	99.63	99.45
Total - LOI	96.68	96.91	98.04	95.12	94.72	98.66
Trace elements (ppm)						
Zn	61.30	19.10	3.70	23.90	38.40	9.6
Cu	6.50	100.70	27.80	16.30	3.90	1.4
Ni	2.90	245.60	10.80	9.20	429.40	0.5
Cr	n.d.	1306.70	n.d.	n.d.	1749.00	1.2
V	13.40	134.10	25.90	38.30	151.90	3
Ba	499.40	16.00	373.90	381.30	7.30	446.1
Sc	0.10	52.40	0.80	2.40	52.40	0.3
La	41.80	n.d.	8.80	10.50	n.d.	2.9
Ce	77.00	0.70	16.70	16.70	0.30	7.6
Nd	26.80	1.10	8.20	10.60	2.80	2.5
U_2	3.20	n.d.	1.20	0.90	0.20	2.8
Th	14.20	0.20	4.30	4.00	0.00	1
Pb	8.00	0.10	5.80	6.30	0.50	17.6
Nb	19.30	0.20	7.40	6.80	0.30	17.2
Zr	243.80	1.70	76.90	83.30	1.70	23.9
Y	21.40	2.90	3.50	4.70	4.20	14.6
Sr	303.30	163.20	584.30	383.80	5.90	64
Rb	88.50	0.70	16.60	35.80	0.30	134.1

Table 1.3a. Whole rock major oxide (wt. %) and trace element (ppm) abundances determined by XRF of samples from the Hasançelebi Formation in the Hekimhan Basin.

Hasançelebi Formation

Sample	MB08-8	MB08-18	MB08-20	MB08-140	MB08-183	MB08-223	MB08-224	MB08-225	MB08-227	MB08-228	MB08-232	MB09-H36
Rock type	Basalt	Dolerite	Basalt	Basalt	Basalt	Basalt	Basalt	Skarn	Basalt	Basalt	Basalt	Basalt
Location	MB08-6.4	MB08-6.5	MB08-6.6	MB08-18.2	MB08-22.1	MB08-25.4	MB08-25.4	MB08-25.4	MB08-25.4	MB08-25.4	MB08-25.7	MB09-8.9
latitude	38.8793	38.9416	38.9416	38.9384	38.8770	38.9314	38.9314	38.9314	38.9314	38.9314	38.9007	38.8295
longitude	37.8955	37.8750	37.8750	37.8420	37.8979	37.8792	37.8792	37.8792	37.8792	37.8792	37.8843	37.7500
Majors (wt %)												
SiO_2	55.079	42.473	49.988	50.596	46.347	51.638	56.120	49.957	48.275	58.047	53.837	51.600
Al_2O_3	18.470	15.672	16.906	17.358	20.787	17.611	17.892	1.653	17.696	17.701	20.035	18.498
Fe_2O_3	4.593	3.477	7.503	7.998	5.757	11.072	3.544	6.443	10.558	3.137	8.644	7.011
MgO	2.951	12.049	6.075	5.888	6.503	4.471	3.296	12.939	7.128	2.926	1.336	8.018
CaO	9.273	26.154	10.036	9.908	19.337	7.837	7.336	26.932	6.142	5.999	5.855	9.223
Na_2O	5.924	-0.031	4.787	4.295	0.736	4.208	9.242	0.316	5.123	7.858	4.900	3.895
K_2O	1.071	0.016	2.929	2.271	0.136	1.179	0.570	0.032	2.989	1.960	3.763	0.699
TiO_2	1.963	0.097	1.383	1.146	0.167	1.528	1.199	1.609	1.653	1.751	1.221	0.843
MnO	0.153	0.092	0.089	0.079	0.221	0.135	0.040	0.115	0.038	0.042	0.086	0.099
P_2O_5	0.522	0.002	0.303	0.461	0.009	0.320	0.762	0.004	0.399	0.579	0.323	0.113
LOI	6.34	3.86	5.12	4.64	6.77	0.96	6.30	5.30	4.70	4.42	4.95	3.54
Total	99.51	99.64	99.22	99.41	99.65	99.59	99.60	99.81	98.00	99.57	99.24	99.82
Total - LOI	93.18	95.78	94.09	94.77	92.87	98.63	93.30	94.51	93.30	95.16	94.29	96.28
Trace elements (ppm)												
Zn	228.80	19.90	47.00	33.40	80.10	16.90	17.80	30.90	29.60	80.60	368.50	27.20
Cu	1366.00	109.50	29.40	7.30	885.30	8.10	6.70	15.10	5.20	41.90	13.80	14.20
Ni	25.00	244.20	48.00	32.60	118.70	5.60	9.70	69.00	83.30	86.00	2.40	77.60
Cr	-22.40	2228.10	57.60	131.60	60.70	n.d.	282.80	49.60	16.20	137.40	n.d.	217.50
V	206.10	133.30	197.30	172.60	169.30	66.40	93.20	160.90	163.30	179.80	62.60	227.50
Ba	277.50	10.90	3018.70	281.00	439.90	429.10	130.70	25.90	569.50	294.40	787.90	118.10
Sc	18.90	38.40	23.10	27.70	57.20	5.90	26.10	35.20	29.30	23.10	0.70	35.60
La	38.70	n.d.	52.10	17.60	n.d.	68.40	58.00	55.50	42.90	17.40	68.60	0.50
Ce	75.00	n.d.	61.20	41.80	n.d.	175.70	132.60	122.50	70.10	35.10	114.90	8.70
Nd	33.30	0.40	12.90	22.90	3.10	72.70	65.60	50.60	21.20	20.40	40.30	9.60
U_2	1.60	0.00	7.50	3.90	n.d.	8.90	9.50	8.00	7.90	1.10	5.90	0.30
Th	7.20	0.30	4.00	10.80	0.30	20.30	23.70	17.50	3.50	4.50	18.20	1.00
Pb	28.20	0.50	13.00	0.60	3.20	2.00	12.80	2.20	2.60	5.70	52.30	1.40
Nb	46.60	0.20	15.30	16.60	0.20	54.60	46.30	42.10	12.60	14.60	85.20	4.20
Zr	213.80	1.10	134.40	162.00	7.10	363.80	280.30	79.70	145.90	172.90	330.90	62.20
Y	37.30	3.60	23.90	24.10	9.10	59.00	61.00	43.00	11.90	28.40	39.70	21.00
Sr	410.60	3.50	3383.10	334.60	90.00	382.10	170.70	31.70	353.80	429.80	470.60	267.20
Rb	58.20	0.30	113.40	57.00	6.30	35.40	10.00	1.00	157.90	23.10	108.00	20.40

Table 1.3b. Whole rock major oxide (wt. %) and trace element (ppm) abundances determined by XRF of samples from the Hasançelebi Formation in the Hekimhan Basin.

Hasançelebi Formation continued

Sample	MB09-H93	MB08-131	MB08-132	MB08-135	MB08-200	MB08-203	MB08-204	MB09-D27	MB10-48	MB10-110a	MB10-110b
Rock type	Basalt	Dacite?	Dacite?	Basalt	Dacite?	Basalt	Basalt	Basalt	Basalt	Basalt	Basalt
Location	MB09-15.5	MB08-18.1	MB08-18.1	MB08-18.1	MB08-22.2	MB08-23.1	MB08-23.1	MB09-7.3	MB10-10.2	MB10-20.1	MB10-20.1
latitude	38.8555	38.9687	38.9687	38.9687	38.9159	38.8700	38.8700	38.8123	38.8528	38.8829	38.8829
longitude	37.9178	37.8684	37.8684	37.8684	37.9169	37.9257	37.9257	37.8298	37.9485	37.8925	37.8925
Majors (wt %)											
SiO_2	53.981	53.51	54.61	53.40	59.52	53.90	64.81	54.32	51.99	57.80	58.42
Al_2O_3	16.288	19.35	18.93	17.85	17.65	17.37	14.77	17.08	18.02	14.27	14.29
Fe_2O_3	10.602	7.32	9.63	10.16	4.46	7.77	5.65	8.55	7.53	11.24	11.09
MgO	3.322	2.43	1.88	2.98	1.29	2.00	2.60	3.01	3.49	4.65	4.74
CaO	11.628	7.89	4.75	7.66	6.87	8.12	7.55	6.63	12.09	5.49	4.78
Na_2O	2.642	3.69	3.90	3.23	8.90	3.45	2.50	3.36	3.19	3.77	4.15
K_2O	0.737	3.90	4.34	2.68	0.12	4.65	1.21	4.37	2.21	0.67	0.41
TiO_2	0.611	1.30	1.31	1.48	0.86	1.92	0.73	1.86	0.98	1.82	1.85
MnO	0.135	0.10	0.15	0.20	0.08	0.14	0.05	0.12	0.13	0.19	0.15
P_2O_5	0.054	0.51	0.51	0.36	0.24	0.70	0.12	0.69	0.37	0.10	0.11
LOI	9.74	5.4	2.77	7.01	6.11	5.29	5.39	8.48	7.89	5.25	4.78
Total	99.44	100.07	99.52	100.10	99.82	99.44	99.75	99.98	99.94	99.60	99.72
Total - LOI	89.70	94.67134	96.7479	93.09271	93.70821	94.15018	94.3584	91.50064	92.05	94.35	94.94
Trace elements (ppm)											
Zn	151.00	82.3	69.7	66.7	18.8	231.5	351.9	98.7	137.8	553.8	311.2
Cu	11.90	13.5	13.9	9.7	4.3	20.7	10.3	80.9	9.4	49.4	30.6
Ni	33.80	11.5	10.4	9.6	13.1	24.9	26.8	78.1	8.8	5.8	6.3
Cr	39.80	n.d.	n.d.	n.d.	n.d.	62.3	58.2	2.4	8.1	5.7	6.1
V	275.10	154.2	92.8	142.7	5.9	163.2	162.1	260.7	111.8	261.7	259.2
Ba	45.40	1107.8	1066.2	552	17.3	933.8	865.4	218.1	656.7	40.3	28.7
Sc	47.90	5.7	6.4	19.5	n.d.	16.7	15.2	25.7	12.8	48.5	49.2
La	n.d.	56.1	52.2	30.7	90.2	72.1	68.1	6.3	60.8	-1.8	-2.1
Ce	2.70	101.9	92.8	65.5	159.3	138.5	131.9	20.7	119.2	6.6	7.8
Nd	4.60	40.9	35.6	28.7	60.6	57.3	54.1	12.5	49.8	6	5.3
U_2	0.00	6.6	3.4	1	3.4	6.2	5.9	0.1	5.5	0	0.2
Th	0.10	16.6	17.3	8.4	16.7	20.9	20.2	1.4	19.1	0.2	0
Pb	10.40	13.2	9.7	7.8	2.2	20.2	21.2	14.6	13.9	7.2	6.5
Nb	1.40	35.1	34.8	20.5	92.9	63.2	61.2	5.2	52.5	1.3	1.3
Zr	29.70	256.9	260.5	156.4	407.5	364.9	350.1	66	345.4	48.7	49.3
Y	15.50	31.5	31.4	25.3	49.1	32.4	31.2	18.5	31	25.3	21.2
Sr	91.20	563.2	529.4	351.3	64.3	588.2	567.1	353.5	395.6	69.6	66.7
Rb	33.30	110.4	124.9	50	2.2	137.8	122.8	9.1	126.4	9.4	6.2

Table 1.4. Whole rock major oxide (wt. %) and trace element (ppm) abundances determined by XRF of samples from the volcaniclastic sediments of the Hasançelebi Formation in the Hekimhan Basin.

Hasançelebi Formation (volcaniclastic sediments)

Sample	MB08-09	MB08-10	MB08-11	MB08-12	MB08-14	MB08-49
Rock type	Mudstone	Mudstone	Mudstone	Mudstone	Mudstone	Mudstone
Location	6.4	6.4	6.4	6.4	6.4	9.1
latitude	38.8793	38.8793	38.8793	38.8793	38.8793	38.8802
longitude	37.8955	37.8955	37.8955	37.8955	37.8955	37.8945
Majors (wt %)						
SiO_2	43.51	43.89	53.69	53.56	55.53	54.59
Al_2O_3	9.54	13.47	16.52	11.68	14.86	16.31
Fe_2O_3	30.73	21.24	13.42	20.13	9.96	10.65
MgO	5.00	7.73	5.56	3.74	7.39	5.55
CaO	3.75	4.77	2.12	2.55	6.33	4.81
Na_2O	0.65	0.92	0.94	0.65	4.49	6.79
K_2O	1.70	2.66	4.67	2.75	0.25	0.24
TiO_2	0.42	0.61	0.80	0.50	0.86	0.76
MnO	4.27	4.36	1.92	3.93	0.27	0.20
P_2O_5	0.42	0.36	0.38	0.50	0.06	0.07
LOI	4.52	6.38	6.041	5.5	5.05	4.94
Total	99.30	99.83	99.51	99.51	99.69	99.37
Total - LOI	94.77941	93.45328	93.468015	94.01	94.639845	94.430336
Trace elements (ppm)						
Zn	298	270.7	158.8	216.4	86.9	64.9
Cu	156.5	3783.6	1427.8	619.9	675.9	62.3
Ni	249.9	310.5	201.8	246.8	98.8	121.1
Cr	83.7	109.4	158.7	55.5	354.2	409.4
V	780.8	356.2	143	302.3	269.8	201.8
Ba	108.5	227.4	149.1	173.3	30	36.3
Sc	18.3	24.5	32.9	21	45	42.3
La	86.2	75.9	56.3	76.8	n.d.	4.7
Ce	72	86.7	101.8	82.2	8.6	13.4
Nd	84.2	65	52.5	65.3	5	7.7
U_2	0.7	0.1	0.8	0.1	n.d.	0
Th	2.6	5.4	9.1	3.9	n.d.	n.d.
Pb	150.6	61.5	51.4	138.6	4.9	11
Nb	9.7	10.8	14.5	10.5	1.3	2.3
Zr	115.6	109.9	127.7	105.1	43.9	43.3
Y	79	58.9	56.5	60.5	19.9	20.2
Sr	73.8	149.3	87.1	313.5	78.4	62.3
Rb	53.6	77.5	125.1	84.9	2.6	4.3

Table 1.5. Whole rock major oxide (wt. %) and trace element (ppm) abundances determined by XRF of samples from the Yüceşafak Member in the Hekimhan Basin.

Yüceşafak Member

Sample	MB08-17	MB08-18	MB08-25	MB10-97	MB10-111a	MB10-111b
Rock type	Syenite	Syenite	Carbonitite	Syenite	Monzogranite?	Monzogranite?
Location	6.5	6.5	6.7	17.5	20.3	20.3
latitude	38.9416	38.9416	38.9219	39.0017	38.9143	38.9143
longitude	37.8750	37.8750	37.8834	37.7606	37.8779	37.8779
Majors (wt %)						
SiO_2	65.661	42.473	24.08	68.74	59.07	58.30
Al_2O_3	17.184	15.672	2.96	16.31	16.77	16.38
Fe_2O_3	0.413	3.477	5.70	2.91	2.04	2.29
MgO	0.148	12.049	3.38	1.23	4.29	4.99
CaO	6.127	26.154	44.66	3.83	7.66	8.53
Na_2O	9.721	-0.031	0.00	4.15	7.45	7.52
K_2O	0.223	0.016	1.54	2.24	1.79	1.01
TiO_2	0.387	0.097	0.79	0.38	0.90	0.93
MnO	0.038	0.092	0.08	0.04	0.05	0.05
P_2O_5	0.098	0.002	16.80	0.16	0.00	0.00
LOI	4.70	3.86	15.03	0.73	3.47	3.59
Total	99.98	99.64	99.35	99.90	100.04	99.66
Total - LOI	95.28	95.78	84.31683	99.17	96.57	96.07
Trace elements (ppm)						
Zn	n.d.	19.90	31.2	36.2	2.1	0.9
Cu	6.00	109.50	8.5	13.6	3.4	3.6
Ni	n.d.	244.20	84.5	8	13.7	17.1
Cr	n.d.	2228.10	n.d.	13.7	0	3.9
V	15.50	133.30	107.4	42.3	22.5	22.9
Ba	366.90	10.90	345.4	382.4	717.1	439.8
Sc	n.d.	38.40	22.5	5.1	3.1	6.8
La	31.30	n.d.	653.3	28.4	49.7	51.4
Ce	77.70	n.d.	943.9	48.8	104.2	109.7
Nd	34.70	0.40	283.4	17.7	44.3	48.2
U_2	8.00	0.00	15.3	2.3	8.8	7.1
Th	26.00	0.30	79.1	7.6	17.7	16.6
Pb	0.30	0.50	4.4	10	1.2	1.8
Nb	34.10	0.20	16.7	10.8	56.5	54.4
Zr	372.40	1.10	40.5	193.3	375	387.2
Y	34.00	3.60	218.8	12.6	50.4	58.4
Sr	137.70	3.50	193.9	322	309.5	319.9
Rb	n.d.	0.30	76.6	46.5	22.8	12.3

Table 1.6. Whole rock major oxide (wt. %) and trace element (ppm) abundances determined by XRF of samples from the Kocaözü Member in the Hekimhan Basin.

	Kocaözü Member					
Sample	**MB10-70a**	**MB10-70b**	**MB10-70c**	**MB10-84a**	**MB10-84b**	**MB10-84c**
Rock type	Basalt	Basalt	Basalt	Basalt	Basalt	Basalt
Location	MB10-12.1	MB10-12.1	MB10-12.1	MB10-14.3	MB10-14.3	MB10-14.3
latitude	38.8190	38.8190	38.8190	38.7316	38.7316	38.7316
longitude	38.0402	38.0402	38.0402	37.8932	37.8932	37.8932
Majors (wt %)						
SiO_2	373.12	111.71	44.35	2.31	10.59	10.66
Al_2O_3	240.97	9.20	59.79	0.00	0.62	1.79
Fe_2O_3	207.99	226.70	29.32	11.14	25.24	13.94
MgO	212.12	225.98	29.53	13.56	29.08	14.15
CaO	200.35	216.17	27.77	10.51	27.52	15.31
Na_2O	160.47	1169.97	19.48	89.78	149.98	58.38
K_2O	237.26	398.20	31.81	23.34	44.35	21.75
TiO_2	242.35	397.18	30.77	23.02	46.01	19.95
MnO	237.79	390.03	31.08	23.76	44.77	21.22
P_2O_5	44.86	390.84	5.28	29.86	50.69	18.69
LOI	1.49	1.57	1.28	2.76	2.82	2.67
Total	99.33	100.49	99.43	99.54	99.29	99.61
Total - LOI	97.84	98.92	98.15	96.78	96.47	96.94
Trace elements (ppm)						
Zn	60	55.4	102.3	84	83.6	84.6
Cu	32.8	46.2	9.3	71.4	73.8	66.4
Ni	126.6	131.3	32	56.5	55.1	57.4
Cr	275	288.2	128.5	182.2	178.7	181.1
V	200	188.9	151.3	223.7	228.5	224.2
Ba	221.1	211.5	1144.7	389.6	388.6	381.6
Sc	28.5	26.8	18.8	30.7	29.7	30
La	12.9	10	85.4	22.2	21.9	22.6
Ce	28	26.5	144.4	42.7	44.3	43.1
Nd	13.4	14.5	55.3	20.6	18.9	20.1
U_2	0.3	0.1	4.6	2.5	2.1	2.3
Th	2.3	2.9	20.5	7.7	7.9	7.7
Pb	3.2	4.5	15.5	8.3	9	9.1
Nb	8.8	8.8	24.4	12.6	12.8	12.6
Zr	94.1	94.2	157.3	153.9	156.1	153.6
Y	22	21.8	24.6	28.2	28.5	28.2
Sr	315.1	311.7	862.3	308.9	308.9	304.9
Rb	9.6	8.2	57.4	46.1	47.7	46.2

Table 1.7. Whole rock major oxide (wt. %) and trace element (ppm) abundances determined by XRF of samples from the Leylek Member in the Hekimhan Basin.

	Leylek Member			
Sample	MB10-34a	MB10-34b	MB10-51	MB10-120
Rock type	Andesite	Andesite	Andesite	Andesite
Location	MB10-8.1	MB10-8.1	MB10-10.4	MB10-24.3
latitude	38.8778	38.8778	38.8914	38.8632
longitude	37.7877	37.7877	37.8152	37.8057
Majors (wt %)				
SiO_2	70.57	69.48	54.90	59.98
Al_2O_3	16.45	16.48	18.58	17.88
Fe_2O_3	1.90	1.92	6.55	5.91
MgO	1.05	1.34	1.43	3.61
CaO	1.84	2.28	8.16	6.08
Na_2O	5.78	6.10	3.73	3.49
K_2O	1.94	1.87	4.38	2.20
TiO_2	0.34	0.34	1.67	0.62
MnO	0.02	0.03	0.13	0.10
P_2O_5	0.13	0.15	0.46	0.14
LOI	1.21	1.10	4.72	1.39
Total	99.35	99.93	99.69	99.44
Total - LOI	98.14	98.83	94.97	98.05
Trace elements (ppm)				
Zn	31.2	31.3	117.3	47.7
Cu	18.2	17.2	62.9	13.7
Ni	22	24.3	25.8	9.1
Cr	16.2	15.5	20.6	33.1
V	36.9	38.9	581.8	139.8
Ba	551.9	530.8	22.7	421.7
Sc	5.7	4.3	48	20.5
La	20.2	18	1.4	19.3
Ce	28	29.7	11.7	39.3
Nd	12.4	10.5	10.1	16.2
U_2	1.5	1.6	0.1	1.6
Th	5.5	5.5	n.d.	7.2
Pb	5.7	7.1	2	4.4
Nb	12.2	12.2	1.4	10.1
Zr	95.9	95.8	82.5	119.1
Y	9.9	6.6	32.2	20.1
Sr	446.4	515.3	172.4	277.2
Rb	43.3	42	4	63.7

Appendix 2: Structural data

Structural orientation and kinematic data were extensively measured in the field. Strike, dip and dip-direction were used to measure fault and fold axial planes. Lineations (e.g. slickensides, axial hinges) were measured using their azimuth and plunge. The data were analysed with Steronet7 (Allmendinger 2011) or FaultKin5.2 (Allmendinger 1992; 1995) initially in order to visual and spatial patterns in structural orientation. Subsequently data were quantitatively analysed with TectonicsFP (Ortner *et al.* 2002).

'Angelier plots' (Angelier 1979) are lower hemisphere stereonet plots that display fault planes as great circles and the relative slip of the hanging wall as an arrow on the great circle. In order to calculate this, a given data set must be corrected so that any lineations lie at 0^{o} to their respective fault plane. This operation is conducted using TectonicsFP (Ortner *et al.* 2002).

Fault data were analysed in terms of their P (pressure)-, B- and T (tension)-axes (Turner 1953). For a given fault zone, the P-axis is aligned at 45^{o}, the T-axis is perpendicular to the P-axis and the B-axis is normal to both P-and T-axes (Sperner *et al.* 1993). The P- and T-axes are, therefore, interpreted as representing the orientation of $\sigma 1$ and $\sigma 3$, respectively and give an indication of palaeostress. TectonicsFP contains a feature which calculates the 'PT' function for a given data set and generates a stereonet. Clustering of the P-, B- and T- axes data on the stereonet are a good indication that the faults analysed were created under the same stress regime. Heterogeneity indicates the inverse. TectonicsFP automatically calculates the R values (the probability) of homogeneity in the data set.

These are first order analysis methods and do not take into account the mechanical rock properties, anisotropy of the medium or the coefficients of friction and cohesion, which lie outside of the remit of this thesis.

Table 2. 8a. Fault planes and kinematic features with a normal sense of slip from the Darende Basin.

Structural Data Type	Azimuth	Dip	Direction	Kinematics	Loc.	Fm
2010 data						
fault plane	231	83	SW	Normal	1.6	Asartepe?
fault plane	060	50	NE	Normal ?	5.2	Ophiolite
fault plane	274	72	W	normal	6.3	Ulupinar
fault plane	280	80	W	normal	6.3	Ulupinar
fault plane	115	79	E	normal	6.3	Ulupinar
fault plane	175	64	S	Normal	7.2	Ulupinar
2009 Autumn data						
fault plane	207	43	SW	extension	2.1	Asartepe
CS-fabric	223	41	SW	extension	2.1	Asartepe
Slickenline		41		extension	2.1	Asartepe
fault plane	160	82	SE	extension	3.3	Eocene
Slickenline		26		extension	3.3	Eocene
Slickenline		28		extension	3.3	Eocene
fault plane	108	53	E	transtension	3.3	Eocene
Slickenline		43		transtension	3.3	Eocene
fault plane	256	58	W	normal	7.3	Hekimhan
fault plane	187	79	S	normal	7.3	Huyuk
2009 Spring data						
fault plane	246	65	SW	Normal	9.1	Darende
fault plane	059	83	ENE	Normal	9.1	Darende
fault plane	291	79	W	Normal	9.1	Darende
fault plane	069	47	E	Normal	12.1	Yenice
Slickenlines		44			12.1	Yenice
fault plane	075	45	E	Normal	12.1	Yenice
fault plane	067	46	E		12.1	Yenice
fault plane	100	33	E	Normal	12.1	Yenice
fault plane	092	18	E		12.1	Yenice
fault plane	325	20	NW		12.1	Yenice
fault plane	140	25	SE	Normal	12.1	Yenice
fault plane	157	33	SE	Normal	12.1	Yenice
fault plane	201	49	S		12.1	Yenice
fault plane	076	38	E	Normal	12.1	Yenice
fault plane	076	57	E	Normal	12.1	Yenice
fault plane	105	47	E	Normal	12.1	Yenice
fault plane	111	61	E	Normal	12.1	Asartepe
fault plane	086	31	E	Normal	12.1	Asartepe
fault plane	074	32	E	Normal	12.1	Asartepe
fault plane	175	65	S	Normal	12.1	Asartepe
fault plane	295	86	W	(Normal?)	14.2	Korgantepe
fault plane	282	68	W	(Normal?)	14.2	Korgantepe
fault plane	342	80	N	(Normal?)	14.2	Korgantepe
fault plane	349	67	N	(Normal?)	14.2	Korgantepe
fault plane	178	72	S	(Normal?)	14.2	Korgantepe
fault plane	161	70	S	(Normal?)	14.2	Korgantepe
fault plane	349	77	N	(Normal?)	14.2	Korgantepe
fault plane	344	74	N	(Normal?)	14.2	Korgantepe
fault plane	341	71	N	(Normal?)	14.2	Korgantepe
fault plane	335	66	NW	(Normal?)	14.2	Korgantepe
fault plane	358	65	N	(Normal?)	14.2	Korgantepe
fault plane	333	75	NW	(Normal?)	14.2	Korgantepe
fault plane	033	67	N	Normal	14.2	Korgantepe
fault plane	155	69	SE	Normal	15	Korgantepe
fault plane	256	62	W	Normal	15	Korgantepe

Table 2. 1b

fault plane	286	41	W	Normal	15	Korgantepe
fault plane	293	38	W	Normal	15	Korgantepe
fault plane	260	64	W	Normal	15	Korgantepe
fault plane	274	68	W	Normal	15	Korgantepe
fault plane	269	63	W	Normal	15	Korgantepe
fault plane	261	71	W	Normal	15	Korgantepe
cs fabric	349	32	N	Normal	16.1	Yenice
cs fabric	345	63	N	Normal	16.1	Yenice
cs fabric	358	68	N	Normal	16.1	Yenice
cs fabric	352	74	N	Normal	16.1	Yenice
fault plane	313	84	NW	Normal	16.1	Yenice
fault plane	281	65	W	Normal	16.1	Yenice
fault plane	301	84	W	Normal	16.1	Yenice
fault plane	311	87	NW	Normal	16.1	Yenice
fault plane	312	86	NW	Normal	16.1	Yenice
fault plane	303	87	NW	Normal	16.1	Yenice
fault plane	306	89	NW	Normal	16.1	Yenice
fault plane	309	78	NW	Normal	16.1	Yenice
fault plane	322	85	NW	Normal	16.1	Yenice
fault plane	321	75	NW	Normal	16.1	Yenice
fault plane	313	85	NW	Normal	16.1	Yenice
fault plane	323	86	NW	Normal	16.1	Yenice
fault plane	326	87	NW	Normal	16.1	Yenice
fault plane	306	80	NW	Normal	16.1	Asartepe
fault plane	161	79	S	normal	21.2	Yenice
fault plane	172	61	S	normal	21.2	Yenice
fault plane	172	41	S	normal	21.2	Yenice
fault plane	333	82	N	normal	21.2	Yenice
fault plane	346	85	N	normal	21.2	Yenice
2008 data						
fault plane	316	78	NE	oblique normal	10.1	kirankaya
slickenline	40/321			oblique normal	10.1	kirankaya
fault plane	036	87	E	normal	10.2	Yenice
fault plane	030	86	E	normal	10.2	Yenice

Table 2.9a. Fault planes and kinematic features with a reverse sense of slip from the Darende Basin.

Structural Data						
Type	**Azimuth**	**Dip**	**Direction**	**Kinematics**	**Loc.**	**Formation**
2010 data						
Fault plane	200	48	ESE	Thrust	2.3	Asartepe
Fault plane	46	30	NE	Thrust	2.3	Asartepe
Fault plane	008	37	N	Thrust		
Fault plane	355	41	N	Thrust		
Fault plane	14	48	N	transpression	5.1	Korgantepe
CS fabric	57	66	NE	transpression	5.1	Korgantepe
Fault plane	106	85	E		7.2	Geniz
Slickenlines	003	31		transpression	7.2	Geniz
Fault plane	127	78	SE		7.2	Geniz
Slickenlines	041	18		transpression	7.2	Geniz
Fault plane	038	79	NE		7.2	Tohma
Fault plane	45	83	NE	Reverse ?	7.2	Tohma
Slickenlines	036	83			7.2	Tohma
Slickenlines	131	12			7.2	Tohma
Fault plane	66	80	E	Thrust	7.2	Ulupinar
Fault plane	250	32	W	Thrust	7.2	Ulupinar
Slickenlines	090	36			7.2	Ulupinar
2009 Autumn data						
Fault plane	246	26	SW	thrust	1.4	Darende
CS-fabric	198	59	S	thrust	1.4	Darende
CS-fabric	178	46	S	thrust	1.4	Darende
CS-fabric	189	55	S	thrust	1.4	Darende
Fault plane	343	15	N	compression	1.2	Yenice
Slickenline	053	09		compression	1.2	Yenice
Fault plane	017	65	NE	compression	1.2	Yenice
Slickenline	057	54		compression	1.2	Yenice
Fault plane	246	26	SW	thrust	1.4	Darende
CS-fabric	188	59	S	thrust	1.4	Darende
CS-fabric	178	46	S	thrust	1.4	Darende
CS-fabric	189	55	S	thrust	1.4	Darende
Fault plane	159	51	SW	thrust	2.1	Asartepe
Fault plane	162	53	SW	thrust	2.1	Asartepe
Fault plane	166	05	N		2.1	Asartepe
CS-fabric	186	37	N	thrust to S	2.1	Asartepe
Fault plane	151	40	SE	thrust	2.1	Asartepe
Slickenline	058	61		thrust	2.1	Asartepe
Slickenline	063	52		thrust	2.1	Asartepe
Fault plane	239	42	SW	thrust	2.1	Asartepe
Slickenline	026	32		thrust	2.1	Asartepe
Fault plane	187	42	SW	thrust	2.1	Asartepe
Slickenline	021	41		thrust	2.1	Asartepe
Fault plane	200	32	SW	thrust	2.1	Asartepe
Slickenline	220	19		thrust	2.1	Asartepe
Slickenline	061	41		thrust	2.1	Asartepe
Slickenline	045	62		thrust	2.1	Asartepe
Slickenline	025	11		thrust	2.1	Asartepe
Fault plane	184	37	S	thrust	2.1	Asartepe
Slickenline	020	35		thrust	2.1	Asartepe
Fault plane	034	38	NW	thrust	3.2	?
Slickenline	210	15		thrust	3.2	?
2009 Spring data						
fault plane	355	32	NE	thrust	7.2B	Darende
fault plane	206	35	SW	thrust	7.2B	Darende

Table 2.2b

fault plane	214	45	SE	oblique	7.2B	Darende
Slickenlines	283	18			7.2B	Darende
cs fabric	252	56	W	to E	7.3	Darende
fault plane	004	76	N	transpression	10.3	Darende
Slickenlines	122	34		dextral	10.3	Darende
2008 data						
fault plane	187	36	S	thrust	3.2	
Shear Fabric	178	50	S	thrust	3.2	
fault plane	337	47	NW	thrust	10.1	kirankaya
fault plane	351	38	SW	thrust	10.1	kirankaya
fault plane	227	50	SW	thrust	10.1	kirankaya
fault plane	181	28	S		14.2	Darende
slickenline	23/207			thrust	14.2	Darende

Table 2.10a. Fault planes and kinematic features with a strike-slip sense of slip from the Darende Basin.

Structural Data						
Type	**Azimuth**	**Dip**	**Direction**	**Kinematics**	**Loc.**	**Fm**
2010 data						
Fault plane	076	78	E	Dextral	1.2	Asartepe
Slickenlines	167	06		Dextral	1.2	Asartepe
Fault plane	132	90		strike-slip	1.2	Asartepe
Fault plane	010	90		strike-slip	1.2	Asartepe
Fault plane	126	79	E	strike-slip	1.2	Asartepe
Fault plane	148	82	SE	strike-slip	1.2	Asartepe
Fault plane	161	80	S	strike-slip	1.2	Asartepe
Fault plane	141	85	E	strike-slip	1.2	Asartepe
Fault plane	012	85	N	Dextral	1.3	Asartepe
Slickenlines	101	05		Dextral	1.3	Asartepe
Fault plane	014	48	N	transpression	5.1	Korgantepe
CS fabric	057	66	NE	transpression	5.1	Korgantepe
Fault plane	106	85	E	oblique sinistral	7.2	Geniz
Slickenlines	003	31		oblique sinistral	7.2	Geniz
Fault plane	127	78	SE	transpression	7.2	Geniz
Slickenlines	041	18		transpression	7.2	Geniz
Fault plane	086	32	E	Sinistral	7.2	Tohma
Slickenlines	132	22		Sinistral	7.2	Tohma
2009 Autumn data						
Fault plane	187	44	S	oblique extension	1.2	Yenice
Slickenline	272	54		oblique extension	1.2	Yenice
Fault plane	057	87	E	oblique extension	1.2	Yenice
Slickenline	150	09		oblique extension	1.2	Yenice
Fault plane	058	86	NE	dextral	1.2	Yenice
Slickenline	146	19		dextral	1.2	Yenice
Fault plane	277	85	W	strike-slip	1.2	Yenice
Slickenline	011	19		strike-slip	1.2	Yenice
Fault plane	046	62	NE	oblique extension	1.4	Darende
Slickenline	139	23		oblique extension	1.4	Darende
Fault plane	043	85	NE	oblique extension	1.4	Darende
Slickenline	138	42		oblique extension	1.4	Darende
Fault plane	231	63	W	dextral	1.4	Darende
Slickenline	132	18		dextral	1.4	Darende
Fault plane	235	64	SW	sinistral	3.1	Asartepe
Slickenline	144	22		sinistral	3.1	Asartepe
Fault plane	236	64	W	dextral	3.1	Q
Slickenline	136	39		dextral	3.1	Q
Fault plane	298	62	NW	sinistral	3.2	?
Slickenline	050	26		sinistral	3.2	?
Fault plane	266	58	W	dextral	3.2	?
Fault plane	348	63	N	dextral	3.2	?
Fault plane	108	53	E	transtension	3.3	Eocene
Slickenline	201	43		transtension	3.3	Eocene
Fault plane	187	70	S	dextral	5.4	Darende
2009 Spring data						
fault plane	034	45	SE	oblique compression	7.2B	Ophiolite
Slickenlines	283	18		oblique compression	7.2B	Ophiolite
fault plane	092	45	E	oblique compression	8.1	Darende
Slickenlines	064	09		oblique compression	8.1	Darende
fault plane	004	76	N	transpression	11.3	Darende
Slickenlines	122	34		dextral	11.3	Darende
fault plane	213	85	SW	dextral	12.1	Yenice
fault plane	108	84	E	strike-slip	14.2	Yenice

Table 2.3b.

fault plane	096	75	E	strike-slip	15	Korgantepe
fault plane	297	62	NW	strike-slip	16.1	Yenice
fault plane	282	71	W	strike-slip	16.1	Yenice
2008 data						
fault plane	096	39	E	strike-slip	1.1	Asartepe
slickenline	011	07		strike-slip	1.1	
fault plane	052			strike-slip	1.12	Darende
fault plane	113	51	E	sinistral	1.12	Darende
fault plane	091	69	E	sinistral	1.12	Darende
fault plane	137			strike-slip	1.12	Darende
fault plane	045			strike-slip	2.1	
fault plane	055	42	NE	strike-slip	2.5	
slickenline	145	06		strike-slip	2.5	
fault plane	099	35	E	sinistral	3.2	Asartepe
fault plane	077	43	E	sinistral	3.2	Asartepe
fault plane	084	32	E	sinistral	3.2	Asartepe
fault plane	073	37	E	dextral	3.2	
slickenline	163	11		dextral	3.2	
slickenline	217	10			3.2	
slickenline	237	42			3.2	
fault plane	149	90		sinistral	4.5	
slickenline	059	00		sinistral	4.5	
fault plane	115	90		sinistral	4.5	
slickenline	025	10		sinistral	4.5	
fault plane	243	69	W	sinistral	10.1	kirankaya
fault plane	248	84	W	sinistral	10.1	kirankaya
fault plane	046	78	NE	oblique normal	10.1	kirankaya
slickenline	321	40		oblique normal	10.1	kirankaya
fault plane	261	38	SW	thrust	10.1	kirankaya
fault plane	261	80	W	sinistral	10.1	kirankaya
fault plane	245	59	W	sinistral	10.1	kirankaya
fault plane	125			sinistral	10.2	Yenice
fault plane	097			sinistral	12.1	Yenice
fault plane	296	81	W	oblique normal	14.2	Darende
slickenline	024	07		oblique normal	14.2	Darende

Table 2.11. Fold planes and features from the Darende Basin.

Structural Data Type	Azimuth	Dip	Direction	Loc.	Fm
2010 data					
Axial plane S	032	82	NE	5.5	Yenice
Axial plane S	364	22	W	6.1	Darende
2009 Spring data					
Axial plane A		71	SSW	10.1	Darende
Axial plane S	008	40	N	10.1	Darende
Axial plane A	331	62	NW	10.1	Darende
Axial plane A	058	76	NE	10.2B	Darende
Axial plane A	080	79	E	10.2B	Darende
Axial plane S	095	75	E	10.2B	Darende
Axial plane A	086	73	E	10.2B	Darende
Axial plane A	021	58	N	16.1	Yenice
Axial plane S	017	61	N	16.1	Yenice
Axial plane A	076	70	E	21.2	Yenice
Axial plane A	350	65	N	21.2	Yenice
Axial plane S	270	51	S	21.2	Yenice
Axial plane A	154	53	S	21.2	Yenice
Axial plane A	348	47	N	21.2	Yenice
Axial plane S	002	51	N	21.2	Yenice
2008 data					
Axial plane A	272	36	W	3.2	
Axial plane A	229	59	SW	10.2	Yenice
Anticline Plunge	319			10.2	Yenice
Axial plane S	248	80	N	10.2	Yenice
Syncline Plunge	258			10.2	Yenice
Axial plane A	205	54	SW	10.2	Yenice
Anticline Plunge	295			10.2	Yenice
Axial plane S	226	68	SW	10.2	Yenice
Syncline Plunge	316			10.2	Yenice
Axial plane A	226	80	SW	10.2	Yenice
Anticline Plunge	316			10.2	Yenice
Axial plane S	206	72	SW	10.2	Yenice
Syncline Plunge	296			10.2	Yenice
Axial plane A	090			12.1	Ulupinar
Anticline Plunge	090			12.1	Ulupinar

Table 2.12. Fault planes and kinematic features with a normal sense of slip from the Hekimhan Basin.

Structural Data Type	Azimuth	Dip	Direction	Kinematics	Loc.	Fm
2010 data						
fault plane	260	84	W	normal	8.1	Tohma
slickenline	007	70		normal	8.1	Tohma
fault plane	010	60	N	normal	15.5	Hekimhan
slickenlines	100	80		normal	15.5	Hekimhan
fault plane	045	79	NE	normal	17.1	Karadere
fault plane	307	90		normal	17.1	Karadere
fault plane	004	87	N	normal	18.2	trachyte
fault plane	000	80	N	normal	18.2	trachyte
fault plane	346	63	NW	normal	20.1	Akpinar
fault plane	358	69	N	normal	20.1	Akpinar
fault plane	017	56	N	normal	21.1	Karadere
fault plane	017	78	N	normal	21.1	Karadere
fault plane	058	75	NE	normal	23.1	Karadere
slickenline	130	51		normal	23.1	Karadere
fault plane	151	85	SE	normal?	19.3	Tohma
fault plane	199	82	S	normal?	22.1	hasancelebi
fault plane	256	58	W	normal	7.3	Hekimhan
2009 Autumn data						
fault plane	187	79	S	normal	7.3	Huyuk
fault plane	148	74	SE	normal?	9.4	Huyuk?
fault plane	049	75	NE	normal?	9.4	Huyuk?
fault plane	031	62	NE	Normal	14.2	Akpinar ?
2008 data						
fault plane	039	84	NE	Normal	14.2	Akpinar ?
fault plane	060	88	NE	Normal	14.2	Akpinar ?
fault plane	099	86	E	Normal ?	15.1	Akpinar
fault plane	108	77	E	Normal ?	16.2	Hekimhan
fault plane	076	85	E	Oblique	16.3	Hekimhan
Slickenlines	163	24			16.3	Hekimhan
fault plane	333	49	NW	Normal	16.4	Akpinar ?
fault plane	340	57	NW	Normal	16.4	Akpinar ?
fault plane	325	46	NW	Normal	16.4	Akpinar ?
fault plane	326	52	NW	Normal	16.4	Akpinar ?
fault plane	334	61	NW	Normal	16.4	Akpinar ?
fault plane	312	60	NW	Normal	16.4	Akpinar ?
fault plane	338	55	NW	Normal	16.4	Akpinar ?
fault plane	309	64	NW	Normal	17.2	Kamatlar
fault plane	253	70	W	Normal	17.2	Kamatlar
fault plane	012	79	N	Normal	19.1	Hekimhan
fault plane	067	84	E	Normal ?	21.3	Akpinar ?
fault plane	075	78	E	Normal	23.1	Geniz
fault plane	094	84	E	Normal ?	23.2	Geniz
fault plane	002	60	N	normal?	15.2	Akpinar
Slickenlines	116	70		normal?	15.2	Akpinar

Table 2.13. Fault planes and kinematic features with a reverse sense of slip from the Hekimhan Basin.

Structural Data Type	Azimuth	Dip	Direction	Kinematics	Loc.	Fm
2010 data						
Fault plane	064	63	E	Reverse ?	14.3	Akpinar
Fault plane	253	60	SW	Reverse ?	15.2	Akpinar
Fault plane	081	43	E	Reverse	17.2	Kamatlar
Fault plane	092	62	E	Reverse	17.2	Kamatlar
Fault plane	096	70	E	Reverse	17.2	Kamatlar
Fault plane	078	57	E	Reverse	17.2	Kamatlar
Fault plane	106	60	E	Reverse	17.2	Kamatlar
Fault plane	085	63	E	Reverse	17.2	Kamatlar
Fault plane	114	59	E	Reverse	17.2	Kamatlar
Fault plane	079	27	E	Reverse	17.2	Kamatlar
Fault plane	103	79	E	Reverse	17.2	Kamatlar
Fault plane	157	47	E	Reverse	17.2	Kamatlar
Fault plane	182	80	S	Reverse ?	18.1	Hekimhan
2009 Autumn data						
Fault plane	209	35	SW	thrust?	9.4	Huyuk?
Fault plane	024	55	N	thrust?	12.1	Hasancelebi
2008 data						
fault plane	137	47	SE	thrust	8.2	Hekimhan
fault plane	052	41	E	thrust	8.2	Hekimhan
fault plane	078	58	E	thrust	17.1	Karadere
fault plane	313	40	NW	thrust	19.4	Hekimhan
fault plane	305	71	NW	thrust	19.4	Hekimhan
fault plane	052	49	NE	thrust	20.2	Hekimhan
fault plane	221	35	SW	thrust	20.2	Hekimhan
fault plane	186	31	S	thrust	20.2	Hekimhan
fault plane	311	15	NW	thrust	22.1	Hasancelebi
fault plane	310	65	NW	thrust?	15.5	Hekimhan

Table 2.14a. Fault planes and kinematic features with a strike-slip sense of slip from the Hekimhan Basin.

Structural Data Type	Azimuth	Dip	Direction	Kinematics	Loc.	Fm
2010 data						
fault plane	173	90		dextral	8.1	Tohma
slickenline	165	22		dextral	8.1	Tohma
fault plane	091	88	E	dextral	8.1	Tohma
slickenline	175	21		dextral	8.1	Tohma
fault plane	104	88	E	dextral	8.1	Tohma
slickenline	008	12		dextral	8.1	Tohma
fault plane	094	86	E	dextral	8.1	Tohma
slickenline	011	09		dextral	8.1	Tohma
fault plane	053	89	E	dextral	8.1	Tohma
slickenline	161	05		dextral	8.1	Tohma
fault plane	257	90		sinistral	16.1	Hekimhan
slickenlines	258	25		sinistral	16.1	Hekimhan
fault plane	270	65	W	sinistral	17.1	Karadere
fault plane	056	83	NE	sinistral	17.1	Karadere
fault plane	225	80	SW	dextral	18.2	trachyte
fault plane	120	84	SE	sinistral	19.3	Tohma
fault plane	052	90		sinistral	19.3	Tohma
fault plane	157	78	SE	sinistral	19.3	Tohma
fault plane	264	79	W	dextral	19.3	Tohma
fault plane	267	81	W	dextral	19.3	Tohma
fault plane	276	75	W	dextral	19.3	Tohma
fault plane	085	80	E	sinistral	19.3	Tohma
fault plane	260	76	W	dextral	19.3	Tohma
fault plane	341	68	NW	dextral	22.1	hasancelebi
fault plane	347	69	NW	dextral	22.1	hasancelebi
fault plane	348	80	NW	dextral	22.1	hasancelebi
fault plane	250	80	W	strike-slip	15.5	Hekimhan
fault plane	263	70	W	strike-slip	18.2	trachyte
fault plane	115	77	SE	strike-slip	19.3	Tohma
fault plane	090	78	E	strike-slip	19.3	Tohma
fault plane	147	80	SE	strike-slip	19.3	Tohma
fault plane	057	78	E	strike-slip	19.3	Tohma
fault plane	027	90		strike-slip	19.3	Tohma
2009 Autumn data						
Fault plane	108	69	E	sinistral	7.3	Karadere
Slickenline	012	39		sinistral	7.3	Karadere
Slickenline	087	39		sinistral	7.3	Huyuk
Fault plane	171	82	S	sinistral	7.3	Huyuk
Slickenline	081	15		sinistral	7.3	Huyuk
Fault plane	019	80	N	dextral	10.1	oph/kara
Slickenline	107	08		dextral	10.1	oph/kara
Fault plane	359	71	N	sinistral	12.1	Hasancelebi
Fault plane	027	90		strike-slip	12.1	Hasancelebi
Fault plane	311	75	NW	sinistral	14.3	Tohma
Slickenline	046	08		sinistral	14.3	Tohma
2008 data						
Fault plane	065	90		strike-slip	8.2	Leylek
Fault plane	085	70	E	Dextral	10.2	Leylek
Slickenlines	175	07		Dextral	10.2	Leylek
Fault plane	009	81	N	Sinistral	10.2	Leylek
Slickenlines	099	12		Sinistral	10.2	Leylek
Fault plane	217	82	SW	Sinistral	11.1	Zorebehan
Fault plane	212	84	SW	Sinistral	11.1	Zorebehan

Table 2.7b.

Slickenlines	120	18		Sinistral	11.1	Zorebehan
Fault plane	262	70	W	strike-slip	12.3	Evaporite
Slickenlines	170	17		strike-slip	12.3	Evaporite
Slickenlines	170	35		strike-slip	12.3	Evaporite
Fault plane	322	86	NW	SS	13.4	Miocene?
Fault plane	030	58	NE	Dextral	15.2	Akpinar
Slickenlines	125	15		Dextral	15.2	Akpinar
Cleavage	017	63	N		15.2	Akpinar
Fault plane	012	86	N	Dextral	22.2	Karadere
Slickenlines	283	32		Dextral	22.2	Karadere
Fault plane	263	76	W	sinistral?	17.2	Kamatlar
Slickenlines	172	38		sinistral?	17.2	Kamatlar
Fault plane	316	88	NW	strike-slip	19.1	Hekimhan